PARP/XRCC1 Surveillance of the Human Genome

A thesis submitted to the University of Sussex for the degree of Doctor of Philosophy

By William Gittens

August 2017

Declaration

I hereby declare that this thesis has not been and will not be, submitted in whole or in part to another University for the award of any other degree.

William Gittens

Acknowledgements

I would like to thank my supervisor Professor Keith Caldecott for his guidance throughout this project. I am also grateful to the many members of the Caldecott Lab, past and present, who have taught me so much and made it such an enjoyable place to work. I would especially like to thank Fernando, for teaching me his Golden Rules of Science…

Finally, I want to thank all my friends and family for their friendship, and for supporting (and tolerating) me over the last four years.

UNIVERSITY OF SUSSEX

DOCTOR OF PHILOSOPHY BIOCHEMISTRY

PARP/XRCC1 SURVEILLANCE OF THE HUMAN GENOME

SUMMARY

DNA single strand breaks (SSBs) are one of the most common lesions to genomic DNA, arising from various endogenous and exogenous sources. Single strand break repair (SSBR) constitutes a biochemical pathway whereby SSBs are detected, enzymatically processed and ligated. Whilst the general mechanisms of SSBR are relatively well described *in vitro,* there are remaining questions concerning how the pathway operates *in vivo.* For example, an early step in SSBR is thought to be the poly(ADP-ribose) polymerase (PARP)-dependent modification of SSB-proximal proteins with ADP-ribose, which is a signal for the recruitment of downstream repair factors, including the central scaffold XRCC1. Yet, the presence of multiple DNA-dependent PARP genes (*PARP1, PARP2 and PARP3*) has caused confusion regarding their specific roles in SSBR. This thesis potentially clarifies some contentious aspects of PARP function in the repair of SSBs induced by reactive oxygen species (ROS) and by Topoisomerase 1 (Top1). By employing *PARP1*$^{-/-}$*/PARP2*$^{-/-}$ cells generated herein using CRISPR-Cas9 technology, in combination with pre-extraction immunofluorescence imaging and high-content analysis, I demonstrate that both PARP1 and PARP2 contribute towards ROS-induced ADP-ribosylation and XRCC1 chromatin-localization, but that in response to Top1-SSBs, these functions are specifically supported by PARP1 alone. Furthermore, using *TDP1*$^{-/-}$ and *XRCC1*$^{-/-}$*/TDP1*$^{-/-}$ cells also generated herein, I characterize a striking hyper-ADP-ribosylation phenotype in response to Top1-SSBs. The clinical significance of this was confirmed by co-workers, who observed a similar phenotype in an XRCC1-deficient patient, where mutations in *XRCC1* underlie a novel cerebellar neurodegenerative disease. This phenotype could be utilized in future to screen for genes with novel functions in SSBR. Finally, I investigate the functional implications of disrupted SSBR genes for rates of repair and cellular viability using alkaline single-cell electrophoresis and clonogenic survival assay. In doing so, I unexpectedly discovered that deletion of PARP1 suppresses CPT-induced comet tail moments of WT and *XRCC1*$^{-/-}$ cells.

Contents

Abbreviations

ADP	Adenosine Diphosphate
AIF	Apoptosis inducing factor
ALS	Amyotrophic lateral sclerosis
AMP	Adenosine monophosphate
ANOVA	Analysis of variance
AOA	Ataxia with oculomotor apraxia
AP	Apurinic/apyrimidinic
APE1	Apurinic/apyrimidinic endonuclease 1
APLF	Aprataxin and PNKP-like factor
APS	Ammonium persulphate
APTX	Aprataxin
ART	ADP-ribosyltransferase
ARTD	Diphtheria toxin-like ADP-ribosyltransferase
AT	Ataxia telangiectasia
ATCC	American type culture collection
ATM	Ataxia telangiectasia mutated
ATP	Adenosine triphosphate
ATR	ATM and Rad3 – related protein
ATRIP	ATR interacting protein
BCA	Bicinchroninic acid
BER	Base excision repair
BIR	Break-induced replication
BLAST	Basic local alignment search tool
BLM	Bloom syndrome RecQ -like helicase
BRCT	BRCA1 C-terminus domain
BSA	Bovine serum albumin
BTR	BLM-TopoIIIα-RMI1-RMI2 complex
CDS	Coding sequence
CHFR	*Checkpoint with forkhead and ring finger domains*
CHO	Chinese hamster ovary
CPT	Camptothecin
CRISPR	Clustered regularly interspaced short palindromic repeat
CSK	Cytoskeleton
CTD	C-terminal domain

DAPI	4',6-diamidino-2-phenylindole
DDR	DNA damage response
DMEM	Dulbecco's modified essential medium
DMS	Dimethyl sulphide
DMSO	Dimethyl sulphoxide
DNA	Deoxyribonucleic acid
DRB	5,6-Dichloro-1-β-D-ribofuranosylbenzimidazole
DSB	Double-strand break
DSBR	DSB repair
DTT	Dithiothreitol
ECL	Electrochemiluminescence
EDTA	Ethylenediaminetetraacetic acid
EGFP	Enhanced GFP
EMA	European medicines agency
FCS	Fetal calf serum
FDA	Food and drug administration
FHA	Forkhead- associated
FITC	Fluorescein isothiocyanate
FL	Full length
FOS	*Fos proto-oncogene*
FP	Fluorescent protein
FRDA	Freidreich ataxia
GFP	Green fluorescent protein
GOI	Gene of interest
HBSS	Hank's balanced salt solution
HCA	High content analysis
HD	Helical domain
HEPES	4-(2-hydroxyethyl)-1-piperazineethanesulfonic acid
HR	Homologous recombination
ICL	Interstrand crosslink
IED	Immediate early response genes
IF	Immunofluorescence
IHC	Immunohistochemistry
IP	Immunoprecipitation
IR	Ionising radiation
JM	Joint molecules

KO	Knockout
LB	Lysogeny broth
LDH	Lactate dehydrogenase
LP-BER	Long-patch base excision repair
MAR	Mono(ADP-ribose)
MCSZ	Microcephaly, seizures, and developmental delay
MEFS	Murine embryonic fibroblasts
MEM	Minimum essential medium
MIF	Macrophage migration inhibitory factor
MMR	Mismatch repair
MMS	Methyl methanesulphonate
MPG	*3 methyladenine DNA glycosylase*
MRN	MRE11-RAD50-NBS1 complex
MUTYH	*mutY DNA glycosylase*
NAD^+	Nicotinamide adenine dinucleotide
NADPH	Nicotinamide adenine dinucleotide phosphate
NCBI	National centre for biotechnology information
NER	Nucleotide excision repair
NHEJ	Non-homologous end joining
NLS	Nuclear localisation sequence
NMD	Nonsense mediated decay
NMDA	N-Methyl-D-aspartate
NMR	Nuclear magnetic resonance
NNK	Nicotine derived nitrosamine ketone
NO	Nitric oxide
NTD	N-terminal domain
NTR	N-terminal region
OAR	Oligo(ADP-ribose)
OB	Oligonucleotide/oligosaccharide-binding
OH	Hydroxyl
$ONOO^-$	Peroxynitrite
PAGE	Polyacrylamide gel electrophoresis
PAM	Protospacer adjacent motif
PAR	Poly(ADP-ribose)
PARG	*Poly(ADP-ribose) glycohydrolase*
PARP	*Poly(ADP-ribose) polymerase*

PBM	PAR-binding motif
PBS	Phosphate buffered saline
PBZ	PAR-binding zinc finger
PCNA	*Proliferating cell nuclear antigen*
PCR	Polymerase chain reaction
PG	Phosphoglycol
PGA	Phosphoglycolaldehyde
PIC	Proteinase inhibitor cocktail
PIKK	Phosphoinositide 3-kinase-related kinase
PLD	*Phospholipase D*
PMSF	phenylmethane sulphonyl fluoride
PNK	*Polynucleotide kinase*
PNKP	*Polynucleotide kinase phosphatase*
POLB	*DNA polymerase β*
PUA	α,β unsaturated aldehyde
RFP	Red fluorescent protein
RNA	Ribonucleic acid
RNAPII	*RNA polymerase 2*
RNAse	Ribonuclease
ROS	Reactive oxygen species
RPA	*Replication protein A*
RPE-1	Retinal pigmented epithelium cell line 1
SAM	S-adenosyl methionine
SB	Sample buffer
SDS	Sodium dodecyl sulphate
SDSA	Synthesis-dependent strand annealing
SEM	Standard error of the mean
SETX	*Senataxin*
SOD	*Superoxide dismutase*
SP-BER	Short-patch base excision repair
SSB	Single-strand break
SSBR	Single-strand break repair
SUMO	*Small ubuitin-like modifier*
TAE	Tris-acetate-EDTA
TBE	Tris-borate-EDTA
TBST	Tris-buffered saline with Tween-20

TDG	*Thymine DNA glycosylase*
TDP1	*Tyrosyl-DNA phosphodiesterase 1*
TDP2	*Tyrosyl-DNA phosphodiesterase 2*
TE	Tris-EDTA
TEMED	Tetramethylethylenediamine
TOP1	*Topoisomerase 1*
TOP2	*Topoisomerase 2*
TOP3	*Topoisomerase 3*
TSS	Transcription start site
TTS	Transcription termination site
UNG	*Uracil DNA glycosylase*
UV	Ultraviolet
WB	Western blot
WGR	Tryptophan-Glycine-Arginine (domain)
WRN	*Werner syndrome helicase*
WT	Wild-type
WWE	Tryptophan-Tryptophan-Glutamic acid (domain)
XLF	*XRCC4-like factor*
XRCC1	*X-ray cross-complementing protein 1*
ZFD	Zinc finger domain

List of Figures

List of Tables

Chapter One

Introduction

1.1. General introduction

Genomic DNA is constantly at threat from a variety of endogenous and exogenous chemicals, and from electromagnetic and particle radiation originating on Earth, in the Sun, and beyond. Whilst it is true that natural selection relies upon the sporadic mutations that may result from genetic lesions or their inaccurate repair, life itself would be impossible without near-perfect molecular maintenance. It is for this reason that DNA repair pathways have developed in complexity throughout Evolution; from the minimal collection of genes found in prokaryotes, to the paralogous and often-redundant multitude in multicellular eukaryotes.

By far the most frequently occurring DNA lesions are the substrates of base excision repair (BER) and single-strand break repair (SSBR) (Lindahl 1993). Collectively, these lesions have been estimated to occur in humans with a frequency in the order of 10^4 to 10^5 cell^{-1} day^{-1}, depending on the cell type (Lindahl 1993, Nakamura and Swenberg 1999, Hegde, Hazra et al. 2008, Swenberg, Lu et al. 2011). This introduction will review the various sources and types of BER/SSBR substrates (see section 1.2), the pathways that operate to repair them in human cells (see section 1.5), and the consequences for our understanding of human disease (see section 1.6). This thesis is particularly focussed on the formation and repair of two types of physiologically-relevant DNA single-strand breaks (SSBs): those resulting from reactions with reactive oxygen species (ROS), and those resulting from the abortive activity of Topoisomerase I. As the formation of ROS-induced SSBs can occur indirectly as intermediates within BER, this introduction will also provide an overview of the substrates and mechanisms of this pathway.

BER/SSBR comprises a front-line repair system which when perturbed or overburdened can lead to the formation of more dangerous lesions, such as double strand breaks (DSBs) during replication (see section 1.3). To aid in understanding the cellular and physiologically consequences of unrepaired SSBs, this chapter will therefore also provide a brief overview of DSB repair (DSBR) mechanisms and the DNA Damage Response (DDR) (see section 1.4).

1.2. Base Modifications and SSBs

There are numerous sources of DNA SSBs, including chemical agents, ionising radiation, and endogenous enzymes. Some of these agents, such as ROS, can cause SSBs both directly, and indirectly as intermediates in the BER of modified nucleobases. This section will begin by introducing the various sources of SSBs and base modifications, and the chemistry of the resulting lesions (sections 1.2.1 to 1.2.4).

1.2.1. Reactive Oxygen Species (ROS)

ROS is a collective term for a group of molecules containing incompletely reduced and therefore highly reactive forms of oxygen. This includes the superoxide radical anion ($O_2^{\bullet-}$), hydroxyl radical ($OH^{\bullet}$), hydrogen peroxide (H_2O_2), hydroperoxyl radical ($HO_2^{\bullet}$), peroxynitrite ($ONOO^-$), Ozone (O_3) and singlet oxygen ($^1O_2$) (Krumova and Cosa 2016), amongst others. Of these, hydroxyl radicals, singlet oxygen and peroxynitrite are the most relevant direct DNA damage sources (Cooke, Evans et al. 2003). The primary endogenous source of hydroxyl radicals and peroxynitrites is superoxide radical anions generated in the mitochondria by low levels of electron leakage from the electron transport chain (1-3% of electrons; (Valko, Leibfritz et al. 2007)), or at the plasma membrane by NADPH oxidases. The anionic nature of the superoxide radical anion restricts diffusion across plasma membranes, but it may react to form more freely diffusible ROS. One such reaction is with a nitric oxide radical ($^{\bullet}NO$) to produce peroxynitrite (Szabo, Ischiropoulos et al. 2007), which may diffuse to the nucleus and damage DNA directly. Another is the dismutation of two superoxide radicals into hydrogen peroxide or water, which is catalysed by superoxide dismutase (SOD) in a two-step reaction (Hayyan, Hashim et al. 2016). Hydrogen peroxide is much more diffusible than superoxide, being comparable to water in this respect (Chung, Xia et al. 2007). This allows it to cross plasma membranes and permeate into the nucleus. Here it may participate in a Fenton reaction, whereby Fe^{2+} is oxidized to Fe^{3}+, generating the highly reactive hydroxyl radical ($OH^{\bullet}$) (Cooke, Evans et al. 2003). The third species which is thought to contribute appreciably to oxidative DNA damage is singlet oxygen, which can be generated

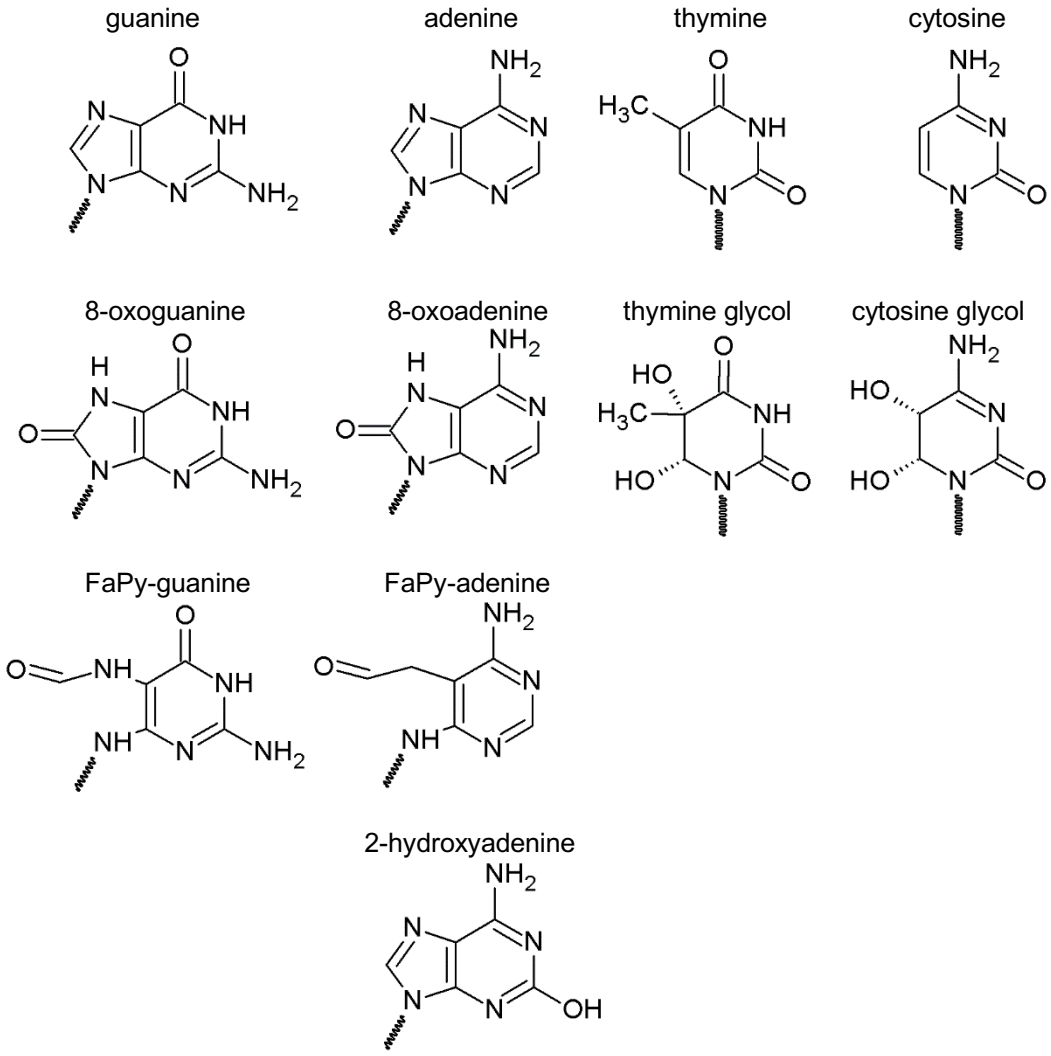

Figure 1.1. Common products of nucleobase oxidation. The structures of the four DNA nucleobases are shown, along with some of the most frequent products of their oxidation. The purines guanine and adenine can be oxidized in ring opening reactions to form formamidopyrimidine (FaPy) derivatives, or oxidized to produce 8-oxo derivatives. Adenine can additionally be oxidized at position 2 to form 2-hydroxyadenine. By comparison, the most common oxidation products of the pyrimidines thymine and cytosol are glycol derivatives.

directly by photoexcitation of molecular oxygen in the presence of a photosensitizing molecule (Valko, Leibfritz et al. 2007) or by the action of several enzymes (Hayaishi and Nozaki 1969, Chan 1971, Kanofsky 1983), often involved in host immune responses (Teixeira, Cunha et al. 1999). ROS can react with all moieties of DNA; leading to strand breaks and oxidization of bases, in a ratio which differs depending on the ROS in question (Kennedy, Moore et al. 1997).

Whilst all four DNA nucleobases can be oxidized *in vivo* to produce a variety of derivatives (Fig. 1.1.), the low redox potential of guanine makes it particularly susceptible (Neeley and Essigmann 2006). Of the many possible guanine oxidation products (Neeley and Essigmann 2006), the most common is 8-oxoguanine (8-oxoG). If not repaired, this lesion is especially deleterious because in its *syn* configuration it can pair with an adenine base (Hsu, Ober et al. 2004), bringing the potential for G-to-T transversion mutations during DNA replication. Oxidized bases are substrates for BER, which will be discussed in section 1.5.1.

In addition to the nucleobases, the deoxyribose-phosphate (dRP) moiety of DNA is susceptible to direct attack by ROS. This generally proceeds by abstraction of one of the seven available hydrogen atoms on deoxyribose, leaving a radical carbon atom which can initiate intramolecular rearrangements and result in strand breakage (Pogozelski and Tullius 1998). Notably, strand scission by these mechanisms does not produce directly ligatable DNA ends, but rather non-canonical 3'-phosphate, 3'-phosphoglycolate, or 3'-phosphoglycolaldehyde termini (Bertoncini and Meneghini 1995, Breen and Murphy 1995). A summary of DNA SSB end chemistry is provided in Fig. 1.2. ROS can also generate SSBs indirectly, as intermediates in the base excision repair (BER) of oxidized bases (see section 1.5.1), or by increasing steady-state levels of Top1ccs via multiple mechanisms (see section 1.2.3). It should also be noted that ROS are also able to generate DSBs directly, but that they do so at a much lower frequency than SSBs (in the case of H_2O_2 treatment, the ratio of SSBs to DSBs is approximately 2000:1 (Bradley and Kohn 1979)).

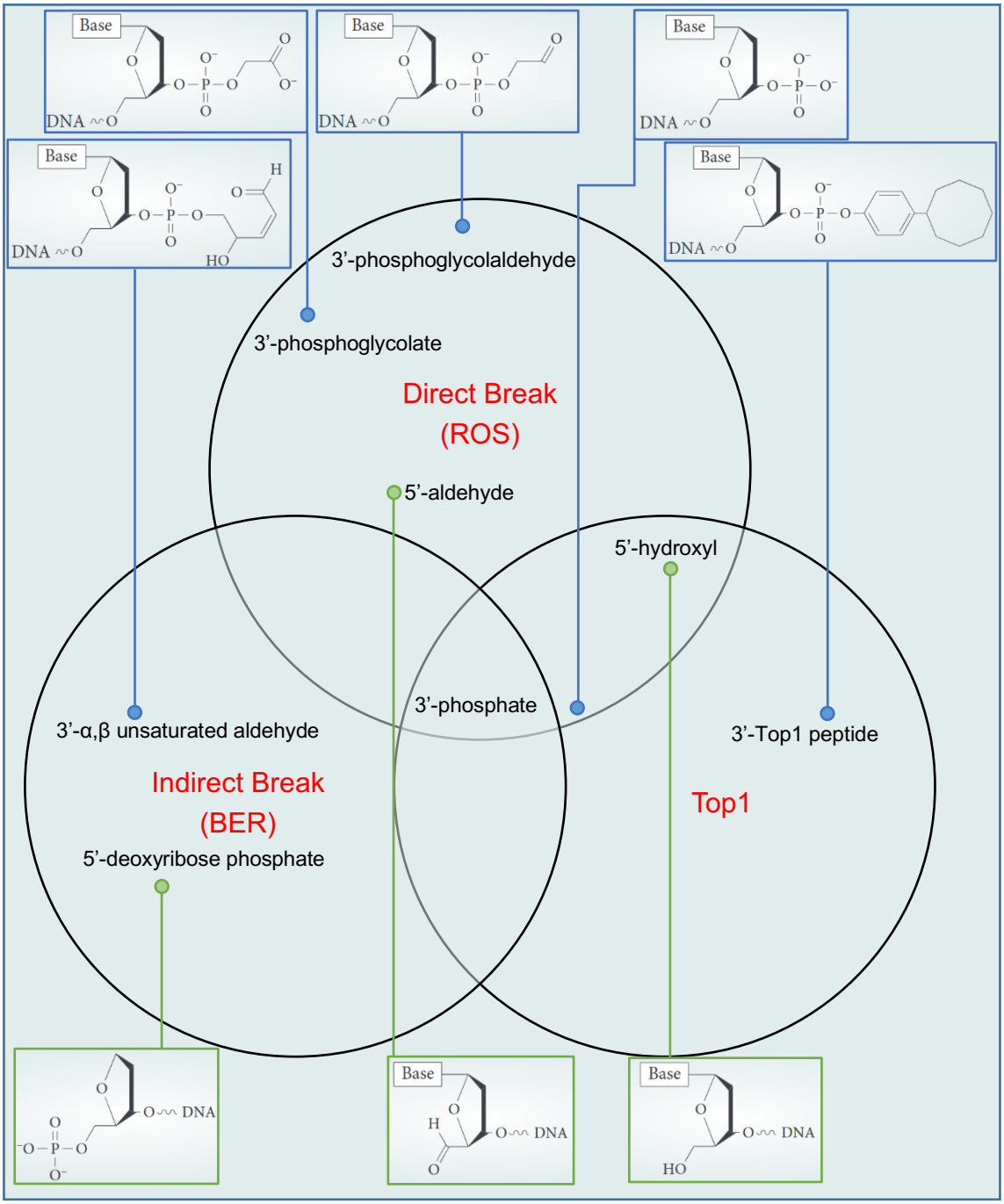

Figure 1.2. The chemistry of non-canonical DNA SSB termini. A summary of some common non-canonical DNA SSB termini is provided, showing lesions which may arise as a result of direct oxidative strand scission (top circle); as intermediates in base excision repair (left circle); or as intermediates in the repair of Top1-SSBs (right circle). Chemical structures of these 3' and 5' termini are shown at the top and bottom of the figure; outlined in blue and green, respectively. **[Figure adapted from (Caldecott 2008)].**

1.2.2. Ionising Radiation

Ionising radiation (IR) is a collective term for types of radiation which have enough energy to remove electrons from substrates, thereby causing their ionisation (WHO 2017). This includes, but is not limited to: alpha (α), beta (β), gamma (γ) and x-ray radiation. There are many natural sources of IR, including decay of radioactive isotopes on earth, nuclear fusion in the sun, and cosmic rays originating outside of the solar system. Different forms of IR are also used for diagnostics and cancer radiotherapy. Ionising radiation causes DNA damage directly by ionising different moieties of the DNA molecule; or indirectly by ionising proximal water molecules, which then react with DNA (Symons 1994), as detailed above (see section 1.2.1).

Ionising radiation causes both DNA single- and double-strand breaks, with the relative amount of each dependent on the ionization density. For example, high ionising density radiation such as α-radiation causes a higher DSB:SSB ratio (Scholz, Weidner et al. 1997) than low ionising density radiation, such as γ-radiation (Roots, Kraft et al. 1985). Although specific estimates of these ratios vary due to the break detection method (Balagurumoorthy, Adelstein et al. 2011), it is important to note that all forms of ionising radiation cause a greater DSB:SSB ratio than oxidising agents, due to clustering of ionisation events in a small area.

1.2.3. Topoisomerase I

The double helical nature of DNA raises a topological problem whenever metabolic processes such as transcription or replication occur. In order for a DNA or RNA polymerase to read the template DNA, the helix must be unwound and denatured. For long or circular molecules, this results in the accumulation of positive supercoils ahead of the point of unwinding (Liu and Wang 1987, Giaever and Wang 1988, Gilbert and Allan 2014). In the case of transcription by RNA polymerase, negative supercoils also accumulate behind the transcription elongation complex, whereas in replication, the two daughter strands are in a relaxed conformation (Pruss, Manes et al. 1982, Wang 2009, Gilbert and Allan 2014). Whilst a certain degree of supercoiling might be important for some functions, over-accumulation produces topological stress which can impede

progression of replication and transcription complexes (Brill, DiNardo et al. 1987, Gartenberg and Wang 1992, Bermejo, Doksani et al. 2007, Gilbert and Allan 2014). Additional topological problems are encountered in mitosis when intertwined sister chromatids must be physically separated (Sundin and Varshavsky 1980, Baxter 2015). The solution to all of these topological problems involves the cleavage of one or both DNA strands, followed by the rotation or passage of DNA relative to the cut strand, and finally resealing of the break (Wang 2002). The topoisomerases comprise a dedicated family of enzymes which perform these essential roles in all domains of life. However, topoisomerases have the potential to become abortive, resulting in the persistence of topoisomerase-linked single- or double-strand breaks (Pommier, Leo et al. 2010). Humans possess six Topoisomerases of three types; type IA, type IB and type IIA. Type I topoisomerases are those that cleave a single strand of DNA, including the type IA Topoisomerase III (Top3α and Top3β in humans), and the type IB Topoisomerase I (Top1 and Top1mt in humans). Type II topoisomerases, by comparison, cleave both strands of DNA and include the type IIA Topoisomerase II (Top2α and Top2β in humans). Top1 is of particular relevance to this project, because of its roles in facilitating both transcription and replication, and its liability to create permanent SSBs (Pommier, Leo et al. 2010).

Eukaryotic Top1 relaxes both negative and positive supercoiled DNA (Brill, DiNardo et al. 1987, Pommier, Sun et al. 2016). It does this by cleaving a single strand, forming a free 5'-hydroxyl DNA end and a transient 3'-phosphotyrosine covalent linkage between the catalytic tyrosine residue in its active site and the 3'-phosphate group of DNA; this intermediate is termed the Top1-cleavage complex (Top1cc) (Fig. 1.3.) (Champoux 1977, Tse, Kirkegaard et al. 1980, Lynn and Wang 1989, Redinbo, Stewart et al. 1998, Stewart, Redinbo et al. 1998). Rotation of the broken strand can then proceed spontaneously, due to the potential energy stored in the supercoiled DNA. This rotation occurs in a controlled fashion, due to the presence of two minimal contacts between Top1 and the DNA helix downstream of the cleavage position (Redinbo, Stewart et al. 1998, Stewart, Redinbo et al. 1998). Finally, the break is resealed by nucleophilic attack of the DNA 5'-hydroxyl group on the 3'-phosphotyrosine linkage. The

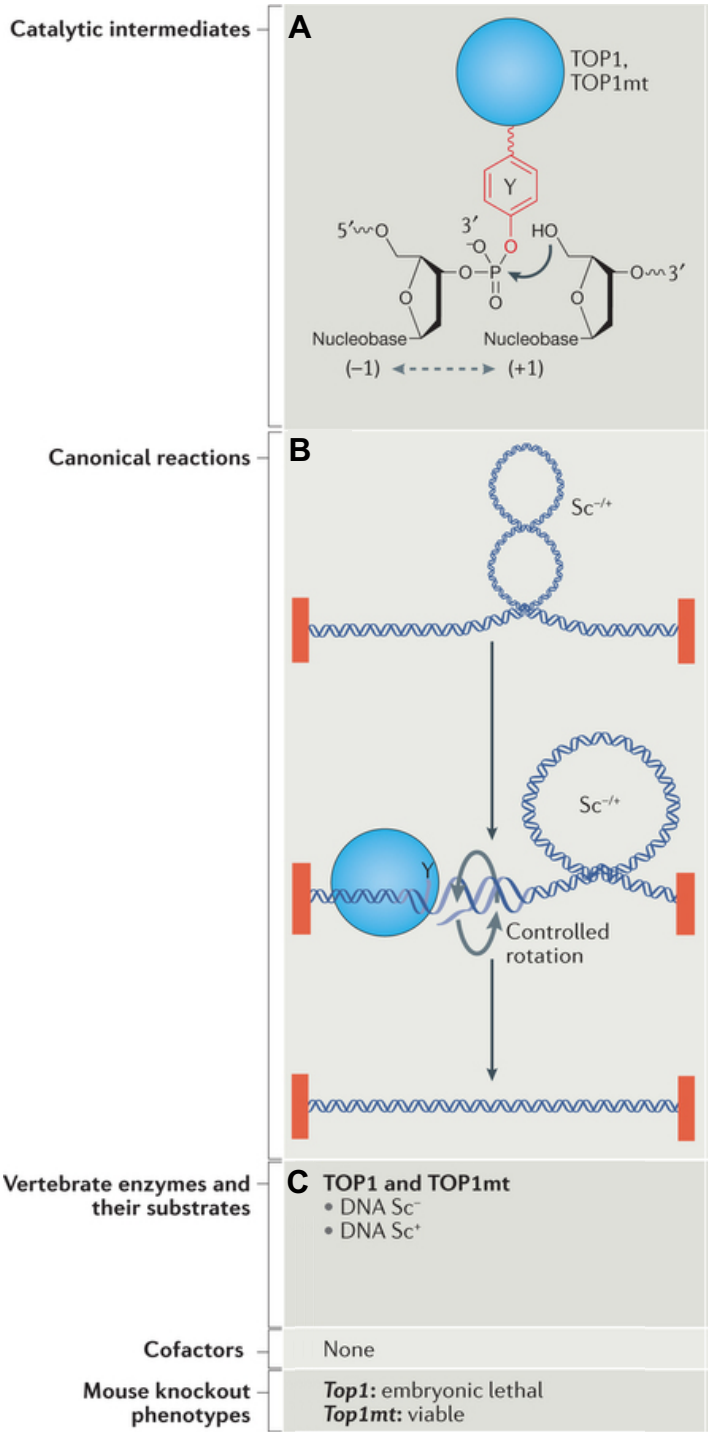

Figure 1.3. The catalytic mechanism and biological roles of vertebrate Top1. The enzymatic mechanism of Top1 proceeds via a protein-DNA covalent intermediate, involving a DNA 3'-tyrosyl phosphodiester bond **(A).** This Top1 cleavage complex (Top1cc) allows controlled spontaneous rotation of DNA downstream of the cleavage site, relieving positive or negative supercoils ($Sc^{-/+}$), prior to religation of the DNA **(B)**. Vertebrates possess two TOP1 genes: nuclear (TOP1) and mitochondrial (TOP1mt) **(C). [Figure taken from (Pommier, Sun et al. 2016)].**

cleavage and ligation steps are catalysed by a pentad of amino acids (Arg488, Lys532, Arg590, His632 and Tyr723) in the Top1 active site (Champoux 2001).

Whilst Top1 does not display strict sequence specificity, cleavage maps do reveal favoured sites (Been, Burgess et al. 1984, Francis Stewart, Herrera et al. 1990). Furthermore, base frequency analysis has suggested some sequence preferences between the -4 and -1 base pairs (relative to Top1cc) (Jaxel, Capranico et al. 1991), the most important of which being a T in the -1 position. Lesions such as 8-oxoG (Pourquier, Ueng et al. 1999), 5-hydroxyC (Pourquier, Ueng et al. 1999) and uracil (Pourquier, Ueng et al. 1997) at the +1 position have also been reported to increase Top1cc formation by increasing DNA binding.

Several factors can prevent ligation, leading to formation of a permanent Top1-SSB. One factor is the presence of other proximal lesions. For efficient ligation, the 5'-hydroxyl group must be positioned correctly for reaction with the 3'-phosphotyrosine linkage (Wang 2009). This generally requires that the +1 nucleobase (relative to the Top1cc) be correctly annealed by hydrogen bonding and base stacking with its complementary and neighbouring nucleobases, respectively. This is thought to explain the diversity of proximal lesions which can trap Top1ccs, including alkylated nucleobases (Pourquier, Bjornsti et al. 1998), mismatched nucleobases (Yeh, Liu et al. 1994), ribonucleotides (Pourquier, Ueng et al. 1997), abasic sites (Pourquier, Ueng et al. 1997), and UV photoproducts (Lanza, Tornaletti et al. 1996). Additionally, trapping of Top1 can occur if there are proximal SSBs on the Top1-cleaved strand, leading to formation of gaps; or proximal SSBs on the Top1-uncleaved strand, leading to DSB formation (Pourquier, Pilon et al. 1997). Finally, Top1ccs can be reversibly stabilized by the quinoline alkaloid camptothecin (CPT) and its analogs. These small molecules intercalate between the -1 and +1 base pairs (relative to Top1cc), displacing the +1 nucleotide and preventing ligation (Redinbo, Stewart et al. 1998, Staker, Hjerrild et al. 2002). The extended lifetime of the CPT-stabilized Top1cc renders it susceptible to conversion into an irreversible Top1-SSB. It is a common misconception that the oxidized bases 8-oxoG and 5-hydroxyC stabilize the Top1cc by inhibition of religation; instead, as noted above, these increase the

steady-state levels of Top1cc by stimulating the forward cleavage reaction (Pourquier, Ueng et al. 1999, Pourquier, Takebayashi et al. 2000).

A major mechanism by which a Top1cc can become irreversible is by collision with the transcription or replication machinery (Wu and Liu 1997) (Hsiang, Lihou et al. 1989). Both events are thought to displace the 5'-hydroxyl terminus, preventing restoration of the phosphodiester bond (Hsiang, Lihou et al. 1989, Wu and Liu 1997). The outcomes of the two events are different, both at the molecular level and in terms of cytotoxicity. In the case of replication fork collision, a Top1cc on the leading strand results in replication run-off, producing a blunt DSB with a 5'-hydroxyl terminus, which must be repaired by homologous recombination (see section 1.4.2) (Strumberg, Pilon et al. 2000). Lagging strand synthesis is likely to proceed past the lesion at least one Okazaki fragment length due to uncoupling of DNA synthesis (Pag, xe et al. 2003). The result of a Top1cc on the lagging strand is less well defined, but they may not impede progression of the replication fork because Okazaki fragment synthesis might initiate beyond the lesion. The impediment to DNA replication, coupled with the possible formation of large numbers of one-ended DSBs (Furuta, Takemura et al. 2003), can explain the significant S-phase selectivity of CPT cell killing (Li, Fraser et al. 1972, Tobey 1972).

Collision of the transcription elongation complex with a Top1cc results in stalling of RNAPII and the formation of regions of DNA:RNA hybridization known as R-loops (Sordet, Redon et al. 2009), which have been implicated in causing genomic instability (see section 1.3.1). Cells which rely on high levels of transcription, such as neurons, may be particularly sensitive to the depletion of essential mRNAs which results from CPT-induced Top1ccs (Morris and Geller 1996). Additionally, apoptosis may be triggered by several mechanisms, which are discussed below (see sections 1.4.3.2 and 1.5.2.1).

1.2.4. Alkylation, Deamination and AP-site Formation

In addition to ROS, IR and Top1, there are other damage sources which result in the formation of BER/SSBR substrates. One example is DNA alkylating agents,

which are found as environmental and dietary contaminants (Hecht and Hoffmann 1989, Hotchkiss 1989), as well as endogenously, such as in the gastric juice (Pignatelli, Malaveille et al. 1993, Xu and Reed 1993, Kyrtopoulos 1998). Probably the most significant examples of these agents are the (predominately exogenous) N-nitroso compounds N-nitrosodimethylamine (NMDA) and 4-(methylnitrosamino)-1-(3-pyridyl)-1-butanone (AKA nicotine-derived nitrosamine ketone, NNK), and the endogenous methylation cofactor S-Adenosyl methionine (SAM). These agents generate methyl adducts on nitrogen and oxygen atoms of the nucleobases, particularly N^7-methylguanine (7-MeA), O^6-methylguanine (6-MeG), N^3-methyladenine (3-MeA) and O^4-methylthymine (4-MeT) (Beranek 1990, Kyrtopoulos 1998); and on oxygen atoms of the DNA phosphate moiety, giving rise to methylphosphotriesters (Beranek 1990). Of these lesions, 7-MeG is the most prevalent, accounting for approximately 70% of all adducts formed (Beranek 1990). Whilst not the major lesion, occurring at an approximately ~20-fold lower frequency than 7-MeG, 6-MeG is thought to contribute heavily to mutagenesis (Swenberg, Bedell et al. 1982, Zaidi, Allay et al. 1995, Zaidi, Pretlow et al. 1995, Kyrtopoulos 1998). This has been attributed to G-to-A transversion mutations (Saffhill and Hall 1985); which result from an increase in the rate of incorporation of thymine opposite 6-MeG, and of the immediate subsequent nucleotide (Tan, Swann et al. 1994). Additionally, although 3-MeA is thought to occur ~7-fold less frequently than 7-MeG, it is highly cytotoxic due to its capacity to block DNA replication (Engelward, Allan et al. 1998, Plosky, Frank et al. 2008).

Abasic sites (AKA apurinic/apyrimidinic site; AP site) constitute another prevalent type of BER substrate (and intermediate). These form when the glycosidic bond linking a nucleobase to the deoxyribose moiety of DNA is hydrolysed, which can occur spontaneously, or by glycosylase enzyme activity operating early within BER (see section 1.5.1) (Lindahl 1993). The rate of spontaneous loss of a purine is ~20-fold that of a pyrimidine, occurring with a frequency of approximately 10,000 vs 500 $cell^{-1}day^{-1}$ in humans, respectively (Lindahl and Nyberg 1972, Lindahl and Karlstrom 1973, Lindahl 1993). AP sites themselves are labile, and can result in strand scission via β-elimination (Lindahl 1993). In addition, AP sites are potentiators of other types of DNA damage, such

as topoisomerase associated strand breaks (see section 1.2.3), and if replicated can lead to base substitution or frameshift mutations (Boiteux and Guillet 2004).

In addition to the spontaneous reactions of the DNA backbone, the nucleobases themselves are prone to spontaneous deamination (Lindahl 1993). The pyrimidines cytosine and 5-methylcytosine are particularly susceptible to this, being converted to uracil and thymine, respectively (Lindahl 1993). The rate of cytosine deamination has been estimated to be approximately 60-500 cell-^{1}day^{-1} in humans (Krokan, Standal et al. 1997), and the rate of deamination of 5-methylcytosine is estimated to be ~3-4-fold faster than this (Lindahl and Nyberg 1974, Wang, Kuo et al. 1982). If unrepaired, the resulting mismatched bases can lead to C-to-T transition mutations upon DNA replication (Duncan and Miller 1980).

1.3. Blockage of Transcription and Replication by SSBs

As detailed above, the collision of elongating replication or transcription complexes can convert a reversible Top1cc to a Top1-SSB requiring repair, whilst simultaneously arresting the progression of the DNA or RNA polymerase. Moreover, blockage of replication and transcription is a general consequence common to many types of SSB and some base modifications. This section will focus on the transcription and replication block imposed by SSBs.

1.3.1. Transcription Blockage

When SSBs occur in gene bodies they are an impediment to transcription elongation (Zhou and Doetsch 1993, Zhou and Doetsch 1994, Kathe, Shen et al. 2004). This effect is dependent on both end-chemistry and gap length, with bulkier groups and longer gaps proving the strongest block to transcription (Neil, Belotserkovskii et al. 2012). Transcription blockage may result in the depletion of essential mRNAs, which could trigger cell death indirectly (Rulten and Caldecott 2013). Additionally, stalling of RNAPII at transcription-blocking lesions, including SSBs (Roy, Zhang et al. 2010), can cause accumulation of R-loops, which have been implicated in causing genomic instability; and of RPA-bound ssDNA

regions, which trigger an ATR-p53 apoptotic programme (see section 1.4.3.2) (Ljungman and Zhang 1996, Ljungman, Zhang et al. 1999, Vrouwe, Pines et al. 2011, Rulten and Caldecott 2013).

In recent years there has been much interest in the mechanisms of formation, repair and genotoxicity of R-loops (Aguilera and Garcia-Muse 2012). Whilst R-loops have physiological functions, such as in immunoglobulin class switch recombination (Skourti-Stathaki and Proudfoot 2014) and the termination of transcription (Mischo, Gómez-González et al. 2011, Skourti-Stathaki, Proudfoot et al. 2011), their excessive accumulation is believed to have genotoxic effects (Aguilera and Garcia-Muse 2012). There are several hypotheses to explain R-loop induced genetic instability, such as the increased susceptibility of the displaced ssDNA to damage by endogenous enzymes (Petersen-Mahrt, Harris et al. 2002, Chaudhuri and Alt 2004) and chemical reactions (Frederico, Kunkel et al. 1990). Furthermore, R-loops themselves are a strong impediment to replication forks, which is thought to be a significant mechanism in generating genetic instability (Tuduri, Crabbe et al. 2009, Alzu, Bermejo et al. 2012, Castellano-Pozo, Garcia-Muse et al. 2012).

1.3.2. Replication Blockage and the Formation of DSBs

Like CPT exposure, UV irradiation results in the formation of single strand interruptions; however, in the case of UV irradiation this occurs indirectly, following the excision of a single-stranded DNA tract containing UV photoproducts by the nucleotide excision repair pathway (NER) (Marteijn, Lans et al. 2014). Early experiments showed that exposure to either CPT or UV radiation caused DNA replication arrest and/or S-phase specific cell-killing (Hanawalt 1966, Li, Fraser et al. 1972), and subsequently it was revealed that these phenotypes were accompanied by the replication-coupled formation of DSBs (Tsao, Russo et al. 1993). This mechanism was generalized to other types of single strand interruption, after similar observations were made in a study utilizing DNA nicks induced by the site-specific single-strand endonuclease gpII (Kuzminov 2001). Furthermore, genetic or chemical perturbation of SSBR (see section 1.5.2), causes elevated levels of spontaneous S-phase DSBs (Bryant,

Schultz et al. 2005, Saleh-Gohari, Bryant et al. 2005), and inhibition of the SSB-sensing PARP enzymes (see section 1.5.2.1) renders cells heavily reliant on functional homologous recombination (HR) (Bryant, Schultz et al. 2005), which repairs replication-coupled DSBs (see sections 1.4.2 and 1.6.1) (Arnaudeau, Lundin et al. 2001, Saleh-Gohari, Bryant et al. 2005).

1.4. Double Strand Break Repair and the DNA Damage Response

The previous section detailed how persistent SSBs can cause replication fork collapse and the generation of DSBs during S-phase. In addition, DSBs can be caused directly in all phases of the cell cycle, by clustered oxidative damage, such as that resulting from IR (see section 1.2.2). DSBs are extremely dangerous for genome integrity, and for this reason multiple pathways have evolved both to repair DSBs, and to trigger cell-cycle arrest or apoptotic mechanisms. A brief overview of some of these mechanisms will be provided below.

1.4.1. Non-Homologous End Joining

Non-homologous end joining (NHEJ) is a collective term for two known molecular pathways which join DNA ends directly; without requiring the presence of a homologous template, and thus able to occur in all phases of the cell cycle (Chang, Pannunzio et al. 2017). The first of these pathways to be identified is now termed classical-NHEJ (C-NHEJ), to distinguish it from the more recently identified alternative-NHEJ (A-NHEJ) pathway (Chang, Pannunzio et al. 2017).

C-NHEJ constitutes the major repair pathway for the repair of DSBs in human cells (Lieber 2010), and is able to be completed very rapidly. The recognition system is composed of an abundant ring-like heterodimer of two similar proteins, Ku70 and Ku80, which threads over each DNA end, limiting DSB mobility (Downs and Jackson 2004) and acting as a scaffold for the recruitment of downstream factors (Yang, Guo et al. 2016), which are, similarly to SSBR (see section 1.5.2), involved in scaffolding, end-processing, polymerisation, and ligation. An early interactor with the DSB-Ku complex is the DNA-dependent

protein kinase catalytic subunit (DNA-PKcs), a member of the phosphoinositide 3 kinase-related kinase (PIKK) family, which includes ataxia-telangiectasia mutated (ATM) and ataxia-telangiectasia and Rad3 related (ATR) kinases. DNA-PKcs is activated upon binding to the C-terminal 12aa of Ku80 (Gell and Jackson 1999); phosphorylating many protein targets, including itself, to positively regulate C-NHEJ. Another interactor to the DSB-Ku complex is the XRCC4-XLF-Lig4 complex (Nick McElhinny, Snowden et al. 2000), which has been reported to tether DNA termini by bridging DSBs (Pang, Yoo et al. 1997, Brouwer, Sitters et al. 2016). The processing of complex DNA termini is carried out by several proteins, including those shared with SSBR (see section 1.5.2.3), such as polynucleotide kinase 3'-phosphatase (PNKP), Aprataxin (APTX) and Aprataxin and PNKP-like factor (APLF); and those which are unique to C-NHEJ, such as the specialized nucleases Artemis and Werner syndrome protein (WRN), and the PolX family polymerases Polλ and Polμ (Davis and Chen 2013). Finally, ligation is conducted by Lig4, in complex with XLF and XRCC4 (Grawunder, Wilm et al. 1997, Schär, Herrmann et al. 1997).

More recently, another mechanism for direct end-joining of DSBs has been described; this is termed alternative-NHEJ (A-NHEJ) (Sfeir and Symington 2015). Some believe that this is an independent pathway whilst others suggest that it performs a backup or rescue function when C-NHEJ stalls. A-NHEJ relies on aligning DNA ends using microhomologous regions of 5-25 bp, often leading to significant deletions at the repair junctions (McVey and Lee 2008). The mechanisms surrounding A-NHEJ are still being elucidated, but are thought to involve the actions of PARP1 and the MRN complex (see section 1.4.2) (Wang, Wu et al. 2006).

1.4.2. Homologous Recombination

The replication of DNA provides a backup of the genome, allowing for potentially error-free repair of DSBs arising in S or G2 phases of the cell cycle by utilizing the undamaged sister chromatid as a template (Heyer, Ehmsen et al. 2010). This process competes with the NHEJ pathways described above, which also function in S and G2.

Homologous recombination involves the resection of a DSB into a 3'-overhang by the combined nuclease activities of the MRE11-RAD50-NBS1 (MRN) complex (Trujillo, Yuan et al. 1998, Williams, Williams et al. 2007), Exo1 (Moreau, Morgan et al. 2001), DNA2 (Bae, Choi et al. 1998, Zhu, Chung et al. 2008) and CtIP (Sartori, Lukas et al. 2007); in cooperation with the helicase BLM (Gravel, Chapman et al. 2008, Huertas 2010). This 3'- ssDNA tail is bound by the single stranded DNA binding protein RPA (Heyer, Rao et al. 1990), which is subsequently displaced by the Rad51 recombinase (Sung 1994). This is accomplished with the aid of a host of mediator proteins including: XRCC2, XRCC3, RAD51B, RAD51C, RAD51D, RAD52, and BRCA2 (Heyer, Ehmsen et al. 2010). Rad51 assembles into a protein-DNA filament, which can carry out an active "homology search" throughout the nucleus (Haber 2013). With the aid of Rad54, the Rad51-DNA filament can coordinate dsDNA regions of homology, by a mechanism which is still unclear (Haber 2013). This results in strand invasion to form a region of heteroduplex DNA, with displacement of a D-loop; a process which is known as synapsis (Heyer, Ehmsen et al. 2010). The invaded 3'-strand then primes DNA synthesis by the replicative polymerase complex, which extends the heteroduplex.

There are three main postsynaptic pathways, termed break-induced replication (BIR), synthesis-dependent strand annealing (SDSA), and double Holliday junction (dHJ) formation (Heyer, Ehmsen et al. 2010). These pathways differ in their molecular outcomes, and in the proteins required. If another DNA end is not available, such as in the case of replication fork collapse at a single strand break (see section 1.3.2), BIR allows polymerisation to occur as far as the next replication fork (or to the end of the chromatid) (Heyer, Ehmsen et al. 2010). This can result in large losses of heterozygosity. When a second DNA end exists, such as for DSBs arising in G2, the predominant mechanism is thought to be SDSA, whereby the newly synthesized 3'-overhang is displaced from its intact template and anneals with the resected region of the other end (Haber 2013). This minimises loss of heterozygosity, as the subsequent gap-filling and ligation always results in a non-crossover product. A final possibility for DSB processing is the formation of a dHJ. This involves annealing the other resected DNA end to the D-loop displaced by the first strand invasion, followed by extension and

ligation of both ends (Heyer, Ehmsen et al. 2010). These joint molecules (JM) can migrate; prior to resolution by the endonucleases GEN1, SLX1-SLX4 and Mus81-Eme1 (Wyatt, Sarbajna et al. 2013), generating crossover or non-crossover products; or dissolution by the BLM-TopoIIIα-RMI1-RMI2 (BTR) complex, generating non-crossover products. In mitotic cells, dissolution by the BTR complex is the preferred pathway choice (Heyer, Ehmsen et al. 2010).

1.4.3. The DNA Damage Response

The serine/threonine kinases ATM and ATR act as molecular sensors of activated MRN and RPA-coated ssDNA regions, respectively; both of which are signals of DSBs (see section 1.4.2) (Marechal and Zou 2013). Furthermore, RPA-coated ssDNA is a structure present in many repair pathways, including nucleotide excision repair (NER), mismatch repair (MMR), long-patch base excision repair (LP-BER), interstrand crosslink (ICL) repair; and at stalled replication forks and transcription complexes, thus allowing ATR to function as a sensor of diverse damage and replication stresses (Zou, Liu et al. 2006). ATR and ATM phosphorylate diverse protein targets involved in repair, replication, cell cycle, and apoptotic mechanisms; promoting cell survival and/or preventing oncogenesis (Marechal and Zou 2013). These complex signalling networks are collectively known as the DNA damage response (DDR).

1.4.3.1. ATM

The MRN complex is thought to be the initial sensor of the DSB, which recruits and activates the PIKK ATM (Falck, Coates et al. 2005, Lavin 2007). Activated ATM phosphorylates a wide range of protein targets, promoting repair mechanisms and the DDR (Marechal and Zou 2013). One important target of ATM is the histone variant H2AX, which is phosphorylated on Ser139 in the vicinity of a DSB (Rogakou, Pilch et al. 1998). This signal has significant roles in promoting chromatin restructuring and DSBR mechanisms, including resection (Marechal and Zou 2013). Other important targets of ATM are BRCA1, Checkpoint kinase 2 (Chk2) and P53; which have roles in repair, cell cycle control and apoptosis, respectively (Marechal and Zou 2013). The involvement of ATM in such diverse cellular signalling programmes explains the complexity and

multisystemic-nature of the disease which is associated with its mutation: Ataxia telangiectasia (AT) (Savitsky, Barshira et al. 1995). AT patients are sensitive to DSB-inducing agents; prone to cancer; and exhibit neurodegeneration, leading to early-onset ataxia (Taylor, Harnden et al. 1975, Rothblum-Oviatt, Wright et al. 2016).

1.4.3.2. ATR

ATR is recruited to RPA-coated ssDNA by ATR interacting protein (ATRIP), causing its activation (Zou and Elledge 2003). Activated ATR phosphorylates Checkpoint kinase 1, which is integral in promoting intra-S and G2/M cell-cycle arrest. Additionally, ATR phosphorylates targets involved in modulating origin firing and replisome stability, highlighting its role in the tolerance of replication stress. These functions are generally unique to ATR, which, unlike ATM and DNA-PK, is essential in replicating cells (de Klein, Muijtjens et al. 2000, Nam and Cortez 2011). Hypomorphic mutations in ATR cause the extremely rare autosomal recessive disease Seckel syndrome, which is characterized by a severe growth defect resulting in microcephallic primordial dwarfism (O'Driscoll, Gennery et al. 2004).

1.5. DNA Base Excision and Single Strand Break Repair

The mechanisms of DSBR and the DDR described above are essential to prevent the severe genotoxic consequences of DSBs. However, the vast majority of DNA breaks which arise in cells are SSBs (see section 1.2). Complex molecular mechanisms have evolved to detect and repair these SSBs, and to prevent their conversion to DSBs during replication. The focus of this thesis is the detection and repair of oxidative and Top1-linked SSBs; therefore, most attention will be paid to these topics in the following sections. As discussed above (see section 1.2.1), both the deoxyribose and nucleobase moieties of DNA are susceptible to attack by ROS, resulting in the formation of not only direct SSBs but also oxidized bases. Oxidized bases are excised during BER, resulting in the formation of intermediate SSBs which are the substrates of SSBR. These processes, which

are thought to be tightly coordinated *in vivo* (Wilson and Kunkel 2000), will be discussed in detail in the following sections.

1.5.1. Base Excision Repair

As detailed above, DNA nucleobases can be oxidized (see section 1.2.1), alkylated (see section 1.2.4), lost by spontaneous hydrolysis (see section 1.2.4) or deaminated to produce non-canonical types (see section 1.2.4). Collectively, these lesions constitute a substantial proportion of the total arising in cells every day (Lindahl 1993). Consequently, an extremely efficient and degenerate pathway has evolved to deal with these lesions: base excision repair (BER). This makes up the earliest activities involved in BER/SSBR, DNA glycosylase and AP lyase or AP endonuclease.

The first step of BER, recognition and excision of the base by a DNA glycosylase, is enzymatically diverse. There are eleven known human DNA glycosylases (Hendrich, Hardeland et al. 1999, Hazra, Izumi et al. 2002, Hegde, Hazra et al. 2008, Jacobs and Schär 2012, Liu, Doublié et al. 2013). Whilst they each tend to have a preferred substrate there is a great deal of functional redundancy. The glycosylases involved in excising uracil (U) and its derivatives from DNA, as well as thymine (T) mispaired with guanine (G), include the monofunctional DNA glycosylases uracil DNA glycosylase, (UNG) (Lindahl 1993), single-strand selective monofunctional DNA glycosylase (SMUG1) (Haushalter, Todd Stukenberg et al. 1999), thymine DNA glycosylase (TDG) (Wiebauer and Jiricny 1989), and methyl-CpG-binding domain protein 4 (MBD4) (Hendrich, Hardeland et al. 1999). Other monofunctional DNA glycosylases include 3-methyladenine DNA glycosylase (MPG) (O'Connor and Laval 1990) and MutY DNA glycosylase (MUTYH) (McGoldrick, Yeh et al. 1995), which excise alkylated purines and 8-oxoG-paired adenine, respectively (Hegde, Hazra et al. 2008). Monofunctional glycosylases catalyse the removal of the nucleobase to generate an AP site, which is subsequently incised by AP endonuclease (APE1) (See section 1.5.2.3.1 for a detailed overview of APE1) (Hegde, Hazra et al. 2008).

By comparison, glycosylases which recognize oxidized bases, such as 8-oxoguanine DNA glycosylase (OGG1) (Lu, Nash et al. 1997), endonuclease II-like protein 1 (NTH1) (Dizdaroglu, Karahalil et al. 1999); endonuclease VIII-like 1 (NEIL1) (Hazra, Izumi et al. 2002), endonuclease VIII-like 2 (NEIL2) (Morland, Rolseth et al. 2002), and endonuclease VIII-like 3 (NEIL3) (Liu, Bandaru et al. 2010) are all bifunctional enzymes, meaning that they also possess intrinsic AP lyase (AKA AP endonuclease class I) activity (Hazra, Izumi et al. 2002, David, O'Shea et al. 2007, Hegde, Hazra et al. 2008, Liu, Doublié et al. 2013). It is important to note that there is thought to be considerable redundancy between these pathways, such that AP sites generated by the monofunctional glycosylases can be substrates for the AP lyase activity of bifunctional glycosylases (Wiederhold, Leppard et al. 2004), and AP sites generated by the bifunctional glycosylases can be substrates for APE1 (Allinson, Dianova et al. 2001).

The AP endonuclease catalytic mechanism differs for APE1, OGG1/NTH1, and NEIL1/NEIL2, resulting in different product termini (Hegde, Hazra et al. 2008). APE1 catalyses cleavage 5’ relative to the AP site, resulting in 3’-OH and 5’-dRP termini. This is defined as a class II AP endonuclease activity (Levin and Demple 1990). By comparison, the bifunctional glycosylases employ a class I AP endonuclease mechanism (Levin and Demple 1990), more commonly referred to as an AP lyase mechanism, whereby the cleavage is made 3’ relative to the AP site. OGG1 and NTH1 use a β-elimination mechanism, which opens the deoxyribose ring and results in 3’-phospho α,β-unsaturated aldehyde (3’-PUA) and 5’-phosphate termini. By comparison, NEIL1, NEIL2 and NEIL3 catalyse a βδ elimination mechanism, resulting in 3’ and 5’- phosphate termini. APE1 therefore produces canonical 3’ and blocked 5’ termini, whereas for the bifunctional glycosylases the opposite is true. The presence of blocked termini necessitates an end-processing step to yield substrates suitable for gap filling and ligation (Hegde, Hazra et al. 2008). Top1-SSBs and direct SSBs induced by ROS also have blocked termini (see section 1.2.1 and 1.2.3), and it is at this stage that SSBR converges with BER.

1.5.2. Single Strand Break Repair

The current consensus model of SSBR can be divided into five major steps: recognition of a SSB by a PARP enzyme; PAR-dependent recruitment of the XRCC1 scaffolding protein and its interactors; end-processing of damaged DNA termini by several XRCC1-interacting enzymes; gap-filling by DNA polymerases; and finally, ligation to restore the intact duplex. These simplified steps are summarised in Fig. 1.4., and will be discussed in detail below.

1.5.2.1. Break detection and ADP-ribosylation

DNA single-strand break repair (SSBR) repairs SSBs arising directly from oxidative sugar damage (see section 1.2.1), from the excision of non-canonical nucleotides and AP-sites in BER (see section 1.5.1), and from the abortive action of Top1 (see section 1.2.3). The sum frequency of these SSBs in mammals is estimated to be approximately 10^4 to 10^5 $cell^{-1}$ day^{-1} (Lindahl 1993), necessitating an extremely sensitive surveillance system in higher eukaryotes (Caldecott 2008). This system employs several Diphtheria toxin-like adenosine diphosphate-ribosyltransferases (ARTDs) to detect strand interruptions and signal their presence. It is important to note that there is evidence that SSBs generated as intermediates in BER do not always require this signalling mechanism (Allinson, Dianova et al. 2003, Strom, Johansson et al. 2011), as they may be passed from one enzyme to the next in a coordinated fashion (Wilson and Kunkel 2000).

Of the eighteen known human ARTDs (Citarelli, Teotia et al. 2010, Hottiger, Hassa et al. 2010), three have been shown to be activated by DNA strand interruptions; these are ARTD1, ARTD2 and ARTD3 (Okayama, Edson et al. 1977, Amé, Rolli et al. 1999, Boehler, Gauthier et al. 2011). These enzymes are more commonly known by their previous names: poly(ADP-ribose) polymerase 1, 2, and 3 (PARP1, PARP2, and PARP3), which is how they will be referred to throughout this thesis. PARP1, PARP2 and PARP3 catalyse the post-translational modification of local acceptor proteins with units of adenosine diphosphate-ribose (ADP-ribose) (Fig. 1.5.). This reaction involves the transfer of

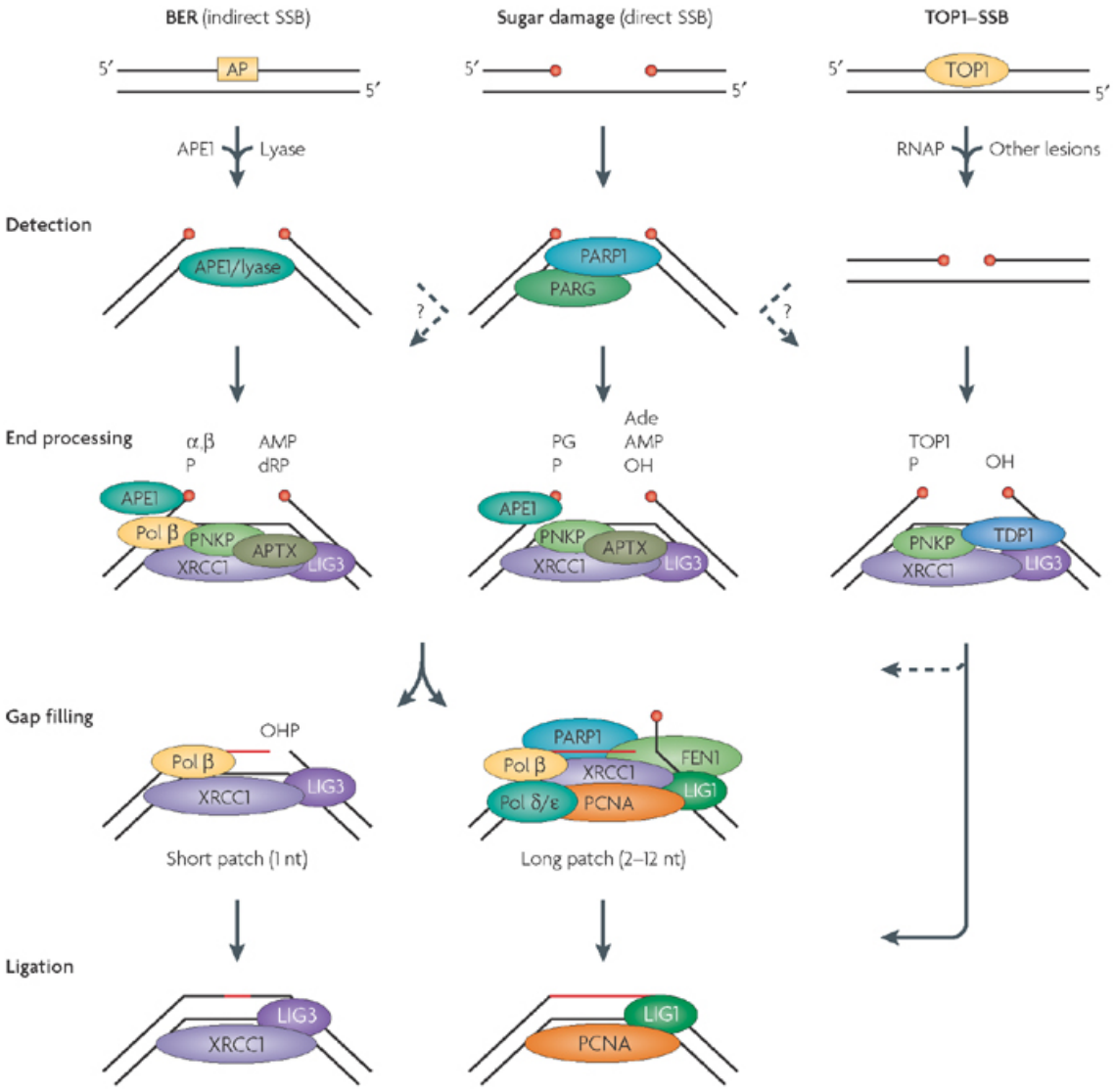

Figure 1.4. A simplified overview of SSBR pathways. SSBs can arise directly, from oxidation of the deoxyribose phosphate backbone; indirectly, as BER intermediates; or from abortive activity of Top1. SSBs are primarily detected by PARP1, which modifies local proteins, including itself, at the site of the lesion. PAR serves as a signal for the recruitment of a complex of enzymes involved in end-processing, gap-filling, and ligation; the stabilities and activities of which are stimulated by the scaffolding protein XRCC1. End-processing restores canonical 3'-hydroxl and 5'-phosphate termini from diverse blocked-SSBs. Gap-filling of 1 nucleotide is conducted by Polβ (short patch); gap-filling of 2-12 nucleotides is conducted by Polδ/ε (long patch), displacing a 5'-flap which is removed by FEN1. Finally, ligation of short patch and long patch products is conducted by Lig3 and Lig1, respectively. **[Figure taken from (Caldecott 2008)].**

ADP-ribose from the substrate nicotinamide adenine dinucleotide (NAD+), to a suitable nucleophilic acceptor. Known acceptor amino acids of the damage-responsive PARPs include aspartate (D), glutamate (E), lysine (K), arginine (R), and serine (S) (Messner, Altmeyer et al. 2010, Martello, Leutert et al. 2016, Bonfiglio, Fontana et al. 2017). Modification with a single unit of ADP-ribose is known as mono ADP-ribosylation (MARylation). The subsequent polymerisation of ADP-ribose to form oligo and poly ADP-ribose (OAR and PAR, respectively), occurs via transfer of another ADP-ribose unit to the 2' position of the preceding adenosine moiety (Hottiger, Hassa et al. 2010). Occasionally an ADP-ribose unit may be transferred to the 2' position of the ribose 5'-phosphate moiety, forming a branch point in the chain (Juarez-Salinas, Levi et al. 1982, Hottiger, Hassa et al. 2010). The percentage of ADP-ribose moieties with a branch point in a PAR chain has been estimated to be between 0.8 and 1.6% (Juarez-Salinas, Levi et al. 1982), but further insights into PAR branch structure are limited. The various abilities of PARP1, PARP2 and PARP3 to generate MAR, OAR and linear/ branched PAR is still being studied; but the consensus is that PARP1 and PARP2 generate long and branched PAR, whereas PARP3 generates predominantly MAR (Vyas, Matic et al. 2014). PARylation of local proteins at the site of DNA strand breaks leads to relaxation of chromatin (Poirier, de Murcia et al. 1982), allowing repair processes to take place (see section 1.5.2.1.1). Simultaneously, PAR and MAR serve as molecular signals for the local enrichment of numerous DNA repair and DDR proteins (see section 1.5.2.1.4), which interact directly and indirectly with this highly-charged molecule.

Similarly to other post translational modifications involved in signalling, PAR is removed by a number of "eraser" enzymes, such as poly(ADP-ribose) glycohydrolase (PARG) (Miwa and Sugimura 1971), which possesses endo and exoglycohydrolase activities (Brochu, Duchaine et al. 1994). This enzyme cleaves the bonds between ribose moieties of a PAR chain, but is unable to remove the terminal protein-linked MAR (Slade, Dunstan et al. 2011). The removal of this terminal moiety has been shown recently to be accomplished by the activities of the catalytic macro domain-containing proteins MacroD1, MacroD2 and O-acyl-ADP-ribose deacylase 1 (OARD1) (see section 1.5.2.1.4 for further discussion) (Jankevicius, Hassler et al. 2013, Rosenthal, Feijs et al. 2013).

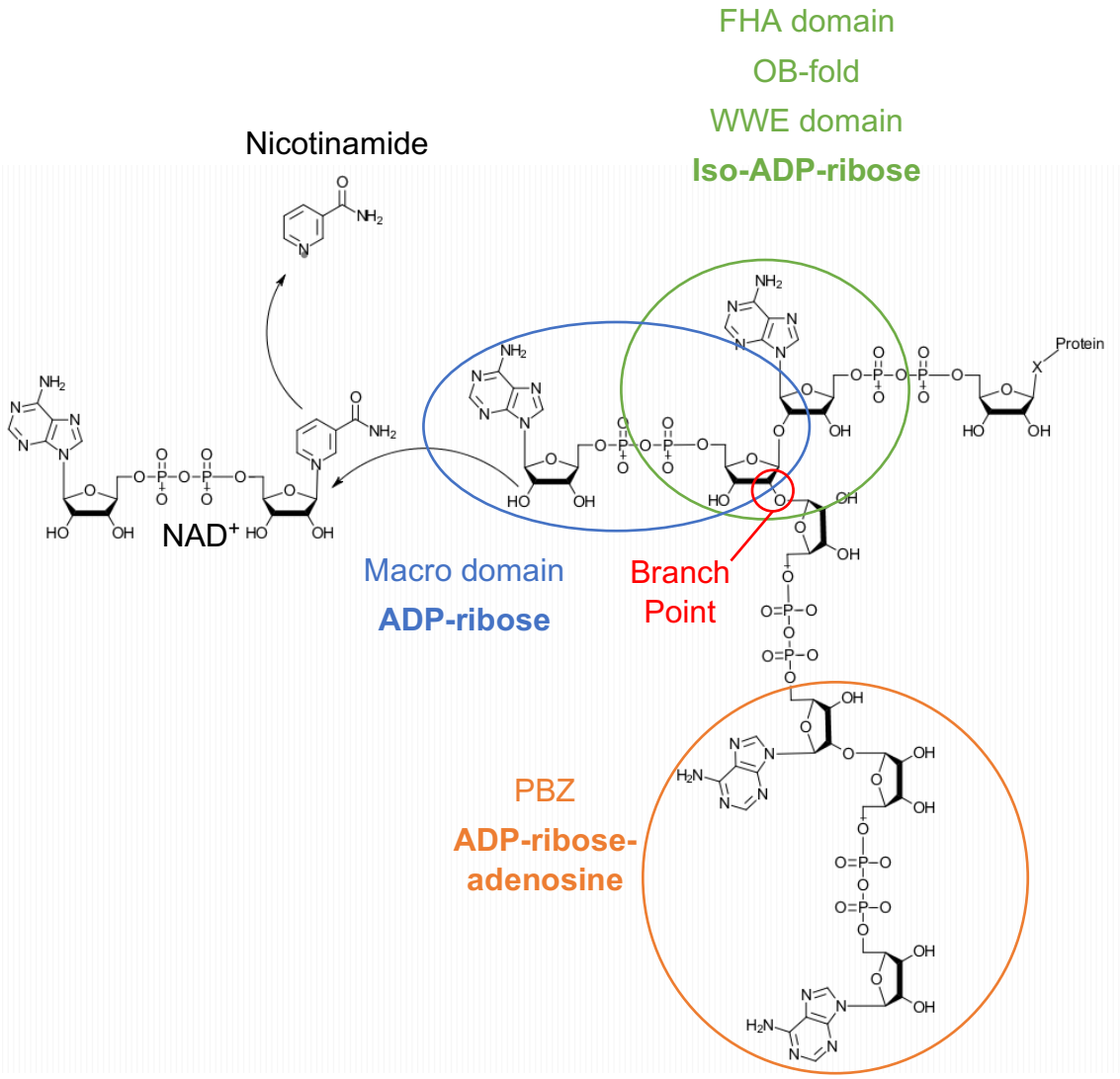

Figure 1.5. The structure of PAR. A simple representation of a PAR chain, showing: ADP-ribose, iso-ADP-ribose and ADP-ribose-adenosine moieties (blue, green and orange ovals, respectively), and the domains which bind them; the branch point at the 2' position of ribose (red circle); the substrate coenzyme NAD^+, and leaving group nicotinamide; and the position of linkage with an amino acid sidechain (X).

The balance of PAR generation and removal has important consequences for cellular metabolism and programmed cell death. Excessive PARP activity can trigger a mechanism of programmed cell death called Parthanatos, which acts independently of the caspase axis (Yu, Wang et al. 2002), and is particularly prevalent in neurons, where it is associated with several common neurological pathologies, such as Parkinson's (Mandir, Przedborski et al. 1999, Lee, Kang et al. 2014), Huntington's (Vis, Schipper et al. 2005) and Alzheimer's diseases (Love, Barber et al. 1999, Abeti and Duchen 2012, Strosznajder, Czapski et al. 2012); amyotrophic lateral sclerosis (ALS) (Hivert, Cerruti et al. 1998); cerebral ischemia (Eliasson, Sampei et al. 1997, Narne, Pandey et al. 2017); and with the recessive ataxias caused by genetic disruption of SSBR (see section 1.6) (Hoch, Hanzlikova et al. 2017). This pathway is dependent on the translocation of the flavoprotein apoptosis inducing factor (AIF) from the mitochondria to the nucleus (Yu, Wang et al. 2002), the trigger for which was originally thought to be depletion of the PARP substrate NAD+, but more recent evidence has cast doubt on this. For example, it was recently shown that PARG inactivation leads to PARthanatos without depletion of NAD+ (Goto, Xue et al. 2002, Zhou, Feng et al. 2011). This has led some to suggest that free PAR or a PARylated protein may mediate AIF release directly (Andrabi, Kim et al. 2006, Yu, Andrabi et al. 2006, Fatokun, Dawson et al. 2014). Until recently, the mechanism by which AIF mediates nuclear DNA fragmentation was similarly unclear. In 2016 *Wang et al* published that in mammals, macrophage migration inhibitory factor (MIF) is an endo/exonuclease which associates with AIF and is essential for the DNA fragmentation which accompanies PARthanatos (Wang, An et al. 2016).

Elucidating the specific biological roles of the DNA dependent PARPs has been the subject of much research in recent years. A summary comparison of some key structural and functional features of PARP1, PARP2 and PARP3 is provided in Fig. 1.6, and these enzymes will be discussed in detail in the following sections.

A

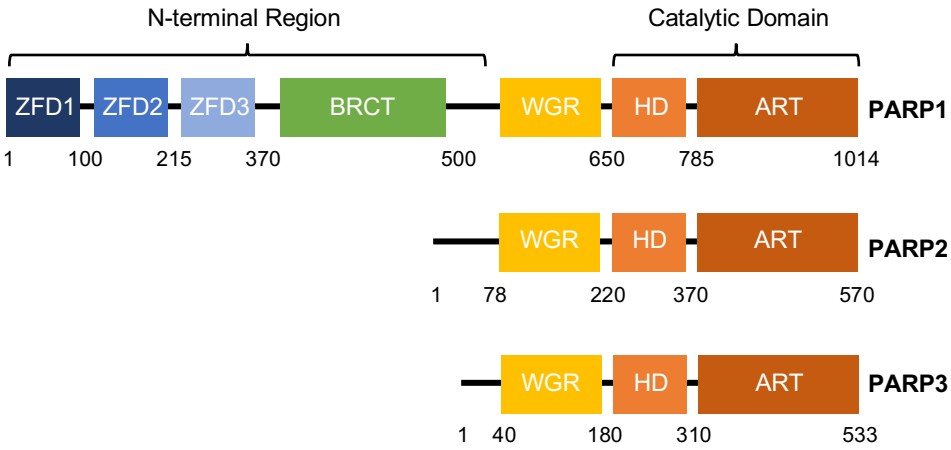

B

Gene	Protein size (aa)	Primary break recognition domains	Break termini preference	Type of ADPr produced
PARP1	1014	ZFD1 & ZFD2	None	Branched PAR
PARP2	570	WGR	5'-phosphate	Branched PAR
PARP3	533	WGR	5'-phosphate	MAR

Figure 1.6. Summary comparison of PARP1, PARP2, and PARP3 structure and function. The domain structure of PARP1, PARP2 and PARP3 is shown, including those conserved between all three enzymes: Trp-Gly-Arg domain (WGR), helical domain (HD), ADP-ribosyl transferase domain (ART); and those unique to PARP1: zinc finger domains 1, 2, and 3 (ZFD1, ZFD2, and ZFD3, respectively); and BRCA1 c-terminus domain (BRCT). The approximate amino acid positions of the domain boundaries are included (Langelier, 2014) **(A)**. A summary of some key features of PARP1, PARP2 and PARP3 structure and function are provided in **B.**

1.5.2.1.1. PARP1

PARP1 was initially identified in 1971, following its partial purification from rat liver nuclei (Yamada, Miwa et al. 1971). In this early study, and in a subsequent publication (Okayama, Edson et al. 1977), it was noted that the activity of the enzyme *in vitro* was dependent on the presence of DNA, and was stimulated 2-3-fold by the addition of purified histones (Yamada, Miwa et al. 1971, Okayama, Edson et al. 1977). Subsequent studies of ADP-ribose production in x-ray-irradiated or endonuclease-treated mammalian cell "ghosts" (detergent-permeabilized cells) revealed the dramatic activation of PARP1 by DNA strand breaks (Berger, Weber et al. 1978, Halldorsson, Gray et al. 1978, Benjamin and Gill 1980). Then, in 1980, the authors of a seminal study demonstrated that inhibition of PARP1 with 3-aminobenzamide reduced the repair rate of SSBs induced by the alkylating agent dimethyl sulphide (DMS) (Durkacz, Omidiji et al. 1980), indicating a role for PARP1 in DNA repair.

Subsequent work from the *Poirier* laboratory used electron microscopy (EM) to show that *in vitro* PARP1-mediated poly(ADP-ribosyl)ation (PARylation) of polynucleosomes causes them to adopt a relaxed, "beads-on-a-string structure" (Poirier, de Murcia et al. 1982, de Murcia, Huletsky et al. 1986), which is characteristic of chromatin depleted of the linker histone H1 (Thoma, Koller et al. 1979), and prompted the hypothesis that PARP1 was involved in the relaxation of chromatin to allow repair processes to take place. In these reactions, H1 was found to be the major PARylated histone, which is supported by recent *in vitro* experiments (Grundy, Polo et al. 2016). Other more recent work has demonstrated that PARP1 itself is a ubiquitous component of undamaged chromatin (Kraus 2008, Muthurajan, Hepler et al. 2014), competing with H1 for overlapping sites on the linker DNA (Kim, Mauro et al. 2004). In a study employing reconstituted chromatinized plasmids, it was shown that both PARP1 and H1 binding could dramatically condense chromatin structures, leading to extension of the nucleosome repeat length by 11% and 14%, respectively (Kim, Mauro et al. 2004). Furthermore, this effect saturated at a 1:1 ratio of nucleosomes to PARP1 or H1, suggesting stoichiometric binding with the linker DNA sites (Kim, Mauro et al. 2004). In the same study, it was demonstrated that inclusion of PARP1 reduced *in vitro* transcription of chromatinized plasmids, similar to the

regulation conferred by H1-mediated chromatin condensation; and that in the case of PARP1 but not H1, this could be reversed by addition of NAD+ (Kim, Mauro et al. 2004, Muthurajan, Hepler et al. 2014). In addition to this *in vitro* work, PAR-mediated decondensation of chromatin has also been reported *in vivo* (Tulin and Spradling 2003, Strickfaden, McDonald et al. 2016), and has become a central paradigm of the PARP field.

PARP1 is a highly active enzyme, accounting for 80-90% of the total cellular PARylation in mammalian cells (Shieh, Ame et al. 1998), and is known to generate branched chains of up to 200 residues in length, on diverse protein targets, including itself. PARP1 is also an extremely abundant molecule in the nucleus, with the PARP1:nucleosome ratio estimated to be approximately 1:20 (Muthurajan, Hepler et al. 2014). The high abundance of PARP1, coupled with its integral association with chromatin, make it perfectly poised to rapidly detect proximal strand breaks as they occur in the genomic DNA. To perform this sensory role, PARP1 uses its N-terminal zinc finger domains (ZFD) to detect strand interruptions (Gradwohl, Menissier de Murcia et al. 1990). This allosteric signal is transmitted to the catalytic domain, which stimulates activity up to 500-fold (Rouleau, Patel et al. 2010). PARP1 is potently stimulated by breaks with diverse termini, including: canonical, 3'-phosphate and 5'-hydroxyl termini; with gaps and overhangs also being well tolerated (Langelier, Riccio et al. 2014).

How PARP1 achieves such a broad sensitivity as a receptor was unclear, until a recent study elucidated the structural basis of SSB recognition by PARP1 (Eustermann, Wu et al. 2015). In its DNA-free conformation, PARP1 is a highly flexible protein, in which the six constituent domains behave like beads-on-a-string (Lilyestrom, van der Woerd et al. 2010, Eustermann, Wu et al. 2015). Strand break-stimulation of PARP1 involves a stepwise multi-domain folding pathway (Fig. 1.7.), which begins with ZFD1 and ZFD2 binding to DNA in a directional manner (Eustermann, Wu et al. 2015). This deforms the DNA in such a way that a cryptic binding interface is exposed for ZFD3, encompassing parts of ZFD1 and the DNA 5'-stem. Similarly, ZFD3 association generates a binding interface for the WGR domain, encompassing parts of ZFD1, ZFD3 and the DNA. The assembly of the three ZFDs with the WGR domain finally creates an interface

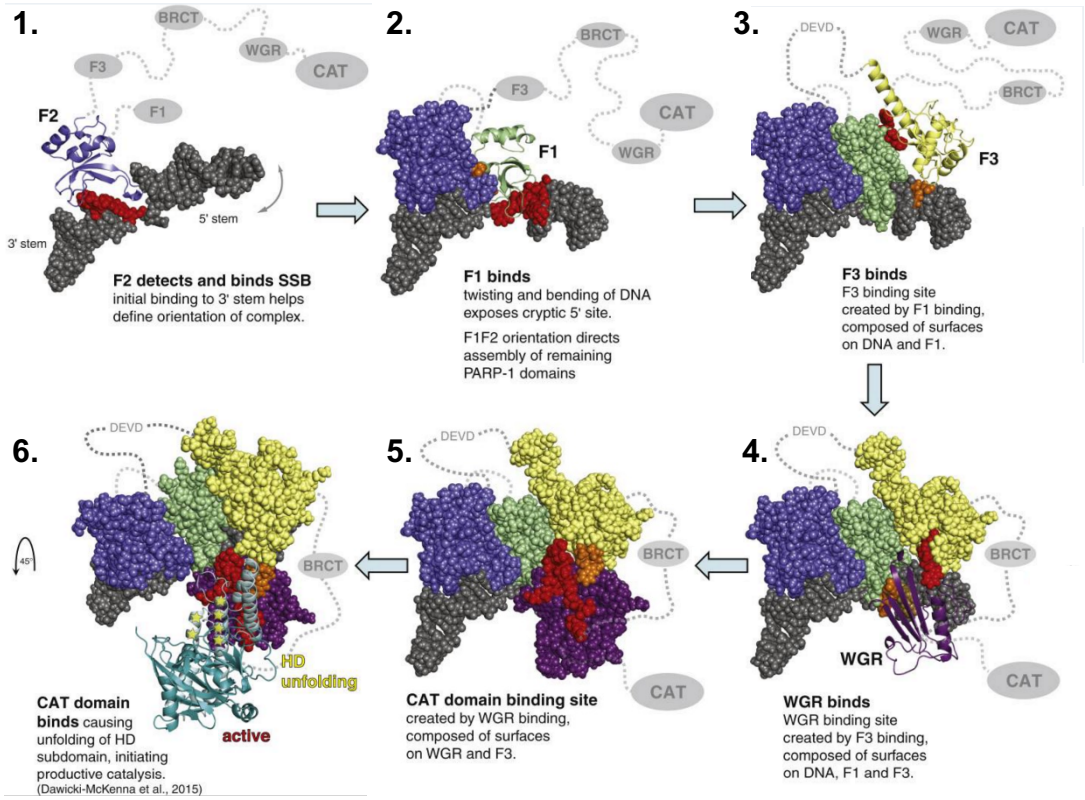

Figure 1.7. The structural basis of SSB detection by PARP1. A model of the allosteric mechanism by which PARP1 detects a SSB is depicted **[figure taken from (Eustermann, Wu et al. 2015), in accordance with the Creative Commons Attribution Licence (CC BY)].** In this model, initial recognition of DNA deformability by the zinc finger domains 1 and 2 (F1 and F2) triggers a sequential folding-up of the flexible PARP1 structure; with each association creating the binding interface for the next. This cumulates in binding of the catalytic (CAT) domain to an interface on the tryptophan-glycine-arginine (WGR) and zinc finger 3 (F3) domains, which destabilizes an autoinhibitory helical domain (HD) and allows productive catalysis. Note that the BRCT domain and proximal linker regions remain flexible, suggesting that they may reach the active site, which might explain their elevated automodification.

for the association of the CAT domain, encompassing parts of ZFD3 and the WGR domain. Binding of the CAT domain triggers the unfolding of an autoinhibitory helical subdomain (HD), resulting in stimulation of PARP1 activity (Dawicki-McKenna, Langelier et al. 2015). An elucidating feature of this break recognition model is the absence of contacts between the DNA termini and the amino acids of ZFDs; detection is instead based on the extreme deformability of SSBs compared to intact DNA (Eustermann, Wu et al. 2015). This explains the ability of PARP1 to recognise breaks with diverse termini. Furthermore, the flexibility of the ZFD1-ZFD2 linker region allows for a “fly-casting” mechanism; whereby initial ZFD2 binding to the 3’ DNA stem tethers PARP1 at the break site, allowing for subsequent scanning by ZFD1 for a 5’ DNA stem. This feature explains the ability of PARP1 to detect breaks with varying gap length (Eustermann, Wu et al. 2015).

The automodification of PARP1 accounts for a large proportion of its activity (D'Amours, Desnoyers et al. 1999, Langelier, Planck et al. 2012), and is thought to predominately occur at Glu, Asp and Lys residues within an automodification domain (373 to 525aa), including: D387, E488, E491 (Tao, Gao et al. 2009), K498, K521 and K524 (Altmeyer, Messner et al. 2009) (Kameshita, Matsuda et al. 1984). More recent work has revealed that automodification is by no means restricted to this region, and appears to occur throughout the protein to some degree (Gagne, Ethier et al. 2015). Despite these recent revelations, it is clear that the BRCT-WGR linker domain is subject to especially extensive automodification (Kameshita, Matsuda et al. 1984). This fits well with the structural model of PARP1-SSB interaction proposed by *Eustermann et al*; in which the BRCT-WGR linker remains flexible, and can reach the active site in *cis* (Eustermann, Wu et al. 2015). Previously, a model of PARP1 break detection was proposed in which the protein functioned as a homodimer, leading to automodification in *trans* (Ali, Timinszky et al. 2012). However, the work of *Eustermann et al* has shown that *trans* automodification of PARP1 occurs only when the DNA substrate contains proximal termini; such as a short linear dsDNA molecule, with breaks at either end. By comparison, no *trans* modification was observed when employing a nicked dumbbell DNA substrate, which mimics an isolated SSB (Eustermann, Wu et al. 2015).

Besides PARP1 itself, histones constituent the major acceptor of PAR modification (Adamietz and Rudolph 1984, Adamietz 1987); as mentioned above, this includes primarily the linker histone H1 (Poirier, de Murcia et al. 1982, Aubin, Fréchette et al. 1983, Gibson, Zhang et al. 2016, Grundy, Polo et al. 2016), but also all core histones (H2A, H2B, H3, and H4) to a lesser extent, which are modified on their flexible N-terminal tails (Messner, Altmeyer et al. 2010, Gibson, Zhang et al. 2016). Recent work has identified histone PARylation factor 1 (HPF1), a novel protein involved in attenuating PARP1 and PARP2 hyper-automodification and promoting their trans modification of histones (Gibbs-Seymour, Fontana et al. 2016). Subsequent work by the same group has clarified the role of HPF1 as a PARP1/PARP2 interactor which is necessary and sufficient for the ADP-ribosylation of Ser residues in many target proteins, including both histones and itself (Bonfiglio, Fontana et al. 2017). The recent unexpected identification of Ser as an acceptor of ADP-ribosylation, indeed a particularly prominent one, has dramatically altered our understanding of the ADP-ribosylated proteome (Leidecker, Bonfiglio et al. 2016, Bonfiglio, Fontana et al. 2017, Leung 2017). Intriguingly, it has been suggested that direction of PARP1 and PARP2 activity towards Ser by HPF1 may also be accompanied by a shift in the polymer chain length; possibly even to MARylation (Bonfiglio, Fontana et al. 2017, Leung 2017).

Recent work has highlighted a potentially novel function of PARP1-mediated PARylation: the nuclear generation of adenosine triphosphate (ATP) (Wright, Lioutas et al. 2016). The remodelling of chromatin which accompanies DNA transcription, replication and repair requires the activities of ATP-consuming enzymes. In this study, the authors demonstrated that ATP can be generated by the nuclear enzyme NUDIX5 (nucleoside diphosphate linked moiety X hydrolase 5) from pyrophosphate and free ADP-ribose (the product of PARG-mediated hydrolysis of PAR) (Wright, Lioutas et al. 2016). The authors further demonstrate than when this mechanism is perturbed by inhibition of PARP1, PARG or NUDIX5, there is a reduction in chromatin modelling associated with progesterone-induced gene expression. The authors postulate that the nuclear ATP generation might also be required for repair processes, and that PAR may

therefore serve as a means of concentrating ATP generation at sites of DNA damage (Wright, Lioutas et al. 2016).

Independently of its role as a SSB sensor, PARP1 has been implicated in the tolerance of replication, following initial immunofluorescence experiments which demonstrated colocalization of PARP1 with replication foci in S-phase cells stress (Sugimura, Takebayashi et al. 2008, Bryant, Petermann et al. 2009). This was followed by observations that inhibition, knockdown or genetic loss of PARP1 prevents the replication fork restart following Top1 poisoning by CPT (Sugimura, Takebayashi et al. 2008, Berti, Ray Chaudhuri et al. 2013) or depletion of the dNTP pool by hydroxyurea (HU) (Bryant, Petermann et al. 2009). This effect was found to be epistatic with loss of the HR nuclease MRE11, leading the authors to propose that PARP1 promotes MRE11 recruitment to stalled replication forks which promotes their restart via HR (Bryant, Petermann et al. 2009). Interestingly, it was seen that depletion of either PARP1 or PARP2 significantly reduced recombination at replication forks stalled by HU or thymidine (dT), and increased sensitivity to these agents in a non-additive manner, suggesting that the two proteins may collaborate in promoting replication stress tolerance (Bryant, Petermann et al. 2009).

1.5.2.1.2. PARP2

Parp2 (*PARP2* in humans) was the second of the PARP/ARTD gene family to be identified, following the observation of residual PAR synthesis in *Parp1*$^{-/-}$ MEFS (Amé, Rolli et al. 1999). PARP2 protein shares significant homology (62% identical or similar amino acids) with the C-terminal half of PARP1; including the WGR domain, HD, and ART domain (NCBI 2016). The homology is even more pronounced when considering only the active site region (amino acids 859 to 908 of PARP1) of the ART domain (92% identical or similar amino acids) (NCBI 2016). This explains the strikingly similar products of PARP1 and PARP2 catalytic activity: branched, high molecular weight PAR (Amé, Rolli et al. 1999).

PARP2 lacks the ~500aa N-terminal region (NTR) of PARP1, containing the ZFDs (Fig. 1.6.) (NCBI 2016). Instead, it has an NTR of only 78 aa, the

function of which is unclear. The lack of the ZFDs means that PARP2 relies more than PARP1 on its WGR and CAT domains, in addition to its NTR, for DNA-binding (Riccio, Cingolani et al. 2016). The NTR is natively disordered, as evidenced by circular dichroism and limited proteolysis experiments (Riccio, Cingolani et al. 2016); and contains a bipartite NLS, which has been characterized by X-ray crystallography (Riccio, Cingolani et al. 2016). Recently, *Riccio* et al reported that the NTR contributes significantly to DNA binding *in vitro*, especially to nicked SSB substrates (Riccio, Cingolani et al. 2016). This is evident from the 358-fold loss of affinity for a nicked dumbbell oligonucleotide of the ΔNTR truncation (K_d =13.3 μM) relative to full length (FL) PARP2 (K_d = 37 nM) (Riccio, Cingolani et al. 2016). Additionally, the isolated NTR has significantly higher affinity for DSB, nicked SSB and gapped SSB substrates than the isolated WGR or CAT domain, *in vitro* (Riccio, Cingolani et al. 2016). However, GFP-tagged NTR is unable to be recruited to laser microirradiated sites; unlike the ΔNTR truncation, which displays kinetics similar to FL PARP2 (Riccio, Cingolani et al. 2016). These discrepancies between *in vitro* and *in vivo* experiments may reflect differences in break recognition in chromatin vs naked DNA, and will require further study.

Despite the structural differences between PARP1 and PARP2, biologically-relevant functional differences remain unclear. It is known that *Parp1*$^{-/-}$ and *Parp2*$^{-/-}$ mice are viable, but embryonic fibroblasts from both display sensitivity to IR and alkylating agents (Ménissier de Murcia, Ricoul et al. 2003). *Parp1*$^{-/-}$*/Parp2*$^{-/-}$ mice, by comparison, are not viable, with embryogenesis arresting around the onset of gastrulation (embryonic day 6; E6) (Ménissier de Murcia, Ricoul et al. 2003). This result suggests that PARP1 and PARP2 may fulfil overlapping or redundant roles during unperturbed embryogenesis.

Recent work has suggested that whereas PARP1 displays broad recognition of strand breaks with diverse termini, PARP2 is preferentially activated by 5'-phosphorylated breaks, a property that it shares with PARP3 (Langelier, Riccio et al. 2014). This led *Langelier et* al to propose a role for PARP2 in the late stages of break repair, immediately prior to ligation (Langelier, Riccio et al. 2014). It was further suggested that this might involve a final burst of

PARylation as a signal to recruit or stimulate ligase complexes for the ligation reaction (see section 1.5.2.4). Whilst this is perhaps an appealing hypothesis, there are several discrepancies. For example, PARP1 is also highly stimulated by 5'-phosphorylated breaks, and would presumably also be able to fulfil the proposed role. As noted above, *Parp2*$^{-/-}$ mice are viable; further suggesting that the proposed role is not essential *in vivo*.

In addition to differences in break recognition specificity, it has been suggested that PARP1 and PARP2 may also differ in terms of protein substrate preference (Oliver, Amé et al. 2004) (Messner, Altmeyer et al. 2010). Structural evidence for this hypothesis stems from the fact that the PARP2 catalytic domain, whilst being largely homologous to that of PARP1, possesses a three-amino acid insertion, resulting in an extended six-residue deviation from the backbone observed in the PARP1 (Oliver, Ame et al. 2004). Within this loop, Tyr528 points directly into the acceptor site. This is not predicted to affect ADP-ribosyltransferase activity on ADP-ribose acceptors (e.g poly(ADP-ribosyl)ation activity) but it may confer a different protein acceptor specificity (Oliver, Ame et al. 2004). Despite these structural predictions, biochemical evidence of differing protein substrate specificity for PARP1 and PARP2 is lacking. One recent study employed a chemical genetics and proteomics strategy to identify the proteins specifically ADP-ribosylated by PARP1, PARP2 or PARP3 (Gibson, Zhang et al. 2016). This innovative approach enabled the authors to assess the degree of overlap between the protein targets of these three enzymes. However, there are a number of caveats to this work. Firstly, due to the impermeability of the cell membrane to the NAD analogs employed in the technique, the experiments were undertaken *in vitro* using recombinant PARPs and cell extracts. This may limit how accurately the data reflect the physiological activity of the enzymes *in vivo*. Secondly, the technique was limited to identifying ADP-ribosylated glutamate and aspartate residues. Given the fact that other residues are known to be acceptors of ADP-ribosylation, including lysine, arginine, and serine; the ADP-ribosylated proteome identified in the study is unlikely to be exhaustive. Future work will be required to fully elucidate the protein targets of the DNA-dependent PARPs *in vivo*.

1.5.2.1.3. PARP3

PARP3 was the third of the DNA break-stimulated ARTD/PARP family to be identified, being shown to be stimulated by DSBs *in vitro* and being implicated in promoting XRCC4-Lig4 function in NHEJ (see section 1.4.1) (Rulten, Fisher et al. 2011). Subsequently it was revealed that PARP3 is even more potently stimulated by 5'-phosphorylated SSBs than by DSBs *in vitro* (Grundy, Polo et al. 2016). *Grundy and Polo et al* were able to show that PARP3 specifically transmodifies H2B, primarily at Glu2, in response to a restriction enzyme-mediated single strand break. Furthermore, they showed that PARP3 stimulation was dependent on the break being 5'-phosphorylated, supporting the findings of *Langelier et al* (Langelier, Riccio et al. 2014). NMR observations of chemical shift perturbations in the WGR domain, upon addition of an oligonucleotide harbouring a 5'-phosphorylated nick, allowed a model of binding to be proposed (Grundy, Polo et al. 2016). In this model, the DNA resides on one face of the WGR domain, interacting with a basic patch that is highly conserved amongst PARP3 orthologs. Interestingly, important residues of this basic patch (Y83, R103, K127, and K149) are conserved with PARP2 (Grundy, Polo et al. 2016), suggesting that this may be the DNA-binding interface in both enzymes.

Based on conservation between PARP1-3 of a triad of residues in the active site (H887, Y919 and E988), amongst other structural features, PARP3 was previously predicted to exhibit poly(ADP-ribose) polymerase activity (Kleine, Poreba et al. 2008). It has been subsequently demonstrated that this is not the case and that PARP3 functions as a mono(ADP-ribose) transferase *in vivo* and *in vitro* (Loseva, Jemth et al. 2010, Vyas, Matic et al. 2014, Grundy, Polo et al. 2016). The functional consequences of this for PARP3-mediated DNA damage signalling remain to be fully understood. More generally, the potential role of PARP3 in SSBR remains to be fully elucidated. Experiments in chicken DT40 cells have confirmed that stable depletion of PARP3 slows repair of γ-radiation induced SSBs (Grundy, Polo et al. 2016), but as chickens lack a PARP2 gene it is unclear to what extent this represents the role of PARP3 in humans.

1.5.2.1.4. ADP-ribose binding domains

In addition to the chromatin decondensation mediated by auto-PARylation and PARylation of H1 (see section 1.5.2.1.1), ADP-ribosylation of core histones and other local proteins serves as a signal for the recruitment of factors involved in chromatin remodelling and DNA repair (Althaus, Kleczkowska et al. 1999). There are several types of protein domains which have been reported to bind to ADP-ribose PTMs, including: Macro domain, Trp-Trp-Glu (WWE) domain, PAR-binding zinc finger (PBZ) motif, PAR-binding motif (PBM), BRCA1 C-terminal (BRCT) domain, OB-fold, and forkhead-associated (FHA) domain (Malanga, Pleschke et al. 1998, Pleschke, Kleczkowska et al. 2000, Karras, Kustatscher et al. 2005, Ahel, Ahel et al. 2008, Kang, Lee et al. 2011, Zhang, Liu et al. 2011, Barkauskaite, Jankevicius et al. 2013, Li, Lu et al. 2013, Zhang, Chen et al. 2014, Breslin, Hornyak et al. 2015). These domains recognize different moieties of MAR and/or PAR (Fig. 1.5.), and are contained in effector proteins with diverse roles in many signalling pathways. The most well described of these domains (PBM, PBZ, Macro domain, and WWE domain), along with the novel PAR-binding BRCT domain of the core BER/SSBR scaffolding protein X-ray cross-complementing protein 1 (XRCC1), will be discussed below.

The first of the PAR-binding modules to be identified was the PBM (Malanga, Pleschke et al. 1998), a domain of 22-25 amino acids which has now been identified in many nuclear proteins; including the core and linker histones, and proteins involved in BER/SSBR, NER, HR, NHEJ and the DDR (Gagné, Isabelle et al. 2008, Teloni and Altmeyer 2016). This flexible motif lacks any strict consensus sequence, but has been proposed to generally conform to: [HKR][X][X][AIQVY][KR][KR][AILV][FILPV] (Gagné, Isabelle et al. 2008, Barkauskaite, Jankevicius et al. 2013). The flexibility of this domain has precluded structural work, preventing identification of the PAR moiety to which it binds. By comparison, the PBZ, Macro domain, and WWE domain all bind to well defined moieties of PAR.

The second of the PAR binding domains to be identified was the macro domain, a globular protein domain of 130-190 amino acids, which interacts with ADP-ribose in various metabolites, including PAR (Karras, Kustatscher et al.

2005, Teloni and Altmeyer 2016). These domains are found in the macro histone variants macroH2A1.1, macroH2A1.2, and macroH2A2, as well as in some members of the ARTD family (PARP9, PARP14, and PARP15) (Teloni and Altmeyer 2016). Because these domains are modular and contain a ADP-ribose binding pocket, some have evolved catalytic activity (Chen, Vollmar et al. 2011). This includes Macro domains which can degrade PAR, such as that found in MacroD1, MacroD2, and OARD1 (Peterson, Chen et al. 2011). The structure of the macroH2A1.1 macrodomain, in complex with ADP-ribose, has been solved by x-ray crystallography (Timinszky, Till et al. 2009). Significant interactions were observed between the 2-OH' and 3'-OH of the adenosine ribose with D352 and S355; which has led to suggestions that macrodomains cap PAR chains, rather than interacting with non-terminal ADP-ribose units (Timinszky, Till et al. 2009). This binding mode also allows macrodomains to interact with MAR, making them unique amongst the ADP-ribose binding domains, and allowing the catalytic macrodomains to remove terminal protein-linked ADP-ribose units (Jankevicius, Hassler et al. 2013, Rosenthal, Feijs et al. 2013).

Three years following the identification of the macro domain as a PAR binding domain, the PBZ was identified (Ahel, Ahel et al. 2008). The PBZ is a comparable size to the PBM (<30 residues); but with a well-defined structure, which has been solved by NMR and X-ray crystallography (Eustermann, Brockmann et al. 2010, Isogai, Kanno et al. 2010, Li, McCulloch et al. 2010, Oberoi, Richards et al. 2010). The consensus sequence ([K/R]-X-X-C-X-[F/Y]-G-X-X-C-X-[K/R]-[K/R]- X-X-X-X-H-X-X-X-[F/Y]-X-H) has been identified in only three human proteins: Aprataxin and PNKP-like factor (APLF), checkpoint with forkhead and ring finger domains (CHFR), and DNA crosslink repair protein 1A (DCLRE1A) (Ahel, Ahel et al. 2008). Of these, only the APLF and CHFR PBZ motifs have been shown to bind PAR; the DCLRE1A PBZ is predicted not to (Oberoi, Richards et al. 2010). The relative rarity of the PBZ is notable in comparison to the ubiquitous PBM. The PBZ is also unique in that it appears to bind to the ADP-ribose-adenosine moiety of a consecutive residues (Eustermann, Brockmann et al. 2010, Li, McCulloch et al. 2010).

Another three years from the discovery of the PBZ, the WWE domain was identified as a PAR binding domain (Kang, Lee et al. 2011, Zhang, Liu et al.

2011).This globular domain of ~80 amino acids, has since been identified in 12 human proteins, in two classes (Kang, Lee et al. 2011, Zhang, Liu et al. 2011, Wang, Michaud et al. 2012, Teloni and Altmeyer 2016). The first class is those that are present in a subgroup of the ARTD/PARP family (PARP7, PARP11, PARP12, and PARP14); notably these are all incapable of generating PAR (Wang, Michaud et al. 2012). The second class is made up of nine ubiquitin ligases of several types, including the PAR-dependent E3 ligase RNF146/Iduna (Wang, Michaud et al. 2012). This protein is particularly notable, as it binds to PARP1, PARP2, and XRCC1, amongst other repair proteins and chromatin factors (Kang, Lee et al. 2011). The WWE domain has been shown to bind to the iso-ADP-ribose moiety of PAR, which contains moieties of consecutive ADP-ribose residues (Wang, Michaud et al. 2012). This domain is therefore unable to bind MAR.

The identification of not one, but four unique PAR-binding domains, appeared to explain the PAR-dependent recruitment kinetics of many DNA repair and DDR proteins, including the crucial SSBR factor XRCC1, which possesses a putative PBM. However, this was not the case. In the following section, the history of XRCC1 research will be reviewed, including the elucidation of its true PAR-binding domain.

1.5.2.2. XRCC1

XRCC1 was originally identified (Thompson, Brookman et al. 1985) and cloned (Thompson, Brookman et al. 1990) by complementation of a mutant Chinese hamster ovary (CHO) cell line designated EM9. These cells were originally shown to be extremely sensitive to alkylating agents, to have attenuated rates of DNA strand break repair, and have a dramatically elevated frequency of sister chromatid exchanges (SCEs) (Thompson, Brookman et al. 1982). Subsequently, they have also been found to be sensitive to many other DNA-damaging agents, including: H_2O_2 (Cantoni, Murray et al. 1987), CPT (Caldecott and Jeggo 1991), IR (Thompson, Brookman et al. 1990), amongst others. The XRCC1 locus was sequenced in EM9 cells and a point mutation was identified which substitutes Gln221 for a stop codon, truncating the protein approximately 1/3rd into the CDS.

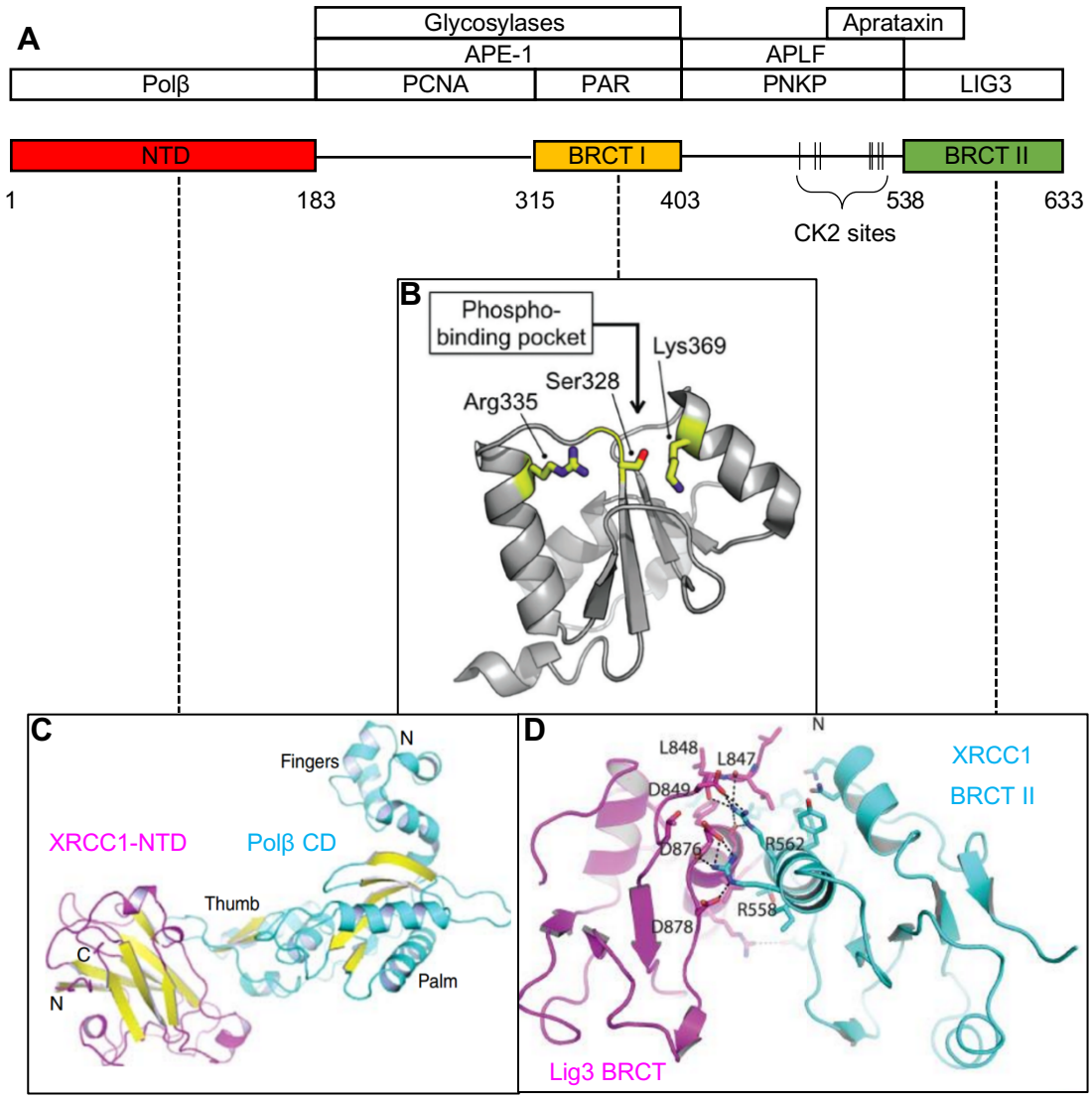

Figure 1.8. The domain structure and interacting partners of XRCC1. The domain structure of XRCC1 is depicted, along with the known regions of interaction with other protein partners [adapted from (Hanssen-Bauer, Solvang-Garten et al. 2012)] **(A)**. A crystal structure of the central BRCT I domain is shown; with highlighted residues comprising the phosphate-binding pocket, which mediates interaction with PAR [taken from (Breslin, Hornyak et al. 2015)] **(B).** Crystal structures of the XRCC1-NTD:Polβ-CD and the XRCC1-BRCTII:Lig3-BRCT interfaces are shown in **(C)** and **(D)**, respectively [taken from (Cuneo and London 2010) and (Cuneo, Gabel et al. 2011), respectively].

This truncated polypeptide is presumably degraded by nonsense-mediated decay (NMD), as no XRCC1 is detected by WB. This cell line has been the predominant model of XRCC1 deficiency since its original identification thirty-five years ago.

XRCC1 is rapidly recruited to sites of SSBs; acting as a scaffolding protein which recruits, stabilizes and stimulates enzymes involved in end-processing (see section 1.5.2.3), gap-filling and ligation (see section 1.5.2.4) (Fig. 1.8.) (Caldecott 2008). The rapid recruitment of XRCC1 to DNA damage sites led to hypotheses of PAR-binding. As mentioned above, this was originally ascribed to the C-terminal region of the BRCT I domain, which contains a putative PBM (Pleschke, Kleczkowska et al. 2000). However, mutation of five of the basic residues in the motif to alanine failed to impact on XRCC1 function (C. Breslin, unpublished observations). Furthermore, subsequent studies have demonstrated the importance of a conserved phosphate-binding pocket upstream of the putative PBM, in the centre of the BRCT I domain (Li, Lu et al. 2013, Breslin, Hornyak et al. 2015). Mutation of two constituent residues which are predicted to be involved in phosphate binding, Arg335 and Lys369, leads to: attenuated PAR-binding *in vitro,* reduced accumulation at sites of UVA laser and H_2O_2-induced damage, and cellular sensitivity to MMS and H_2O_2 (Breslin, Hornyak et al. 2015). Whilst the exact moiety to which this BRCT-domain binds has not been identified, it appears to be specific to PAR. This is evidenced by the inability of excess MAR to compete with WT XRCC1$^{161\text{-}406}$ binding to adsorbed, PARylated PARP1 or H1 (Breslin, Hornyak et al. 2015). By comparison, auto-PARylated PARP1 could compete with this binding. Interestingly, mutant (R335A, K369A) XRCC1$^{161\text{-}406}$ was still able to bind to adsorbed proteins which had been PARylated with an excessive NAD^+ concentration (Breslin, Hornyak et al. 2015). This may suggest that there are other motifs which contribute to XRCC1 PAR-binding, perhaps including the putative PBM described above.

XRCC1 is thought to adopt a rod-like structure in solution (Mani, Karimi-Busheri et al. 2004); which has been proposed to be characteristic of other proteins with multiple BRCT domains, often fulfilling scaffolding roles (Williams, Green et al. 2001). The proposed rod-like structure is thought to extend the

surface area for interaction with other proteins. Many of these protein-protein interfaces have been mapped to specific regions of XRCC1 (Fig. 1.8.). One such interaction is of the XRCC1 CTD with Lig3α (see section 1.5.2.4). This is a constitutive interaction, being unaffected by DNA damage induction; and significantly stabilizes Lig3α, such that loss of XRCC1 results in an ~80% reduction in Lig3α levels (Caldecott, Tucker et al. 1995). The NTD of XRCC1 interacts with the nucleotide-binding thumb domain of repair polymerase Polβ, facilitating the recruitment of this end-processing (see section 1.5.2.3.4) and gap-filling (see section 1.5.2.4) enzyme to DNA breaks. XRCC1 also interacts with the end-processing factors Aprataxin (see section 1.5.2.3.5) and PNKP (see section 1.5.2.3.2), and the more recently identified partner Aprataxin and PNKP-like factor (APLF) (Whitehouse, Taylor et al. 2001, Clements, Breslin et al. 2004, Loizou, El-Khamisy et al. 2004, Iles, Rulten et al. 2007). These interactions are mediated by the forkhead associated (FHA) domains of Aprataxin, PNKP and APLF; which bind to a phosphorylated region of XRCC1 in the linker region between the central BRCT I and C-terminal BRCT II domains. This region contains eight serine/threonine phosphorylation consensus sites for the constitutively-expressed casein kinase 2 (CK2) (Kubota, Nash et al. 1996). The phosphorylation marks are independent of DNA-damage, and appear to be constitutive (Luo, Chan et al. 2004). The binding of one FHA domain-containing partner is thought to preclude interaction with the others; suggesting that XRCC1 forms distinct complexes in cells (Luo, Chan et al. 2004).

The BRCT I domain of XRCC1 has been previously reported to interact with the PARP1 BRCT domain, in a PAR-independent fashion (Masson, Niedergang et al. 1998, Beernink, Hwang et al. 2005). However, other reports have contradicted this (Loeffler, Cuneo et al. 2011, Kim, Stegeman et al. 2015), and the consensus now is that the XRCC1-PARP1 interaction is mediated largely or entirely by PAR (London 2015).

XRCC1 has been reported to interact with various glycosylases (Marsin, Vidal et al. 2003, Campalans, Marsin et al. 2005, Akbari, Solvang-Garten et al. 2010, Hegde, Hegde et al. 2012) involved in base excision repair (see section 1.5.1), and with APE1 (Vidal, Boiteux et al. 2001). Some of these interactions

have been suggested to be direct, whilst others are likely to occur via interaction with other partners of XRCC1. In this way, products of BER are thought to be passed directly to the SSBR system (Wilson and Kunkel 2000). The interaction with APE-1 may also serve to recruit this enzyme in its role of end-processing at 3'-phosphoglyocolate and 3'-phosphoglycolaldehyde SSB termini (see section 1.2.1).

In addition to promoting the PAR-dependent recruitment of SSBR factors at DNA strand breaks, *in vitro* reconstitution of SSBR reactions has revealed that XRCC1 also stimulates the overall reaction (Whitehouse, Taylor et al. 2001). In these experiments, the activity of the core SSBR complex containing XRCC1, Polβ, PNKP, and Lig3α was investigated using a DNA substrate harbouring 5'-hydroxyl and 3'-phosphate termini and a one bp gap. As shall be discussed below in detail (see section 1.5.2.3), this substrate requires the activities of PNKP, Polβ and Lig3α to be successfully repaired. Omission of XRCC1 from these reactions significantly slowed the completion of SSBR when the concentrations of the other factors were limiting. Intriguingly, this was not the case when employing a substrate with canonical termini. As this substrate does not require the activity of PNKP, this suggested that XRCC1 predominately stimulates PNKP activity, which was confirmed with further experiments (Whitehouse, Taylor et al. 2001).

In this section, XRCC1 has been introduced as a scaffolding protein which helps to recruit and stimulate the activities of enzymes required for the end-processing, gap-filling and ligation of SSBs. In the following sections, these enzymes will be discussed in more detail, beginning with the most enzymatically-diverse of the three stages: end-processing.

1.5.2.3. End-processing

As discussed above, single strand breaks from various sources rarely contain canonical termini. This necessitates a host of enzymes to process these termini prior to gap-filling and ligation steps, many of which are interaction partners of

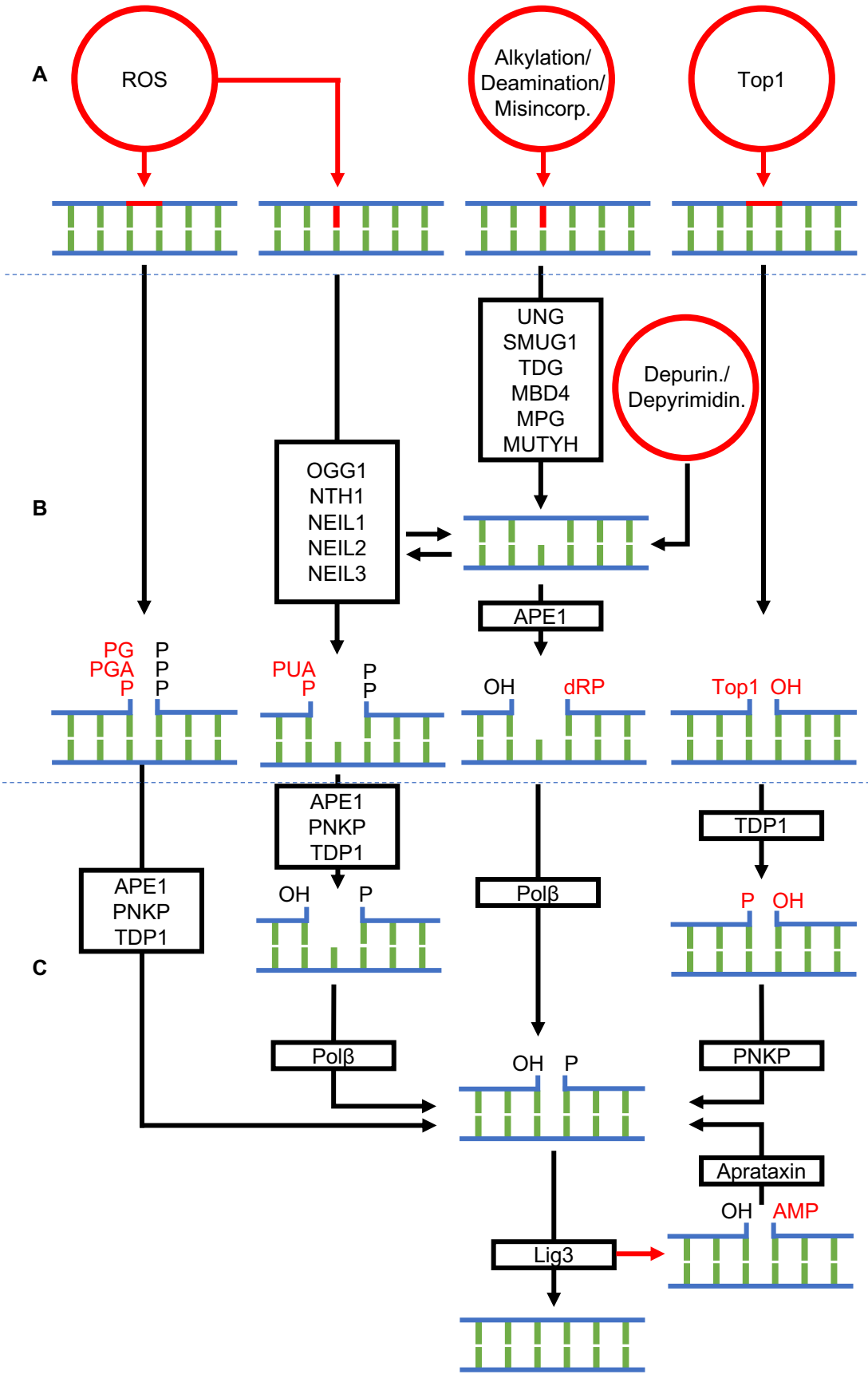
A
ROS
Alkylation/
Deamination/
Misincorp.
Top1
B
UNG
SMUG1
TDG
MBD4
MPG
MUTYH
Depurin./
Depyrimidin.
OGG1
NTH1
NEIL1
NEIL2
NEIL3
APE1
PG
PGA
P
P
P
P
PUA
P
P
P
OH
dRP
Top1
OH
C
APE1
PNKP
TDP1
APE1
PNKP
TDP1
OH
P
Polβ
TDP1
P
OH
Polβ
OH
P
PNKP
Aprataxin
OH
AMP
Lig3

Figure 1.9. Simplified model of the end-processing enzymatic activities required for the BER/SSBR of different lesions. SSBs can arise directly or indirectly as a result of various agents. Direct SSBs can arise by reaction of reactive oxygen species (ROS) with the deoxyribose phosphate moiety of DNA, or the through cleavage by Top1. Alternatively, DNA bases are susceptible to oxidation, alkylation or deamination, producing non-canonical bases which are the substrates of BER **(A).** ROS-induced direct SSBs often have a canonical 5'-phosphate (P) terminus and a non-canonical 3'-phosphoglycolate (PG), 3'-phosphoglycolaldehyde (PGA) or 3'-phosphate (P) terminus. By comparison, Top1-induced direct SSBs have non-canonical 5'-hydroxyl (OH) and non-canonical 3'-Top1 peptide termini. ROS-induced indirect SSBs result from the dual glycosylase and endonuclease activities of OGG1, NTH1, NEIL1, NEIL2 or NEIL3 at oxidized bases. These bifunctional glycosylases produce a canonical 5'-phosphate terminus and either a non-canonical 3'-phospho α,β-unsaturated aldehyde (PUA) terminus (OGG1 and NTH1), or a non-canonical 3'-phosphate terminus (NEIL1, NEIL2 and NEIL3). By comparison, the monofunctional glycosylases (UNG, SMUG1, TDG, MBD4, MPG and MUTYH) are variously responsible for excision of alkylated bases, deaminated bases, and misincorporated ribonucleotides and deoxyribonucleotides. The glycosylation activity of these enzymes produces an apurinic/apyrimidinic (AP) site, which is the substrate of the AP endonuclease (APE1). APE1 generates a SSB with a non-canonical 5'-deoxyribose phosphate (dRP) terminus and a canonical 3'-hydroxyl terminus. **(B)**. 3'-PG, 3'-PGA and 3'-PUA termini are substrates for APE1 and tyrosyl-DNA phosphodiesterase 1 (TDP1). The 5'-dRP terminus is a substrate for DNA polymerase β (Polβ). 3'-Top1 peptide termini are substrates for TDP1. 5'-OH and 3'-P termini are substrates for the dual activities of polynucleotide kinase 3'-phosphatase (PNKP). Finally, the 5'-adenosine monophosphate (AMP) terminus that can result from abortive ligation is a substrate for Aprataxin.

XRCC1 (Fig. 1.8.). An overview of the enzymatic activities required for the repair of some common damaged termini is shown in (Fig. 1.9.).

Three enzymes are implicated in processing blocked termini which result from direct oxidation of the dRP moiety of DNA: APE1, PNKP, and tyrosyl-DNA phosphodiesterase 1 (TDP1). These enzymes are also involved in processing blocked termini which result from excision of oxidized bases by the bifunctional glycosylases. By comparison, the 5'-dRP terminus which results from base excision by the monofunctional glycosylases and the subsequent endonuclease activity of APE1 requires processing by DNA polymerase β (Polβ). The blocked terminus which results from abortive Top1 activity is processed by proteolysis and the activities of TDP1 and PNKP. Finally, a special type of damaged terminus, which result from abortive ligation, is processed by APTX. These end-processing enzymes, and the reactions they catalyse, will be discussed in more detail below.

1.5.2.3.1. APE1

The first definitive proof of an endonuclease activity specific for AP sites was in 1972 (Paquette, Crine et al. 1972, Verly and Paquette 1972), following observations of this activity copurifying with *E. coli* endonuclease II preparations (Hadi and Goldthwait 1971). This AP endonuclease (APE) activity was subsequently demonstrated to belong to the previously characterized exonuclease III (ExoIII) (Weiss 1976, Lindahl 1979). *E. coli xth*$^{-}$ mutants, which are deficient for ExoIII, retain a residual level of APE activity that was attributed to another enzyme: endonuclease IV (EndoIV), encoded by the gene *nfo*. Homologs of ExoIII and EndoIV are now known to make up two types of APEs which exist throughout all domains of life. ExoIII-like APEs constitute the major APE activity in *E. coli* and most studied eukaryotes; many of which, including mammals, lack an EndoIV-like APE (Hadi and Wilson 2000).

In addition to its APE activity at intact AP sites, ExoIII-like human APE1 also possesses an ~200-fold lower activity for hydrolysis of 3'-P, 3'-PG, 3'-PGA and 3'-PUA termini in vitro (Chen, Herman et al. 1991), and is thus implicated in

processing 3'-termini of direct ROS-induced SSBs and those generated by the AP lyase activity of the bifunctional glycosylases (Fig. 1.9.) (Wallace 1998, Evans, Limp-Foster et al. 2000, Hegde, Hazra et al. 2008).

Human APE1 is a ~35 KDa protein, composed of a 61 aa N-terminal extension linked to a globular α/β region composed of two domains (Gorman, Morera et al. 1997). The globular region shares structural homology with *E. coli* ExoIII and DNAse I. APE1 and ExoIII share similar loop motifs which are notably absent in DNAse I, which led to the hypothesis that these loops were responsible for the DNA substrate specificity of APE1 and ExoIII, compared to DNAse I, which is highly promiscuous (Gorman, Morera et al. 1997). This hypothesis was subsequently proven correct when it was shown that APE1 inserts its loop motifs into both the major and minor groove of DNA, coordinating the AP-site in such a way as to exclude DNA bases (Mol, Izumi et al. 2000). The absence of APE-1 leads to early embryonic lethality in mice (Xanthoudakis, Smeyne et al. 1996) and induces apoptosis within 24 h at the cellular level (Izumi, Brown et al. 2005), highlighting the importance of APE1 in BER and SSBR.

As noted above, APE1 is able to process a range of 3'-termini, including the 3'-phosphate terminus *in vitro* (Chen, Herman et al. 1991). However, the kinetics of APE1 3'-phosphatase activity are very slow, with a turnover number (k_{cat}) of ~0.03 min^{-1} (Wiederhold, Leppard et al. 2004). Indeed, APE1 is not the dominant 3'-phosphatase in cells. This is the role of PNKP, which will be discussed below.

1.5.2.3.2. PNKP

The first enzymes to be identified which were capable of phosphorylating RNA and DNA 5'-hydroxyl termini were found in the bacteriophages T2 and T4 (Novogrodsky and Hurwitz 1966), which was followed in quick succession by the identification of a comparable activity in rat liver nuclei (Novogrodsky, Tal et al. 1966). The T4 polynucleotide kinase (PNK) became widely employed in the radiolabelling of nucleic acids with ^{32}P for use in downstream applications, including early methods for sequencing DNA (Maxam and Gilbert 1977). Over ten years after the identification of T4 PNK, it was discovered that the enzyme also

catalysed another reaction: the removal of phosphate from a 3'-phosphate terminus (Cameron and Uhlenbeck 1977), which is a feature common to mammalian PNK orthologs, including the 57 KDa human enzyme, PNKP (Karimi-Busheri, Daly et al. 1999). The possession of both 3'-DNA phosphatase and 5'-DNA kinase activities makes PNKP a critical end-processing enzyme, required not only in the repair of direct oxidative SSBs; but also in those arising as intermediates in BER and following abortive Top1 activity (Fig. 1.9.).

Mammalian PNKPs are comprised of an N-terminal forkhead-associated (FHA) domain joined via a flexible linker to tandem kinase and phosphatase domains at the C-terminus (Bernstein, Williams et al. 2005). This bipartite C-terminal domain shares homology with that of T4 PNK (Wang, Lima et al. 2002), although in T4 the phosphatase domain is C-terminal to the kinase domain. The kinase domain of mammalian PNKP differs from that of T4 PNK, in that it has a wider nucleic acid binding cleft, which is able to accommodate a double-stranded DNA substrate (Bernstein, Williams et al. 2005) and therefore prefers to phosphorylate 5'-hydroxyl termini at DNA nicks, gaps, and DSBs with 3'- single-stranded overhangs (Karimi-Busheri and Weinfeld 1997, Bernstein, Hammel et al. 2009). The PNKP phosphatase domain is similarly able to act on double-stranded DNA substrates, but unlike the kinase domain it lacks a substrate cleft wide enough to accommodate these substrates without prior DNA denaturation and/or protein conformational change (Bernstein, Williams et al. 2005, Havali-Shahriari, Weinfeld et al. 2017). The N-terminal FHA domain, which is absent in T4 PNK, mediates the interaction of mammalian PNKP not only with the phosphorylated CK2 sites of XRCC1 (see section 1.5.2.2) (Whitehouse, Taylor et al. 2001), but also with the similar sites in the NHEJ protein XRCC4 (Koch, Agyei et al. 2004) (see section 1.4.1). This promotes its recruitment to DSBs, which also often harbour 5'-hydroxyl and 3'-phosphate termini requiring repair (Chappell, Hanakahi et al. 2002).

The ubiquitous role of PNKP in many BER/SSBR sub-pathways (Fig. 1.9.) explains how its depletion results in cellular sensitivity to such a wide range of genotoxic agents, including: IR, CPT, H_2O_2, and MMS (Rasouli-Nia, Karimi-Busheri et al. 2004). Moreover, in unchallenged cells, PNKP depletion results in

an approximately seven-fold increased frequency of spontaneous mutation (Rasouli-Nia, Karimi-Busheri et al. 2004), highlighting its importance for the maintenance of genome integrity. More recently, hypomorphic PNKP mutations have been identified in patients with the neurological disease microcephaly, seizures, and developmental delay (MCSZ) (Shen, Gilmore et al. 2010), and in the neurodegenerative disease ataxia with oculomotor apraxia type 4 (AOA4) (Bras, Alonso et al. 2015), which will be discussed in detail in section 1.6.2.

PNKP is unlike APE1 in that it is apparently unable to process a broad range of 3'-termini (Wiederhold, Leppard et al. 2004) (Inamdar, Pouliot et al. 2002). However, there is another human 3'-end processing enzyme with broad substrate specificity: TDP1. This enzyme will be discussed in detail below.

1.5.2.3.3. TDP1

TDP1 was first cloned in 1999 (Pouliot, Yao et al. 1999), three years after researchers purified an enzyme capable of hydrolysing DNA 3'-phosphotyrosyl bonds in *S. cerevisiae* (Yang, Burgin et al. 1996). These initial publications identified the importance of TDP1 in the repair of abortive Top1-linked SSBs, because inactivating mutations in the gene sensitised HR-compromised cells to the Top1 poison CPT (Pouliot, Yao et al. 1999). Subsequent work has further improved our understanding of the role of TDP1 both in the repair of Top1-SSBs, and in the repair of other types of SSBs.

SSBs which arise as a result of abortive Top1 activity (see section 1.2.3) possess unique polypeptide-linked 3'-termini. Following Cullin 3-dependent polyubiquitylation (Desai, Liu et al. 1997), these Top1 polypeptides are degraded by the proteasome (Zhang, Tomida et al. 2004). Both the CPT-induced polyubiquitylation and degradation of Top1 seem to be dependent upon transcription, rather than replication, as they are blocked by inhibitors of the former (DRB and α-amanitin), but not the latter (aphidicolin) (Desai, Liu et al. 1997, Desai, Zhang et al. 2003, Lin, Ban et al. 2008). Using the expression of dominant negative ubiquitin mutants, polyubiquitylation was shown to occur via

K48-ubiquitin linkages (Lin, Ban et al. 2008), which are known to serve as a molecular signal for degradation by the 26S proteasome (Pickart 1997).

Following degradation of Top1 to an oligopeptide, TDP1 can catalyse cleavage of the 3'-tyrosyl phosphodiester bond (Yang, Burgin et al. 1996, Pouliot, Yao et al. 1999). *In vitro* activity assays have shown that TDP1 has very low cleavage activity upon the full length Top1cc, instead preferring oligopeptide substrates < 13 amino acids in length (Debethune, Kohlhagen et al. 2002). This can be rationalised by the inaccessibility of the Top1 active site, and therefore the DNA-tyrosyl phosphodiester linkage, in the native Top1cc structure (Redinbo, Stewart et al. 1998). TDP1 is a member of the phospholipase D (PLD) superfamily, and has been shown to be widely conserved amongst eukaryotic organisms (Pouliot, Yao et al. 1999, El-Khamisy and Caldecott 2006), since its original discovery in *S. cerevisiae.* The PLD superfamily catalyse phosphoryl transferase reactions, fulfilling diverse roles in all domains of life (Interthal, Pouliot et al. 2001). These PLD enzymes typically contain two copies of a highly-conserved active site motif: $HXK(X)_4D(X)_6GSXN$. Human TDP1, and its orthologs, possess unusual "HKD" motifs, in that the aspartate residue is not conserved. The histidine and lysine residues are conserved, however, and their mutation has been shown to dramatically attenuate TDP1 activity in vitro (Interthal, Pouliot et al. 2001). Interestingly, similar to other PLD enzymes, the TDP1 catalytic mechanism has been shown to proceed via 3'-phosphohistidyl-DNA covalent intermediate, which is subsequently hydrolysed by nucleophilic attack of an activated water molecule (Interthal, Pouliot et al. 2001). The histidines of the two HKD motifs are crucial for both steps. H263 is the nucleophile which attacks the 3'-phosphotyrosyl linkage in the first step; with protonated H493 acting as a general acid catalyst by protonating the tyrosine oxygen. Subsequently, H493 acts as a general base in the activation of the second nucleophile: water. Interestingly, H493 is the mutated residue in the hereditary neurodegenerative disease spinocerebellar ataxia with axonal neuropathy (SCAN1) (see section 1.6.2).

The product of TDP1 activity is a 3'-phosphate terminus which, along with the 5'-hydroxyl terminus generated initially by Top1 incision, requires the activity

of PNKP to be converted to a canonical terminus. In addition to its tyrosyl phosphodiesterase activity, TDP1 is also able to process other 3'-termini in vitro, including 3'-phosphoglycolate and 3'-PUA termini (Inamdar, Pouliot et al. 2002, Interthal, Chen et al. 2005, Zhou, Akopiants et al. 2009, Lebedeva, Rechkunova et al. 2011). This has implicated TDP1 in the repair of SSBs arising directly and indirectly from oxidation of DNA (Fig 1.9.) (Interthal, Chen et al. 2005, Zhou, Lee et al. 2005).

Human TDP1 possess an N-terminal 140aa domain which is unconserved with its orthologs in lower eukaryotes (Interthal, Pouliot et al. 2001, El-Khamisy and Caldecott 2006). This domain does not influence catalytic activity, but is nonetheless important for TDP1 function *in vivo*. In lower eukaryotes, the primary role of TDP1 appears to be in repairing replication induced Top1-DSBs (Liu, Pouliot et al. 2004). This is evidenced by its epistatic relationships with components of the homologous recombination repair pathway in *S. cerevisiae (Vance and Wilson 2002).* In higher eukaryotes, TDP1 function appears to be more intimately linked with SSBR. This is likely to be in part achieved by interaction of TDP1, via its N-terminal domain, with Lig3α (El-Khamisy, Saifi et al. 2005). Incidentally, XRCC1-Lig3α is absent in *S. cerevisiae*, perhaps indicating less strict requirements for coordination of SSBR in lower eukaryotes (Caldecott 2008).

TDP1 has been shown by multiple groups to be phosphorylated by ATM and DNA-PK at S81, within its N-terminal domain (Das, Antony et al. 2009, Chiang, Carroll et al. 2010). Both groups reported that this phosphorylation stabilizes TDP1 protein, and that its mutation to alanine compromises survival following treatment with CPT. Using an anti-pS81 antibody, *Das et al* could show that the phosphorylation of S81 is induced by CPT, and that it is reduced by both transcription and replication inhibition (with DRB and Aphidicolin, respectively). Furthermore, *Das et al* report a colocalization of anti-pS81 and γ-H2AX foci, suggesting that the modification may be induced at DSBs which result from replication collision with Top1ccs (Das, Antony et al. 2009). Lacking a specific anti-pS81 antibody, *Chiang et al* instead utilized a yeast two-hybrid (Y2H)

approach to identify that S81 is critical for the interaction of TDP1 with Lig3α (Chiang, Carroll et al. 2010).

The N-terminal domain of TDP1 also contains a SUMOylation site (K111), which is conserved amongst vertebrates (Hudson, Chiang et al. 2012). Mutation of this site to arginine, or depletion of the obligate SUMO-conjugating enzyme UBC9, has been shown to reduce TDP1 accumulation at sites of DNA damage (Hudson, Chiang et al. 2012). More recently, a direct interaction between the TDP1 N-terminal domain and PARP1 has been reported by *Das et al*. The authors report that this interaction is independent of damage induction or PARP1 activity, and serves to recruit TDP1 upstream of the XRCC1 repair complex (Das, Huang et al. 2014). They also report that PARP1 can poly ADP-ribosylate TDP1 in vitro, but that this does not impact TDP1 enzyme activity; instead they suggest that this may stabilize TDP1 (Das, Huang et al. 2014). It has been further reported that the PARP1-TDP1 interaction may promote an intrinsic AP-endonuclease activity of TDP1 (Lebedeva, Anarbaev et al. 2015). The existence of this activity remains controversial, however, as it is not universally observed in other recombinant TDP1 preparations (Pouliot, Robertson et al. 2001). Furthermore, the original authors did not observe the activity in TDP1 preparations which had been renatured following further purification by SDS-PAGE, suggesting that it may be have been caused by a contaminating endonuclease in the original preparation (Lebedeva, Rechkunova et al. 2011). Finally, it is important to note that abasic sites are prone to thermal degradation (Sugiyama, Fujiwara et al. 1994, Zheng and Sheppard 2004) and alkaline lysis (Lindahl and Andersson 1972), which can potentially introduce spurious results when conducting AP endonuclease assays *in vitro*.

1.5.2.3.4. Polβ

SSBs generated by the class II AP endonuclease activity of APE1 harbour canonical 3’-hydroxyl and non-canonical 5’-dRP termini. These 5’-blocked SSBs contrast with the 3’-blocked SSBs which predominate following direct oxidation of the deoxyribose phosphate backbone, and those generated by the AP lyase activity of the bifunctional glycosylases. The removal of 5’-dRP is catalysed by

Polβ, a PolX family polymerase which is also responsible for the gap-filling step in short patch repair (see section 1.5.2.4).

Polβ was discovered in 1971, following its purification from rabbit bone marrow (Chang and Bollum 1971). The authors of this early work noted that the 39 KDa polymerase was considerably smaller than the first identified mammalian polymerase catalytic subunit pol α (~165 KDa). Observations that Polβ could fill small gaps in DNA (Wang and Korn 1980), coupled with its constant expression throughout the cell cycle (Zmudzka, Fornace et al. 1988), lead to suggestions that it was the predominant DNA polymerase involved in BER. This hypothesis was subsequently confirmed, following *in vitro* experiments with mammalian and frog cell extracts (Wiebauer and Jiricny 1990, Dianov, Price et al. 1992, Matsumoto, Kim et al. 1994, Singhal, Prasad et al. 1995).

In 1995, it was shown that Polβ also possesses a 5'-dRP lyase activity in addition to its polymerase activity, and that this was attributable to its 8 KDa N-terminal domain (absent in the replicative polymerases α, δ and ε) (Matsumoto and Kim 1995). *Polb*$^{-/-}$ mice die *in utero*, before day 10.5 of gestation (Gu, Marth et al. 1994). However, *Polb*$^{-/-}$ mouse embryonic fibroblasts have been isolated and have been shown to be sensitive to alkylating agents and hydrogen peroxide (Sobol, Horton et al. 1996, Fortini, Pascucci et al. 2000), and this can be complemented by expression of *Polb* harbouring mutations in the catalytic, but not dRP lyase domain (Sobol, Prasad et al. 2000). These experiments highlight the importance of Polβ as an end-processing enzyme.

1.5.2.3.5. Aprataxin

One of the most recently identified DNA end-blocking groups results from the catalytic mechanism of DNA ligases, which involves the formation of a transient DNA 5'-AMP intermediate (see section 1.5.2.4) (Ahel, Rass et al. 2006, Tomkinson, Vijayakumar et al. 2006). In productive ligation, nucleophilic attack by the 3'-hydroxyl DNA end then results in formation of the phosphodiester bond, with concurrent release of AMP. If the 3'-DNA end is not in proximity, as is the case in a single-strand gap; or if it harbours a non-canonical chemical group, then

the adenylate moiety will remain on the 5'-DNA terminus. In 2006, Aprataxin was identified as the enzyme which removes the adenylate, restoring a 5'-phosphate terminus (Ahel, Rass et al. 2006). The gene encoding Aprataxin, APTX, was originally described following the identification of its mutation in a subset of Freidreich ataxia (FRDA)–like patients (Date, Onodera et al. 2001). The similarity in the clinical presentations of these patients to those with ataxia with oculomotor apraxia (AOA) was noted, and the disease was subsequently named ataxia with oculomotor apraxia type 1 (AOA1). It was shown that AOA1 patient cells were sensitive to MMS, H_2O_2 and CPT (Clements, Breslin et al. 2004, Gueven, Becherel et al. 2004, Luo, Chan et al. 2004, Mosesso, Piane et al. 2005). This sensitivity to diverse SSB-inducing agents is unsurprising, because all SSBR pathways must end in ligation, regardless of the initial type of lesion. Further highlighting its importance as an integral component of SSBR, Aprataxin was identified as an interaction partner of XRCC1 (see section 1.5.2.2) (Clements, Breslin et al. 2004).

1.5.2.4. Gap-filling and ligation

The restoration of a canonical 3'-OH terminus through the activities of APE1, TDP1 and/or PNKP allows gap-filling to be conducted by DNA polymerases. It is important to note that the repair of some SSBs does not require this activity, because they do not involve DNA gaps (for example some types of Top1-SSBs and direct ROS-induced SSBs) (Caldecott 2008). By comparison, SSBs generated by the DNA glycosylases in BER harbour a one nucleotide gap. Furthermore it has been suggested that proximal tandem SSBs can result in the loss of an oligonucleotide and the formation of longer gaps (Sage and Harrison 2011, Schiml, Fauser et al. 2016), which would also require polymerase activity for repair.

Gap-filling can occur via a short-patch (SP-SSBR; AKA SP-BER) or long-patch (LP-SSBR; AKA LP-BER) mechanism (Fig. 1.10.). SP-SSBR refers to the synthesis of one nucleotide, usually by the PolX family repair polymerase Polβ (see section 1.5.2.3.4), whereas LP-SSBR refers to the synthesis of a longer DNA tract of 2-12 nucleotides, usually by the replicative polymerases δ and ε in

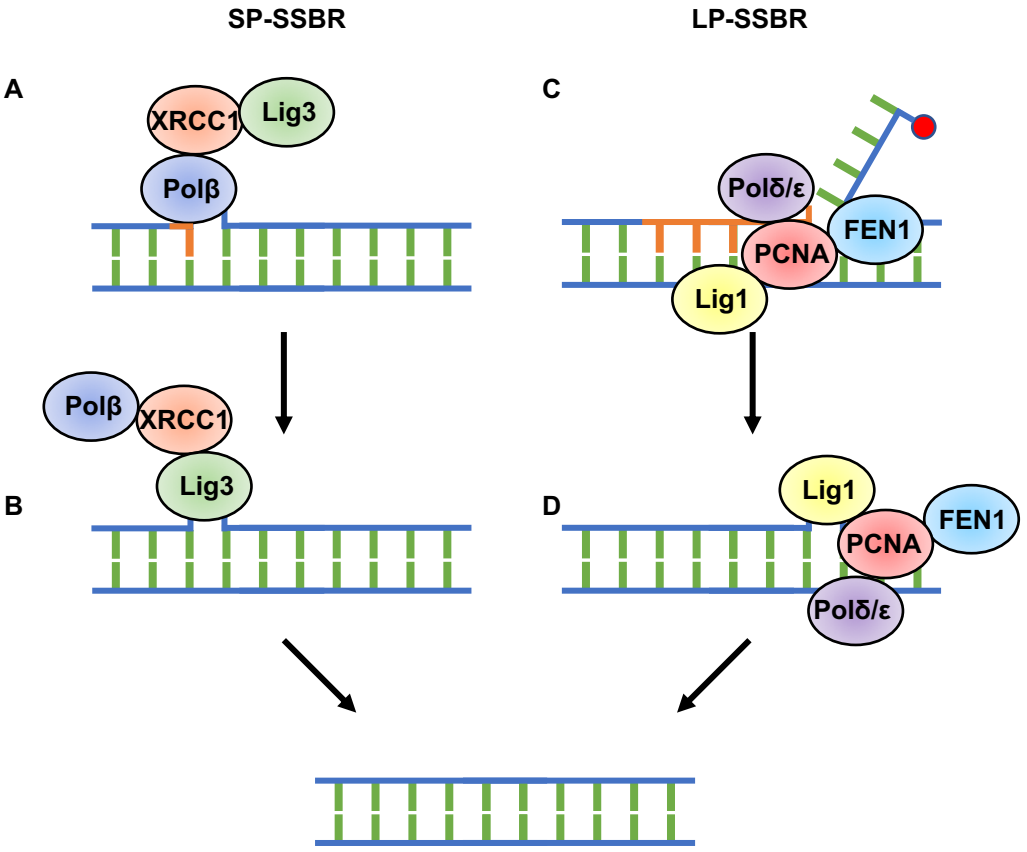

Figure 1.10. Simplified model of the gap-filling and ligation steps of SSBR. Following end-processing, SSBR can proceed by a short patch (SP-SSBR) or long patch (LP-SSBR) mechanism. SP-SSBR involves one nucleotide gap-filling by Polβ (in complex with XRCC1-Lig3). This step is closely coordinated with the end-processing 5'-dRP lyase activity of Polβ **(A)**. SP-SSBR is usually completed by Lig3-mediated ligation of the DNA nick **(B)**. By comparison, LP-SSBR involves polymerisation of a 2-12 nucleotide tract of DNA, usually by Polδ/ε (in complex with the accessory clamp PCNA), displacing a 5'-DNA flap which is cleaved by FEN1. This pathway is thought to be important when processing breaks with 5'-blocking lesions which cannot be removed by Polβ **(C)**. LP-SSBR is completed by Lig1-mediated ligation of the DNA nick **(D).**

complex with proliferating cell nuclear antigen (PCNA) (Frosina, Fortini et al. 1996). This displaces a 5'-DNA flap which is cleaved by flap endonuclease 1 (FEN1) (Klungland and Lindahl 1997, Kim, Biade et al. 1998). The long-patch system averts the requirement to directly recognize and remove a 5'-blocking lesion, and may serve as an important mechanism when 5'-dRP termini are oxidized, reduced, or otherwise modified, preventing their removal by Polβ (Klungland and Lindahl 1997).

The final ligation of the nicked DNA is conducted by either ligase III (LIG3), in complex with its constitutive partner XRCC1 (exclusive to SP-BER); or by ligase I (LIG1), via its interaction with PCNA (predominately in LP-BER) (Barnes, Tomkinson et al. 1992, Cappelli, Taylor et al. 1997, Sleeth, Robson et al. 2004). As mentioned above (see section 1.5.2.3.5), the mechanism catalysed by these ligases (and by LIG4-XRCC4, operating in NHEJ) involves a DNA 5'-AMP intermediate (Tomkinson, Vijayakumar et al. 2006). When ligases become abortive, this adenylated DNA terminus remains; and it must be removed by Aprataxin prior to a successful ligation attempt (Ahel, Rass et al. 2006).

1.6. SSBR and Human Disease

The previous sections have reviewed the mechanisms of SSBR which defend the integrity of the genome. This has implications for our understanding and treatment of human diseases. In this section, two areas of clinical significance will be reviewed: the rationale for the use of PARP inhibitors in treating HR-deficient cancers, and the neurodegenerative genetic diseases associated with defective SSBR.

1.6.1. Synthetic Lethality of PARP1 inhibition and HR deficiency

In proliferating cells, SSBs are an impediment to replication forks, and can cause their collapse to produce one-ended DSBs (see section 1.3.2). The absence of another DNA end necessitates that these lesions be repaired by Homologous Recombination (HR – see section 1.4.2), which gives rise to the selective sensitivity of HR-deficient cells to SSBR-blocking PARP inhibitors (Bryant,

Schultz et al. 2005, Farmer, McCabe et al. 2005, Saleh-Gohari, Bryant et al. 2005). This mechanism is the rationale behind the FDA and EMA-approved use of PARP inhibitors for the treatment of *BRCA1/BRCA2* -deficient tumours in patients with advanced ovarian cancer (EMA 2014, FDA 2014).

Synthetic lethality is a term used to describe a lethal genetic interaction between two genes which only exists upon their coincident deficiency, and not upon deficiency of either individually. Since the late 1990s, it was suggested that this might be used in the selective killing of tumour cells, which often have mutations in genes involved in DNA repair or the maintenance of genome stability (Hartwell, Szankasi et al. 1997); and in 2005 this effect was definitively demonstrated for the first time between *PARP1* and *BRCA2* (Bryant, Schultz et al. 2005). In this original publication, the authors noted that *BRCA2*$^{-/-}$ cells were more sensitive to PARP inhibition than genetic loss of *PARP1*, which they suggested could be due to the formation of a more dangerous lesion upon inhibition of the enzyme (Bryant, Schultz et al. 2005). This hypothesis was supported by the observation of increased sensitivity of WT cells cotreated with PARP inhibitors and SSB-inducing agents, relative to *Parp1*$^{-/-}$ cells treated with MMS alone (Horton, Stefanick et al. 2005). It was subsequently demonstrated that PARP inhibitors trap PARP1 and PARP2 bound to DNA breaks (Kedar, Stefanick et al. 2012, Murai, Huang et al. 2012, Murai, Huang et al. 2012), and these complexes are suspected to be a more robust block to replication (Helleday 2011) and/or to preclude redundant repair pathways which could act on naked SSBs. This effect can be understood from the mechanism described above (see section 1.5.2.1.1), whereby PARP automodification normally mediates release from DNA strand breaks, but inhibition or genetic loss of this activity prevents release (Satoh and Lindahl 1992).

Further supporting the hypothesis that this example of synthetic lethality results from a more complex mechanism than a reduction in SSBR kinetics mediated by catalytic inhibition of PARP1, it has been shown that other SSBR genes do not exhibit the same genetic relationship with *BRCA1/BRCA2*. For example, depletion of *XRCC1*, which significantly slows SSBR (Thompson, Brookman et al. 1982), does not reduce survival of *BRCA2*$^{-/-}$ cells (Patel, Sarkaria

et al. 2011). Furthemore, limiting NHEJ by depletion of Ku80 or inhibition of DNA-PKcs results in suppression of the PARP inhibitor sensitivity of *BRCA2*$^{-/-}$ cells (Patel, Sarkaria et al. 2011), suggesting that this pathway is involved in the mechanism of cell death.

1.6.2. Defective SSBR and Neurodegeneration

The proficiency of HR has been suggested to account for the fact that genetic defects in SSBR do not result in significant pathology in proliferating tissues (Rulten and Caldecott 2013). This is evidenced by the fact that defective SSBR results in an increased frequency of sister chromatid exchanges – one hallmark of HR (El-Khamisy, Saifi et al. 2005). By contrast, SSBR is thought to be particularly important in postmitotic cells, where SSBs cannot be repaired by replication coupled-HR processes (Rulten and Caldecott 2013). In recent years, a group of recessive human diseases have been identified which are caused by mutations in the SSBR genes *TDP1, APTX, PNKP* and, recently, *XRCC1* (SCAN1, AOA1, AOA4, and AOA-XRCC1, respectively) (Date, Onodera et al. 2001, Takashima, Boerkoel et al. 2002, El-Khamisy, Saifi et al. 2005, Shen, Gilmore et al. 2010, Bras, Alonso et al. 2015, Hoch, Hanzlikova et al. 2017). A hallmark of all of these diseases is neurodegeneration: typically, peripheral axonal neuropathy (dysfunction of the neurons which control sensory and motor functions), and early onset cerebellar ataxia (defective control and coordination of muscle movements resulting from degeneration in a region of the brain called the cerebellum) (Rulten and Caldecott 2013). Patients with AOA1, AOA2 or AOA-XRCC1 additionally also exhibit oculomotor apraxia (defective control and coordination of eye movements) (Rulten and Caldecott 2013).

There are several hypotheses to explain why neurons are more sensitive to defective SSBR than other terminally differentiated cell types. Firstly, oxidative stress is thought to be particularly high in the brain (Barzilai, Rotman et al. 2002), due to a combination of relatively high metabolic rate (Wang, Ying et al. 2010), low levels of antioxidants (Uttara, Singh et al. 2009), and the production of the ROS cellular signalling molecule nitric oxide (NO) by neuronal NO synthase (nNOS) (Eliasson, Sampei et al. 1997). This combination of factors is thought to

elevate the frequency of SSBs (Rulten and Caldecott 2013). Another hypothesis implicates the reliance of neurons on very high levels of transcription, which may increase the frequency of Top1-SSBs whilst simultaneously rendering the cells more dependent on production of essential mRNAs, and more susceptible to apoptosis mechanisms which result from transcription blockage (Hetman, Vashishta et al. 2010, Rulten and Caldecott 2013). Finally, it appears that neurons are particularly sensitive to programmed cell death via Parthanatos (see section 1.5.2.1), which is illustrated by the current model of cerebral ischaemia, a brain injury caused by a focal loss of blood supply. In cerebral ischaemia, tissue damage is thought to result from blood reperfusion of the deprived region, triggering an excessive release of the neurotransmitter glutamate which is bound by several receptors of the N-methyl-D-aspartate (NMDA) class (Curtis and Watkins 1965, Watkins and Olverman 2000). The excitation of these receptors triggers an influx of Ca^{2+} into the neurons, which in turn stimulates the production of ROS by enzymes such as nNOS (Bredt, Hwang et al. 1991, Rameau, Chiu et al. 2004). It has been shown that genetic loss of *Parp1* protects cultured cerebral cortical cells from NMDA-induced cell death, and reduces the extent of brain injury following induction of cerebral ischaemia in mice (Eliasson, Sampei et al. 1997), suggesting that Parthanatos may be the mechanism responsible for excitotoxicity. More recent evidence has implicated Parthanatos as a mechanism of neuronal cell death in mice with brain specific loss of *Xrcc1* (Hoch, Hanzlikova et al. 2017). Co-workers in the Caldecott laboratory found that genetic loss of *Parp1* reduced the loss of cerebellar neurons and ataxia in these mice (Hoch, Hanzlikova et al. 2017).

1.7. General Aims of the Thesis

SSBR is a complex and multifaceted pathway which repairs SSBs arising from various endogenous and exogenous sources. Despite great advances in our knowledge of how this pathway operates, many questions remain. Developing our understanding of SSBR from a basic research perspective is crucial for the comprehension and treatment of human diseases. The broad and general aim of this thesis is to elucidate novel features of how SSBR operates on physiological substrates *in vivo,* in human cells.

Chapter Three will focus on attempting to establish a single gene system for studying how CPT-induced Top1-SSBs influence transcription and recruitment of the central SSBR scaffold XRCC1.

Chapter Four will focus on establishing novel knockout human diploid cell lines using CRISPR-Cas9, for use in subsequent parts of the project, and in future work.

Chapter Five will focus on establishing controlled high-content microscopic methods for measuring cellular ADP-ribosylation and the recruitment of endogenous XRCC1 into the chromatin.

Chapter Six will use cell lines and methods developed in Chapter Four and Five to investigate the role of the three DNA-dependent PARPs in cellular responses to oxidative DNA damage, including: ADP-ribosylation, recruitment of XRCC1 to the chromatin, and rates of SSBR.

Chapter Seven will use cell lines and methods developed in Chapter Four and Five to investigate cellular responses to Top1-SSBs induced by CPT; with a focus on the genetic relationships between *TDP1, XRCC1* and the DNA dependent *PARPs.*

Chapter Two

Materials and Methods

2.1. Materials

2.1.1. Primary antibodies

Primary Antibody	Supplier	Reported Target	Host	WB Cond.	IF Cond.	ChIP Cond.
A300-231A	Bethyl	XRCC1	Rabbit	1/5000 10% milk TBST	Not used	2 µg / IP
ABC738	Millipore	XRCC1	Rabbit	1/2000 10% milk TBST	1/200 10% FCS	Not used
MCA1522G	Serotec	PARP1	Mouse	1/2000 10% milk TBST	Not used	Not used
39743	Active Motif	PARP2	Rabbit	1/500 10% milk TBST	1/200 10% FCS	Not used
4699	Gift of F. Dantzer	PARP3	Rabbit	1/500 10% milk TBST	Not used	Not used
MABE1016	Millipore	PAR	Rabbit	1/2000 10% milk TBST	1/1000 10% FCS	Not used
8WG16	Santa Cruz	RNAP2	Mouse	1/1000 3% BSA TBST	Not used	1 µg / IP
A301-618A	Bethyl	TDP1	Rabbit	1/500 10% milk TBST	Not used	Not used
SK3195	Own hybridoma	PNKP	Rabbit	1/500 10% milk TBST	1/1000 10% FCS	Not used
TL25	Own hybridoma	Lig3α	Rabbit	1/1500 10% milk TBST	Not used	Not used
66009	Protein Tech	β-Actin	Mouse	1/2000 10% milk TBST	Not used	Not used
Ab6160	Abcam	α-Tubulin	Rat	1/5000 10% milk TBST	Not used	Not used
Ab17677	Abcam	Histone 1.2	Rabbit	1/2000 10% milk TBST	Not used	Not used
4974-7808	Serotec	Histone 1	Mouse	Not used	1/500 10% FCS	Not used
Ab3825	Abcam	Top1	Rabbit	1/200 10% milk TBST	Not used	Not used

Table 2.1. Details of primary antibodies used in this project. The catalogue or clone number is indicated, together with the supplier, the reported protein target, and the host species in which the antibody was generated. Also indicated are the conditions in which the antibody was used for Western Blot (WB), Immunofluorescence (IF), or Chromatin Immunoprecipitation (ChIP), where relevant.

2.1.2. Secondary antibodies

Secondary Antibody	Supplier	Reported Target	Host	WB Cond.	IF Cond.	ChIP Cond.
P0448 HRP-GαR	Dako	Rabbit Ig	Goat	1/10,000 10% milk	Not used	Not used
P0260 HRP-MαR	Dako	Mouse Ig	Rabbit	1/10,000 10% milk	Not used	Not used
Ab6734	Abcam	Rat Ig	Rabbit	1/10,000 10% milk	Not used	Not used
Alexa 488 - GαR	Life	Rabbit Ig	Goat	Not used	1/1000 10% FCS	Not used
Alexa 647 - DαM	Life	Mouse Ig	Donkey	Not used	1/1000 10% FCS	Not used

Table 2.2. Details of secondary antibodies used in this project. The catalogue or clone number is indicated, together with the supplier, the reported protein target, and the host species in which the antibody was generated. Also indicated are the conditions in which the antibody was used for Western Blot (WB), Immunofluorescence (IF), or Chromatin Immunoprecipitation (ChIP), where relevant.

2.1.3. Mammalian expression plasmids

Name	Plasmid	Expresses	Bacterial Antibiotic Resistance	Mammalian Antibiotic Resistance	Created by
pEGFP-XRCC1	pEGFP-C1	EGFP-XRCC1	Kan	G418	Akira Yasui
pEGFP	pEGFP-C1	EGFP	Kan	G418	Commercial
pGR.TDP1.1	Addgene #41824	gRNA TDP1.1	Kan	Bleomycin	William Gittens
pGR.TDP1.2	Addgene #41824	gRNA TDP1.2	Kan	Bleomycin	William Gittens
pGR.PARP2.	Addgene #41824	gRNA PARP2.2	Kan	Bleomycin	Zhihong Zeng
pCas9	Addgene #41815	Cas9	Amp	G418	(Mali, Yang et al. 2013)

Table 2.3. Details of mammalian expression plasmids used in this project. The name of the plasmid is indicated, together with the parent vector, and the expressed construct. Also indicated are the antibiotic resistances conferred for bacterial or mammalian selection, and the original creator of the plasmid.

2.1.4. siRNAs

siRNA	Target	Supplier	Type
D-001810-10-05	Non-targetting	Dharmacon	ON-TARGETplus SmartPool
L-010127-02-005	PARP2	Dharmacon	ON-TARGETplus SmartPool
L-009297-00-0005	PARP3	Dharmacon	ON-TARGETplus SmartPool

Table 2.4. Details of siRNAs used in this project. The catalogue number of the siRNA is indicated, together with the reported target, the supplier, and the type of reagent.

2.1.5. qPCR primers

qPCR Primer Name	Name on tube	qRT-PCR	ChIP-qPCR	Sequence
H.s FOS A (fw)	*FOS*.ChIP.F(fw)	No	Yes	AGGTTTCCACGGCCTTTCC
H.s FOS A (r)	*FOS*.ChIP.F(r)	No	Yes	TTTCGCAGTTCCTGTCTCAGAG
H.s FOS B (fw)	*FOS*.ChIP.A(fw)	No	Yes	ACTCATTCATAAAACGCTTG
H.s FOS B (r)	*FOS*.ChIP.A(r)	No	Yes	GTAGGAGCACGGTCACTG
H.s FOS C (fw)	*FOS*.ChIP.H(fw)	No	Yes	TTCGTTCTGAGCAACCTCTGG
H.s FOS C (r)	*FOS*.ChIP.H(r)	No	Yes	TTAGCGAGTTTGTGCTTGGG
H.s FOS D (fw)	*FOS*.ChIP.C(fw)	Yes	Yes	ATTCCATCCCAACTCAGAC
H.s FOS D (r)	*FOS*.ChIP.C(r)	Yes	Yes	AGATCCTCAGCAAGAGAAC
H.s FOS E (fw)	RT-*FOS*fw(E4)	Yes	No	GCTTCCCTTGATCTGACTGG
H.s FOS E (r)	RT-*FOS*r(E4)	Yes	No	GCTGCTGATGCTCTTGACAG
H.s FOS F (fw)	*FOS*.ChIP.D(fw)	Yes	Yes	CTTCCCTTGATCTGACTGG
H.s FOS F (r)	*FOS*.ChIP.D(r)	Yes	Yes	CTGATGCTCTTGACAGGTTC
H.s FOS G (fw)	*FOS*.ChIP.P(fw)	No	Yes	ATTAGCCTGGTGTGGTGGTG
H.s FOS G (r)	*FOS*.ChIP.P(r)	No	Yes	TCTCAGTTCGCTGCAACATC
H.s Actin (fw)	hACTBrv	Yes	No	CTCGTCATACTCCTGCTTGC
H.s Actin (r)	hACTBfw	Yes	No	GAAGTGTGACGTGGACATCC
H.s MLN51 (fw)	hMLN51fw	Yes	No	CTAAGGAAGCCAGTCACCTT
H.s MLN51 (r)	hMLN51rv	Yes	No	AGGAATCTCTTCCACAGAGG
C.g FOS E4 (fw)	CHO.C-*FOS*.3414.fw	No	Yes	TTTCCTTGTGCAGGAGACAG
C.g FOS E4 (r)	CHO.C-*FOS*.3414.r	No	Yes	GCTGCCAAAATGAACTCCAG

Table 2.5. Details of qPCR primers used in this project. The name of the qPCR primer is given, both as it is referred to within this thesis, and as it appears on the tube. Whether the primer was used for qRT-PCR or ChIP-qPCR is also indicated, along with the sequence of the primer.

2.2. Methods

2.2.1. Molecular cloning methods

2.2.1.1. Polymerase Chain Reaction (PCR)

PCR was conducted using Phusion High Fidelity Polymerase (NEB) as per the manufacturer's instructions. Reaction products were purified using a PCR purification kit (QIAGEN).

2.2.1.2. Restriction digests

Restriction of plasmid or PCR product DNA was conducted with Restriction enzymes (NEB, Roche) as per the manufacturer's instructions. Digest products were purified using a PCR purification kit (QIAGEN) or Gel extraction kit (QIAGEN), depending on the downstream application.

2.2.1.3. Ligation

Ligations were conducted with T4 DNA Ligase (NEB) as per the manufacturer's instructions. Briefly, a 3:1 molar ratio of insert to vector was combined with T4 DNA Ligase and 1x T4 Ligase Buffer. The reaction was incubated overnight at 16˚C, prior to bacterial transformation (see section 2.2.1.7), and plating on LB-agar with suitable antibiotic selection.

2.2.1.4. Gibson assembly

Gibson assembly was conducted with Gibson Assembly Master Mix (NEB), as per the manufacturer's instructions. Briefly, 0.02 pmol linearized plasmid and 0.3 pmol insert (15:1 molar ratio) were combined with master mix (2X) and deionized water to a final master mix concentration of 1X. Reactions were incubated at 50˚C for 1 hr, prior to bacterial transformation (see section 2.2.1.7) and plating on LB-agar with suitable antibiotic selection.

2.2.1.5. TOPO TA cloning

TOPO cloning was conducted with TOPO TA Cloning Kit (ThermoFisher) as per the manufacturer's instructions. Briefly, 2-5 µg of unpurified PCR products were

combined with pCR 2.1-TOPO plasmid, Salt Solution and deionized water (final NaCl and $MgCl_2$ concentration: 200 mM and 10 mM $MgCl_2$, respectively). Reactions were incubated at room temperature (RT) for 1 h, prior to bacterial transformation (see section 2.2.1.7) and plating on LB-agar with suitable antibiotic selection and X-gal (0.2 mg/ml), for blue-white colony screening.

2.2.1.6. DNA TAE-agarose electrophoresis

Agarose gels were prepared by dissolving Agarose powder (Sigma) in 1X TAE Buffer (40 mM Tris-acetate, 1 mM EDTA) with heating, to a percentage suitable for the downstream application. Prior to casting, the mixture was cooled and ethidium bromide was added to a final concentration of 0.3 µg/ml. DNA samples were prepared in 1X GelPilot DNA Loading Dye (QIAGEN). Electrophoresis was conducted at 4 V/cm, with 1X TAE Running Buffer. 1 kb Plus DNA Ladder (ThermoFisher) was included as a size marker. DNA was visualised by UV illumination (UV Transilluminator Appligene Inc QBiogene).

2.2.1.7. Bacterial transformation, amplification and preparation of plasmid DNA

Unless otherwise stated, 0.1-2 µg plasmid DNA was mixed with 50 µL chemically competent DH5α cells and incubated on ice for 10 min. The mixture was subjected to heat shock in a 42˚C water bath for 30 s, before being returned to ice for 2 min. 500 µL of LB was added and cultures were incubated at 37 ˚C for 1 h with agitation. Cultures were centrifuged at 6000 g and pellets were suspended in a small volume of supernatant and plated on LB-agar with kanamycin or ampicillin (both 50 µg/ml). Plates were incubated at 37˚C overnight to allow colony formation. Single colonies were selected and transferred to 3 ml or 100 ml LB containing kanamycin or ampicillin (both 50 µg/ml), depending on the scale of preparation. Cultures were incubated overnight at 37˚C, and pellets were processed with QIAprep Spin Miniprep Kit (QIAGEN) or QIAfilter Plasmid Midi Kit (QIAGEN), according to the manufacturer's instructions.

2.2.2. Mammalian cell culture

2.2.2.1. General Maintenance of Cell lines

A431 cells (ATCC) were maintained as monolayers in DMEM (Gibco) supplemented with 10% fetal calf serum (FCS), 2 mM L-glutamine (Gibco), 100 U/ml Penicillin (Gibco) and 100 µg/ml Streptomycin (Gibco). CHO EM9 derivative cell lines were maintained in α-MEM (Gibco) supplemented with 10% FCS, 100 U/ml Penicillin (Gibco) and 100 µg/ml Streptomycin (Gibco). RPE-1 cells (ATCC) and derivatives were maintained in DMEM/F12 (Sigma) supplemented with 10% FCS, 100 U/ml Penicillin (Gibco) and 100 µg/ml Streptomycin (Gibco). A431 and CHO cells were maintained in a humidified atmosphere at 37˚C with atmospheric O_2 and 5% CO_2. RPE-1 cells were maintained in a humidified atmosphere at 37˚C with 3% O_2 and 5% CO_2. Care was taken to passage all cell lines before 100% confluence. Monolayers were washed with PBS prior to RT incubation with 0.25% Trypsin (w/v), 2.21 mM EDTA in Hank's Balanced Salt Solution (HBSS) (Litmus Scientific), until detachment was observed. Trypsin activity was quenched with complete media and cells were pelleted by centrifugation at 300 g for 5 min. Cells were then resuspended in complete media. Cells were counted, as required, with a haemocytometer, prior to plating as necessary.

2.2.2.2. Neon nucleofection of plasmid DNA

The Neon nucleofection system (ThermoFisher) was used to transfect RPE-1 cells with plasmid DNA, according to the manufacturer's instructions. Briefly, $1.2x10^6$ tyrpsinised and PBS-washed cells were resuspended in 30 µL buffer R and combined with a total of 3 µg plasmid DNA. The mixture was electroporated with the device (2 x 20 ms 1350 V pulses), prior to immediate plating in complete DMEM/F12. A plating density of $4x10^5$ cells per 35 mm dish was used.

2.2.2.3. Amaxa transfection of plasmid DNA

The Amaxa Kit T nucleofection system (Lonza) was used to transfect A431 cells with plasmid DNA, according to the manufacturer's instructions. Briefly, $1x10^6$ trypsinised and PBS-washed cells were resuspended in 100 µL Nucleofector Solution and combined with 2 µg plasmid DNA. The mixture was electroporated

with the device, using program X-001 as per the manufacturer's recommendation, prior to immediate plating in complete DMEM. A plating density of $1X10^6$ cells per 35 mm dish was used.

2.2.2.4. RNAimax transfection of siRNA

The Lipofectamine RNAimax Reagent (ThermoFisher) was used to reverse transfect RPE-1 cells with siRNA according to the following method. 90 µL Optimem (Gibco) was combined with 12.5 µL siRNA solution in water (1 µM) in a microcentrifuge tube. Separately, 100 µL Optimem was combined with 2.7 µL Lipofectamine RNAimax reagent and mixed with a pipette tip. The mixtures were combined and mixed gently with a pipette tip, prior to dropwise distribution of 200 µL of the mixture over the surface of a 35 mm dish. The dish was then incubated for 20 min at RT. $7x10^5$ trypsinised and PBS-washed cells were resuspended in 1 ml complete DMEM/F12 and added dropwise to the dish, prior to overnight incubation at 37˚C. 0.8 ml complete DMEM/F12 was then added. Unless otherwise stated, all subsequent experiments were conducted 72 h after transfection.

2.2.2.5. Generation of A431 cell lines stably expression GFP and GFP-XRCC1

A431 cells were transfected with 2 µg pEGFP or pEGFP-XRCC1 using Amaxa Kit T (Lonza) (see section 2.2.2.3). 24 h later, GFP positive cells were observed by live fluorescent microscopy to assess transfection efficiency. G418 was then added to a final concentration of 0.6 mg/ml and cells were incubated for 7 days, prior to passaging to 10 cm dishes for single colony formation. 2-3 weeks later, single GFP +ve colonies were individually passaged to 12 well plates using cloning cylinders (Agar Scientific). Cells were then expanded prior to screening for presence of protein expression by Western Blot (WB) (see section 2.2.6).

2.2.3. qRT-PCR

2.2.3.1. Total RNA extraction

Cells growing in 35 mm dishes were treated according to specific time courses detailed in the results. At the indicated time points, cells were washed with 1 ml ice cold PBS and scraped into 500 µL ice cold PBS. The cells were then pelleted by 500 g centrifugation (4˚C). The supernatant was aspirated and cells were snap frozen in liquid nitrogen. Pellets were stored at -80˚C until further use. Total RNA was extracted using the RNAeasy Mini Kit (QIAGEN), according to manufacturer's instructions with a few modifications. All centrifugation steps were conducted at 21,000 g for 1 min. Pellets were lysed in 350 µL Buffer RLT with vortexing. The lysate was transferred to a gDNA Eliminator spin column and centrifuged. 350 µL 70% EtOH was added to the flow through and the mixture was transferred to a RNAeasy spin column and centrifuged. The flow through was discarded and the column was washed with 700 µL Buffer RW1, with centrifugation. The column was washed with 400 µL Buffer RPE. 10 µL of a solution of DNAse I (NEB) in 1X DNAse I Reaction Buffer (4 units), was added to the centre of the column, prior to incubation for 5 min at RT. The column was washed with 400 µL Buffer RPE, with centrifugation. The column was then washed once more with 200 µL Buffer RPE, with centrifugation. The flow through was discarded and the column was dried by centrifugation. Finally, RNA was eluted in 50 µL milli-q filtered water. RNA samples were maintained on ice and used immediately.

2.2.3.2. RNA integrity analysis by TBE-Agarose Electrophoresis

1.5% Agarose gels were prepared as described (see section 2.2.1.6), with the exception that 1X TAE buffer was replaced with 1X TBE buffer (89 Mm Tris-Borate, 2 mM EDTA). 2 µL of RNA sample was prepared in 1X RNA Loading Dye (NEB) and loaded onto the gel. Electrophoresis was conducted at 60 V for 45 min. RNA was visualised by UV illumination (UV Transilluminator Appligene Inc QBiogene).

2.2.3.3. DNA Synthesis

Total RNA concentration of samples was measured using the Nanodrop 2000c Spectrophotometer. 0.5-1 µg RNA was combined with 0.5 µL of 100 µM oligo-dT primer solution (Eurogentec) and Milli-Q filtered water, to a final volume of 12.5 µL. The mixture was incubated at 70˚C for 5 min, before being returned to ice for 2 min. 37.25 µL of the following mixture was added: 10 µL 5X RT-buffer (NEB), 2 µL 25 mM dNTPs (NEB), 1 µL Murine RNASE Inhibitor (NEB), 0.25 µL Reverse Transcriptase (NEB), and 24 µL milli-q water. Reactions were incubated at 42˚C for 1 h. Reactions were spiked with a further 0.25 µL Reverse Transcriptase and incubated at 42˚C for 1 h. Finally, 1 µL RNAse A (ThermoFisher) was added and the reactions were incubated at 37˚C for 30 min. Reactions were purified using PCR Purification Kit (QIAGEN) and eluted in 100 µL milli-Q purified water. cDNA samples were used immediately or maintained at -20˚C until further use.

2.2.3.4. Identification of qRT-PCR primer pairs

FOS qRT-PCR primer pairs were identified using the Primer3Plus web application operating in qPCR mode (Rozen and Skaletsky 1999). The following parameters were specified: product length of 90-150 bp, and primer dissociation temperature of 55˚C.

2.2.3.5. Validation of primers used for *FOS* qRT-PCR

To quantify the relative abundance of *FOS* mRNA accurately by qRT-PCR, primer sets (see table 2.5) were carefully validated to ensure specific amplification of the target sequence. The human *FOS* genomic locus is shown in Fig. 2.1.a, together with the mRNA and protein maps. The positions of the amplicons of three pairs of primers (D, E and F) are shown. Primer pair D targets the region 1499-1617 bp downstream of the transcription start site (TSS), within intron 2. Primer pairs E and F target an almost identical region in exon 4 (2163-2291 and 2164-2287 bp downstream of the TSS, respectively). Total RNA, from untreated A431 cells, was extracted and used as a template for cDNA synthesis with oligo-dT primers, to amplify poly(A)-tailed mRNA (see sections 2.2.3.1 and 2.2.3.3). This cDNA was then subjected to qPCR with primers pairs D, E, and F targeting *FOS* (see section 2.2.3.6). In addition, primers targeting human *Actin* or *MLN51* were used,

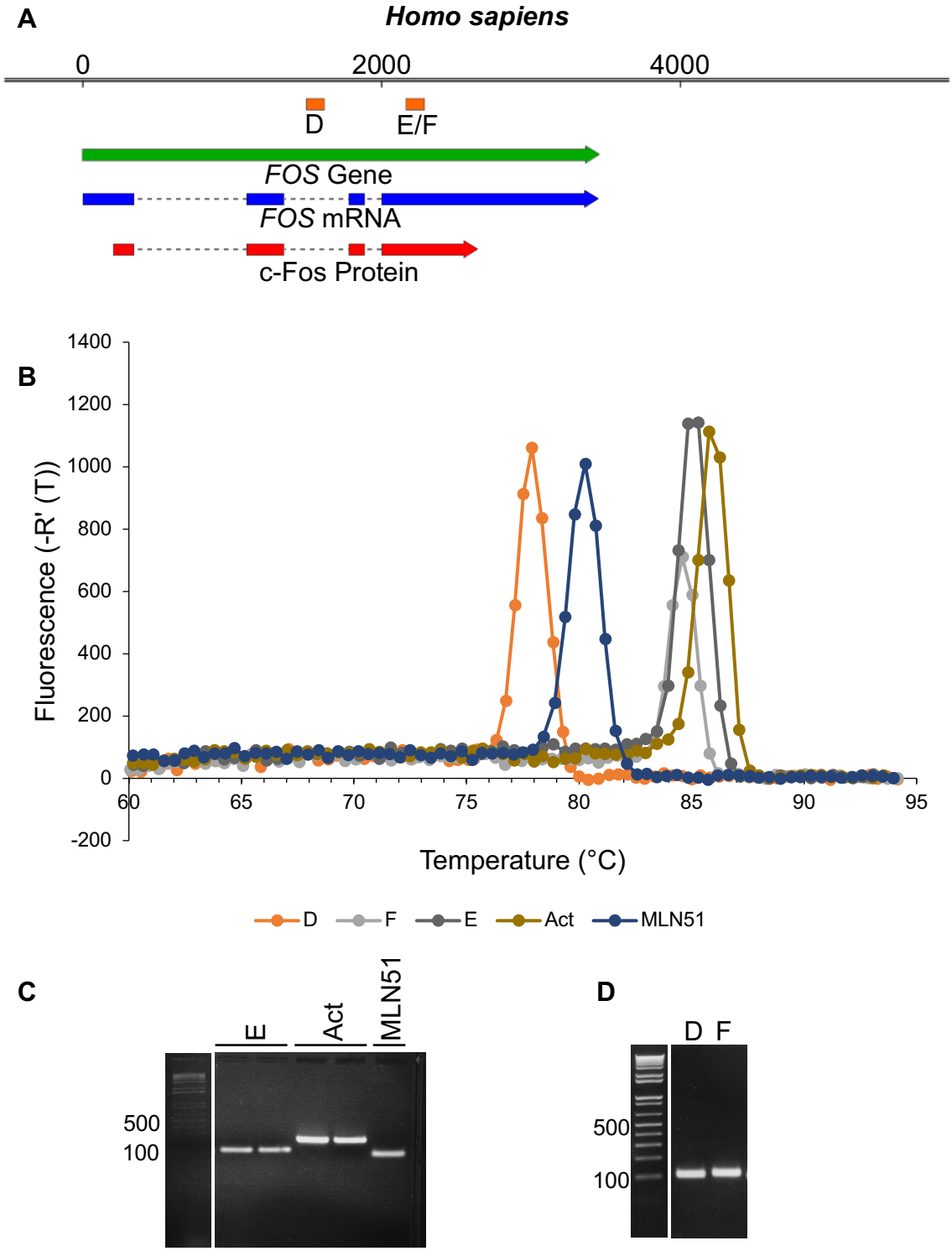

Figure 2.1. Validation of primers used for RT-qPCR with human cells. The positions of primers pairs used for RT-PCR are shown in a diagram of the human *FOS* gene (numbers are bp). Orange rectangles represent the amplicon of each primer pair. The amplicon of primer pair E is almost identical to that of primer pair F (see section 2.2.3.5), so both are indicated by a single orange rectangle. **(A)**. Dissociation curves of the products of qPCR reactions using primer pairs D, E, F, Act and MLN51 are shown in (see Table 2.5. for sequences) **(B)**. PCR products were separated and visualised by 1.5% agarose electrophoresis and ethidium bromide staining. A molecular weight marker has been included, showing size in bp **(C) and (D).**

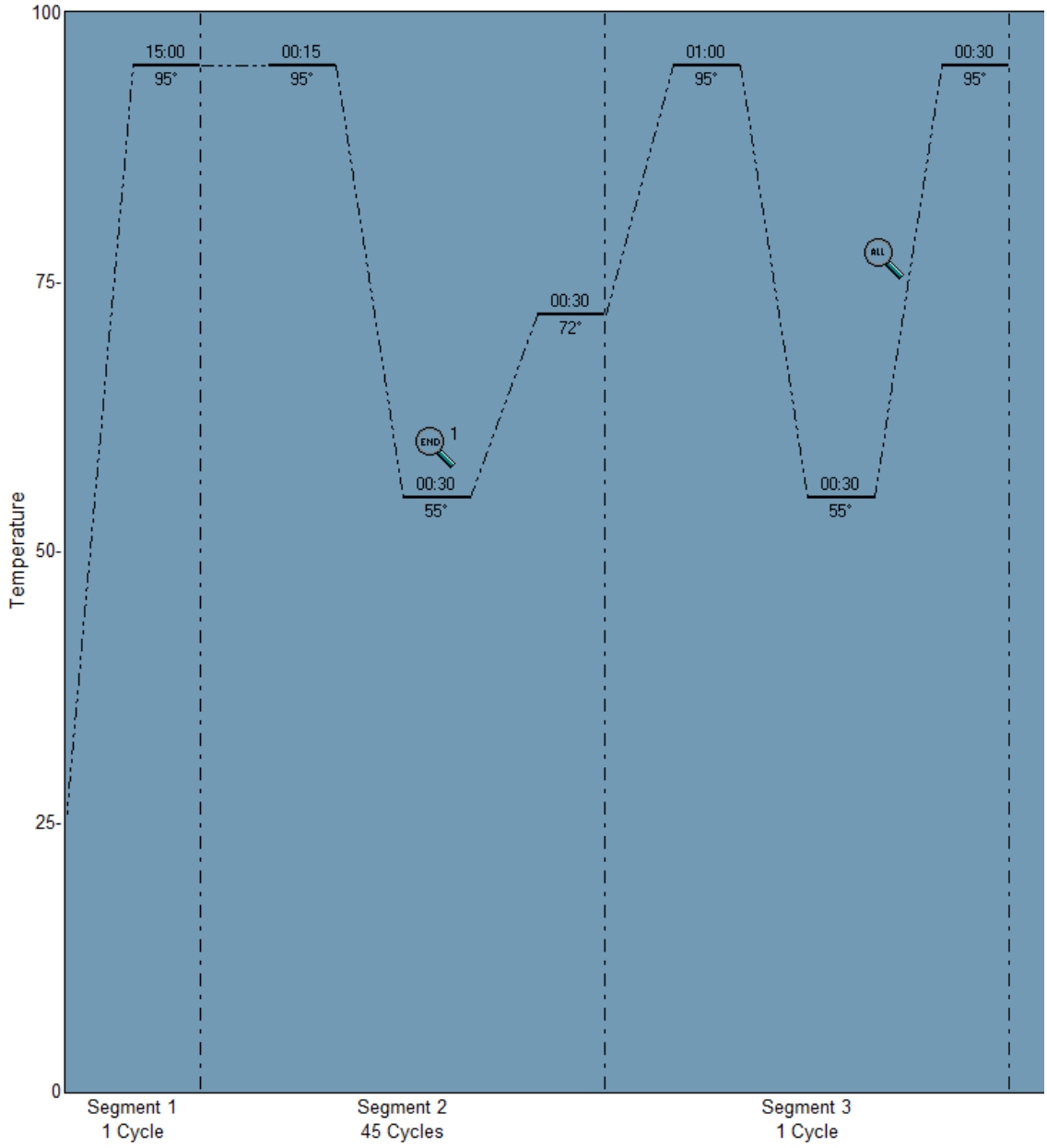

Figure 2.2. qRT-PCR Reaction Steps. The temperature and duration of each step of the qRT-PCR is illustrated. Segment 1,2 and 3 correspond to the hot-start polymerase activation, the PCR itself, and the dissociation curve, respectively. The source of the image is a screen capture from the MxPro software.

as these genes are expressed at relatively constant rates and serve as internal sample controls. Following amplification by PCR, the reactions were subjected to a temperature gradient with constant fluorescence detection. A dissociation curve was generated, which reveals the melting temperature of the products (Fig. 2.1.b). For each primer set a single sharp peak was observed in the graph of the first derivative of the fluorescence (-Rn' (T)) vs temperature. This is a good indicator that PCR with each of the primer sets produces a single specific product. To confirm this, the products of the qPCRs were separated and visualised by 1.5% agarose EtBr electrophoresis (Fig. 2.1.c and d). In each case, a single band corresponding to the expected amplicon size was detected.

2.2.3.6. qPCR and Data Analysis

Per qPCR well and for each primer pair of interest, the following mixture was assembled: 10 µL 2X SYBR G qPCR Master Mix (ThermoFisher), 0.8 µL 10 µM each fw/rv primer mix, 7.2 µL milli-Q filtered water. 18 µL of this was added to each tube of 8 x optical plastic tube strips (Agilent Technologies), as required. 2 µL of each cDNA sample was added to each tube, as required. Each sample / primer combination was conducted in technical triplicate. qPCR reactions were conducted with the Mx3000p (Agilent Technologies). The reaction steps are illustrated in Fig. 2.2. mRNA fold changes were calculated by the ΔΔct method, using *Actin* as the internal control gene. The threshold cycle (ct) of *Actin* was subtracted from that of the gene of interest (GOI), for each sample to calculate the Δct. Then, the Δct of the untreated sample was subtracted from the Δct of each time point sample, to calculate the ΔΔct. Finally, the following equation was used to find the fold change:

$$mRNA\ fold\ change = 2^{-\Delta\Delta ct}$$

2.2.4. ChIP-qPCR

2.2.4.1. Identification of ChIP-qPCR primer pairs

FOS ChIP-qPCR primer pairs were identified using the Primer3Plus web application operating in qPCR mode (Rozen and Skaletsky 1999). The following

parameters were specified: product length of 90-110 bp, and primer dissociation temperature of 55˚C.

2.2.4.2. Validation of primers used for ChIP-qPCR in A431 cells

To investigate the effect of RNAPII and XRCC1 occupancy at *FOS* following CPT treatment, ChIP-qPCR was employed. As described for RT-PCR primer sets, ChIP-qPCR primer sets (see table 2.5) were carefully validated to ensure specific amplification of the target sequence. The human *FOS* genomic locus is shown, together with the mRNA and protein maps (Fig. 2.3.a). The positions of the amplicons of primer pairs (A, B, C, D, F, and G) are shown. Note that primer pairs D and F (targeting intron 2 and exon 4, respectively) were used for both qRT-PCR and ChIP-qPCR. Primer pair A targets the promoter region (-236 to -139 bp relative to the TSS). Primer pair B targets a region immediately downstream of the TSS, where RNAPII is known to pause after initiation (1 to 138 bp downstream of the TSS). Primer pair C targets a region in intron 1 (565 to 651 bp downstream of the TSS). Primer pair G targets a region 690 to 793 bp downstream of the transcription termination site (TTS). qPCR was conducted using each of the ChIP-qPCR primer pairs and A431 gDNA as the template (see section 2.2.3.6). Following this, a dissociation curve was generated as described above (Fig. 2.3.b). qPCRs conducted with primer pairs A-F had dissociation curves with a single clear peak, suggesting single products. qPCR with primer pair G also produced a strong peak in the dissociation curve at 83.9˚C. However, there was elevated region of the curve centred at ~ 78˚C. This is likely to be due to an intermediate state between single and double strand product, rather than multiple products; because when separated and visualised on 1.5% agarose EtBr gels, a single band was observed for each qPCR product (Fig. 2.3.c.).

2.2.4.3. Validation of primers used for ChIP-qPCR in EM9 cells.

A map of the *Cricetulus griseus FOS* genomic locus is depicted (Fig. 2.4.a), together with the mRNA and protein maps. A qPCR primer pair (*cg*E4) was identified in exon 4 (1990 to 2097 bp downstream of TSS), slightly upstream of the locus orthologous to F in human *FOS* (2164 to 287 bp downstream of TSS). qPCR was conducted using the *cg*E4 primer pair and EM9 XH gDNA as the

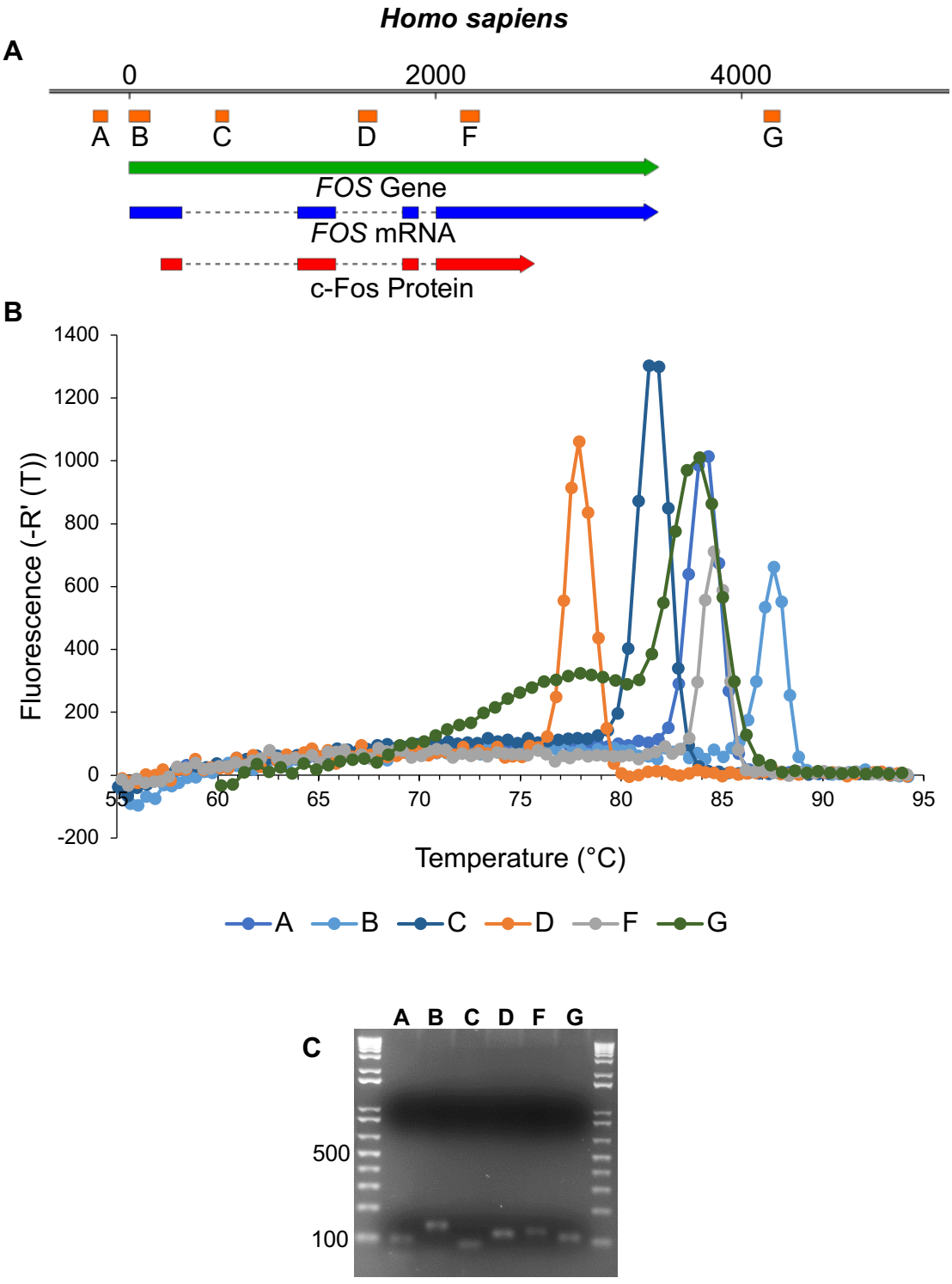

Figure 2.3. Validation of primers used for ChIP-qPCR with human cells. The positions of primer pairs used for ChIP-qPCR are shown in a diagram of the FOS gene (numbers are bp from the TSS) **(A)**. Orange rectangles represent the amplicon of each primer pair. Dissociation curves of the products of qPCR reactions using primer pairs A, B, C, D, F and G are shown (see Table 2.5. for sequences) **(B)**. PCR products were separated and visualised by 1.5% agarose electrophoresis and ethidium bromide staining. A molecular size marker is included, showing sizes in bp. **(C).**

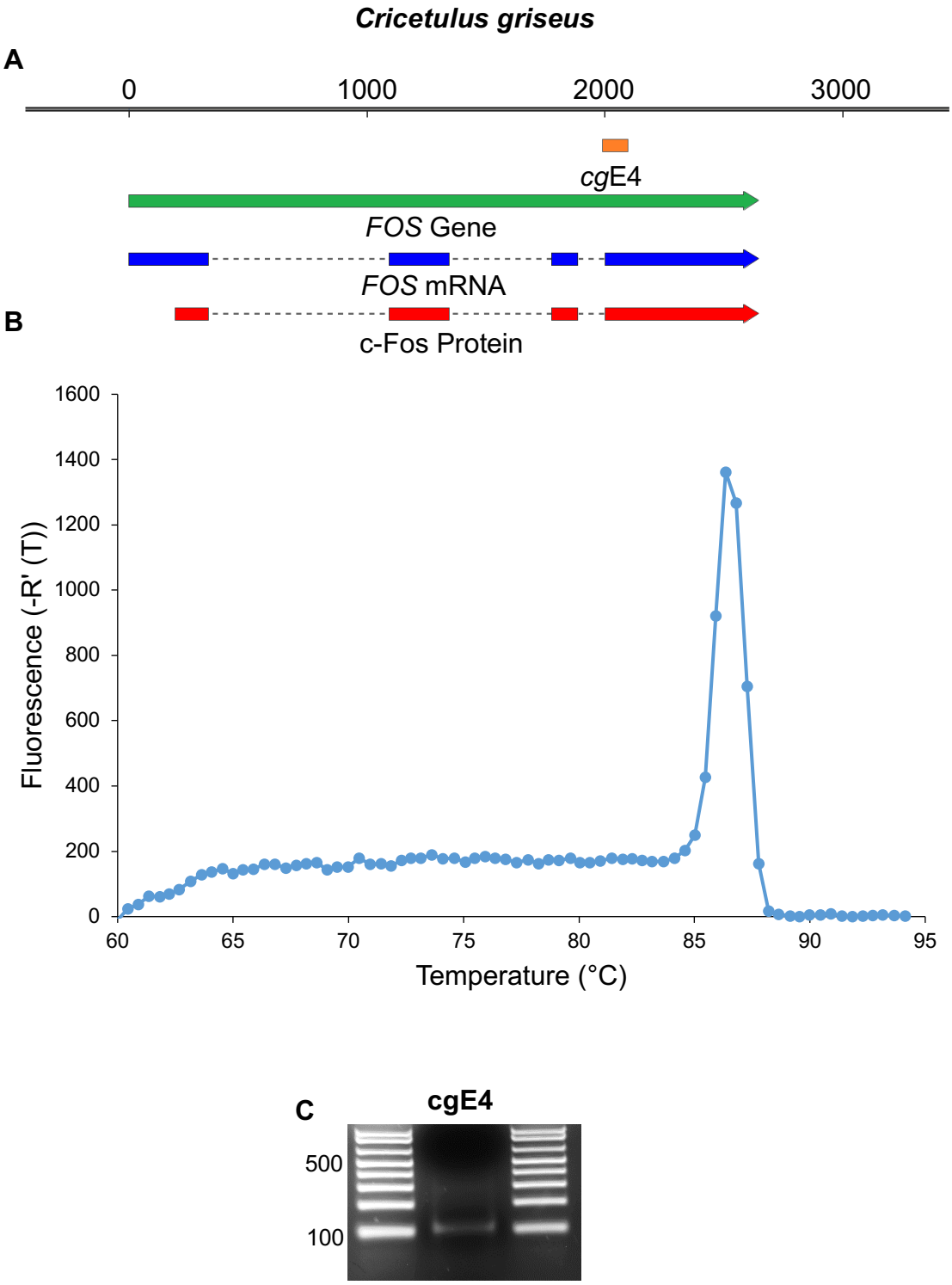

Figure 2.4. Validation of primers used for ChIP-qPCR in CHO cells. The positions of primer set *cg*E4 used for ChIP-qPCR is shown in a diagram of the *FOS* gene (numbers are bp from the TSS). The orange rectangle represents the amplicon of the primer pair **(A)**. Dissociation curves of the product of qPCR reaction using primer set *cg*E4 is shown in **(B)** (see Table 2.5. for sequences). PCR products were separated and visualised by 1.5% agarose electrophoresis and ethidium bromide staining **(C).**

template (see section 2.2.3.6). Dissociation curve analysis of a qPCR reaction conducted with *cg*E4 indicated a single product with a melting point of 86.4˚C (Fig. 2.4.b), and this was confirmed by 1.5% Agarose EtBr (Fig. 2.4.c).

2.2.4.4. Formaldehyde crosslinking

Crosslinking of 8x10^6 A431, A431 GFP, A431 GFP-XRCC1, or CHO cells was conducted by direct addition of 0.27 ml 37% w/v Formaldehyde with 10-15% methanol stabilizer (Sigma) cells in 10 ml complete media, to a final concentration of 1% formaldehyde. Cells were incubated with gentle rocking at RT for 10 min, prior to quenching of fixation by addition of 1.25 ml 1M Glycine 1M, to a final concentration of 111 mM. Cells were collected by scraping and centrifugation at 4˚C. The flask was washed with 3 x 15 ml ice cold PBS. The pellet was resuspended and washed in these PBS volumes. Finally, cell pellets were snap frozen and maintained at -80˚C until further use.

2.2.4.5. Lysis and sonication

Immediately prior to lysis, ChIP Lysis Buffer (1% SDS, 50 mM Tris-HCl pH 8.0, 10 mM EDTA) was completed with 1X Protease Inhibitor Cocktail (Sigma), 50 µg/ml PMSF (Sigma) and 1 mM DTT (ThermoFisher). 8x10^6 fixed cells were lysed by resuspension of the pellet in 610 µL Complete ChIP Lysis Buffer (4˚C), with agitation by pipetting. The lysate was divided into 2x300 µL fractions in 1.5 ml Bioruptor Pico Microtubes (Diagenode), and each was subjected to 3 cycles (30 s ON/ 30 s OFF) sonication using a Bioruptor Pico (Diagenode) water bath sonicator (4˚C), as per the protocol identified by optimization detailed in Chapter Three (See Fig. 3.6., Fig. 3.10. and Fig. 3.12.). The fractions were then recombined and clarified by centrifugation at 10,000 g for 10 min (4˚C). The supernatant of each was removed to a separate tube on ice. Chromatin immunoprecipitation was conducted immediately.

2.2.4.6. Chromatin Immunoprecipitation with A300-231A and 8WG16

Immediately prior to dilution, ChIP Dilution Buffer (1.1% Triton X-100, 167 mM NaCl, 16.7 mM Tris-HCl pH 8.0, 1.2 mM EDTA) was completed with 1X Protease

Inhibitor Cocktail (Sigma) and 50 µg/ml PMSF (Sigma). 10 µL of sonicated and clarified cell lysate was preserved on ice as an input sample. 150 µL (~2x10^6 cells) was diluted 10-fold with 1.35 ml Complete ChIP Dilution Buffer. 10 µL Saturated Protein G Dynabeads (ThermoFisher) were added and the mixture was incubated for 1 h on a rotary mixer (4˚C). The Dynabeads were pelleted using the DynaMag (ThermoFisher) magnet. The supernatant was removed a new microcentrifuge tube on ice. This preclearing step was conducted to remove any material which binds non-specifically to the Protein G Dynabeads, and might therefore increase background qPCR signal. Antibody (2 µg A300-231A anti-XRCC1, 1 µg 8WG16 anti-RNAPII, 1 µg Rabbit -ve IgG) was added directly to the precleared material and immunoprecipitation was carried out for 16 h on a rotary mixer (4˚C). 20 µL Saturated Protein G Dynabeads were added and the mixture was incubated for 3 h on a rotary mixer (4˚C). The beads were then pelleted on the DynaMag magnet, the supernatant was discarded. The beads were washed serially with 2x500 µL ice cold NaCl Wash Buffer (0.1% SDS, 1% Triton-X100, 20 mM Tris-HCl pH 8.0, 500 mM NaCl, 2 mM EDTA), , 2x500 µL ice cold LiCl Wash Buffer (1% Deoxycholate, 1% NP-40, 10 mM Tris-HCl, 250 mM LiCl, 1 mM EDTA) and 2x500 µL ice cold 1X TE (10 mM Tris-HCL pH 8.0, 1 mM EDTA). The immunoprecipitation was eluted by addition of 110 µL ChIP Elution Buffer (2% SDS, 10 mM Tris-HCl pH 8.0, 1 mM EDTA) to the beads, vortexing and 10 min incubation (65˚C), followed by removal of 100 µL supernatant to a separate tube. This process was repeated with a further 100 µL ChIP Elution Buffer, and the fractions were combined. 190 µL Elution Buffer was added to the input samples. The Input and IP samples were incubated overnight at 65˚C to reverse formaldehyde crosslinks. Samples were then incubated with 100 µg Proteinase K (Sigma) for 1.5 h at 50˚C. Finally, the samples were purified with the PCR Purification Kit (QIAGEN), and eluted in 100 µL milli-Q filtered water. The samples were maintained at -20˚C until further use.

2.2.4.7. Chromatin Immunoprecipitation with ab290

Immediately prior to dilution, ChIP Dilution Buffer (1.1% Triton X-100, 167 mM NaCl, 16.7 mM Tris-HCl pH 8.0, 1.2 mM EDTA) was completed with 1X Protease Inhibitor Cocktail (Sigma) and 50 µg/ml PMSF (Sigma). 10 µL of sonicated and

clarified cell lysate was preserved on ice as an input sample. 300 µL (~4x10^6 cells) was diluted 5-fold with 1.2 ml Complete ChIP Dilution Buffer. 10 µL Saturated Protein A Dynabeads (ThermoFisher) were added and the mixture was incubated for 1 h on a rotary mixer (4˚C). The Dynabeads were pelleted using the DynaMag (ThermoFisher) magnet. The supernatant was removed a new microcentrifuge tube on ice. This preclearing step was conducted to remove any material which binds non-specifically to the Protein A Dynabeads, and might therefore increase background qPCR signal. Antibody (10 µg ab290 anti-GFP) was added directly to the precleared material and immunoprecipitation was carried out for 16 h on a rotary mixer (4˚C). 30 µL Saturated Protein G Dynabeads were added and the mixture was incubated for 3 h on a rotary mixer (4˚C). The beads were then pelleted on the DynaMag magnet, the supernatant was discarded. The beads were washed serially with 2x500 µL ice cold NaCl Wash Buffer (0.1% SDS, 1% Triton-X100, 20 mM Tris-HCl pH 8.0, 500 mM NaCl, 2 mM EDTA), 2x500 µL ice cold LiCl Wash Buffer (1% Deoxycholate, 1% NP-40, 10 mM Tris-HCl, 250 mM LiCl, 1 mM EDTA) and 2x500 µL ice cold 1X TE (10 mM Tris-HCL pH 8.0, 1 mM EDTA). The immunoprecipitation was eluted by addition of 110 µL ChIP Elution Buffer (2% SDS, 10 mM Tris-HCl pH 8.0, 1 mM EDTA) to the beads, vortexing and 10 min incubation (65˚C), followed by removal of 100 µL supernatant to a separate tube. This process was repeated with a further 100 µL ChIP Elution Buffer, and the fractions were combined. 190 µL Elution Buffer was added to the input samples. The Input and IP samples were incubated overnight at 65˚C to reverse formaldehyde crosslinks. Samples were then incubated with 100 µg Proteinase K (Sigma) for 1.5 h at 50˚C. Finally, the samples were purified with the PCR Purification Kit (QIAGEN), and eluted in 100 µL milli-Q filtered water. The samples were maintained at -20˚C until further use.

2.2.4.8. qPCR and Data Analysis

Per qPCR well and for each primer pair of interest, the following mixture was assembled: 10 µL 2X SYBR G qPCR Master Mix, 0.8 µL fw/rv primer mix (10 µM each), 6.8 µL milli-Q filtered water. 17.6 µL of this was added to each tube of 8 x optical plastic tube strips, as required. 2.4 µL of each ChIP sample was added to each tube, as required. Each sample / primer combination was conducted in

technical triplicate. qPCR reactions were conducted with the Mx3000p. A standard curve was prepared by 10-fold serial dilution of one untreated input sample. This standard curve was measured for each primer pair, along with the input and IP samples. Each input sample was diluted 10-fold. All input and IP samples were quantified using the standard curve. Enrichments were then calculated as % of input.

2.2.5. CRISPR-Cas9

2.2.5.1. Identification of gRNA target sequences in *TDP1*

gRNA sequences targeting TDP1 were identified using the web application Benchling (https://benchling.com). The following parameters were specified: target sequence length of 17 bp (Tru-gRNA); target sequence begins with a G; PAM is of the form NGG. Potential off-target sites were assessed by BLAST (https://blast.ncbi.nlm.nih.gov).

2.2.5.2. Cloning of gRNAs targeting *TDP1* into gRNA expression plasmid

Oligodeoxynucleotides composed of the sense and antisense Tru-gRNA sequences fused to left and right homology arms were annealed and extended using Phusion polymerase. Separately, the gRNA expression plasmid was linearized with AflII. The two fragments were combined by Gibson Assembly (see section 2.2.1.4). This process was conducted for two gRNA sequences targeting *TDP1* (shown below), to produce the plasmids pGR.TDP1.1 and pGR.TDP1.2.

gRNA	Primer	Sequence
TDP1.1	fw	TTTCTTGGCTTTATATATCTTGTGGAAAGGACGAAACACCGAGGTAGATGGCTTGTC
TDP1.1	r	GACTAGCCTTATTTTAACTTGCTATTTCTAGCTCTAAAACGACAAGCCATCTACCTC
TDP1.2	fw	TTTCTTGGCTTTATATATCTTGTGGAAAGGACGAAACACCGACGAGTATGAGACATC
TDP1.2	r	GACTAGCCTTATTTTAACTTGCTATTTCTAGCTCTAAAACGATGTCTCATACTCGTC

2.2.5.3. Generation of *TDP1*$^{-/-}$ (#4A2, #5B3, #5B4 and #5B5) RPE-1 cells

RPE-1 cells were co-transfected with 1.5 µg hCas9 expression plasmid and 1.5 µg pGR.TDP1.1 or pGR.TDP1.2 by Neon nucleofection (see section 2.2.2.2). Following overnight incubation, the cells were passaged to 10 cm dishes and

incubated for 5 days with complete DMEM/F12 containing 1 mg/ml G418. After selection, cells were trypsinised and plated at density of 50 cells per 10 cm dish. Following 2-week incubation in G418-free media, colonies were selected and passaged individually to duplicate wells of a 24-well plates using cloning cylinders (Agar Scientific). After a subsequent week of incubation, confluent wells were lysed in LB and subjected to SDS-PAGE and WB with anti-TDP1 (A301-618A) and anti-actin (66009) antibodies. Clones with apparently absent TDP1 protein (#4A2, #4A4, #5B3, #5B4 and #5B5) were selected and expanded further into T75 flasks. A second WB was conducted at this stage to confirm the absence of TDP1 protein. Clone #4A4 had a small remaining TDP1 band. All clones with absent TDP1 protein (#4A2, #5B3, #5B4 and #5B5) were passaged to T175. After this expansion step, cells were trypsinised; resuspended in complete DMEM/F12 with 10% DMSO; and multiple aliquots were frozen in cryovials at -80˚C, using a Mr Frosty Freezing Containing (ThermoFisher). Vials were maintained by cell cryopreservation in the vapor phase of liquid nitrogen.

2.2.5.4. Generation of *XRCC1*$^{-/-}$/*TDP1*$^{-/-}$ (#3A2) RPE-1 cells

XRCC1$^{-/-}$ RPE-1 (#3) cells were co-transfected with 1.5 µg hCas9 expression plasmid and 1.5 µg pGR.TDP1.1 or pGR.TDP1.2 by Neon nucleofection (see section 2.2.2.2). Following overnight incubation, the cells were trypsinised and plated at density of 50 cells per 10 cm dish. Following 2-week incubation, colonies were selected and passaged individually to duplicate wells of multiple 24-well plates using cloning cylinders (Agar Scientific). After a subsequent week of incubation, confluent wells were lysed in LB and subjected to SDS-PAGE and WB with anti-TDP1 (A301-618A) and anti-actin (66009) antibodies. 2 clones had apparently absent TDP1 protein (#1D2 and #3A2). These were selected and expanded further into T75 flasks. A second WB was conducted at this stage to confirm the absence of TDP1 and XRCC1 proteins. Clone #1D6 had a small remaining TDP1 band. Clone #3A2 had absent TDP1 and XRCC1 protein, and was passaged to T175. After this expansion step, cells were trypsinised; resuspended in complete DMEM/F12 with 10% DMSO; and multiple aliquots were frozen in cryovials at -80˚C, using a Mr Frosty Freezing Containing

(ThermoFisher). Vials were maintained by cell cryopreservation in the vapor phase of liquid nitrogen.

2.2.5.5. Generation of *PARP1*$^{-/-}$/*PARP2*$^{-/-}$ (#E6) RPE-1 cells

PARP1$^{-/-}$ RPE-1 (#G7) cells were co-transfected with 1.5 µg hCas9 expression plasmid and 1.5 µg pGR.PARP2.2 by Neon nucleofection (see section 2.2.2.2). Following overnight incubation, the cells were trypsinised and plated at density of 50 cells per 10 cm dish. Following 2-week incubation, colonies were selected and passaged individually to wells of 1x96 and 2x24-well plates, using cloning cylinders (Agar Scientific). After 2 days, cells in the 96-well plate were fixed with formaldehyde and subjected to anti-PARP2 (39743) IF (see section 2.2.7). Cells were observed manually on an Olympus IX83 fluorescence; 13 clones with absent or low anti-PARP2 IF signal were noted. These clones were selected from one of the 24-well plates, lysed in LB, and subjected to SDS-PAGE and WB with anti-PARP2 (39743) and anti-actin (66009) antibodies (see section 2.2.6). 1 clone exhibited PARP2 absence by WB (#E6). Clone #E6 was expanded further into a T75 flask. A second WB was conducted at this stage to confirm the absence of PARP1 and PARP2 proteins. Clone #E6 was passaged to T175. After this expansion step, cells were trypsinised; resuspended in complete DMEM/F12 with 10% DMSO; and multiple 1 ml aliquots were frozen in cryovials at -80˚C, using a Mr Frosty Freezing Containing (ThermoFisher). Vials were maintained by cell cryopreservation in the vapor phase of liquid nitrogen.

2.2.5.6. Sequencing of TDP1 gRNA 2 locus in WT, *TDP1*$^{-/-}$ (#5B5) and *XRCC1*$^{-/-}$/*TDP1*$^{-/-}$ (#3A2) RPE-1 cells

Genomic DNA was extracted from 1x10^6 WT, *TDP1*$^{-/-}$ (#5B5) and *XRCC1*$^{-/-}$/*TDP1*$^{-/-}$ (#3A2) RPE-1 cells using Extract-N-Amp Tissue PCR kit (Sigma). A pair of primers were designed which spanned 277 bp around the TDP1 gRNA 2 target locus (TDP1.2.seq.fw and TDP1.2.seq.rv; see below for sequences), using Primer3Plus. PCR was conducted using the gDNA and this primer pair (see section 2.2.1.1). PCR products were separated and visualised by TAE-agarose electrophoresis (see section 2.2.1.6). PCR products were Topo-cloned into pCR 2.1-TOPO plasmid and single colonies were mini-prepped

(see section 2.2.1.5). Plasmid DNA from individual colonies was subjected to a diagnostic restriction digest with EcoRI-HF (see section 2.2.1.2), and those containing an insert were sent for sanger sequencing (Genewiz) with M13 fw primers. Sequences were aligned to the TDP1 gDNA sequence (NCBI) and mutations were noted.

Primer	Sequence
TDP1.2.seq.fw	GAAGCAGGCTGAGAAAGTGG
TDP1.2.seq.r	CTTGACACCCAGCATCCTCT

2.2.6. Western Blot (WB)

2.2.6.1. Total protein extraction with Laemmli Buffer or Sample Buffer

Cell pellets or adherent cells were washed twice with PBS, prior to direct addition of 95˚C 1X Laemmli Buffer (2% SDS, 10% glycerol, 5% 2-mercaptoethanol, 0.001% bromophenol blue, 62.5 µM Tris-HCl pH 6.8) or 1X Sample Buffer (2% SDS, 10% glycerol, 62.5 µM Tris-HCl pH 6.8). Samples were boiled for 10 min (95˚C) in a Thermomixer R (Eppendorf) hot block shaker, at 2000rpm. One cycle of sonication (30 s ON/ 30 s OFF) in the Bioruptor Pico was used where necessary to reduce viscosity. Samples were cooled on ice and used immediately, or maintained at -20˚C until further use.

2.2.6.2. Chromatin fractionation

Immediately prior to the experiment, all buffers were completed with 1X Protease Inhibitor Cocktail (Sigma) and 1X Phosphatase Inhibitor Cocktail (Sigma). $2x10^6$ RPE-1 cells were scraped into ice cold PBS and pelleted by centrifugation at 400 g. The pellet was resuspended in 200 µL complete LB1 (0.1% Triton-X100, 1X PIC, 1X PhIC, 50 mM HEPES pH 7.5, 150 mM NaCl, 1 mM EDTA). 20 µL of this was snap frozen as input. The remaining 180 µL was incubated on ice for 3 min, prior to centrifugation at 21,000 g for 3 min. The supernatant was snap frozen as fraction S1. The pellet was washed once with 200 µL LB2 (1X PIC, 1X PhIC, 50 mM HEPES pH 7.5, 150 mM NaCl, 1 mM EDTA), with centrifugation at 21,000 g for 3 min. The supernatant was discarded and the pellet was resuspended in 100

µL LB3 (0.2 mg/ml RNAse A, 1X PIC, 1X PhIC, 50 mM HEPES pH 7.5, 150 mM NaCl, 1 mM EDTA). The suspension was incubated on a rotary mixer for 30 min at RT, prior to centrifugation at 21,000 g for 3 min. The supernatant was snap frozen as fraction S2. The pellet was snap frozen as fraction P2, containing the chromatin. All samples were maintained at -80˚C until further use.

2.2.6.3. Total protein quantification by BCA assay

2 µL of total protein extract in 1X SB (see section 2.2.6.1) was combined with 8 µL deionized water and 200 µL BCA Working Reagent (Pierce) (3.9 µL BCA reagent B, 196.1 µL BCA reagent A) in triplicate wells of an optical 96-well plate. 10 µL of protein standards A-I was combined with 200 µL BCA working reagent in separate wells. The 96-well plate was covered with Parafilm (Sigma) and incubated for 30 min at 36˚C. Absorbance was measured at 562 nm using a POLARstar Omega Microplate Spectrophotometer (BMG Lab Tech). Protein concentration of each sample was calculated from the average absorbance of triplicate wells, using the standard curve. DTT and Bromophenol Blue were added to final concentrations of 100 mM DTT and 0.001%, respectively.

2.2.6.4. SDS-PAGE

Resolving polyacrylamide gels of various acrylamide percentages were cast as described previously (Sambrook and Russell, 2001); by combining different volumes of deionized water, 30% acrylamide mix (Flowgen), 1.5M Tris-HCl pH 8.8, 10% (w/v) SDS, 10% (w/v) APS and TEMED (ThermoFisher). After polymerisation of the resolving gel, stacking gels were cast by combining different volumes of deionized water, 30% acrylamide mix (Flowgen), 1M Tris-HCl pH 6.8, 10% (w/v) SDS, 10% (w/v) APS and TEMED (ThermoFisher). Samples were loaded along with protein marker (Biorad), and electrophoresis was conducted at 150V in a Mini-PROTEAN Tetra Cell electrophoresis tank (Biorad), using 1X Running Buffer (25 mM Tris-Hcl, 250 mM glycine, 0.01% SDS).

2.2.6.5. Gel-Membrane Transfer

After SDS-PAGE, proteins were electrophoretically transferred from polyacrylamide gels to nitrocellulose membrane (ThermoFisher) at 90 V for 90 min, in the Mini-PROTEAN Tetra Cell tank, using 1X Towbin buffer (25 mM Tris-HCl, 192 mM glycine, 20% methanol). Membranes were stained with 0.1% (w/v) Ponceau S in 5% acetic acid (Sigma) to visualise total protein levels. Ponceau S staining was imaged using an Epson Perfection 2400 PHOTO desktop scanner. Ponceau S staining was removed by serial washing with 1x TBST (20 mM Tris-HCl, 150 mM NaCl, 0.1% Tween-20). The membrane was blocked with 10% milk in 1X TBST for 1 h with rocking at RT.

2.2.6.6. Immunodetection

The blocked membrane was probed with various primary antibodies diluted in 10% milk-TBST (see Table 2.1), either for 1 h at RT, or overnight at 4˚C. Following primary antibody incubation, the membrane was washed for with 4x20 ml TBST for 5 min each, with rocking at RT. The membrane was then probed with a secondary antibody-HRP, according to the host of the primary antibody (see Table 2.2), for 1 h with rocking at RT. The membrane was then washed for 4x5 min with 20 ml TBST. Finally, the membrane was incubated for 1 min in enhanced chemiluminescence (ECL) detection reagent (GE Healthcare), prior to exposure to blue autoradiography film (GRI) and developing.

2.2.7. Immunofluorescence (IF)

2.2.7.1. Fixation

Cells growing on glass coverslips were fixed for 10 min with 0.3 ml 4% formaldehyde in PBS, at RT. Cells were then washed for 3x2 min with 0.5 ml PBS; prior to being used immediately, or maintained in 0.5 ml PBS at 4˚C until further use.

2.2.7.2. Detergent Pre-extraction of soluble proteins

Cells growing on glass coverslips in 24-well plates were washed with 0.3 ml ice cold Pre-extraction Buffer (0.2% Triton-X100 in PBS) for 2 min on ice with gentle

rocking (5 rpm), prior to immediate fixation with 0.3 ml 4% formaldehyde in PBS, at RT. Cells were then washed for 3x2 min with 0.5 ml PBS; prior to being used immediately, or maintained in 0.5 ml PBS at 4˚C until further use.

2.2.7.3. Immunodetection

Fixed cells were permeabilized with 0.3 ml methanol/acetone (1:1) for 5 min at -20˚C, prior to washing for 3x2 min with 0.5 ml PBS. Cells were blocked with 0.3 ml IF Buffer (10% Fetal Calf Serum in PBS) for 1 h at RT. Primary antibody dilutions were made in IF buffer (see Table 2.1). Coverslips were carefully placed inverted on 30 µL droplets of primary antibody dilution, on a sheet of parafilm. Incubations were conducted in a humidified chamber for 1.5 h at RT. Coverslips were then turned face-up and washed for 3x5 min with 0.3 ml PBS. Fluorescently labelled-secondary antibody dilutions were made in IF buffer (see Table 2.2). 80 µL secondary antibody dilution was carefully added to the surface of the coverslip. Incubations were conducted in a humidified chamber for 1 h at RT. Coverslips were washed for 3x5 min with 0.3 ml PBS and 1x2 min with 0.3 ml deionised water. Coverslips were then allowed to dry for 10 min on Whatman Filter Paper (ThermoFisher), prior to mounting on glass slides with 4 µL Vectashield Antifade Mounting Medium with DAPI (Vector Laboratories). Slides were imaged immediately or maintained at 4˚C until further use.

2.2.8. ScanR Microscopy

Automated widefield microscopy was performed on an Olympus ScanR system (motorized IX83 microscope) with ScanR Image Acquisition and Analysis Software, 20x/0.45 (LUCPLFLN 20x PH) and 40x/0.6 (LUCPLFLN 40x PH) dry objectives and a Hamamatsu ORCA-R2 digital CCD camera C10600. Definition of the main object was based on an intensity threshold of DAPI signal. Definition of the sub-object was based on an intensity threshold of B23-Alexa 647 signal, as illustrated in Chapter Five (See Fig. 5.5.). In this way, it was possible to derive the mean ex-nucleolar signal with the following formula:

$$Mean\ Exnucleolar\ Signal = \frac{\sum Total\ nuclear\ signal - \sum Total\ nucleolar\ signal}{Number\ of\ nuclei}$$

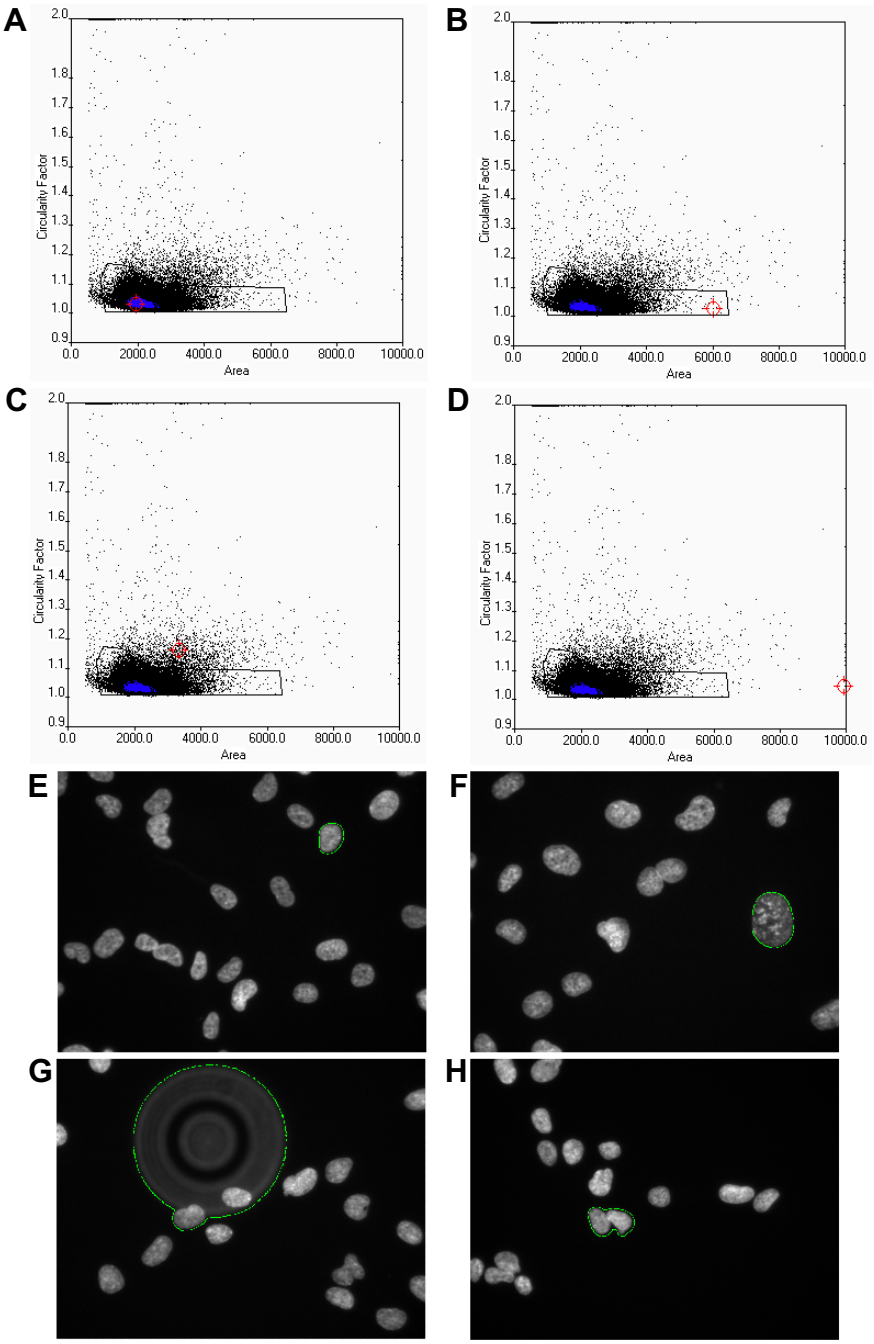

Figure 2.5. Population gating removes unwanted anomalies. RPE-1 cells were formaldehyde fixed, stained with DAPI and imaged using the ScanR system. ScanR Analysis software was used to assess nuclear area and circularity factor from DAPI signal. Scatterplots of area vs circularity factor (**A-D**) showing the defined gate region and position of a representative average nucleus (**E**), large nucleus (**F**), imaging aberration (**G**) and double nucleus (**H**), respectively.

To further improve the accuracy of the method, gating was applied to exclude factors which might skew the data (Fig. 2.5.). The first such gate was defined following visual examination of the scatter plot of nuclear size vs circularity factor. This plot revealed that while most correctly identified single nuclei were distributed in a single population of low size and low circularity factor (Fig. 2.5.a and e), there were also some of significantly larger size (Fig. 2.5.b and f). In contrast, those objects with a high circularity factor were predominantly caused by failure of watershedding, resulting in multiple adjacent nuclei being detected as a single object (Fig. 2.5.d and h). Furthermore, some of these anomalies were caused by imaging aberrations such as poor autofocusing, or fluorescence of debris (Fig. 2.5.c and g). A 2d region was defined on the scatterplot to exclude as many of these anomalies whilst still retaining a complete size range of nuclei. The second gate employed was used to exclude those nuclei with undetectable nucleoli, as these were generally due to poor B23-Alexa 647 signal detection.

2.2.9. Single Cell Alkaline Electrophoresis (Comet assay)

2.2.9.1. H_2O_2 Treatment

A total of $3x10^6$ RPE-1 cells were trypsinised, washed and resuspended in ice cold PBS. A total of $5x10^5$ cells were removed and stored on ice ('undamaged' sample). The remaining cells were then treated with H_2O_2 (50 µM) in PBS for 10 min on ice, before mixing with complete DMEM/F12 medium, and recovery of the cells by centrifugation and resuspension in ice cold complete DMEM/F12. A total of $5x10^5$ cells were removed and stored on ice ('no repair' sample) and the remaining cells resuspended in complete DMEM/F12 (37◦C) and incubated at 37◦C for the indicated repair period. At 7.5, 15 and 30 min, $5x10^5$ cells were removed and stored on ice.

2.2.9.2. CPT Treatment

Per condition, $5x10^5$ RPE-1 cells were trypsinised, washed and resuspended in 0.5 ml complete DMEM/F12 (37˚C), containing 10 or 100 µM CPT or an equivalent concentration of DMSO vehicle. Cells were incubated for 1 h (37˚C) in a water bath, prior to being returned to ice.

2.2.9.3. Single Cell Alkaline Electrophoresis

Finally, all samples were resuspended in 200 µL ice cold PBS, rapidly mixed with 200 µL 1.2% low melting point agarose (Sigma) in PBS and plated on frosted glass slides coated with 0.6% ultrapure agarose (ThermoFisher), on ice. The agarose was allowed to solidify prior to incubation in Comet Lysis Buffer (2.5 M NaCl, 100 mM EDTA, 10 mM Tris-HCl pH 10) for 1 h at 4◦C. Slides were washed 3 times with 4◦C H_2O and incubated for 45 min in Comet Electrophoresis Buffer (1 mM EDTA, 50 mM NaOH). Electrophoresis was carried out at 12V for 25 min, prior to overnight neutralization with 1 M Tris-HCl. Finally, slides were stained with 1 M Tris-HCl containing SYBR-G (1:10000) and Antifade (40 µg/ml), and imaged (Nikon Eclipse 50i). Average tail moments from 100 cells per sample were obtained using Comet Assay IV software (Perceptive Instruments).

2.2.10. Clonogenic Survival Assay

2.2.10.1. Plating Cells

Each condition was performed on triplicate dishes per replicate. RPE-1 cells were trypsinised, washed and resuspended at a density of 33.3 ml^{-1} in complete DMEM/F12 (37˚C). 9 ml of this suspension was added to each 10 cm dish (300 cells per dish). Dishes were rocked gently to evenly distribute single cells, prior to being incubated for 4 h (37˚C) to allow adherence.

2.2.10.2. H_2O_2Treatment

Plating media was removed by aspiration. 6 ml PBS (RT) containing 10, 20, 35, 50 µM H_2O_2, was added to each dish. The dishes were incubated for 20 min (RT), prior to aspiration of the treatment buffer, washing with 6 ml PBS, and addition of 10 ml complete DMEM/F12. The dishes were incubated for 12 days (37˚C) to allow colony formation.

2.2.10.3. CPT treatment

1 ml of DMEM/F12 containing 5, 10, 15, 20 nM CPT, or an equivalent concentration of DMSO vehicle was added to each dish (final concentrations of

CPT: 0.5, 1, 1.5 and 2 nM CPT, respectively). The dishes were incubated for 12 days (37˚C) to allow colony formation.

2.2.10.4. Staining and Scoring of Colonies

Dishes were washed once with 6 ml PBS (RT), fixed with 6 ml industrial methylated spirit for 5 min (RT), and stained with 10 ml 2% (w/v) methylene blue in 70% (v/v) ethanol for 30 min (RT). The staining solution was removed and recycled, and the dishes were washed collectively in a large volume of tap water (0˚C). The dishes were finally allowed to dry, prior to scoring of colonies of >50 cells using a digital colony counter (Stuart SC6Plus).

Chapter Three

Investigating SSBR at a Highly-Transcribed Gene Locus

3.1. Introduction and Aims

Defective SSBR resulting from mutation of *TDP1, APTX, PNKP* and *XRCC1* is associated with the neurodegenerative genetic diseases SCAN1, AOA1, AOA4 and AOA-XRCC1, respectively (Date, Onodera et al. 2001, Takashima, Boerkoel et al. 2002, El-Khamisy, Saifi et al. 2005, Shen, Gilmore et al. 2010, Bras, Alonso et al. 2015, Hoch, Hanzlikova et al. 2017). These diseases share the common clinical presentation of cerebellar atrophy resulting in progressive ataxia. Several hypotheses have been suggested to explain the sensitivity of post-mitotic neuronal subtypes to defective SSBR. High levels of oxygen consumption and low levels of antioxidant enzymes may result in high oxidative stress in the brain (Barzilai, Rotman et al. 2002, Caldecott 2003). This in turn is likely to elevate levels of various lesions repaired by BER and SSBR (Barzilai, Rotman et al. 2002, Caldecott 2003, El-Khamisy and Caldecott 2006, Caldecott 2008). Additionally, in the absence of redundant replication-coupled repair mechanisms, single-strand lesions may accumulate in post-mitotic cells (Rulten and Caldecott 2013). However, other tissues of the body containing post-mitotic cells seem largely unaffected by disruption of SSBR, for example the skeletal muscle. A further hypothesis to explain neurodegeneration implicates the reliance of neurons upon a high rate of transcription, often of particularly long genes (Zylka, Simon et al. 2015). Single-strand lesions block transcription of essential mRNAs and non-coding RNAs (Zhou and Doetsch 1993, Zhou and Doetsch 1994, Lehmann 2003, Kathe, Shen et al. 2004), and may trigger apoptosis via the detection of persistent single stranded DNA by RPA/ATR and the subsequent phosphorylation of p53 (Ljungman and Zhang 1996, Ljungman, Zhang et al. 1999, Derheimer, O'Hagan et al. 2007, Vrouwe, Pines et al. 2011). One aim of this chapter is to investigate the effect of defective SSBR on transcription directly.

Nucleotide excision repair (NER), which repairs a subset of single strand lesions (cyclobutene primidine dimers, 6-4 photoproducts and bulky adducts), operates in a specialised mode for repair of transcribed DNA (transcription coupled- nucleotide excision repair; TC-NER). Genetic defects in this specialised pathway lead to neurological symptoms which are less frequently seen when only global genome-NER (GG-NER) is disrupted (Lehmann 2003). By comparison to NER, our understanding of SSBR processes at the gene level remains limited.

Consequently, another aim of this chapter is to investigate any specialised SSBR mechanisms which may operate at transcribed loci.

FOS is an immediate early-response gene which is induced to a very high level of transcription in response to external stimuli, including in the brain where it is a marker of neuronal activity (Morgan and Curran 1986, Morgan, Cohen et al. 1987, Day, Masini et al. 2004). Given its ease of manipulation and relevance as a highly-transcribed locus in neurons, it is a good model system for investigating SSBR processes at the gene level. Furthermore, the body of the gene has been previously demonstrated to contain multiple Top1 cleavage sites (Francis Stewart, Herrera et al. 1990, Listerman, Sapra et al. 2006), allowing SSBs to be induced with camptothecin (CPT). This chapter will utilize ChIP-qPCR and RT-PCR to investigate the interplay between SSBR and transcription occurring at the *FOS* locus.

3.2. Results

3.2.1. *FOS* induction with A23187 calcium ionophore

FOS is rapidly induced by diverse external stimuli; including application of A23187, a calcium ionophore that increases intracellular calcium levels (Francis Stewart, Herrera et al. 1990). To test this, confluent A431 cells were treated with 5 µM A23187 or an equal concentration of DMSO vehicle; prior to snap freezing of samples at 30, 60 or 90 minutes and subsequent quantitation of *FOS* mRNA by qRT-PCR (Fig. 3.1.). Serum is another known *FOS* transcription stimulus. For this reason, incubation in the absence of serum is necessary to pre-sensitise the cells before addition of A23187. qRT-PCR was conducted with primer set E, targeting exon 4 of *FOS*, and primer sets targeting *Actin* and *MLN51*. A rapid and transient induction of *FOS* was observed, which peaked 60 min after A23187 addition. Little difference was seen in the *FOS* expression profile when *MLN51* was used as an internal control (Fig. 3.1.b), instead of *Actin* (Fig. 3.1.a). Notably, the addition of DMSO alone caused some induction of *FOS* mRNA at 30 min (14.5-fold over untreated), highlighting the diversity of *FOS* stimuli. This was transient, as it was significantly reduced by 60 min. By comparison, induction with A23187 caused significantly greater (ANOVA p-value = 2.71×10^{-4}) increase in

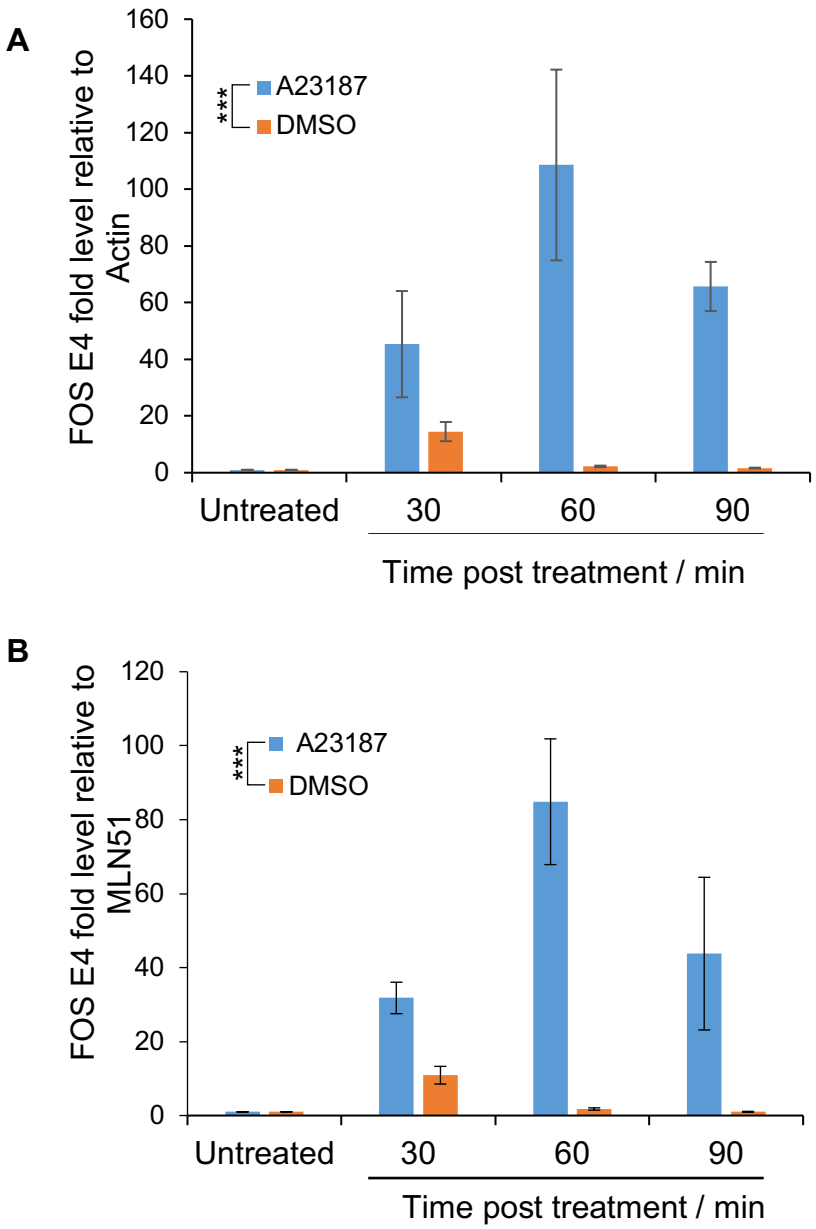

Figure 3.1. FOS can be rapidly induced with A23187 calcium ionophore. Subconfluent A431 cells were incubated in serum-free media for 2.5 hr prior to treatment with serum-free media containing 5 μM A23187, or an equivalent concentration of DMSO vehicle. At the indicated timepoints cells were collected by scraping and snap freezing in liquid nitrogen. Subsequently, total RNA was extracted and cDNA was synthesized with oligo-dT primers, using 1 μg total RNA as the template. RNA was degraded with RNAse A and samples were purified. Finally, samples were subjected to qPCR using primer set E, targeting FOS Exon 4. Data were calculated by the ΔΔct method and are presented as fold over untreated, relative to Actin (**A**) or MLN51 (**B**). Data are mean ±SEM of 3 biological replicates. Statistical significance was calculated by two-factor ANOVA.

FOS mRNA abundance by 60 min (108.6-fold over untreated), which decreased by 90 min (65.7-fold over untreated). This experiment highlights the transient nature of *FOS* transcription induction and *FOS* mRNA stability, which has been noted previously (Francis Stewart, Herrera et al. 1990).

3.2.2. *FOS* induction is inhibited by treatment with CPT

CPT has been reported previously to block transcription of *FOS* and lead to the formation of Top1-SSBs within the gene (Francis Stewart, Herrera et al. 1990). To test this, A431 cells were pre-incubated in serum-free media prior to induction with A23187. 10 µM CPT or DMSO vehicle was added 20 min after A23187 induction and samples were collected at the time points indicated (Fig. 3.2.a). Upon A23187 induction alone, qRT-PCR with primer set F revealed an accumulation of exon 4-containing mRNA which peaked at 60 min (113.1-fold over untreated) (Fig. 3.2.b). Treatment with CPT significantly reduced (ANOVA p-value = 1.83×10^{-4}) the accumulation of exon 4-containing mRNA at 30, 60 and 90 min (28.7, 45.0 and 30.4-fold over untreated, respectively), suggesting transcriptional inhibition. qPCR was also conducted with primer set D, targeting intron 2 (Fig. 3.2.c). By comparison with exon 4-containing mRNA, the fold change of intron 2-containing mRNA was notably lower after addition of A23187 alone (51.5, 40.1 and 29.1-fold at 30, 60 and 90 min, respectively). Furthermore, the fold change of intron 2-containing mRNA peaked earlier than exon 4-containing mRNA. This is unsurprising, as splicing of *FOS* mRNA occurs rapidly and co-transcriptionally (Listerman, Sapra et al. 2006). Co-treatment with CPT lead to a gradual accumulation of intron 2-containing transcripts (13.9, 29.1 and 42.5-fold at 30, 60 and 90 min, respectively), which was significantly different from that observed in the absence of CPT (ANOVA p-value = 7.02×10^{-3}).

3.2.3. *FOS* transcription in the presence of CPT and/or PARP inhibitor

The sustained accumulation of *FOS* mRNA in the presence of CPT, albeit at lower levels than in the absence of CPT, could be dependent on SSBR at transcription-blocking lesions. To test this, A431 cells were pre-incubated in serum-free media for 4 h prior to treatment with A23187 (5 µM) in the presence

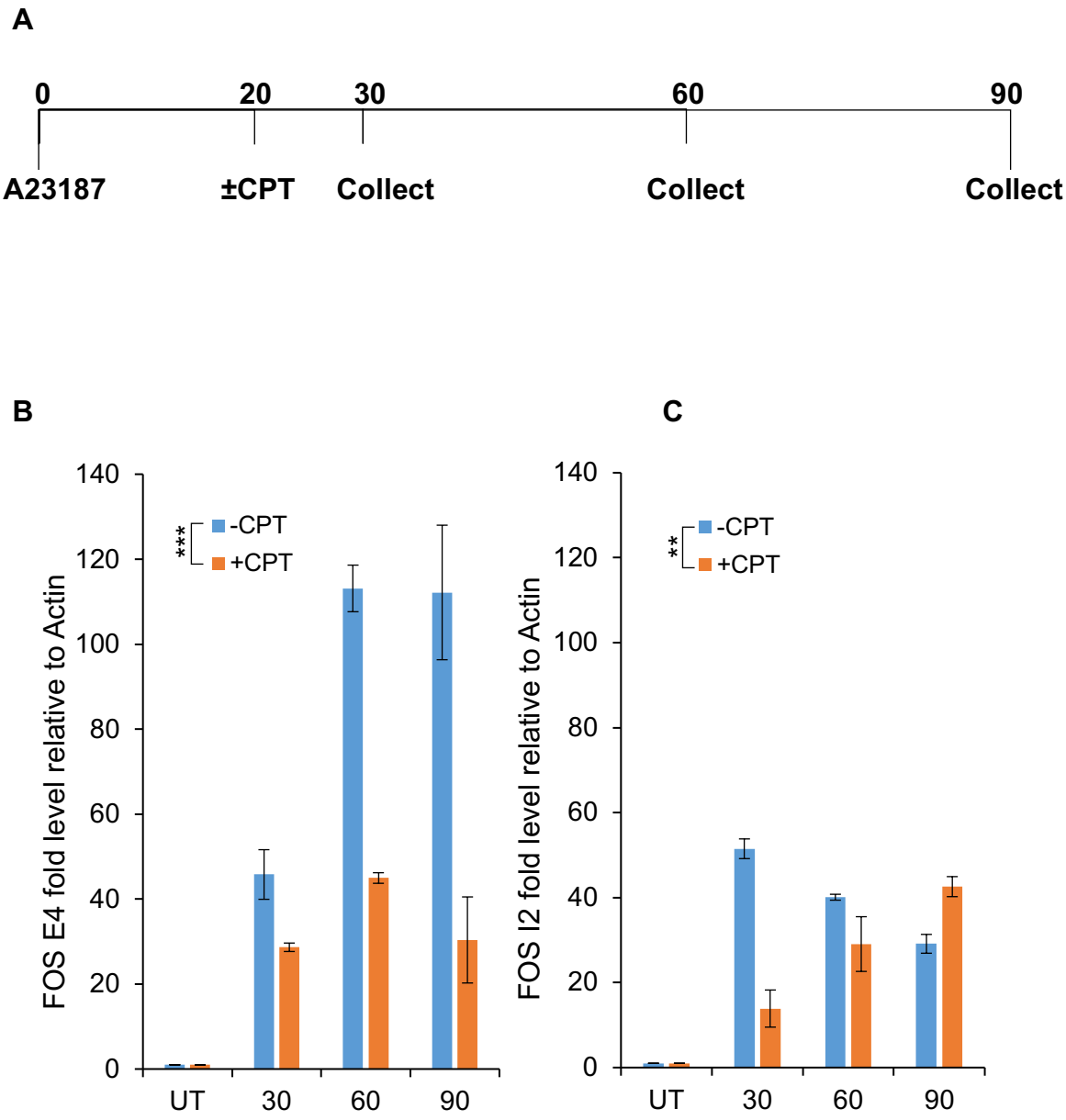

Figure 3.2. CPT treatment inhibits A23187-induced transcription of *FOS*. Subconfluent A431 cells were incubated in serum-free media for 2.5 hr prior to treatment with serum-free media containing 5 μM A23187. After 20 min, 10 μM CPT or DMSO vehicle was added. At the indicated timepoints cells were collected by scraping and snap freezing in liquid nitrogen **(A)**. Subsequently, total RNA was extracted and cDNA was synthesized with oligo-dT primers, using 1 μg total RNA as the template. RNA was degraded with RNAse A and samples were purified. Finally, samples were subjected to qPCR using primer sets F and D, targeting Exon 4 **(B)** and Intron 2 **(C)**, respectively. Data were calculated by the ΔΔct method and are presented as fold over untreated, relative to the level of Actin mRNA. Data are mean ±SEM of 3 biological replicates. Statistical significance was calculated by two-factor ANOVA.

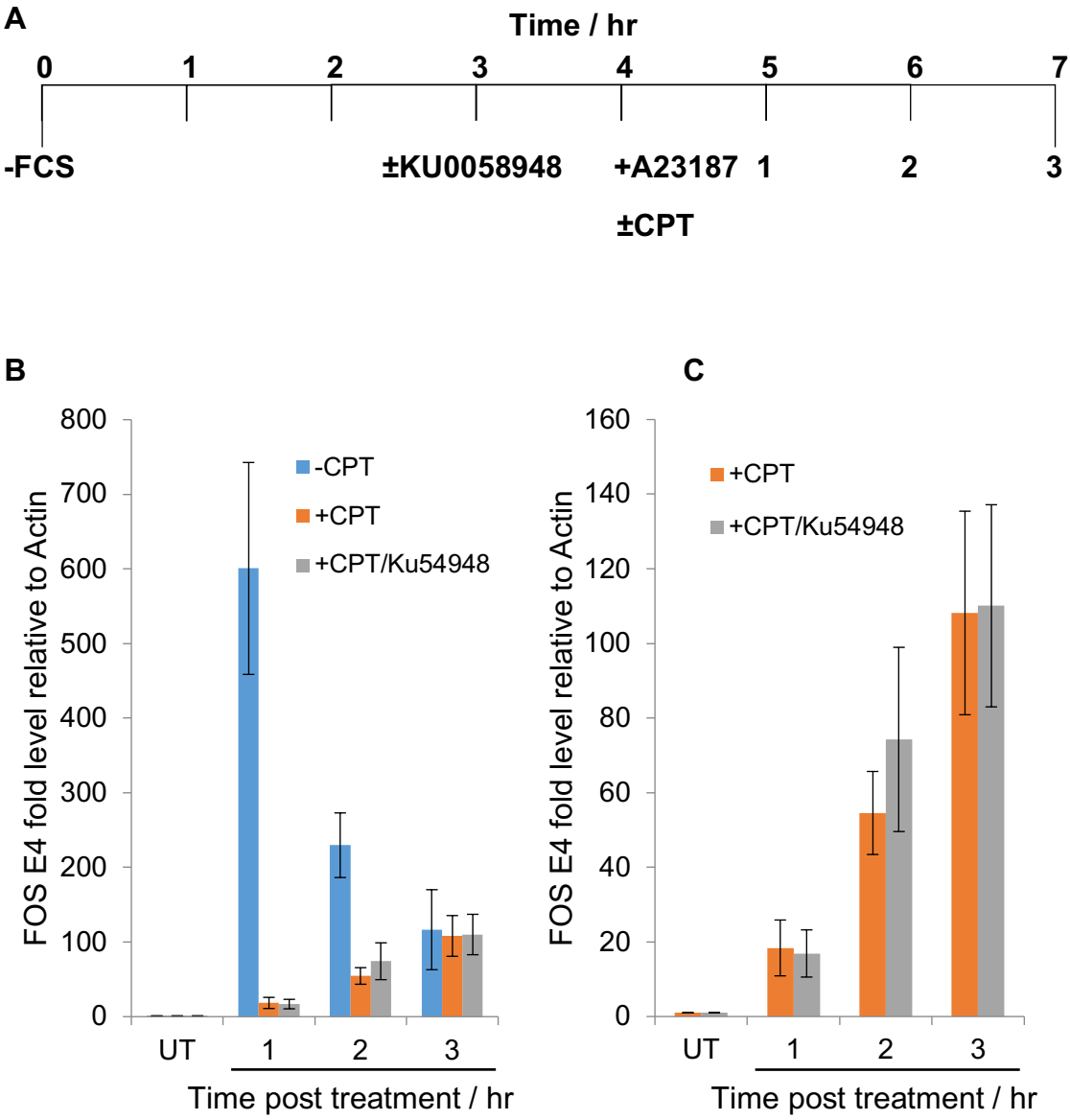

Figure 3.3. PARP inhibition does not prevent A23187-induced *FOS* transcription in the presence of CPT. Subconfluent A431 cells were treated according to the depicted **(A)**. At the indicated time points cells were collected by scraping and snap freezing in liquid nitrogen. Subsequently total RNA was extracted and cDNA was synthesized with oligo-dT primers. RNA was degraded with RNAse A and samples were purified. Finally, samples were subjected to qPCR using primer set F, targeting *FOS* Exon 4. Data were calculated by the ΔΔct method and are presented as fold over untreated, relative to the level of Actin mRNA **(B)**. For clarity, data are replotted after omitting samples treated with A23187 only **(C)**. All data are mean ±SEM of 4 biological replicates.

or absence of CPT (10 µM) and/or KU0058948 PARP inhibitor (500 nM) (Fig. 3.3.a). Where KU0058948 was used, cells were incubated with the drug for 1 h prior to induction with A23187, and throughout the time course. A longer pre-incubation in serum-free medium was conducted to increase *FOS* mRNA fold induction. This was evidently the case, as treatment with A23187 alone lead to a notably higher fold change in *FOS* exon 4-containing mRNA (primer set F) at 1 h (600.7-fold over untreated) (Fig. 3.3.b). Upon co-treatment with CPT, accumulation of *FOS* mRNA was significantly delayed. Notably, whilst the induction of *FOS* in the absence of CPT lead to a transient induction (Fig. 3.2.b and Fig. 3.3.b) the continued presence of CPT throughout lead to a continued gradual accumulation of exon 4-containing transcripts. Co-incubation with PARP inhibitor KU0058948 failed to prevent *FOS* mRNA accumulation in the presence of CPT (Fig. 3.3.b and c). This suggests that *FOS* induction in the presence of CPT is independent of PARP activity. Whilst this result might indicate that SSBR is not required for the residual induction of *FOS* observed in the presence of CPT, alternatively it might indicate that SSBR following CPT treatment is PARP1 independent.

3.2.4. *FOS* transcription in the presence of CPT and/or proteasome inhibitor

Proteasomal degradation of Top1-SSBs has been shown to occur prior to downstream steps of SSBR (Zhang, Tomida et al. 2004, Lin, Ban et al. 2008). To further investigate the Top1-SSB repair-dependence of *FOS* transcription in the presence of CPT, cells were co-incubated with MG132 proteasome inhibitor (50 µM) (Fig. 3.4.a). In this case, MG132 was found to significantly reduce (ANOVA p-value = 3.95×10^{-3}) accumulation of *FOS* exon 4-containing mRNA (primer set F) in the presence of CPT (Fig. 3.4.b and c). Whilst this could suggest that transcription in the presence of CPT is dependent on repair of Top1-SSBs, it could also be due to a general effect of proteasome inhibition on *FOS* transcription. To test this, serum starved A431 cells were pre-treated with MG132 (50 µM) for 1 h prior to treatment with A23187 in the continued presence or absence of MG132 (Fig. 3.5.a). It was found that MG132 did indeed limit *FOS* mRNA accumulation in the absence of CPT (Fig. 3.5.b).

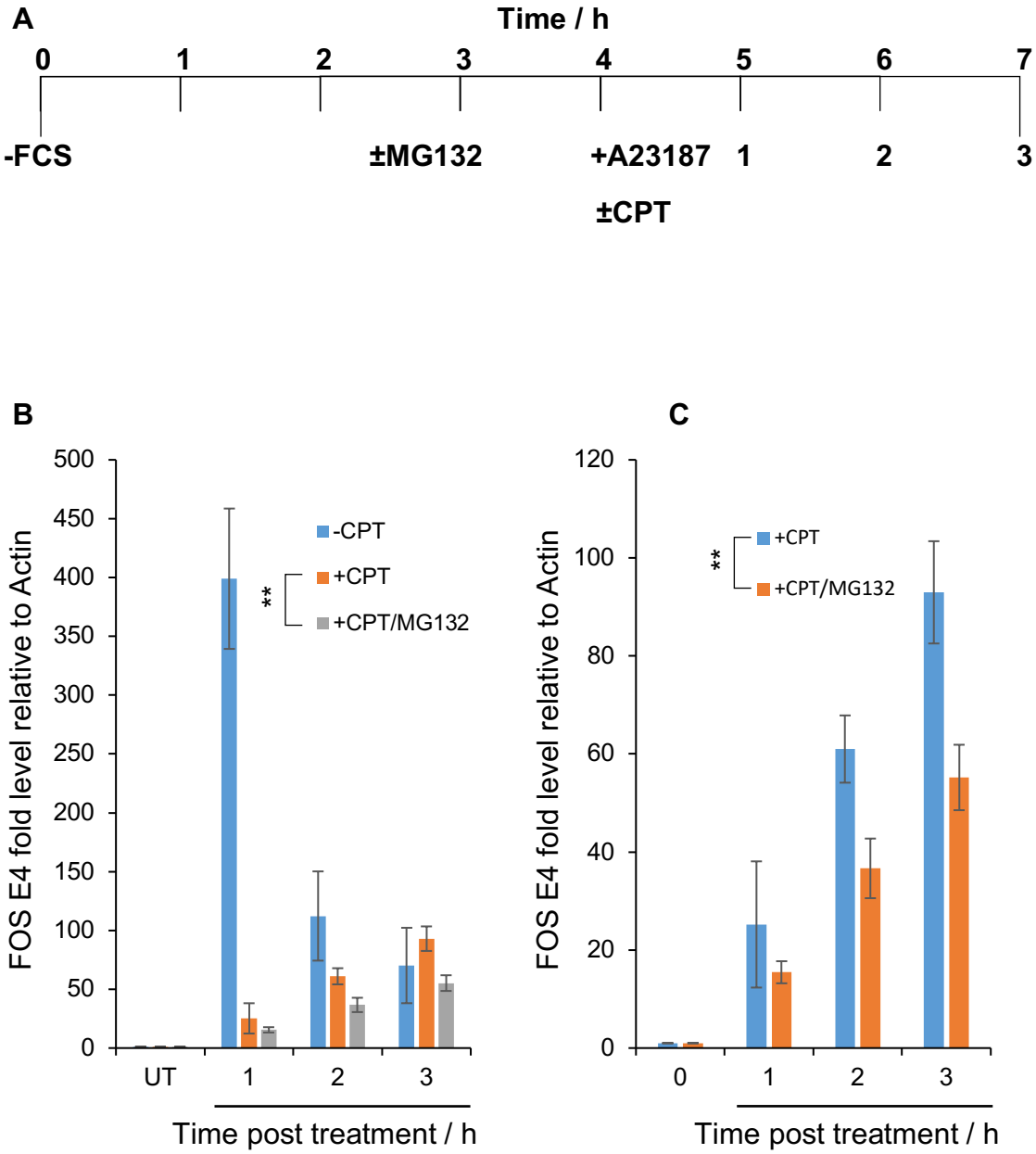

Figure 3.4. Proteasome inhibition limits A23187-induced *FOS* transcription in the presence of CPT. Subconfluent A431 cells were treated according to the time course depicted **(A)**. At the indicated time points cells were collected by scraping and snap freezing in liquid nitrogen. Subsequently total RNA was extracted and cDNA was synthesized with oligo-dT primers. RNA was degraded with RNAse A and samples were purified. Finally, samples were subjected to qPCR using primer set F, targeting *FOS* Exon 4. Data were calculated by the ΔΔct method and are presented as fold over untreated, relative to the level of Actin mRNA **(B)**. For clarity, data are replotted after omitting samples treated with A23187 only **(C)**. All data are mean ±SEM of 4 biological replicates. Statistical significance was calculated using two-factor ANOVA.

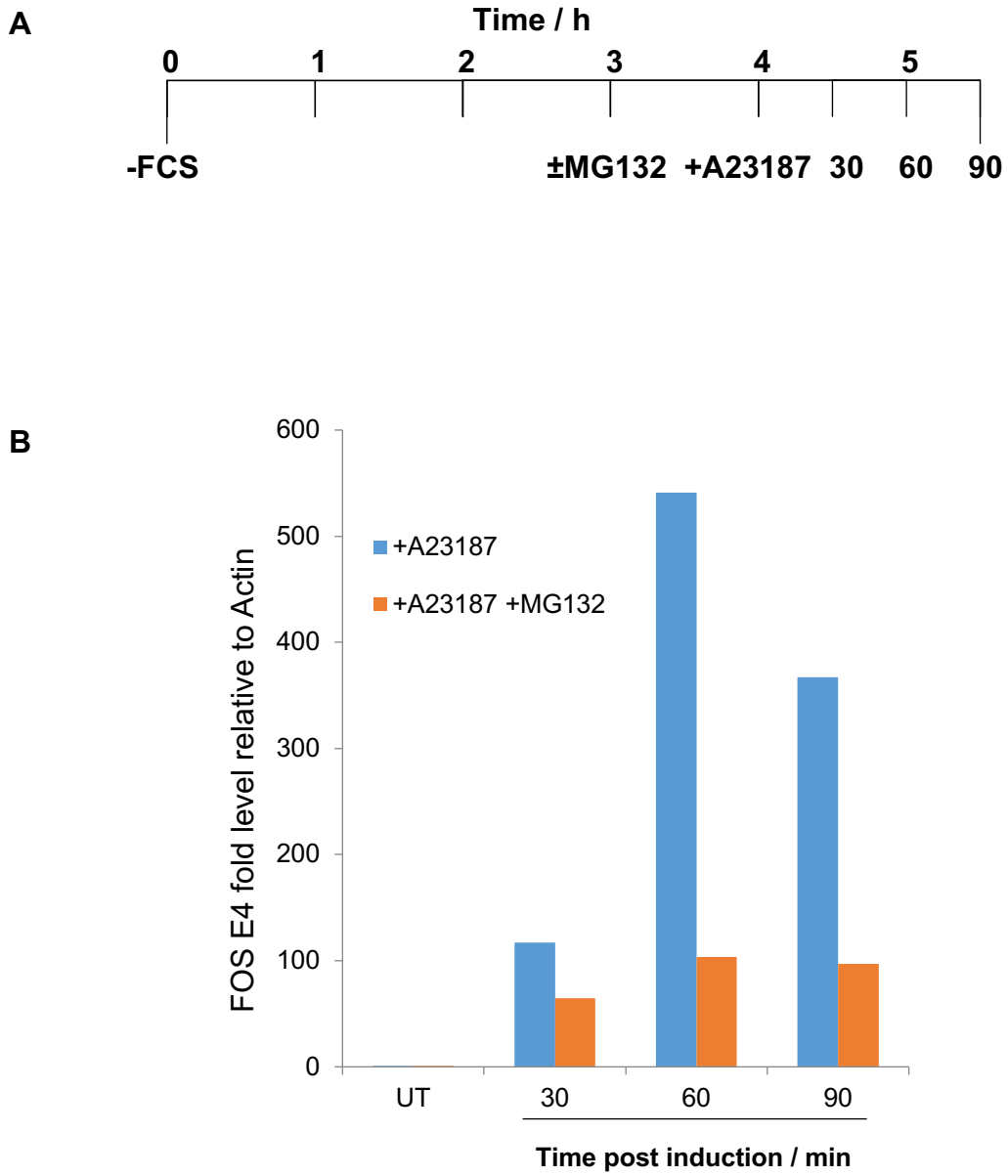

Figure 3.5. Proteasome inhibition limits A23187-induced *FOS* transcription in the absence of CPT. Subconfluent A431 cells were treated according to the time course depicted (**A**). At the indicated time points cells were collected by scraping and snap freezing in liquid nitrogen. Subsequently total RNA was extracted and cDNA was synthesized with oligo-dT primers. RNA was degraded with RNAse A and samples were purified. Finally, samples were subjected to qPCR using primer set F, targeting *FOS* Exon 4. Data were calculated by the ΔΔct method and are presented as fold over untreated, relative to the level of Actin mRNA. Data are presented for one experiment. **(B).**

3.2.5. Optimization of A431 ChIP sonication conditions

Successful ChIP is reliant upon many different variables which must be carefully optimized for every cell line and antibody combination. One particularly important factor is the quality of chromatin sonication. Sonication should be sufficient to produce chromatin fragments with an average size of 300-500 bp, whilst minimising degradation of the epitope of interest. Optimization was conducted by subjecting 4% formaldehyde -fixed A431 cells to lysis in 1% SDS buffer, followed by water bath sonication for increasing numbers of cycles (30 s ON / 30 s OFF). Samples were then divided into two to allow separate analysis of chromatin fragments by 1% agarose EtBr (Fig. 3.6.a and b) and XRCC1 protein by WB (Fig. 3.6.c). Three cycles were sufficient to produce chromatin fragments with an average size of 300-500 bp. Three cycles also resulted in minimal XRCC1 protein loss, which was very apparent with increasing sonication cycles.

3.2.6. RNAPII binding at *FOS* measured by ChIP.

The genomic distribution of RNAPII has been measured previously using ChIP-seq/qPCR with several different antibodies. The most commonly used are H5, H14 and 8WG16 monoclonal antibodies. These all target the C-terminal domain of RNAPII, which is differentially phosphorylated at specific residues in its YSPTSPS repeat motif, depending on the stage of transcription in which the polymerase is engaged. The CTD of RNAPII is hypophosphorylated in the pre-initiation complex. Phosphorylation of CTD Ser5 is found in early elongating complexes, and Ser2 is additionally phosphorylated in productively elongating complexes. H14 and H5 antibodies recognise CTD epitopes with Ser5 or Ser2 Ser5 phosphorylation. By comparison 8WG16 recognizes unphosphorylated CTD and CTD phosphorylated on Ser5 but not Ser2 (Morris, Michelotti et al. 2005). However, given that even productively elongating RNAPII complexes will contain some unphosphorylated CTD sequences, 8WG16 has traditionally been used as a measure of total RNAPII. For this reason, 8WG16 was selected for use in this study.

A431 cells were treated with A23187 (5 µM) and/or CPT (10 µM) prior to fixation, according to the time course in (Fig. 3.7.a). ChIP was conducted with

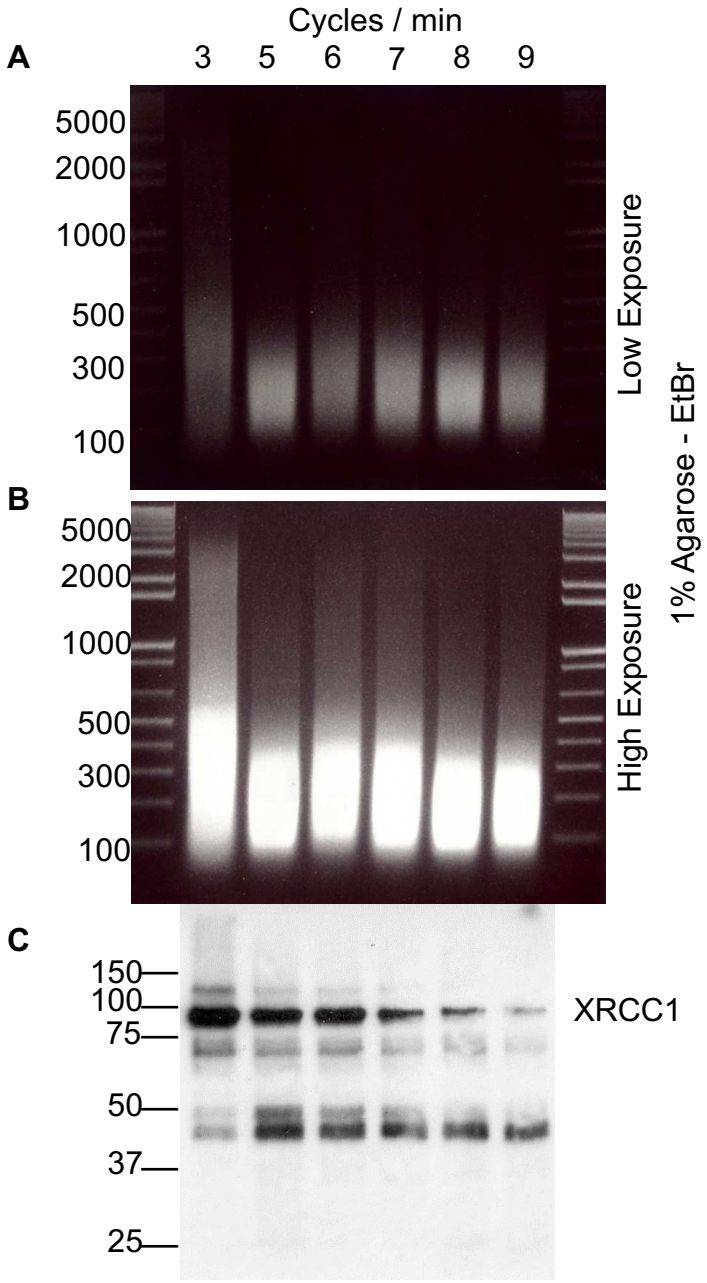

Figure 3.6. Optimization of sonication conditions for ChIP with A431 cells. A431 cells were formaldehyde fixed and collected by scraping and centrifugation. Pellets were lysed in 1% SDS ChIP lysis buffer and sonicated for the indicate number of cycles (1 cycle = 30 s ON, 30 s OFF). One aliquot of each sample was incubated at 65°C overnight to reverse formaldehyde crosslinks, prior to separation and visualisation of chromatin fragments by agarose electrophoresis with ethidium bromide staining. A molecular weight marker is included, showing sizes in bp. **(A).** A longer exposure is shown in **(B).** The other fraction of each sample was boiled immediately in LB and subjected to SDS-PAGE and WB with anti-XRCC1 antibody A231-300A. A molecular weight marker is included, showing sizes in KDa. **(C).**

8WG16 antibody or anti-IgG antibody as detailed in the methods, using the sonication conditions established above. qPCR was subsequently conducted using primer sets A, B, C, D, F and G (Fig. 3.7.b). The profile of RNAPII distribution in untreated cells is characteristic of many immediate early response (IED) genes, with a significant fraction being located immediately downstream of the TSS in a state of promoter proximal pausing. Upon induction with A23187, RNAPII association increased at all gene loci, but did not significantly increase at the downstream locus G. This indicates that sonication is optimal to produce small enough fragments for high resolution ChIP-qPCR. Whilst an increase in RNAPII association was detected at all gene loci, the fold increase was particularly pronounced at the downstream loci detected by primer sets C, D, and F (t-test p-values: $3.06x10^{-3}$, $1.17x10^{-3}$, and $1.34x10^{-3}$, respectively). This enrichment of RNAPII at downstream loci indicates release from a paused state to productive elongation upon induction with A23187. Upon treatment with A23187 and CPT, a significant reduction in RNAPII association at all loci was detected, relative to A23187 treatment alone (ANOVA p-value = $1.05x10^{-2}$). It is important to note that treatment with CPT in the absence of *FOS* induction did not result in any significant alteration of the RNAPII distribution within *FOS* (ANOVA p-value = $6.86x10^{-1}$).

3.2.7. Optimization of XRCC1 ChIP immunoprecipitation with A431 cells

Next, protocols were established for the direct measurement of XRCC1 recruitment to *FOS*, by ChIP. First, the immunoprecipitation (IP) of XRCC1 was optimized by ChIP-WB. Fixed and lysed A431 cells were sonicated for 3 cycles prior to dilution and overnight IP with 1, 2, or 5 µg A300-231A antibody. This polyclonal antibody is affinity purified using an immobilized peptide encompassing the phosphorylated S485 and T488 residues. It has been used extensively in the literature for WB, IF, IP, and IHC, but not for ChIP. Following IP, Protein G -conjugated dynabeads were added to precipitate antibody-antigen complexes, prior to washing and elution. Fractions of input, unbound, washes and elution were subjected to 10% SDS-PAGE and WB with A300-231 anti-XRCC1 antibody (Fig. 3.8.). XRCC1 was successfully recovered in all IPs to a varying extent. IP with 2 µg of antibody resulted in the best recovery of XRCC1,

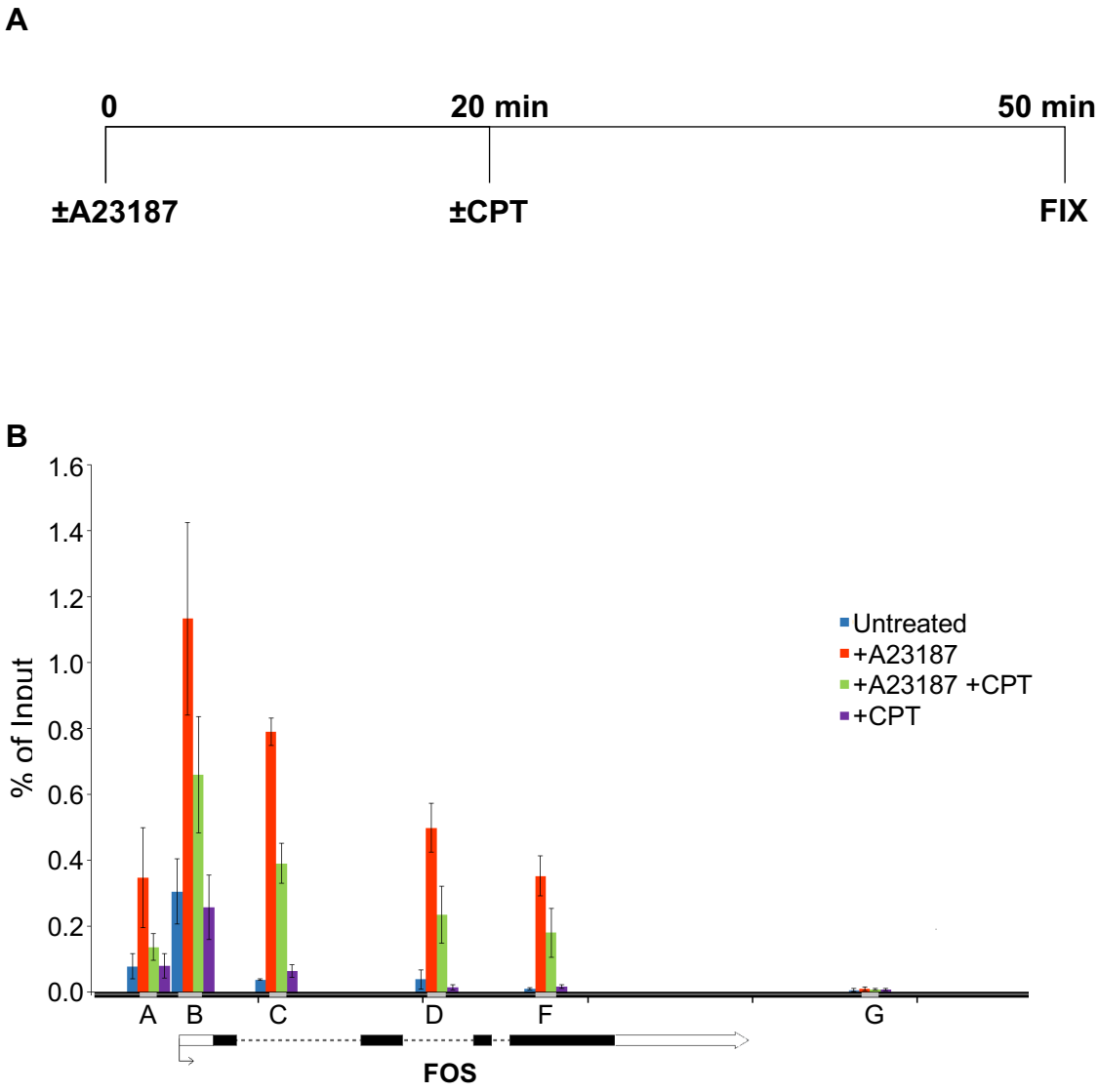

Figure 3.7. ChIP reveals distribution of RNAPII within *FOS* in cells treated with A23187 and/or CPT. A431 cells were treated or not with A23187 (5 µM) and/or CPT (10 µM) as in **(A).** RNAPII ChIP-qPCR was conducted with 8WG16 antibody, as described in section 2.2.4.6. The enrichment values of the primer pairs A, B, C, D, F, and G are expressed as % of input. The positions of these primer pairs relative to the FOS gene are indicated **(B).** All data are mean ±SEM of at least 2 biological replicates.

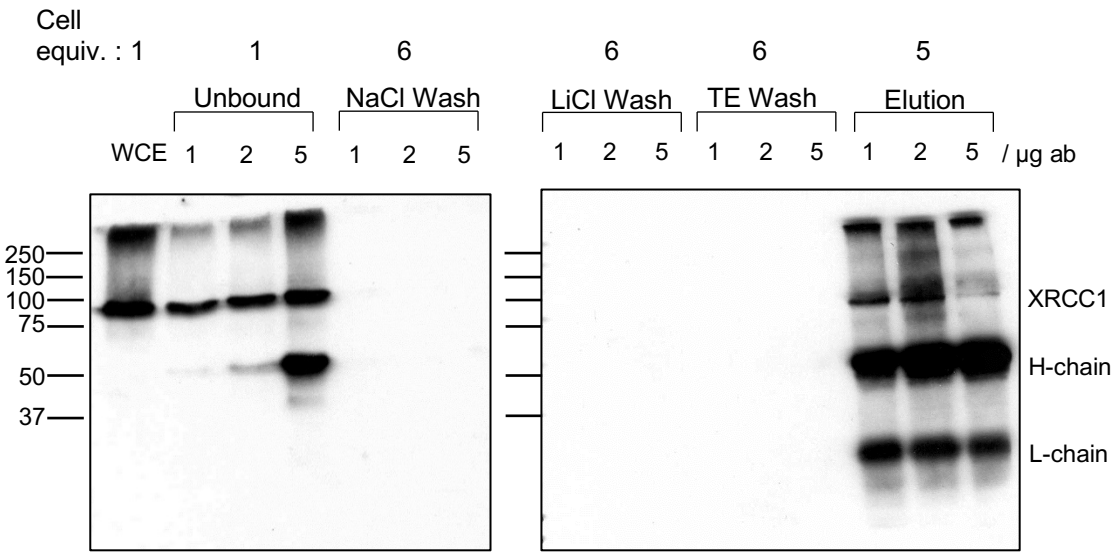

Figure 3.8. Optimization of immunoprecipitation conditions for XRCC1 ChIP with A431 cells. A431 cells were formaldehyde fixed and subjected to anti-XRCC1 ChIP-WB as described in the methods. For the immunoprecipitation, a titration of 1, 2 or 5 uL of A300-231A antibody was used. Samples of input, unbound, washes and elution were retained and subjected to WB with anti-XRCC1 antibody (A300-231A). The loaded cell equivalents are expressed relative to input. The position of XRCC1 and the heavy and light antibody chains is indicated.

whereas IP with 5 µg resulted in the worst recovery. This is likely to be due to saturation of the binding capacity of the Protein G beads. Protein G dynabeads have an estimated capacity of 0.24 µg of IgG per 1 µL beads, which would be an estimated 4.8 µg A300-231A for the 20 uL beads used here. However, this estimate is for human rather than rabbit IgG, and was estimated by the manufacturer using different IP conditions. In the unbound fraction of the 5 µg IP there is a strong band at ~50 KDa corresponding to the heavy chain of the A300-231A antibody, indicating that the capacity of the protein G beads has indeed been exceeded. This may result in lower recovery of XRCC1 in the IP, as some of the recoverable fraction remains associated with the unbound A300-231A antibody. It may be possible to increase the volume of beads used in the IP to recover more XRCC1 with 5 µg A300-231A. However, the recovery was deemed sufficient for the purposes of the ChIP-qPCR with 2 µg A300-231A.

3.2.8. XRCC1 localization at *FOS* measured by ChIP

Untreated cells, and cells treated with A23198 and/or CPT were fixed according to the time course depicted in (Fig. 3.9.a). Cells were then subjected to anti-XRCC1 ChIP with A300-231A antibody, using the sonication and IP conditions established above (see section 2.2.4.6 for detailed protocol). As for RNAPII ChIP, primer sets A, B, C, D, F, and G were used to measure XRCC1 localization at the *FOS* locus (Fig. 3.9.b). A300-231A signal was low at all tested loci in untreated cells. Upon treatment with A23187, A300-231A ChIP signal significantly increased in the gene body at loci C, D and F (t-test p-values: 1.61×10^{-2}, 1.12×10^{-2} and 2.10×10^{-3}, respectively). By comparison, the small increases in ChIP signal at the promoter locus (A), the transcription pausing locus (B) and the downstream locus (G) were not significant (t-test p-values: 1.09×10^{-1}, 6.49×10^{-2}, 9.51×10^{-2}, respectively). The signal increase was correlated with distance from the TSS, with the downstream loci D and F having the largest fold changes (3.6 and 3.5-fold respectively). By comparison, the signal at the promoter (A) and RNAPII pause site (B) remained relatively low. Upon treatment with A23187 and CPT, A300-231A signal at all *FOS* loci was not significantly different to treatment with A23187 alone (t-test p-values: 9.76×10^{-1}, 7.67×10^{-1}, 8.09×10^{-1}, 5.29×10^{-1} and 2.54×10^{-1} for A, B, C, D and F, respectively). This result

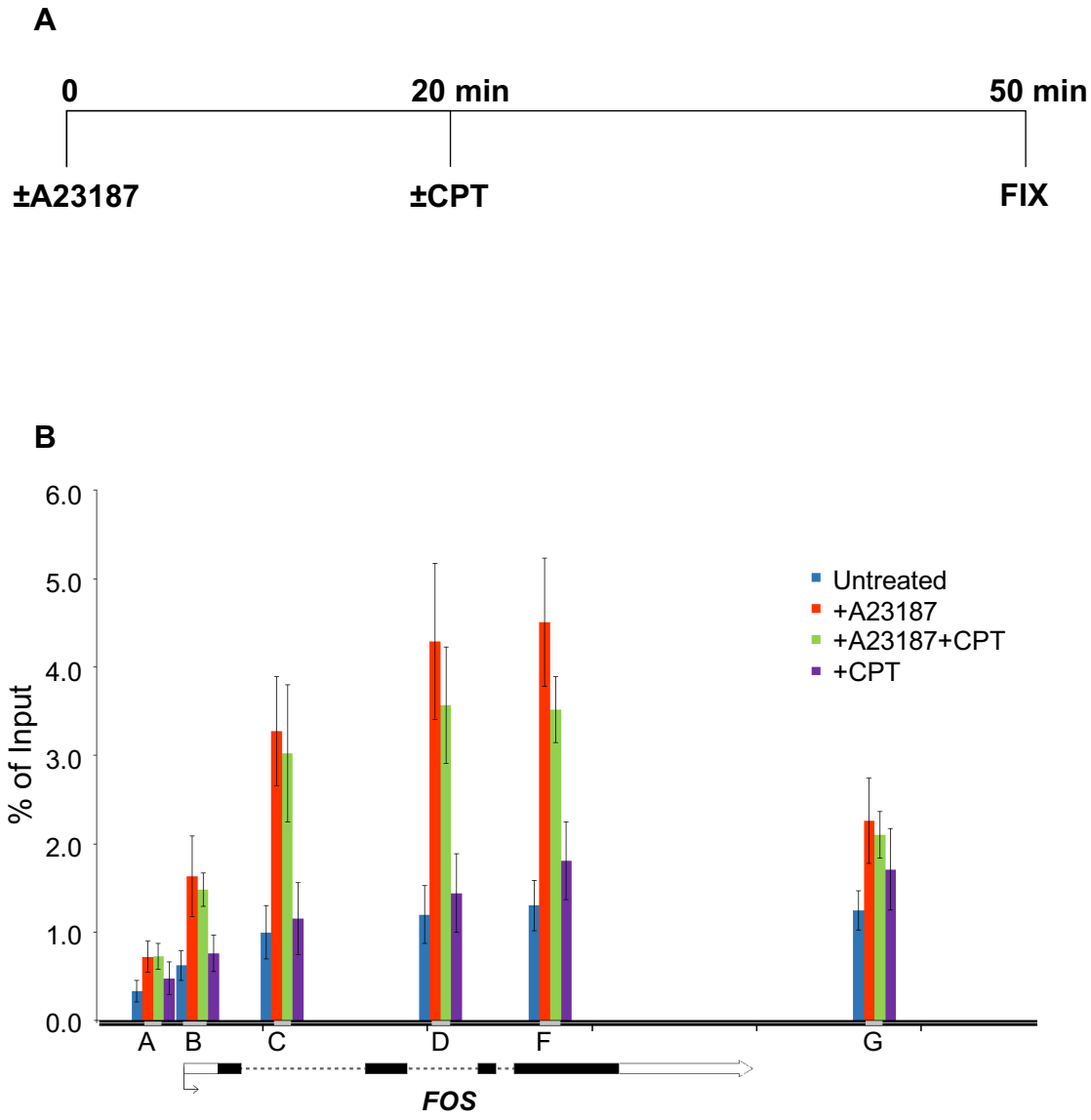

Figure 3.9. ChIP reveals apparent distribution of XRCC1 within *FOS* in cells treated with A23187 and/or CPT. A431 cells were treated or not with A23187 (5 μM) and/or CPT (10 μM) in the manner depicted in **(A)**. XRCC1 ChIP-qPCR was conducted with A231-300A antibody, as described in section 2.2.4.6. The enrichment values of the primer pairs A, B, C, D, F and G are expressed as % of input. The positions of these primer pairs relative to the *FOS* gene are indicated **(B)**. All data are mean ±SEM of at least 2 biological replicates.

was surprising as it implied that XRCC1 recruitment might occur co-transcriptionally, in the absence of DNA damage. To validate that the results of the A300-231A ChIP specifically reflected XRCC1 localization, further experiments were conducted.

3.2.9. Optimization of conditions for XRCC1 ChIP with EM9 cells.

At the time that these experiments were being conducted, a human XRCC1 KO cell line was not available for use as an antigen negative control. Instead, the Chinese Hamster Ovary (CHO) XRCC1 KO cell line EM9 was the most suitable choice to test the specificity of the A300-231A antibody. ChIP sonication and IP conditions were established in EM9 cells stably complemented with WT XRCC1 (EM9-XH) (Fig. 3.10.). Three cycles of sonication produced suitable chromatin fragments of 300-500 bp (Fig. 3.10.a). The IP resulted in a good recovery of XRCC1, with little remaining in the unbound fraction (Fig. 3.10.b).

3.2.10. XRCC1 ChIP with A300-231A antibody in EM9 cells reveals non-specific signal.

EM9 cells complemented with wild type human XRCC1-His or vector, denoted XRCC1-XH (XH) or EM9-V (V), respectively were treated or not with A23187 and/or CPT, prior to fixation according to the time course as for A431 cells (Fig. 3.9.a). Cells were then subjected to ChIP with A300-231A anti-XRCC1 antibody, or a negative control antibody targeting rabbit IgG, as per the sonication and IP conditions identified above (see section 2.2.4.6 for detailed protocol). qPCR was conducted with pimer set *cg*E4, targeting a comparable region of *FUS* exon 4 to primer set F in A431 cells (see section 2.2.4.3). Unfortunately, a strong A300-231A ChIP signal was observed in both EM9 XH and EM9 V cells upon treatment with A23187 and/or CPT (Fig. 3.11.a). Moreover, the signal was even higher in EM9 V than EM9 XH cells, indicating that the signal observed with this antibody is not specific to XRCC1. The signal was two orders of magnitude higher than the background signal observed in the mock anti-IgG ChIP. A WB with A300-231A antibody was conducted in parallel with the ChIP, demonstrating the absence of XRCC1 protein in EM9 V cells (Fig. 3.11.b). The WB did not detect

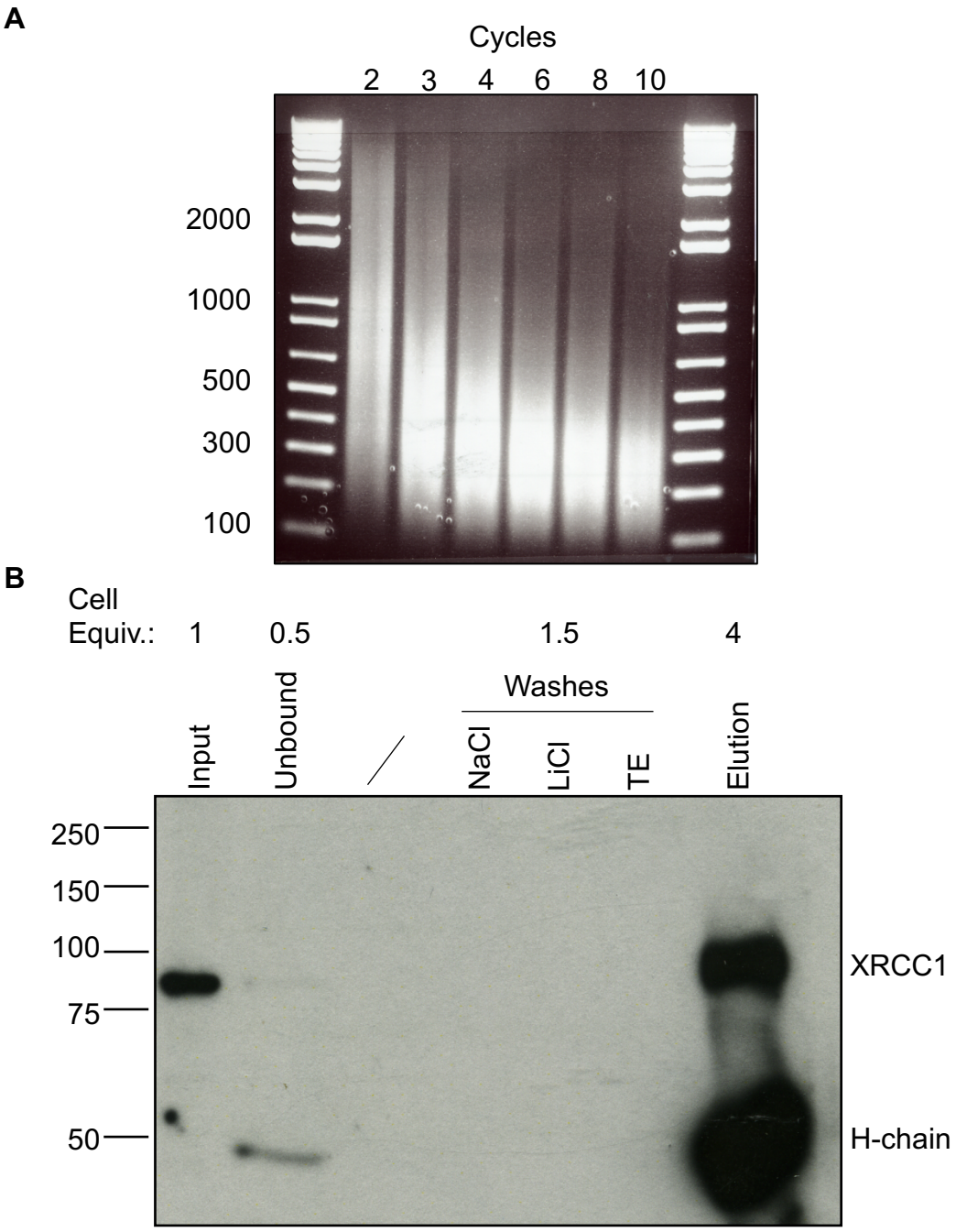

Figure 3.10. Optimization of conditions for XRCC1 ChIP with EM9 cells. EM9 cells were formaldehyde fixed, lysed in 1% SDS lysis buffer and subjected to sonication for the indicated number of cycles (1 cycle = 30 s ON/ 30 s OFF); prior to 65ºC incubation overnight to reverse crosslinks. Chromatin fragments were separated and visualised by 1% agarose electrophoresis with EtBr staining **(A)**. EM9 cells stably expressing XRCC1 were subjected to anti-XRCC1 ChIP-WB with A231A-300A antibody as described in the methods. Samples of input, unbound, washes and elution were retained and subjected to WB with anti-XRCC1 antibody (A300-231A). The loaded cell equivalents are expressed relative to input. The position of XRCC1 and the heavy antibody chain are indicated **(B)**.

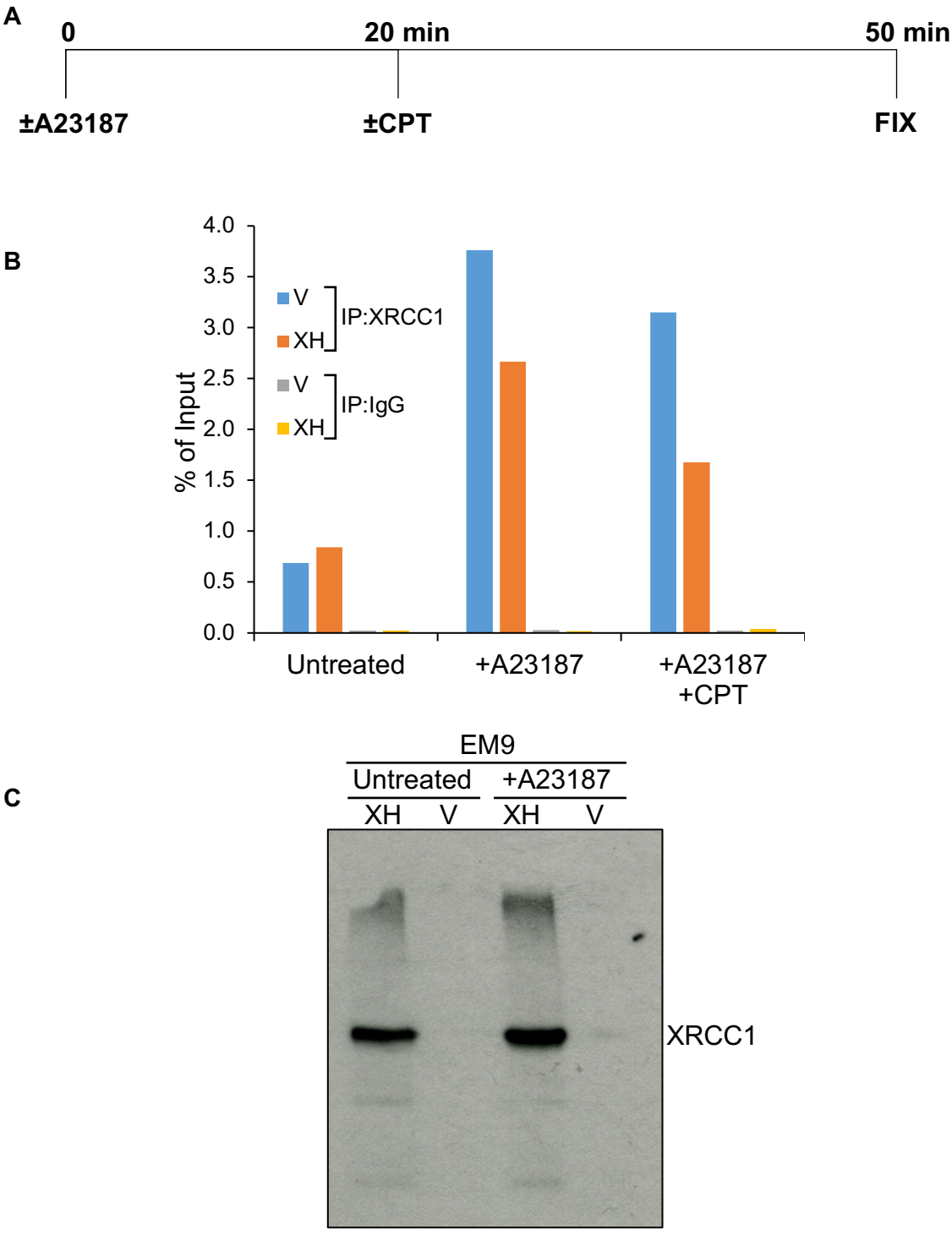

Figure 3.11. XRCC1 ChIP with A300-231A antibody in EM9 cells reveals non-specific signal. EM9 cells stably complemented with wild type XRCC1 (XH) or vector (V) were treated with A23187 (5 μM) and/or CPT (10 μM) according to the time course depicted in **(A)**, before being subjected to ChIP with anti-XRCC1 A300-231A antibody and anti-IgG antibody, as described in section 2.2.4.6. qPCR was conducted with the Exon 4 primer pair **(B).** Enrichments are expressed as % of input. A representative experiment is shown. A fraction of the indicated sample inputs was boiled in LB and subjected to SDS-PAGE and WB with anti-XRCC1 antibody A300-231A **(C)**.

any obvious non-specific bands in the EM9 V cells. However, this may be because A300-231A recognizes non-specific epitopes in the ChIP that are destroyed by the denaturing conditions of the WB.

Many proteins localize to actively transcribing genes, any of which may be non-specific targets of A300-231A. In addition, the relaxed conformation of active genes is thought to lead to their overrepresentation in ChIP data, possibly due to an increased susceptibility to formaldehyde fixation (Park, Lee et al. 2013, Teytelman, Thurtle et al. 2013) (see section 3.3 for further discussion). These details are likely to explain the A23187-inducible nature of the non-specific signal.

3.2.11. A431 GFP-XRCC1 ChIP optimization

Due to the inherent bias of ChIP data towards transcriptionally active DNA (Park, Lee et al. 2013, Teytelman, Thurtle et al. 2013), the enrichment of any nuclear protein could be falsely detected at *FOS*. To try to control for this, and to circumvent a lack of other suitable anti-XRCC1 antibodies available at the time of these experiments, a new strategy was devised. A431 cells were transfected with GFP-XRCC1 or GFP expression plasmids. Transfected cells were subjected to antibiotic selection with G418, prior to isolation of single clones by observation of GFP fluorescence. To confirm the expression of the transgenes, a WB with anti-GFP antibody (ab290) was performed on cell lysates from these two cell lines (Fig. 3.12.a). Next, using A431 GFP-XRCC1 cells ChIP sonication conditions were again optimized: for minimal degradation of GFP-XRCC1 (Fig. 3.12.b), and to produce chromatin fragments of 300-500 bp (Fig. 3.12.c). In each case, three cycles produced optimum results. Finally, the IP of GFP-XRCC1 with anti-GFP antibody (AB290) was tested (Fig. 3.12.d). Approximately 10-15% of input GFP-XRCC1 was recovered in the IP (compare GFP-XRCC1 band in input vs 10-fold elution).

3.2.12. Anti-GFP ChIP cannot detect GFP-XRCC1 enrichment in C-*FOS* following transcription induction or CPT exposure

A431, A431 GFP, or A431 GFP-XRCC1 cells were treated or not with A23187 and/or CPT, prior to fixation according to the time course depicted in (Fig. 3.13.a).

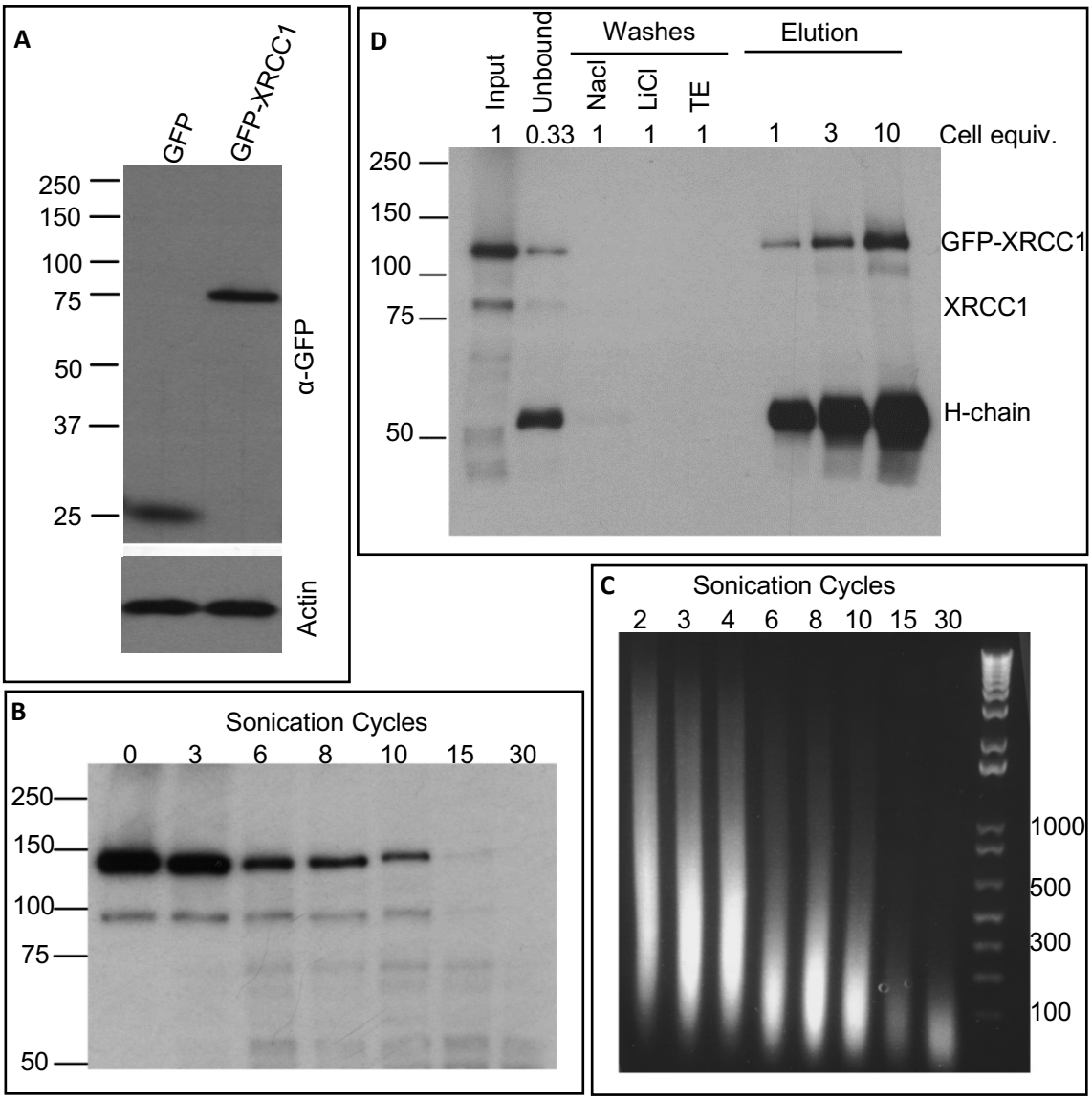

Figure 3.12. GFP-XRCC1 ChIP optimization. A431 cells stably expressing GFP or GFP-XRCC1 were generated by transfection and selection in G418 (see section 2.2.2.5), prior to western blotting of whole cell extracts with anti-GFP (α-GFP) and anti-Actin antibodies **(A).** GFP-XRCC1 cells were fixed with 4% formaldehyde and collected by scraping and centrifugation. Cells were lysed in 1% SDS lysis buffer and sonicated for the indicated number of cycles (30 s ON/ 30 s OFF), prior to being subjected to SDS-PAGE and western blotting with anti-XRCC1 antibody (A300-231A) **(B)**, or agarose electrophoresis and ethidium bromide staining (**C**). GFP-XRCC1 cells were subjected to anti-GFP ChIP-WB as described in the section 2.2.4.7 (3 cycles of sonication). Samples of input, unbound, washes and elution were retained and subjected to western blotting with anti-XRCC1 antibody (A300-231A) **(D)**. The loaded cell equivalents are expressed relative to input. A molecular weight marker was included in all electrophoresis experiments and sizes are indicated in bp **(C)** or KDa **(A, B and D)**.

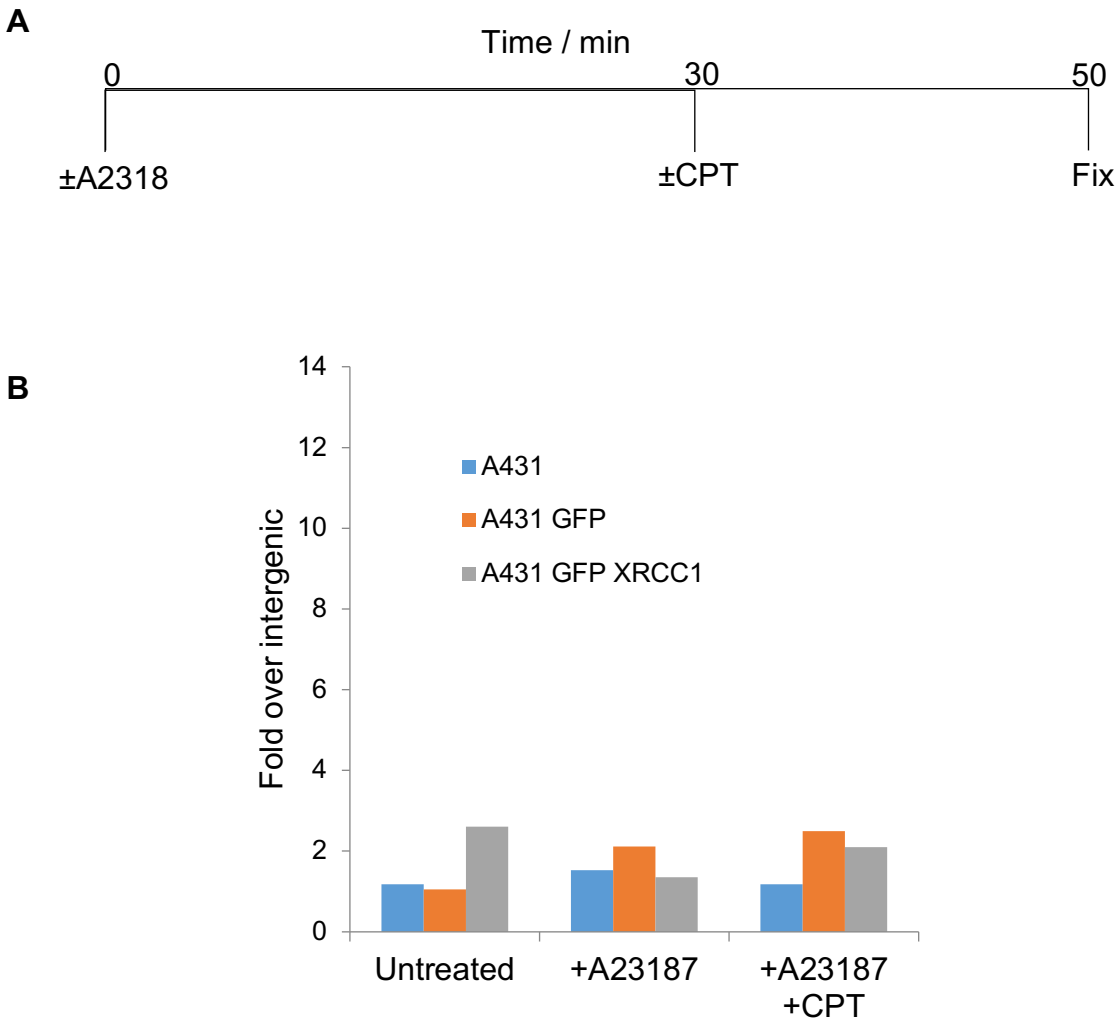

Figure 3.13. Anti-GFP ChIP cannot detect GFP-XRCC1 enrichment in *FOS* following transcription induction or CPT. A431, A431 GFP or A431 GFP-XRCC1 cells were treated or not with A23187 (5 μM) in the presence or absence of CPT (10 μM), according to the time course illustrated in **(A)**. Fixed cells were then subjected to anti-GFP ChIP-qPCR (primer set F) as described in section 2.2.4.7. A representative experiment is shown **(B).**

Cells were then subjected to ChIP with anti-GFP antibody (ab290), as per the sonication and IP conditions identified above (see section 2.2.4.7 for detailed protocol). qPCR was conducted with primer set F, and the results of a representative experiment are shown in (Fig. 3.13.b). Unfortunately, despite repeated attempts (not shown), ChIP-qPCR failed to detect any enrichment of GFP-XRCC1 in *FOS* following A23187 and/or CPT.

3.3. Conclusions and Discussion

This chapter attempted to establish a model system for studying the interplay between SSBR and transcription at the level of a single endogenous gene. Induction of *FOS* transcription with the calcium ionophore A23187 was successfully demonstrated by RT-PCR and RNAPII ChIP-qPCR. The accumulation of *FOS* mRNA was shown to be very transient, which has been noted previously (Francis Stewart, Herrera et al. 1990). This is due to rapid degradation of the *FOS* transcript (Shyu, Greenberg et al. 1989), coupled with an autoinhibitory effect of FOS protein at its own promoter (Schönthal, Herrlich et al. 1988). Upon additional treatment with 10 µM CPT, *FOS* mRNA accumulation was limited but not prevented. Furthermore, in contrast to the kinetics in the absence of CPT, *FOS* mRNA continued to accumulate during the time course of the experiments in the presence of CPT, which may be because *FOS* protein levels are too low in the presence of CPT to trigger the negative feedback mechanism. To test whether ongoing transcription in the presence of CPT was dependent on repair of Top1-SSBs, two known steps in this process were perturbed. Co-treatment with MG132, which blocks proteasomal degradation of Top1-SSBs, was found to limit accumulation of *FOS* mRNA in the presence of CPT. However, subsequent experiments revealed that this was also limited in the absence of CPT, suggesting a more general effect on the regulation of *FOS* transcription. FOS protein, which represses its own transcription (Schönthal, Herrlich et al. 1988), is known to be degraded rapidly by the proteasome (Ito, Inoue et al. 2005). Upon treatment with MG132, increased FOS protein levels may therefore repress *FOS* transcription.

Inhibition of PARP activity by co-treatment with KU0058948 failed to limit *FOS* mRNA accumulation in the presence of CPT, suggesting independence of this phenomenon from SSBR involving ADP-ribosylation. There are several possible explanations for this. One possibility is that alternative repair pathways can compensate, such as NER. Supporting this, the endonuclease XPF-ERCC1, which acts in global and transcription coupled-NER, has been reported to function in an alternative pathway for the repair of CPT-induced damage (Zhang, Regairaz et al. 2011). In the future, the accumulation of *FOS* mRNA in the presence of CPT could be measured in a context of XPF or ERCC1 depletion.

The reduced accumulation of *FOS* mRNA upon CPT treatment coincided with a reduction in RNAPII ChIP-qPCR signal at the promoter and in the gene body. Prolonged DNA damage-dependent (Desai, Zhang et al. 2003) and independent (Ratner, Balasubramanian et al. 1998, Karakasili, Burkert-Kautzsch et al. 2014) stalling of transcription leads to proteasomal degradation of Rpb1, the largest subunit of RNAPII, which contains the CTD. A more immediate effect of exposure of cells to CPT is the CDK7-mediated hyperphosphorylation of Rpb1 at Ser5 residues of the CTD repeat motif (Sordet, Larochelle et al. 2008), which may result in reduced affinity of 8WG16 binding and thus also contribute to the loss of RNAPII ChIP-qPCR signal (Cho, Kobor et al. 2001, Jones, Phatnani et al. 2004).

Following successful application of the ChIP protocol to RNAPII, attempts were made then made to apply the same techniques to XRCC1, in order to measure recruitment of this central SSBR scaffold to *FOS* in response to transcription induction with or without DNA damage. Initial experiments, using A300-231A antibody, indicated transcription-dependent XRCC1 recruitment concentrated in downstream transcribed regions of *FOS*. However, concerns about the specificity of this signal prompted further experiments in XRCC1 KO EM9 cells. Unfortunately, it was found that A23187-induced A300-231A ChIP-qPCR signal was present at *FOS* in EM9 V cells, revealing its non-specificity. This finding highlights the importance of including epitope depletion controls when conducting ChIP, especially when using an antibody which has not been verified with the technique. Unfortunately, the majority of published ChIP data includes only a mock IP control (Landt, Marinov et al. 2012).

In this case, the non-specific A300-231A signal is two orders of magnitude greater than the anti-IgG signal, which demonstrates the unsuitability of mock IPs as ChIP negative controls (Landt, Marinov et al. 2012).

Heavily transcribed loci, such as *FOS*, have recently been shown to be overrepresented in ChIP-qPCR/seq data (Auerbach, Euskirchen et al. 2009, Park, Lee et al. 2013, Teytelman, Thurtle et al. 2013, Jain, Baldi et al. 2015), possibly due to increased crosslinking or sonication of active chromatin. This widespread, systematic artifact may be particularly troublesome when attempting to ChIP proteins which interact transiently with chromatin, such as chromatin remodellers and repair proteins (Jain, Baldi et al. 2015). Considering this, a different strategy was devised to conduct anti-GFP ChIP-qPCR in cells stably transfected with GFP or GFP-XRCC1. This approach, which has been suggested previously (Teytelman, Thurtle et al. 2013), should control for the ChIP bias towards transcriptionally active regions. The advantage over other traditionally-used controls, such as mock IPs, is that the negative control involves precipitation of a real epitope (GFP) with the same antibody (anti-GFP), and should therefore be subject to the same inherent ChIP bias as precipitation of the tagged protein of interest (GFP-XRCC1). Unfortunately, despite many attempts to optimise and improve the protocol, anti-GFP ChIP-qPCR was not able to detect GFP-XRCC1 recruitment to *FOS* following treatment with A23187 and/or CPT. There are several reasons why this may not have been successful. Firstly, it is possible that the overexpression of GFP-XRCC1 results in a very large fraction which is not associated with chromatin. As only 10-15% of the input GFP-XRCC1 was recovered by IP, this may reduce the signal to noise ratio appreciably. Secondly, the epitope bound by ab290 may be sterically hindered by the orientation of GFP-XRCC1 chromatin binding. Thirdly, it is important to note that strong ChIP signal is generally only seen for proteins which interact strongly with chromatin for extended periods of time (transcription factors, polymerases etc) (Landt, Marinov et al. 2012). A combination of these issues may result in a signal to background ratio which is below the limit of detection of the assay. Finally, it is possible that GFP-XRCC1 is truly not recruited to *FOS* under the treatment conditions employed here. This final point highlights a significant obstacle which

was faced throughout this research: the lack of a validated genomic locus with enriched XRCC1 association, for use as a positive control.

Establishing the A300-231A ChIP-qPCR protocol in EM9 cells, whilst necessary to check the specificity of the signal, was time consuming. Furthermore, it raised the possibility of detecting non-specific signal unique to CHO cells. If this project were to be reattempted in the future, either with XRCC1 or another SSBR protein, it would be useful to have a panel of KO human cell lines for use as epitope negative controls. With these, it would be possible to screen a panel of antibodies for high specificity and affinity. The advent of CRISPR-Cas9 technology, allowing relatively straightforward modification of genomic DNA *in vivo*, makes the generation of such cells possible. This will be the subject of the following chapter.

Chapter Four

Generation and Characterization of Diploid Human Cells with CRISPR-Cas9 -mediated deletion of SSBR genes

4.1. Introduction and Aims

The previous chapter attempted to establish protocols for XRCC1 ChIP with limited success. One limitation that proved a barrier was the absence of a suitable human XRCC1-deleted cell line for use as an antigen negative control. Eventually this lead to establishing the ChIP protocol in Chinese hamster ovary (CHO) cells, where an XRCC1 KO cell line was available (EM9). This highlights a clear dearth of published human cell lines with SSBR gene KOs, with most studies instead utilizing siRNA-mediated depletion or mouse embryonic fibroblasts (MEFs) derived from transgenic animals. Whilst these tools have greatly advanced our understanding of SSBR gene function, they are not without limitations. Depletion by siRNA can often be incomplete and a seemingly negligible remaining fraction of protein, for example a highly active enzyme such as PARP1, can mask phenotypes and lead to erroneous conclusions. One example of this is the observation that complemented *XRCC1*$^{-/-}$ mice possessing approximately 10% WT levels of XRCC1 protein exhibit normal embryogenesis and post-natal development, and that MEFs generated from these animals display comparable methyl methanesulfonate (MMS) sensitivity to WT cells (Tebbs, Thompson et al. 2003).

By comparison with siRNA depletion, KO MEFs offer complete deletion of gene function and are thought to be a good model of most features of human DNA repair. However, there are known instances where DNA repair pathway choice may differ in human and mouse. For example the relative abundance of Ku80 and DNA-PKcs is dramatically higher in human than mouse cells (Lorenzini, Johnson et al. 2009). Furthermore, there are multiple examples where KO mouse models do not fully recapitulate the phenotypes of human patients (van der Horst, van Steeg et al. 1997, Lombard, Beard et al. 2000, Yeo, Becherel et al. 2014).

For these reasons, it would be useful to have a panel of immortalized human KO cell lines for studying SSBR. With the advent of CRISPR-Cas9 mediated gene editing technology, this is now feasible. This chapter will describe the generation of three novel KO cell lines derived from human diploid retinal pigmented epithelium (RPE-1) cells. These cells were chosen for several reasons. Firstly, they are not tumour-derived and instead were initially generated

by human telomerase reverse transcriptase (hTERT) – mediated immortalization of the non-cancerous RPE-340 cell line, in a landmark study which was first to employ this technique (Bodnar, Ouellette et al. 1998). Consequently, the cells have a relatively normal karyotype (modal chromosome number of 46, present in >90% of cells) when compared to other commonly used human cell lines, which are often remarkably polyploid. This is important because the hyperploidy of tumour-derived cell lines, such as U2OS (hypertriploid), is likely to result in altered gene dosage and may have phenotypic consequences (Birchler and Veitia 2012). Also, from a practical perspective, lower ploidy is likely to improve efficiency of KO generation (H. Hanzlikova and N. Hegarat, personal communication; and (Horii and Hatada 2015).

CRISPR-Cas9 is a technology which utilizes components of the prokaryotic adaptive immune system (Mojica, Diez-Villasenor et al. 2005, Pourcel, Salvignol et al. 2005) to introduce precise and specific site-directed alterations to genomic DNA (Cong, Ran et al. 2013, Mali, Yang et al. 2013). This is typically accomplished by transient coexpression of two components: the RNA-directed deoxyriboendonuclease Cas9, and a guide RNA (gRNA) comprised of a structural region and a region which is complementary to the target genomic locus. NLS-tagged Cas9 binds to the structural region of the gRNA, which is derived from the trans-activating crRNA; and is directed to the target gDNA locus by the complementary region of the gRNA (Cong, Ran et al. 2013, Mali, Yang et al. 2013). This target sequence must precede a Protospacer Adjacent Motif (PAM), which varies for nucleases of different prokaryotic species (Mojica, Díez-Villaseñor et al. 2009). In the case of the most commonly used nuclease from *Streptococcus pyogenes*, spCas9, the PAM sequence is NGG (Mojica, Díez-Villaseñor et al. 2009). Cas9 subsequently makes a blunt double-strand DNA break three base pairs (bp) upstream of the PAM. This double-strand break is subject to homologous recombination (HR) and non-homologous end joining (NHEJ) repair pathways. Error-free events, such as those which predominate in HR, will restore the target sequence and allow successive rounds of Cas9 activity. Eventually an erroneous repair event is likely to occur, introducing an indel (an insertion or deletion) which disrupts the target sequence and prevents further nuclease activity. If this indel is within an exon

and is not a multiple of three nucleotides in length; a frame shift will occur, which will often lead to the introduction of a premature stop codon downstream. These nonsense transcripts are then detected and degraded by a co-translational surveillance pathway termed Nonsense Mediated Decay (NMD), preventing the expression of the target gene at the protein level (Losson and Lacroute 1979).

4.2. Results

4.2.1. Design of gRNAs for deletion of *TDP1* by CRISPR-CAS9

The Benchling web application (https://benchling.com) was used to design two gRNAs for use in deletion of human *TDP1*. The algorithm was constrained to search for gRNA target loci that were of the form:

5'-GNNNNNNNNNNNNNNNNGG-3'

gRNAs were selected that were 17 bp in length (without PAM), as these truncated gRNAs (tru-gRNAs) have been demonstrated to minimize off-target activity of Cas9 nuclease, without compromising the on-target efficiency (Fu, Sander et al. 2014). Secondly, gRNAs were selected with 5'-guaninosine, because this aids efficient transcription from the U6 promoter present on the gRNA expression plasmid. Thirdly, only gRNA loci with a PAM sequence of the form NGG were selected, which is the consensus PAM sequence for the *S. pyogenes* Cas9 used in this protocol (Mojica, Díez-Villaseñor et al. 2009). Finally, the search was confined to the first exon of *TDP1*, to maximise the chance of a frame-shift nonsense mutation at the beginning of the coding sequence. The Benchling algorithm identified a number of potential gRNA sequences which were ranked by an Off-target Score, which is defined based on a previous study (Hsu, Scott et al. 2013). High scoring candidate sequences were aligned to the human genome (BLAST) to look for potential off-target loci (https://blast.ncbi.nlm.nih.gov). Two gRNA sequences were identified (5'-GAGGUAGAUGGCUUGUCUGG and 5'-GACGAGUAUGAGACAUCAGG), and are hereafter referred to as gRNA TDP1.1 and TDP1.2, respectively. The positions of these target loci are indicated in Fig. 4.1.

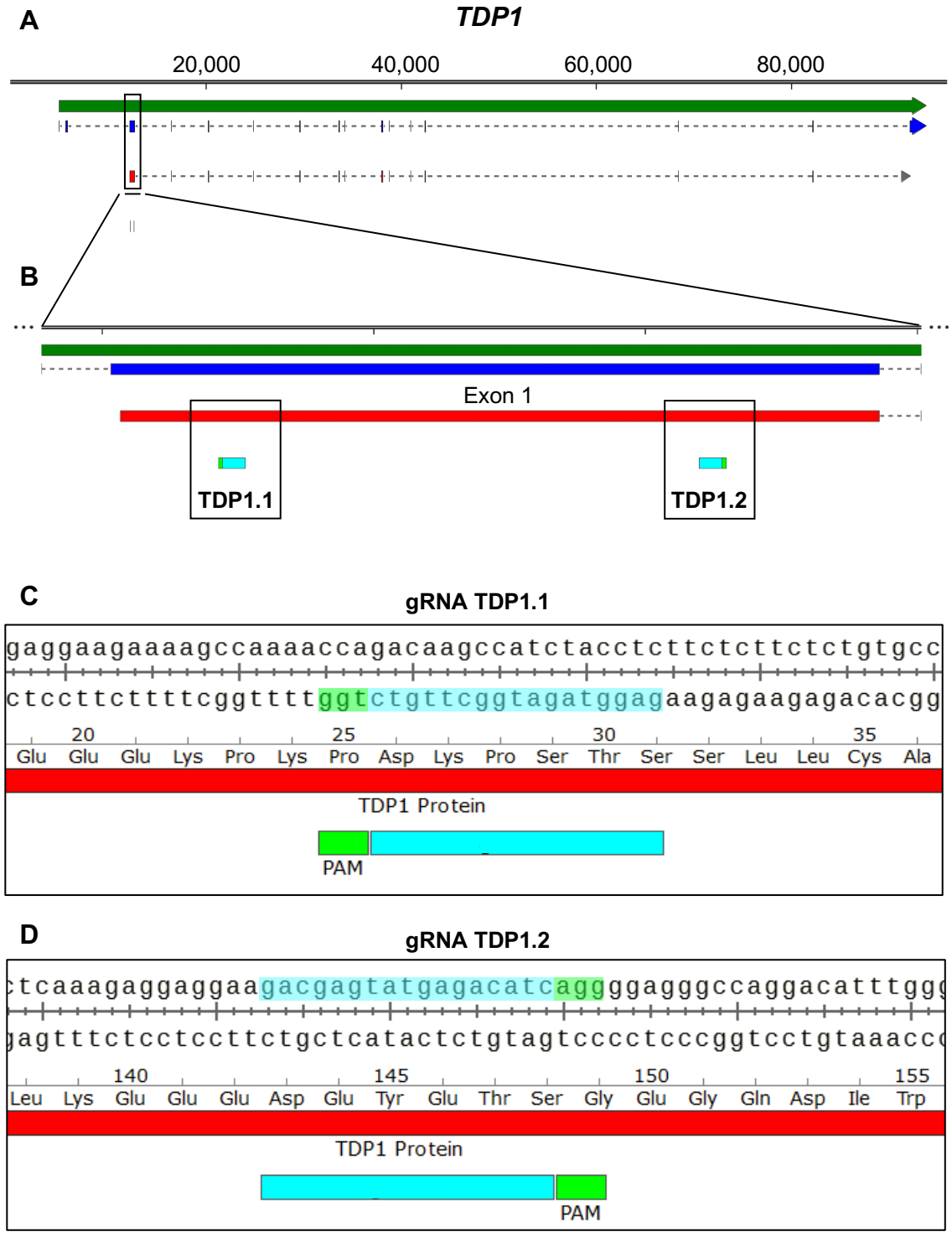

Figure 4.1. The genomic loci targeted by gRNAs TDP1.1 and TDP1.2. Full length *TDP1* gene (dark green), mRNA (dark blue) and protein coding (red) sequences are depicted **(A)**. The region of exon 1 containing the loci targeted by gRNA TDP1.1 and TDP1.2 is enlarged in **(B).** The target loci of gRNAs TDP1.1 and TDP1.2 are further enlarged in **(C)** and **(D)**, respectively.

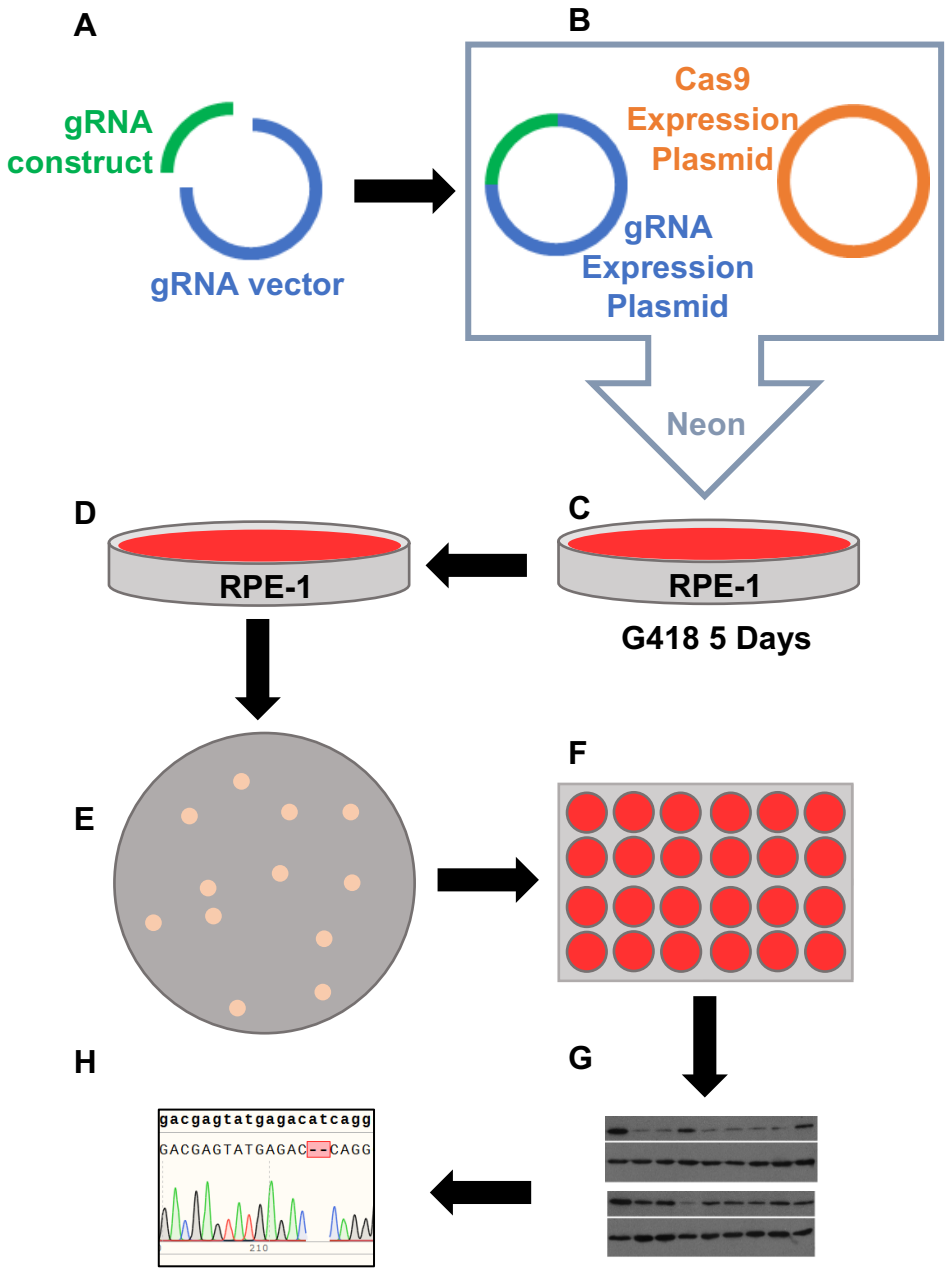

Figure 4.2. An overview of the CRISPR-Cas9 method. gRNA constructs were assembled and cloned into the gRNA vector to generate the gRNA expression plasmid (**A**). This was cotransfected with the Cas9 expression vector into RPE-1 cells by Neon nucleofection (**B**). Cells were selected for five days with G418 antibiotic (**C**), prior to plating at low density (**D**). After two weeks incubation in antibiotic-free media (**E**), single colonies were passaged to duplicate wells of 24-well plates (**F**). After one week, confluent wells were lysed and screened by western blot for absence of the target protein (**G**). Positive KO clones were expanded and further characterized by PCR and Sanger sequencing (**H**).

4.2.2. Generation of *TDP1*$^{-/-}$ and *XRCC1*$^{-/-}$/*TDP1*$^{-/-}$ RPE-1 cells

The CRISPR-Cas9 genome editing protocol employed herein is depicted in Fig. 4.2. Firstly, oligodeoxynucleotides encoding gRNAs TDP1.1 and TDP1.2 were cloned into a previously reported expression plasmid (Mali, Yang et al. 2013), to generate plasmids pGR.TDP1.1 and pGR.TDP1.2, respectively. These plasmids were co-transfected with the Cas9 expression plasmid (Mali, Yang et al. 2013) into RPE-1 cells using the Neon nucleofection system. After twenty-four hours, complete media containing 0.5 mg/ml G418 was added and cells were incubated for five days. This strategy of antibiotic selection for five days only was chosen to eradicate non-transfected cells, based on the G418 resistance cassette present on the Cas9 expression construct, whilst minimising the likelihood of selecting for stable Cas9 integrants. After selection, cells were trypsinised and plated at low density. Following two weeks incubation in antibiotic-free media, colonies were selected and seeded individually into duplicate wells of a 24-well dish. After a subsequent week of incubation, confluent wells were lysed directly in Laemmli Buffer (LB) and subjected to SDS-PAGE and Western Blot (WB) with anti-TDP1 and anti-actin antibodies (Fig. 4.3.a).

TDP1 protein was present in all sixteen clones selected following transfection with pGR.TDP1.1, suggesting inefficient Cas9 nuclease activity with this gRNA sequence. One clone (#5C6) appeared to have a small insertion, leading to a shift in the TDP1 band. Additionally, one clone (#1B2) may have had reduced TDP1 protein levels, but this was inconclusive due to poor loading in this lane. By contrast, five out of ten clones transfected with pGR.TDP1.2 appeared to have absent or minimal TDP1 expression. Five of the apparent KO clones (#4A2, #4A4, #4B3, #4B4 and #4B5) were expanded and the WB repeated (Fig. 4.3.b). WT RPE-1 cell lysate was used as a positive control for TDP1 protein. Lysate from RPE-1 cells transiently transfected with Cas9 expression plasmid alone was used as a positive control for expression of Cas9. Four clones (#4A2, #4B3, #4B4 and #4B5) again exhibited an absence of TDP1 protein, under the conditions employed. These clones also lacked Cas9 expression, suggesting that the Cas9 expression cassette was not stably integrated. A band that migrated slightly faster than WT TDP1 was detected in clone #4A4, suggesting an in-frame

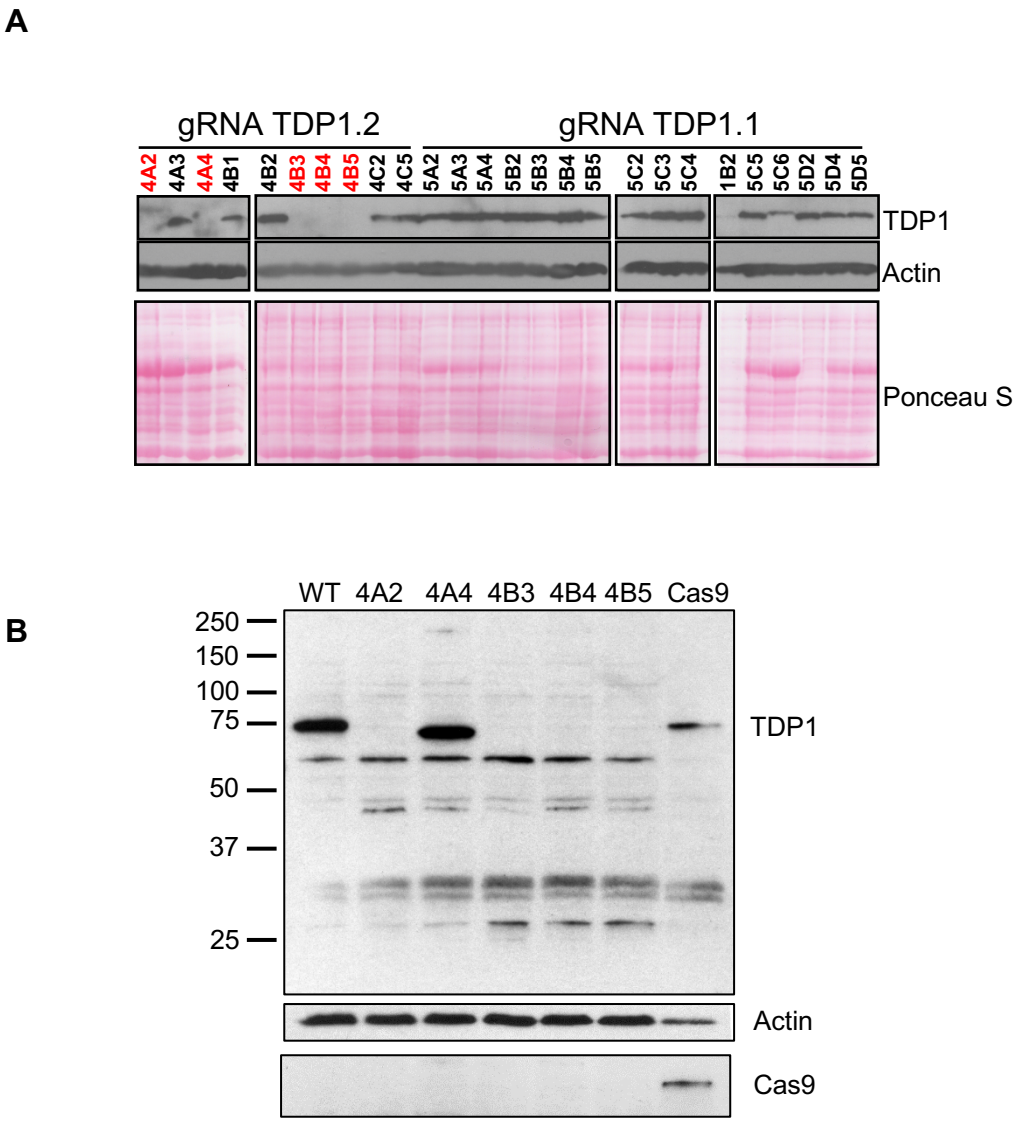

Figure 4.3. Screening for *TDP1*$^{-/-}$ RPE-1 clones by Western blot. Isolated RPE-1 clones processed as in Fig. 4.2. were subjected to Western blotting with anti-TDP1 and anti-actin antibodies (**A**). Highlighted clones (red) were expanded and subjected to repeated WB (**B**). Note the apparent absence of TDP1 protein in #4A2, #4A4, #4B3, #4B4 and #4B5. WT cells transiently expressing Cas9 alone were used as a control to demonstrate the absence of stable Cas9 expression in the *TDP1*$^{-/-}$ RPE-1 clones. A molecular weight marker was included, indicating the approximate molecular weight in KDa.

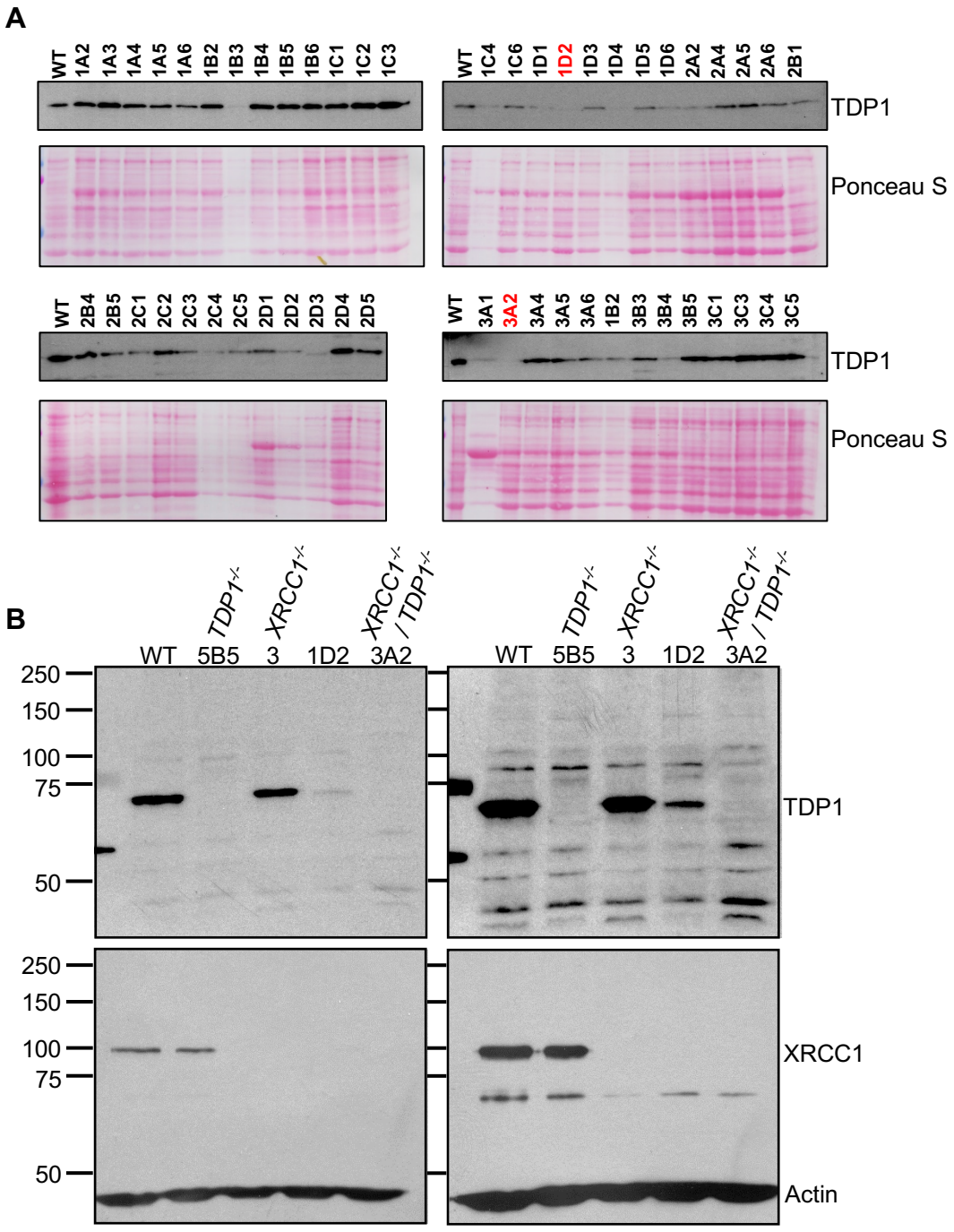

Figure 4.4. Screening for *XRCC1*$^{-/-}$/ *TDP1*$^{-/-}$ RPE-1 clones by Western blot. Isolated RPE-1 clones were subjected to SDS-PAGE and Western blotting with Ponceau S staining and anti-TDP1 antibody (**A**). Highlighted clones (red) #1D2 and #3A2 were expanded and WB repeated. WT, *TDP1*$^{-/-}$, *XRCC1*$^{-/-}$ RPE-1 cell lysates were included as controls (**B**). Note the apparent absence of TDP1 and XRCC1 proteins in #3A2. A molecular weight marker was included, indicating the approximate molecular weight in KDa.

deletion. Clone #4B5 was selected for more extensive characterization by sequencing.

Next, pGR.TDP1.2 was co-transfected with Cas9 expression plasmid to delete TDP1 in *XRCC1*$^{-/-}$ RPE-1 cells (#3). This *XRCC1*$^{-/-}$ RPE-1 cell line was previously generated by co-workers in the Caldecott laboratory. Fifty-one clones were screened by WB for TDP1 (Fig. 4.4.). Of these clones, two appeared to have low or absent TDP1 protein (#1D2 and #3A2), and repeated WB confirmed the absence of both XRCC1 and TDP1 in #3A2. In contrast, a low level of TDP1 was observed in #1D2, suggesting deletion of TDP1 was incomplete.

4.2.3. Sanger sequencing of the gDNA 2 locus in *TDP1*$^{-/-}$ (#4B5) and *XRCC1*$^{-/-}$/*TDP1*$^{-/-}$ (#3A2) RPE-1 cells

To determine the mutations introduced in *TDP1*$^{-/-}$ RPE-1 #4B5 and *XRCC1*$^{-/-}$/*TDP1*$^{-/-}$ RPE-1 #3A2, genomic DNA was extracted and PCR was conducted using primers flanking the gRNA TDP1.2 target locus (277 bp amplicon). As a control, gDNA from WT RPE-1 cells was subjected to the same PCR. Separation of the PCR products by 1% agarose electrophoresis revealed a band in WT and #4B5 at the expected size of 277 bp, indicating that any indels in #4B5 must be smaller than the size resolution of the gel (Fig. 4.5.a). In contrast, the PCR product with #3A2 gDNA was ~200 bp larger, indicating a larger insertion. PCR products were purified and cloned, and expanded in DH5α. DNA prepared from multiple bacterial colonies was then Sanger sequenced (eight bacterial colonies each). Alignment of the resulting sequencing reads to the reference genome revealed mutations in #4B5 and #3A2 cells (Fig. 4.5.b). Of the eight mutated PCR clones in #4B5, five had a deletion of “AT” and three had an insertion of “C” at the target locus. Given that RPE-1 are diploid, the presence of two mutations in a single clone suggests that both alleles have been successfully targeted, resulting in a compound heterozygous mutant. Both the insertion and deletion mutations result in a +1 frame shift and the introduction of premature stop codons at the 161st and 160th amino acids, respectively (Fig. 4.5.c). No evidence was found for a truncated TDP1 protein by WB, using a polyclonal antibody raised against the first fifty amino acids of TDP1. This suggests that the mutant TDP1 mRNA is subject to nonsense-mediated decay (NMD).

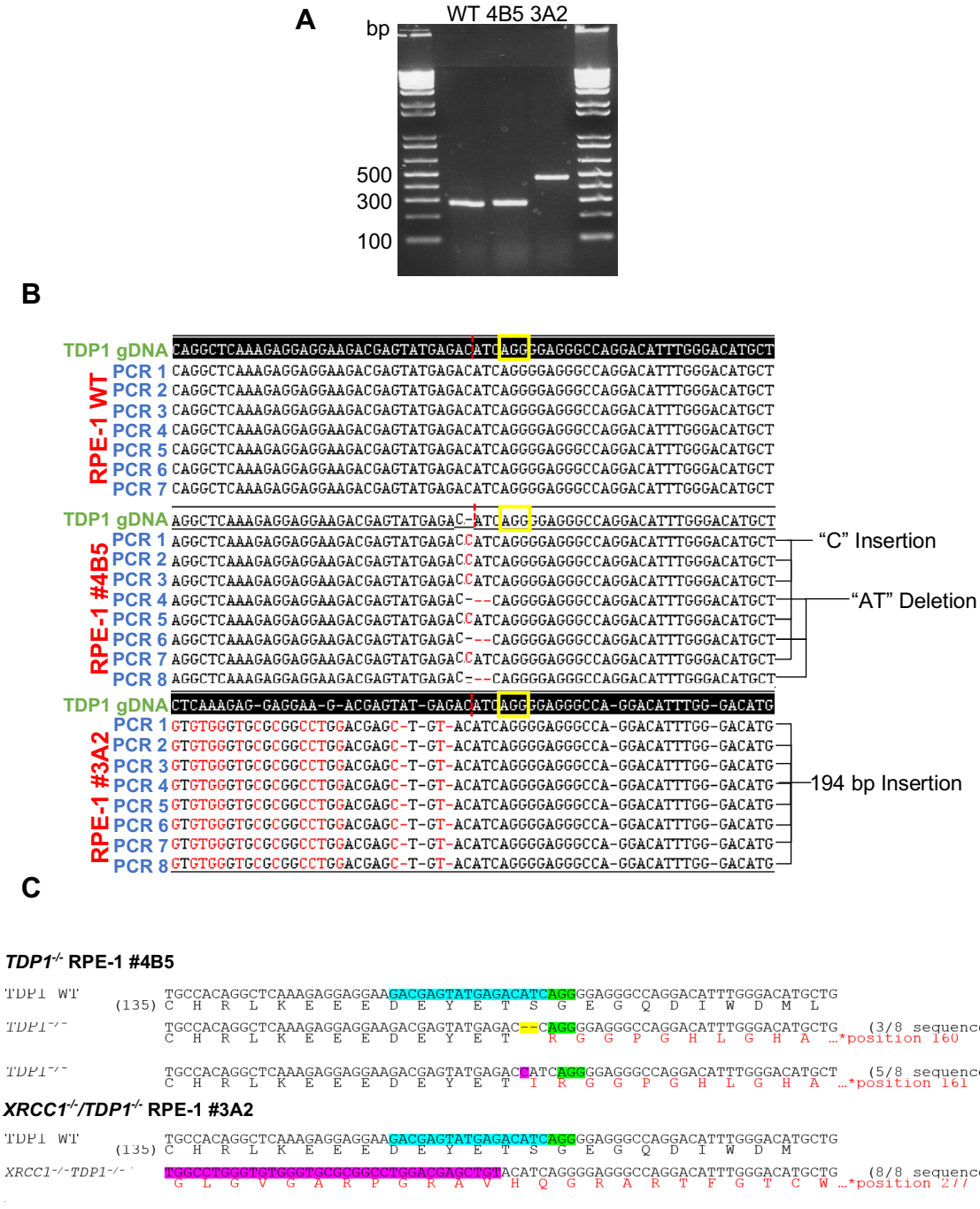

***TDP1*$^{-/-}$ RPE-1 #4B5**

***XRCC1*$^{-/-}$/*TDP1*$^{-/-}$ RPE-1 #3A2**

Figure 4.5. PCR and Sanger sequencing of the gRNA TDP1.2 target locus in RPE-1 WT, *TDP1*$^{-/-}$ #4B5 and *XRCC1*$^{-/-}$/*TDP1*$^{-/-}$ #3A2. The products of PCR with primers spanning the target locus in WT RPE-1, *TDP1*$^{-/-}$ #4B5 and *XRCC1*$^{-/-}$/*TDP1*$^{-/-}$ #3A2 were subjected to 1% agarose electrophoresis **(A)**. PCR products were purified, Topo-cloned, and Sanger sequenced. Alignment to *TDP1* gDNA from the reference genome reveals 7/7 WT PCR clones from RPE-1 WT, 8/8 mutated PCR clones from #4B5 and 8/8 mutated PCR clones from #3A2 **(B)**. The PAM and CRISPR cut site are indicated by a yellow box and red dashed line, respectively. Of the eight mutated PCR clones in #4B5, five had an insertion of "C", and three had a deletion of "AT". Both of the mutations in #4B5 result in a +1 frame shift, leading to premature stop codons being introduced at the 161st and 160th amino acid, respectively. The 194 bp insertion in #3A2 results in a +2 frame shift and leads to a premature stop codon at the 277th amino acid **(C)**.

Sanger sequencing of the #3A2 PCR products confirmed an insertion of 194 bp at the gRNA TDP1.2 target locus in all eight bacterial clones (Fig. 4.5.b), resulting in a +2 frame shift and the introduction of a premature stop codon at the 277th amino acid (Fig. 4.5.c). Comparison of the sequence to those in the NCBI databases using BLAST revealed 100% homology to several plasmid sequences (https://blast.ncbi.nlm.nih.gov). Direct comparison with the known sequence of the gRNA expression plasmid revealed that the insertion comprised an out-of-frame fragment of the bleomycin resistance cassette. As for *TDP1*$^{-/-}$ RPE-1 #4B5, the absence of any TDP1 protein detected by WB suggested that the #3A2 mutant mRNA is subject to NMD.

4.2.4. Generation of *PARP1*$^{-/-}$/*PARP2*$^{-/-}$ RPE-1 cells

To generate *PARP1*$^{-/-}$/*PARP2*$^{-/-}$ cells, *PARP1*$^{-/-}$ RPE-1 (#G7) cells were co-transfected with pGR.PARP2 and Cas9 expression plasmids. Both *PARP1*$^{-/-}$ RPE-1 (#G7) cells and the pGR.PARP2 plasmid were generated previously by co-workers in the Caldecott laboratory. Since an anti-PARP2 antibody suitable for IF was available, 96 colonies were screened in glass-bottomed 96-well plates by immunofluorescence (IF). Thirteen clones were selected and subject to WB with anti-PARP2 antibody (Fig. 4.6.a). Of these clones, only one (#E6) appeared to lack PARP2 protein, and this was confirmed by additional WB, including extracts from WT, *PARP1*$^{-/-}$ (#G7) and *PARP2*$^{-/-}$ (#A1) cells as controls (Fig. 4.6.b and 4.6.c). *PARP2*$^{-/-}$ RPE-1 (#A1) cells were also generated previously by co-workers in the Caldecott laboratory.

4.2.5. Levels of SSBR proteins in a panel of RPE-1 KO cell lines.

The *TDP1*$^{-/-}$, *XRCC1*$^{-/-}$/*TDP1*$^{-/-}$ and *PARP1*$^{-/-}$/*PARP2*$^{-/-}$ RPE-1 cells generated in this chapter join a panel of RPE-1 KO cell lines generated by other members of the laboratory. It is known that many proteins involved in SSBR heterodimerise. Loss of one protein in the heterodimer can destabilise the interacting partner. One example which has been repeatedly demonstrated in the literature is the XRCC1-Lig3α interaction (Caldecott, Tucker et al. 1995). To check for other such interactions, cell lysates from the panel of RPE-1 cell lines were subjected to

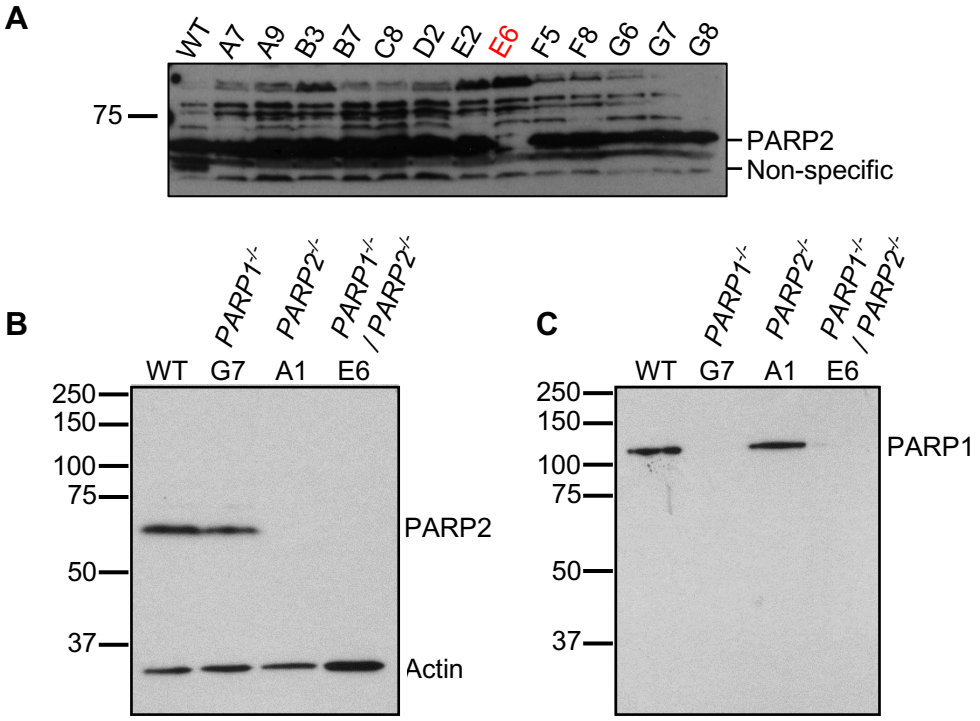

Figure 4.6. Screening for *PARP1*$^{-/-}$/*PARP2*$^{-/-}$ RPE-1 clones by Western blot. Thirteen isolated RPE-1 clones with low or absent PARP2 immunofluorescence were subjected to Western blot with anti-PARP2 antibody (**A**). Clone #E6 was expanded and subjected to Western blotting with anti-PARP2 **(B)**, anti-actin (**B**) and anti-PARP1 antibodies (**C**). Included are cell lysates from WT, *PARP1*$^{-/-}$ and *PARP2*$^{-/-}$ RPE-1 cells. Note the apparent absence of PARP1 and PARP2 proteins in clone #E6. A molecular weight marker was included, indicating the approximate molecular weight in KDa.

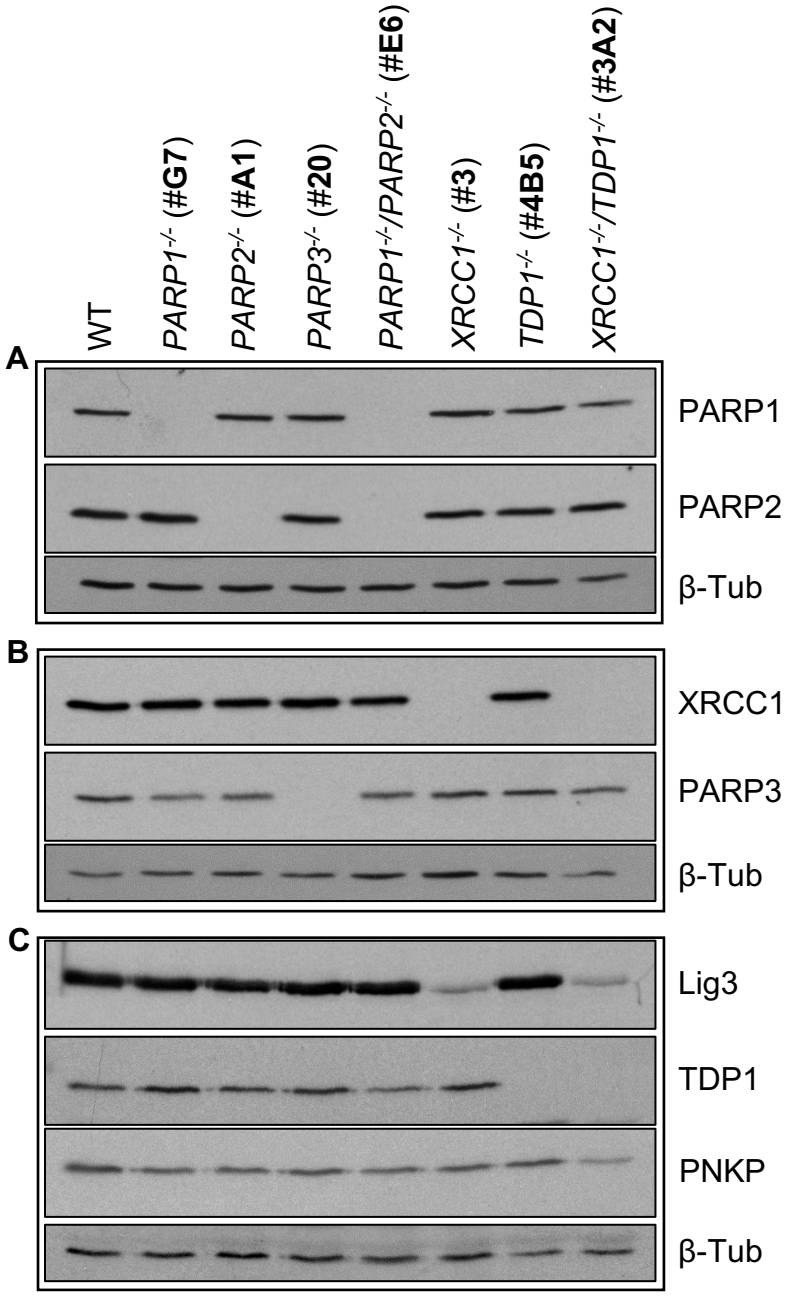

Figure 4.7. The levels of SSBR proteins in a panel of RPE-1 KO cell lines. Cell lysates containing 30 µg of total protein, from the indicated genotypes, were subjected to SDS-PAGE and Western blotting with antibodies targeting PARP1, PARP2, PARP3, XRCC1, TDP1, Lig3, PNKP and β-Tub (**A, B and C**). Total protein loading revealed by Ponceau S staining of **A, B and C** is shown overleaf (**C, D and E,** respectively**)**.

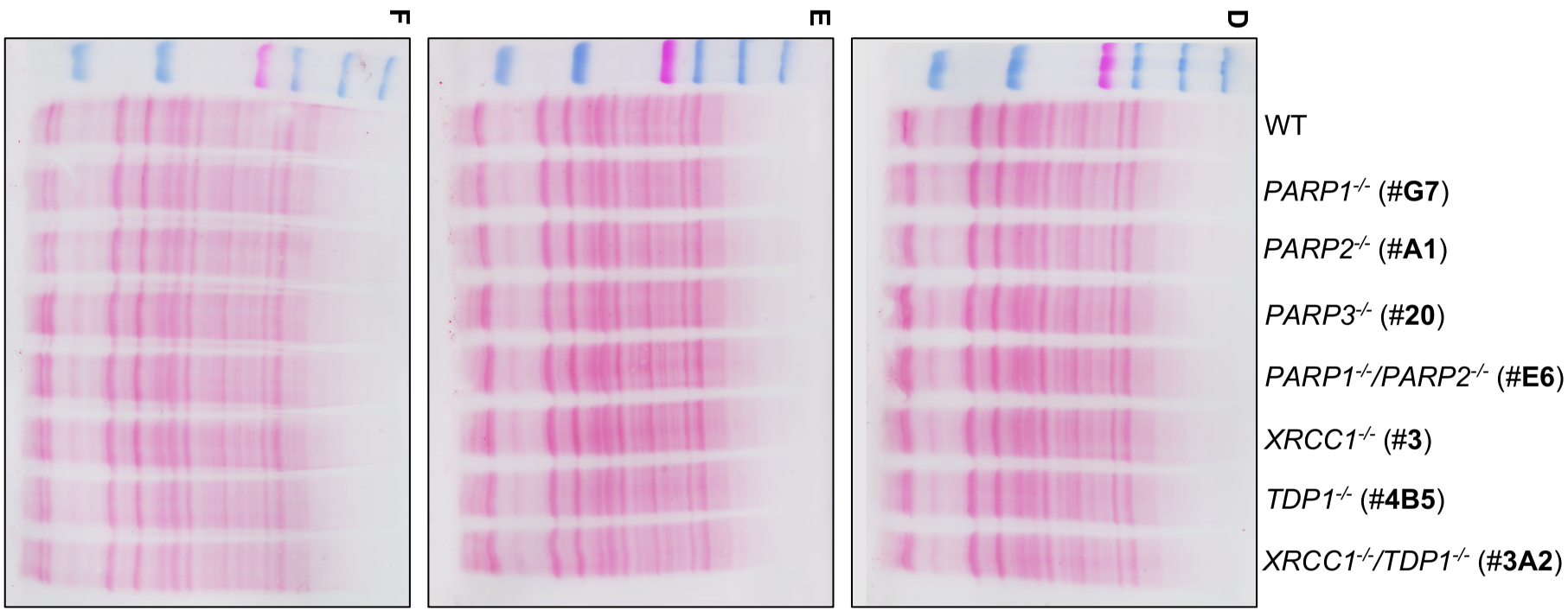
F
E
D
WT
PARP1-/- (#G7)
PARP2-/- (#A1)
PARP3-/- (#20)
PARP1-/-/PARP2-/- (#E6)
XRCC1-/- (#3)
TDP1-/- (#4B5)
XRCC1-/-/TDP1-/- (#3A2)

SDS-PAGE, and WB with antibodies targeting PARP1, PARP2, PARP3, XRCC1, Lig3α, TDP1, PNKP and β-Tub (Fig. 4.7.). As reported previously (Caldecott, Tucker et al. 1995), loss of XRCC1 was seen to significantly destabilize Lig3α. PNKP is another protein which interacts directly with XRCC1 (Whitehouse, Taylor et al. 2001). However, loss of XRCC1 did not appear to destabilize PNKP, nor any of the other proteins examined here. Furthermore, in each of the other knockout cell lines, only the targeted protein was absent, with no apparent depletion of the other examined SSBR factors.

4.3. Conclusions and Discussion

The mutations characterized in *TDP1*$^{-/-}$ and *XRCC1*$^{-/-}$/*TDP1*$^{-/-}$ RPE-1 cells can be compared to those identified in other CRISPR-generated RPE-1 KO cell lines, including the *PARP1*$^{-/-}$/*PARP2*$^{-/-}$ cells generated herein (Fig. 4.8.). In every case, the indels occur precisely at the position of the Cas9-induced double strand break. Seven out of eight of the sequenced mutations were small indels of one or two bp. This is expected based on the prevalent model of CRISPR-Cas9-induced mutagenesis, which posits that the small insertions and deletions introduced at most target loci result from the activity of nucleases (Ma, Pannicke et al. 2002) and the PolX family of DNA polymerases functioning within the NHEJ repair pathway (Yang, Guell et al. 2013, Bétermier, Bertrand et al. 2014). The PolX family can catalyse DNA polymerisation across discontinuous templates. The members of this family are variously able to add entirely untemplated nucleotides or nucleotides templated from downstream positions, resulting in insertions or deletions, respectively (Ramadan, Maga et al. 2003, Ramadan, Shevelev et al. 2004, Bertocci, De Smet et al. 2006).

Only one out of eight of the mutations (detected in *XRCC1*$^{-/-}$/*TDP1*$^{-/-}$ RPE-1 #3A2) was a longer insertion (194 bp). No significant microhomology was found at either end of the insertion, and there was no loss of genomic or gain of untemplated nucleotides, suggesting that this event may have occurred by direct ligation of the blunt-ended fragments within c-NHEJ. It is important to note that mutations detected may be the result of rare events of infidelity. However, given that error-free repair by HR or c-NHEJ would result in restoration of the gRNA

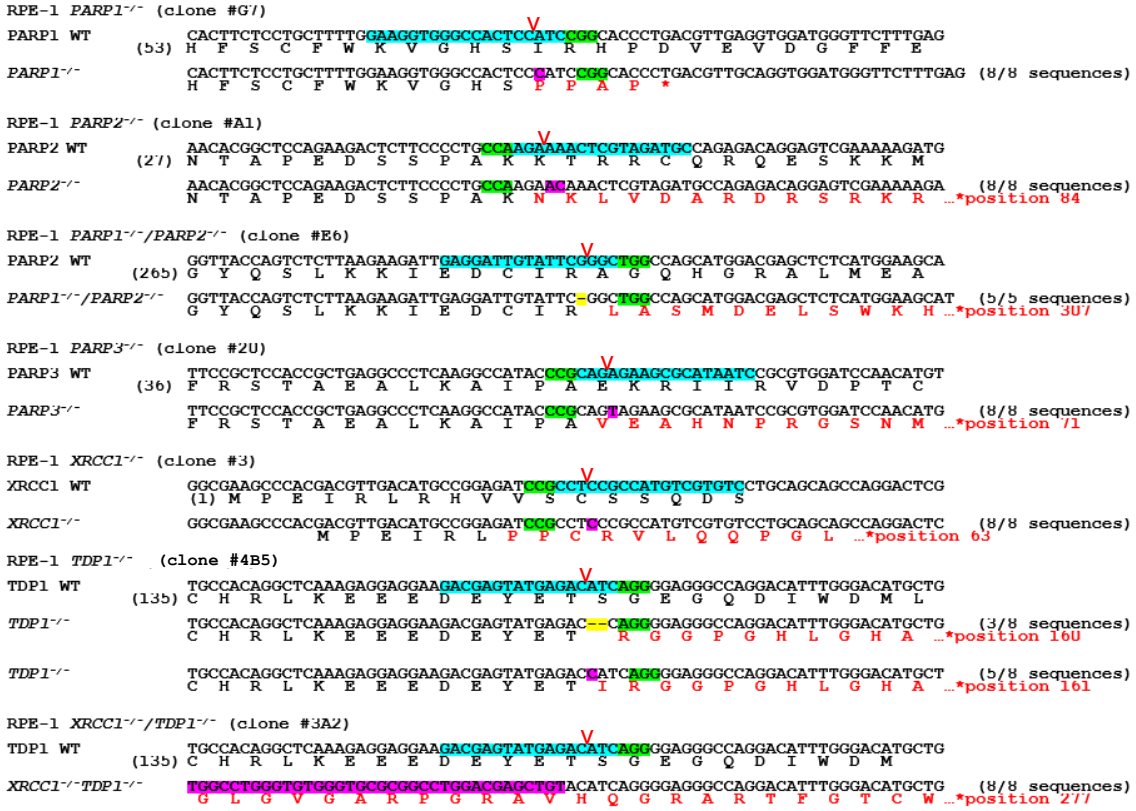

Figure 4.8. Sanger sequenced mutations at gRNA loci in a panel of RPE-1 KO cell lines. The gRNA target loci in the indicated RPE-1 clones were sequenced as described herein for RPE-1 #4B5 and #3A2 **(Z. Zeng)**. The sequenced PCR products were aligned to the target loci sequences from the reference genome. The positions of the gRNA target sequence and PAM are indicated in cyan and green, respectively. The position of the Cas9-induced double-strand break is indicated by a red arrow. Frame-shift insertions and deletions in the sequenced PCR products are indicated in magenta and yellow, respectively. The resulting amino acid changes are indicated in red. Positions of premature stop codons (*) are given in number of amino acids.

target sequence, successive rounds of Cas9 cleavage would likely result in mutation eventually. Notably, in all but one RPE-1 cell line (*TDP1*$^{-/-}$ #4B5) only a single mutation was detected. The surprising frequency of homozygous indels has been reported previously in the literature (Li, Wang et al. 2014). Given that the PCR amplicon was 200-300 bp in each case, it is not possible to rule out that larger indels allow some alleles to escape amplification and lead to their underrepresentation. Alternatively, these may be real homozygous mutations. This could feasibly result from a gene conversion event which transfers the nascent mutation of one allele to the other. The frequency of G1 interallelic HR events is thought to be very low in mammals (Liang, Han et al. 1998, Johnson and Jasin 2000), which is compensated for by the efficiency of NHEJ in G1. However, given the high efficiency of the Cas9 nuclease, an intact sister chromatid may not be available in S/G2; which may bias HR towards utilizing the only available intact and homologous template: that of the other mutated allele.

The RPE-1 knockout cell lines generated herein, along with those generated by co-workers in the Caldecott laboratory, were characterized by WB using antibodies targeting SSBR factors. Lig3α exists as an obligate heterodimer with XRCC1, such that loss of XRCC1 leads to pronounced destabilization of Lig3α (Caldecott, Tucker et al. 1995), as observed here. Given that abortive ligation at non-canonical termini results in 5'-AMP generation (Ahel, Rass et al. 2006), this may be an evolutionary adaption to prevent unscheduled Lig3α activity in the absence of chaperoning by XRCC1. By comparison, no destabilization of PNKP was observed upon loss of XRCC1. This may be explained from an evolutionary perspective by a requirement for a pool of free PNKP. The PNKP-XRCC1 interface overlaps with that of XRCC1-APLF and XRCC1-APTX and these interactions are thought to be mutually exclusive (Luo, Chan et al. 2004, Ahel, Rass et al. 2006, Rass, Ahel et al. 2007). The presence of the CK2 phosphorylation motif in the shared interface suggests that the affinities of these interactions may be fine-tuned by phosphorylation and/or other post-translation modifications (Luo, Chan et al. 2004). CK2 is a ubiquitously-expressed and well conserved eukaryotic kinase, and its regulation has been the subject of controversy and contradiction (Litchfield 2003). It does appear to be the case that levels of CK2 are higher in highly proliferative cells (Munstermann, Fritz et al.

1990). In this way, it is possible that levels of XRCC1-PNKP, XRCC1-APLF and XRCC1-APTX may be regulated according to cell type or proliferative state. More elaborately, the regulation may occur on an *ad-hoc* basis at specific lesions or repair intermediates, although this has yet to be demonstrated. Given the non-constitutive nature of these interactions (as opposed to the XRCC1-Lig3α interaction), XRCC1-free stability of PNKP, APLF and APTX would be required.

PARP1 and PARP2 have been reported to heterodimerise (Schreiber, Amé et al. 2002). Here it was found that loss of either did not result in destabilization of the other, nor indeed of PARP3, confirming that whilst these proteins may heterodimerise, these interactions do not provide reciprocal stabilization. Furthermore, whilst PARP1 has been reported to interact directly with TDP1 (Das, Huang et al. 2014), reciprocal stabilization was not observed here.

In conclusion, this chapter has described the generation and characterization of three novel diploid human cell lines with knockout mutations in *TDP1* (RPE-1 #4B5), *XRCC1* and *TDP1* (RPE-1 #3A2) or *PARP1* and *PARP2* (RPE-1 #E6). These join a panel of RPE-1 cell lines with KO mutations in other SSBR genes. In Chapters Six and Seven these cell lines will be used to investigate fundamental features of human SSBR.

Chapter Five

Establishing High Content Imaging Methods for the Sensitive Quantification of ADP-ribose and Chromatin-associated XRCC1

5.1. Introduction and aims

Rapid and extensive nuclear ADP-ribosylation is a well-documented response to many DNA damaging agents, including H_2O_2 (Schraufstatter, Hinshaw et al. 1986, Cantoni, Cattabeni et al. 1989). One aim of this chapter is to introduce a methodology for the sensitive quantification of this ADP-ribose. In the past, this has typically been achieved by Immunofluorescence (IF) or Western Blot (WB) using an antibody raised against a heterogenous poly(ADP-ribose) (PAR) antigen. One such antibody which has been used extensively in the literature is the 10H monoclonal antibody (Kawamitsu, Hoshino et al. 1984). This has proved popular due to its reported ability to recognise ADP-ribose from a variety of sources, including PARP1, PARP2 and PARP3. However others have reported that 10H fails to recognize mono-ADP-ribose (MAR) and oligo-ADP-ribose (OAR) (Kraus 2015, Vivelo and Leung 2015), such as that produced by PARP3. Indeed, the initial study reporting generation of this antibody found that the PAR-10H interaction was only weakly inhibited by competition with the smallest structural unit of PAR, iso-ADP-ribose, and not at all by ADP-ribose (Kawamitsu, Hoshino et al. 1984). Furthermore, a subsequent study revealed that one 63mer PAR molecule is bound by twenty-one 10H molecules, suggesting a binding stoichiometry of one 10H antibody to every 3-4 ADP-ribose units (Fahrer, Kranaster et al. 2007). In this chapter, the sensitivity of the 10H antibody will be compared with other available reagents, including the pan-ADP-ribose binding reagent. This commercial reagent is a recombinant protein composed of a rabbit immunoglobulin fragment crystallisable (Fc) domain fused to a macrodomain (Kraus 2015). The specific identity of this macrodomain is proprietary but it has been demonstrated to recognize MAR, OAR and PAR with high affinity (Kraus 2015, Gibson, Zhang et al. 2016).

XRCC1 has been demonstrated previously to relocate to into subnuclear foci in response to oxidative DNA damage (El-Khamisy, Masutani et al. 2003), supporting the role of this protein in promoting BER/SSBR. Chromatin binding by a protein of interest has traditionally been observed by several different approaches. Biochemical fractionation of cell extracts can yield chromatin-enriched samples which can then be subjected to SDS-PAGE and WB with appropriate antibodies (Andegeko, Moyal et al. 2001, Cheng, Barboule et al.

2011). Due to the requirement for lengthy serial incubations with various extraction buffers, this method has poor temporal resolution. Other methods have used microscopy to observe relocalization of exogenously overexpressed flurescent protein (FP) -tagged XRCC1 into discrete nuclear foci (El-Khamisy, Masutani et al. 2003). These foci are typically very large and far fewer than the number of H_2O_2-induced single strand breaks reported by more quantitative methods (own observations, and (Breslin, Hornyak et al. 2015)).

Whilst attractive for their ability to be observed in real time in live cells, FP-tagged protein fusions are often exogenously overexpressed at such an elevated level that their behaviour may not accurately reflect that of the endogenous protein (Moriya 2015). Additionally, several high-profile studies have demonstrated that FP-tags have a propensity to dimerise or oligomerise under certain conditions (Zacharias, Violin et al. 2002, Snapp, Hegde et al. 2003, Costantini, Fossati et al. 2012). In particular, a high local concentration of FP-tagged proteins can cause assembly into artefactual macromolecular complexes. Previous studies have investigated this effect for FP-tagged, membrane-associated proteins, where the local concentration is elevated by virtue of 2D confinement (Zacharias, Violin et al. 2002, Snapp, Hegde et al. 2003). It is likely that other mechanisms which dramatically elevate local concentrations of FP-tagged proteins could nucleate similar oligomerisation. One conceivable mechanism is formation of a PAR molecule with multiple binding sites for FP-tagged XRCC1. Initial PAR-binding via the BRCT domain of XRCC1 might be followed by dimerisation via the FP-tag. Conceivably this could lead to clustering of SSBR complexes from independent but proximal lesions. This could explain observation of the large, persisting EGFP-XRCC1 foci which form in response to H_2O_2 exposure (Breslin, Hornyak et al. 2015). It is currently unclear whether endogenous XRCC1 also forms these large macromolecular foci. This chapter aims to establish a method for quantifying endogenous XRCC1 chromatin recruitment which avoids some of the pitfalls of traditional methods.

IF protocols typically involve formaldehyde-fixation of cells prior to a detergent or organic solvent-based membrane permeabilization step which allows access of the antibodies to intracellular epitopes. One notable recent study employed a pre-fixation incubation with cytoskeleton (CSK) buffer containing

Triton X100 and RNAse A to remove soluble nucleoplasmic Ku70, allowing observation of single foci by super resolution microscopy (Britton, Coates et al. 2013). A variation of this method has been widely used in the cytoskeleton field since first being reported (Cramer and Mitchison 1995). The method is attractive for the purposes of this study as it does not require lengthy incubation times prior to fixation, which greatly improves the temporal resolution. During preliminary work on this project it was found that the technique could be adapted further for use with XRCC1 IF (Hana Hanzlikova, unpublished observations). This involved replacing the CSK buffer with PBS, lowering the detergent concentration to 0.2% Triton X100 and shortening the incubation to two min. Additionally, to limit rapid cellular processes during the pre-extraction, the incubation was carried out on ice.

Developments in the automation of microscopy and image processing have led to the emergence of High Content Analysis (HCA). This term is used to describe the algorithmic analysis of multiple parameters of many cells in a population, allowing accurate quantification of cellular phenotypes which would be difficult and time consuming when conducted manually (Zock 2009). Examples of parameters which might be analysed include nuclear size and shape, the distribution of fluorescently labelled proteins and their associated intensity. From these variables, inferences can be made about cell status, such as cell cycle phase (Barabasz, Foley et al. 2006) or apoptosis (Inglefield, Larson et al. 2006). The technique is a particularly powerful drug discovery tool (A. Giuliano, L. DeBiasio et al. 1997), especially when coupled to high throughput screening approaches, such as those employing siRNA (Bjorklund, Taipale et al. 2006) or compound libraries (Vogt, Cooley et al. 2003). In addition to its utility in translational research, HCA is also an effective tool in basic research, owing to the ease with which it can quantify all manner of cellular phenotypes. This chapter will apply HCA to streamline protocols which would be manually unfeasible when conducted with multiple cell lines and treatment conditions.

5.2. Results

5.2.1. Comparison of anti ADP-ribose antibodies and binding reagents

In the interest of establishing protocols with the highest possible sensitivity for ADP-ribose, three detection reagents were tested by WB and IF (Fig. 5.1.). These were the 10H monoclonal antibody, 4336-BPC-100 polyclonal antibody, and the MABE1016 Pan-ADP-ribose binding reagent. For the WB (Fig. 5.1.a, contributing WB from K. Krejcikova), WT RPE-1 cells were pre-incubated or not with 1 or 10 µM KU0058948 PARP inhibitor for one hour prior to treatment with 150 µM H_2O_2 on ice for 10 min in the continued presence of KU0058948. Cells were then lysed and subjected to SDS-PAGE and WB with the three detection reagents. In the absence of H_2O_2 treatment, all three reagents failed to detect any significant immunological signal, suggesting that the level of ADP-ribosylation in unperturbed cells is very low. Upon treatment with H_2O_2, all three reagents successfully detected the presence of ADP-ribosylated proteins. Both the pan-ADP-ribose binding reagent and 4336-BPC-100 polyclonal were able to detect ADP-ribosylation of low molecular weight proteins (<25 KDa), whilst the 10H monoclonal was not. Furthermore, the signal detected with 10H was concentrated at a high molecular weight, possibly reflecting a propensity for binding auto-PARylated PARP1. In all cases, the ADP-ribosylation signal was prevented by co-treatment with 1 and 10 µM KU0058948.

For the IF experiments (Fig. 5.1.b), WT RPE-1 cells growing on glass coverslips were treated as described above, prior to formaldehyde fixation and fluorescent labelling with the three described reagents. In the case of pan-ADP-ribose binding reagent and 4336-BPC-100 polyclonal antibody, a strong pan-nuclear signal was observed upon treatment with H_2O_2. Furthermore, both reagents were able to detect residual H_2O_2-induced ADP-ribosylation signal in the presence of 1 µM but not 10 µM KU0058948. In contrast, the signal detected by 10H monoclonal antibody was dramatically weaker in the H_2O_2 treated cells, and entirely absent upon co-incubation with both 1 and 10 µM KU0058948.

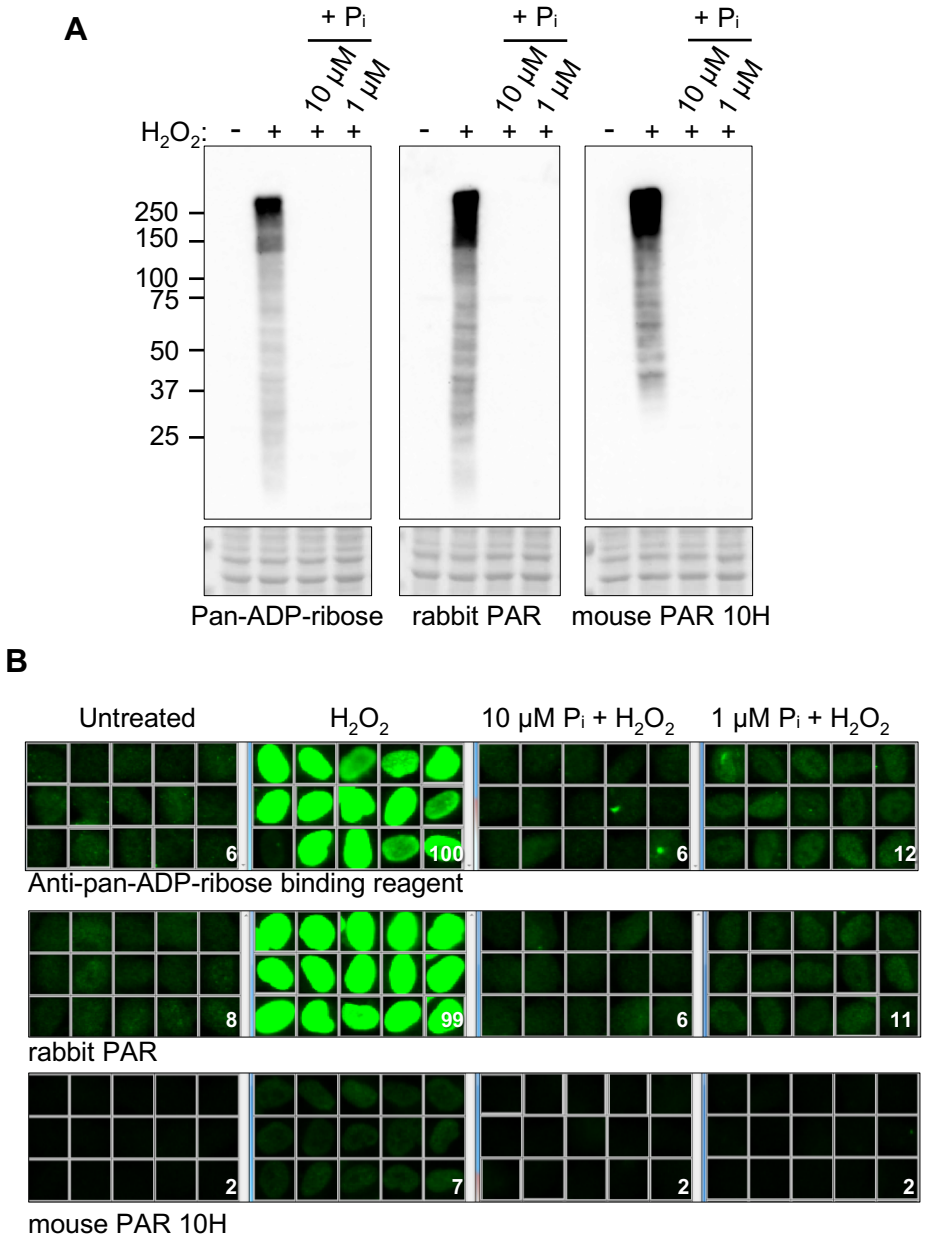

Figure 5.1. Impact of PARP inhibitor on ADP-ribosylation detected using different anti-(ADP-ribose) detection reagents. WT RPE-1 cells were pre-incubated or not with 1 or 10 µM PARP inhibitor KU0058948 (P_i) for 1 h and subsequently treated for 10 min with 150 µM H_2O_2 on ice in the continued presence or absence of PARP inhibitor as indicated. ADP-ribosylated proteins were detected by WB (**A**) or IF (**B**). Corner numbers are the mean nuclear ADP-ribose signal in >1500 cells relative (%) to the signal detected by anti-pan-ADP-ribose binding reagent in H_2O_2-treated cells (set at 100%). Data were quantified by Olympus ScanR acquisition and analysis software. A molecular weight marker was included in the WB, and approximate sizes are indicated in KDa. **Contributing WB from K. Krejcikova**

5.2.2. Limitations of Conventional Chromatin Fractionation Methods

Different techniques were considered for measuring XRCC1 recruitment into chromatin. Firstly, RPE-1 cells were subjected to biochemical fractionation of chromatin by a previously published method (Drouet, Delteil et al. 2005). WT RPE-1 cells were pre-incubated or not with 10 µM KU0058948 PARP inhibitor for 1 hr, and then treated in suspension with 10 mM H_2O_2 for 7 or 15 min in the continued presence or absence of KU0058948. H_2O_2 was quenched with complete media and the cells then lysed and fractionated using buffer containing detergent into soluble and insoluble fractions (see Materials and Methods). Samples were subjected to SDS-PAGE and WB with antibodies targeting XRCC1, Histone 1.2, and with pan-ADP-ribose binding reagent (Fig. 5.2.). Whereas ADP-ribose was not detected in untreated cells in these experiments, a strong ADP-ribose signal was detected in samples from H_2O_2-treated cells which increased with duration of H_2O_2 treatment. This signal was prevented by treatment with the PARP inhibitor KU0058948, consistent with it reflecting protein ADP-ribosylation.

In untreated cells, there was a low level of XRCC1 in the chromatin fraction. Following 7 and 15 min H_2O_2-treatment, XRCC1 progressively increased in the chromatin fraction, and this was inhibited by KU0058948. Despite apparent success in detecting XRCC1 recruitment or retention in chromatin in these experiments, the method was found to be time-consuming and difficult to perform with multiple samples, which resulted in poor reproducibility (data not shown). This makes the technique unsuitable for use with multiple cell lines in parallel. Additionally, whilst quantification is possible, qualitative information, such as the sub-nuclear distribution of signal, is lost. By comparison quantitative IF and high content analysis offer higher throughput and the ability to determine the sub-nuclear distribution of signal. For these reasons, attention turned to a method of chromatin enrichment which could be coupled with IF.

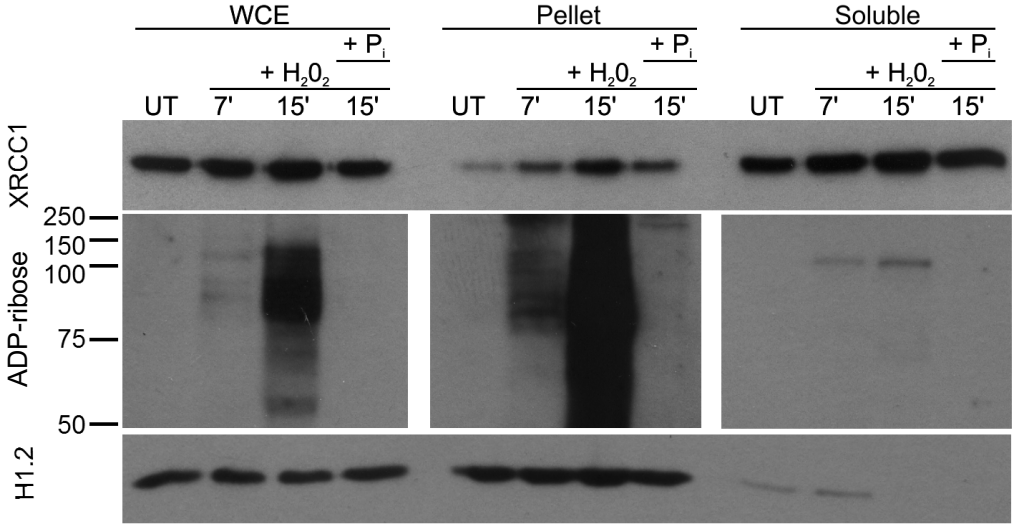

Fig 5.2. H_2O_2 induced DNA damage triggers ADP-ribosylation and recruitment of XRCC1 to the chromatin. RPE-1 cells were trypsinised and washed with PBS prior to being treated for the indicated times with 10 mM H_2O_2 in the presence or absence of 10 μM KU0058948 PARP inhibitor (P_i). H_2O_2 was quenched with complete media and the cells were subjected to biochemical subcellular fractionation. Whole cell extract (WCE), soluble protein and pellet were lysed in Laemmli buffer and subject to 8% SDS-PAGE and WB with antibodies targeting XRCC1, Histone 1.2, or with pan-ADP-ribose binding reagent. A molecular weight marker was included and approximate sizes are indicated in KDa.

5.2.3. Removal of soluble XRCC1 by detergent pre-extraction

Pre-extraction of adherent cells with low concentrations of detergent has been demonstrated previously to remove soluble nuclear proteins, leaving behind chromatin bound proteins and components of the cytoskeleton (Cramer and Mitchison 1995, Britton, Coates et al. 2013). To demonstrate that the pre-extraction is stringent enough to remove soluble nuclear XRCC1, but not chromatin proteins such as histones, untreated WT RPE-1 cells were subjected to IF with anti-XRCC1 and anti-H1 antibodies, with or without pre-extraction (Fig. 5.3.). Without pre-extraction, XRCC1 was observed throughout the nucleus in untreated WT RPE-1 cells. Pre-extraction was found to effectively remove ~90% of the nuclear XRCC1 signal. The residual signal remaining after pre-extraction (10.85%) was specific for XRCC1, as it was further significantly reduced to 4.00% of the non-pre-extracted WT signal in pre-extracted *XRCC1*$^{-/-}$ cells (t-test p-value = 1.02x10^{-2}). Similarly to XRCC1, H1 was observed throughout the nucleus in non-pre-extracted cells, consistent with it being an integral and ubiquitous component of chromatin. However, in comparison to XRCC1, H1 signal was not reduced by pre-extraction (t-test p-value = 2.79x10^{-1}), confirming that the stringency of the technique is suitable for removing only soluble nuclear proteins and not those in the chromatin.

5.2.4. Detergent insoluble XRCC1 co-localizes with the nucleolus in untreated cells

The residual XRCC1 in pre-extracted WT cells appeared to be localized at specific focal sites in the nucleus. To determine if the focal sites reflected nucleoli, pre-extracted WT and *XRCC1*$^{-/-}$ RPE-1 cells were subjected to co-IF with anti-XRCC1 antibody and an antibody targeting the nucleolar phosphoprotein B23 (Fig. 5.4.). The colocalization of B23 and XRCC1 was evident in pre-extracted untreated WT cells. This reflected specific XRCC1 signal because it was absent from *XRCC1*$^{-/-}$ cells immunostained in parallel. In order to delineate the nucleolar and ex-nucleolar XRCC1 fractions, the B23 signal was used to define a sub-object within the DAPI-defined main object (Fig. 5.5.). The main and sub-object, were then used to define nuclear, nucleolar and exnucleolar regions, as detailed in the methods (see section 2.2.8). Unless otherwise stated, all

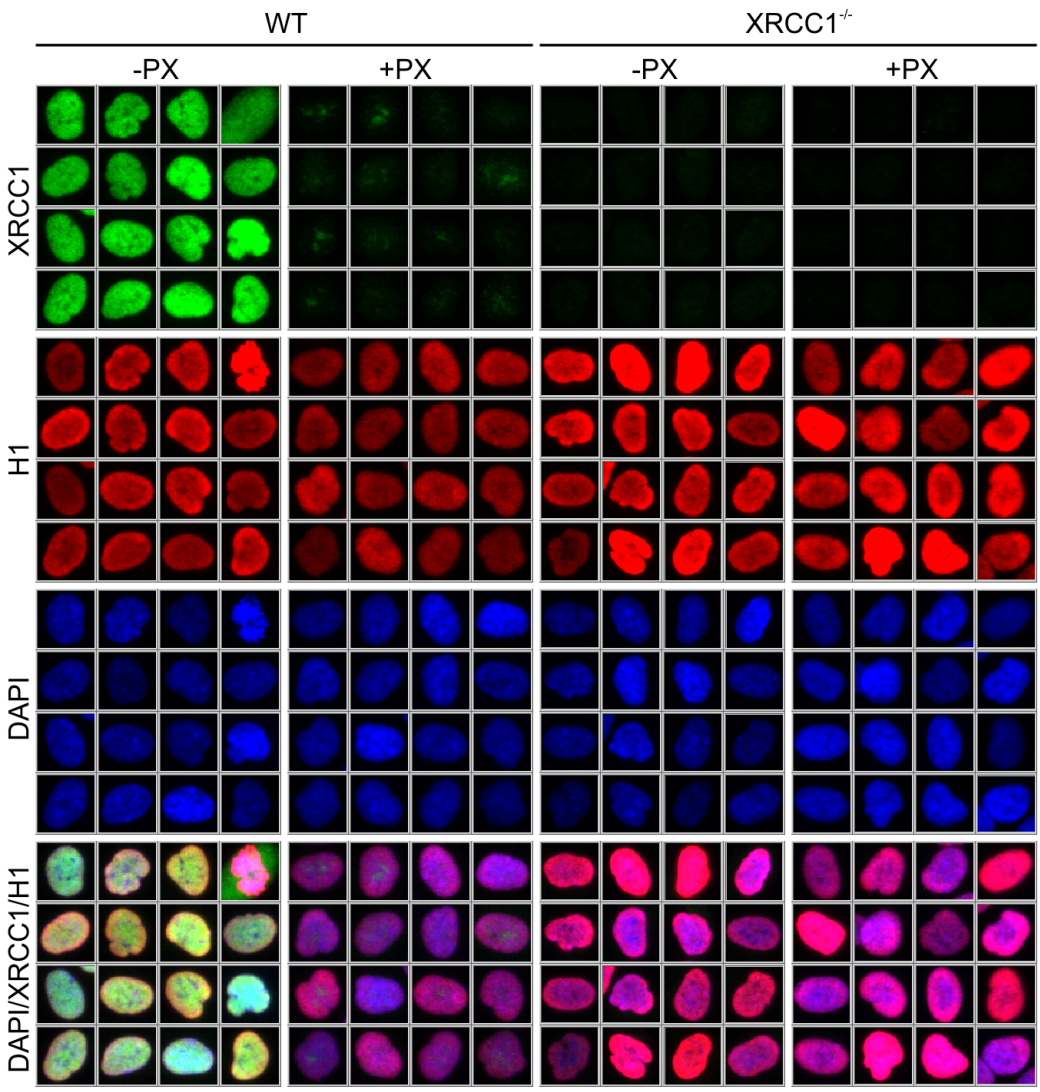

Figure 5.3. Pre-extraction removes soluble nuclear XRRC1 but not chromatin-associated H1. Untreated WT and *XRCC1*$^{-/-}$ RPE-1 cells growing on glass coverslips were formaldehyde fixed with or without pre-extraction (PX). Co-immunolabelling was carried out with antibodies against XRCC1 and H1. Slides were imaged using the Olympus ScanR system and ScanR Analysis software was used to generate galleries of 16 randomly selected cells for each condition **(A)**. XRCC1 fluorescence from >1000 cells was quantified in the nuclear region and is expressed as percentage of WT -PX **(B, overleaf)**. H1 fluorescence from >1000 cells was quantified in the nuclear region and is expressed as percentage of WT -PX **(C, overleaf)**. Data are mean +/- S.E.M from 3 experiments. Statistical significance was calculated by paired student's t-test.

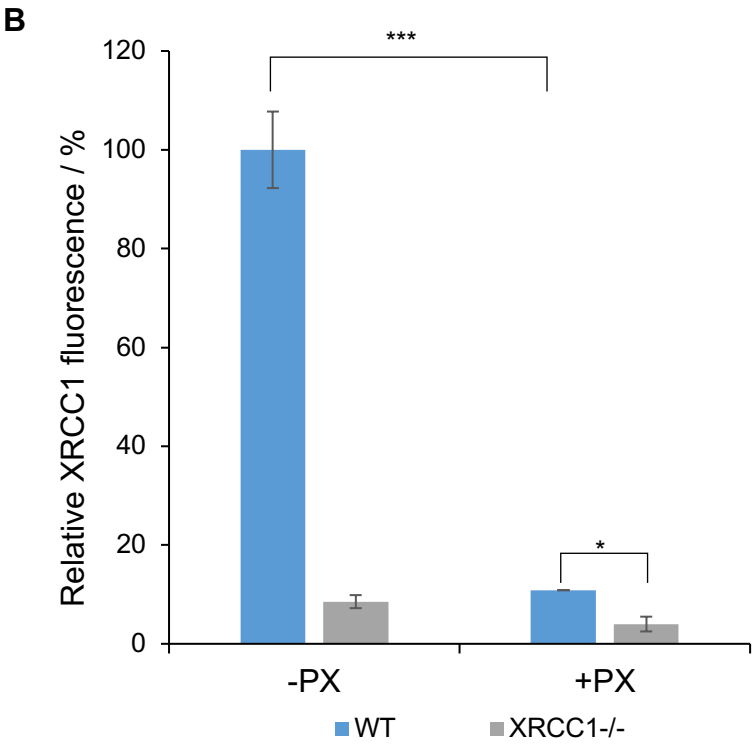
B
***
*
120
100
80
60
40
20
0
Relative XRCC1 fluorescence / %
-PX
+PX
WT
XRCC1-/-

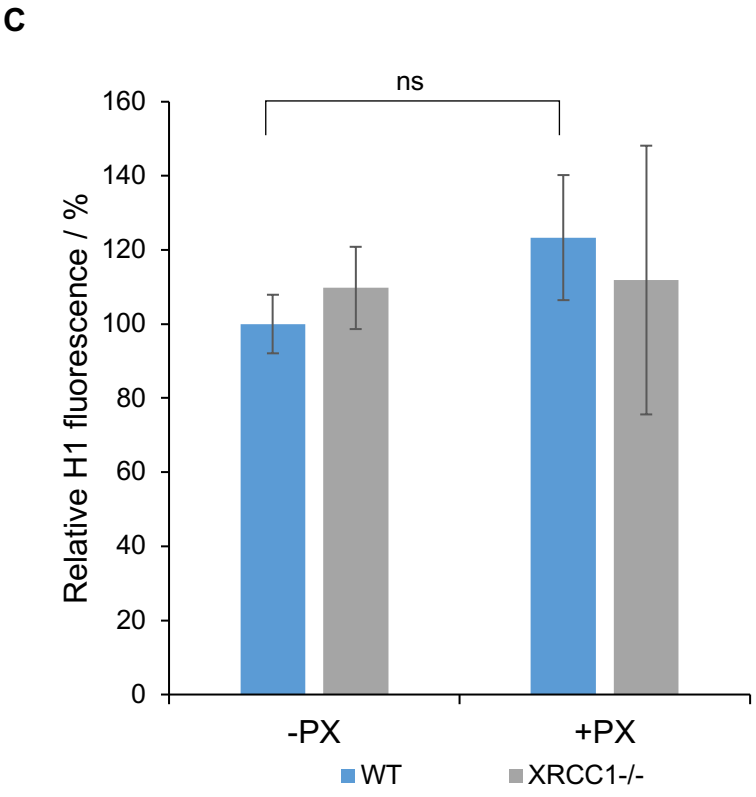
C
ns
160
140
120
100
80
60
40
20
0
Relative H1 fluorescence / %
-PX
+PX
WT
XRCC1-/-

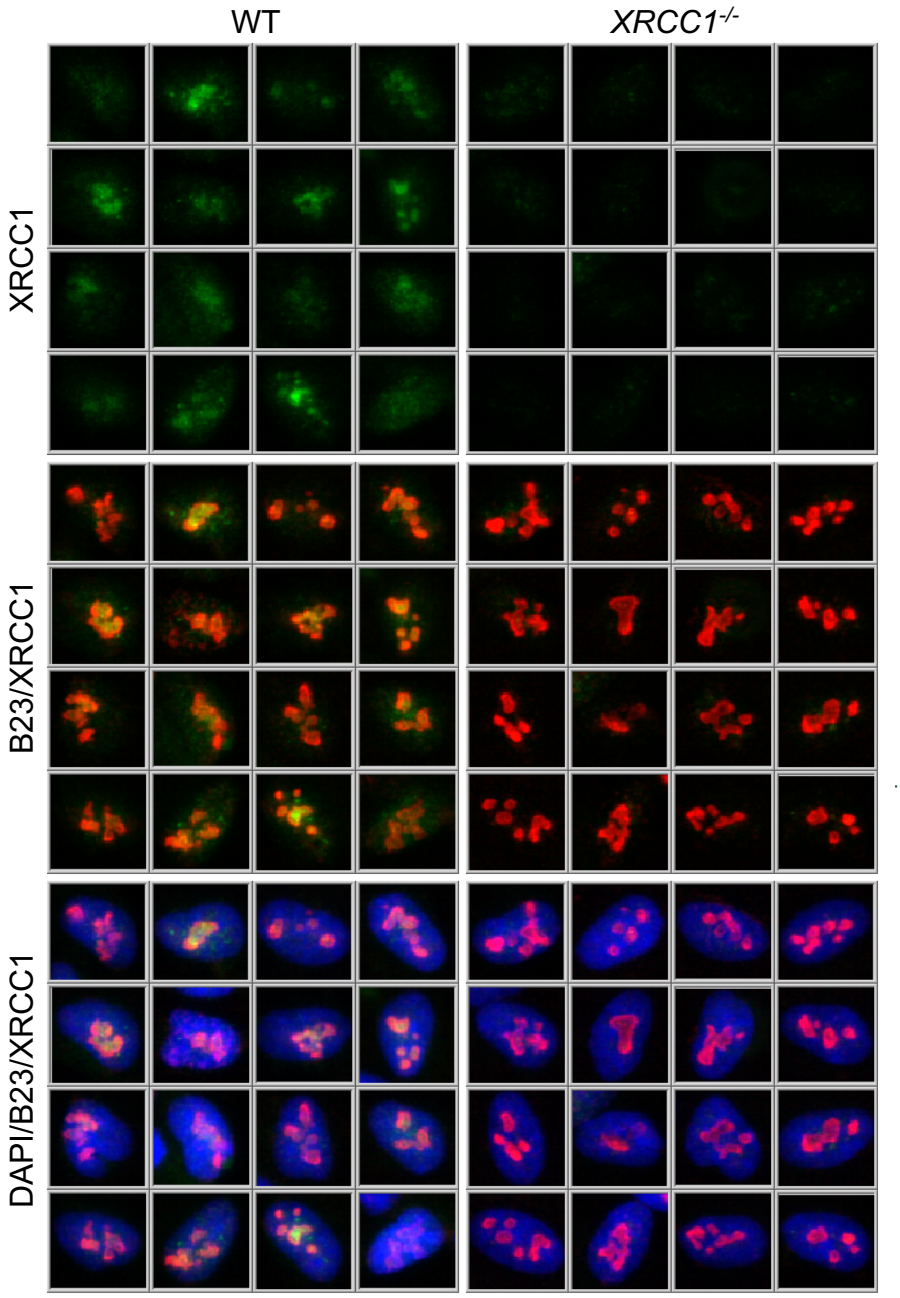

Figure 5.4. XRCC1 is localized to the nucleolus in untreated, pre-extracted cells. Untreated WT and *XRCC1*$^{-/-}$ RPE-1 cells were pre-extracted with 0.2% Triton-X100 for 2 min prior to formaldehyde fixation and immunofluorescence with antibodies targeting XRCC1 (green) and B23 (red), and staining of DNA with DAPI (blue). Slides were imaged using the Olympus ScanR system and ScanR Analysis software was used to generate a gallery of 16 randomly selected cells. The brightness of the residual XRCC1 signal has been increased to demonstrate colocalization with the nucleolar marker, phosphoprotein B23.

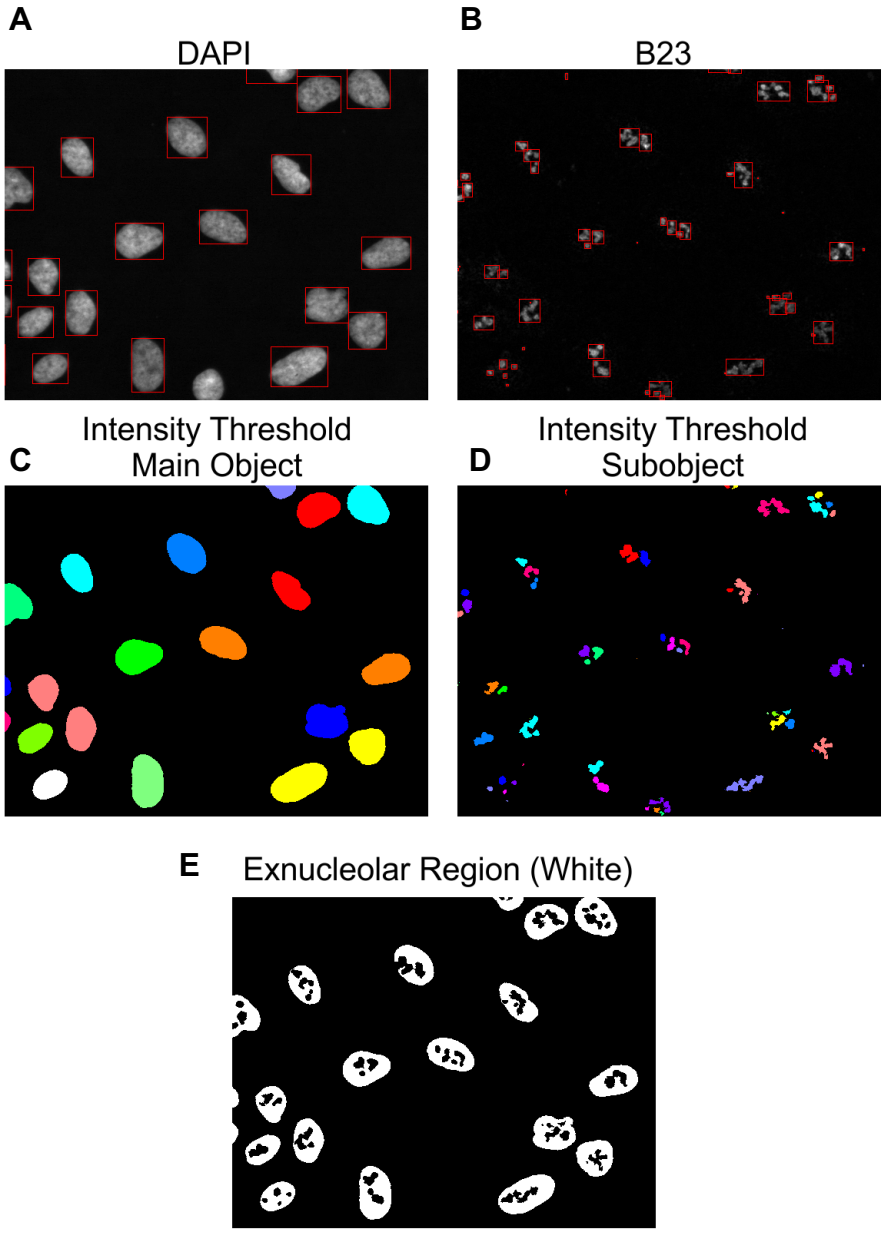

Figure 5.5. The delineation of nuclear, nucleolar and exnucleolar regions. DAPI (**A**) and B23 (**B**) fluorescence signal are thresholded to define the nuclear (**C**) and nucleolar (**D**) regions, respectively. By subtracting the sum total fluorescence intensity of the nucleolar region from that of the nuclear region, the fluorescence intensity in the exnucleolar region (**E**) can be derived. Images A-E are adapted screenshots from ScanR Analysis software.

subsequent XRCC1 fluorescence quantifications are of this exnucleolar region. This was to avoid artefactual replicate-to-replicate variability originating from incomplete washing of the nucleoli (see section 5.3 for further discussion).

5.2.5. H_2O_2-induced recruitment and/or retention of XRCC1 into chromatin

To demonstrate that the pre-extraction method can detect and quantify H_2O_2-induced XRCC1 localization into chromatin, a dose response was conducted (Fig. 5.6.). Cells were treated or not with 50, 100, 400 µM or 10 mM H_2O_2 for 10 min at RT, prior to pre-extraction, fixation and IF with anti-XRCC1 and anti-B23 antibodies. In untreated cells, a very low background anti-XRCC1 signal was observed, and as before this was largely restricted to the nucleolar region. Upon treatment with each dose of H_2O_2, anti-XRCC1 signal increased throughout the nucleus. The increased retention of XRCC1 in detergent-insoluble material suggests that the pre-extraction technique is able to enrich the XRCC1 fraction which is responding to oxidative damage. A 2.19-fold increase in exnuclear anti-XRCC1 signal was detected at the lowest dose of 50 µM and this increased to approximately 3.46-fold at the highest dose of 10 mM. 10 mM H_2O_2 did not result in a dramatically higher response than 400 µM, which may reflect a saturation of the response before this dose. It was observed that the high dose of 10 mM induced some morphological changes the cells, and resulted in some detachment from the coverslip. Therefore, for the purposes of this study 400 µM H_2O_2 will be used, unless otherwise indicated.

To investigate the nature of the detergent-insoluble material further, pre-extracted and fixed cells were subjected to overnight DNAse I digestion, prior to subsequent IF with anti-XRCC1 and anti-H1 antibodies (Fig 5.7.). DNAse I -treated cells exhibited a very low DAPI signal (2.7 and 2.3% that of cells not treated with DNAse I, for undamaged and H_2O_2-treated cells, respectively), demonstrating that the digestion worked as intended. The remaining DAPI signal was enough, however, to allow detection of the main object (nuclear region) by the ScanR analysis software. In addition to reducing of DAPI signal, DNAse I treatment also reduced or ablated the anti-H1 signal of untreated and H_2O_2-treated cells (both 0.2% of H_2O_2-treated, undigested cells), suggesting that

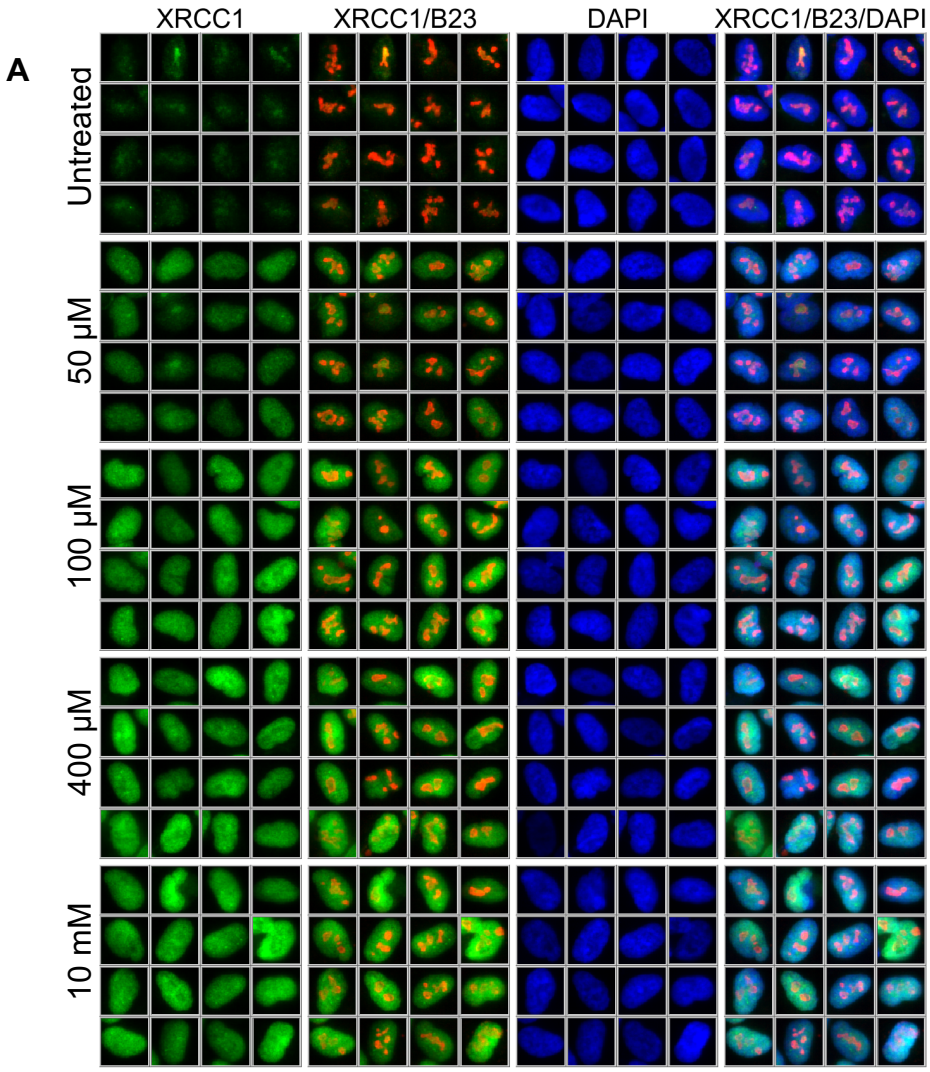

Figure 5.6. H_2O_2 dose response of XRCC1 chromatin-loading in RPE-1 cells. WT and *XRCC1*$^{-/-}$ RPE-1 cells growing on glass coverslips were treated or not with 0, 50, 100, 400 µM or 10 mM H_2O_2 for 10 min, prior to pre-extraction, formaldehyde fixation and immunofluorescence with antibodies against XRCC1 (green) and B23 (red), and DNA-staining with DAPI (blue). Slides were imaged using the Olympus ScanR system and ScanR Analysis software was used to generate galleries of 16 randomly selected WT cells for each condition **(A)**. XRCC1 fluorescence from >1000 cells was quantified in the exnucleolar region and is expressed as fold over untreated WT **(B, overleaf)**. Data are mean +/- S.E.M from 3 experiments.

B

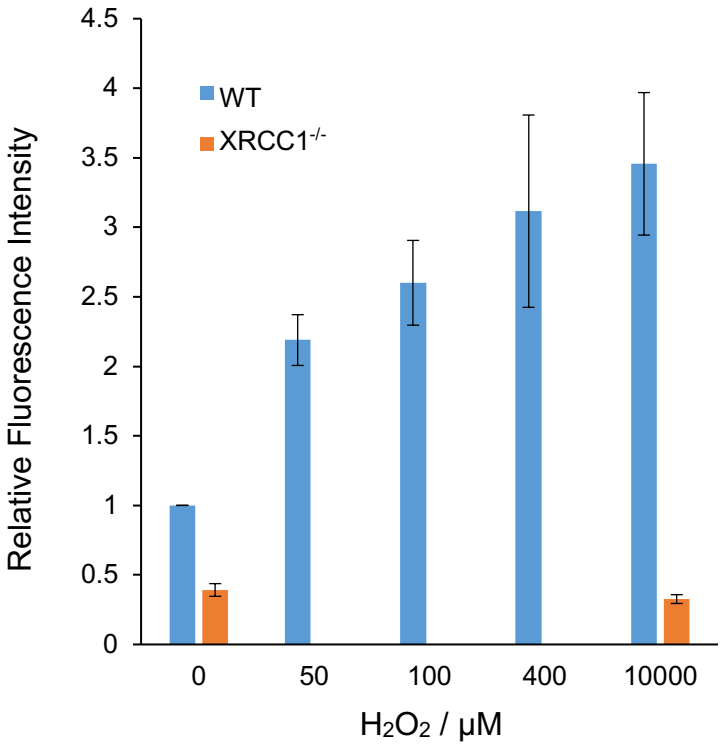
Relative Fluorescence Intensity
4.5
4
3.5
3
2.5
2
1.5
1
0.5
0
WT
XRCC1-/-
0
50
100
400
10000
H2O2 / μM

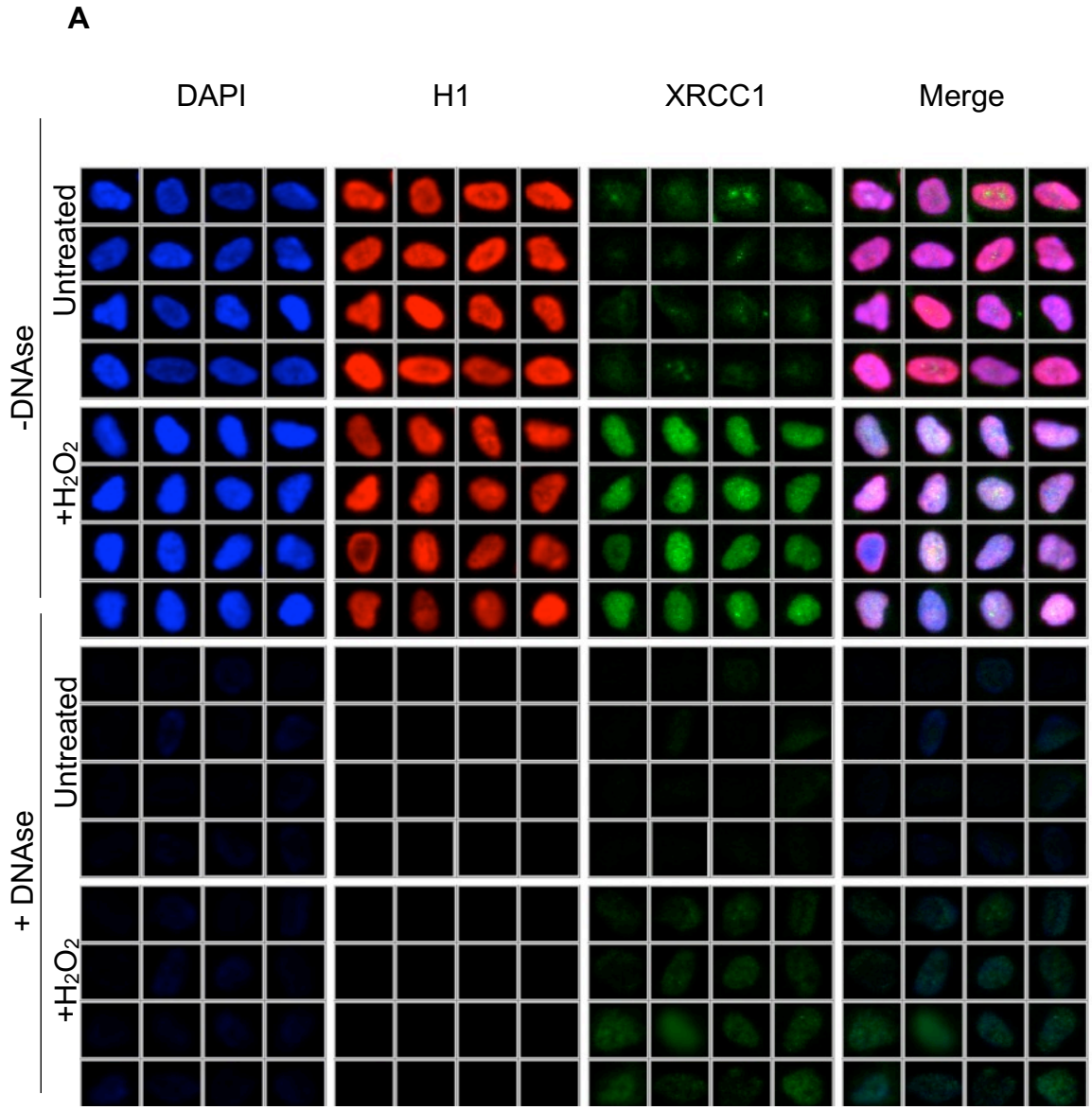

Figure 5.7. Detergent-insoluble XRCC1 signal is associated with chromatin. WT RPE-1 cells growing on glass coverslips were treated or not with 400 µM H_2O_2 for 7 min at RT. Cells were pre-extracted, formaldehyde fixed and subjected to overnight incubation with DNAse I buffer ±DNAse I, prior to immunofluorescence with antibodies targeting XRCC1 (green) and H1 (red), and DNA-staining with DAPI (blue). Slides were imaged using the Olympus ScanR system and ScanR Analysis software was used to generate galleries of 16 randomly selected cells for each condition **(a)**. Total XRCC1 **(b)**, H1 **(c)** and DAPI **(d)** fluorescence from >1000 cells were quantified in the nuclear region and are expressed as percentage of signal in H_2O_2-treated, undigested cells. Data is presented from one experiment.

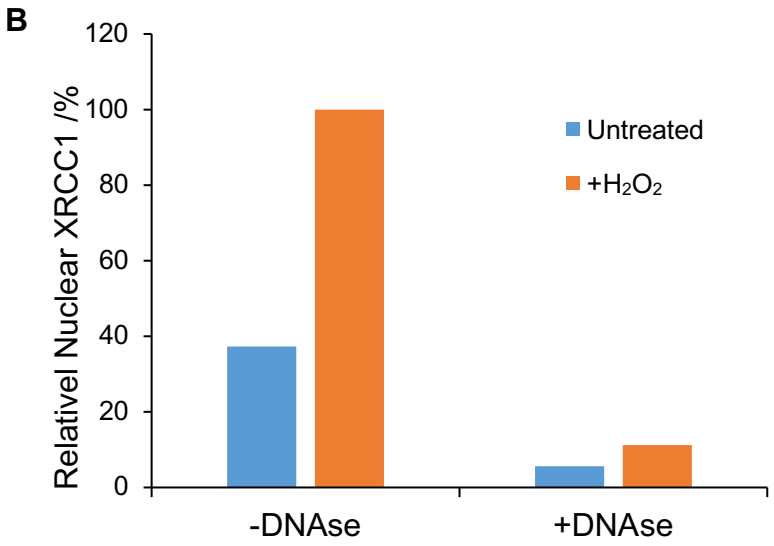
B
Relativel Nuclear XRCC1 /%
120
100
80
60
40
20
0
Untreated
+H2O2
-DNAse
+DNAse

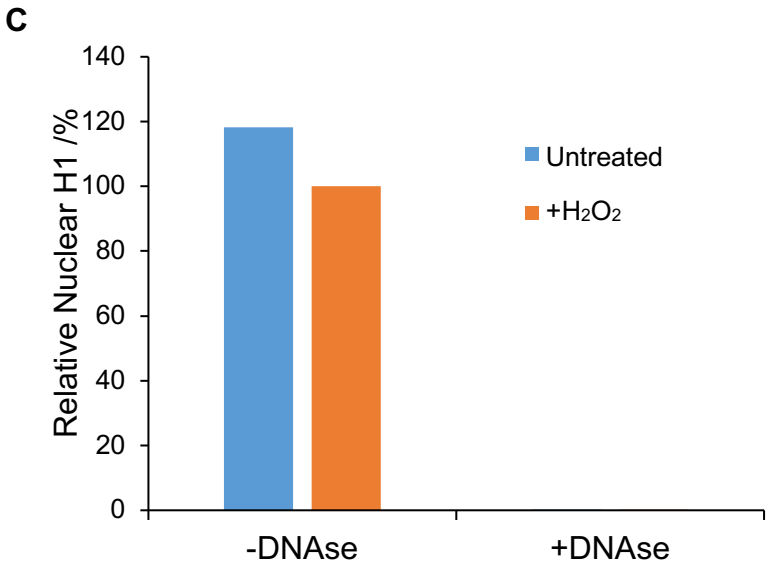
C
Relative Nuclear H1 /%
140
120
100
80
60
40
20
0
Untreated
+H2O2
-DNAse
+DNAse

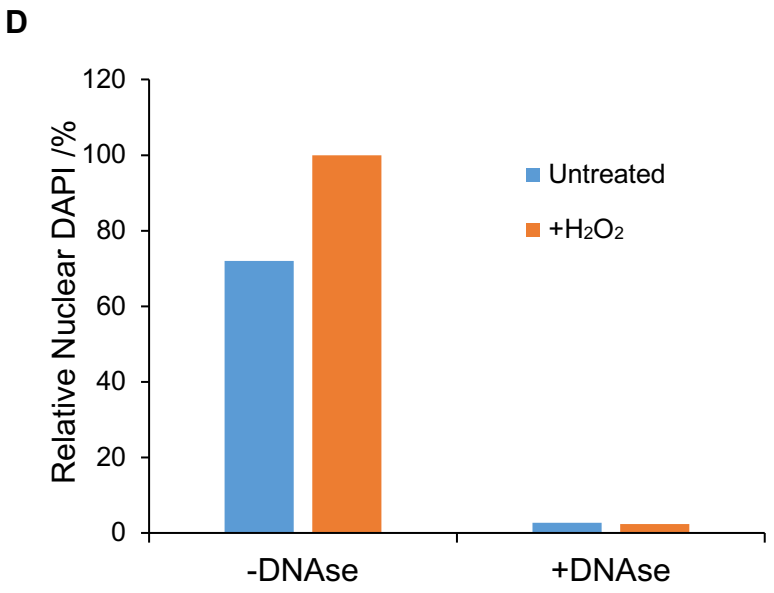
D
Relative Nuclear DAPI /%
120
100
80
60
40
20
0
Untreated
+H2O2
-DNAse
+DNAse

DNA digestion also releases the associated chromatin proteins. DNAse I treatment also decreased the detergent-insoluble XRCC1 signal in untreated and H_2O_2-treated cells (5.3 and 11.1% of H_2O_2-treated, undigested cells, respectively), suggesting that it is indeed reflective of chromatin-associated XRCC1.

5.3. Conclusions and Discussion

Previous attempts to characterize rapid cellular responses to H_2O_2 have had several disadvantages. Traditional methods for the biochemical fractionation of chromatin are often time-consuming to perform with multiple samples, making them unsuitable when many cell lines are assayed in parallel. Alternatively, the use of FP-tags allows the observation of protein localization in real time. However, the overexpression of such constructs may produce responses which are not representative of the endogenous repair proteins (Moriya 2015). Additionally, FP-tags have a propensity to oligomerise (Zacharias, Violin et al. 2002, Snapp, Hegde et al. 2003, Costantini, Fossati et al. 2012), which may explain the large macromolecular FP-XRCC1 foci which form in response to H_2O_2 (Breslin, Hornyak et al. 2015). Here, I employed a detergent pre-extraction-IF approach to demonstrate that endogenous XRCC1 does not form these large foci but rather distributes uniformly throughout the chromatin in H_2O_2-treated cells.

Interest in ADP-ribosylation and the PARP enzymes has increased dramatically over the decades. This is evident from the exponential growth in the yearly number of papers published on the topic (NCBI Resource NCBI 2016). In recent years this has been partly driven by the observation of sensitivity of HR-deficient cells to PARP inhibitors (Bryant, Schultz et al. 2005, Farmer, McCabe et al. 2005) and the resulting U.S. Food and Drug Administration (FDA) and European Medicines Agency (EMA) approval of their use in treating BRCA1 and BRCA2 mutated patients with advanced ovarian cancer (EMA 2014, FDA 2014). Accurate and sensitive quantification of ADP-ribosylation *in vivo* is important for future work in the field. Despite this, the anti-PAR 10H monoclonal antibody (Kawamitsu, Hoshino et al. 1984) remains the most popular detection reagent (NCBI 2016). This chapter conclusively demonstrates its inferior sensitivity when compared to other reagents in parallel. This was particularly true

for the IF application, where the signal detected with 10H was dramatically lower than that detected by pan-ADP-Ribose binding reagent or 4336-BPC-100 polyclonal antibody. By comparison, the signal detected by 10H on a WB was more comparable to that of the other reagents. This difference in sensitivity depending on application might be due to 10H requiring or preferring an epitope which is more accessible under the conditions of a WB. For example, it is possible that interaction of the PAR chain with the nitrocellulose membrane exposes a confirmation preferred by 10H. Alternatively, the formaldehyde-fixation step of IF may alter the PAR epitope normally recognized by 10H. Using the other reagents, it was clear that IF allowed more sensitive detection of PAR than by WB, revealing that very high doses of PARP inhibitor are required to completely block H_2O_2-induced ADP-ribosylation *in vivo*. This has not been widely reported before, and is of particular significance for the validation of future PARP inhibitor therapeutics.

In untreated cells, the detergent-insoluble XRCC1 is largely confined to the nucleolar region. It is tempting to speculate that this may reflect a physiologically relevant role of XRCC1 in concentrating SSBR machinery at regions of high transcriptional activity. Although XRCC1 does not have a clear nucleolar localization signal, PARP1 and PARP2, the major sources of PAR, are both reported to (Meder, Boeglin et al. 2005). However, as demonstrated in Chapter Six, deletion of *PARP1* and *PARP2* does not significantly or specifically reduce XRCC1 nucleolar localization in untreated pre-extracted cells (see section 6.2.6). Whilst it is certainly possible that XRCC1 is enriched in the nucleolus by another mechanism independent of PARP1/PARP2 activity, it is also possible that the residual signal results as an artefact of incomplete extraction from this structure. Nucleoli can be thought of as non-membranous subnuclear organelles (Lam and Trinkle-Mulcahy 2015), with a structure that is maintained by elaborate RNA-protein interactions. These interactions cause the nucleolus to have a significantly higher density than the surrounding nucleoplasm (estimated values of 0.215 g/cm^3 and 0.106 g/cm^3, respectively (Handwerger, Cordero et al. 2005)), which incidentally allows their convenient observation by phase contrast or differential interference contrast microscopy (Zernike 1942), and the relative ease of their isolation by centrifugation (Busch, Adams et al. 1963). It is conceivable

that their higher density also renders them intrinsically less permeable to detergent-containing buffers. In 1992, Melan *et al* conducted a study of the effects of different IF fixation protocols on the apparent distribution of a panel of FITC-labelled proteins (Melan and Sluder 1992), introduced exogenously using a bead-loading technique. The authors tested several pre-fixation detergent extraction steps, including the use of 0.2% Triton-X100 buffer. Interestingly, they observed a strong enrichment in the nucleus and nucleolus for several of the tested proteins, including lactate dehydrogenase (LDH), β-lactoglobulin, and globin. This is particularly pertinent, as β-lactoglobulin and globin have no intracellular role, suggesting that their nucleolar enrichment following pre-extraction is entirely artificial (Melan and Sluder 1992). Notably, a similar localization of residual anti-Ku80 signal has been observed following pre-extraction of cells with CSK buffer (Britton, Coates et al. 2013). In their study, Britton *et al* attribute the residual anti-Ku80 signal that they observe in CSK-extracted cells to Ku80 RNA-binding, citing a previously published interaction with the RNA component of human telomerase hTR (Ting, Yu et al. 2005). This explanation is supported by their observation that inclusion of RNAse A in the CSK pre-extraction buffer dramatically reduces residual Ku80 signal throughout the nucleus. Furthermore, a subsequent publication has reported another specific interaction of Ku80 with RNA; in this case the long non-coding RNA LINP1 (Zhang, He et al. 2016). Britton *et al* do not comment directly on the nucleolar fraction of the residual signal, but there is no reason to suspect that hTR or LINP1 preferentially localize to the nucleolus. It is possible that other Ku80-binding RNAs exist which are generated in or localized to the nucleolus. However, it is notable that the inclusion of RNAse A by Britton *et al* also ablated nucleolin signal, revealing total nucleolar disruption. This is expected, as nucleolar integrity is dependent on its constituent RNA (Caudron-Herger, Pankert et al. 2015).

No evidence was found herein to suggest that the residual XRCC1 signal observed in the nucleolus reflected a functional role, and its inclusion in fluorescence quantification lowered the signal to noise ratio and reproducibility of experiments. For this these reasons, fluorescence quantification was restricted to the ex-nucleolar nuclear region for the remainder of the project.

In summary, this chapter has introduced a method for enrichment of the XRCC1 fraction responding to DNA damage, and provided evidence that this detergent-insoluble fraction represents chromatin-associated protein. In the following chapter, this technique will be combined with the panel of KO RPE-1 cell lines introduced in Chapter Four to investigate the role of PARP1, PARP2 and PARP3 in the recruitment of endogenous XRCC1 into oxidised human chromatin.

Chapter Six

Overlapping roles of PARP1 and PARP2 for the loading of endogenous XRCC1 and PNKP into oxidized human chromatin

6.1. Introduction and Aims

Single-strand breaks (SSBs) are one of the commonest lesions in DNA, arising at a frequency of tens-of-thousands per cell per day (Lindahl 1993, Caldecott 2008). One major source of SSBs are ROS that generate DNA breaks directly by attack of deoxyribose and indirectly by triggering the excision repair of oxidized DNA bases and abasic sites. An early step in the repair of SSBs is the activation of poly (ADP-ribose) polymerases (PARPs); enzymes that covalently modify themselves and other proteins at the site of the break with mono and/or poly (ADP-ribose) and thereby serve as molecular SSB sensors (de Murcia and Menissier de Murcia 1994, Ame, Spenlehauer et al. 2004, Caldecott 2014). Poly(ADP-ribose) (PAR) is then bound by X-ray repair cross-complementing protein 1 (XRCC1), a molecular scaffold protein that interacts with, stabilizes and stimulates multiple enzymatic components of SSB repair (SSBR), and accelerates the overall process (Caldecott 2003, Li, Lu et al. 2013, Caldecott 2014, Breslin, Hornyak et al. 2015). The first PARP to be identified was PARP1 (AKA ARTD1), a 113 KDa enzyme that is responsible for ~85–95% of the total cellular PARP activity triggered in response to DNA breaks (Amé, Rolli et al. 1999). Subsequently, following the observation of residual PAR synthesis in *Parp1*$^{-/-}$ mouse embryonic fibroblasts (MEFs) treated with high doses of damaging agents, *Parp2* (AKA ARTD2) was identified (Amé, Rolli et al. 1999, Johansson 1999). More recently multiple research groups have identified PARP3 (AKA ARTD3) as a third Diphtheria toxin-like ADP-ribosyl transferase (ARTD) that is stimulated by DNA breaks (Boehler, Gauthier et al. 2011, Rulten, Fisher et al. 2011, Langelier, Riccio et al. 2014). PARP1, PARP2 and PARP3 share ~60% homology within their catalytic and tryptophan-glycine-arginine (WGR) domains, but diverge at their N-termini. The N-terminal region of PARP1 is comprised of ~500 amino acids and includes three zinc finger domains, two of which promote binding to DNA breaks and a third that is believed to trigger stimulation of catalytic activity by up to ~500-fold. PARP2 and PARP3 lack these zinc finger domains and instead possess shorter N-terminal regions of 78 and 40 amino acids, respectively, the functions of which are poorly understood. In contrast to PARP1, PARP2 and PARP3 are reliant on their WGR domains for DNA binding, perhaps explaining their lower catalytic activity.

Despite a great deal of interest in the precise roles of PARP enzymes in DNA repair, their relative contribution to specific DNA repair processes remains unclear. Previous studies employing overexpressed GFP-tagged or RFP-tagged XRCC1 have demonstrated that the re-localization of these fusion proteins to focal sites of laser microirradiation or chromatin oxidized by H_2O_2 is largely or entirely dependent upon PARP1 (El-Khamisy, Masutani et al. 2003, Okano, Lan et al. 2003, Fisher, Hochegger et al. 2007, Mortusewicz, Amé et al. 2007). However, the overexpression of tagged XRCC1 might not accurately reflect the behaviour of endogenous XRCC1 (see Chapter Five). Moreover, the role of PARP1 in promoting XRCC1 recruitment to sites of DNA damage has recently been challenged (Parsons, Dianova et al. 2005, Hanssen-Bauer, Solvang-Garten et al. 2011, Abdou, Poirier et al. 2015). Consequently, the *PARP1*$^{-/-}$, *PARP2*$^{-/-}$, *PARP1*$^{-/-}$/*PARP2*$^{-/-}$ and *PARP3*$^{-/-}$ diploid human hTERT RPE-1 cell lines generated herein (See Chapter Four) and by co-workers in the Caldecott laboratory using CRISPR-Cas9 technology will be used to assess the impact of the three DNA strand break-stimulated PARPs on the recruitment of endogenous XRCC1 into oxidized human chromatin. **[Adapted from (Hanzlikova, Gittens et al. 2016) – own writing].**

To further investigate the overlapping roles of PARP1 and PARP2 in SSBR, observations will be extended to another protein involved in this repair pathway. PNKP is an enzyme involved in catalysing the phosphorylation and dephosphorylation of 5'-OH and 3'-phosphate termini, respectively. As such, it is often an essential enzymatic activity prior to DNA synthesis and ligation. PNKP interacts with the XRCC1 CK2 phosphorylation motif via its forkhead associated (FHA) domain. Perturbing this interaction by mutation of XRCC1, or loss of XRCC1 entirely in EM9 cells, has been demonstrated to decrease PNKP recruitment/retention at damage sites (Loizou, El-Khamisy et al. 2004, Della-Maria, Hegde et al. 2012). The prevailing model has been that XRCC1 PAR-binding co-recruits PNKP to damage sites. However, this model has been challenged by others who report direct PAR-binding by PNKP (Li, Lu et al. 2013) and has led to the suggestion that XRCC1-Lig3α recruitment to damage sites might follow binding of end-processing factors, including PNKP.

The previous chapter introduced methodologies for the sensitive quantification of nuclear ADP-ribose and chromatin-localized XRCC1. In this chapter, these methods will be combined with the panel of diploid human cell lines generated by CRISPR, to answer a fundamental question which has been debated in the literature, namely the relative contributions of PARP1, PARP2 and PARP3 to the chromatin loading of XRCC1 and PNKP in response to H_2O_2-induced DNA damage. Finally, the consequences of deletion of *XRCC1, PARP1* and/or *PARP2* for rates of SSBR will be compared.

6.2. Results

6.2.1. PARP Inhibition blocks H_2O_2-induced XRCC1 chromatin recruitment.

To check the requirement for ADP-ribosylation for the chromatin recruitment of XRCC1 in response to H_2O_2, WT RPE-1 cells growing on glass coverslips were preincubated or not with 10 µM KU0058948 PARP inhibitor for 1 h, prior to treatment with 400 µM H_2O_2 for 7 min at room temperature (RT) in the continued absence or presence of 10 µM KU0058948. Cells were then pre-extracted, formaldehyde fixed and subjected to immunofluorescence (IF) with anti-XRCC1 antibody. As previously observed (see Chapter Five), treatment with 400 µM H_2O_2 induced a significant 3.86-fold enrichment of XRCC1 in the chromatin outside of the nucleolus (t-test p-value = $8.58x10^{-4}$) (Fig. 6.1.). This enrichment was significantly reduced (t-test p-value = $1.94x10^{-3}$) by preincubation with 10 µM KU0058948, to a level that was not significantly different from untreated cells (t-test p-value = $1.29x10^{-1}$), confirming that recruitment of endogenous XRCC1 into chromatin requires PARP activity (Masson, Niedergang et al. 1998, El-Khamisy, Masutani et al. 2003). The concentration of KU0058948 used here is likely to potently inhibit PARP1, PARP2 and PARP3 (IC_{50} values of 3.4, 1.5 and 40 nM, respectively) (Farmer, McCabe et al. 2005).

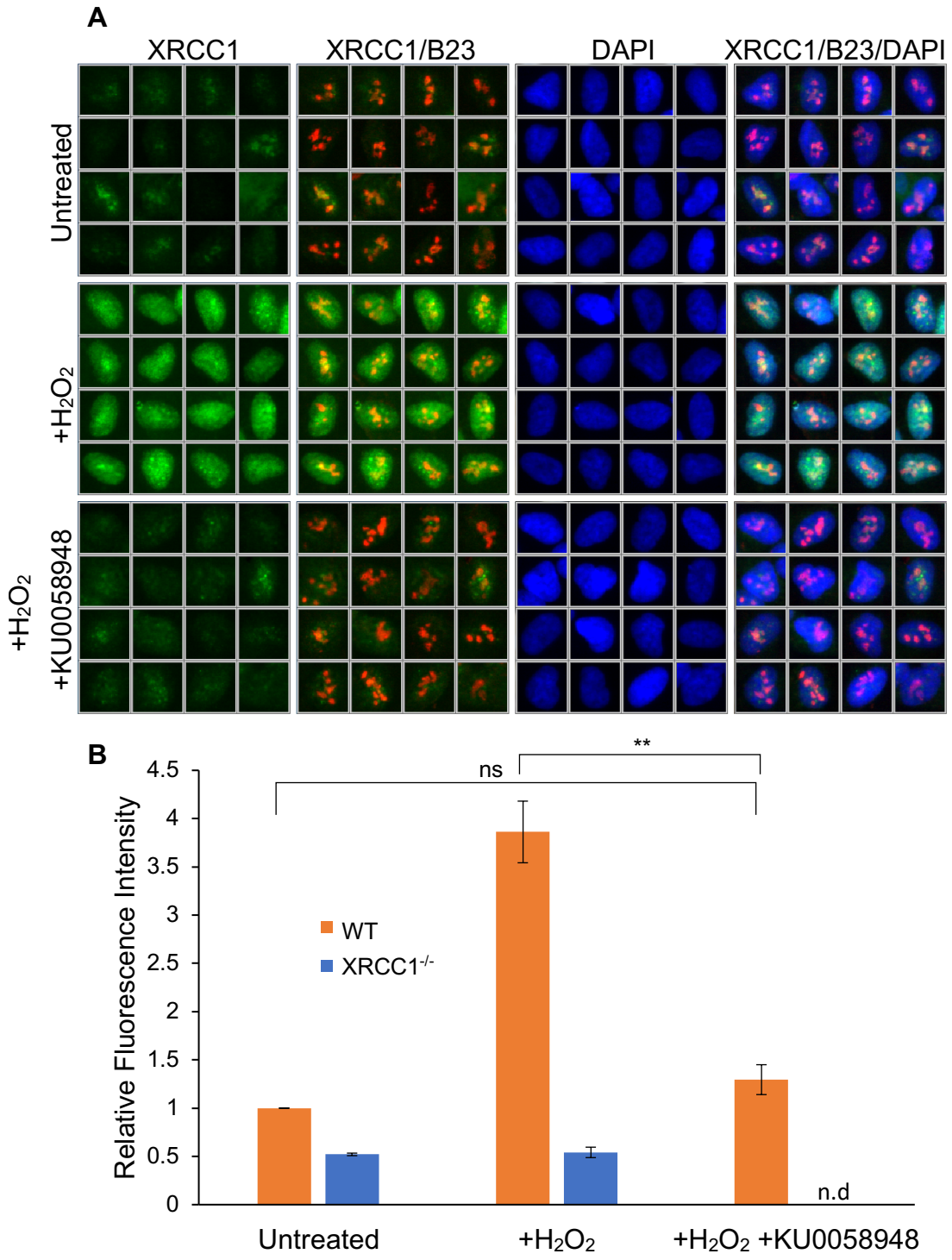

Figure 6.1. H_2O_2-induced XRCC1 chromatin loading is blocked by PARP inhibition. WT and *XRCC1*$^{-/-}$ RPE-1 cells growing on glass coverslips were preincubated or not with 10 μM KUU0058948 PARP inhibitor for 1 h prior to treatment or not with 400 μM H_2O_2 for 7 min at RT. Cells were pre-extracted, formaldehyde fixed and subjected to immunofluorescence with anti-XRCC1 and anti-B23 antibodies. Slides were imaged using the Olympus ScanR system and ScanR Analysis software was used to generate galleries of 16 randomly selected cells for each condition. For clarity, only WT cells are shown **(A)**. XRCC1 fluorescence from >1000 cells was quantified in the nuclear region excluding phosphoprotein B23 signal and is expressed as fold over signal in untreated. All data are mean ± S.E.M of 3 replicates. Statistical significance was calculated by student's t-test. "n.d" (not done) indicates a condition which was not assessed. **(B).**

6.2.2. Levels of H_2O_2-induced ADP-ribosylation in PARP-deleted RPE-1 cells.

Next, H_2O_2 induced ADP-ribosylation was measured in WT, *PARP1*$^{-/-}$, *PARP2*$^{-/-}$ *PARP3*$^{-/-}$ and *XRCC1*$^{-/-}$ RPE-1 cells by Western Blot (WB) and IF. For the WB, asynchronous RPE-1 cells of different genotypes were treated with 400 µM H_2O_2 for 7 min in PBS at RT, prior to lysis, 10% SDS-PAGE and detection with pan-ADP-ribose binding reagent (Fig. 6.2.a). In WT RPE-1 cells, H_2O_2 induces a strong signal corresponding to ADP-ribosylation of targets across the mass range (<20 to >250 kDa). Within this smear, faint bands are visible, corresponding to heavily ADP-ribosylated protein targets. The signal was indistinguishable, both in terms of intensity and pattern, from that observed in *PARP2*$^{-/-}$ and *PARP3*$^{-/-}$ and *XRCC1*$^{-/-}$ cells. In the *PARP1*$^{-/-}$ cells however, the signal was dramatically and uniformly reduced. Despite the clear reduction in intensity, ADP-ribosylation signal was still detected over a wide mass range, albeit more faintly than in the WT cells.

To verify that the ADP-ribosylation pattern observed above in *PARP1*$^{-/-}$ and *PARP2*$^{-/-}$ cells was indeed dependent upon the deletion of these genes, rather than any other clonally inherited characteristic, multiple clones were tested by the same method (Fig. 6.2.b). All three *PARP1*$^{-/-}$ RPE-1 cell clones (#D4, #F5 and #G7) exhibited the same reduced ADP-ribosylation phenotype. Similarly, both *PARP2*$^{-/-}$ cell clones (#A1 and #B1) exhibited levels of ADP-ribosylation that were indistinguishable from that in WT cells. **[Contributing WB from Hana Hanzlikova].**

To more sensitively quantitate the H_2O_2-induced ADP-ribosylation, cells were subjected to IF and ScanR analysis following 400 µM H_2O_2 treatment, as described previously (Fig. 6.3.). Treatment with H_2O_2 increased ADP-ribosylation 25.7-fold in WT cells. This was not significantly reduced in either *PARP2*$^{-/-}$ or *PARP3*$^{-/-}$ cells (t-test p-values: 8.81×10^{-1} and 3.56×10^{-1}, respectively). In contrast, in *PARP1*$^{-/-}$ cells ADP-ribosylation was significantly reduced to 5.5-fold relative to WT untreated (t-test p-value = 1.08×10^{-2}). This 78.4% reduction in the H_2O_2-induced signal is consistent with previous observations demonstrating that PARP1 accounts for 80–90% of total ADP-ribosylation following DNA damage (Amé, Rolli et al. 1999).

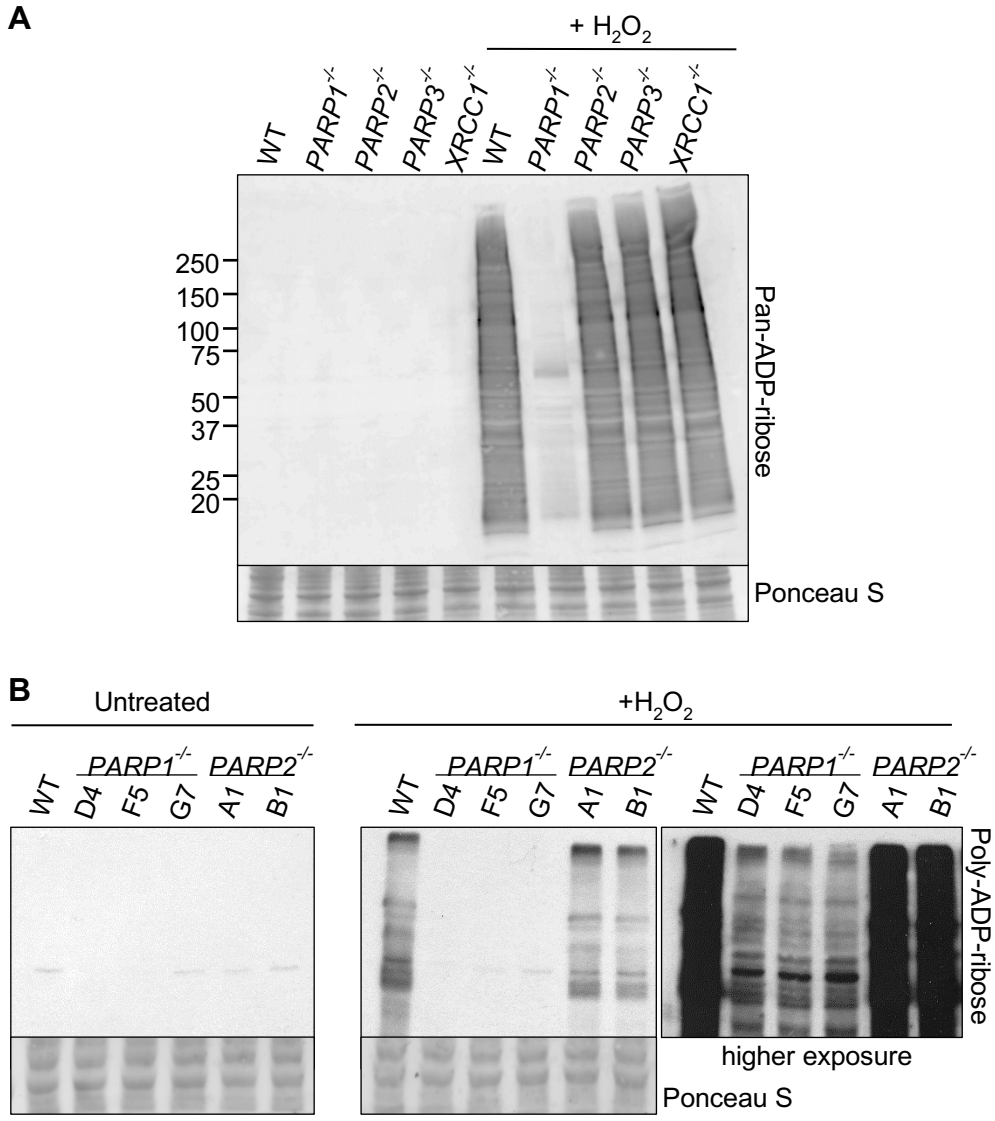

Figure 6.2. Western blots of H_2O_2-induced ADP-ribosylation in WT, *PARP1*$^{-/-}$, *PARP2*$^{-/-}$ and *PARP3*$^{-/-}$ RPE-1 cells. WT, *PARP1*$^{-/-}$ (#G7), *PARP2*$^{-/-}$ (#A1), *PARP3*$^{-/-}$ (#20) and *XRCC1*$^{-/-}$ (#3) RPE-1 cells were treated or not with 400 μM H_2O_2 for 7 min at room temperature, prior to whole cell lysis and immunoblotting with pan-ADP-ribose binding reagent (**A**). Multiple *PARP1*$^{-/-}$ and *PARP2*$^{-/-}$ RPE-1 clones were treated or not with 10 mM H_2O_2 for 10 min at RT, prior to whole cell lysis and immunoblotting with pan-ADP-ribose binding reagent (**B**). **[Contributing WB from Hana Hanzlikova]**

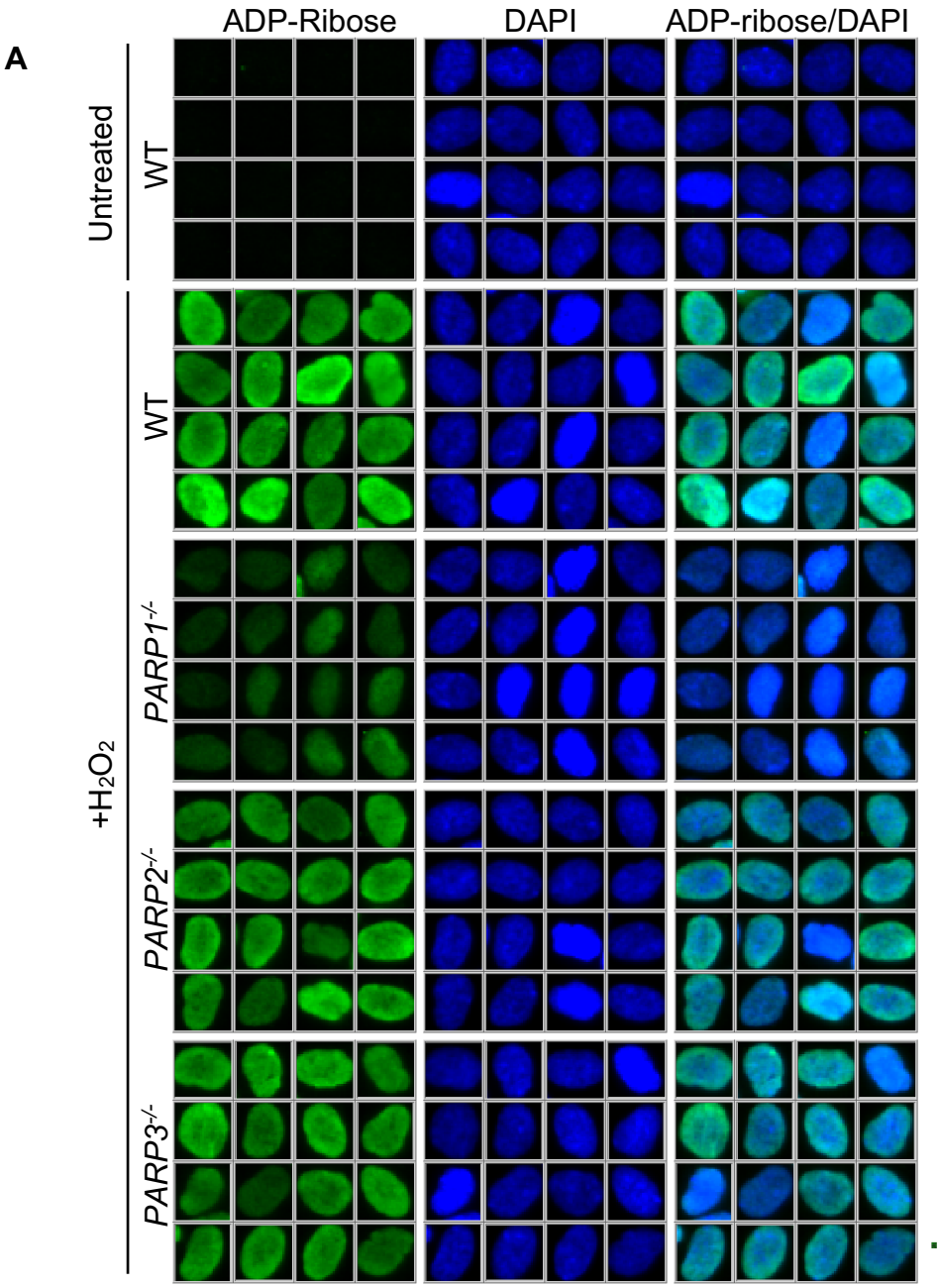

Figure 6.3. Immunofluorescence of H_2O_2-induced ADP-ribosylation in WT, *PARP1*$^{-/-}$, *PARP2*$^{-/-}$ and *PARP3*$^{-/-}$ RPE-1 cells. WT, *PARP1*$^{-/-}$, *PARP2*$^{-/-}$ *and PARP3*$^{-/-}$ RPE-1 cells were treated with 400 µM H_2O_2 for 7 min prior to formaldehyde fixation and labelling with Pan-ADP-ribose binding reagent (green) and DNA-staining with DAPI (blue). Slides were imaged using the Olympus ScanR system and ScanR Analysis software was used to generate galleries of 16 randomly selected cells for each condition **(A)**. ADP-ribose fluorescence from >1000 cells was quantified and is expressed as fold over signal in untreated NT-transfected cells. Data are means ±SEM of 3 experiments. Statistical significance was calculated by students t-test **(B, overleaf).**

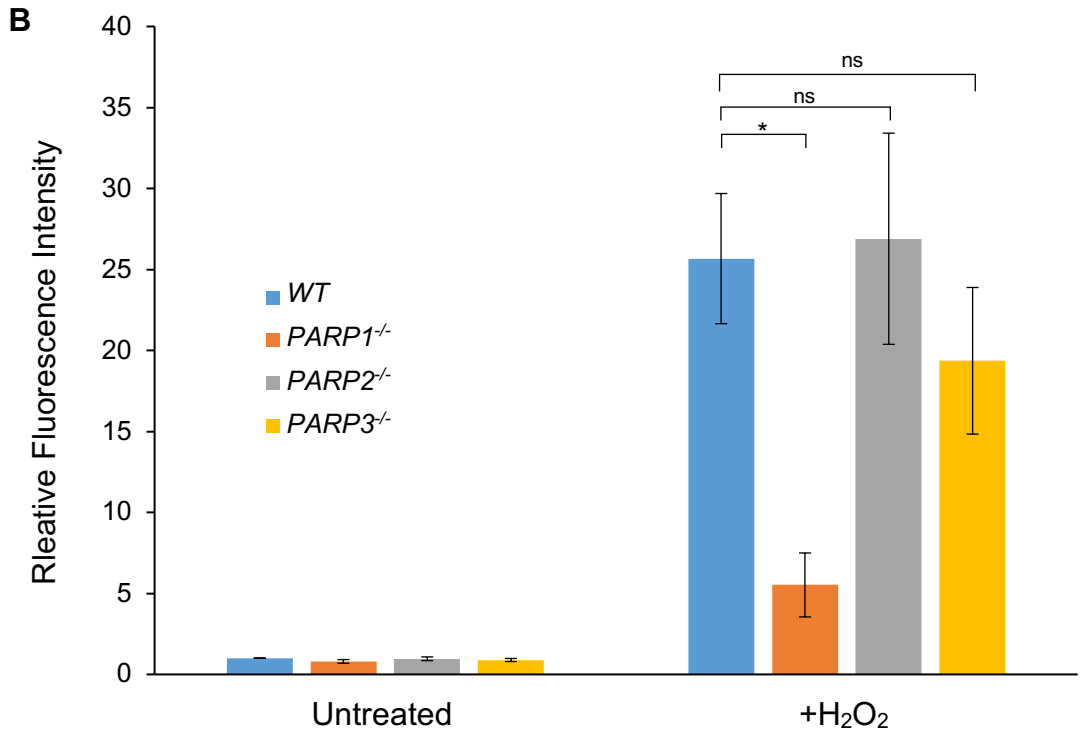
B
Rleative Fluorescence Intensity
40
35
30
25
20
15
10
5
0
WT
PARP1-/-
PARP2-/-
PARP3-/-
ns
ns
*
Untreated
+H2O2

6.2.3. Levels of H_2O_2-induced XRCC1 chromatin recruitment in PARP-deleted cells remain comparable to WT cells.

Next, H_2O_2-induced XRCC1 recruitment was tested in WT, *PARP1*$^{-/-}$, *PARP2*$^{-/-}$ and *PARP3*$^{-/-}$ cell lines, using the pre-extraction method established in the previous chapter. Surprisingly, this was not significantly reduced in any single *PARP*-deleted cell line, including in *PARP1*$^{-/-}$ cells (Fig. 6.4.). Since there is significant remaining ADP-ribosylation in *PARP1*$^{-/-}$ cells (Fig. 6.3.), I hypothesised that the residual ADP-ribosylation in *PARP1*$^{-/-}$ cells is sufficient for near WT levels of XRCC1 chromatin loading. Supporting this, it was found that inhibition of the remaining ADP-ribosylation in *PARP1*$^{-/-}$ cells with 10 µM KU0058948 significantly reduced XRCC1 chromatin recruitment (t-test p-value = 6.21×10^{-3}) (Fig. 6.5.).

6.2.4. Simultaneous depletion of PARP1/PARP2 ablates H_2O_2-induced ADP-ribosylation.

To test which of the other PARPs was responsible for the remaining H_2O_2-induced ADP-ribosylation in the absence of PARP1, siRNA was used to deplete PARP2 and/or PARP3 in *PARP1*$^{-/-}$ RPE-1 cells. Cells were lysed and subjected to anti-PARP2 and anti-PARP3 WB 72 h after transfection with siRNA targeting PARP2, PARP3, PARP2 and PARP3 in combination, or a non-targeting siRNA (Fig. 6.6.c). Depletion of each protein from the whole cell extract was effective. In parallel to the WB, transfected cells were plated onto glass coverslips and subjected to IF protocols at the same 72 h time point (Fig. 6.6.a and b). H_2O_2-induced ADP-ribosylation was significantly reduced in PARP2-depleted and PARP2+PARP3-depleted (t-test p-value = 1.83×10^{-3} and 1.98×10^{-3}, respectively) but not PARP3 depleted *PARP1*$^{-/-}$ cells (t-test p-value = 2.54×10^{-1}). While ADP-ribosylation is entirely absent from most PARP2-depleted *PARP1*$^{-/-}$ cells, it was retained in a small population. This could be due to heterogenous transfection efficiency of the siRNA, with some cells being unsuccessfully depleted of PARP2. This further highlights the superiority of this IF over WB quantification, as the population of ADP-ribose positive cells is likely small enough that it would be below the detection limit by WB. Additionally, there was no significant further reduction in ADP-ribosylation when PARP2 depletion was combined with PARP3 depletion (t-test p-value = 3.65×10^{-1}). These

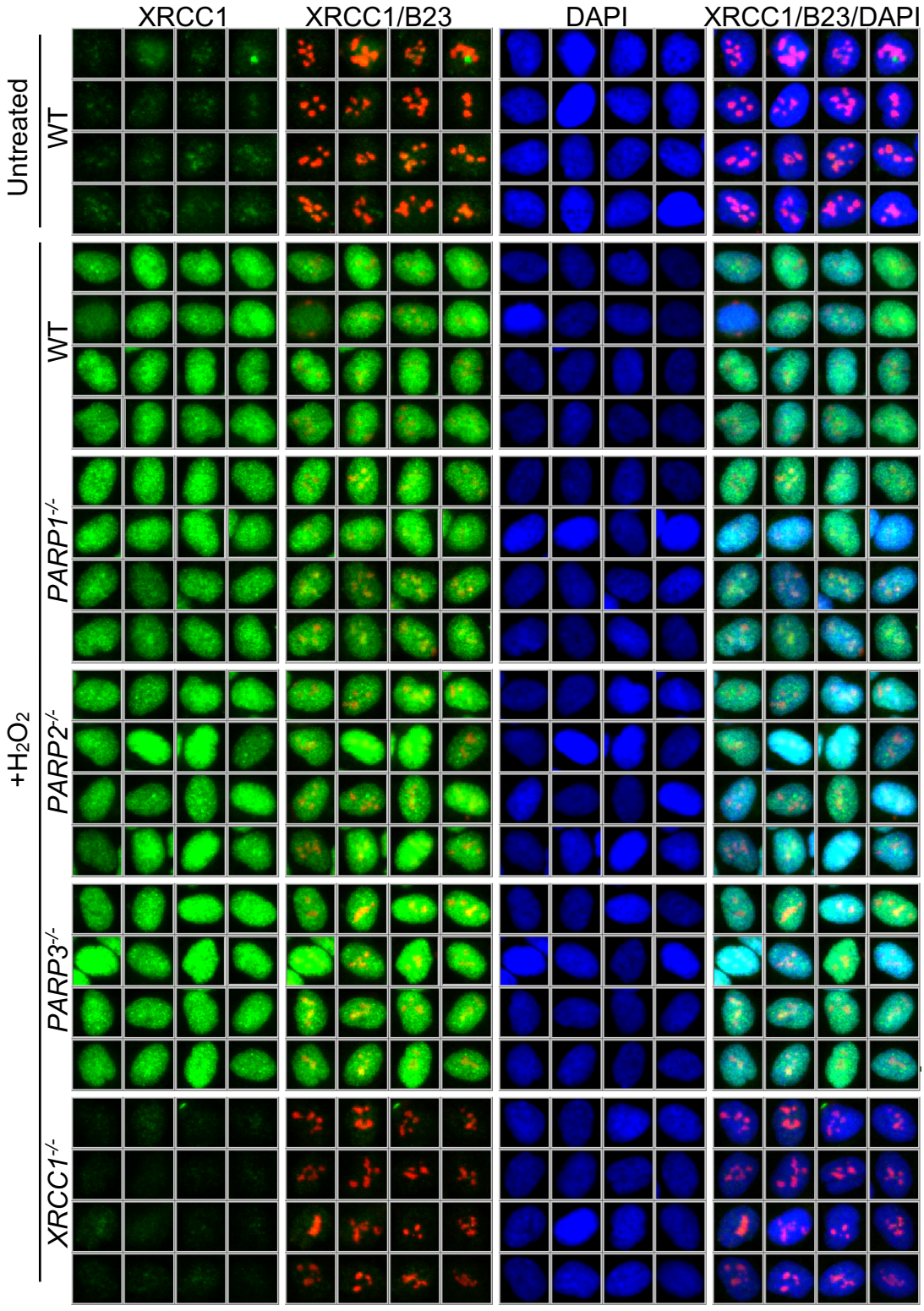

Figure 6.4. H_2O_2-induced XRCC1 chromatin-loading in WT, *PARP1*$^{-/-}$, *PARP2*$^{-/-}$ and *PARP3*$^{-/-}$ RPE-1 cells WT, *PARP1*$^{-/-}$, *PARP2*$^{-/-}$, *PARP3*$^{-/-}$ and *XRCC1*$^{-/-}$ RPE-1 cells were treated with 400 μM H_2O_2 for 7 min prior to pre-extraction, formaldehyde fixation and labelling with antibodies targeting XRCC1 (green) and B23 (red), and DNA staining with DAPI (blue). Slides were imaged using the Olympus ScanR system and ScanR Analysis software was used to generate galleries of 16 randomly selected cells for each condition.

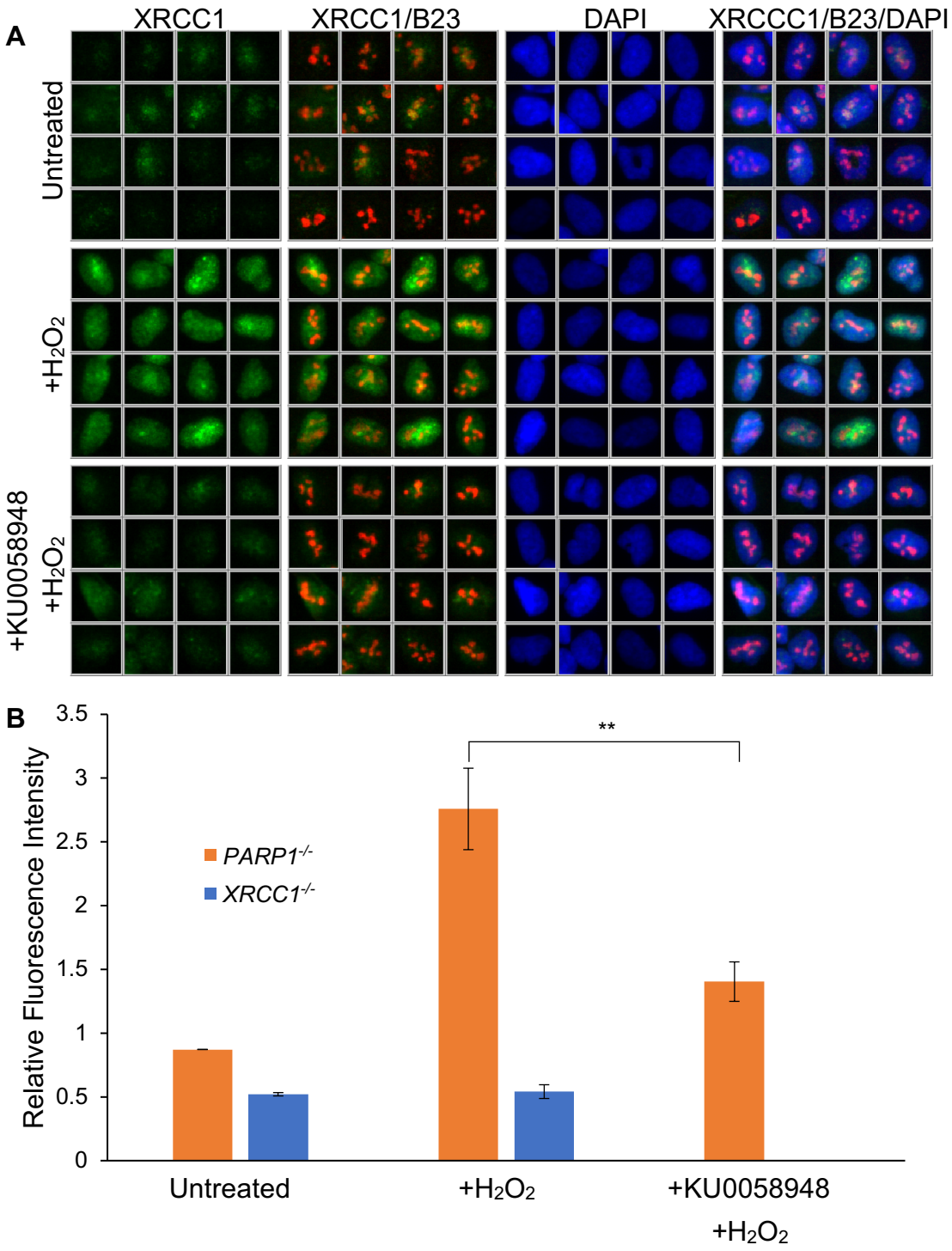

Figure 6.5. XRCC1 chromatin-loading in *PARP1*$^{-/-}$ cells is blocked by PARP inhibition. *PARP1*$^{-/-}$ and *XRCC1*$^{-/-}$ RPE-1 cells growing on glass coverslips were treated or not with 10 μM KU0058948 for 1 hr prior to being treated or not with 400 μM H_2O_2 for 7 min prior to pre-extraction, formaldehyde fixation and immunolabelling with antibodies against XRCC1 (green) and phosphoprotein B23 (red), and DNA-staining with DAPI (blue). Slides were imaged using the Olympus ScanR system and ScanR Analysis software was used to generate galleries of 16 randomly selected *PARP1*$^{-/-}$ cells for each condition **(A)** XRCC1 fluorescence from >1000 cells was quantified in the nuclear region excluding phosphoprotein B23 signal and is expressed as fold over signal in untreated *PARP1*$^{-/-}$ cells. Data are mean ±SEM of 3 biological replicates. Statistical significance was calculated by students t-test **(B)**.

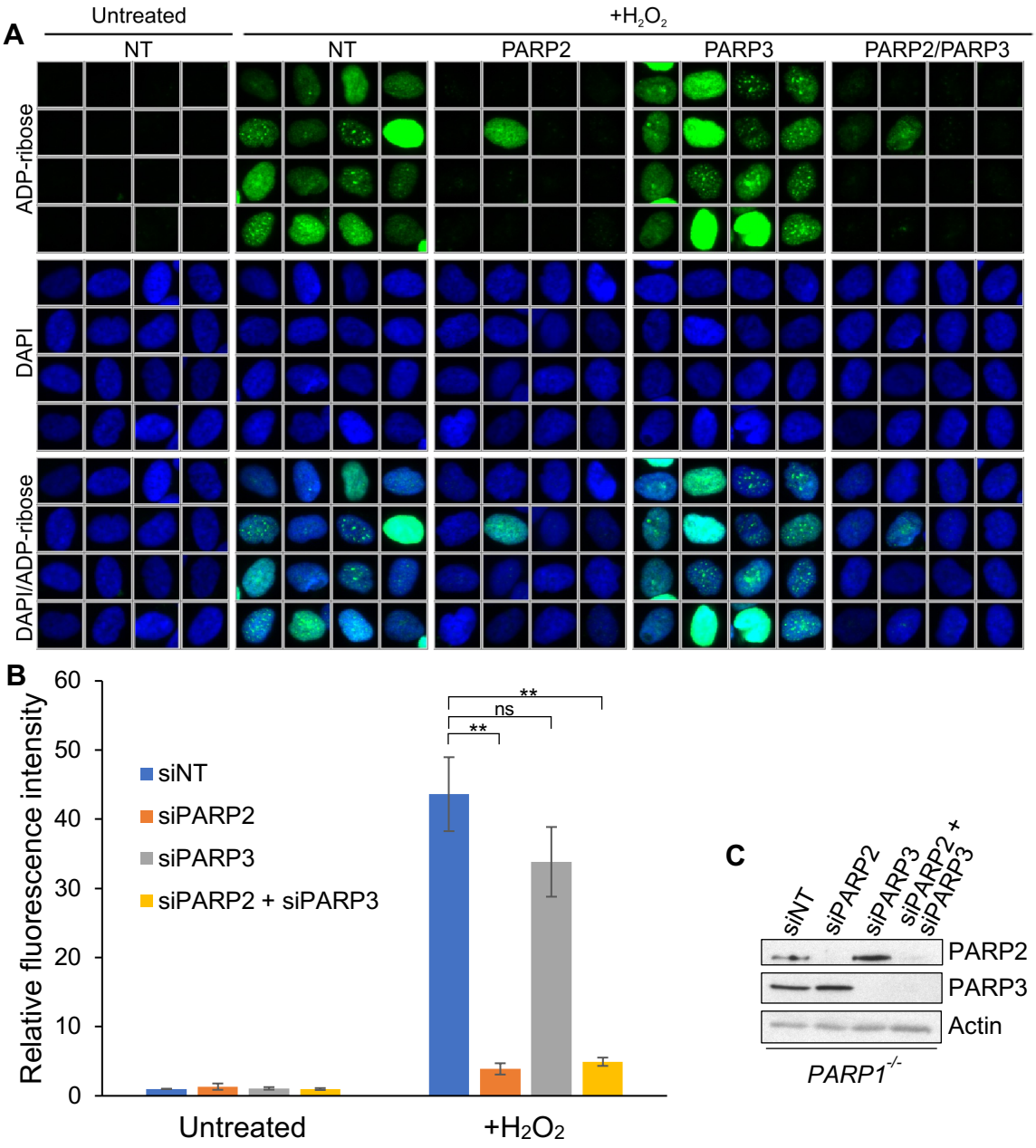

Figure 6.6. Depletion of PARP2 but not PARP3 significantly reduces H_2O_2-induced ADP-ribosylation in *PARP1*$^{-/-}$ RPE-1 cells. *PARP1*$^{-/-}$ RPE-1 cells were reverse transfected with siRNA targeting PARP2, PARP3, PARP2+PARP3 or a non-targeting siRNA. 48 h later, cells were seeded onto glass coverslips. 24 h later cells were treated or not with 400 µM H_2O_2 for 7 min prior to formaldehyde fixation and labelling with Pan ADP-ribose binding reagent (green), and DNA labelling with DAPI (blue). Slides were imaged using the Olympus ScanR system and ScanR Analysis software was used to generate galleries of 16 randomly selected cells for each condition **(A)**. ADP-ribose fluorescence from >1000 cells was quantified and is expressed as fold over signal in untreated NT-transfected cells. Data are means ±SEM of 3 experiments. Statistical significance was calculated by students t-test **(B)**. PARP2 and/or PARP3 depletion is demonstrated by a representative immunoblot **(C)**.

observations therefore do not statistically support the hypothesis that the residual signal is due to PARP3 activity. However, this result does not exclude a role for PARP3 in the response to ROS.

6.2.5. Simultaneous depletion of PARP1/PARP2 significantly reduces H_2O_2-induced XRCC1 chromatin-loading.

In parallel to ADP-ribosylation quantification, XRCC1 chromatin recruitment was measured in PARP2 and PARP3-depleted *PARP1*$^{-/-}$ RPE-1 cells (Fig. 6.7.). In agreement with the reduction in ADP-ribosylation, only PARP2 depletion caused a significant reduction in XRCC1 chromatin-loading in *PARP1*$^{-/-}$ RPE-1 cells (t-test p-values: $2.07x10^{-3}$ and $2.04x10^{-3}$, respectively). Whilst the residual level of H_2O_2-induced XRCC1-loading in PARP2-depleted cells (2.1-fold relative to untreated WT) was significantly greater than in untreated cells (t-test p-value = $1.95x10^{-3}$), this could be explained by incomplete or heterogenous transfection efficiency, as described above. PARP3 depletion did not result in a significant reduction in H_2O_2-induced XRCC1-chromatin loading in *PARP1*$^{-/-}$ cells (t-test p-value = $1.51x10^{-1}$). Furthermore, PARP2 and PARP3 depletion in combination did not result in a significant reduction in XRCC1-chromatin loading vs PARP2 depletion alone (t-test p-value = $4.84x10^{-1}$). These assays therefore find no significant evidence to support a role for PARP3 in the loading of XRCC1 into oxidized chromatin.

6.2.6. *PARP1*$^{-/-}$/*PARP2*$^{-/-}$ RPE-1 cells lack significant H_2O_2-induced ADP-ribosylation and XRCC1 chromatin-loading.

To avoid the problems of incomplete or heterogenous target depletion by siRNA described above, and to determine conclusively if XRCC1 chromatin loading is entirely dependent on PARP1 and PARP2, CRISPR technology was used to generate a cell line in which both *PARP1* and *PARP2* were deleted (see Chapter Four). H_2O_2-induced ADP-ribosylation (Fig. 6.8.) and XRCC1 chromatin-loading (Fig. 6.9.) was measured in these cells as described above. Notably, I failed to detect ADP-ribosylation in H_2O_2-treated *PARP1*$^{-/-}$/*PARP2*$^{-/-}$ cells (t-test p-value = $1.62x10^{-1}$), confirming that PARP2 accounted for the residual ADP-ribosylation in

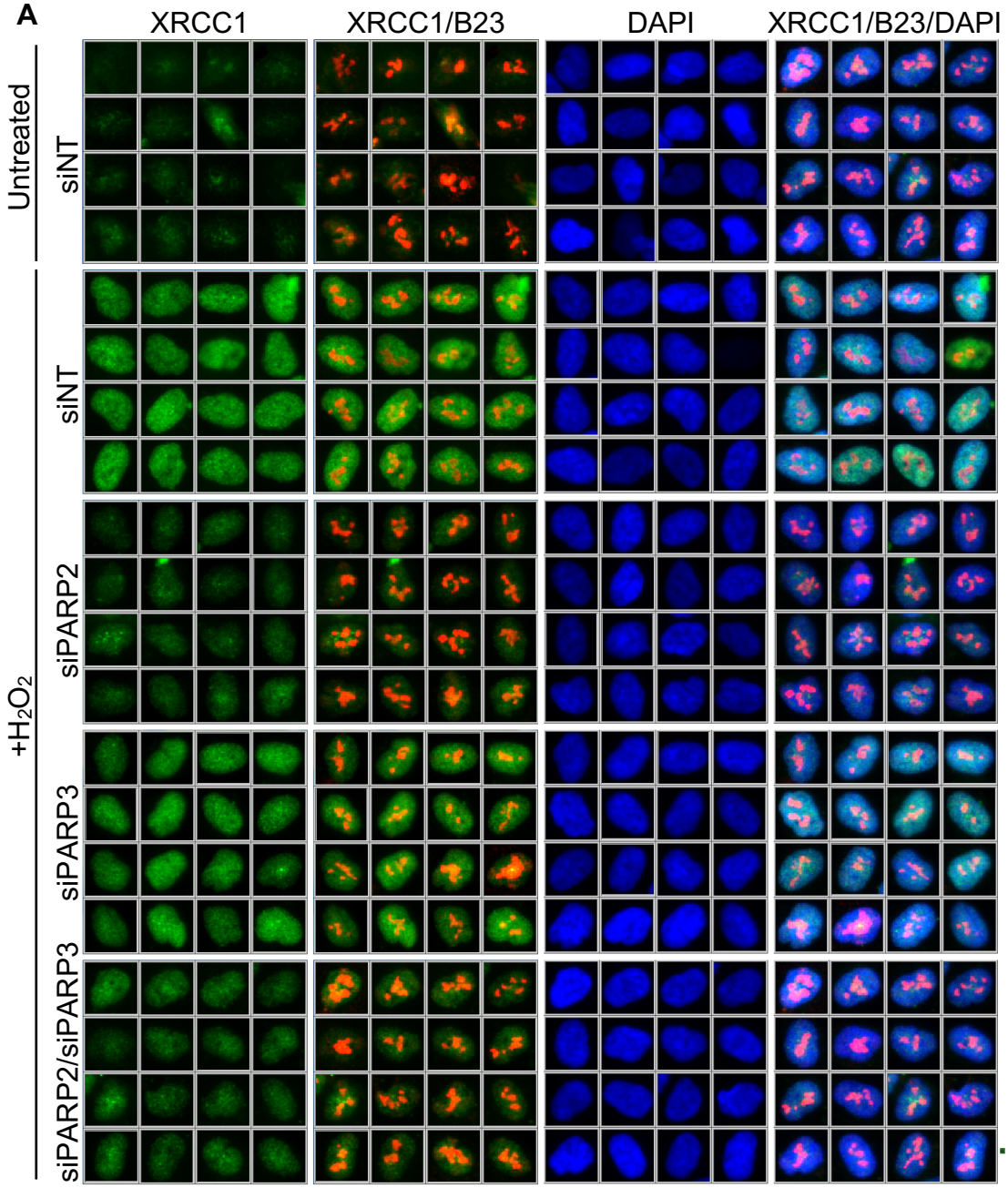

Figure 6.7. Depletion of PARP2 but not PARP3 significantly reduces H_2O_2-induced XRCC1 chromatin loading in *PARP1*$^{-/-}$ RPE-1 cells. *PARP1*$^{-/-}$ RPE-1 cells were reverse transfected with siRNA targeting PARP2, PARP3, PARP2+PARP3 or a non-targeting siRNA. 48 hr later, cells were seeded onto glass coverslips. 24 hr later cells were treated or not with 400 μM H_2O_2 for 7 min prior to pre-extraction, formaldehyde fixation and labelling with anti-XRCC1 (green) and anti-B23 antibodies (red), and DNA-staining with DAPI (blue). Slides were imaged using the Olympus ScanR system and ScanR Analysis software was used to generate galleries of 16 randomly selected cells for each condition **(A)**. XRCC1 from >1000 cells was quantified in the nuclear region excluding the nucleolus and is expressed as fold over signal in untreated NT-transfected cells. Data are means ±SEM of 3 experiments. Statistical significance was calculated by students t-test **(B, overleaf)**.

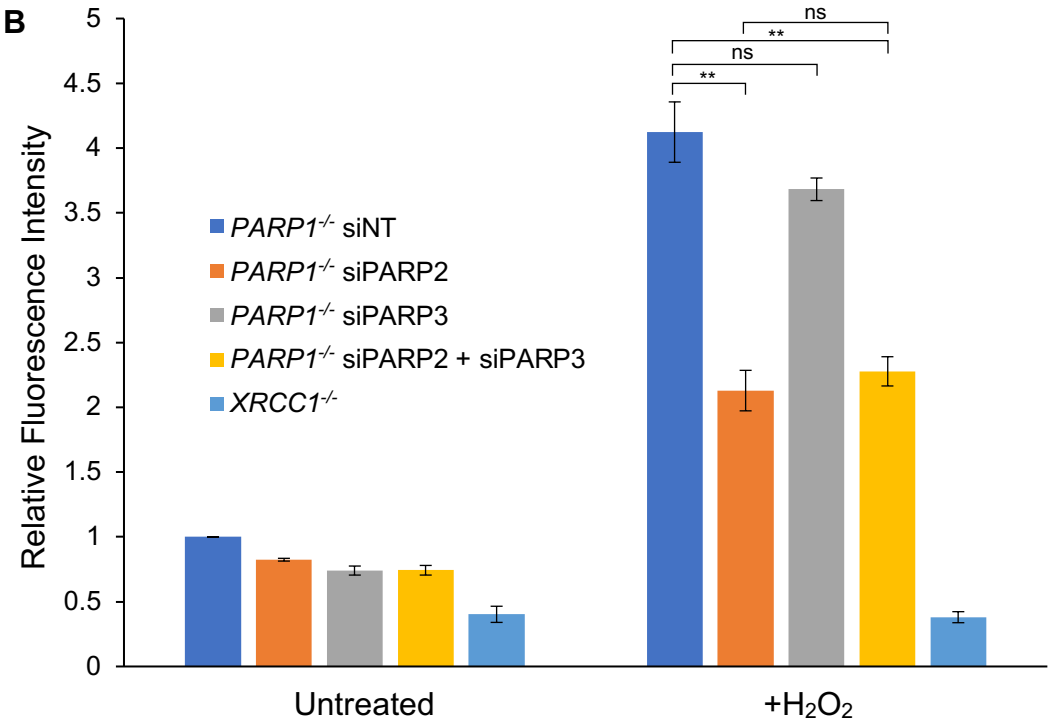
B
Relative Fluorescence Intensity
5
4.5
4
3.5
3
2.5
2
1.5
1
0.5
0
PARP1-/- siNT
PARP1-/- siPARP2
PARP1-/- siPARP3
PARP1-/- siPARP2 + siPARP3
XRCC1-/-
ns
**
ns
**
Untreated
+H2O2

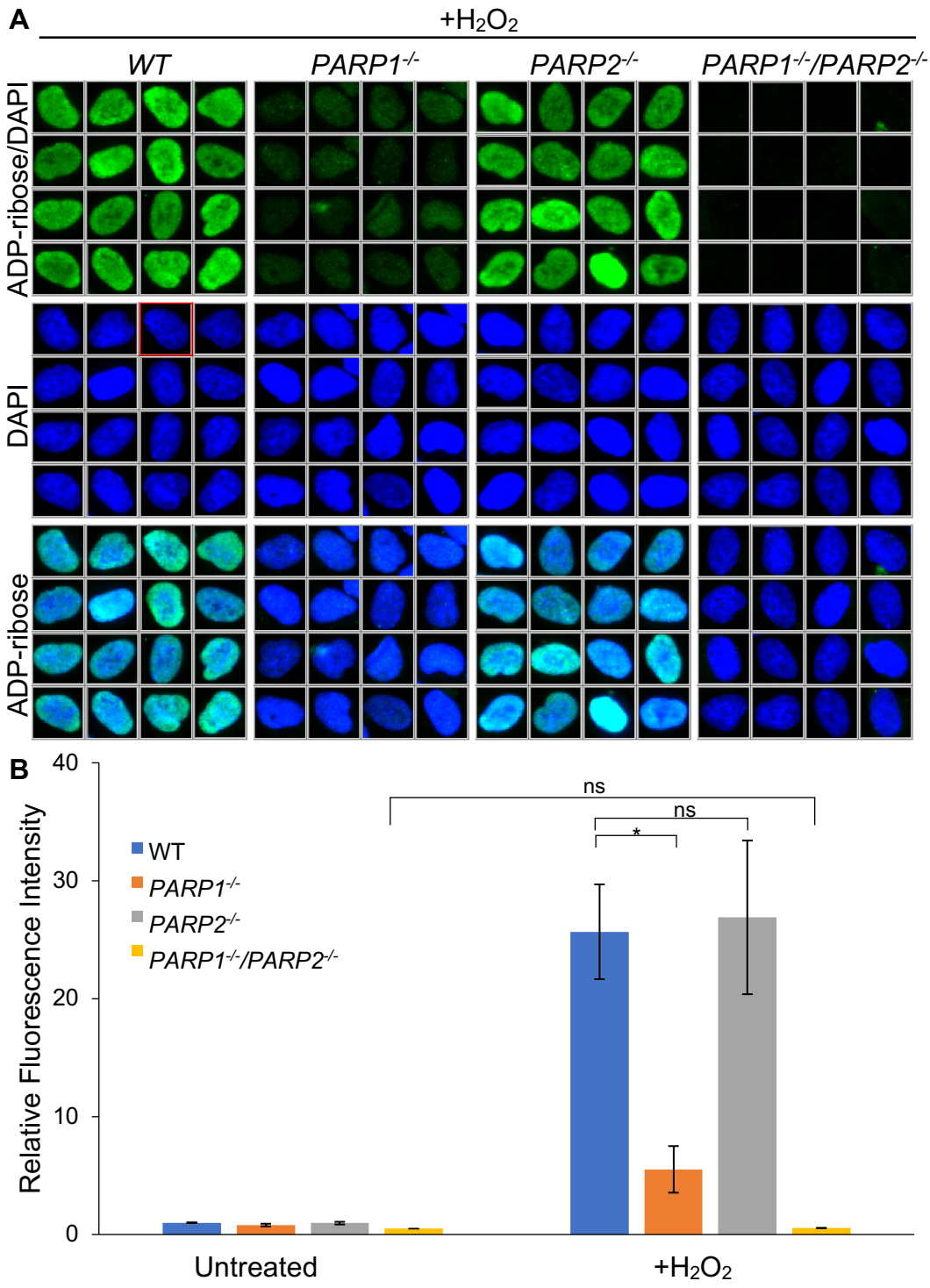

Figure 6.8. Deletion of *PARP1* and *PARP2* significantly reduces H_2O_2-induced ADP-ribosylation. WT, *PARP1*$^{-/-}$, *PARP2*$^{-/-}$ and *PARP1*$^{-/-}$/*PARP2*$^{-/-}$ RPE-1 cells growing on glass coverslips were treated or not with 400 µM H_2O_2 for 7 min prior to formaldehyde fixation and labelling with pan-ADP-ribose binding reagent (green), and DNA-labelling with DAPI (blue). Slides were imaged using the Olympus ScanR system and ScanR Analysis software was used to generate galleries of 16 randomly selected cells for each condition **(A)**. ADP-ribose from >1000 cells was quantified in the nucleus and is expressed as fold over signal in untreated WT cells. Data are mean ±S.E.M of 3 replicates. Statistical significance was calculated by students t-test **(B)**.

PARP1$^{-/-}$ cells. In addition, H_2O_2-induced XRCC1 chromatin-loading (1.34-fold) was significantly reduced in *PARP1*$^{-/-}$/*PARP2*$^{-/-}$ cells, compared to *PARP1*$^{-/-}$ cells (3.56-fold), to a level that was not significantly different from the background level in untreated cells (t-test p-value = $2.10x10^{-1}$).

In untreated *PARP1*$^{-/-}$/*PARP2*$^{-/-}$ cells, the nucleolar signal of XRCC1 was 74% that of untreated WT cells, but this was not significant at the 5% level (t-test p-value: $8.38x10^{-2}$). Furthermore, this reduction was also evident in the exnucleolar region (75% XRCC1 signal in untreated *PARP1*$^{-/-}$/*PARP2*$^{-/-}$ cells relative to untreated WT cells), implying that it is not specific to the nucleolus. As discussed in Chapter Five, there is therefore no significant evidence to suggest that the nucleolar XRCC1 signal in untreated cells is due to elevated association with ADP-ribosylated proteins in these regions. An alternative hypothesis is that the observed effect may be a consequence of poorer detergent extraction from the dense nucleolar region than from the surrounding nucleoplasm (see section 5.3).

6.2.7. H_2O_2- induced PNKP chromatin-loading is significantly reduced in *PARP1*$^{-/-}$/*PARP2*$^{-/-}$ cells.

Next, the chromatin loading of PNKP was investigated by IF following H_2O_2 treatment (Fig. 6.10.). Prior to H_2O_2 treatment, background PNKP signal was observed throughout the nucleus in WT cells, rather than predominately in the nucleolus, in contrast with XRCC1 (Fig. 5.4.). In WT cells, H_2O_2 treatment increased PNKP chromatin-loading 1.85-fold. This was not significantly diminished in *PARP1*$^{-/-}$, *PARP2*$^{-/-}$ or *PARP3*$^{-/-}$ cells (t-test p-values: $9.10x10^{-1}$, $2.15x10^{-1}$ and $4.15x10^{-1}$, respectively). However, in both *XRCC1*$^{-/-}$ and *PARP1*$^{-/-}$/*PARP2*$^{-/-}$ cells, the PNKP signal in chromatin was reduced to 0.69 and 0.95-fold that of WT untreated cells, respectively (t-test p-values: $4.34x10^{-3}$ and $1.16x10^{-2}$, respectively). This result confirms that PNKP localization at damage sites is largely dependent on XRCC1 and PARP1/2 activity. Chromatin-localized PNKP signal was notably more punctate than H_2O_2-induced XRCC1 signal. Co-IF experiments were not possible, due to both the anti-PNKP and anti-XRCC1 antibodies being raised in the same host species. However, the punctate nature

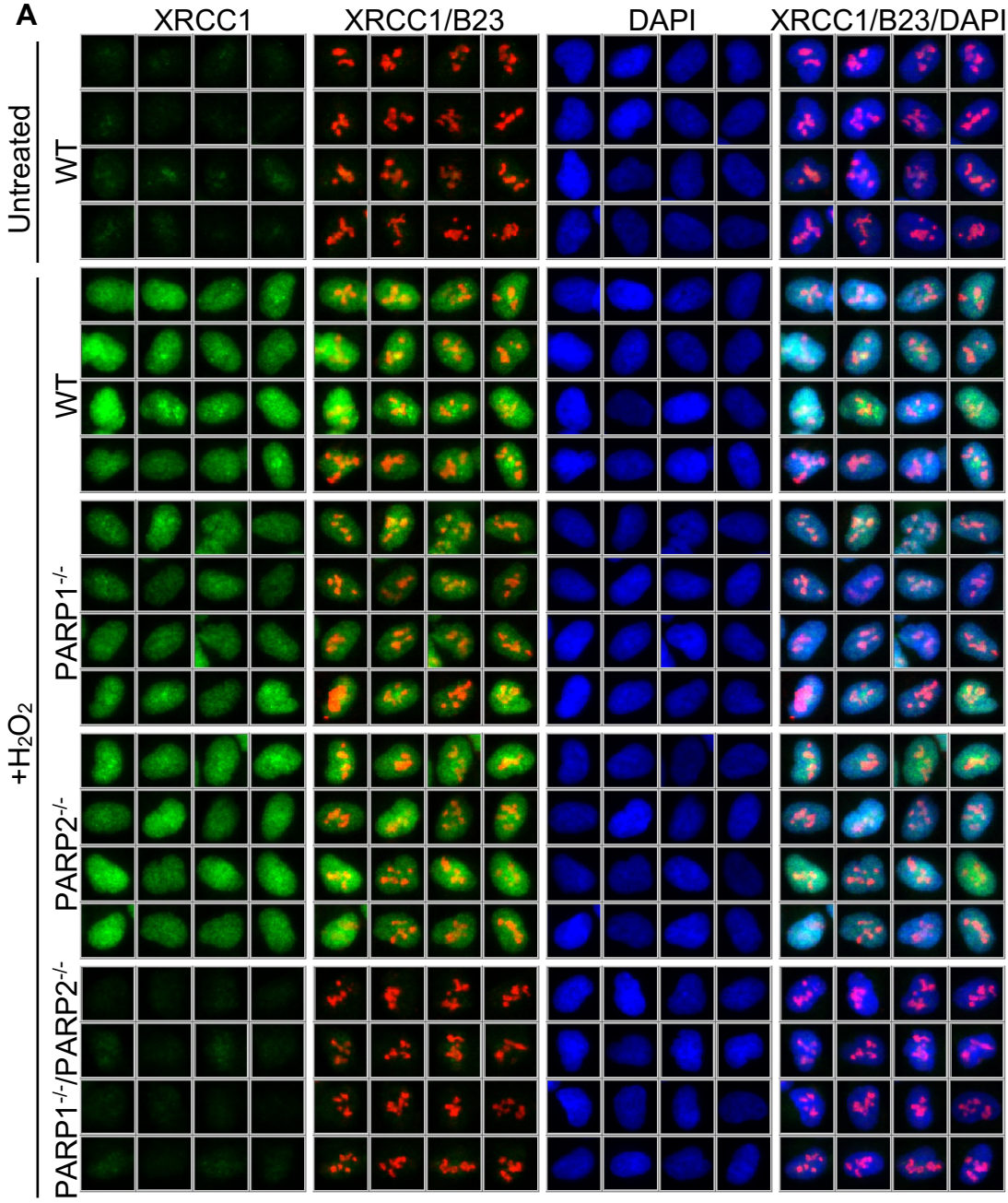

Figure 6.9. Deletion of *PARP1* and *PARP2* significantly reduces H_2O_2-induced XRCC1 chromatin loading. WT, *PARP1*$^{-/-}$, *PARP2*$^{-/-}$, *XRCC1*$^{-/-}$ and *PARP1*$^{-/-}$/*PARP2*$^{-/-}$ RPE-1 cells growing on glass coverslips were treated or not with 400 µM H_2O_2 for 7 min prior to pre-extraction, formaldehyde fixation and immunolabelling with antibodies against XRCC1 (green) and B23 (red), and DNA-staining with DAPI (blue). Slides were imaged using the Olympus ScanR system and ScanR Analysis software was used to generate galleries of 16 randomly selected cells for each condition **(A)**. XRCC1 fluorescence from >1000 cells was quantified in the nuclear region excluding phosphoprotein B23 signal and is expressed as fold over signal in untreated WT cells. Data are mean ± SEM of 3 biological replicates. Statistical significance was calculated by students t-test **(B, overleaf)**.

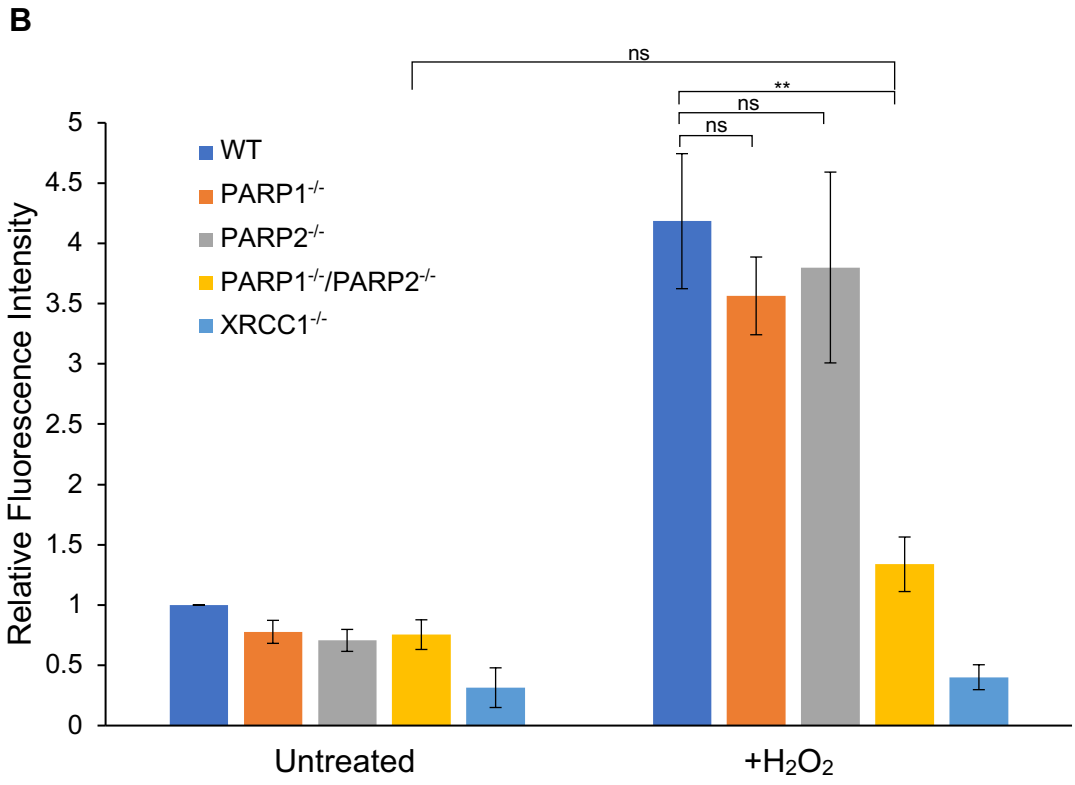
B
ns
**
ns
ns
WT
PARP1-/-
PARP2-/-
PARP1-/-/PARP2-/-
XRCC1-/-
Relative Fluorescence Intensity
5
4.5
4
3.5
3
2.5
2
1.5
1
0.5
0
Untreated
+H2O2

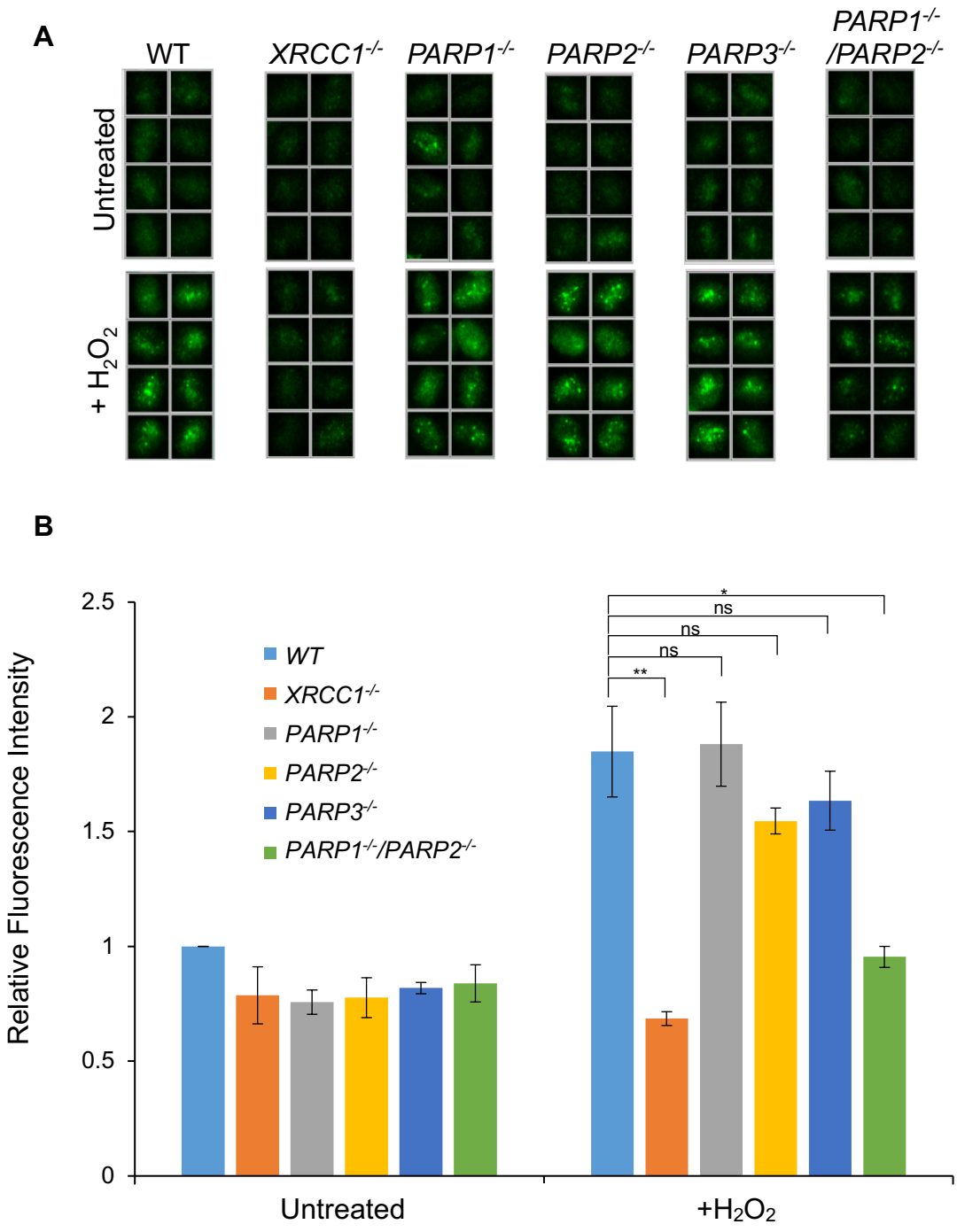

Figure 6.10. Deletion of *XRCC1* or *PARP1* and *PARP2* significantly reduces H_2O_2-induced PNKP chromatin loading. WT, *XRCC1*$^{-/-}$, *PARP1*$^{-/-}$, *PARP2*$^{-/-}$, *PARP3*$^{-/-}$ and *PARP1*$^{-/-}$/*PARP2*$^{-/-}$ RPE-1 cells growing on glass coverslips were treated or not with 400 μM H_2O_2 for 7 min prior to pre-extraction, formaldehyde fixation and immunolabelling with anti-PNKP antibody (green) and DNA-staining with DAPI (not shown). Slides were imaged using the Olympus ScanR system and ScanR Analysis software was used to generate galleries of 8 randomly selected cells for each condition **(A)**. PNKP fluorescence from >1000 cells was quantified in the nucleus and is expressed as fold over signal in untreated WT cells. Data are mean ±SEM of 3 biological replicates. Statistical significance was calculated by students t-test **(B).**

of the PNKP signal may reflect its association with a subset of XRCC1 complexes (see section 6.3 for further discussion).

6.2.8. Rates of SSBR in WT, *PARP1*$^{-/-}$, *PARP2*$^{-/-}$, *PARP1*$^{-/-}$/*PARP2*$^{-/-}$ and *XRCC1*$^{-/-}$ cells.

Thus far, this chapter has dealt specifically with the ADP-ribosylation requirements for H_2O_2-induced chromatin-loading of the repair factors XRCC1 and PNKP. It has been suggested however that ADP-ribosylation at damaged DNA loci might serve additional functions beyond the rapid localization of the XRCC1 repair complex. Some such functions include modulation of chromatin superstructure (de Murcia, Huletsky et al. 1986, Kim, Mauro et al. 2004, Wacker, Ruhl et al. 2007), chromatin remodelling (Messner and Hottiger 2011) and rapid nuclear ATP generation (Wright, Lioutas et al. 2016). It is feasible that whilst either PARP1 or PARP2 is capable of supporting XRCC1 chromatin-recruitment, they are not equivalent for these other potential roles. To approach this problem, the alkaline single cell electrophoresis (Comet) assay was employed to measure levels of DNA breaks and therefore SSBR rates directly (Fig. 6.11.). Previous use of γ-Ray calibration curves in combination with this protocol allows approximate conversion of Comet tail moment to number of breaks per cell (Fisher, Hochegger et al. 2007). Based on this calibration, 1 unit of Comet tail moment is approximately equal to 1000 DNA breaks per cell. Whilst the alkaline Comet assay cannot distinguish single and double strand breaks, it has been previously demonstrated that H_2O_2 induces an approximate DSB:SSB ratio of 1:2000 (Bradley and Kohn 1979), suggesting that the Comet tails observed here are largely a measurement of SSBs.

WT, *PARP1*$^{-/-}$, *PARP2*$^{-/-}$, *PARP1*$^{-/-}$/*PARP2*$^{-/-}$ and *XRCC1*$^{-/-}$ RPE-1 cells were treated in suspension with 50 µM H_2O_2 for 10 min on ice. Samples were taken immediately after this treatment, or following increasing 37˚C incubation repair times. Regardless of genotype, untreated cells had a very low average tail moment (0.12 for WT), indicating that the level of endogenous damage in these cells is below the detection limit of the assay. Immediately following H_2O_2 treatment the Comet tail moment in WT cells increased to ~20.41; indicative of ~20,000 DNA breaks per cell (Fig. 6.11a). There was some variation in the damage induction between genotypes. However, this also varied between

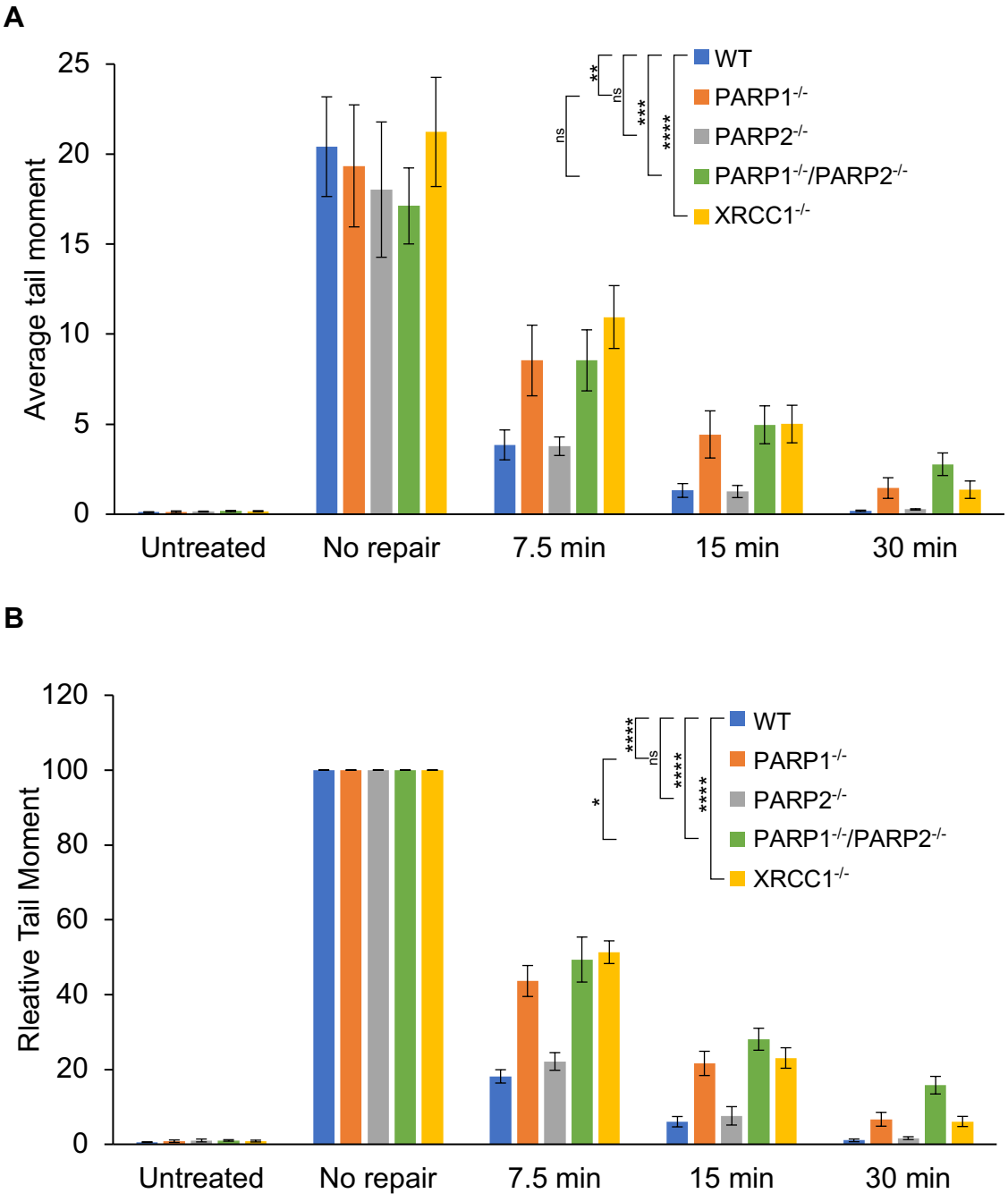

Figure 6.11. Rates of SSBR in H_2O_2-induced WT, *PARP1*$^{-/-}$, *PARP2*$^{-/-}$, *PARP1*$^{-/-}$/*PARP2*$^{-/-}$ and *XRCC1*$^{-/-}$ RPE-1 cells. Subconfluent RPE-1 cells of the indicated genotypes were trypsinised, washed with PBS and resuspended in ice cold 50 μM H_2O_2 PBS on ice for 10 min, prior to quenching, washing and resuspension with ice cold complete media. Samples were taken immediately prior to addition of H_2O_2 (untreated), immediately after treatment and resuspension in ice cold media (no repair), and following 7.5, 15 and 30 min subsequent incubation at 37°C. Samples were subjected to alkaline single cell electrophoresis and comet tail moments were measured with Comet IV software. Data are presented as absolute (**A**) or relative (**B**) values. All data are expressed as mean ±SEM of 4 independent experiments. Statistical significance was calculated by two factor ANOVA.

replicates, indicating that it is likely to be due to experimental variation, rather than cellular genotype. In WT cells, the Comet tail moment decreased to 0.19 within 30 min following drug removal, which was not significantly different from that of untreated cells (t-test p-value = 1.66×10^{-1}), and so indicated complete repair. By comparison, the repair of damage was significantly delayed in *PARP1*$^{-/-}$, *XRCC1*$^{-/-}$ and *PARP1*$^{-/-}$/*PARP2*$^{-/-}$ cells (ANOVA p-values: 2.59×10^{-3}, 5.49×10^{-5} and 1.47×10^{-4}, respectively).

As mentioned above, the induction of damage was variable between replicates, which decreased the reproducibility of the absolute tail moments. For this reason, the data were also expressed as a percentage of the no repair value (Fig. 6.11.b). This method increased the precision of the data, which is evident from a general decrease in the relative SEM values. When expressed as relative Comet tail moments, a significant difference was found between repair in *PARP1*$^{-/-}$ and *PARP1*$^{-/-}$/*PARP2*$^{-/-}$ cells by analysis of variance (ANOVA p-value: 2.97×10^{-2}).

The number of DNA breaks over time follow exponential decay kinetics (Fig. 6.11). To quantify the rates of SSBR in the different genotypes, exponential regression was used to fit an exponential curve to the relative tail moment data, with an equation of the form:

$$N_t = N_0 e^{-\lambda t}$$

This equation relates the proportion of strand breaks remaining (N_t) at a given time (t) to the number of strand breaks without repair (N_0) and the exponential decay constant (λ). The exponential decay constant (λ) was used to calculate the half-life of strand breaks in each genotype (Table 6.1). These calculations reveal a half-life of H_2O_2-induced damage of 3.03 min in WT RPE-1 cells, which is comparable to that estimated from a previous study employing A549 cells (Fisher, Hochegger et al. 2007). Relative to this value, the half-lives in *PARP1*$^{-/-}$ (6.43 min), *XRCC1*$^{-/-}$ (7.44 min) and *PARP1*$^{-/-}$/*PARP2*$^{-/-}$ cells (8.11 min) were all significantly increased (extra sum-of-squares F test p-values $<1 \times 10^{-4}$) In comparison, the half-life of strand breaks in *PARP2*$^{-/-}$ (3.45 min) was not significantly different from that in WT cells (extra sum-of-squares F test p-value = 5.07×10^{-2}). Furthermore, the half-life of H_2O_2-induced strand breaks in *PARP1*$^{-/-}$

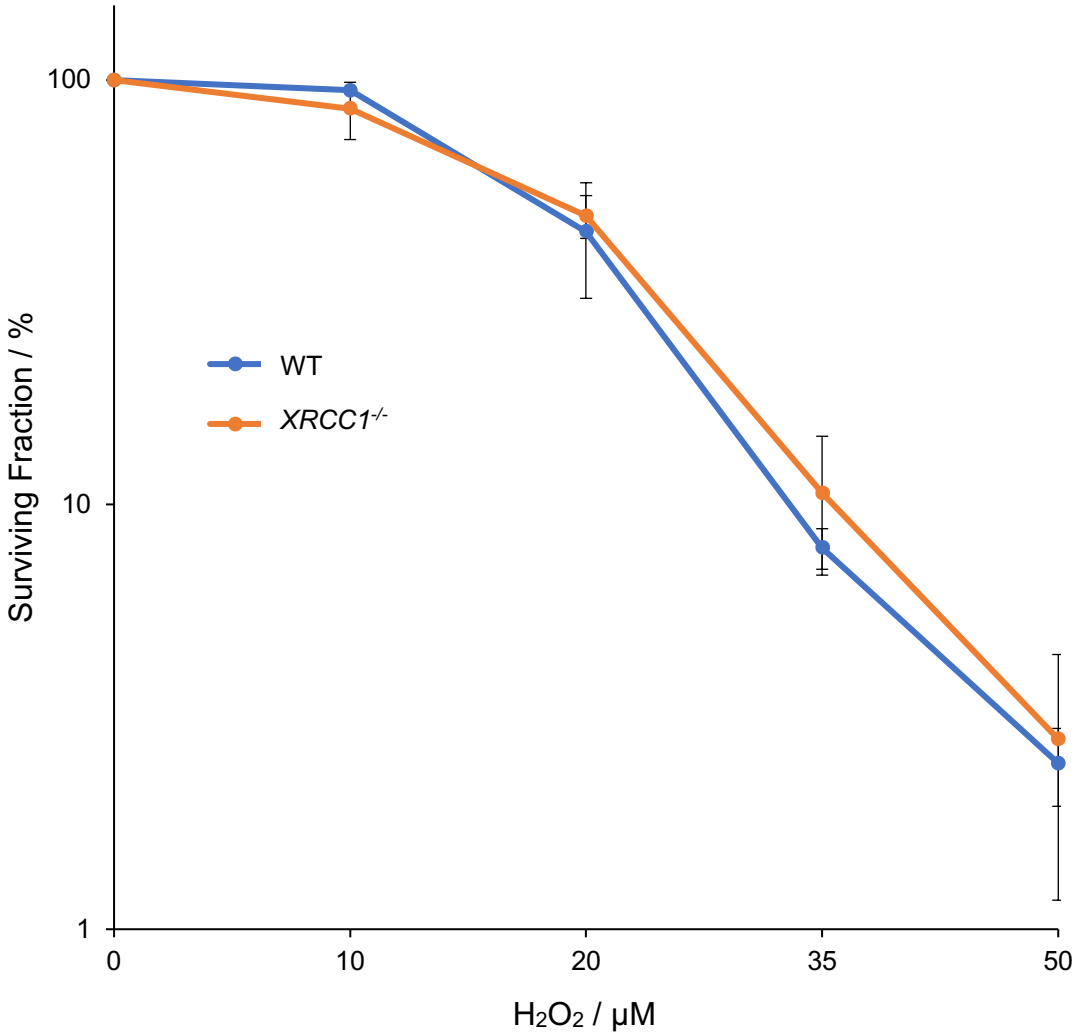

Figure 6.12. Deletion of *XRCC1* does not sensitise RPE-1 cells to H_2O_2. WT and *XRCC1*$^{-/-}$ cells RPE-1 cells were plated at low density (300 per 10 cm dish) and incubated at 37°C for 4 h to allow adherence. Dishes were then treated with the indicated dose of H_2O_2 for 20 min in PBS at RT, prior to washing with PBS and incubation at 37°C in complete DMEM/F12 media for 12 days. Dishes were then stained with 2% methylene blue and colonies of >50 cells were counted. Each dose was conducted on triplicate 10 cm dishes per experiment. The data are expressed as mean ±SEM of 4 independent biological replicates.

Cell Line	Exponential Decay Constant / λ	Half-life / min	R^2
WT	0.229, CI 95% [0.204, 0.253]	3.03, CI 95% [2.74, 3.40]	0.997
PARP1$^{-/-}$	0.108, CI 95% [0.084, 0.131]	6.43, CI 95% [5.28, 8.24]	0.981
PARP2$^{-/-}$	0.201, CI 95% [0.172, 0.230]	3.45, CI 95% [3.02, 4.02]	0.994
XRCC1$^{-/-}$	0.093, CI 95% [0.076, 0.110]	7.44, CI 95% [6.30, 9.08]	0.988
PARP1$^{-/-}$/ *PARP2*$^{-/-}$	0.085, CI 95% [0.054, 0.117]	8.11, CI 95% [5.95, 12.75]	0.949

Table 6.1. Exponential decay equations for the proportion of SSBs remaining (N_t) against time (t) for WT, *PARP1*$^{-/-}$, *PARP2*$^{-/-}$, *XRCC1*$^{-/-}$ and *PARP1*$^{-/-}$/*PARP2*$^{-/-}$ RPE-1 cells. Exponential regression was used to fit equations to the repair kinetics. Exponential decay constants, and half-lives (min), including upper and lower 95% confidence intervals, are provided for each cell line. R^2 values are also provided for each regression, demonstrating high goodness of fit.

/PARP2$^{-/-}$ cells was significantly different from that in *PARP1*$^{-/-}$ cells (extra sum-of-squares F test p-value = $3.32x10^{-2}$), but not significantly different than that in *XRCC1*$^{-/-}$ cells (extra sum-of-squares F test p-value = $3.29x10^{-1}$).

6.2.9. Sensitivity of RPE-1 cells to H_2O_2

Cellular sensitivity of RPE-1 cells to H_2O_2 was investigated by clonogenic survival assay (Fig. 6.12.). Subconfluent WT and *XRCC1*$^{-/-}$ RPE-1 cells were plated at a low density (300 per 10 cm dish) and incubated for 4 h to allow cell adhesion. Cells were then treated with 0, 10, 20, 35 or 50 µM H_2O_2 in PBS for 20 min at RT, prior to PBS washing and incubation for 12 days at 37˚C in complete media. Dishes were then stained with 2% methylene blue to allow counting of colonies of more than 50 cells. Unfortunately, despite clear killing of WT RPE-1 cells over the tested dose range, *XRCC1*$^{-/-}$ cells were not more sensitive. The lack of sensitivity of *XRCC1*$^{-/-}$ vs WT implies that SSBR rate is not the limiting factor for H_2O_2 cytotoxicity in RPE-1 cells. ROS are known to be important signalling molecules in mediating caspase-dependent apoptosis (Pierce, Parchment et al. 1991). It is possible that RPE-1 cells may be particularly sensitive to the pro-apoptotic effects of ROS which are independent of persistent SSBs. In support of this, the EC_{50} for WT RPE-1s (~18 µM) was notably at least an order of magnitude lower than the EC_{50} values of some other commonly used cell lines (Table 6.2.), all of which have been demonstrated to be sensitised to H_2O_2 by XRCC1 loss.

6.3. Conclusions and Discussion

The results of this chapter reveal that whilst *PARP1*$^{-/-}$ cells had significantly reduced H_2O_2-induced ADP-ribosylation, the chromatin-loading of XRCC1 and PNKP was not significantly reduced. Furthermore, individual deletion of *PARP2* or *PARP3* failed to significantly reduce H_2O_2-induced ADP-ribosylation or chromatin-loading of XRCC1 or PNKP. Despite this, the chromatin-loading of XRCC1 in *PARP1*$^{-/-}$ cells was found to be ADP-ribosylation dependent, as it was blocked by PARP inhibition. Considering this, it was found that simultaneous loss of *PARP1* and *PARP2* could ablate H_2O_2-induced ADP-ribosylation and

Cell line	Treatment Time / min	Treatment Buffer	Treatment Temperature / °C	Estimated EC_{50} / µM	Ref.
CHO	15	PBS	37	300	(Breslin, 2004)
MCF-7	30	PBS	20	300	(Nyaga, 2006)
U2OS	30	Serum-free Media	37	185	(Paquet, 2015)
RPE-1	20	PBS	20	18	Fig. 7.13

Table 6.2. Estimated H_2O_2 EC_{50} values of commonly used cell lines. The EC_{50} values for the indicated H_2O_2 treatments, estimated from the referenced publications.

significantly reduce or ablate XRCC1 chromatin-loading. This was demonstrated by siRNA mediated depletion of PARP2 mRNA, and by successful generation of the first reported *PARP1*$^{-/-}$/*PARP2*$^{-/-}$ cell line (Hanzlikova, Gittens et al. 2016). Depletion of PARP3 mRNA did not significantly impact on XRCC1 chromatin-loading in *PARP1*$^{-/-}$ cells, nor did it significantly further reduce XRCC1 chromatin loading in PARP2-depleted *PARP1*$^{-/-}$ cells, suggesting that PARP3 does not function in XRCC1 chromatin-loading in response to H_2O_2.

The complete absence of ADP-ribosylation in H_2O_2-treated *PARP1*$^{-/-}$/*PARP2*$^{-/-}$ cells was notable and requires discussion. PARP3 has been reported previously to interact with components of BER/SSBR (Rouleau, McDonald et al. 2007) and to be stimulated by nicked oligonucleotide substrates (Rulten, Fisher et al. 2011, Langelier, Riccio et al. 2014), leading to speculation about an undescribed role in SSBR in addition to its role in promoting DSBR by NHEJ (Boehler, Gauthier et al. 2011, Rulten, Fisher et al. 2011, Beck, Boehler et al. 2014). Recent work in the Caldecott laboratory has identified H2B^{Glu2} as a site of PARP3 mono-ADP-ribosylation in nucleosomes containing nicks and 3'-overhang DSBs. Considering this, the absence of Pan-ADP-ribose signal in H_2O_2-treated *PARP1*$^{-/-}$/*PARP2*$^{-/-}$ cells is perhaps surprising. Pan-ADP-ribose binding reagent is reported to recognize mono-ADP-ribose on recombinant PARP3 (Kraus 2015). Despite this, it is likely that the multiple terminal ADP-ribose moieties in branched PAR provide many more binding sites than MAR for Pan-ADP-ribose binding reagent, resulting in an amplification of the signal. This may result in PARP3 ADP-ribosylation signal being below the detection limit of this assay. An alternative but not mutually exclusive explanation is that PARP3 acts upon a repair intermediate which is downstream of PARP1/PARP2 activity and thus reduced in *PARP1*$^{-/-}$/*PARP2*$^{-/-}$ cells. Given that, in contrast to PARP1, PARP3 activity is specifically stimulated by 5'-phosphorylated nicks (Langelier, Riccio et al. 2014), these data do not exclude the possibility that the role of these respective enzymes may be to sense SSBs that arise before and after restoration of canonical termini.

In addition to quantification of XRCC1 chromatin-loading and ADP-ribosylation, repair rates were measured directly using the alkaline Comet assay. These data were expressed in terms of absolute values, and also relative to the

no-repair level in each experiment. Additionally, non-linear regression was used to fit exponential decay kinetics to the relative Comet tail moments, allowing quantification of the rates of repair in the different genotypes. By all analyses, the repair in *PARP1*$^{-/-}$, *PARP1*$^{-/-}$/*PARP2*$^{-/-}$ and *XRCC1*$^{-/-}$ cells was significantly slower than in WT cells, whereas repair in *PARP2*$^{-/-}$ cells was not. Whilst the rate of repair in *XRCC1*$^{-/-}$ cells was slower than in *PARP1*$^{-/-}$ cells (indicated by SSB half-lives of 7.44 and 6.43 min, respectively), this was not significant at the 5% level. Given that XRCC1 chromatin-loading is not significantly decreased in *PARP1*$^{-/-}$ cells, this supports PARP1 fulfilling other roles in SSBR independent of XRCC1 chromatin-loading, such as the relaxation of chromatin (Poirier, de Murcia et al. 1982, Aubin, Fréchette et al. 1983, de Murcia, Huletsky et al. 1986, Kim, Mauro et al. 2004, Strickfaden, McDonald et al. 2016). Only when expressed in terms of relative Comet tail moments, was a significant difference was found between H_2O_2-induced Comet tail moments in *PARP1*$^{-/-}$ and *PARP1*$^{-/-}$/*PARP2*$^{-/-}$ cells by analysis of variance (ANOVA). This is likely to be due to the two cell lines having significantly different relative Comet tail moments at 30 min repair (t-test p-value = 2.25×10^{-2}), as the values were not significantly different at 7.5 or 15 min of repair (t-test p-values: 4.62×10^{-1} and 1.9×10^{-1}, respectively). In support of this, an extra sum-of-squares F-test confirmed that the rate of repair in *PARP1*$^{-/-}$/*PARP2*$^{-/-}$ cells (SSB half-life of 8.11 min) was significantly slower than in *PARP1*$^{-/-}$ cells, suggesting a role for PARP2 in SSBR in the absence of PARP1. It is important to note that the Comet tail moment at 30 min of repair was also significantly elevated in *PARP1*$^{-/-}$/*PARP2*$^{-/-}$ relative to *XRCC1*$^{-/-}$ cells, suggesting that this phenotype is not caused by a failure to load XRCC1 into chromatin. Future work could focus on other mechanisms mediated by ADP-ribosylation which may accelerate SSBR in addition to XRCC1 chromatin localization. In particular, the relative contribution of PARP1, PARP2 and PARP3 to these mechanisms must be assessed.

Observation of ablated PNKP chromatin-loading in *XRCC1*$^{-/-}$ cells supports previous observations in EM9 (*XRCC1*$^{-/-}$) cells (Loizou, El-Khamisy et al. 2004), and confirms that PNKP localization to damage sites is largely dependent on its interaction with XRCC1, which has been previously questioned (Parsons, Dianova et al. 2005). In agreement with this, *PARP1*$^{-/-}$/*PARP2*$^{-/-}$ cells, which fail to efficiently load XRCC1, consequently also exhibit reduced PNKP

chromatin-loading. The H_2O_2-induced PNKP signal was notably more punctate than XRCC1 signal. The reason for this is unclear and will require further study. PNKP retention at damage sites has been shown previously to be more transient than XRCC1 retention (Della-Maria, Hegde et al. 2012). Thus, we may not expect PNKP to exactly colocalize with XRCC1 in damaged chromatin. Instead, at a given time point, PNKP might occupy a subset of damage sites, making its focal distribution more apparent.

In summary, this chapter has employed WB, IF, high-content microscopy and the alkaline Comet assay to reveal the contributions of PARP1 and PARP2 to H_2O_2-induced ADP-ribosylation, XRCC1 and PNKP chromatin loading; and to rates of SSBR. In the concluding results chapter, SSBR will be investigated at another type of physiologically relevant SSBs: those which result from abortive Topoisomerase 1 activity.

Chapter Seven

The Role of PARP1, TDP1 and XRCC1 in the Repair of CPT-induced DNA Damage

7.1. Introduction and Aims

The previous chapter utilized a panel of isogenic human cell lines to investigate the roles of PARP1, PARP2 and PARP3 in H_2O_2-induced ADP-ribosylation, XRCC1 chromatin-loading and rates of SSBR. In addition to oxidation of DNA, another physiologically relevant source of SSBs is the abortive action of Topoisomerase 1 (Top1), which will be the focus of this chapter.

Top1 acts to relax torsional stress associated with replication and transcription, via a Top1-DNA covalent intermediate termed the Top1-cleavage complex (Top1cc). Top1ccs can be stabilized under certain physiological conditions, such as by the presence of proximal DNA lesions (Pourquier, Ueng et al. 1997, Lesher, Pommier et al. 2002), which disrupt re-ligation efficiency. Additionally, Top1ccs can be stabilized by exogenous agents such as camptothecin (CPT). Collision of RNA or DNA polymerases (Wu and Liu 1997, Strumberg, Pilon et al. 2000) can convert reversible Top1ccs on the template strand into irreversible Top1-linked SSBs (Top1-SSBs). Repair can proceed by proteolysis of the Top1 polypeptide, followed by the action of Tyrosyl-DNA phosphodiesterase 1 (TDP1) to cleave the tyrosyl-3'-DNA phosphodiester. This reaction reveals a 3'-phosphate DNA terminus which, along with the 5'-hydroxyl terminus generated by the Top1 initially, must be processed by PNKP to restore ligatable 3'-hydroxyl and 5'-phosphate termini. Finally, the nick can be ligated by XRCC1-Lig3 (Fig. 7.1.).

PARP1 activity has been implicated in the repair of Top1-SSBs (Pommier, Barcelo et al. 2006, Zhang, Regairaz et al. 2011, Das, Huang et al. 2014). This has been demonstrated genetically by the sensitivity of *PARP1*$^{-/-}$ Chicken DT40 cells (Das, Huang et al. 2014) to CPT and other Top1 poisons. In contrast, another study employing *PARP1*$^{-/-}$ MEFs found that deletion of *PARP1* did not sensitise cells to CPT (Patel, Flatten et al. 2012). Since DT40 cells do not encode a *PARP2* ortholog (Hochegger, Dejsuphong et al. 2006), we wondered if the conflicting conclusions of these studies might be explained by the availability of *PARP2* in mammalian cells. Therefore, one aim of section is to examine the functional redundancy between PARP1, PARP2 and PARP3 proteins for cellular responses to CPT in human cells.

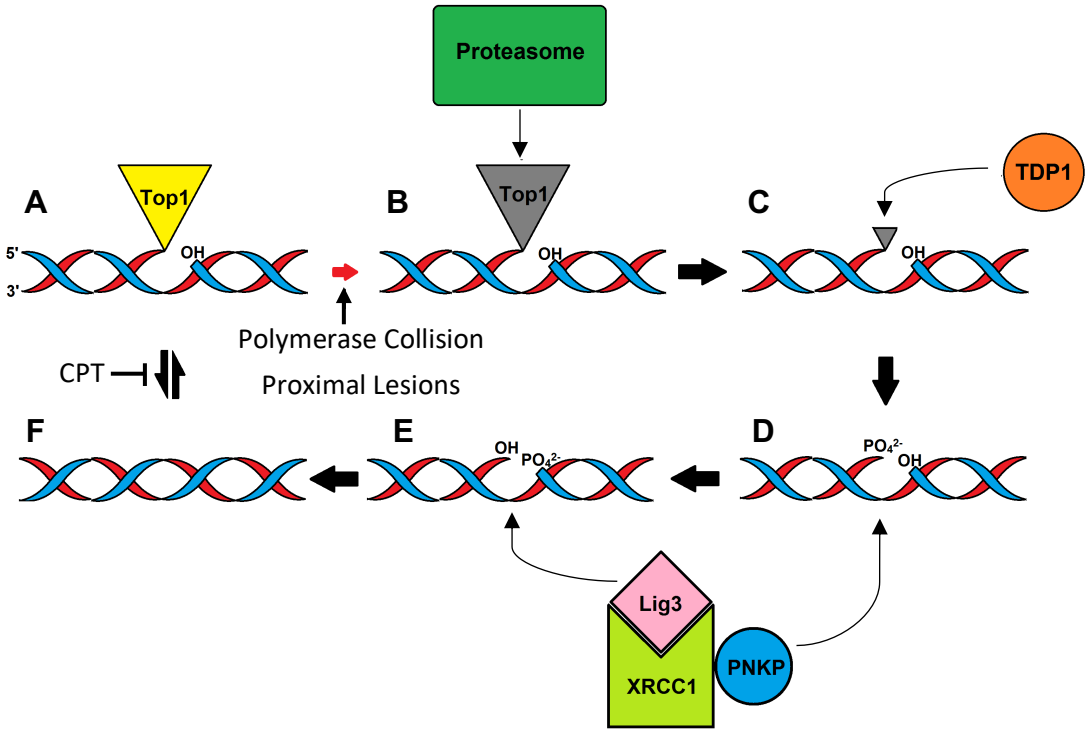

Figure 7.1. A model of Top1-SSB formation and repair. Top1 cleaves a single strand of DNA, forming a DNA 3'-tyrosyl phosphodiester-linked cleavage complex (Top1cc) and a non-canonical 5'-hydroxyl terminus **(A).** Whilst Top1ccs are usually rapidly reversible, they can be stabilized by the exogenous agent camptothecin (CPT). Top1ccs can also be converted into irreversible Top1-SSBs by the presence of other proximal lesions or by the collision of RNA and DNA polymerases (red arrow). Top1-SSBs are degraded by the proteasome, leaving a short peptide **(B),** which can be cleaved from the DNA by tyrosyl-DNA phosphodiesterase 1 (TDP1) **(C)**. Cleavage of the tyrosyl-DNA phosphodiester bond reveals a non-canonical 3'-phosphate terminus. Polynucleotide kinase 3'-phosphatase (PNKP), in complex with the scaffold protein X-ray cross-complementing 1 (XRCC1), restores canonical 5'-phosphate and 3'-hydroxyl termini **(D)**, which can then be ligated by Lig3, also in complex with XRCC1 **(E).** This completes repair of the lesion **(F).**

Recent work by co-workers in the Caldecott laboratory has identified a novel human ataxia caused by hypomorphic mutation of XRCC1 (Hoch, Hanzlikova et al. 2017): AOA-XRCC1. This joins a group of recessive ataxias caused by mutation of other SSBR genes, including TDP1, APTX and PNKP (Date, Onodera et al. 2001, Takashima, Boerkoel et al. 2002, El-Khamisy, Saifi et al. 2005, Shen, Gilmore et al. 2010, Bras, Alonso et al. 2015, Hoch, Hanzlikova et al. 2017)). One hypothesis to explain the neurotoxicity caused by defective SSBR involves programmed cell-death via Parthanatos, in a mechanism involving hyper-ADP-ribosylation triggered by PARP activity at persistent SSBs (Yu, Andrabi et al. 2006) (Hoch, Hanzlikova et al. 2017). For this reason, this chapter will also directly investigate CPT-induced SSB formation and ADP-ribosylation in several models of perturbed SSBR, including: *XRCC1*$^{-/-}$ cells generated by co-workers in the Caldecott laboratory, and *TDP1*$^{-/-}$ and *XRCC1*$^{-/-}$/*TDP1*$^{-/-}$ cells generated in Chapter Four.

7.2. Results

7.2.1. Impact of PARP enzymes on the sensitivity of RPE-1 cells to CPT

To investigate the roles of PARP enzymes in repair of CPT-induced damage, clonogenic survival assays of *PARP1*$^{-/-}$, *PARP2*$^{-/-}$, *PARP3*$^{-/-}$, *PARP1*$^{-/-}$/*PARP2*$^{-/-}$ and *TDP1*$^{-/-}$ RPE-1 cells were conducted (Fig. 7.2.). It is well described that acute treatments with micromolar concentrations of CPT kill predominately S-phase cells, resulting in biphasic survival curves (Bhuyan, Fraser et al. 1973). If the genotypes have different cell cycle profiles this can make comparison of the data difficult. For this reason, continuous rather than acute treatment was chosen.

The clonogenic survival assay revealed that *PARP1*$^{-/-}$ and *TDP1*$^{-/-}$ cells were significantly more sensitive than WT cells (ANOVA p-values : 1.3×10^{-5} and 7.94×10^{-6}, respectively); however, *PARP2*$^{-/-}$ and *PARP3*$^{-/-}$ cells were not (ANOVA p-values: 7.69×10^{-1} and 7.38×10^{-1}, respectively). The sensitivity of *PARP1*$^{-/-}$ cells was notably similar to that of *TDP1*$^{-/-}$ cells, indicating that this is the primary PARP enzyme promoting cellular resistance to CPT-induced lesions. Interestingly, *PARP1*$^{-/-}$/*PARP2*$^{-/-}$ cells were significantly more sensitive than *PARP1*$^{-/-}$ cells

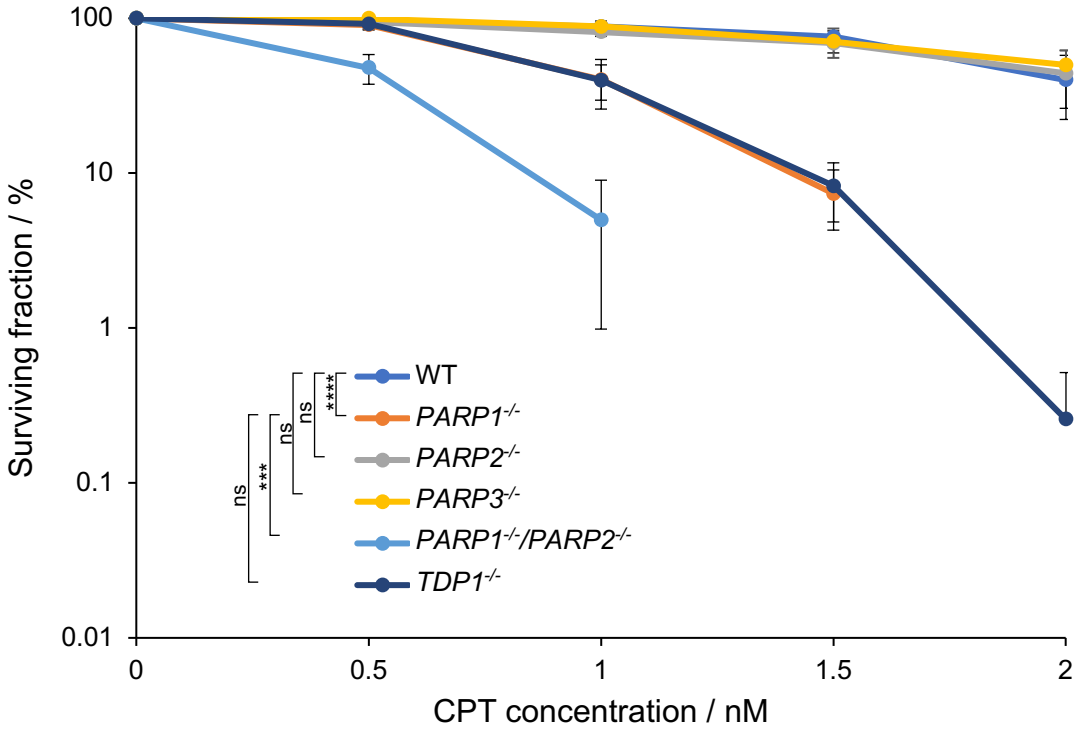

Figure 7.2. Sensitivity of RPE-1 *PARP* KO cell lines to CPT. WT, *TDP1*$^{-/-}$, *PARP1*$^{-/-}$, *PARP2*$^{-/-}$, *PARP3*$^{-/-}$ and *PARP1*$^{-/-}$/*PARP2*$^{-/-}$ RPE-1 cells were plated at a density of 300 cells per 10 cm dish, 4 h prior to addition of complete DMEM/F12 containing 0, 0.5 ,1, 1.5 or 2 nM CPT. Cells were incubated for 12 days prior to staining with 2% methylene blue and scoring of colonies with more than 50 cells. For each biological replicate, the surviving fraction was as calculated from the average number of colonies on duplicate treated plates, expressed as a fraction of average number of colonies on triplicate untreated plates. Data are mean ±SEM of 3 biological replicates. Statistical significance was calculated by two factor ANOVA.

(ANOVA p-value = 3.90×10^{-4}), suggesting that PARP2 promotes cell survival in response to CPT in the absence of PARP1.

7.2.2. PARP1 and XRCC1 are epistatic for cellular resistance to CPT

After identifying PARP1 as the predominant PARP enzyme promoting CPT-resistance in WT cells, its genetic relationship with XRCC1 was investigated. The clonogenic survival assay was employed to determine the sensitivity of WT, *XRCC1*$^{-/-}$, *PARP1*$^{-/-}$ *and XRCC1*$^{-/-}$/*PARP1*$^{-/-}$ cells to continuous CPT treatment (Fig. 7.3.). It was found that *XRCC1*$^{-/-}$, *PARP1*$^{-/-}$ *and XRCC1*$^{-/-}$/*PARP1*$^{-/-}$ cells were significantly more sensitive to CPT than WT cells (ANOVA p-values: 1.75×10^{-7}, 4.19×10^{-10}, 8.14×10^{-7}, respectively). However, *XRCC1*$^{-/-}$/*PARP1*$^{-/-}$ cells were significantly more sensitive than *XRCC1*$^{-/-}$ or *PARP1*$^{-/-}$ cells, suggesting that that *XRCC1* and *PARP1* exhibit an epistatic relationship for cellular resistance to CPT. This epistasis is indicative of PARP1 and XRCC1 operating in the same pathway for the repair of CPT-induced lesions.

7.2.3. XRCC1 and TDP1 are epistatic for cellular resistance to CPT

To investigate the genetic relationship between XRCC1 and TDP1 following CPT-induced damage, clonogenic survival assays were used to determine the sensitivity of WT, *TDP1*$^{-/-}$ *and XRCC1*$^{-/-}$/*TDP1*$^{-/-}$ cells to continuous CPT treatment (Fig. 7.4.). These experiments were conducted together with the *PARP* KO cell lines in Fig. 7.1, but for clarity the data are plotted separately. It was found that *TDP1*$^{-/-}$ and *XRCC1*$^{-/-}$/*TDP1*$^{-/-}$ cells were significantly more sensitive to the anti-proliferative effects of CPT than WT RPE-1 cells (ANOVA p-values: 7.94×10^{-6} and 6.30×10^{-6}, respectively), demonstrating a role of these genes in SSBR at CPT-induced lesions. Importantly, the hypersensitivity of *TDP1*$^{-/-}$ cells to CPT was not further increased by additional loss of *XRCC1* (ANOVA p-value = 9.06×10^{-1}), arguing that TDP1 and XRCC1 operate in the same pathway for repair of CPT-induced lesions. Together with Fig. 7.3., this result suggests that *PARP1, XRCC1* and *TDP1* are in the same epistasis group for cellular resistance to CPT.

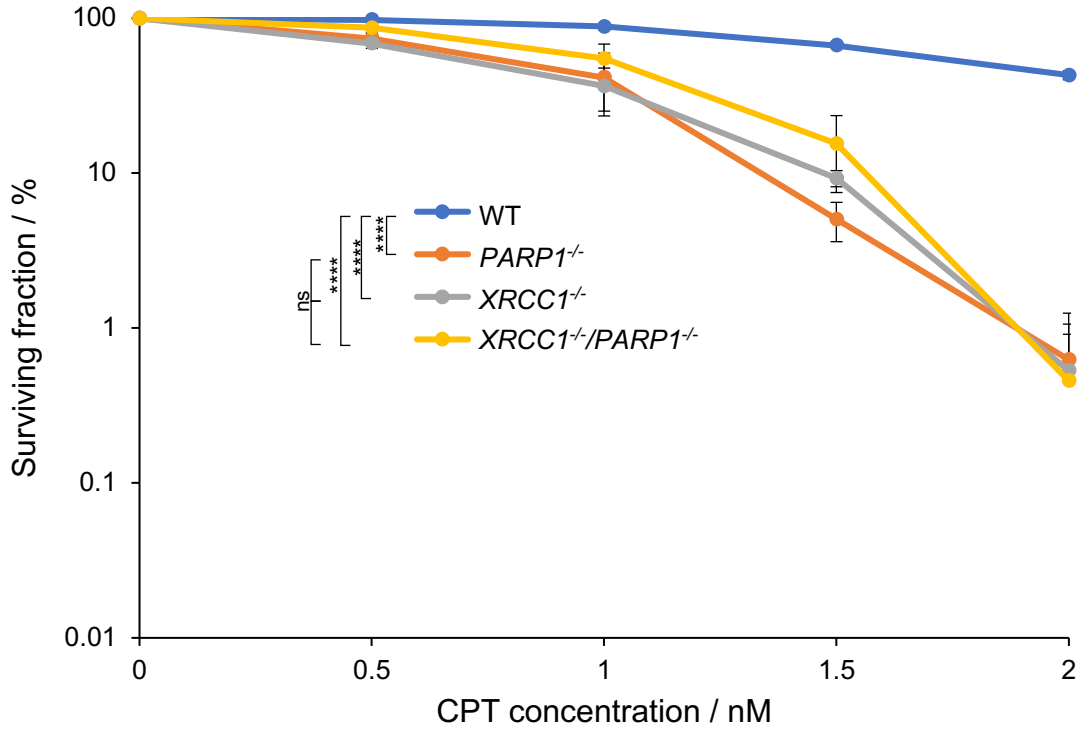

Figure 7.3. *XRCC1* and *PARP1* are epistatic for promoting cell proliferation in the presence of CPT. WT, *PARP1*$^{-/-}$, *XRCC1*$^{-/-}$ and *XRCC1*$^{-/-}$/*PARP1*$^{-/-}$ RPE-1 cells were plated at a density of 300 cells per 10 cm dish 4 h prior to addition of complete DMEM/F12 containing 0, 0.5 ,1, 1.5 or 2 nM CPT. Cells were incubated for 12 days prior to staining with 3% crystal violet and scoring of colonies with more than 50 cells. For each biological replicate, the surviving fraction was as calculated from the average number of colonies on duplicate treated plates, expressed as a fraction of average number of colonies on triplicate untreated plates. Data are mean ±SEM of 3 biological replicates. Statistical significance was calculated by two factor ANOVA.

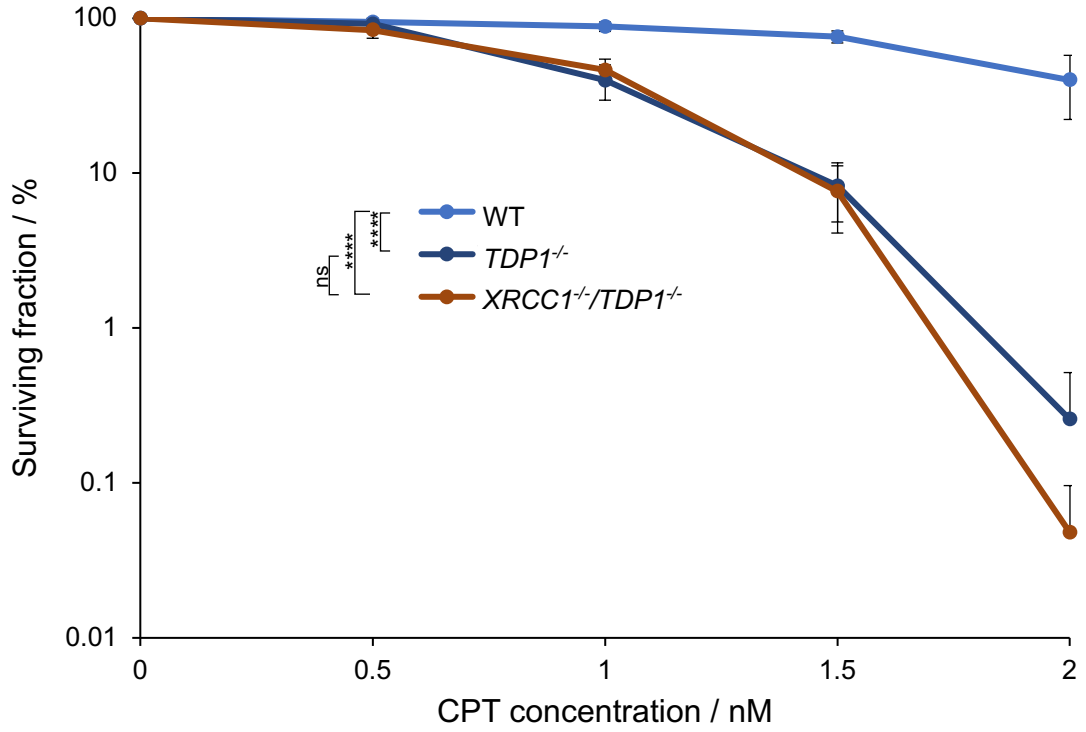

Figure 7.4. *XRCC1* and *TDP1* are epistatic for promoting cell proliferation in the presence of CPT. WT, *TDP1*$^{-/-}$ and *XRCC1*$^{-/-}$/*TDP1*$^{-/-}$ RPE-1 cells were plated at a density of 300 cells per 10 cm dish 4 h prior to addition of complete DMEM/F12 containing 0, 0.5 ,1, 1.5 or 2 nM CPT. Cells were incubated for 12 days prior to staining with 2% methylene blue and scoring of colonies with more than 50 cells. For each biological replicate, the surviving fraction was calculated from the average number of colonies on duplicate treated plates, expressed as a fraction of average number of colonies on triplicate untreated plates. Data are mean ±SEM of 3 biological replicates. Statistical significance was calculated by two factor ANOVA. Data for *TDP1*$^{-/-}$ cells are replotted from Fig. 7.2. for comparison, as these experiments were conducted together.

7.2.4. Levels of CPT-induced DNA strand breaks are elevated in *XRCC1*$^{-/-}$, *TDP1*$^{-/-}$ *and XRCC1*$^{-/-}$/*TDP1*$^{-/-}$ RPE-1 cells

To determine if the loss of cellular resistance to CPT in *XRCC1*$^{-/-}$ and *TDP1*$^{-/-}$ cells reflected reduced repair of CPT-induced strand breaks, the alkaline Comet assay was used to directly compare the steady-state levels of CPT-induced strand breakage in *WT, XRCC1*$^{-/-}$*, TDP1*$^{-/-}$ *and XRCC1*$^{-/-}$/*TDP1*$^{-/-}$ RPE-1 cells (Fig. 7.5.). Without treatment, all genotypes had very low Comet tail moments (0.19, 0.15, 0.16 and 0.18 for WT, *XRCC1*$^{-/-}$*, TDP1*$^{-/-}$ and *XRCC1*$^{-/-}$/*TDP1*$^{-/-}$, respectively), indicating that the level of endogenous lesions is not significantly elevated by loss of TDP1 and/or XRCC1, or that this is below the detection limit of the assay. Upon treatment with 10 or 100 µM CPT, the Comet tail moment in WT cells increased to 0.63 and 1.43, respectively. Whilst dramatically lower than the Comet tail moments resulting from H_2O_2 treatment, these values were nonetheless significantly higher than those of untreated cells (t-test p-values: 5.45×10^{-4} and 2.55×10^{-2}, respectively). In comparison, Comet tail moments in CPT treated *TDP1*$^{-/-}$*, XRCC1*$^{-/-}$ and *XRCC1*$^{-/-}$/*TDP1*$^{-/-}$ cells were significantly greater (ANOVA p-values: 5.95×10^{-5}, 3.13×10^{-4} and 4.22×10^{-7}, respectively), indicating perturbed SSBR and elevated steady-state numbers of strand breaks in all three cell lines. No significant difference was found between *TDP1*$^{-/-}$ and *XRCC1*$^{-/-}$ cells (ANOVA p-value = 5.38×10^{-1}), indicating that deletion of *TDP1* or *XRCC1* results in comparable blockage of SSBR. Moreover, combined deletion of both genes imposed only a very minor additional effect on the level of strand breakage induced by CPT, consistent with these proteins operating in the same SSBR pathway and supporting the results of the clonogenic survival assay (Fig. 7.4.).

7.2.5. CPT-induced Comet tail moments are not elevated in *PARP1*$^{-/-}$, *PARP2*$^{-/-}$, *PARP3*$^{-/-}$, or *PARP1*$^{-/-}$/*PARP2*$^{-/-}$ RPE-1 cells

Given that *PARP1*$^{-/-}$ cells exhibit a similar CPT-sensitivity to *XRCC1*$^{-/-}$ and *TDP1*$^{-/-}$ cells, it was hypothesised that the level of CPT-induced strand breaks would be similarly elevated. To investigate this, the alkaline Comet assay was conducted with WT, *PARP1*$^{-/-}$*, PARP2*$^{-/-}$*, PARP3*$^{-/-}$ and *PARP1*$^{-/-}$/*PARP2*$^{-/-}$ RPE-1 cells (Fig. 7.6.). These experiments were conducted together with *TDP1*$^{-/-}$*, XRCC1*$^{-/-}$ and *XRCC1*$^{-/-}$/*TDP1*$^{-/-}$ (Fig. 7.5.), but for clarity are plotted separately.

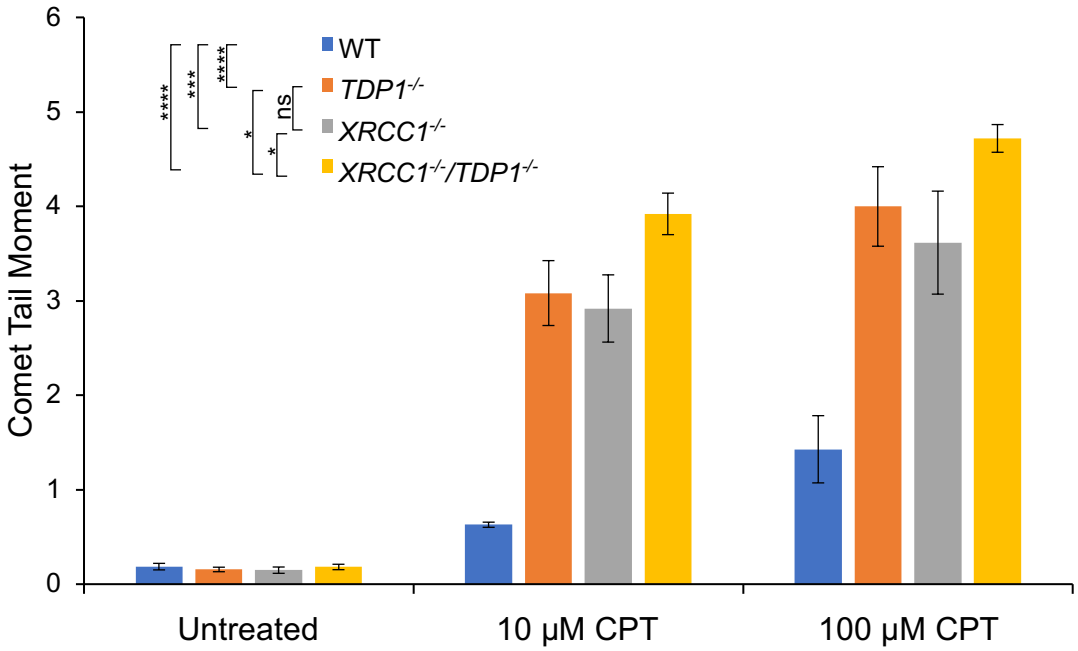

Figure 7.5. Steady-state levels of CPT-induced strand breaks in WT, *TDP1*$^{-/-}$, *XRCC1*$^{-/-}$ and *XRCC1*$^{-/-}$/*TDP1*$^{-/-}$ RPE-1 cells. Subconfluent RPE-1 cells of the indicated genotypes were trypsinised, washed with DMEM/F12 and resuspended in DMEM/F12 containing 0, 10 or 100 μM CPT. Cells were incubated for 1 h at 37°C prior to being subjected to alkaline single cell electrophoresis. Comet tail moments from 100 cells per condition were measured with Comet IV software. Data are expressed as mean ±SEM of 3 independent experiments. Statistical significance was calculated by two factor ANOVA.

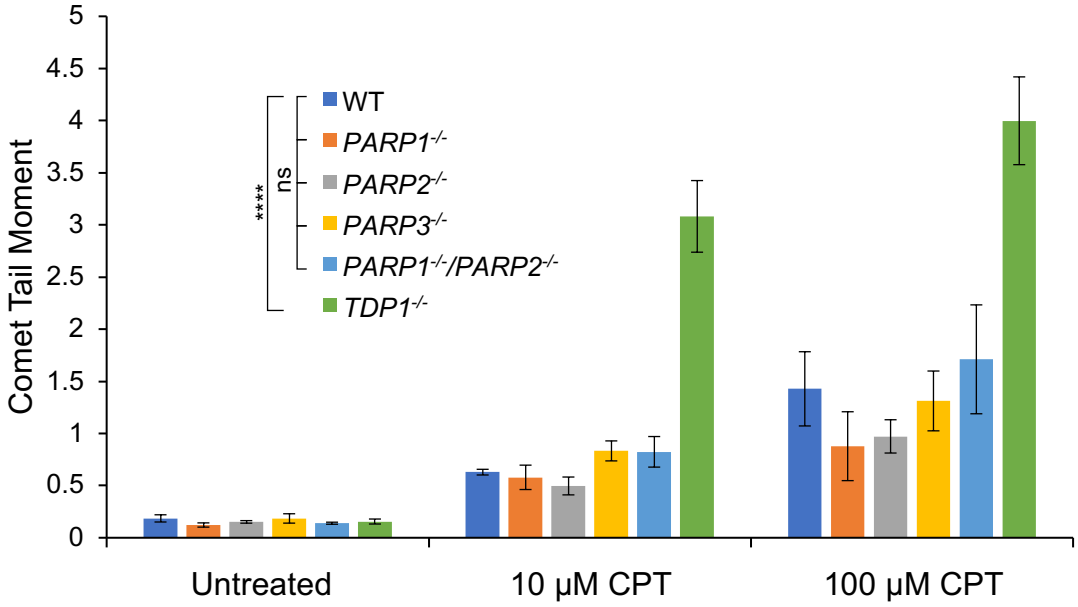

Figure 7.6. Steady-state levels of CPT-induced strand breaks in WT, *PARP1*$^{-/-}$, *PARP2*$^{-/-}$, *PARP3*$^{-/-}$, *PARP1*$^{-/-}$/*PARP2*$^{-/-}$ and *TDP1*$^{-/-}$ RPE-1 cells. Sub-confluent RPE-1 cells of the indicated genotypes were trypsinised, washed with DMEM/F12 and resuspended in DMEM/F12 containing 0, 10 or 100 μM CPT. Cells were incubated for 1 h at 37°C prior to being subjected to alkaline single cell electrophoresis. Comet tail moments from 100 cells per condition were measured with Comet IV software. Data are expressed as mean ±SEM of 3 independent experiments. Statistical significance was calculated by two factor ANOVA. Data for *TDP1*$^{-/-}$ cells are replotted from Fig. 7.5. for comparison, as these experiments were conducted together.

For comparison, the data for *TDP1*$^{-/-}$ is replotted. Surprisingly, it was found that the average tail moment was not significantly elevated in any of the *PARP* KO cell lines.

7.2.6. Deletion of *PARP1* supresses the elevated CPT-induced Comet tail moment in *XRCC1*$^{-/-}$ cells

It was observed that *PARP1*$^{-/-}$ cells generally appeared to have slightly lower CPT-induced Comet tails than WT cells. Whilst this was not significant at the 5% level, it was evident in all 4 replicates following treatment with 100 µM CPT. This led to the hypothesis that *PARP1* loss might supress elevated Comet tail moments seen in other cell lines. To investigate this, the alkaline Comet assay was conducted with WT, *PARP1*$^{-/-}$, *XRCC1*$^{-/-}$ and *XRCC1*$^{-/-}$/*PARP1*$^{-/-}$ cells (Fig. 7.7.). Strikingly, it was found that the Comet tail moment of CPT-treated *XRCC1*$^{-/-}$/*PARP1*$^{-/-}$ cells (1.44) was indeed supressed to 0.41-fold that of CPT-treated *XRCC1*$^{-/-}$ cells (3.52; t-test p-value = 2.75×10^{-4}). The suppression was not complete, in that the Comet tail moment of CPT-treated *XRCC1*$^{-/-}$/*PARP1*$^{-/-}$ cells was still 2.84-fold that of CPT-treated WT cells (0.51; t-test p-value = 5.88×10^{-4}).

7.2.7. CPT induces very low steady-state levels of ADP-ribose in WT cells.

In summary of the chapter so far, the clonogenic survival assays in Fig. 7.3. and 7.4. demonstrate that *PARP1, XRCC1* and *TDP1* are epistatic for cellular resistance to CPT. However, the alkaline Comet assays in Fig. 7.5, 7.6. and 7.7. demonstrate that whereas *TDP1* and *XRCC1* appear to be in the same epistasis group for levels of CPT-induced DNA strand breakage, *PARP1* behaves differently. To investigate this in more detail, CPT-induced ADP-ribosylation was measured directly by quantitative immunofluorescence (IF). WT RPE-1 cells growing on glass coverslips were treated with 30 µM CPT in complete DMEM/F12 for 1 h at 37°C, prior to formaldehyde fixation and IF with pan-ADP-ribose binding reagent. ScanR image analysis was used to quantify nuclear pan-ADP-ribose signal as described for H_2O_2-treated cells (Fig. 7.8.). The ADP-ribose signal induced by CPT in WT cells (1.09-fold), whilst significantly greater than the background in untreated cells (t-test p-value = 8.08×10^{-3}), was dramatically lower

A

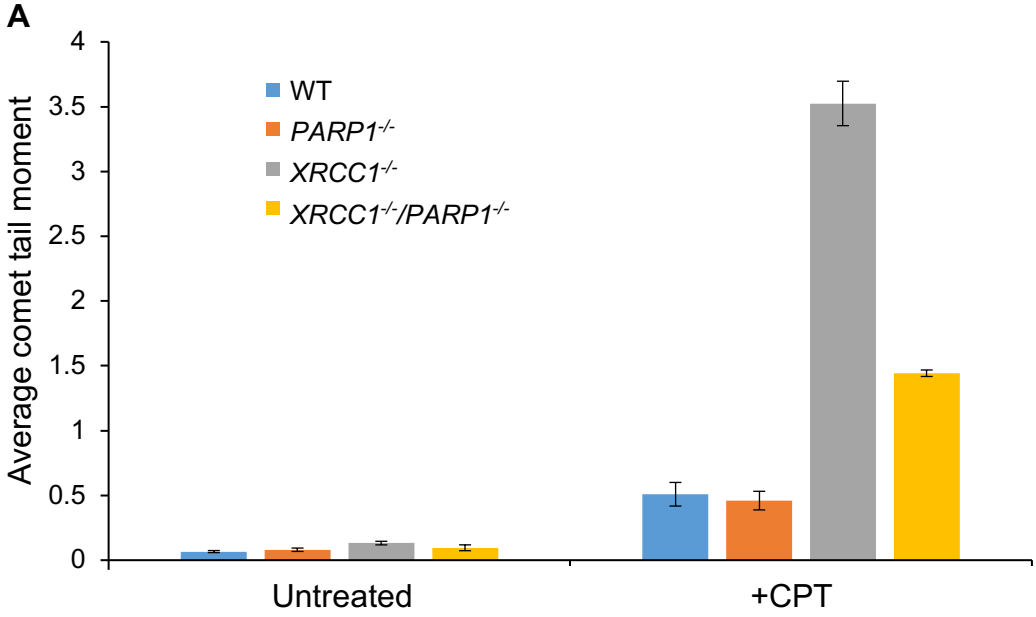

B

vs		Untreated				+CPT			
		WT	*PARP1*$^{-/-}$	*XRCC1*$^{-/-}$	*XRCC1*$^{-/-}$/*PARP1*$^{-/-}$	WT	*PARP1*$^{-/-}$	*XRCC1*$^{-/-}$	*XRCC1*$^{-/-}$/*PARP1*$^{-/-}$
Untreated	WT		4.06E-01	1.48E-02	2.87E-01	8.40E-03	5.53E-03	3.58E-05	8.07E-07
	PARP1$^{-/-}$	4.06E-01		5.34E-02	5.89E-01	9.62E-03	6.53E-03	3.67E-05	1.11E-06
	XRCC1$^{-/-}$	1.48E-02	5.34E-02		2.43E-01	1.50E-02	1.10E-02	3.90E-05	1.38E-06
	XRCC1$^{-/-}$/*PARP1*$^{-/-}$	2.87E-01	5.89E-01	2.43E-01		1.17E-02	8.43E-03	3.82E-05	2.37E-06
+CPT	WT	8.40E-03	9.62E-03	1.50E-02	1.17E-02		6.94E-01	1.00E-04	5.88E-04
	PARP1$^{-/-}$	5.53E-03	6.53E-03	1.10E-02	8.43E-03	6.94E-01		7.92E-05	2.07E-04
	XRCC1$^{-/-}$	3.58E-05	3.67E-05	3.90E-05	3.82E-05	1.00E-04	7.92E-05		2.75E-04
	XRCC1$^{-/-}$/*PARP1*$^{-/-}$	8.07E-07	1.11E-06	1.38E-06	2.37E-06	5.88E-04	2.07E-04	2.75E-04	

Key:

ns	*	**	***	****
(0.05<p)	(0.01<p<0.05)	(0.001<p<0.01)	(0.0001<p<0.001)	(p<0.0001)

Figure 7.7. Steady-state levels of CPT-induced strand breaks in WT, *PARP1*$^{-/-}$, *XRCC1*$^{-/-}$ and *XRCC1*$^{-/-}$/*PARP1*$^{-/-}$ RPE-1 cells. Sub-confluent RPE-1 cells of the indicated genotypes were trypsinised, washed with DMEM/F12 and resuspended in DMEM/F12 containing 0 or 10 μM CPT. Cells were incubated for 1 h at 37°C prior to being subjected to alkaline single cell electrophoresis. Comet tail moments from 100 cells per condition were measured with Comet IV software. Data are expressed as mean ±SEM of at 3 independent experiments **(A)**. T-test p values between pairwise CPT-treated data are tabulated. Cell colour coding indicates the significance level, according to the key (bottom) **(B)**.

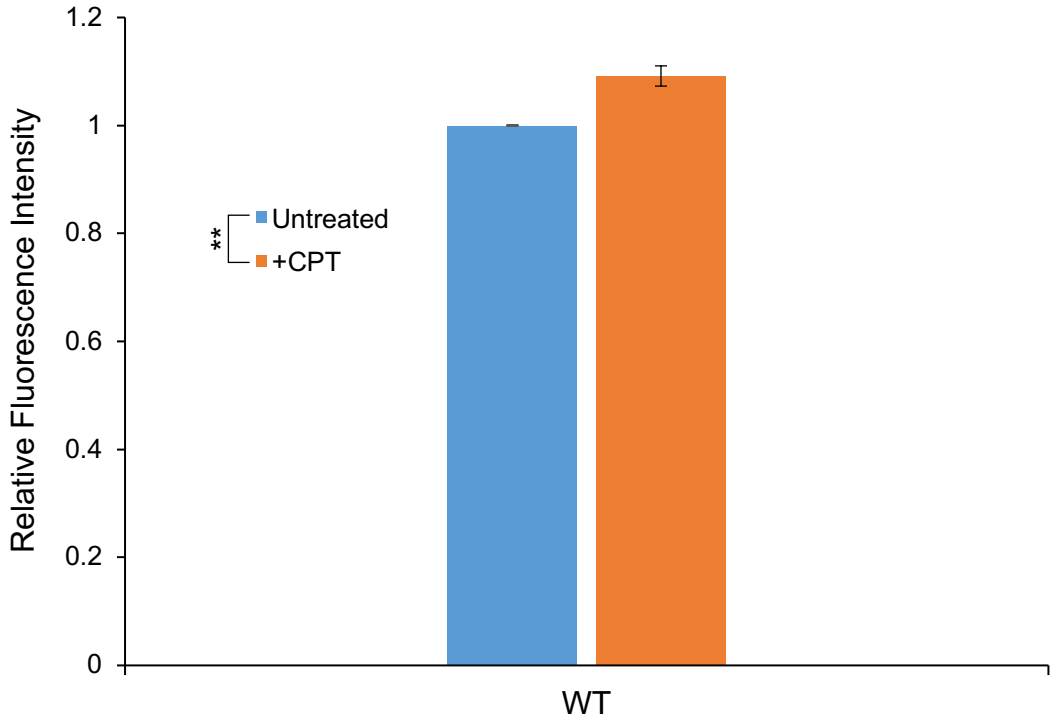

Figure 7.8. CPT induces a very low steady state level of ADP-ribosylation in WT RPE-1 cells. WT RPE-1 cells growing on glass coverslips were treated or not with 30 μM CPT for 1 h prior to formaldehyde fixation and immunolabelling with Pan-ADP-ribose binding reagent. Slides were imaged using the Olympus ScanR system and ScanR Analysis software. Pan-ADP-ribose fluorescence from >1000 cells was quantified in the nucleus and is expressed as fold over signal in untreated WT. Data are mean ±SEM of 6 independent replicates.

than that induced by 400 µM H_2O_2 (>25-fold; see Fig. 6.8.). It was hypothesised that this was due to the kinetics of the damage induction, which are likely to be slower than for H_2O_2 as they are dependent on other factors such as active transcription and replication. In the presence of competent and rapid downstream SSBR, this would result in a low steady state level of Top1-SSB lesions and a low steady state ADP-ribose signal. Alternatively, the level of PARP activation per SSB could be less for CPT-induced lesions than H_2O_2-induced lesions. A prediction of the first hypothesis is that disruption of the downstream repair of Top1-SSBs might lead to an increase in the observed CPT-induced ADP-ribosylation; this was investigated next.

7.2.8. Loss of *XRCC1* or *TDP1* causes a dramatic elevation of CPT-induced ADP-ribosylation

The level of CPT-induced ADP-ribosylation was compared in WT, *TDP1*$^{-/-}$ and *XRCC1*$^{-/-}$ cells (Fig. 7.9.). As predicted, the level of CPT-induced ADP-ribosylation in *XRCC1*$^{-/-}$ RPE-1 cells (8.95-fold) was dramatically higher than in WT cells (t-test p-value = 3.39×10^{-3}). The level of ADP-ribosylation observed in four independent *TDP1*$^{-/-}$ cell lines (#4A2, #5B3, #5B4 and #5B5), was also dramatically elevated relative to WT cells (3.11, 2.96, 3.35 and 3.78-fold relative to WT untreated, respectively). However, this was ~30% of that observed in *XRCC1*$^{-/-}$ cells. Importantly, the phenotype of *TDP1*$^{-/-}$ RPE-1 cells was unlikely to be attributable to any other clonal characteristic, as it was comparable in all four clonally isolated *TDP1*$^{-/-}$ RPE-1 cell lines.

7.2.9. PARP1 is responsible for the CPT-induced ADP-ribosylation observed in *XRCC1*$^{-/-}$ cells

To test which PARP was responsible for the elevated CPT-induced ADP-ribosylation observed in the absence of XRCC1, *XRCC1*$^{-/-}$/*PARP1*$^{-/-}$ cells were compared with WT and *XRCC1*$^{-/-}$ cells. Simultaneous loss of *XRCC1* and *PARP1* resulted in a significant (t-test p-value = 5.03×10^{-3}) ablation in CPT-induced ADP-ribosylation (1.00 ± 0.02 fold relative to WT untreated), to a level that was not significantly different from that in untreated WT or

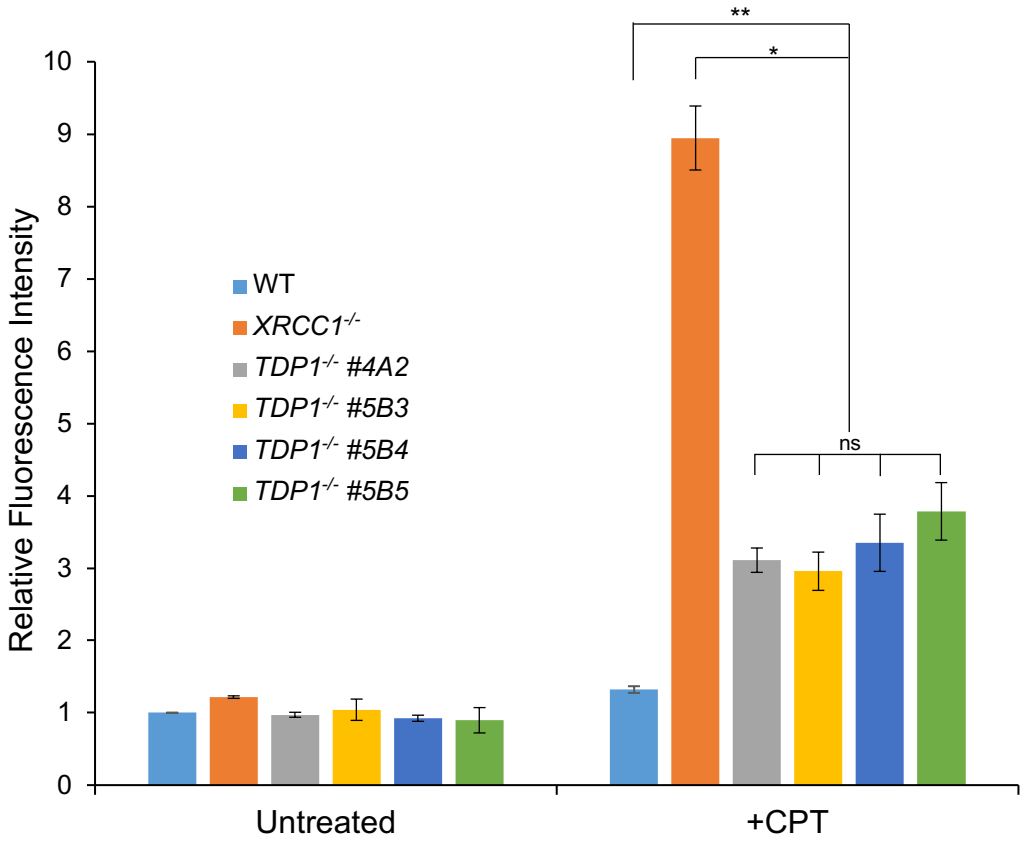

Figure 7.9. CPT-induced ADP-ribosylation is elevated in *XRCC1*$^{-/-}$ and four clonally-isolated *TDP1*$^{-/-}$ RPE-1 cell lines. WT, *XRCC1*$^{-/-}$ and four independent *TDP1*$^{-/-}$ RPE-1 clones (#4A2, #5B3, #5B4, #5B5) growing on glass coverslips were treated or not with 30 μM CPT for 1 h prior to formaldehyde fixation and immunolabelling with pan-ADP-ribose binding reagent (green), and DNA staining with DAPI (blue). Slides were imaged using the Olympus ScanR system. Pan-ADP-ribose fluorescence from >1000 cells was quantified in the nucleus and is expressed as fold over signal in untreated WT **(A)**. ScanR Analysis software was used to generate galleries of 16 randomly selected cells for each condition **(B, overleaf)**. Data are mean ±SEM of 2 independent replicates.

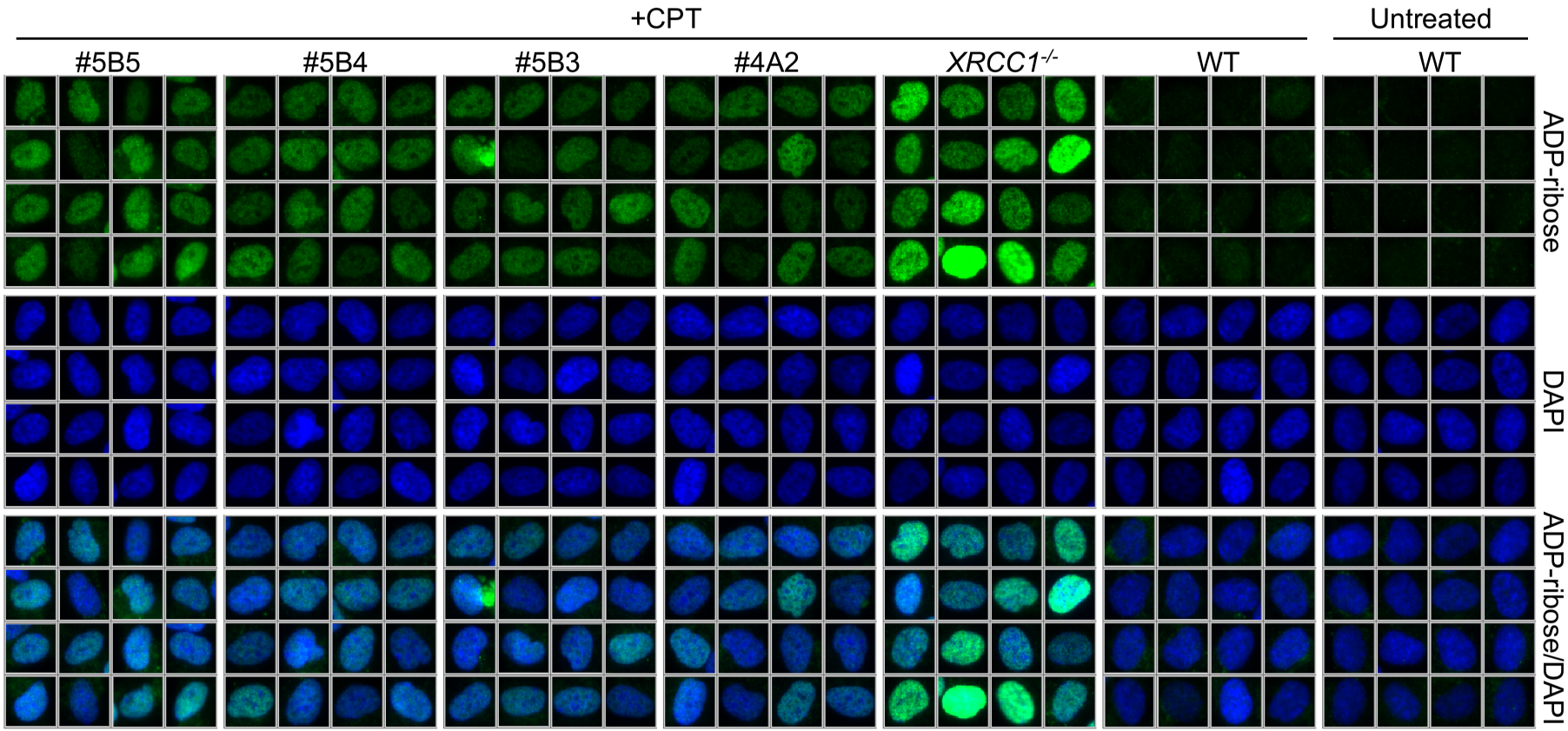
+CPT
Untreated
#5B5
#5B4
#5B3
#4A2
XRCC1-/-
WT
WT
ADP-ribose
DAPI
ADP-ribose/DAPI

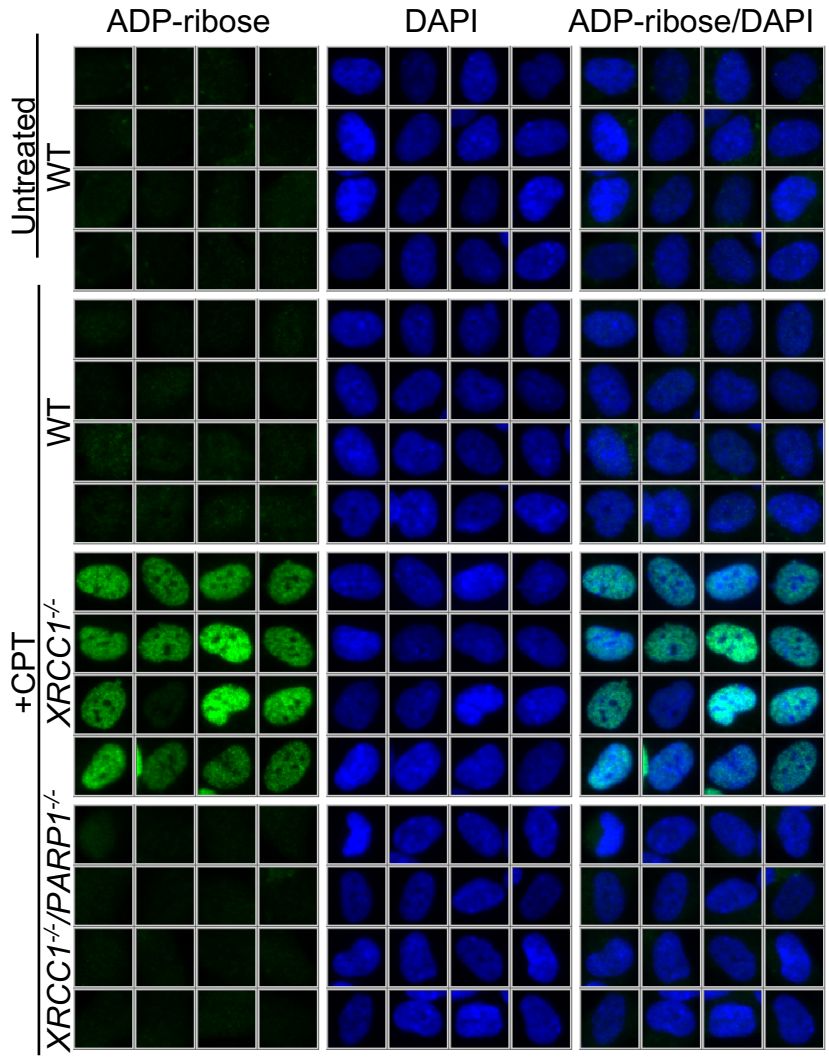

Figure 7.10. PARP1 is responsible for the elevated CPT-induced ADP-ribosylation in *XRCC1*$^{-/-}$ RPE-1 cells. WT, *XRCC1*$^{-/-}$ and *XRCC1*$^{-/-}$/*PARP1*$^{-/-}$ RPE-1 cells growing on glass coverslips were treated or not with 30 μM CPT for 1 hr prior to formaldehyde fixation and immunolabelling with pan-ADP-ribose binding reagent (green), and DNA labelling with DAPI (blue). Slides were imaged using the Olympus ScanR system and ScanR Analysis software was used to generate galleries of 16 randomly selected cells for each condition. See Fig. 7.14. for quantification.

XRCC1$^{-/-}$/*PARP1*$^{-/-}$ cells (t-test p-values: 3.86x10^{-1} and 9.68x10^{-1}, respectively) (Fig. 7.10. and 7.14.). This result suggests that PARP1 contributes significantly to the elevated ADP-ribosylation observed in CPT-treated *XRCC1*$^{-/-}$ cells.

7.2.10. PARP1 is responsible for CPT-induced loading of XRCC1 into the chromatin

In order to test which PARP was responsible for loading XRCC1 into the chromatin in response to CPT, the IF assay developed in Chapter Five was employed. WT, *PARP1*$^{-/-}$, *PARP2*$^{-/-}$, *PARP3*$^{-/-}$, *PARP1*$^{-/-}$/*PARP2*$^{-/-}$ and *XRCC1*$^{-/-}$ RPE-1 cells growing on glass coverslips were treated for 1 h with 30 µM CPT, prior to detergent pre-extraction, fixation and IF with antibodies targeting XRCC1 and B23. XRCC1 fluorescence was quantified in the region excluding the nucleolus, as described above. In WT cells, CPT-induced a low but reproducible increase in XRCC1 fluorescence in the chromatin (1.4-fold relative to untreated) (Fig. 7.11.a). In all other genotypes, the level of XRCC1 fluorescence in CPT-treated cells was lower than this. However, it is notable that in all other genotypes the level of chromatin-localized XRCC1 fluorescence was also lower in untreated cells, perhaps due to a loss of PARP activity in unchallenged cells. To account for this, the CPT-induced change in XRCC1 fluorescence is also plotted, in arbitrary units (Fig. 7.11.b). It was found that the CPT-induced change in XRCC1 fluorescence in the chromatin was not significantly different between WT and *PARP2*$^{-/-}$ or *PARP3*$^{-/-}$ cells (t-test p-values: 9.90x10^{-1} and 3.96x10^{-1}, respectively). By comparison, in *PARP1*$^{-/-}$ and *PARP1*$^{-/-}$/*PARP2*$^{-/-}$ cells this increase was completely abolished, which was significantly different from the increase observed in WT cells (t-test p-values: 9.46x10^{-3} and 1.35x10^{-2}, respectively).

7.2.11. XRCC1 and TDP1 are epistatic for the level of CPT-induced ADP-ribosylation

TDP1 has recently been reported to be recruited to CPT-induced damage sites upstream of XRCC1 recruitment, via a direct interaction with PARP1 (Das, Huang et al. 2014). Given that cleavage of the DNA 3'-tyrosyl phosphodiester bond must occur prior to subsequent catalytic activities of the XRCC1 interaction partners

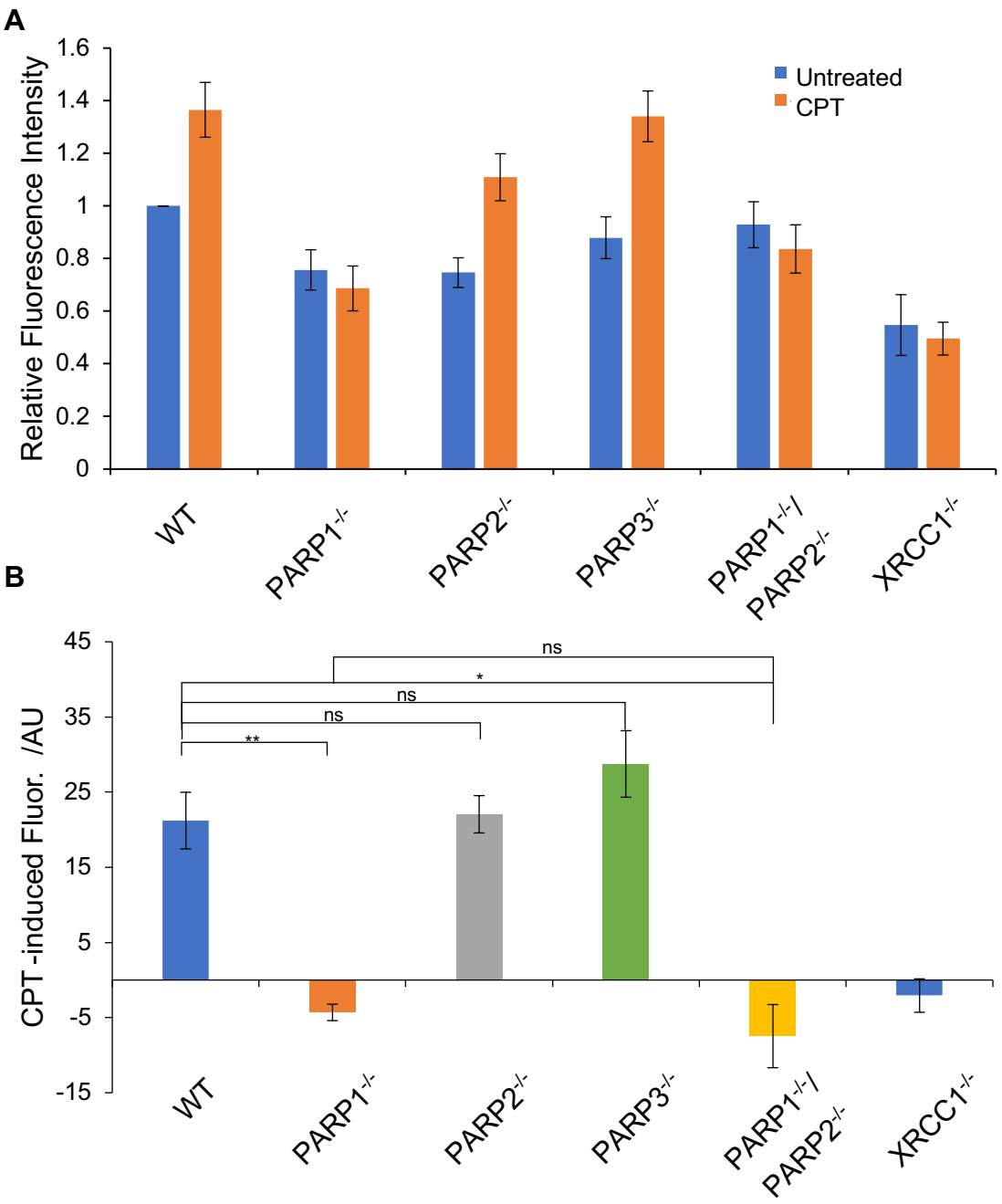

Figure 7.11. Deletion of *PARP1* prevents a CPT-induced increase in XRCC1 chromatin-localization. WT, *PARP1*$^{-/-}$, *PARP2*$^{-/-}$, *PARP3*$^{-/-}$, *PARP1*$^{-/-}$/*PARP2*$^{-/-}$ and *XRCC1*$^{-/-}$ RPE-1 cells growing on glass coverslips were treated or not with 30 μM CPT for 1 h prior to pre-extraction, formaldehyde fixation and immunolabelling with antibodies against XRCC1 and B23, and DNA-staining with DAPI. Slides were imaged using the Olympus ScanR system. XRCC1 fluorescence from >1000 cells was quantified in the nuclear region excluding phosphoprotein B23 signal and is expressed as fold over signal in untreated WT cells **(A)**. Data are also expressed as CPT-induced change in XRCC1 fluorescence, calculated by subtracted the level of XRCC1 fluorescence in untreated cells from that of CPT-treated cells, for each genotype **(B).** Data are mean ± SEM of 4 biological replicates. Statistical significance was calculated by students t-test.

PNKP and Lig3α, it was expected that TDP1 or XRCC1 deletion would result in a comparable block to repair of CPT-induced SSBs. This was demonstrated by the accumulation of similar levels of DNA strand breaks in CPT-treated *TDP1*$^{-/-}$ and *XRCC1*$^{-/-}$ by alkaline Comet assay (Fig. 7.5.). The fact that *TDP1*$^{-/-}$ cells exhibited a lower level of CPT-induced ADP-ribosylation than *XRCC1*$^{-/-}$ cells therefore suggests that the level of PARP1 activation is not directly proportional to the level of DNA strand breaks. One possibility is that repair intermediates that accumulate in *TDP1*$^{-/-}$ cells do not activate PARP1 to the same extent as those which accumulate in *XRCC1*$^{-/-}$ cells. To investigate this relationship in more detail, *XRCC1*$^{-/-}$/*TDP1*$^{-/-}$ cells were compared to WT, *XRCC1*$^{-/-}$ and *TDP1*$^{-/-}$ cells (Fig. 7.12 and 7.14.). As before, *XRCC1*$^{-/-}$ and *TDP1*$^{-/-}$ (#5B5) cells exhibited an elevated level of CPT-induced ADP-ribosylation (11.46 and 5.03-fold relative to WT untreated, respectively). The effects of XRCC1 and TDP1 loss were not additive, as CPT-induced ADP-ribosylation in *XRCC1*$^{-/-}$/*TDP1*$^{-/-}$ cells (11.80-fold relative to WT untreated) was not significantly different from in *XRCC1*$^{-/-}$ cells (t-test p-value = 8.39×10^{-1}). This epistatic relationship suggests that the two proteins operate in the same pathway for repair of CPT-induced DNA strand breaks. However, this result does not support a model in which the difference in the level of PARP1 hyperactivation between *TDP1*$^{-/-}$ and *XRCC1*$^{-/-}$ cells is only due to the accumulation of different repair intermediates in each cell line. This is because based on the order of events in SSBR, we would expect *XRCC1*$^{-/-}$/*TDP1*$^{-/-}$ cells to accumulate the same repair intermediates as *TDP1*$^{-/-}$ cells: SSBs with 3'-phosphotyrosyl-linked Top1 peptides (see section 7.3 for further discussion).

7.2.12. Loss of *TDP2* further elevates CPT-induced ADP-ribosylation in *TDP1*$^{-/-}$ cells.

The combined loss of *XRCC1* and *TDP1* resulted in a small but significant additive increase in CPT-induced DNA strand breaks by alkaline Comet assay (Fig. 7.5.). This might suggest that loss of either protein is not a complete block to SSBR of CPT-induced DNA strand breaks, such that their combined loss causes a more severe block to SSBR than loss of either protein alone. If this is the case, the presence of alternative redundant activities which circumvent the

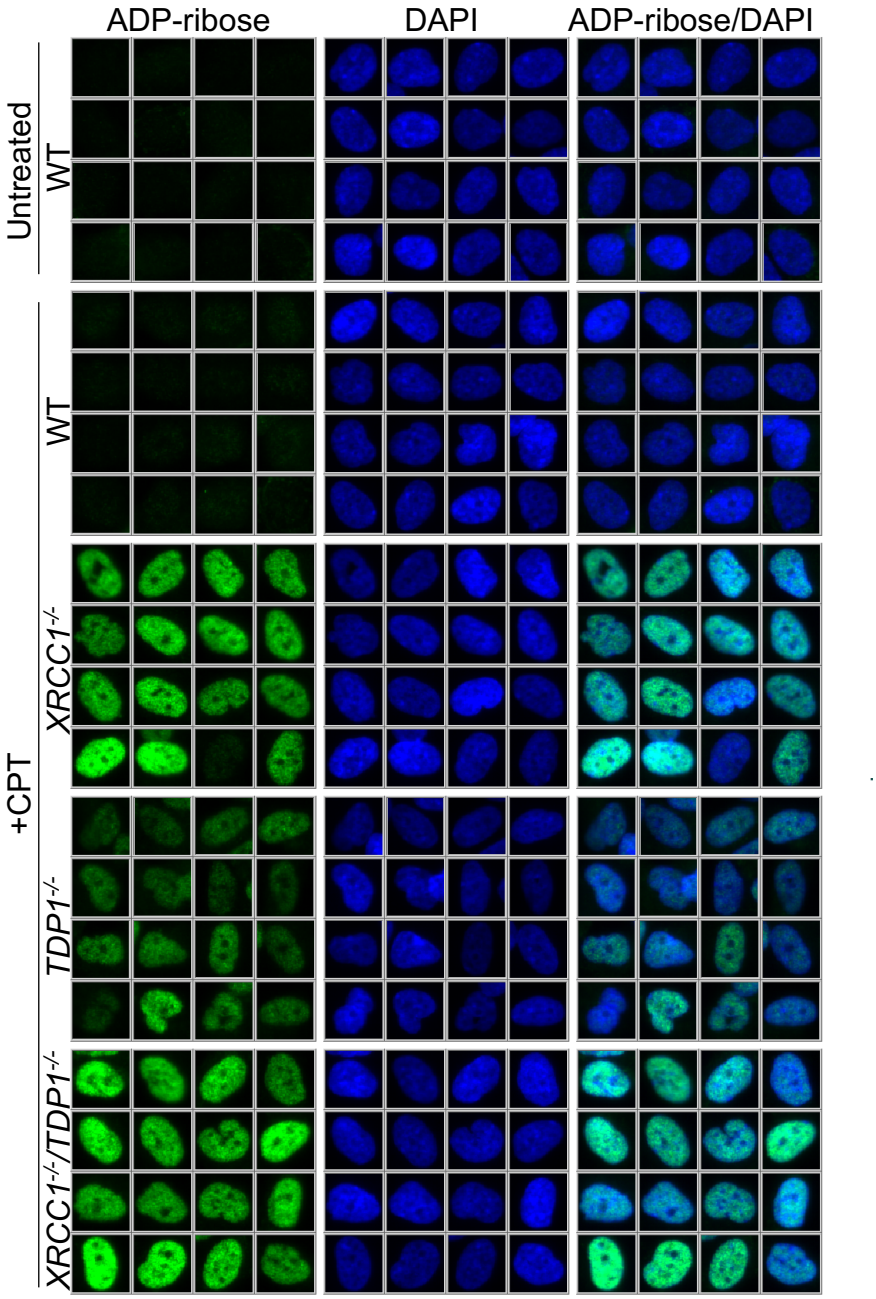

Figure 7.12. *XRCC1* and *TDP1* are epistatic for the level of CPT-induced ADP-ribosylation. WT, *XRCC1*$^{-/-}$, *TDP1*$^{-/-}$ and *XRCC1*$^{-/-}$/*TDP1*$^{-/-}$ RPE-1 cells growing on glass coverslips were treated or not with 30 μM CPT for 1 h prior to formaldehyde fixation and immunolabelling with pan-ADP-ribose binding reagent (green), and DNA labelling with DAPI (blue). Slides were imaged using the Olympus ScanR system and ScanR Analysis software was used to generate galleries of 16 randomly selected cells for each condition. See Fig. 7.14. for quantification.

requirement for TDP1 might be a contributing factor to the lower level of CPT-induced ADP-ribosylation observed in *TDP1*$^{-/-}$ cells. This could also explain why the *XRCC1*$^{-/-}$/*TDP1*$^{-/-}$ cells exhibit similar levels of CPT-induced ADP-ribosylation to *XRCC1*$^{-/-}$ cells, rather than *TDP1*$^{-/-}$ cells. In addition to TDP1, cells possess another tyrosyl-DNA phosphodiesterase: TDP2. Whilst this enzyme's primary activity is hydrolysis of DNA 5'-phosphotyrosyl bonds which result from abortive Top2 action, it has been shown to also have a weaker activity upon DNA 3'-phosphotyrosyl bonds *in vitro* (Cortes Ledesma, El Khamisy et al. 2009, Zeng, Sharma et al. 2012). It was hypothesised that TDP2 could act on SSBs with 3'-phosphotyrosyl termini in the absence of TDP1. To test this, the level of CPT-induced ADP-ribose was measured in *TDP2*$^{-/-}$ and *TDP1*$^{-/-}$/*TDP2*$^{-/-}$ RPE-1 cells (Fig. 7.13. and 7.14.), which were generated by a coworker in the Caldecott laboratory: G. Zagnoli. It was found that the level of CPT-induced ADP-ribose observed in *TDP1*$^{-/-}$/*TDP2*$^{-/-}$ cells (8.03 +1.23-fold relative to WT untreated) was significantly higher than in *TDP1*$^{-/-}$ cells (t-test p-value = 9.23×10^{-3}), suggesting that TDP2 does act on CPT-induced lesions in the absence of TDP1. Notably, however, the loss of *TDP2* alone did not result in elevated levels of CPT-induced ADP-ribose relative to WT cells (t-test p-value = 1.17×10^{-1}), indicating that TDP2 does not act appreciably in the presence of TDP1. Interestingly, the level of CPT-induced ADP-ribosylation in *TDP1*$^{-/-}$/*TDP2*$^{-/-}$ cells was lower than in *XRCC1*$^{-/-}$ cells (11.46-fold). Whilst not significant at the 5% level, this result may indicate that TDP2 activity does not account entirely for the difference in CPT-induced ADP-ribosylation between *XRCC1*$^{-/-}$ and *TDP1*$^{-/-}$ cells. It is possible that there are other pathways which circumvent the requirement for TDP1 activity, or that the types of breaks which accumulate in *TDP1*$^{-/-}$/*TDP2*$^{-/--}$ cells do not stimulate ADP-ribosylation to the same extent as those which accumulate in *XRCC1*$^{-/-}$ cells, as suggested above. Alternatively, it is possible that XRCC1 deletion causes hyperactivation of PARP1 by another mechanism, independent from the repair of DNA strand breaks (see section 7.3 for further discussion).

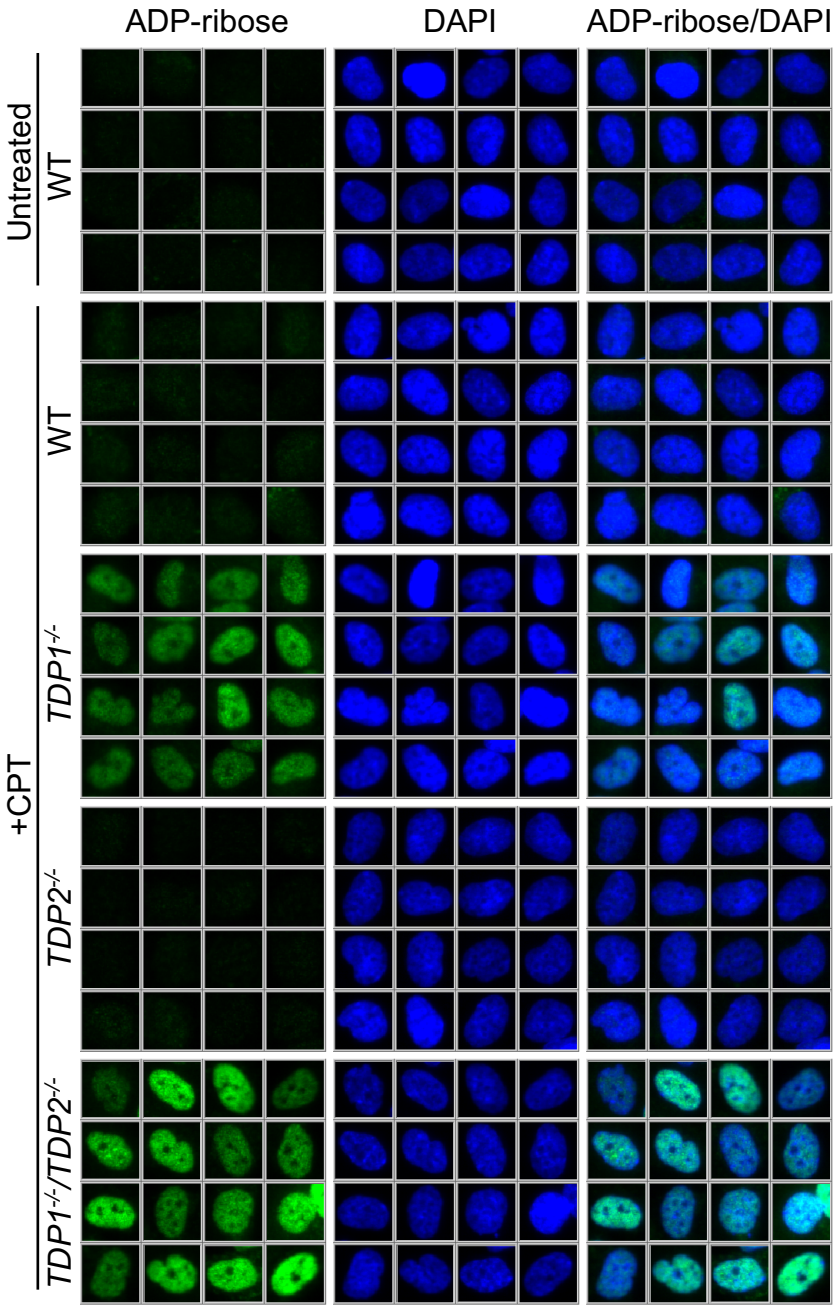

Figure 7.13. Deletion of *TDP2* further elevates CPT-induced ADP-ribosylation in *TDP1*$^{-/-}$ cells. WT, *TDP1*$^{-/-}$, *TDP1*$^{-/-}$/*TDP2*$^{-/-}$ *and TDP2*$^{-/-}$ RPE-1 cells growing on glass coverslips were treated or not with 30 μM CPT for 1 h prior to formaldehyde fixation and immunolabelling with pan-ADP-ribose binding reagent (green), and DNA labelling with DAPI (blue). Slides were imaged using the Olympus ScanR system and ScanR Analysis software was used to generate galleries of 16 randomly selected cells for each condition. See Fig. 7.14. for quantification.

A

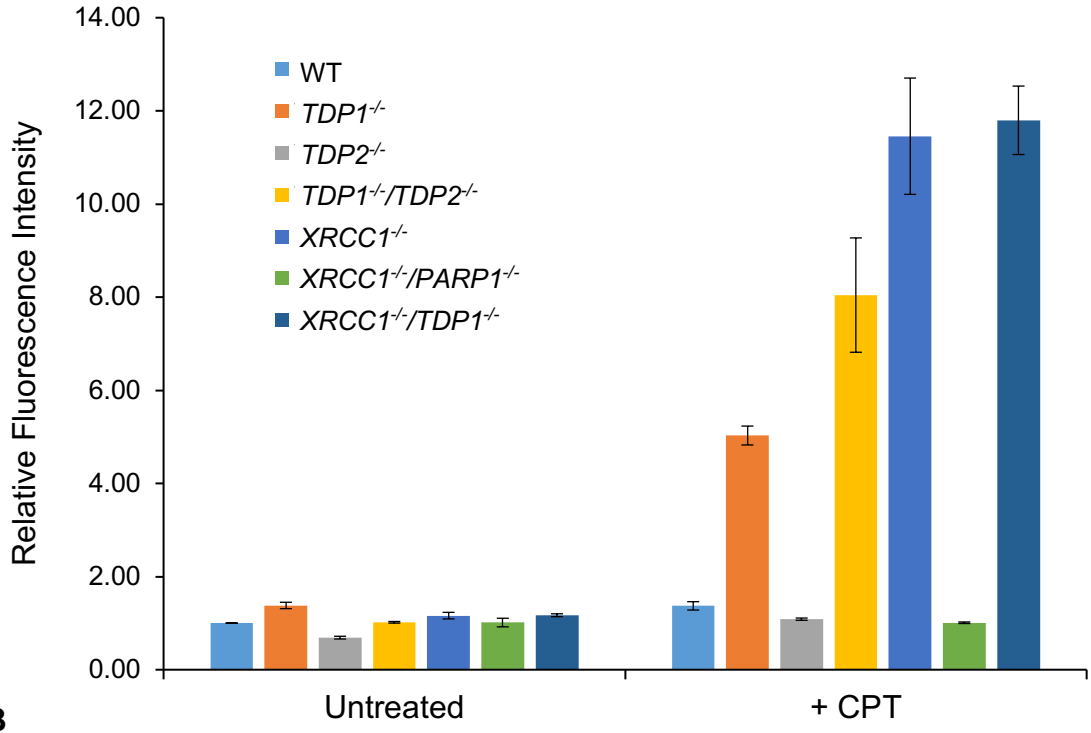

B

V.S		+CPT						
		WT	*TDP1*$^{-/-}$	*TDP2*$^{-/-}$	*TDP1*$^{-/-}$/*TDP2*$^{-/-}$	*XRCC1*$^{-/-}$	*XRCC1*$^{-/-}$/*PARP1*$^{-/-}$	*XRCC1*$^{-/-}$/*TDP1*$^{-/-}$
+CPT	WT		1.90E-07	1.20E-01	1.70E-04	3.80E-05	6.10E-02	1.40E-06
	TDP1-/-	1.90E-07		8.30E-05	9.20E-03	7.10E-04	7.60E-05	2.90E-05
	TDP2-/-	1.20E-01	8.30E-05		3.00E-02	5.20E-03	1.20E-01	1.50E-03
	TDP1-/-/TDP2-/-	1.70E-04	9.20E-03	3.00E-02		1.70E-01	2.90E-02	6.50E-02
	XRCC1-/-	3.80E-05	7.10E-04	5.20E-03	1.70E-01		5.10E-03	8.40E-01
	XRCC1-/-/PARP1-/-	6.10E-02	7.60E-05	1.20E-01	2.90E-02	5.10E-03		1.50E-03
	XRCC1-/-/TDP1-/-	1.40E-06	2.90E-05	1.50E-03	6.50E-02	8.40E-01	1.50E-03	

Key:

ns (0.05<p)	* (0.01<p<0.05)	** (0.001<p<0.01)	*** (0.0001<p<0.001)	**** (p<0.0001)

Figure 7.14. CPT-induced ADP-ribosylation levels in RPE-1 knockout cell lines. Quantification of Pan-ADP-ribose fluorescence in untreated and CPT-treated RPE-1 cells of the indicated genotypes. Representative images are presented in Fig. 7.10, 7.12. and 7.13. Pan-ADP-ribose fluorescence from >1000 cells was quantified in the nucleus and is expressed as fold over signal in untreated WT. Data are mean ±SEM of at least 2 independent replicates **(A).** T-test p-values between pairwise CPT-treated data are tabulated. Cell colour coding indicates the significance level, according to the key (bottom) **(B)**.

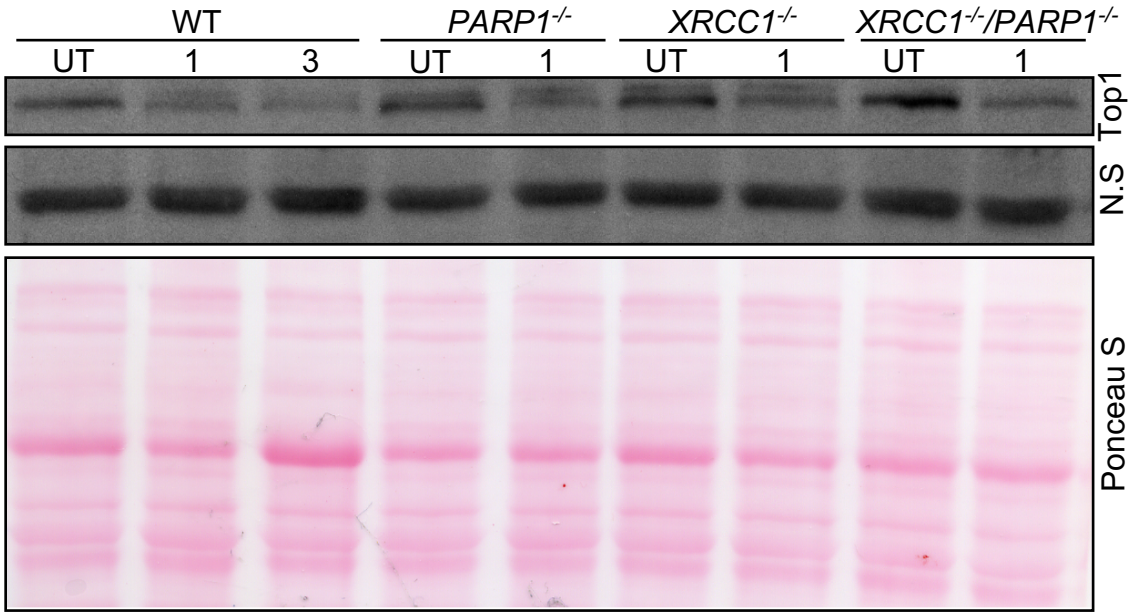

Figure 7.15. CPT-induced degradation of Top1 is not blocked by loss of PARP1. Sub-confluent RPE-1 cells of different genotypes were treated or not with complete DMEM/F12 containing 30 μM CPT for 1 or 3 h, prior to PBS washing and recovery in complete DMEM/F12 for 30 min. Cells were then washed, lysed, and subjected to 10% SDS-PAGE with anti-Top1 antibody. Equal loading is demonstrated by equivalence of Ponceau S staining, and equivalence of a non-specific (N.S) band detected by the anti-Top1 antibody.

7.2.13. Loss of *PARP1* does/does not block CPT-induced degradation of Top1

Having demonstrated that PARP1 is activated by CPT-induced DNA strand breaks which accumulate in *XRCC1*$^{-/-}$ cells (Fig. 7.10. and 7.14.), the mechanism by which PARP1 deletion suppresses the elevated Comet tail moment of CPT-treated *XRCC1*$^{-/-}$ cells was investigated. One explanation for how this might occur is by affecting the proteasomal degradation of Top1-SSBs. It has been reported previously that pre-treating cells with MG132 proteasome inhibitor reduces CPT-induced Comet tails (Alagoz, Chiang et al. 2013). To test whether PARP1 is involved in the proteasomal degradation of Top1-SSBs, WT, *PARP1*$^{-/-}$, *XRCC1*$^{-/-}$ and *XRCC1*$^{-/-}$/*PARP1*$^{-/-}$ RPE-1 cells were treated or not with 30 µM CPT for 1 or 3 h (WT only), prior to washing and recovery in complete media. Whole cell lysates were subjected to SDS-PAGE and anti-Top1 Western Blot (WB) (Fig. 7.15.). CPT-induced degradation of Top1 was evident in WT cells by 1 h, with limited further degradation by 3 h. Strikingly, all other genotypes exhibited comparable degradation of Top1 by 1 h; suggesting that neither PARP1 nor XRCC1 are involved in this step of Top1-SSB repair, and arguing against this hypothesis to explain the results of the Comet assay (see section 7.3 for further discussion).

7.3. Conclusions and Discussion

In this chapter, the genetic relationship between *PARP1, XRCC1* and *TDP1* in the cellular response to CPT was investigated by three main methodologies: clonogenic survival, Comet assay and PAR IF. Deletion of *PARP1, XRCC1* or *TDP1* was found to result in comparable sensitivity to CPT by clonogenic survival assay. Unfortunately, the generation of *PARP1*$^{-/-}$/*TDP1*$^{-/-}$ cells was unsuccessful here. However, by using *XRCC1*$^{-/-}$/*PARP1*$^{-/-}$ and *XRCC1*$^{-/-}$/*TDP1*$^{-/-}$ cells to demonstrate epistatic relationships between *PARP1* and *XRCC1*, and between *XRCC1* and *TDP1*, we can infer that all three genes are in the same epistasis group for cellular resistance to CPT. The very similar sensitivity of *PARP1*$^{-/-}$ and *TDP1*$^{-/-}$ cells is in agreement with a previous study which reported epistasis of these two genes for resistance of chicken DT40 cells to continuous CPT

treatment (Das, Huang et al. 2014). Notably, this result contradicts a previous study which found no sensitivity of *PARP1*$^{-/-}$ MEFs or PARP1-depleted A2780 human cells to CPT (Patel, Flatten et al. 2012). The explanation for this discrepancy is unclear. In the cited publication, cells were exposed to CPT for 24 h prior to washing and incubation in drug-free media, which contrasts with the continuous treatment used here. It is possible that these different treatment protocols could be a factor in the different responses observed.

Here it was found that loss of PARP2 sensitised *PARP1*$^{-/-}$ but not WT cells to CPT. This suggests that in the presence of PARP1, PARP2 does not play any appreciable role in the repair of CPT-induced damage, but that it may be providing a backup role in the absence of PARP1. As PARP1 deletion fully blocked CPT-induced ADP-ribosylation in *XRCC1*$^{-/-}$ cells, this backup role of PARP2 is unclear. Either the function is independent of the catalytic activity of PARP2, or the catalytic activity is so low that it is below the detection limit of the IF assay. Alternatively, it may be a catalytic role which is downstream of the rate-limiting SSBR step in *XRCC1*$^{-/-}$ cells. For example PARP2 is likely to respond to 5'-phosphate termini which result after PNKP activity (Langelier, Riccio et al. 2014). If this activity is the rate-limiting step in *XRCC1*$^{-/-}$ cells, we might be unlikely to detect PARP2-mediated ADP-ribosylation in these cells. Alternatively, if Lig3 activity is rate-limiting in *XRCC1*$^{-/-}$ cells we might expect an accumulation of 5'-phosphate termini which would be expected to activate PARP2. In the future, this model could be tested by quantification of CPT-induced ADP-ribosylation in *PARP1*$^{-/-}$ and *PARP1*$^{-/-}$/*PARP2*$^{-/-}$ cells depleted of PNKP or Lig3α.

PARP1 was shown in this chapter to be entirely responsible for the CPT-induced increase in chromatin-localized XRCC1. This is contrast to the findings of Chapter Six, which revealed overlapping functions of PARP1 and PARP2 in H_2O_2-induced XRCC1 chromatin-localization. One model to explain this difference involves differences in the types of termini generated following exposure to the two damaging agents. It is notable that SSBs generated both by direct oxidation of the dRP moiety, or by excision of oxidized bases by the bifunctional glycosylases, often harbour a 5'-phosphate terminus. CPT, on the other hand, induces SSBs which do not harbour a 5'-phosphate terminus until after processing by TDP1 and PNKP (see Fig. 7.1.). As mentioned above, 5'-

phosphate termini have been demonstrated previously to stimulate PARP2 to a greater degree than other types of termini (Langelier, Riccio et al. 2014); by comparison, PARP1 exhibits no such selectivity. This may explain the apparent involvement of PARP2 in XRCC1 chromatin-localization following H_2O_2, but not CPT treatment.

Alkaline single cell electrophoresis revealed that *PARP1*$^{-/-}$ cells do not exhibit the elevated CPT-induced Comet tail moments of *TDP1*$^{-/-}$ or *XRCC1*$^{-/-}$ cells; nor indeed do any of the other *PARP* KO cell lines, including *PARP1*$^{-/-}$/*PARP2*$^{-/-}$ cells. Furthermore, deletion of *PARP1* supressed the elevated CPT-induced Comet tail moment observed in *XRCC1*$^{-/-}$ cells. These surprising results are notably distinct from the published effect of PARP inhibitors, which reportedly do cause elevated CPT-induced Comet tail moments (Lin, Ban et al. 2008, Znojek, Willmore et al. 2014). In order to investigate the role of PARP1 at Top1-SSBs in more detail, quantitative IF was used to measure CPT-induced ADP-ribosylation directly. As discussed above, it was found that deletion of PARP1 in *XRCC1*$^{-/-}$ cells completely abolished CPT-induced ADP-ribosylation, suggesting that at least in the absence of XRCC1, the CPT-induced lesions which accumulate trigger activation of PARP1 alone. It has been reported previously that inhibition of the proteasome blocks CPT-induced Comet tail moments (Alagoz, Chiang et al. 2013). Inclusion of a proteinase K digestion step in the Comet protocol removes this block, suggesting that it is probably due to retarded electrophoretic mobility of unproteolyzed Top1-SSBs (Alagoz, Chiang et al. 2013). It was therefore hypothesised that PARP1 may be playing a previously unreported role in this process. However, WB failed to detect a difference in CPT-induced degradation of Top1 between WT, *PARP1*$^{-/-}$ or *XRCC1*$^{-/-}$/*PARP1*$^{-/-}$ cells. This approach has been used previously to establish a link between ATM loss and suppressed Top1 degradation (Katyal, Lee et al. 2014). It is important to note that the reported difference in CPT-induced Top1 degradation between WT and *ATM*$^{-/-}$ cells was small (59% and 37%, respectively), and not immediately apparent by eye. This suggests that the assay may not be sufficiently sensitive for detecting proteolysis of Top1-SSBs. Future work will focus more directly on the ubiquitylation and sumoylation which is known to be involved in this process (Mao, Sun et al. 2000, Lin, Ban et al. 2008, Lin, Ban

et al. 2009). Unfortunately, the suppression of elevated CPT-induced Comet tail moments in PARP1-deficient cell lines was observed at a late stage of this project, and time constraints have prevented further investigation here. These observations will therefore serve as preliminary work for future experiments concerning this intriguing phenotype.

Previous work has identified the human neurodegenerative disease SCAN1, caused by mutations in *TDP1* (Takashima, Boerkoel et al. 2002, El-Khamisy, Saifi et al. 2005). Recent work in this laboratory has identified a novel human disease (AOA-XRCC1) with similar clinical features, caused by mutation of *XRCC1* (Hoch, Hanzlikova et al. 2017). In this chapter, a common feature of *XRCC1*$^{-/-}$ and *TDP1*$^{-/-}$ RPE-1 cells was identified: hyper-ADP-ribosylation in response to CPT. This result is pertinent for several reasons. Firstly, one mechanism of cell death which is thought to act in SSBR-defective neurons is the programmed response Parthanatos, which is initiated by excessive PAR generation and concurrent depletion of NAD. The relevance of this mechanism is demonstrated by the fact that heterozygous and homozygous deletion of *Parp1* suppresses disease-associated phenotypes of an *Xrcc1* brain-specific knockout mouse (Hoch, Hanzlikova et al. 2017), and that cells derived from the AOA-XRCC4 patient also exhibit CPT-induced hyper-ADP-ribosylation (Hoch, Hanzlikova et al. 2017). Here it is reported for the first time that *TDP1*$^{-/-}$ RPE-1 cells also exhibit a PARP hyperactivation phenotype. It remains to be seen whether this phenotype is present upon mutation of other SSBR genes associated with autosomal recessive cerebellar ataxias, such as APTX and PNKP. More generally, it is conceivable that PARP hyperactivation might be a contributing factor in the onset or progression of other more common neurodegenerative diseases, such as Parkinson's (Cosi, Chopin et al. 1996, Mandir, Przedborski et al. 1999, Martire, Mosca et al. 2015) and Alzheimer's diseases (Love, Barber et al. 1999, Kauppinen, Suh et al. 2011, Martire, Fuso et al. 2013, Martire, Mosca et al. 2015). If this is indeed the case, the development of small molecules which inhibit PARP activity, without trapping the enzyme at the site of damage, could provide a therapeutic opportunity. Furthermore, the strikingly elevated levels of ADP-ribosylation in CPT-treated *XRCC1*$^{-/-}$ and

TDP1$^{-/-}$ cells suggests a paradigm which could be used to identify other genes with novel functions in SSBR.

Whilst elevated relative to WT, the CPT-induced ADP-ribosylation in *TDP1*$^{-/-}$ cells was found to be significantly lower than in *XRCC1*$^{-/--}$ cells. When combined, deletion of *XRCC1* and *TDP1* did not result in an additive effect in CPT-induced ADP-ribosylation, or on cell proliferation in the presence of CPT, and had only a very small additive effect on levels of CPT-induced strand breakage. Together these data indicate that these proteins operate in the same repair pathway for CPT-induced DNA damage. A number of factors could explain the lower levels of CPT-induced ADP ribosylation observed in *TDP1*$^{-/-}$ cells relative to *XRCC1*$^{-/-}$ cells. Firstly, it is possible that there are alternative enzymatic activities in the cell which bypass the requirement for TDP1 and allow downstream XRCC1-dependent repair. In this case, the loss of TDP1 might not be a robust block to SSBR, leading to a lower steady state number of CPT-induced Top1-SSBs and lower ADP-ribosylation. Some evidence was found for this hypothesis, as the combined deletion of *TDP1* and *TDP2* (which possesses a weak 3'-tyrosyl-phosphodiesterase activity) (Cortes Ledesma, El Khamisy et al. 2009, Zeng, Sharma et al. 2012) led to significantly higher levels of CPT-induced ADP-ribosylation than loss of TDP1 alone. This finding is in agreement with a previous study which observed elevated levels of CPT-induced strand breaks in *TDP1*$^{-/-}$/*TDP2*$^{-/-}$ vs *TDP1*$^{-/-}$ MEFs by alkaline Comet assay (Zeng, Sharma et al. 2012). Here, however, steady state levels of strand breaks were found by alkaline Comet assay to be approximately equivalent in *XRCC1*$^{-/-}$ and *TDP1*$^{-/-}$ cells. This result suggests that the steady-state level of ADP-ribosylation is not directly proportional to the number of CPT-induced DNA strand-breaks and that circumvention of TDP1 activity is unlikely to be the sole explanation for the lower hyper-ADP-ribosylation in *TDP1*$^{-/-}$ vs *XRCC1*$^{-/-}$ cells. CPT-treated *TDP1*$^{-/-}$ cells are likely to accumulate DNA 3'-tyrosyl-linked SSBs, whereas the identity of the lesions which accumulate in CPT-treated *XRCC1*$^{-/-}$ cells is less clear. XRCC1 promotes the stability, recruitment and activity of several SSBR enzymes involved in the repair of Top1-SSBs downstream of TDP1 activity, including PNKP and Lig3α. Additionally XRCC1 interacts with TDP1 itself via its constitutive partner Lig3α and may promote the recruitment and activity of TDP1

(Plo, Liao et al. 2003). It remains to be seen which enzymatic step is rate-limiting in *XRCC1*$^{-/-}$ cells, but if it is PNKP or Lig3α activity we would expect the accumulation of 5'-hydroxyl and 3'-phosphate, or DNA nicks, respectively. It is possible that repair intermediates that accumulate in CPT-treated *XRCC1*$^{-/-}$ cells may activate PARP1 to a greater extent than those which accumulate in CPT-treated *TDP1*$^{-/-}$ cells. Interestingly, recent work in this laboratory found that the levels of CPT-induced ADP-ribosylation were 2-fold greater in PNKP patient fibroblasts than XRCC1 patient fibroblasts (Hoch, Hanzlikova et al. 2017). This might suggest that the PARP1 hyperactivation phenotype in *XRCC1*$^{-/-}$ RPE-1 cells and XRCC1 patient fibroblasts results indirectly from a failure to efficiently recruit PNKP, although further work would be required to confirm this. For example, generation of *PNKP*$^{-/-}$ and *XRCC1*$^{-/-}$*/PNKP*$^{-/-}$ isogenic RPE-1 cells would allow the genetic relationship to be examined in more detail. Additionally, complementation of *XRCC1*$^{-/-}$ cells with XRCC1^{A482T}, which has disrupted PNKP binding, would allow separation of XRCC1 PAR-binding from PNKP recruitment.

A final hypothesis for the elevated level of hyper-ADP-ribosylation observed in *XRCC1*$^{-/-}$ cells is direct inhibition of PARP1 activity by XRCC1. In this case, XRCC1 recruitment could inhibit the level of ADP-ribosylation regardless of blocked repair in *TDP1*$^{-/-}$ cells. This has been suggested previously in the literature based on the observation that titration with recombinant XRCC1 reduces the activity of PARP1 *in vitro* (Masson, Niedergang et al. 1998, Keil, Gröbe et al. 2006). However, another study found that in contrast to overexpression of full length XRCC1, overexpression of the PAR-binding BRCT I domain alone actually stimulated ADP-ribosylation in untreated and H_2O_2-treated cells (Lévy, Oehlmann et al. 2009). This could be due to the BRCT I domain competing with the endogenous XRCC1 complex and thus inhibiting repair, but further work will be required to fully clarify this.

Chapter Eight

Final Summary and Concluding Remarks

8.1. Introduction

In this thesis, new data have been provided which clarify mechanisms of SSBR as they occur *in vivo* in human cells. The scope of the project was relatively broad, encompassing two subpathways of SSBR: the repair of oxidative SSBs and the repair of Top1-SSBs. In this concluding section, the notable findings of each chapter will be briefly summarised and discussed in relation to one another, and in relation to the recent literature. In particularly, suggestions will be made for future work in this area.

8.2. Chapter Summaries

8.2.1. Chapter Three – Investigating SSBR at a Highly-transcribed Gene Locus

Chapter Three constituted some of the early work undertaken on this project, which began with the aim of investigating the interplay between transcription and SSBR at the inducible early-response gene *FOS*: a marker of neuronal activity (Morgan and Curran 1986, Morgan, Cohen et al. 1987, Day, Masini et al. 2004) with known Top1 cleavage sites within its transcribed region (Francis Stewart, Herrera et al. 1990). A23187-induced *FOS* transcription and its inhibition by CPT was successfully demonstrated by qRT-PCR and RNAPII ChIP-qPCR.

Attention was focussed on the minimal level of transcription which persisted in the presence of CPT, as we hypothesised that this might be dependent upon functional SSBR. This hypothesis was first tested with the use of the PARP inhibitor KU0058948, which was found not to reduce transcription in the presence of CPT. At the time of these experiments, the consensus amongst myself and co-workers was that incubation of cells with 500 nM KU0058948 would essentially abolish cellular ADP-ribosylation by PARP1, PARP2 and PARP3. In latter stages of the project (see section 5.2.1), it was found that even a 2-fold higher concentration of KU0058948 (1 µM) failed to completely abolish H_2O_2-induced ADP-ribose IF signal. In the future, the level of *FOS* transcription in the presence of CPT could be tested with a higher concentration of KU0058948, or in the various *PARP*-deleted cell lines now available in the laboratory.

Inhibition of the proteasome with MG132 was used to block proteolysis of Top1-SSBs, in another attempt to determine if ongoing transcription in the presence of CPT was dependent on repair. This was problematic, as it was found that MG132 treatment lowered *FOS* transcription even in the absence of CPT. In the future, the *TDP1*$^{-/-}$ RPE-1 cells generated in subsequent stages of this project (see section 4.2.2) could be used to more specifically perturb repair of Top1-SSBs.

The primary aim of this chapter was to establish ChIP methods to detect enrichment of XRCC1 at *FOS* following gene induction and/or CPT treatment. Early attempts were apparently successful, suggesting an increased localization of XRCC1 to *FOS* upon gene induction. To test the specificity of this signal, the protocol was then established in CHO cells, where an *XRCC1* KO (EM9) was available. It became evident that the ChIP-qPCR signal detected with the A300-231A antibody was not specific to XRCC1, which prompted further experiments employing a GFP-tagging strategy (Teytelman, Thurtle et al. 2013). At the time of these experiments, there were not adequate tools to easily test the specificity of anti-XRCC1 signal in human cells. Following the generation of the *XRCC1*$^{-/-}$ RPE-1 cells by co-workers, these experiments would be far more tractable. For example, it was possible to select the anti-XRCC1 antibody used for many of the subsequent stages of the project (ABC738) based on its lack of immunoreactivity with *XRCC1*$^{-/-}$ cells by Western Blot (WB) and Immunofluorescence (IF). In the future, this antibody may also find use for the XRCC1 ChIP experiments.

8.2.2. Chapter Four - Generation and Characterization of Diploid Human Cells with CRISPR/Cas9 Mediated Deletion of SSBR Genes.

In attempting to develop a specific XRCC1 ChIP-qPCR protocol at an early stage of this project, it became apparent that there was a lack of human cell lines with KO mutations in SSBR genes, which would have been very useful as antigen depletion controls. In the year that this work was initiated, two pioneering publications detailed the RNA-guided genetic modification of human cells using CRISPR/Cas9 technology (Cong, Ran et al. 2013, Mali, Yang et al. 2013). Myself and other co-workers began employing this technology to generate a panel of

isogenic diploid human cells with deletions of SSBR genes. I successfully generated *TDP1*$^{-/-}$, *XRCC1*$^{-/-}$/*TDP1*$^{-/-}$ and *PARP1*$^{-/-}$/*PARP2*$^{-/-}$ RPE-1 cells, and characterized them by WB and sequencing of the mutations introduced.

The previous literature does not include any mention of cell lines which are doubly deleted of *XRCC1* and *TDP1*, or of *PARP1* and *PARP2*: implying that these may be the first such cell lines to be generated. In particular, the successful generation of *PARP1*$^{-/-}$/*PARP2*$^{-/-}$ cells was very exciting, because this combination of mutations leads to early embryonic lethality in mice (Ménissier de Murcia, Ricoul et al. 2003), and had an unknown phenotype at the cellular level. Since the observation of a synthetically lethal interaction between PARP inhibition and HR-deficiency (Bryant, Schultz et al. 2005), and the subsequent FDA and EMA approval of PARP inhibitors for the treatment of BRCA1/BRCA2 deficient ovarian cancers (EMA 2014, FDA 2014), clinical research into poly(ADP-ribosyl)ation has increased dramatically (NCBI 2016). The *PARP1*$^{-/-}$/*PARP2*$^{-/-}$ cells generated here may useful for future work in this area, for example in testing the specificity, potency, and DNA-PARP trapping propensity of novel PARP inhibitors. In support of this, since publication of the cell line (Hanzlikova, Gittens et al. 2016), it has been requested by and distributed to several external research groups.

In the future, it would be useful to generate a complete panel of cell lines with combined deletion of the three known DNA-dependent PARPs. This would involve generation of *PARP1*$^{-/-}$/*PARP3*$^{-/-}$, *PARP2*$^{-/-}$/*PARP3*$^{-/-}$ and *PARP1*$^{-/-}$/*PARP2*$^{-/-}$/*PARP3*$^{-/-}$ cells. This complete panel might prove useful, for example in identifying the ADP-ribosylation targets of the three enzymes *in vivo*.

8.2.3. Chapter Five – Establishing High-Content Imaging Methods for the Sensitive Quantification of ADP-ribose and Chromatin-associated XRCC1.

The aim of Chapter Five was to develop and characterize a method for the quantification of endogenous ADP-ribosylation and XRCC1 chromatin-association which avoided some negative aspects of previously-employed methods, such as: poor signal from the use of insensitive detection reagents, artefacts caused by overexpression of fluorescent protein (FP) –tagged

constructs, and poor reproducibility and temporal resolution of chromatin fractionation methods. In the case of ADP-ribosylation, this involved comparing the sensitivity of multiple available antibodies/ recombinant reagents. In the case of detecting the chromatin localization of XRCC1, a pre-extraction technique based on previous work (Cramer and Mitchison 1995, Britton, Coates et al. 2013) was employed. Both IF methods were coupled to a high-content imaging platform which allowed the sensitive quantification of ADP-ribosylation and chromatin-associated endogenous XRCC1 in thousands of single cells.

It was found that the ADP-ribose binding reagent MABE1016 (Kraus 2015) was significantly more sensitive than the 10H monoclonal in widespread use, and furthermore it appeared to detect a broader molecular weight range of ADP-ribosylated protein targets. High content imaging of IF conducted with this reagent revealed that treatment with 1 μM KU0058948 fails to abolish H_2O_2-induced ADP-ribosylation.

XRCC1 appeared to be localized predominately to the nucleolar chromatin in unchallenged cells, which may be explained by a resistance of these structures to detergent-extraction (Melan and Sluder 1992, Britton, Coates et al. 2013), or alternatively may reflect a functional role of XRCC1 in the nucleolus. PARP1 and PARP2 both possess nucleolar localization sequences, which might suggest a model of XRCC1 nucleolar localization involving elevated ADP-ribosylation at these regions. However, no enrichment of ADP-ribosylation was detected in the nucleolus in unchallenged cells, and in Chapter Six, it was demonstrated that there was no specific reduction in nucleolar XRCC1 signal in *PARP1*$^{-/-}$*/PARP2*$^{-/-}$ cells. Both of these observations suggest that if the nucleolar XRCC1 signal reflects a functional enrichment, then this enrichment is independent of PARP1/PARP2 mediated ADP-ribosylation.

8.2.4. Chapter Six – Overlapping Roles of PARP1 and PARP2 for the Loading of Endogenous XRCC1 and PNKP into Oxidised Human Chromatin

Chapter Six aimed to utilize the techniques developed in Chapter Five to assess the contributions of PARP1, PARP2 and PARP3 to H_2O_2-induced ADP-ribosylation, XRCC1 and PNKP chromatin-loading, and to rates of SSBR. The

pattern of H_2O_2-induced ADP-ribosylated targets in WT, *PARP1*$^{-/-}$, *PARP2*$^{-/-}$ and *PARP3*$^{-/-}$ cell extracts were visually similar by WB, as was the distribution of nuclear signal detected by high-content IF. The levels of total H_2O_2-induced ADP-ribosylation were comparable in WT, *PARP2*$^{-/-}$ and *PARP3*$^{-/-}$ cells, but were significantly lower in *PARP1*$^{-/-}$ cells, in agreement with previous research (Ame, Rolli et al. 1999). Surprisingly, the remaining level of ADP-ribosylation, which was shown to be PARP2-dependent, was found to be sufficient for proficient XRCC1 chromatin-localization (Hanzlikova, Gittens et al. 2016). These experiments were first conducted using siRNA-mediated depletion of PARP2 and/or PARP3 in a *PARP1*$^{-/-}$ background, and subsequently repeated following the generation of the *PARP1*$^{-/-}$/*PARP2*$^{-/-}$ RPE-1 cell line.

The role of PARP2-mediated ADP-ribosylation in recruiting XRCC1 to sites of DNA damage had been previously questioned, in part due to observations that the relocalization of overexpressed GFP-XRCC1 into H_2O_2-induced foci or to sites of UVA laser-mediated damage was entirely reliant on PARP1 activity (El-Khamisy, Masutani et al. 2003, Okano, Lan et al. 2003, Fisher, Hochegger et al. 2007, Mortusewicz, Amé et al. 2007). As detailed in Chapter Seven, the role of PARP2 in promoting XRCC1 recruitment to sites of oxidative damage does not appear to extend to the other type of lesion considered in this project: Top1-SSBs (see section 7.2.10). This can be rationalised by considering that 5'-phosphate termini, which most stimulate PARP2 activity, are commonly generated following direct oxidative scission of the dRP DNA moiety, or excision of oxidized bases by the bifunctional glycosylases; but are not generated at Top1-SSBs until after end-processing by TDP1 and PNKP. By comparison, PARP1 is potently stimulated by SSBs with diverse chemical termini, owing to the mechanism by which it coordinates them (Dawicki-McKenna, Langelier et al. 2015, Eustermann, Wu et al. 2015). This is likely to explain its involvement in CPT-induced XRCC1 chromatin localization.

The role of PARP3 was also investigated, as it has been previously reported to be a sensor of nicked nucleosomes and to be implicated in SSBR in chicken DT40 cells (Grundy, Polo et al. 2016). In this human cell system, PARP3 appeared to play no role in either H_2O_2-induced ADP-ribosylation, XRCC1 chromatin-localization, or rates of SSBR in H_2O_2 -treated cells. It is possible that

H_2O_2-induced damage does stimulate PARP3 activity, but that this technique is not sensitive enough to detect mono(ADP-ribosyl)ated targets. However, it does seem clear that any PARP3-mediated ADP-ribosylation does not have a role in XRCC1 recruitment into oxidised chromatin, and if present must instead promote other aspects of SSBR.

The mechanism of PNKP recruitment at sites of DNA damage has been the subject of controversy in the literature, with some suggesting that this is mediated by its interaction with XRCC1 (Loizou, El-Khamisy et al. 2004, Della-Maria, Hegde et al. 2012), and others suggesting that PNKP interacts with PAR directly (Li, Lu et al. 2013). Here it was shown that *XRCC1*$^{-/-}$ cells had significantly reduced or ablated PNKP chromatin-loading in response to H_2O_2 treatment, which is consistent with the former model. In comparison to XRCC1, the PNKP signal was notably punctate, which might indicate recruitment of PNKP to only a subset of H_2O_2-induced lesions. This will require further study, for example by using an anti-PNKP antibody raised in a different host to the anti-XRCC1 antibody, which would allow an analysis of signal colocalization.

PARP1$^{-/-}$ and *XRCC1*$^{-/-}$ cells exhibited similarly delayed SSBR kinetics following H_2O_2 treatment. Given that XRCC1 chromatin-loading is proficient in the *PARP1*$^{-/-}$ cells, this implies that this is not the source of their SSBR defect. In the future, other known roles of PARylation must be assessed in this system, for example relaxation of chromatin superstructure (Aubin, Fréchette et al. 1983, de Murcia, Huletsky et al. 1986, Kim, Mauro et al. 2004, Strickfaden, McDonald et al. 2016). The extent to which PARP2 can support these other functions will be particularly interesting. At the time of these experiments, a *PARP1*$^{-/-}$*/XRCC1*$^{-/-}$ cell line was not available, but this has been subsequently generated by co-workers. Using these cells, we have reported that loss of *PARP1* and *XRCC1* does not have an additive effect in delaying SSBR (Hoch, Hanzlikova et al. 2017), which would support the consensus model whereby the additional roles of *PARP1* in modulating chromatin structure, for example, are in the same pathway and thus epistatic with *XRCC1*.

8.2.5. Chapter Seven - The Role of PARP1, TDP1 and XRCC1 in the Repair of CPT-induced DNA Damage

Chapter Seven aimed to use the cell lines generated in Chapter Four, and the methods developed in Chapter Five, to investigate the SSBR of CPT-induced Top1-SSBs. It was found by clonogenic survival assay that *PARP1*$^{-/-}$ cells, but not *PARP2*$^{-/-}$ or *PARP3*$^{-/-}$ cells, were sensitive to CPT. *PARP1*$^{-/-}$/*PARP2*$^{-/-}$ cells were more sensitive than *PARP1*$^{-/-}$ cells, implying that in the absence of *PARP1*, *PARP2* may be able to support some of its roles in promoting cellular resistance to CPT. Despite this, the absence of sensitivity of *PARP2*$^{-/-}$ cells to CPT suggests that in WT cells, *PARP1* is mainly responsible for promoting cellular resistance to CPT. This was supported by the finding that loss of *PARP1*, but not *PARP2* or *PARP3*, ablated the CPT-induced increase in XRCC1 chromatin-localization.

Unfortunately, the generation of *PARP1*$^{-/-}$/*TDP1*$^{-/-}$ cells was unsuccessful here. However, the similarity of the CPT survival curves of *PARP1*$^{-/-}$, *TDP1*$^{-/-}$ and *XRCC1*$^{-/-}$ cells, coupled with the demonstration of epistasis between *PARP1* and *XRCC1* and between *TDP1* and *XRCC1*, strongly suggests that these three genes all operate in the same epistasis group for CPT tolerance. In support of this, it was found that *TDP1*$^{-/-}$ and *XRCC1*$^{-/-}$ cells exhibited comparably elevated levels of CPT-induced SSBs, relative to WT. However, unexpectedly, *PARP1*$^{-/-}$ cells did not exhibit the same elevated Comet tail moment, and it was subsequently shown that loss of *PARP1* was able to supress the Comet tail moment of *XRCC1*$^{-/-}$ cells. This intriguing phenotype has not been reported previously in the literature, and is the subject of ongoing research in the Caldecott laboratory. Since completion of this project, the phenotype has been confirmed with siRNA-mediated depletion of PARP1 in *XRCC1*$^{-/-}$ cells (J. Wang, personal communication), arguing that it is not due to any other clonal characteristic of *XRCC1*$^{-/-}$/*PARP1*$^{-/-}$ cells. At the point of writing, the focus is on two potential models. Firstly, PARP1 may have a previously undescribed role in promoting the proteolysis of Top1-SSBs, such that its loss leads to an accumulation of unproteolysed Top1-SSBs, which are undetectable by alkaline Comet assay ((Alagoz, Chiang et al. 2013) and J. Wang, personal communication). Another hypothesis is that PARP1 is actively involved in converting Top1ccs to Top1-SSBs. Whilst the induction of Top1ccs by CPT appears to be comparable in WT

and *PARP1*$^{-/-}$ cells (J. Wang, personal communication), the level of Top1-SSBs which remain after CPT removal has yet to be assessed. If PARP1-mediated ADP-ribosylation prevents the reversal of CPT-stabilized Top1ccs which otherwise might occur under the conditions of the alkaline Comet assay, this could explain the phenotype. To test this, the levels of Top1-SSBs should be determined following removal of CPT in WT vs *PARP1*$^{-/-}$ cells, using an assay which directly quantifies covalently linked DNA-Top1 molecules.

In Chapter Seven, a striking phenotype of *XRCC1*$^{-/-}$ and *TDP1*$^{-/-}$ cells was reported: hyper-ADP-ribosylation in response to CPT. This was rationalised by a model in which perturbation of SSBR causes an accumulation of CPT-induced SSBs which would otherwise be rapidly repaired, and these SSBs activate ADP-ribosylation. In the case of *XRCC1*$^{-/-}$ RPE-1 cells, the CPT-induced ADP-ribosylation was shown to be entirely dependent on PARP1, because in *XRCC1*$^{-/-}$*/PARP1*$^{-/-}$ cells it was completely ablated. In the future, it will be important to demonstrate whether PARP1 is similarly entirely responsible for the hyper-ADP-ribosylation observed in CPT-treated *TDP1*$^{-/-}$ cells. It will also be important to identify the types of SSB which accumulate in *TDP1*$^{-/-}$ and *XRCC1*$^{-/-}$ cells, as these appear to activate ADP-ribosylation to differing degrees.

The hyper-ADP-ribosylation phenotype described above was subsequently observed in fibroblasts derived from patients with mutations in *XRCC1* and *PNKP* (Hoch, Hanzlikova et al. 2017), by co-workers in the Caldecott lab. It was further demonstrated that deletion of *Parp1* was able to reduce cerebellar neurodegeneration and ataxic phenotypes of *Xrcc1* brain-specific KO mice, indicating that PARthanatos is involved in the pathogenesis (Hoch, Hanzlikova et al. 2017), and that non-trapping PARP inhibition might provide a therapeutic opportunity for human diseases in which this cell death programme is implicated. This publication additionally demonstrated that the hyper-ADP-ribosylation phenotype was also observed 1 h after H_2O_2 treatment, demonstrating that other types of persistent SSB also trigger hyper-ADP-ribosylation (Hoch, Hanzlikova et al. 2017). Given the work presented in this thesis, it will be interesting to determine whether H_2O_2-induced hyper-ADP-ribosylation in *XRCC1*$^{-/-}$ cells is entirely dependent on PARP1, or whether PARP2 also contributes in this case. More generally, by treating various SSBR-deficient

cells with different types of SSB-inducing agent, it should be possible to elucidate the roles of the DNA-dependent PARPs in each subpathway of SSBR. Finally, by coupling high-content analysis of hyper-ADP-ribosylation with a high-throughput screening approach, it should be possible to identify genes with novel functions in promoting SSBR.

Uncategorized References

A. Giuliano, K., R. L. DeBiasio, R. Terry Dunlay, A. Gough, J. M. Volosky, J. Zock, G. Pavlakis and D. Taylor (1997). *High-Content Screening: A New Approach to Easing Key Bottlenecks in the Drug Discovery Process*.

Abdou, I., G. G. Poirier, M. J. Hendzel and M. Weinfeld (2015). "DNA ligase III acts as a DNA strand break sensor in the cellular orchestration of DNA strand break repair." *Nucleic Acids Res* **43**(2): 875-892.

Abeti, R. and M. R. Duchen (2012). "Activation of PARP by oxidative stress induced by beta-amyloid: implications for Alzheimer's disease." *Neurochem Res* **37**(11): 2589-2596.

Adamietz, P. (1987). "Poly(ADP-ribose) synthase is the major endogenous nonhistone acceptor for poly(ADP-ribose) in alkylated rat hepatoma cells." *Eur J Biochem* **169**(2): 365-372.

Adamietz, P. and A. Rudolph (1984). "ADP-ribosylation of nuclear proteins invivo - identification of histone H2B as a major acceptor for mono(ADP-ribose) and poly(ADP-ribose) in dimethyl sulfate-treated hepatoma ah 7974 cells." *Journal of Biological Chemistry* **259**(11): 6841-6846.

Aguilera, A. and T. Garcia-Muse (2012). "R Loops: From Transcription Byproducts to Threats to Genome Stability." *Molecular Cell* **46**(2): 115-124.

Ahel, I., D. Ahel, T. Matsusaka, A. J. Clark, J. Pines, S. J. Boulton and S. C. West (2008). "Poly(ADP-ribose)-binding zinc finger motifs in DNA repair/checkpoint proteins." *Nature* **451**(7174): 81-85.

Ahel, I., U. Rass, S. F. El-Khamisy, S. Katyal, P. M. Clements, P. J. McKinnon, K. W. Caldecott and S. C. West (2006). "The neurodegenerative disease protein aprataxin resolves abortive DNA ligation intermediates." *Nature* **443**(7112): 713-716.

Akbari, M., K. Solvang-Garten, A. Hanssen-Bauer, N. V. Lieske, H. S. Pettersen, G. K. Pettersen, D. M. Wilson Iii, H. E. Krokan and M. Otterlei (2010). "Direct interaction between XRCC1 and UNG2 facilitates rapid repair of uracil in DNA by XRCC1 complexes." *DNA Repair* **9**(7): 785-795.

Alagoz, M., S.-C. Chiang, A. Sharma and S. F. El-Khamisy (2013). "ATM Deficiency Results in Accumulation of DNA-Topoisomerase I Covalent Intermediates in Neural Cells." *PLOS ONE* **8**(4): e58239.

Ali, A. A. E., G. Timinszky, R. Arribas-Bosacoma, M. Kozlowski, P. O. Hassa, M. Hassler, A. G. Ladurner, L. H. Pearl and A. W. Oliver (2012). "The zinc-finger domains of PARP1 cooperate to recognize DNA strand breaks." *Nature Structural & Molecular Biology* **19**(7): 685-+.

Allinson, S. L., Dianova, II and G. L. Dianov (2003). "Poly(ADP-ribose) polymerase in base excision repair: always engaged, but not essential for DNA damage processing." *Acta Biochim Pol* **50**(1): 169-179.

Allinson, S. L., I. I. Dianova and G. L. Dianov (2001). "DNA polymerase β is the major dRP lyase involved in repair of oxidative base lesions in DNA by mammalian cell extracts." *The EMBO Journal* **20**(23): 6919-6926.

Althaus, F. R., H. E. Kleczkowska, M. Malanga, C. R. Müntener, J. M. Pleschke, M. Ebner and B. Auer (1999). Poly ADP-ribosylation: A DNA break signal mechanism. *ADP-Ribosylation Reactions: From Bacterial Pathogenesis to Cancer*. R. Alvarez-Gonzalez. Boston, MA, Springer US**:** 5-11.

Altmeyer, M., S. Messner, P. O. Hassa, M. Fey and M. O. Hottiger (2009). "Molecular mechanism of poly(ADP-ribosyl)ation by PARP1 and identification of lysine residues as ADP-ribose acceptor sites." *Nucleic Acids Research* **37**(11): 3723-3738.

Alzu, A., R. Bermejo, M. Begnis, C. Lucca, D. Piccini, W. Carotenuto, M. Saponaro, A. Brambati, A. Cocito, M. Foiani and G. Liberi (2012). "Senataxin associates with replication forks to protect fork integrity across RNA-polymerase-II-transcribed genes." *Cell* **151**(4): 835-846.

Amé, J.-C., V. Rolli, V. Schreiber, C. Niedergang, F. Apiou, P. Decker, S. Muller, T. Höger, J. M.-d. Murcia and G. de Murcia (1999). "PARP-2, A Novel Mammalian DNA Damage-dependent Poly(ADP-ribose) Polymerase." *Journal of Biological Chemistry* **274**(25): 17860-17868.

Ame, J. C., V. Rolli, V. Schreiber, C. Niedergang, F. Apiou, P. Decker, S. Muller, T. Hoger, J. Menissier-de Murcia and G. de Murcia (1999). "PARP-2, A novel mammalian DNA damage-dependent poly(ADP-ribose) polymerase." *J Biol Chem* **274**.

Ame, J. C., C. Spenlehauer and G. de Murcia (2004). "The PARP superfamily." *Bioessays* **26**.

Andegeko, Y., L. Moyal, L. Mittelman, I. Tsarfaty, Y. Shiloh and G. Rotman (2001). "Nuclear retention of ATM at sites of DNA double strand breaks." *J Biol Chem* **276**(41): 38224-38230.

Andrabi, S. A., N. S. Kim, S. W. Yu, H. Wang, D. W. Koh, M. Sasaki, J. A. Klaus, T. Otsuka, Z. Zhang, R. C. Koehler, P. D. Hurn, G. G. Poirier, V. L. Dawson and T. M. Dawson (2006). "Poly(ADP-ribose) (PAR) polymer is a death signal." *Proc Natl Acad Sci U S A* **103**(48): 18308-18313.

Arnaudeau, C., C. Lundin and T. Helleday (2001). "DNA double-strand breaks associated with replication forks are predominantly repaired by homologous recombination involving an exchange mechanism in mammalian cells." *J Mol Biol* **307**(5): 1235-1245.

Aubin, R. J., A. Fréchette, G. de Murcia, P. Mandel, A. Lord, G. Grondin and G. G. Poirier (1983). "Correlation between endogenous nucleosomal hyper(ADP-ribosyl)ation of histone H1 and the induction of chromatin relaxation." *The EMBO Journal* **2**(10): 1685-1693.

Auerbach, R. K., G. Euskirchen, J. Rozowsky, N. Lamarre-Vincent, Z. Moqtaderi, P. Lefrancois, K. Struhl, M. Gerstein and M. Snyder (2009). "Mapping accessible chromatin regions using Sono-Seq." *Proc Natl Acad Sci U S A* **106**(35): 14926-14931.

Bae, S. H., E. Choi, K. H. Lee, J. S. Park, S. H. Lee and Y. S. Seo (1998). "Dna2 of Saccharomyces cerevisiae possesses a single-stranded DNA-specific endonuclease activity that is able to act on double-stranded DNA in the presence of ATP." *J Biol Chem* **273**(41): 26880-26890.

Balagurumoorthy, P., S. J. Adelstein and A. I. Kassis (2011). "Novel method for quantifying radiation-induced single-strand-break yields in plasmid DNA highlights 10-fold discrepancy." *Anal Biochem* **417**(2): 242-246.

Barabasz, A., B. Foley, J. C. Otto, A. Scott and J. Rice (2006). "The use of high-content screening for the discovery and characterization of compounds that modulate mitotic index and cell cycle progression by differing mechanisms of action." *Assay Drug Dev Technol* **4**(2): 153-163.

Barkauskaite, E., G. Jankevicius, A. G. Ladurner, I. Ahel and G. Timinszky (2013). "The recognition and removal of cellular poly(ADP-ribose) signals." *Febs Journal* **280**(15): 3491-3507.

Barnes, D. E., A. E. Tomkinson, A. R. Lehmann, A. D. B. Webster and T. Lindahl (1992). "Mutations in the DNA ligase-I gene of an individual with immunodeficiencies and cellular-hypersensitivity to DNA-damaging agents." *Cell* **69**(3): 495-503.

Barzilai, A., G. Rotman and Y. Shiloh (2002). "ATM deficiency and oxidative stress: a new dimension of defective response to DNA damage." *DNA Repair* **1**(1): 3-25.

Baxter, J. (2015). ""“Breaking Up Is Hard to Do”: The Formation and Resolution of Sister Chromatid Intertwines." *Journal of Molecular Biology* **427**(3): 590-607.

Beck, C., C. Boehler, J. Guirouilh Barbat, M. E. Bonnet, G. Illuzzi, P. Ronde, L. R. Gauthier, N. Magroun, A. Rajendran, B. S. Lopez, R. Scully, F. D. Boussin, V. Schreiber and F. Dantzer (2014). "PARP3 affects the relative contribution of homologous recombination and nonhomologous end-joining pathways." *Nucleic Acids Res* **42**(9): 5616-5632.

Been, M. D., R. R. Burgess and J. J. Champoux (1984). "DNA strand breakage by wheat germ type 1 topoisomerase." *Biochimica et Biophysica Acta (BBA) - Gene Structure and Expression* **782**(3): 304-312.

Beernink, P. T., M. Hwang, M. Ramirez, M. B. Murphy, S. A. Doyle and M. P. Thelen (2005). "Specificity of Protein Interactions Mediated by BRCT Domains of the XRCC1 DNA Repair Protein." *Journal of Biological Chemistry* **280**(34): 30206-30213.

Benjamin, R. C. and D. M. Gill (1980). "ADP-ribosylation in mammalian cell ghosts. Dependence of poly(ADP-ribose) synthesis on strand breakage in DNA." *J Biol Chem* **255**(21): 10493-10501.

Beranek, D. T. (1990). "Distribution of methyl and ethyl adducts following alkylation with monofunctional alkylating agents." *Mutat Res* **231**(1): 11-30.

Berger, N. A., G. Weber and A. S. Kaichi (1978). "Characterization and comparison of poly(adenosine dephosphoribose) synthesis and DNA synthesis in nucleotide-permeable cells." *Biochim Biophys Acta* **519**(1): 87-104.

Bermejo, R., Y. Doksani, T. Capra, Y. M. Katou, H. Tanaka, K. Shirahige and M. Foiani (2007). "Top1- and Top2-mediated topological transitions at replication forks ensure fork progression and stability and prevent DNA damage checkpoint activation." *Genes Dev* **21**(15): 1921-1936.

Bernstein, N. K., M. Hammel, R. S. Mani, M. Weinfeld, M. Pelikan, J. A. Tainer and J. N. Glover (2009). "Mechanism of DNA substrate recognition by the mammalian DNA repair enzyme, Polynucleotide Kinase." *Nucleic Acids Res* **37**(18): 6161-6173.

Bernstein, N. K., R. S. Williams, M. L. Rakovszky, D. Cui, R. Green, F. Karimi-Busheri, R. S. Mani, S. Galicia, C. A. Koch, C. E. Cass, D. Durocher, M. Weinfeld and J. N. Glover (2005). "The molecular architecture of the mammalian DNA repair enzyme, polynucleotide kinase." *Mol Cell* **17**(5): 657-670.

Berti, M., A. Ray Chaudhuri, S. Thangavel, S. Gomathinayagam, S. Kenig, M. Vujanovic, F. Odreman, T. Glatter, S. Graziano, R. Mendoza-Maldonado, F. Marino, B. Lucic, V. Biasin, M. Gstaiger, R. Aebersold, J. M. Sidorova, R. J. Monnat, Jr., M. Lopes and A. Vindigni (2013). "Human RECQ1 promotes restart of replication forks reversed by DNA topoisomerase I inhibition." *Nat Struct Mol Biol* **20**(3): 347-354.

Bertocci, B., A. De Smet, J. C. Weill and C. A. Reynaud (2006). "Nonoverlapping functions of DNA polymerases mu, lambda, and terminal deoxynucleotidyltransferase during immunoglobulin V(D)J recombination in vivo." *Immunity* **25**(1): 31-41.

Bertoncini, C. R. A. and R. Meneghini (1995). "DNA strand breaks produced by oxidative stress in mammalian-cells exhibit 3'-phosphoglycolate termini." *Nucleic Acids Research* **23**(15): 2995-3002.

Bétermier, M., P. Bertrand and B. S. Lopez (2014). "Is Non-Homologous End-Joining Really an Inherently Error-Prone Process?" *PLOS Genetics* **10**(1): e1004086.

Bhuyan, B. K., T. J. Fraser, L. G. Gray, S. L. Kuentzel and G. L. Neil (1973). "Cell-Kill Kinetics of Several S-Phase-specific Drugs." *Cancer Research* **33**(4): 888-894.

Birchler, J. A. and R. A. Veitia (2012). "Gene balance hypothesis: Connecting issues of dosage sensitivity across biological disciplines." *Proceedings of the National Academy of Sciences* **109**(37): 14746-14753.

Bjorklund, M., M. Taipale, M. Varjosalo, J. Saharinen, J. Lahdenpera and J. Taipale (2006). "Identification of pathways regulating cell size and cell-cycle progression by RNAi." *Nature* **439**(7079): 1009-1013.

Bodnar, A. G., M. Ouellette, M. Frolkis, S. E. Holt, C.-P. Chiu, G. B. Morin, C. B. Harley, J. W. Shay, S. Lichtsteiner and W. E. Wright (1998). "Extension of Life-Span by Introduction of Telomerase into Normal Human Cells." *Science* **279**(5349): 349-352.

Boehler, C., L. R. Gauthier, O. Mortusewicz, D. S. Biard, J.-M. Saliou, A. Bresson, S. Sanglier-Cianferani, S. Smith, V. Schreiber, F. Boussin and F. Dantzer (2011). "Poly(ADP-ribose) polymerase 3 (PARP3), a newcomer in cellular response to DNA damage and mitotic progression." *Proceedings of the National Academy of Sciences of the United States of America* **108**(7): 2783-2788.

Boiteux, S. and M. Guillet (2004). "Abasic sites in DNA: repair and biological consequences in Saccharomyces cerevisiae." *DNA Repair* **3**(1): 1-12.

Bonfiglio, J. J., P. Fontana, Q. Zhang, T. Colby, I. Gibbs-Seymour, I. Atanassov, E. Bartlett, R. Zaja, I. Ahel and I. Matic (2017). "Serine ADP-Ribosylation Depends on HPF1." *Molecular Cell* **65**(5): 932-940.e936.

Bradley, M. O. and K. W. Kohn (1979). "X-ray induced DNA double strand break production and repair in mammalian cells as measured by neutral filter elution." *Nucleic Acids Research* **7**(3): 793-804.

Bras, J., I. Alonso, C. Barbot, M. M. Costa, L. Darwent, T. Orme, J. Sequeiros, J. Hardy, P. Coutinho and R. Guerreiro (2015). "Mutations in PNKP cause recessive ataxia with oculomotor apraxia type 4." *Am J Hum Genet* **96**(3): 474-479.

Bredt, D. S., P. M. Hwang, C. E. Glatt, C. Lowenstein, R. R. Reed and S. H. Snyder (1991). "Cloned and expressed nitric oxide synthase structurally resembles cytochrome P-450 reductase." *Nature* **351**(6329): 714-718.

Breen, A. P. and J. A. Murphy (1995). "Reactions of oxyl radicals with DNA." *Free Radic Biol Med* **18**(6): 1033-1077.

Breslin, C., P. Hornyak, A. Ridley, S. L. Rulten, H. Hanzlikova, A. W. Oliver and K. W. Caldecott (2015). "The XRCC1 phosphate-binding pocket binds poly (ADP-ribose) and is required for XRCC1 function." *Nucleic Acids Research* **43**(14): 6934-6944.

Brill, S. J., S. DiNardo, K. Voelkel-Meiman and R. Sternglanz (1987). "Need for DNA topoisomerase activity as a swivel for DNA replication for transcription of ribosomal RNA." *Nature* **326**(6111): 414-416.

Britton, S., J. Coates and S. P. Jackson (2013). "A new method for high-resolution imaging of Ku foci to decipher mechanisms of DNA double-strand break repair." *The Journal of Cell Biology* **202**(3): 579-595.

Brochu, G., C. Duchaine, L. Thibeault, J. Lagueux, G. M. Shah and G. G. Poirier (1994). "Mode of action of poly(ADP-ribose) glycohydrolase." *Biochim Biophys Acta* **1219**(2): 342-350.

Brouwer, I., G. Sitters, A. Candelli, S. J. Heerema, I. Heller, A. J. Melo de, H. Zhang, D. Normanno, M. Modesti, E. J. G. Peterman and G. J. L. Wuite (2016). "Sliding sleeves of XRCC4–XLF bridge DNA and connect fragments of broken DNA." *Nature* **535**(7613): 566-569.

Bryant, H. E., E. Petermann, N. Schultz, A. S. Jemth, O. Loseva, N. Issaeva, F. Johansson, S. Fernandez, P. McGlynn and T. Helleday (2009). "PARP is activated at stalled forks to mediate Mre11-dependent replication restart and recombination." *Embo j* **28**(17): 2601-2615.

Bryant, H. E., N. Schultz, H. D. Thomas, K. M. Parker, D. Flower, E. Lopez, S. Kyle, M. Meuth, N. J. Curtin and T. Helleday (2005). "Specific killing of BRCA2-deficient tumours with inhibitors of poly (ADP-ribose) polymerase." *Nature* **434**.

Busch, H., H. Adams, W. J. Steele, K. Smetana, M. C. Liau and M. Muramatsu (1963). "Isolation of nucleoli." *Experimental Cell Research* **24**: 50-63.

Caldecott, K. and P. Jeggo (1991). "Cross-sensitivity of gamma-ray-sensitive hamster mutants to cross-linking agents." *Mutation Research* **255**(2): 111-121.

Caldecott, K. W. (2003). "DNA Single-Strand Break Repair and Spinocerebellar Ataxia." *Cell* **112**(1): 7-10.

Caldecott, K. W. (2003). "XRCC1 and DNA strand break repair." *DNA Repair (Amst)* **2**(9): 955-969.

Caldecott, K. W. (2008). "Single-strand break repair and genetic disease." *Nat Rev Genet* **9**(8): 619-631.

Caldecott, K. W. (2014). "DNA single-strand break repair." *Exp Cell Res* **329**(1): 2-8.

Caldecott, K. W. (2014). "Protein ADP-ribosylation and the cellular response to DNA strand breaks." *DNA Repair (Amst)* **19**: 108-113.

Caldecott, K. W., J. D. Tucker, L. H. Stanker and L. H. Thompson (1995). "Characterization of the XRCC1-DNA ligase III complex in vitro and its absence from mutant hamster cells." *Nucleic Acids Research* **23**(23): 4836-4843.

Cameron, V. and O. C. Uhlenbeck (1977). "3'-Phosphatase activity in T4 polynucleotide kinase." *Biochemistry* **16**(23): 5120-5126.

Campalans, A., S. Marsin, Y. Nakabeppu, R. O'Connor T, S. Boiteux and J. P. Radicella (2005). "XRCC1 interactions with multiple DNA glycosylases: a model for its recruitment to base excision repair." *DNA Repair (Amst)* **4**(7): 826-835.

Cantoni, O., F. Cattabeni, V. Stocchi, R. E. Meyn, P. Cerutti and D. Murray (1989). "Hydrogen peroxide insult in cultured mammalian cells: relationships between DNA single-strand breakage, poly(ADP-ribose) metabolism and cell killing." *Biochimica et Biophysica Acta (BBA) - Molecular Cell Research* **1014**(1): 1-7.

Cantoni, O., D. Murray and R. E. Meyn (1987). "Induction and repair of DNA single-strand breaks in EM9 mutant cho cells treated with hydrogen-peroxide." *Chemico-Biological Interactions* **63**(1): 29-38.

Cappelli, E., R. Taylor, M. Cevasco, A. Abbondandolo, K. Caldecott and G. Frosina (1997). "Involvement of XRCC1 and DNA ligase III gene products in DNA base excision repair." *Journal of Biological Chemistry* **272**(38): 23970-23975.

Castellano-Pozo, M., T. Garcia-Muse and A. Aguilera (2012). "R-loops cause replication impairment and genome instability during meiosis." *EMBO Rep* **13**(10): 923-929.

Caudron-Herger, M., T. Pankert, J. Seiler, A. Németh, R. Voit, I. Grummt and K. Rippe (2015). "Alu element-containing RNAs maintain nucleolar structure and function." *The EMBO Journal* **34**(22): 2758-2774.

Champoux, J. J. (1977). "Strand breakage by DNA untwisting enzyme results in covalent attachment of enzyme to DNA - (superhelical simian virus-40 DNA-DNA strand breakage DNA replication DNA-protein complex hydroxylamine)." *Proceedings of the National Academy of Sciences of the United States of America* **74**(9): 3800-3804.

Champoux, J. J. (2001). "DNA topoisomerases: structure, function, and mechanism." *Annu Rev Biochem* **70**: 369-413.

Chan, H. W. S. (1971). "Singlet oxygen analogs in biological systems. Coupled oxygenation of 1,3-dienes by soybean lipoxidase." *Journal of the American Chemical Society* **93**(9): 2357-2358.

Chang, H. H. Y., N. R. Pannunzio, N. Adachi and M. R. Lieber (2017). "Non-homologous DNA end joining and alternative pathways to double-strand break repair." *Nature Reviews Molecular Cell Biology* **18**(8): 495-506.

Chang, L. M. S. and F. J. Bollum (1971). "Low Molecular Weight Deoxyribonucleic Acid Polymerase in Mammalian Cells." *Journal of Biological Chemistry* **246**(18): 5835-5837.

Chappell, C., L. A. Hanakahi, F. Karimi-Busheri, M. Weinfeld and S. C. West (2002). "Involvement of human polynucleotide kinase in double-strand break repair by non-homologous end joining." *The EMBO Journal* **21**(11): 2827-2832.

Chaudhuri, J. and F. W. Alt (2004). "Class-switch recombination: interplay of transcription, DNA deamination and DNA repair." *Nat Rev Immunol* **4**(7): 541-552.

Chen, D., M. Vollmar, M. N. Rossi, C. Phillips, R. Kraehenbuehl, D. Slade, P. V. Mehrotra, F. von Delft, S. K. Crosthwaite, O. Gileadi, J. M. Denu and I. Ahel (2011). "Identification of Macrodomain Proteins as Novel O-Acetyl-ADP-ribose Deacetylases." *Journal of Biological Chemistry* **286**(15): 13261-13271.

Chen, D. S., T. Herman and B. Demple (1991). "Two distinct human DNA diesterases that hydrolyze 3'-blocking deoxyribose fragments from oxidized DNA." *Nucleic Acids Res* **19**(21): 5907-5914.

Cheng, Q., N. Barboule, P. Frit, D. Gomez, O. Bombarde, B. Couderc, G.-S. Ren, B. Salles and P. Calsou (2011). "Ku counteracts mobilization of PARP1 and MRN in chromatin damaged with DNA double-strand breaks." *Nucleic Acids Research* **39**(22): 9605-9619.

Chiang, S. C., J. Carroll and S. F. El-Khamisy (2010). "TDP1 serine 81 promotes interaction with DNA ligase IIIalpha and facilitates cell survival following DNA damage." *Cell Cycle* **9**(3): 588-595.

Cho, E.-J., M. S. Kobor, M. Kim, J. Greenblatt and S. Buratowski (2001). "Opposing effects of Ctk1 kinase and Fcp1 phosphatase at Ser 2 of the RNA polymerase II C-terminal domain." *Genes & Development* **15**(24): 3319-3329.

Chung, Y.-H., J. Xia and C. J. Margulis (2007). "Diffusion and Residence Time of Hydrogen Peroxide and Water in Crowded Protein Environments." *The Journal of Physical Chemistry B* **111**(46): 13336-13344.

Citarelli, M., S. Teotia and R. S. Lamb (2010). "Evolutionary history of the poly(ADP-ribose) polymerase gene family in eukaryotes." *BMC Evolutionary Biology* **10**(1): 308.

Clements, P. M., C. Breslin, E. D. Deeks, P. J. Byrd, L. M. Ju, P. Bieganowski, C. Brenner, M. C. Moreira, A. M. R. Taylor and K. W. Caldecott (2004). "The ataxia-oculomotor apraxia 1 gene product has a role distinct from ATM and interacts with the DNA strand break repair proteins XRCC1 and XRCC4." *DNA Repair* **3**(11): 1493-1502.

Cong, L., F. A. Ran, D. Cox, S. Lin, R. Barretto, N. Habib, P. D. Hsu, X. Wu, W. Jiang, L. A. Marraffini and F. Zhang (2013). "Multiplex Genome Engineering Using CRISPR/Cas Systems." *Science (New York, N.Y.)* **339**(6121): 819-823.

Cooke, M. S., M. D. Evans, M. Dizdaroglu and J. Lunec (2003). "Oxidative DNA damage: mechanisms, mutation, and disease." *Faseb j* **17**(10): 1195-1214.

Cortes Ledesma, F., S. F. El Khamisy, M. C. Zuma, K. Osborn and K. W. Caldecott (2009). "A human 5'-tyrosyl DNA phosphodiesterase that repairs topoisomerase-mediated DNA damage." *Nature* **461**(7264): 674-678.

Cosi, C., P. Chopin and M. Marien (1996). "Benzamide, an inhibitor of poly(ADP-ribose) polymerase, attenuates methamphetamine-induced dopamine neurotoxicity in the C57B1/6N mouse." *Brain Res* **735**(2): 343-348.

Costantini, L. M., M. Fossati, M. Francolini and E. L. Snapp (2012). "Assessing the Tendency of Fluorescent Proteins to Oligomerize under Physiologic Conditions." *Traffic (Copenhagen, Denmark)* **13**(5): 643-649.

Cramer, L. P. and T. J. Mitchison (1995). "Myosin is involved in postmitotic cell spreading." *The Journal of Cell Biology* **131**(1): 179-189.

Curtis, D. R. and J. C. Watkins (1965). "The pharmacology of amino acids related to gamma-aminobutyric acid." *Pharmacol Rev* **17**(4): 347-391.

D'Amours, D., S. Desnoyers, I. D'Silva and G. G. Poirier (1999). "Poly(ADP-ribosyl)ation reactions in the regulation of nuclear functions." *Biochem J* **342 (Pt 2)**: 249-268.

Das, B. B., S. Antony, S. Gupta, T. S. Dexheimer, C. E. Redon, S. Garfield, Y. Shiloh and Y. Pommier (2009). "Optimal function of the DNA repair enzyme TDP1 requires its phosphorylation by ATM and/or DNA-PK." *Embo j* **28**(23): 3667-3680.

Das, B. B., S.-y. N. Huang, J. Murai, I. Rehman, J.-C. Amé, S. Sengupta, S. K. Das, P. Majumdar, H. Zhang, D. Biard, H. K. Majumder, V. Schreiber and Y. Pommier (2014). "PARP1–TDP1 coupling for the repair of topoisomerase I–induced DNA damage." *Nucleic Acids Research* **42**(7): 4435-4449.

Date, H., O. Onodera, H. Tanaka, K. Iwabuchi, K. Uekawa, S. Igarashi, R. Koike, T. Hiroi, T. Yuasa, Y. Awaya, T. Sakai, T. Takahashi, H. Nagatomo, Y. Sekijima, I. Kawachi, Y. Takiyama, M. Nishizawa, N. Fukuhara, K. Saito, S. Sugano and S. Tsuji (2001). "Early-onset ataxia with ocular motor apraxia and hypoalbuminemia is caused by mutations in a new HIT superfamily gene." *Nat Genet* **29**(2): 184-188.

Date, H., O. Onodera, H. Tanaka, K. Iwabuchi, K. Uekawa, S. Igarashi, R. Koike, T. Hiroi, T. Yuasa, Y. Awaya, T. Sakai, T. Takahashi, H. Nagatomo, Y. Sekijima, I. Kawachi, Y. Takiyama, M.

Nishizawa, N. Fukuhara, K. Saito, S. Sugano and S. Tsuji (2001). "Early-onset ataxia with ocular motor apraxia and hypoalbuminemia is caused by mutations in a new HIT superfamily gene." *Nat Genet* **29**(2): 184-188.

David, S. S., V. L. O'Shea and S. Kundu (2007). "Base-excision repair of oxidative DNA damage." *Nature* **447**(7147): 941-950.

Davis, A. J. and D. J. Chen (2013). "DNA double strand break repair via non-homologous end-joining." *Transl Cancer Res* **2**(3): 130-143.

Dawicki-McKenna, Jennine M., M.-F. Langelier, Jamie E. DeNizio, Amanda A. Riccio, Connie D. Cao, Kelly R. Karch, M. McCauley, Jamin D. Steffen, Ben E. Black and John M. Pascal (2015). "PARP-1 Activation Requires Local Unfolding of an Autoinhibitory Domain." *Molecular Cell* **60**(5): 755-768.

Day, H. E. W., C. V. Masini and S. Campeau (2004). "The pattern of brain c-fos mRNA induced by a component of fox odor, 2,5-dihydro-2,4,5-Trimethylthiazoline (TMT), in rats, suggests both systemic and processive stress characteristics." *Brain Research* **1025**(1–2): 139-151.

de Klein, A., M. Muijtjens, R. van Os, Y. Verhoeven, B. Smit, A. M. Carr, A. R. Lehmann and J. H. Hoeijmakers (2000). "Targeted disruption of the cell-cycle checkpoint gene ATR leads to early embryonic lethality in mice." *Curr Biol* **10**(8): 479-482.

de Murcia, G., A. Huletsky, D. Lamarre, A. Gaudreau, J. Pouyet, M. Daune and G. G. Poirier (1986). "Modulation of chromatin superstructure induced by poly(ADP-ribose) synthesis and degradation." *J Biol Chem* **261**(15): 7011-7017.

de Murcia, G. and J. Menissier de Murcia (1994). "Poly(ADP-ribose) polymerase: a molecular nick-sensor." *Trends Biochem Sci* **19**(4): 172-176.

Debethune, L., G. Kohlhagen, A. Grandas and Y. Pommier (2002). "Processing of nucleopeptides mimicking the topoisomerase I-DNA covalent complex by tyrosyl-DNA phosphodiesterase." *Nucleic Acids Res* **30**(5): 1198-1204.

Della-Maria, J., M. L. Hegde, D. R. McNeill, Y. Matsumoto, M. S. Tsai, T. Ellenberger, D. M. Wilson, 3rd, S. Mitra and A. E. Tomkinson (2012). "The interaction between polynucleotide kinase phosphatase and the DNA repair protein XRCC1 is critical for repair of DNA alkylation damage and stable association at DNA damage sites." *J Biol Chem* **287**(46): 39233-39244.

Derheimer, F. A., H. M. O'Hagan, H. M. Krueger, S. Hanasoge, M. T. Paulsen and M. Ljungman (2007). "RPA and ATR link transcriptional stress to p53." *Proceedings of the National Academy of Sciences* **104**(31): 12778-12783.

Desai, S. D., L. F. Liu, D. Vazquez-Abad and P. D'Arpa (1997). "Ubiquitin-dependent destruction of topoisomerase I is stimulated by the antitumor drug camptothecin." *J Biol Chem* **272**(39): 24159-24164.

Desai, S. D., H. Zhang, A. Rodriguez-Bauman, J.-M. Yang, X. Wu, M. K. Gounder, E. H. Rubin and L. F. Liu (2003). "Transcription-Dependent Degradation of Topoisomerase I-DNA Covalent Complexes." *Molecular and Cellular Biology* **23**(7): 2341-2350.

Dianov, G., A. Price and T. Lindahl (1992). "Generation of single-nucleotide repair patches following excision of uracil residues from DNA." *Molecular and Cellular Biology* **12**(4): 1605-1612.

Dizdaroglu, M., B. Karahalil, S. Senturker, T. J. Buckley and T. Roldan-Arjona (1999). "Excision of products of oxidative DNA base damage by human NTH1 protein." *Biochemistry* **38**(1): 243-246.

Downs, J. A. and S. P. Jackson (2004). "A means to a DNA end: the many roles of Ku." *Nat Rev Mol Cell Biol* **5**(5): 367-378.

Drouet, J., C. Delteil, J. Lefrancois, P. Concannon, B. Salles and P. Calsou (2005). "DNA-dependent protein kinase and XRCC4-DNA ligase IV mobilization in the cell in response to DNA double strand breaks." *J Biol Chem* **280**(8): 7060-7069.

Duncan, B. K. and J. H. Miller (1980). "Mutagenic deamination of cytosine residues in DNA." *Nature* **287**(5782): 560-561.

Durkacz, B. W., O. Omidiji, D. A. Gray and S. Shall (1980). "(ADP-ribose)n participates in DNA excision repair." *Nature* **283**(5747): 593-596.

El-Khamisy, S. F. and K. W. Caldecott (2006). "TDP1-dependent DNA single-strand break repair and neurodegeneration." *Mutagenesis* **21**(4): 219-224.

El-Khamisy, S. F., M. Masutani, H. Suzuki and K. W. Caldecott (2003). "A requirement for PARP-1 for the assembly or stability of XRCC1 nuclear foci at sites of oxidative DNA damage." *Nucleic Acids Res* **31**(19): 5526-5533.

El-Khamisy, S. F., G. M. Saifi, M. Weinfeld, F. Johansson, T. Helleday, J. R. Lupski and K. W. Caldecott (2005). "Defective DNA single-strand break repair in spinocerebellar ataxia with axonal neuropathy-1." *Nature* **434**(7029): 108-113.

Eliasson, M. J. L., K. Sampei, A. S. Mandir, P. D. Hurn, R. J. Traystman, J. Bao, A. Pieper, Z.-Q. Wang, T. M. Dawson, S. H. Snyder and V. L. Dawson (1997). "Poly(ADP-ribose) polymerase gene disruption renders mice resistant to cerebral ischemia." *Nat Med* **3**(10): 1089-1095.

EMA (2014). "Lynparza EMA/648393/2014 approval letter."

Engelward, B. P., J. M. Allan, A. J. Dreslin, J. D. Kelly, M. M. Wu, B. Gold and L. D. Samson (1998). "A chemical and genetic approach together define the biological consequences of 3-methyladenine lesions in the mammalian genome." *J Biol Chem* **273**(9): 5412-5418.

Eustermann, S., C. Brockmann, P. V. Mehrotra, J. C. Yang, D. Loakes, S. C. West, I. Ahel and D. Neuhaus (2010). "Solution structures of the two PBZ domains from human APLF and their interaction with poly(ADP-ribose)." *Nat Struct Mol Biol* **17**(2): 241-243.

Eustermann, S., W.-F. Wu, M.-F. Langelier, J.-C. Yang, Laura E. Easton, Amanda A. Riccio, John M. Pascal and D. Neuhaus (2015). "Structural Basis of Detection and Signaling of DNA Single-Strand Breaks by Human PARP-1." *Molecular Cell* **60**(5): 742-754.

Evans, A. R., M. Limp-Foster and M. R. Kelley (2000). "Going APE over ref-1." *Mutation Research/DNA Repair* **461**(2): 83-108.

Fahrer, J., R. Kranaster, M. Altmeyer, A. Marx and A. Bürkle (2007). "Quantitative analysis of the binding affinity of poly(ADP-ribose) to specific binding proteins as a function of chain length." *Nucleic Acids Research* **35**(21): e143-e143.

Falck, J., J. Coates and S. P. Jackson (2005). "Conserved modes of recruitment of ATM, ATR and DNA-PKcs to sites of DNA damage." *Nature* **434**(7033): 605-611.

Farmer, H., N. McCabe, C. J. Lord, A. N. J. Tutt, D. A. Johnson, T. B. Richardson, M. Santarosa, K. J. Dillon, I. Hickson, C. Knights, N. M. B. Martin, S. P. Jackson, G. C. M. Smith and A. Ashworth (2005). "Targeting the DNA repair defect in BRCA mutant cells as a therapeutic strategy." *Nature* **434**(7035): 917-921.

Fatokun, A. A., V. L. Dawson and T. M. Dawson (2014). "Parthanatos: mitochondrial-linked mechanisms and therapeutic opportunities." *British Journal of Pharmacology* **171**(8): 2000-2016.

FDA, U. S. (2014). "Lynparza NDA 206162 approval letter."

Fisher, A. E., H. Hochegger, S. Takeda and K. W. Caldecott (2007). "Poly(ADP-ribose) polymerase 1 accelerates single-strand break repair in concert with poly(ADP-ribose) glycohydrolase." *Mol Cell Biol* **27**(15): 5597-5605.

Fisher, A. E. O., H. Hochegger, S. Takeda and K. W. Caldecott (2007). "Poly(ADP-Ribose) Polymerase 1 Accelerates Single-Strand Break Repair in Concert with Poly(ADP-Ribose) Glycohydrolase." *Molecular and Cellular Biology* **27**(15): 5597-5605.

Fortini, P., B. Pascucci, F. Belisario and E. Dogliotti (2000). "DNA polymerase β is required for efficient DNA strand break repair induced by methyl methanesulfonate but not by hydrogen peroxide." *Nucleic Acids Research* **28**(16): 3040-3046.

Francis Stewart, A., R. E. Herrera and A. Nordheimt (1990). "Rapid induction of c-fos transcription reveals quantitative linkage of RNA polymerase II and DNA topoisomerase I enzyme activities." *Cell* **60**(1): 141-149.

Frederico, L. A., T. A. Kunkel and B. R. Shaw (1990). "A sensitive genetic assay for the detection of cytosine deamination: determination of rate constants and the activation energy." *Biochemistry* **29**(10): 2532-2537.

Frosina, G., P. Fortini, O. Rossi, F. Carrozzino, G. Raspaglio, L. S. Cox, D. P. Lane, A. Abbondandolo and E. Dogliotti (1996). "Two pathways for base excision repair in mammalian cells." *Journal of Biological Chemistry* **271**(16): 9573-9578.

Fu, Y., J. D. Sander, D. Reyon, V. M. Cascio and J. K. Joung (2014). "Improving CRISPR-Cas nuclease specificity using truncated guide RNAs." *Nat Biotech* **32**(3): 279-284.

Furuta, T., H. Takemura, Z.-Y. Liao, G. J. Aune, C. Redon, O. A. Sedelnikova, D. R. Pilch, E. P. Rogakou, A. Celeste, H. T. Chen, A. Nussenzweig, M. I. Aladjem, W. M. Bonner and Y. Pommier (2003). "Phosphorylation of Histone H2AX and Activation of Mre11, Rad50, and Nbs1 in Response to Replication-dependent DNA Double-strand Breaks Induced by Mammalian DNA Topoisomerase I Cleavage Complexes." *Journal of Biological Chemistry* **278**(22): 20303-20312.

Gagné, J.-P., M. Isabelle, K. S. Lo, S. Bourassa, M. J. Hendzel, V. L. Dawson, T. M. Dawson and G. G. Poirier (2008). "Proteome-wide identification of poly(ADP-ribose) binding proteins and poly(ADP-ribose)-associated protein complexes." *Nucleic Acids Research* **36**(22): 6959-6976.

Gagne, J. P., C. Ethier, D. Defoy, S. Bourassa, M. F. Langelier, A. A. Riccio, J. M. Pascal, K. M. Moon, L. J. Foster, Z. Ning, D. Figeys, A. Droit and G. G. Poirier (2015). "Quantitative site-specific ADP-ribosylation profiling of DNA-dependent PARPs." *DNA Repair (Amst)* **30**: 68-79.

Gartenberg, M. R. and J. C. Wang (1992). "Positive supercoiling of DNA greatly diminishes mRNA synthesis in yeast." *Proc Natl Acad Sci U S A* **89**(23): 11461-11465.

Gell, D. and S. P. Jackson (1999). "Mapping of protein-protein interactions within the DNA-dependent protein kinase complex." *Nucleic Acids Res* **27**(17): 3494-3502.

Giaever, G. N. and J. C. Wang (1988). "Supercoiling of intracellular DNA can occur in eukaryotic cells." *Cell* **55**(5): 849-856.

Gibbs-Seymour, I., P. Fontana, Johannes Gregor M. Rack and I. Ahel (2016). "HPF1/C4orf27 Is a PARP-1-Interacting Protein that Regulates PARP-1 ADP-Ribosylation Activity." *Molecular Cell* **62**(3): 432-442.

Gibson, B. A., Y. Zhang, H. Jiang, K. M. Hussey, J. H. Shrimp, H. Lin, F. Schwede, Y. Yu and W. L. Kraus (2016). "Chemical genetic discovery of PARP targets reveals a role for PARP-1 in transcription elongation." *Science* **353**(6294): 45-50.

Gilbert, N. and J. Allan (2014). "Supercoiling in DNA and chromatin." *Current Opinion in Genetics & Development* **25**: 15-21.

Gorman, M. A., S. Morera, D. G. Rothwell, E. de La Fortelle, C. D. Mol, J. A. Tainer, I. D. Hickson and P. S. Freemont (1997). "The crystal structure of the human DNA repair endonuclease HAP1 suggests the recognition of extra-helical deoxyribose at DNA abasic sites." *The EMBO Journal* **16**(21): 6548-6558.

Goto, S., R. Xue, N. Sugo, M. Sawada, K. K. Blizzard, M. F. Poitras, D. C. Johns, T. M. Dawson, V. L. Dawson, B. J. Crain, R. J. Traystman, S. Mori and P. D. Hurn (2002). "Poly(ADP-ribose) polymerase impairs early and long-term experimental stroke recovery." *Stroke* **33**(4): 1101-1106.

Gradwohl, G., J. M. Menissier de Murcia, M. Molinete, F. Simonin, M. Koken, J. H. Hoeijmakers and G. de Murcia (1990). "The second zinc-finger domain of poly(ADP-ribose) polymerase determines specificity for single-stranded breaks in DNA." *Proc Natl Acad Sci U S A* **87**(8): 2990-2994.

Gravel, S., J. R. Chapman, C. Magill and S. P. Jackson (2008). "DNA helicases Sgs1 and BLM promote DNA double-strand break resection." *Genes Dev* **22**(20): 2767-2772.

Grawunder, U., M. Wilm, X. Wu, P. Kulesza, T. E. Wilson, M. Mann and M. R. Lieber (1997). "Activity of DNA ligase IV stimulated by complex formation with XRCC4 protein in mammalian cells." *Nature* **388**(6641): 492-495.

Grundy, G. J., L. M. Polo, Z. Zeng, S. L. Rulten, N. C. Hoch, P. Paomephan, Y. Xu, S. M. Sweet, A. W. Thorne, A. W. Oliver, S. J. Matthews, L. H. Pearl and K. W. Caldecott (2016). "PARP3 is a sensor of nicked nucleosomes and monoribosylates histone H2BGlu2." *Nature Communications* **7**: 12404.

Gu, H., J. Marth, P. Orban, H. Mossmann and K. Rajewsky (1994). "Deletion of a DNA polymerase beta gene segment in T cells using cell type-specific gene targeting." *Science* **265**(5168): 103-106.

Gueven, N., O. J. Becherel, A. W. Kijas, P. Chen, O. Howe, J. H. Rudolph, R. Gatti, H. Date, O. Onodera, G. Taucher-Scholz and M. F. Lavin (2004). "Aprataxin, a novel protein that protects against genotoxic stress." *Human Molecular Genetics* **13**(10): 1081-1093.

Haber, J. E. (2013). *Genome Stability*, Taylor & Francis Group.

Hadi, M. Z. and D. M. Wilson, 3rd (2000). "Second human protein with homology to the Escherichia coli abasic endonuclease exonuclease III." *Environ Mol Mutagen* **36**(4): 312-324.

Hadi, S. M. and D. A. Goldthwait (1971). "Endonuclease II of Escherichia coli. Degradation of partially depurinated deoxyribonucleic acid." *Biochemistry* **10**(26): 4986-4994.

Halldorsson, H., D. A. Gray and S. Shall (1978). "Poly(ADP-ribose) polymerase activity in nucleotide permeable cells." *FEBS Letters* **85**(2): 349-352.

Hanawalt, P. C. (1966). "The U.V. sensitivity of bacteria: its relation to the DNA replication cycle." *Photochem Photobiol* **5**(1): 1-12.

Handwerger, K. E., J. A. Cordero and J. G. Gall (2005). "Cajal bodies, nucleoli, and speckles in the Xenopus oocyte nucleus have a low-density, sponge-like structure." *Mol Biol Cell* **16**(1): 202-211.

Hanssen-Bauer, A., K. Solvang-Garten, O. Sundheim, J. Pena-Diaz, S. Andersen, G. Slupphaug, H. E. Krokan, D. M. Wilson, 3rd, M. Akbari and M. Otterlei (2011). "XRCC1 coordinates disparate responses and multiprotein repair complexes depending on the nature and context of the DNA damage." *Environ Mol Mutagen* **52**(8): 623-635.

Hanzlikova, H., W. Gittens, K. Krejcikova, Z. Zeng and K. W. Caldecott (2016). "Overlapping roles for PARP1 and PARP2 in the recruitment of endogenous XRCC1 and PNKP into oxidized chromatin." *Nucleic Acids Res* **45**(5): 2546-2557.

Hartwell, L. H., P. Szankasi, C. J. Roberts, A. W. Murray and S. H. Friend (1997). "Integrating genetic approaches into the discovery of anticancer drugs." *Science* **278**(5340): 1064-1068.

Haushalter, K. A., M. W. Todd Stukenberg, M. W. Kirschner and G. L. Verdine (1999). "Identification of a new uracil-DNA glycosylase family by expression cloning using synthetic inhibitors." *Curr Biol* **9**(4): 174-185.

Havali-Shahriari, Z., M. Weinfeld and J. N. Glover (2017). "Characterization of DNA Substrate Binding to the Phosphatase Domain of the DNA Repair Enzyme Polynucleotide Kinase/Phosphatase." **56**(12): 1737-1745.

Hayaishi, O. and M. Nozaki (1969). "Nature and mechanisms of oxygenases." *Science* **164**(3878): 389-396.

Hayyan, M., M. A. Hashim and I. M. AlNashef (2016). "Superoxide Ion: Generation and Chemical Implications." *Chemical Reviews* **116**(5): 3029-3085.

Hazra, T. K., T. Izumi, I. Boldogh, B. Imhoff, Y. W. Kow, P. Jaruga, M. Dizdaroglu and S. Mitra (2002). "Identification and characterization of a human DNA glycosylase for repair of modified bases in oxidatively damaged DNA." *Proc Natl Acad Sci U S A* **99**(6): 3523-3528.

Hecht, S. S. and D. Hoffmann (1989). "The relevance of tobacco-specific nitrosamines to human cancer." *Cancer Surv* **8**(2): 273-294.

Hegde, M. L., T. K. Hazra and S. Mitra (2008). "Early steps in the DNA base excision/single-strand interruption repair pathway in mammalian cells." *Cell Res* **18**(1): 27-47.

Hegde, M. L., P. M. Hegde, D. Arijit, I. Boldogh and S. Mitra (2012). "Human DNA Glycosylase NEIL1's Interactions with Downstream Repair Proteins Is Critical for Efficient Repair of Oxidized DNA Base Damage and Enhanced Cell Survival." *Biomolecules* **2**(4): 564-578.

Helleday, T. (2011). "The underlying mechanism for the PARP and BRCA synthetic lethality: Clearing up the misunderstandings." *Molecular Oncology* **5**(4): 387-393.

Hendrich, B., U. Hardeland, H. H. Ng, J. Jiricny and A. Bird (1999). "The thymine glycosylase MBD4 can bind to the product of deamination at methylated CpG sites." *Nature* **401**(6750): 301-304.

Hetman, M., A. Vashishta and G. Rempala (2010). "Neurotoxic mechanisms of DNA damage: focus on transcriptional inhibition." *Journal of Neurochemistry* **114**(6): 1537-1549.

Heyer, W. D., K. T. Ehmsen and J. Liu (2010). "Regulation of homologous recombination in eukaryotes." *Annu Rev Genet* **44**: 113-139.

Heyer, W. D., M. R. Rao, L. F. Erdile, T. J. Kelly and R. D. Kolodner (1990). "An essential Saccharomyces cerevisiae single-stranded DNA binding protein is homologous to the large subunit of human RP-A." *The EMBO Journal* **9**(7): 2321-2329.

Hivert, B., C. Cerruti and W. Camu (1998). "Hydrogen peroxide-induced motoneuron apoptosis is prevented by poly ADP ribosyl synthetase inhibitors." *Neuroreport* **9**(8): 1835-1838.

Hoch, N. C., H. Hanzlikova, S. L. Rulten, M. Tétreault, E. Komulainen, L. Ju, P. Hornyak, Z. Zeng, W. Gittens, S. A. Rey, K. Staras, G. M. S. Mancini, P. J. McKinnon, Z.-Q. Wang, J. D. Wagner, C. Care4Rare Canada, G. Yoon and K. W. Caldecott (2017). "XRCC1 mutation is associated with PARP1 hyperactivation and cerebellar ataxia." *Nature* **541**(7635): 87-91.

Hochegger, H., D. Dejsuphong, T. Fukushima, C. Morrison, E. Sonoda, V. Schreiber, G. Y. Zhao, A. Saberi, M. Masutani, N. Adachi, H. Koyama, G. de Murcia and S. Takeda (2006). "Parp-1 protects homologous recombination from interference by Ku and Ligase IV in vertebrate cells." *Embo j* **25**(6): 1305-1314.

Horii, T. and I. Hatada (2015). "Genome Editing Using Mammalian Haploid Cells." *International Journal of Molecular Sciences* **16**(10): 23604-23614.

Horton, J. K., D. F. Stefanick, J. M. Naron, P. S. Kedar and S. H. Wilson (2005). "Poly(ADP-ribose) Polymerase Activity Prevents Signaling Pathways for Cell Cycle Arrest after DNA Methylating Agent Exposure." *Journal of Biological Chemistry* **280**(16): 15773-15785.

Hotchkiss, J. H. (1989). "Preformed N-nitroso compounds in foods and beverages." *Cancer Surv* **8**(2): 295-321.

Hottiger, M. O., P. O. Hassa, B. Lüscher, H. Schüler and F. Koch-Nolte (2010). "Toward a unified nomenclature for mammalian ADP-ribosyltransferases." *Trends in Biochemical Sciences* **35**(4): 208-219.

Hsiang, Y.-H., M. G. Lihou and L. F. Liu (1989). "Arrest of replication forks by drug-stabilized topoisomerase I-DNA cleavable complexes as a mechanism of cell killing by camptothecin." *Cancer Res* **49**.

Hsu, G. W., M. Ober, T. Carell and L. S. Beese (2004). "Error-prone replication of oxidatively damaged DNA by a high-fidelity DNA polymerase." *Nature* **431**(7005): 217-221.

Hsu, P. D., D. A. Scott, J. A. Weinstein, F. A. Ran, S. Konermann, V. Agarwala, Y. Li, E. J. Fine, X. Wu, O. Shalem, T. J. Cradick, L. A. Marraffini, G. Bao and F. Zhang (2013). "DNA targeting specificity of RNA-guided Cas9 nucleases." *Nat Biotech* **31**(9): 827-832.

Hudson, J. J. R., S.-C. Chiang, O. S. Wells, C. Rookyard and S. F. El-Khamisy (2012). "SUMO modification of the neuroprotective protein TDP1 facilitates chromosomal single-strand break repair." *Nat Commun* **3**: 733.

Huertas, P. (2010). "DNA resection in eukaryotes: deciding how to fix the break." *Nat Struct Mol Biol* **17**(1): 11-16.

Iles, N., S. Rulten, S. F. El-Khamisy and K. W. Caldecott (2007). "APLF (C2orf13) is a novel human protein involved in the cellular response to chromosomal DNA strand breaks." *Molecular and Cellular Biology* **27**(10): 3793-3803.

Inamdar, K. V., J. J. Pouliot, T. Zhou, S. P. Lees-Miller, A. Rasouli-Nia and L. F. Povirk (2002). "Conversion of phosphoglycolate to phosphate termini on 3' overhangs of DNA double strand breaks by the human tyrosyl-DNA phosphodiesterase hTdp1." *J Biol Chem* **277**(30): 27162-27168.

Inglefield, J. R., C. J. Larson, S. J. Gibson, H. Lebrec and R. L. Miller (2006). "Apoptotic responses in squamous carcinoma and epithelial cells to small-molecule toll-like receptor agonists evaluated with automated cytometry." *J Biomol Screen* **11**(6): 575-585.

Interthal, H., H. J. Chen and J. J. Champoux (2005). "Human Tdp1 Cleaves a Broad Spectrum of Substrates, Including Phosphoamide Linkages." *Journal of Biological Chemistry* **280**(43): 36518-36528.

Interthal, H., J. J. Pouliot and J. J. Champoux (2001). "The tyrosyl-DNA phosphodiesterase Tdp1 is a member of the phospholipase D superfamily." *Proc Natl Acad Sci U S A* **98**(21): 12009-12014.

Isogai, S., S. Kanno, M. Ariyoshi, H. Tochio, Y. Ito, A. Yasui and M. Shirakawa (2010). "Solution structure of a zinc-finger domain that binds to poly-ADP-ribose." *Genes Cells* **15**(2): 101-110.

Ito, Y., D. Inoue, S. Kido and T. Matsumoto (2005). "c-Fos degradation by the ubiquitin-proteasome proteolytic pathway in osteoclast progenitors." *Bone* **37**(6): 842-849.

Izumi, T., D. B. Brown, C. V. Naidu, K. K. Bhakat, M. A. Macinnes, H. Saito, D. J. Chen and S. Mitra (2005). "Two essential but distinct functions of the mammalian abasic endonuclease." *Proc Natl Acad Sci U S A* **102**(16): 5739-5743.

Jacobs, A. L. and P. Schär (2012). "DNA glycosylases: in DNA repair and beyond." *Chromosoma* **121**(1): 1-20.

Jain, D., S. Baldi, A. Zabel, T. Straub and P. B. Becker (2015). "Active promoters give rise to false positive 'Phantom Peaks' in ChIP-seq experiments." *Nucleic Acids Research* **43**(14): 6959-6968.

Jankevicius, G., M. Hassler, B. Golia, V. Rybin, M. Zacharias, G. Timinszky and A. G. Ladurner (2013). "A family of macrodomain proteins reverses cellular mono-ADP-ribosylation." *Nat Struct Mol Biol* **20**(4): 508-514.

Jaxel, C., G. Capranico, D. Kerrigan, K. W. Kohn and Y. Pommier (1991). "Effect of local DNA sequence on topoisomerase I cleavage in the presence or absence of camptothecin." *J Biol Chem* **266**(30): 20418-20423.

Johansson, M. (1999). "A human poly(ADP-ribose) polymerase gene family (ADPRTL): cDNA cloning of two novel poly(ADP-ribose) polymerase homologues." *Genomics* **57**.

Johnson, R. D. and M. Jasin (2000). "Sister chromatid gene conversion is a prominent double-strand break repair pathway in mammalian cells." *The EMBO Journal* **19**(13): 3398-3407.

Jones, J. C., H. P. Phatnani, T. A. Haystead, J. A. MacDonald, S. M. Alam and A. L. Greenleaf (2004). "C-terminal Repeat Domain Kinase I Phosphorylates Ser2 and Ser5 of RNA Polymerase II C-terminal Domain Repeats." *Journal of Biological Chemistry* **279**(24): 24957-24964.

Juarez-Salinas, H., V. Levi, E. L. Jacobson and M. K. Jacobson (1982). "Poly(ADP-ribose) has a branched structure in vivo." *Journal of Biological Chemistry* **257**(2): 607-609.

Kameshita, I., Z. Matsuda, T. Taniguchi and Y. Shizuta (1984). "Poly (ADP-Ribose) synthetase. Separation and identification of three proteolytic fragments as the substrate-binding domain, the DNA-binding domain, and the automodification domain." *J Biol Chem* **259**.

Kang, H. C., Y. I. Lee, J. H. Shin, S. A. Andrabi, Z. K. Chi, J. P. Gagne, Y. J. Lee, H. S. Ko, B. D. Lee, G. G. Poirier, V. L. Dawson and T. M. Dawson (2011). "Iduna is a poly(ADP-ribose) (PAR)-dependent E3 ubiquitin ligase that regulates DNA damage." *Proceedings of the National Academy of Sciences of the United States of America* **108**(34): 14103-14108.

Kanofsky, J. R. (1983). "Singlet oxygen production by lactoperoxidase." *J Biol Chem* **258**(10): 5991-5993.

Karakasili, E., C. Burkert-Kautzsch, A. Kieser and K. Strasser (2014). "Degradation of DNA damage-independently stalled RNA polymerase II is independent of the E3 ligase Elc1." *Nucleic Acids Res* **42**(16): 10503-10515.

Karimi-Busheri, F., G. Daly, P. Robins, B. Canas, D. J. C. Pappin, J. Sgouros, G. G. Miller, H. Fakhrai, E. M. Davis, M. M. Le Beau and M. Weinfeld (1999). "Molecular Characterization of a Human DNA Kinase." *Journal of Biological Chemistry* **274**(34): 24187-24194.

Karimi-Busheri, F. and M. Weinfeld (1997). "Purification and substrate specificity of polydeoxyribonucleotide kinases isolated from calf thymus and rat liver." *J Cell Biochem* **64**(2): 258-272.

Karras, G. I., G. Kustatscher, H. R. Buhecha, M. D. Allen, C. Pugieux, F. Sait, M. Bycroft and A. G. Ladurner (2005). "The macro domain is an ADP-ribose binding module." *EMBO J* **24**.

Kathe, S. D., G.-P. Shen and S. S. Wallace (2004). "Single-Stranded Breaks in DNA but Not Oxidative DNA Base Damages Block Transcriptional Elongation by RNA Polymerase II in HeLa Cell Nuclear Extracts." *Journal of Biological Chemistry* **279**(18): 18511-18520.

Kathe, S. D., G. P. Shen and S. S. Wallace (2004). "Single-stranded breaks in DNA but not oxidative DNA base damages block transcriptional elongation by RNA polymerase II in HeLa cell nuclear extracts." *J Biol Chem* **279**(18): 18511-18520.

Katyal, S., Y. Lee, K. C. Nitiss, S. M. Downing, Y. Li, M. Shimada, J. Zhao, H. R. Russell, J. H. J. Petrini, J. L. Nitiss and P. J. McKinnon (2014). "Aberrant topoisomerase-1 DNA lesions are pathogenic in neurodegenerative genome instability syndromes." *Nat Neurosci* **17**(6): 813-821.

Kauppinen, T. M., S. W. Suh, Y. Higashi, A. E. Berman, C. Escartin, S. J. Won, C. Wang, S. H. Cho, L. Gan and R. A. Swanson (2011). "Poly(ADP-ribose)polymerase-1 modulates microglial responses to amyloid beta." *J Neuroinflammation* **8**: 152.

Kawamitsu, H., H. Hoshino, H. Okada, M. Miwa, H. Momoi and T. Sugimura (1984). "Monoclonal antibodies to poly(adenosine diphosphate ribose) recognize different structures." *Biochemistry* **23**(16): 3771-3777.

Kedar, P. S., D. F. Stefanick, J. K. Horton and S. H. Wilson (2012). "Increased PARP-1 association with DNA in alkylation damaged, PARP-inhibited mouse fibroblasts." *Mol Cancer Res* **10**(3): 360-368.

Keil, C., T. Gröbe and S. Li Oei (2006). "MNNG-induced Cell Death Is Controlled by Interactions between PARP-1, Poly(ADP-ribose) Glycohydrolase, and XRCC1." *Journal of Biological Chemistry* **281**(45): 34394-34405.

Kennedy, L. J., K. Moore, J. L. Caulfield, S. R. Tannenbaum and P. C. Dedon (1997). "Quantitation of 8-oxoguanine and strand breaks produced by four oxidizing agents." *Chemical Research in Toxicology* **10**(4): 386-392.

Kim, I. K., R. A. Stegeman, C. A. Brosey and T. Ellenberger (2015). "A Quantitative Assay Reveals Ligand Specificity of the DNA Scaffold Repair Protein XRCC1 and Efficient Disassembly of Complexes of XRCC1 and the Poly(ADP-ribose) Polymerase 1 by Poly(ADP-ribose) Glycohydrolase." *Journal of Biological Chemistry* **290**(6): 3775-3783.

Kim, K., S. Biade and Y. Matsumoto (1998). "Involvement of flap endonuclease 1 in base excision DNA repair." *J Biol Chem* **273**(15): 8842-8848.

Kim, M. Y., S. Mauro, N. Gevry, J. T. Lis and W. L. Kraus (2004). "NAD+-dependent modulation of chromatin structure and transcription by nucleosome binding properties of PARP-1." *Cell* **119**(6): 803-814.

Kleine, H., E. Poreba, K. Lesniewicz, P. O. Hassa, M. O. Hottiger, D. W. Litchfield, B. H. Shilton and B. Luscher (2008). "Substrate-assisted catalysis by PARP10 limits its activity to mono-ADP-ribosylation." *Mol Cell* **32**.

Klungland, A. and T. Lindahl (1997). "Second pathway for completion of human DNA base excision-repair: reconstitution with purified proteins and requirement for DNase IV (FEN1)." *The EMBO Journal* **16**(11): 3341-3348.

Koch, C. A., R. Agyei, S. Galicia, P. Metalnikov, P. O'Donnell, A. Starostine, M. Weinfeld and D. Durocher (2004). "Xrcc4 physically links DNA end processing by polynucleotide kinase to DNA ligation by DNA ligase IV." *The EMBO Journal* **23**(19): 3874-3885.

Kraus, L. W. C., TX, US), Gibson, Bryan A. (Dallas, TX, US) (2015). ADP-RIBOSE DETECTION REAGENTS. United States, The Board of Regents of the University of Texas System (Austin, TX, US).

Kraus, W. L. (2008). "Transcriptional control by PARP-1: chromatin modulation, enhancer-binding, coregulation, and insulation." *Curr Opin Cell Biol* **20**(3): 294-302.

Krokan, H. E., R. Standal and G. Slupphaug (1997). "DNA glycosylases in the base excision repair of DNA." *Biochem J* **325 (Pt 1)**: 1-16.

Krumova, K. and G. Cosa (2016). Chapter 1 Overview of Reactive Oxygen Species. *Singlet Oxygen: Applications in Biosciences and Nanosciences, Volume 1*, The Royal Society of Chemistry. **1:** 1-21.

Kubota, Y., R. A. Nash, A. Klungland, P. Schar, D. E. Barnes and T. Lindahl (1996). "Reconstitution of DNA base excision-repair with purified human proteins: interaction between DNA polymerase beta and the XRCC1 protein." *Embo j* **15**(23): 6662-6670.

Kuzminov, A. (2001). "Single-strand interruptions in replicating chromosomes cause double-strand breaks." *Proc Natl Acad Sci U S A* **98**(15): 8241-8246.

Kyrtopoulos, S. A. (1998). "DNA adducts in humans after exposure to methylating agents." *Mutation Research/Fundamental and Molecular Mechanisms of Mutagenesis* **405**(2): 135-143.

Lam, Y. W. and L. Trinkle-Mulcahy (2015). "New insights into nucleolar structure and function." *F1000Prime Reports* **7**: 48.

Landt, S. G., G. K. Marinov, A. Kundaje, P. Kheradpour, F. Pauli, S. Batzoglou, B. E. Bernstein, P. Bickel, J. B. Brown, P. Cayting, Y. Chen, G. DeSalvo, C. Epstein, K. I. Fisher-Aylor, G. Euskirchen, M. Gerstein, J. Gertz, A. J. Hartemink, M. M. Hoffman, V. R. Iyer, Y. L. Jung, S. Karmakar, M. Kellis, P. V. Kharchenko, Q. Li, T. Liu, X. S. Liu, L. Ma, A. Milosavljevic, R. M. Myers, P. J. Park, M. J. Pazin, M. D. Perry, D. Raha, T. E. Reddy, J. Rozowsky, N. Shoresh, A. Sidow, M. Slattery, J. A. Stamatoyannopoulos, M. Y. Tolstorukov, K. P. White, S. Xi, P. J. Farnham, J. D. Lieb, B. J. Wold and M. Snyder (2012). "ChIP-seq guidelines and practices of the ENCODE and modENCODE consortia." *Genome Research* **22**(9): 1813-1831.

Langelier, M.-F., J. L. Planck, S. Roy and J. M. Pascal (2012). "Structural basis for DNA-dependent poly(ADP-ribosyl)ation by human PARP-1." *Science (New York, N.Y.)* **336**(6082): 728-732.

Langelier, M.-F., A. A. Riccio and J. M. Pascal (2014). "PARP-2 and PARP-3 are selectively activated by 5’ phosphorylated DNA breaks through an allosteric regulatory mechanism shared with PARP-1." *Nucleic Acids Research* **42**(12): 7762-7775.

Lanza, A., S. Tornaletti, C. Rodolfo, M. C. Scanavini and A. M. Pedrini (1996). "Human DNA Topoisomerase I-mediated Cleavages Stimulated by Ultraviolet Light-induced DNA Damage." *Journal of Biological Chemistry* **271**(12): 6978-6986.

Lavin, M. F. (2007). "ATM and the Mre11 complex combine to recognize and signal DNA double-strand breaks." *Oncogene* **26**(56): 7749-7758.

Lebedeva, Natalia A., Rashid O. Anarbaev, M. Sukhanova, Inna A. Vasil'eva, Nadejda I. Rechkunova and Olga I. Lavrik (2015). "Poly(ADP-ribose)polymerase 1 stimulates the AP-site cleavage activity of tyrosyl-DNA phosphodiesterase 1." *Bioscience Reports* **35**(4): e00230.

Lebedeva, N. A., N. I. Rechkunova and O. I. Lavrik (2011). "AP-site cleavage activity of tyrosyl-DNA phosphodiesterase 1." *FEBS Letters* **585**(4): 683-686.

Lee, Y., H. C. Kang, B. D. Lee, Y.-I. Lee, Y. P. Kim and J.-H. Shin (2014). "Poly (ADP-ribose) in the pathogenesis of Parkinson's disease." *BMB Reports* **47**(8): 424-432.

Lehmann, A. R. (2003). "DNA repair-deficient diseases, xeroderma pigmentosum, Cockayne syndrome and trichothiodystrophy." *Biochimie* **85**(11): 1101-1111.

Leidecker, O., J. J. Bonfiglio, T. Colby, Q. Zhang, I. Atanassov, R. Zaja, L. Palazzo, A. Stockum, I. Ahel and I. Matic (2016). "Serine is a new target residue for endogenous ADP-ribosylation on histones." *Nat Chem Biol* **12**(12): 998-1000.

Lesher, D. T., Y. Pommier, L. Stewart and M. R. Redinbo (2002). "8-Oxoguanine rearranges the active site of human topoisomerase I." *Proc Natl Acad Sci U S A* **99**(19): 12102-12107.

Leung, A. K. L. (2017). "SERious Surprises for ADP-Ribosylation Specificity: HPF1 Switches PARP1 Specificity to Ser Residues." *Molecular Cell* **65**(5): 777-778.

Levin, J. D. and B. Demple (1990). "Analysis of class II (hydrolytic) and class I (beta-lyase) apurinic/apyrimidinic endonucleases with a synthetic DNA substrate." *Nucleic Acids Research* **18**(17): 5069-5075.

Lévy, N., M. Oehlmann, F. Delalande, H. P. Nasheuer, A. Van Dorsselaer, V. Schreiber, G. de Murcia, J. Ménissier-de Murcia, D. Maiorano and A. Bresson (2009). "XRCC1 interacts with the p58 subunit of DNA Pol α-primase and may coordinate DNA repair and replication during S phase." *Nucleic Acids Research* **37**(10): 3177-3188.

Li, G. Y., R. D. McCulloch, A. L. Fenton, M. Cheung, L. Meng, M. Ikura and C. A. Koch (2010). "Structure and identification of ADP-ribose recognition motifs of APLF and role in the DNA damage response." *Proc Natl Acad Sci U S A* **107**(20): 9129-9134.

Li, K., G. Wang, T. Andersen, P. Zhou and W. T. Pu (2014). "Optimization of Genome Engineering Approaches with the CRISPR/Cas9 System." *PLoS ONE* **9**(8): e105779.

Li, L. H., T. J. Fraser, E. J. Olin and B. K. Bhuyan (1972). "Action of Camptothecin on Mammalian Cells in Culture." *Cancer Research* **32**(12): 2643-2650.

Li, M., L.-Y. Lu, C.-Y. Yang, S. Wang and X. Yu (2013). "The FHA and BRCT domains recognize ADP-ribosylation during DNA damage response." *Genes & Development* **27**(16): 1752-1768.

Liang, F., M. Han, P. J. Romanienko and M. Jasin (1998). "Homology-directed repair is a major double-strand break repair pathway in mammalian cells." *Proceedings of the National Academy of Sciences of the United States of America* **95**(9): 5172-5177.

Lieber, M. R. (2010). "The mechanism of double-strand DNA break repair by the nonhomologous DNA end-joining pathway." *Annu Rev Biochem* **79**: 181-211.

Lilyestrom, W., M. J. van der Woerd, N. Clark and K. Luger (2010). "Structural and biophysical studies of human PARP-1 in complex with damaged DNA." *J Mol Biol* **395**(5): 983-994.

Lin, C.-P., Y. Ban, Y. L. Lyu, S. D. Desai and L. F. Liu (2008). "A Ubiquitin-Proteasome Pathway for the Repair of Topoisomerase I-DNA Covalent Complexes." *Journal of Biological Chemistry* **283**(30): 21074-21083.

Lin, C.-P., Y. Ban, Y. L. Lyu and L. F. Liu (2009). "Proteasome-dependent Processing of Topoisomerase I-DNA Adducts into DNA Double Strand Breaks at Arrested Replication Forks." *Journal of Biological Chemistry* **284**(41): 28084-28092.

Lindahl, T. (1979). "DNA Glycosylases, Endonucleases for Apurinic/Apyrimidinic Sites, and Base Excision-Repair." *Progress in Nucleic Acid Research and Molecular Biology* **22**: 135-192.

Lindahl, T. (1993). "Instability and decay of the primary structure of DNA." *Nature* **362**(6422): 709-715.

Lindahl, T. and A. Andersson (1972). "Rate of chain breakage at apurinic sites in double-stranded deoxyribonucleic acid." *Biochemistry* **11**(19): 3618-3623.

Lindahl, T. and O. Karlstrom (1973). "Heat-induced depyrimidination of deoxyribonucleic acid in neutral solution." *Biochemistry* **12**(25): 5151-5154.

Lindahl, T. and B. Nyberg (1972). "Rate of depurination of native deoxyribonucleic acid." *Biochemistry* **11**(19): 3610-3618.

Lindahl, T. and B. Nyberg (1974). "Heat-induced deamination of cytosine residues in deoxyribonucleic acid." *Biochemistry* **13**(16): 3405-3410.

Listerman, I., A. K. Sapra and K. M. Neugebauer (2006). "Cotranscriptional coupling of splicing factor recruitment and precursor messenger RNA splicing in mammalian cells." *Nat Struct Mol Biol* **13**(9): 815-822.

Litchfield, D. W. (2003). "Protein kinase CK2: structure, regulation and role in cellular decisions of life and death." *Biochem J* **369**(Pt 1): 1-15.

Liu, C., J. J. Pouliot and H. A. Nash (2004). "The role of TDP1 from budding yeast in the repair of DNA damage." *DNA Repair (Amst)* **3**(6): 593-601.

Liu, L. F. and J. C. Wang (1987). "Supercoiling of the DNA template during transcription." *Proceedings of the National Academy of Sciences of the United States of America* **84**(20): 7024-7027.

Liu, M., V. Bandaru, J. P. Bond, P. Jaruga, X. Zhao, P. P. Christov, C. J. Burrows, C. J. Rizzo, M. Dizdaroglu and S. S. Wallace (2010). "The mouse ortholog of NEIL3 is a functional DNA glycosylase in vitro and in vivo." *Proc Natl Acad Sci U S A* **107**(11): 4925-4930.

Liu, M., S. Doublié and S. S. Wallace (2013). "Neil3, the final frontier for the DNA glycosylases that recognize oxidative damage." *Mutation research* **0**: 4-11.

Ljungman, M. and F. Zhang (1996). "Blockage of RNA polymerase as a possible trigger for u.v. light-induced apoptosis." *Oncogene* **13**(4): 823-831.

Ljungman, M., F. Zhang, F. Chen, A. J. Rainbow and B. C. McKay (1999). "Inhibition of RNA polymerase II as a trigger for the p53 response." *Oncogene* **18**(3): 583-592.

Loeffler, P. A., M. J. Cuneo, G. A. Mueller, E. F. DeRose, S. A. Gabel and R. E. London (2011). "Structural studies of the PARP-1 BRCT domain." *Bmc Structural Biology* **11**.

Loizou, J. I., S. F. El-Khamisy, A. Zlatanou, D. J. Moore, D. W. Chan, J. Qin, S. Sarno, F. Meggio, L. A. Pinna and K. W. Caldecott (2004). "The Protein Kinase CK2 Facilitates Repair of Chromosomal DNA Single-Strand Breaks." *Cell* **117**(1): 17-28.

Lombard, D. B., C. Beard, B. Johnson, R. A. Marciniak, J. Dausman, R. Bronson, J. E. Buhlmann, R. Lipman, R. Curry, A. Sharpe, R. Jaenisch and L. Guarente (2000). "Mutations in the WRN gene in mice accelerate mortality in a p53-null background." *Mol Cell Biol* **20**(9): 3286-3291.

London, R. E. (2015). "The structural basis of XRCC1-mediated DNA repair." *DNA Repair* **30**: 90-103.

Lorenzini, A., F. B. Johnson, A. Oliver, M. Tresini, J. S. Smith, M. Hdeib, C. Sell, V. J. Cristofalo and T. D. Stamato (2009). "Significant Correlation of Species Longevity with DNA Double Strand Break-Recognition but not with Telomere Length." *Mechanisms of ageing and development* **130**(11-12): 784-792.

Loseva, O., A.-S. Jemth, H. E. Bryant, H. Schüler, L. Lehtiö, T. Karlberg and T. Helleday (2010). "PARP-3 Is a Mono-ADP-ribosylase That Activates PARP-1 in the Absence of DNA." *Journal of Biological Chemistry* **285**(11): 8054-8060.

Losson, R. and F. Lacroute (1979). "Interference of nonsense mutations with eukaryotic messenger RNA stability." *Proc Natl Acad Sci U S A* **76**(10): 5134-5137.

Love, S., R. Barber and G. K. Wilcock (1999). "Increased poly(ADP-ribosyl)ation of nuclear proteins in Alzheimer's disease." *Brain* **122 (Pt 2)**: 247-253.

Lu, R., H. M. Nash and G. L. Verdine (1997). "A mammalian DNA repair enzyme that excises oxidatively damaged guanines maps to a locus frequently lost in lung cancer." *Curr Biol* **7**(6): 397-407.

Luo, H., D. W. Chan, T. Yang, M. Rodriguez, B. P.-C. Chen, M. Leng, J.-J. Mu, D. Chen, Z. Songyang, Y. Wang and J. Qin (2004). "A New XRCC1-Containing Complex and Its Role in Cellular Survival of Methyl Methanesulfonate Treatment." *Molecular and Cellular Biology* **24**(19): 8356-8365.

Lynn, R. M. and J. C. Wang (1989). "Peptide sequencing and site-directed mutagenesis identify tyrosine-319 as the active-site tyrosine of escherichia-coli DNA topoisomerase-I." *Proteins-Structure Function and Genetics* **6**(3): 231-239.

Ma, Y., U. Pannicke, K. Schwarz and M. R. Lieber (2002). "Hairpin opening and overhang processing by an Artemis/DNA-dependent protein kinase complex in nonhomologous end joining and V(D)J recombination." *Cell* **108**(6): 781-794.

Malanga, M., J. M. Pleschke, H. E. Kleczkowska and F. R. Althaus (1998). "Poly(ADP-ribose) Binds to Specific Domains of p53 and Alters Its DNA Binding Functions." *Journal of Biological Chemistry* **273**(19): 11839-11843.

Mali, P., L. Yang, K. M. Esvelt, J. Aach, M. Guell, J. E. DiCarlo, J. E. Norville and G. M. Church (2013). "RNA-guided human genome engineering via Cas9." *Science* **339**(6121): 823-826.

Mandir, A. S., S. Przedborski, V. Jackson-Lewis, Z. Q. Wang, C. M. Simbulan-Rosenthal, M. E. Smulson, B. E. Hoffman, D. B. Guastella, V. L. Dawson and T. M. Dawson (1999). "Poly(ADP-ribose) polymerase activation mediates 1-methyl-4-phenyl-1, 2,3,6-tetrahydropyridine (MPTP)-induced parkinsonism." *Proc Natl Acad Sci U S A* **96**(10): 5774-5779.

Mani, R. S., F. Karimi-Busheri, M. Fanta, K. W. Caldecott, C. E. Cass and M. Weinfeld (2004). "Biophysical characterization of human XRCC1 and its binding to damaged and undamaged DNA." *Biochemistry* **43**(51): 16505-16514.

Mao, Y., M. Sun, S. D. Desai and L. F. Liu (2000). "SUMO-1 conjugation to topoisomerase I: A possible repair response to topoisomerase-mediated DNA damage." *Proc Natl Acad Sci U S A* **97**(8): 4046-4051.

Marechal, A. and L. Zou (2013). "DNA damage sensing by the ATM and ATR kinases." *Cold Spring Harb Perspect Biol* **5**(9).

Marsin, S., A. E. Vidal, M. Sossou, J. Menissier-de Murcia, F. Le Page, S. Boiteux, G. de Murcia and J. P. Radicella (2003). "Role of XRCC1 in the coordination and stimulation of oxidative DNA damage repair initiated by the DNA glycosylase hOGG1." *J Biol Chem* **278**(45): 44068-44074.

Marteijn, J. A., H. Lans, W. Vermeulen and J. H. J. Hoeijmakers (2014). "Understanding nucleotide excision repair and its roles in cancer and ageing." *Nature Reviews Molecular Cell Biology* **15**(7): 465-481.

Martello, R., M. Leutert, S. Jungmichel, V. Bilan and S. C. Larsen (2016). "Proteome-wide identification of the endogenous ADP-ribosylome of mammalian cells and tissue." **7**: 12917.

Martire, S., A. Fuso, D. Rotili, I. Tempera, C. Giordano, I. De Zottis, A. Muzi, P. Vernole, G. Graziani, E. Lococo, M. Faraldi, B. Maras, S. Scarpa, L. Mosca and M. d'Erme (2013). "PARP-1 modulates amyloid beta peptide-induced neuronal damage." *PLoS One* **8**(9): e72169.

Martire, S., L. Mosca and M. d'Erme (2015). "PARP-1 involvement in neurodegeneration: A focus on Alzheimer's and Parkinson's diseases." *Mechanisms of Ageing and Development* **146–148**: 53-64.

Masson, M., C. Niedergang, V. Schreiber, S. Muller, J. Menissier-de Murcia and G. de Murcia (1998). "XRCC1 is specifically associated with poly(ADP-ribose) polymerase and negatively regulates its activity following DNA damage." *Mol Cell Biol* **18**(6): 3563-3571.

Matsumoto, Y. and K. Kim (1995). "Excision of deoxyribose phosphate residues by DNA polymerase beta during DNA repair." *Science* **269**(5224): 699-702.

Matsumoto, Y., K. Kim and D. F. Bogenhagen (1994). "Proliferating cell nuclear antigen-dependent abasic site repair in xenopus-laevis oocytes - an alternative pathway of base excision DNA-repair." *Molecular and Cellular Biology* **14**(9): 6187-6197.

Maxam, A. M. and W. Gilbert (1977). "A new method for sequencing DNA." *Proc Natl Acad Sci U S A* **74**(2): 560-564.

McGoldrick, J. P., Y. C. Yeh, M. Solomon, J. M. Essigmann and A. L. Lu (1995). "Characterization of a mammalian homolog of the Escherichia coli MutY mismatch repair protein." *Mol Cell Biol* **15**(2): 989-996.

McVey, M. and S. E. Lee (2008). "MMEJ repair of double-strand breaks (director's cut): deleted sequences and alternative endings." *Trends Genet* **24**(11): 529-538.

Meder, V. S., M. Boeglin, G. de Murcia and V. Schreiber (2005). "PARP-1 and PARP-2 interact with nucleophosmin/B23 and accumulate in transcriptionally active nucleoli." *J Cell Sci* **118**(Pt 1): 211-222.

Melan, M. A. and G. Sluder (1992). "Redistribution and differential extraction of soluble proteins in permeabilized cultured cells. Implications for immunofluorescence microscopy." *Journal of Cell Science* **101**(4): 731-743.

Ménissier de Murcia, J., M. Ricoul, L. Tartier, C. Niedergang, A. Huber, F. Dantzer, V. Schreiber, J.-C. Amé, A. Dierich, M. LeMeur, L. Sabatier, P. Chambon and G. de Murcia (2003). "Functional interaction between PARP-1 and PARP-2 in chromosome stability and embryonic development in mouse." *The EMBO Journal* **22**(9): 2255-2263.

Messner, S., M. Altmeyer, H. Zhao, A. Pozivil, B. Roschitzki, P. Gehrig, D. Rutishauser, D. Huang, A. Caflisch and M. O. Hottiger (2010). "PARP1 ADP-ribosylates lysine residues of the core histone tails." *Nucleic Acids Research* **38**(19): 6350-6362.

Messner, S. and M. O. Hottiger (2011). "Histone ADP-ribosylation in DNA repair, replication and transcription." *Trends in Cell Biology* **21**(9): 534-542.

Mischo, H. E., B. Gómez-González, P. Grzechnik, A. G. Rondón, W. Wei, L. Steinmetz, A. Aguilera and N. J. Proudfoot (2011). "Yeast Sen1 Helicase Protects the Genome from Transcription-Associated Instability." *Molecular Cell* **41**(1): 21-32.

Miwa, M. and T. Sugimura (1971). "Splitting of the ribose-ribose linkage of poly(adenosine diphosphate-robose) by a calf thymus extract." *J Biol Chem* **246**(20): 6362-6364.

Mojica, F. J., C. Diez-Villasenor, J. Garcia-Martinez and E. Soria (2005). "Intervening sequences of regularly spaced prokaryotic repeats derive from foreign genetic elements." *J Mol Evol* **60**(2): 174-182.

Mojica, F. J. M., C. Díez-Villaseñor, J. García-Martínez and C. Almendros (2009). "Short motif sequences determine the targets of the prokaryotic CRISPR defence system." *Microbiology* **155**(3): 733-740.

Mol, C. D., T. Izumi, S. Mitra and J. A. Tainer (2000). "DNA-bound structures and mutants reveal abasic DNA binding by APE1 DNA repair and coordination." *Nature* **403**(6768): 451-456.

Moreau, S., E. A. Morgan and L. S. Symington (2001). "Overlapping functions of the Saccharomyces cerevisiae Mre11, Exo1 and Rad27 nucleases in DNA metabolism." *Genetics* **159**(4): 1423-1433.

Morgan, J. I., D. R. Cohen, J. L. Hempstead and T. Curran (1987). "Mapping patterns of c-fos expression in the central nervous system after seizure." *Science* **237**(4811): 192-197.

Morgan, J. I. and T. Curran (1986). "Role of ion flux in the control of c-fos expression." *Nature* **322**(6079): 552-555.

Moriya, H. (2015). "Quantitative nature of overexpression experiments." *Molecular Biology of the Cell* **26**(22): 3932-3939.

Morland, I., V. Rolseth, L. Luna, T. Rognes, M. Bjoras and E. Seeberg (2002). "Human DNA glycosylases of the bacterial Fpg/MutM superfamily: an alternative pathway for the repair of 8-oxoguanine and other oxidation products in DNA." *Nucleic Acids Res* **30**(22): 4926-4936.

Morris, D. P., G. A. Michelotti and D. A. Schwinn (2005). "Evidence That Phosphorylation of the RNA Polymerase II Carboxyl-terminal Repeats Is Similar in Yeast and Humans." *Journal of Biological Chemistry* **280**(36): 31368-31377.

Morris, E. J. and H. M. Geller (1996). "Induction of neuronal apoptosis by camptothecin, an inhibitor of DNA topoisomerase-I: evidence for cell cycle-independent toxicity." *J Cell Biol* **134**(3): 757-770.

Mortusewicz, O., J.-C. Amé, V. Schreiber and H. Leonhardt (2007). "Feedback-regulated poly(ADP-ribosyl)ation by PARP-1 is required for rapid response to DNA damage in living cells." *Nucleic Acids Research* **35**(22): 7665-7675.

Mosesso, P., M. Piane, F. Palitti, G. Pepe, S. Penna and L. Chessa (2005). "The novel human gene aprataxin is directly involved in DNA single-strand-break repair." *Cell Mol Life Sci* **62**(4): 485-491.

Munstermann, U., G. Fritz, G. Seitz, Y. P. Lu, H. R. Schneider and O. G. Issinger (1990). "Casein kinase-II is elevated in solid human tumors and rapidly proliferating non-neoplastic tissue." *European Journal of Biochemistry* **189**(2): 251-257.

Murai, J., S.-y. N. Huang, B. B. Das, A. Renaud, Y. Zhang, J. H. Doroshow, J. Ji, S. Takeda and Y. Pommier (2012). "Differential trapping of PARP1 and PARP2 by clinical PARP inhibitors." *Cancer research* **72**(21): 5588-5599.

Murai, J., S.-y. N. Huang, B. B. Das, A. Renaud, Y. Zhang, J. H. Doroshow, J. Ji, S. Takeda and Y. Pommier (2012). "Trapping of PARP1 and PARP2 by Clinical PARP Inhibitors." *Cancer Research* **72**(21): 5588-5599.

Muthurajan, U. M., M. R. D. Hepler, A. R. Hieb, N. J. Clark, M. Kramer, T. Yao and K. Luger (2014). "Automodification switches PARP-1 function from chromatin architectural protein to

histone chaperone." *Proceedings of the National Academy of Sciences of the United States of America* **111**(35): 12752-12757.

Nakamura, J. and J. A. Swenberg (1999). "Endogenous Apurinic/Apyrimidinic Sites in Genomic DNA of Mammalian Tissues." *Cancer Research* **59**(11): 2522-2526.

Nam, Edward A. and D. Cortez (2011). "ATR signalling: more than meeting at the fork." *Biochemical Journal* **436**(3): 527-536.

Narne, P., V. Pandey, P. K. Simhadri and P. B. Phanithi (2017). "Poly(ADP-ribose)polymerase-1 hyperactivation in neurodegenerative diseases: The death knell tolls for neurons." *Seminars in Cell & Developmental Biology* **63**: 154-166.

NCBI (2016). "Database resources of the National Center for Biotechnology Information." *Nucleic Acids Research* **44**(Database issue): D7-D19.

Neeley, W. L. and J. M. Essigmann (2006). "Mechanisms of formation, genotoxicity, and mutation of guanine oxidation products." *Chem Res Toxicol* **19**(4): 491-505.

Neil, A. J., B. P. Belotserkovskii and P. C. Hanawalt (2012). "Transcription blockage by bulky end termini at single-strand breaks in the DNA template: differential effects of 5' and 3' adducts." *Biochemistry* **51**(44): 8964-8970.

Nick McElhinny, S. A., C. M. Snowden, J. McCarville and D. A. Ramsden (2000). "Ku recruits the XRCC4-ligase IV complex to DNA ends." *Mol Cell Biol* **20**(9): 2996-3003.

Novogrodsky, A. and J. Hurwitz (1966). "The Enzymatic Phosphorylation of Ribonucleic Acid and Deoxyribonucleic Acid: I. PHOSPHORYLATION AT 5'-HYDROXYL TERMINI." *Journal of Biological Chemistry* **241**(12): 2923-2932.

Novogrodsky, A., M. Tal, A. Traub and J. Hurwitz (1966). "The enzymatic phosphorylation of ribonucleic acid and deoxyribonucleic acid. II. Further properties of the 5'-hydroxyl polynucleotide kinase." *J Biol Chem* **241**(12): 2933-2943.

O'Connor, T. R. and F. Laval (1990). "Isolation and structure of a cDNA expressing a mammalian 3-methyladenine-DNA glycosylase." *EMBO J* **9**(10): 3337-3342.

O'Driscoll, M., A. R. Gennery, J. Seidel, P. Concannon and P. A. Jeggo (2004). "An overview of three new disorders associated with genetic instability: LIG4 syndrome, RS-SCID and ATR-Seckel syndrome." *DNA Repair* **3**(8-9): 1227-1235.

Oberoi, J., M. W. Richards, S. Crumpler, N. Brown, J. Blagg and R. Bayliss (2010). "Structural basis of poly(ADP-ribose) recognition by the multizinc binding domain of checkpoint with forkhead-associated and RING Domains (CHFR)." *J Biol Chem* **285**(50): 39348-39358.

Okano, S., L. Lan, K. W. Caldecott, T. Mori and A. Yasui (2003). "Spatial and Temporal Cellular Responses to Single-Strand Breaks in Human Cells." *Molecular and Cellular Biology* **23**(11): 3974-3981.

Okayama, H., C. M. Edson, M. Fukushima, K. Ueda and O. Hayaishi (1977). "Purification and properties of poly(adenosine diphosphate ribose) synthetase." *Journal of Biological Chemistry* **252**(20): 7000-7005.

Okayama, H., C. M. Edson, M. Fukushima, K. Ueda and O. Hayaishi (1977). "Purification and properties of poly(adenosine diphosphate ribose) synthetase - role of histone in poly(ADP-ribose) synthesis." *Journal of Biological Chemistry* **252**(20): 7000-7005.

Oliver, A. W., J.-C. Amé, S. M. Roe, V. Good, G. de Murcia and L. H. Pearl (2004). "Crystal structure of the catalytic fragment of murine poly(ADP-ribose) polymerase-2." *Nucleic Acids Research* **32**(2): 456-464.

Oliver, A. W., J. C. Ame, S. M. Roe, V. Good, G. de Murcia and L. H. Pearl (2004). "Crystal structure of the catalytic fragment of murine poly(ADP-ribose) polymerase-2." *Nucleic Acids Res* **32**.

Pag, xe, V. s and R. P. Fuchs (2003). "Uncoupling of Leading- and Lagging-Strand DNA Replication during Lesion Bypass in Vivo." *Science* **300**(5623): 1300-1303.

Pang, D., S. Yoo, W. S. Dynan, M. Jung and A. Dritschilo (1997). "Ku proteins join DNA fragments as shown by atomic force microscopy." *Cancer Res* **57**(8): 1412-1415.

Paquette, Y., P. Crine and W. G. Verly (1972). "Properties of endonuclease for depurinated DNA from escherichia-coli." *Canadian Journal of Biochemistry* **50**(11): 1199-1209.

Park, D., Y. Lee, G. Bhupindersingh and V. R. Iyer (2013). "Widespread Misinterpretable ChIP-seq Bias in Yeast." *PLoS ONE* **8**(12): e83506.

Parsons, J. L., Dianova, II, S. L. Allinson and G. L. Dianov (2005). "DNA polymerase beta promotes recruitment of DNA ligase III alpha-XRCC1 to sites of base excision repair." *Biochemistry* **44**(31): 10613-10619.

Parsons, J. L., I. I. Dianova, E. Boswell, M. Weinfeld and G. L. Dianov (2005). "End-damage-specific proteins facilitate recruitment or stability of X-ray cross-complementing protein 1 at the sites of DNA single-strand break repair." *FEBS Journal* **272**(22): 5753-5763.

Patel, A. G., K. S. Flatten, P. A. Schneider, N. T. Dai, J. S. McDonald, G. G. Poirier and S. H. Kaufmann (2012). "Enhanced Killing of Cancer Cells by Poly(ADP-ribose) Polymerase Inhibitors and Topoisomerase I Inhibitors Reflects Poisoning of Both Enzymes." *Journal of Biological Chemistry* **287**(6): 4198-4210.

Patel, A. G., J. N. Sarkaria and S. H. Kaufmann (2011). "Nonhomologous end joining drives poly(ADP-ribose) polymerase (PARP) inhibitor lethality in homologous recombination-deficient cells." *Proceedings of the National Academy of Sciences* **108**(8): 3406-3411.

Petersen-Mahrt, S. K., R. S. Harris and M. S. Neuberger (2002). "AID mutates E. coli suggesting a DNA deamination mechanism for antibody diversification." *Nature* **418**(6893): 99-104.

Peterson, F. C., D. Chen, B. L. Lytle, M. N. Rossi, I. Ahel, J. M. Denu and B. F. Volkman (2011). "Orphan macrodomain protein (human C6orf130) is an O-acyl-ADP-ribose deacylase: solution structure and catalytic properties." *J Biol Chem* **286**(41): 35955-35965.

Pickart, C. M. (1997). "Targeting of substrates to the 268 proteasome." *Faseb Journal* **11**(13): 1055-1066.

Pierce, G. B., R. E. Parchment and A. L. Lewellyn (1991). "Hydrogen peroxide as a mediator of programmed cell death in the blastocyst." *Differentiation* **46**(3): 181-186.

Pignatelli, B., C. Malaveille, A. Rogatko, A. Hautefeuille, P. Thuillier, N. Muñoz, B. Moulinier, F. Berger, H. De Montclos, R. Lambert, P. Correa, B. Ruiz, G. M. Sobala, C. J. Schorah, A. T. R. Axon and H. Bartsch (1993). "Mutagens, N-nitroso compounds and their precursors in gastric juice from patients with and without precancerous lesions of the stomach." *European Journal of Cancer* **29**(14): 2031-2039.

Pleschke, J. M., H. E. Kleczkowska, M. Strohm and F. R. Althaus (2000). "Poly(ADP-ribose) Binds to Specific Domains in DNA Damage Checkpoint Proteins." *Journal of Biological Chemistry* **275**(52): 40974-40980.

Plo, I., Z.-Y. Liao, J. M. Barceló, G. Kohlhagen, K. W. Caldecott, M. Weinfeld and Y. Pommier (2003). "Association of XRCC1 and tyrosyl DNA phosphodiesterase (Tdp1) for the repair of topoisomerase I-mediated DNA lesions." *DNA Repair* **2**(10): 1087-1100.

Plosky, B. S., E. G. Frank, D. A. Berry, G. P. Vennall, J. P. McDonald and R. Woodgate (2008). "Eukaryotic Y-family polymerases bypass a 3-methyl-2'-deoxyadenosine analog in vitro and methyl methanesulfonate-induced DNA damage in vivo." *Nucleic Acids Research* **36**(7): 2152-2162.

Pogozelski, W. K. and T. D. Tullius (1998). "Oxidative strand scission of nucleic acids: Routes initiated by hydrogen abstraction from the sugar moiety." *Chemical Reviews* **98**(3): 1089-1107.

Poirier, G. G., G. de Murcia, J. Jongstra-Bilen, C. Niedergang and P. Mandel (1982). "Poly(ADP-ribosyl)ation of polynucleosomes causes relaxation of chromatin structure." *Proc Natl Acad Sci U S A* **79**(11): 3423-3427.

Pommier, Y., J. Barcelo, V. A. Rao, O. Sordet, A. G. Jobson, L. Thibaut, Z. Miao, J. Seiler, H. Zhang, C. Marchand, K. Agama and C. Redon (2006). "Repair of Topoisomerase I-Mediated DNA Damage." *Progress in nucleic acid research and molecular biology* **81**: 179-229.

Pommier, Y., E. Leo, H. L. Zhang and C. Marchand (2010). "DNA Topoisomerases and Their Poisoning by Anticancer and Antibacterial Drugs." *Chemistry & Biology* **17**(5): 421-433.

Pommier, Y., Y. Sun, S.-y. N. Huang and J. L. Nitiss (2016). "Roles of eukaryotic topoisomerases in transcription, replication and genomic stability." *Nat Rev Mol Cell Biol* **17**(11): 703-721.

Pouliot, J. J., C. A. Robertson and H. A. Nash (2001). "Pathways for repair of topoisomerase I covalent complexes in Saccharomyces cerevisiae." *Genes Cells* **6**(8): 677-687.

Pouliot, J. J., K. C. Yao, C. A. Robertson and H. A. Nash (1999). "Yeast gene for a Tyr-DNA phosphodiesterase that repairs topoisomerase I complexes." *Science* **286**(5439): 552-555.

Pourcel, C., G. Salvignol and G. Vergnaud (2005). "CRISPR elements in Yersinia pestis acquire new repeats by preferential uptake of bacteriophage DNA, and provide additional tools for evolutionary studies." *Microbiology* **151**(Pt 3): 653-663.

Pourquier, P., M. A. Bjornsti and Y. Pommier (1998). "Induction of topoisomerase I cleavage complexes by the vinyl chloride adduct 1,N6-ethenoadenine." *J Biol Chem* **273**(42): 27245-27249.

Pourquier, P., A. A. Pilon, G. Kohlhagen, A. Mazumder, A. Sharma and Y. Pommier (1997). "Trapping of Mammalian Topoisomerase I and Recombinations Induced by Damaged DNA Containing Nicks or Gaps: Importance of DNA end phosphorylation and camptothecin effects." *Journal of Biological Chemistry* **272**(42): 26441-26447.

Pourquier, P., Y. Takebayashi, Y. Urasaki, C. Gioffre, G. Kohlhagen and Y. Pommier (2000). "Induction of topoisomerase I cleavage complexes by 1-β-d-arabinofuranosylcytosine (ara-C) in vitro and in ara-C-treated cells." *Proceedings of the National Academy of Sciences of the United States of America* **97**(4): 1885-1890.

Pourquier, P., L.-M. Ueng, J. Fertala, D. Wang, H.-J. Park, J. M. Essigmann, M.-A. Bjornsti and Y. Pommier (1999). "Induction of Reversible Complexes between Eukaryotic DNA Topoisomerase I and DNA-containing Oxidative Base Damages: 7,8-DIHYDRO-8-OXOGUANINE AND 5-HYDROXYCYTOSINE." *Journal of Biological Chemistry* **274**(13): 8516-8523.

Pourquier, P., L. M. Ueng, G. Kohlhagen, A. Mazumder, M. Gupta, K. W. Kohn and Y. Pommier (1997). "Effects of uracil incorporation, DNA mismatches, and abasic sites on cleavage and religation activities of mammalian topoisomerase I." *J Biol Chem* **272**(12): 7792-7796.

Pruss, G. J., S. H. Manes and K. Drlica (1982). "Escherichia coli DNA topoisomerase I mutants: Increased supercoiling is corrected by mutations near gyrase genes." *Cell* **31**(1): 35-42.

Ramadan, K., G. Maga, I. V. Shevelev, G. Villani, L. Blanco and U. Hübscher (2003). "Human DNA Polymerase λ Possesses Terminal Deoxyribonucleotidyl Transferase Activity And Can Elongate RNA Primers: Implications for Novel Functions." *Journal of Molecular Biology* **328**(1): 63-72.

Ramadan, K., I. V. Shevelev, G. Maga and U. Hubscher (2004). "De novo DNA synthesis by human DNA polymerase lambda, DNA polymerase mu and terminal deoxyribonucleotidyl transferase." *J Mol Biol* **339**(2): 395-404.

Rameau, G. A., L. Y. Chiu and E. B. Ziff (2004). "Bidirectional regulation of neuronal nitric-oxide synthase phosphorylation at serine 847 by the N-methyl-D-aspartate receptor." *J Biol Chem* **279**(14): 14307-14314.

Rasouli-Nia, A., F. Karimi-Busheri and M. Weinfeld (2004). "Stable down-regulation of human polynucleotide kinase enhances spontaneous mutation frequency and sensitizes cells to genotoxic agents." *Proc Natl Acad Sci U S A* **101**(18): 6905-6910.

Rass, U., I. Ahel and S. C. West (2007). "Defective DNA Repair and Neurodegenerative Disease." *Cell* **130**(6): 991-1004.

Ratner, J. N., B. Balasubramanian, J. Corden, S. L. Warren and D. B. Bregman (1998). "Ultraviolet radiation-induced ubiquitination and proteasomal degradation of the large subunit of RNA polymerase II. Implications for transcription-coupled DNA repair." *J Biol Chem* **273**(9): 5184-5189.

Redinbo, M. R., L. Stewart, P. Kuhn, J. J. Champoux and W. G. J. Hol (1998). "Crystal Structures of Human Topoisomerase I in Covalent and Noncovalent Complexes with DNA." *Science* **279**(5356): 1504-1513.

Riccio, A. A., G. Cingolani and J. M. Pascal (2016). "PARP-2 domain requirements for DNA damage-dependent activation and localization to sites of DNA damage." *Nucleic Acids Research* **44**(4): 1691-1702.

Rogakou, E. P., D. R. Pilch, A. H. Orr, V. S. Ivanova and W. M. Bonner (1998). "DNA double-stranded breaks induce histone H2AX phosphorylation on serine 139." *J Biol Chem* **273**(10): 5858-5868.

Roots, R., G. Kraft and E. Gosschalk (1985). "The formation of radiation-induced dna breaks: The ratio of double-strand breaks to single-strand breaks." *International Journal of Radiation Oncology • Biology • Physics* **11**(2): 259-265.

Rosenthal, F., K. L. Feijs, E. Frugier, M. Bonalli, A. H. Forst, R. Imhof, H. C. Winkler, D. Fischer, A. Caflisch, P. O. Hassa, B. Luscher and M. O. Hottiger (2013). "Macrodomain-containing proteins are new mono-ADP-ribosylhydrolases." *Nat Struct Mol Biol* **20**(4): 502-507.

Rothblum-Oviatt, C., J. Wright, M. A. Lefton-Greif, S. A. McGrath-Morrow, T. O. Crawford and H. M. Lederman (2016). "Ataxia telangiectasia: a review." *Orphanet Journal of Rare Diseases* **11**: 21.

Rouleau, M., D. McDonald, P. Gagné, M. E. Ouellet, A. Droit, J. M. Hunter, S. Dutertre, C. Prigent, M. J. Hendzel and G. G. Poirier (2007). "PARP-3 associates with polycomb group bodies and with components of the DNA damage repair machinery." *Journal of Cellular Biochemistry* **100**(2): 385-401.

Rouleau, M., A. Patel, M. J. Hendzel, S. H. Kaufmann and G. G. Poirier (2010). "PARP inhibition: PARP1 and beyond." *Nature Reviews Cancer* **10**(4): 293-301.

Roy, D., Z. Zhang, Z. Lu, C. L. Hsieh and M. R. Lieber (2010). "Competition between the RNA transcript and the nontemplate DNA strand during R-loop formation in vitro: a nick can serve as a strong R-loop initiation site." *Mol Cell Biol* **30**(1): 146-159.

Rozen, S. and H. Skaletsky (1999). Primer3 on the WWW for General Users and for Biologist Programmers. *Bioinformatics Methods and Protocols*. S. Misener and S. A. Krawetz. Totowa, NJ, Humana Press**:** 365-386.

Rulten, S. L. and K. W. Caldecott (2013). "DNA strand break repair and neurodegeneration." *DNA Repair* **12**(8): 558-567.

Rulten, S. L., A. E. O. Fisher, I. Robert, M. C. Zuma, M. Rouleau, L. Ju, G. Poirier, B. Reina-San-Martin and K. W. Caldecott (2011). "PARP-3 and APLF Function Together to Accelerate Nonhomologous End-Joining." *Molecular Cell* **41**(1): 33-45.

Saffhill, R. and J. A. Hall (1985). "The incorporation of O6-methyldeoxyguanosine monophosphate and O4-methyldeoxythymidine monophosphate into polynucleotide templates leads to errors during subsequent in vitro DNA synthesis." *Chemico-Biological Interactions* **56**(2): 363-370.

Sage, E. and L. Harrison (2011). "Clustered DNA lesion repair in eukaryotes: relevance to mutagenesis and cell survival." *Mutation research* **711**(1-2): 123-133.

Saleh-Gohari, N., H. E. Bryant, N. Schultz, K. M. Parker, T. Cassel and T. Helleday (2005). "Spontaneous homologous recombination is induced by collapsed replication forks that are caused by ebdogenous DNA single-strand breaks." *Mol Cell Biol* **25**.

Sartori, A. A., C. Lukas, J. Coates, M. Mistrik, S. Fu, J. Bartek, R. Baer, J. Lukas and S. P. Jackson (2007). "Human CtIP promotes DNA end resection." *Nature* **450**(7169): 509-514.

Satoh, M. S. and T. Lindahl (1992). "Role of poly(ADP-ribose) formation in DNA repair." *Nature* **356**(6367): 356-358.

Savitsky, K., A. Barshira, S. Gilad, G. Rotman, Y. Ziv, L. Vanagaite, D. A. Tagle, S. Smith, T. Uziel, S. Sfez, M. Ashkenazi, I. Pecker, M. Frydman, R. Harnik, S. R. Patanjali, A. Simmons, G. A. Clines, A. Sartiel, R. A. Gatti, L. Chessa, O. Sanal, M. F. Lavin, N. G. J. Jaspers, A. Malcolm, R. Taylor, C. F. Arlett, T. Miki, S. M. Weissman, M. Lovett, F. S. Collins and Y. Shiloh (1995). "A single ataxia-telangiectasia gene with a product similar to PI-3 kinase." *Science* **268**(5218): 1749-1753.

Schär, P., G. Herrmann, G. Daly and T. Lindahl (1997). "A newly identified DNA ligase of Saccharomyces cerevisiae involved in RAD52-independent repair of DNA double-strand breaks." *Genes & Development* **11**(15): 1912-1924.

Schiml, S., F. Fauser and H. Puchta (2016). "Repair of adjacent single-strand breaks is often accompanied by the formation of tandem sequence duplications in plant genomes." *Proceedings of the National Academy of Sciences of the United States of America* **113**(26): 7266-7271.

Scholz, V., J. Weidner, W. Kohnlein, D. Frekers and H. J. Wortche (1997). "Induction of single- and double-strand breaks in plasmid DNA by monoenergetic alpha-particles with energies below the Bragg-maximum." *Z Naturforsch C* **52**(5-6): 364-372.

Schönthal, A., P. Herrlich, H. J. Rahmsdorf and H. Ponta (1988). "Requirement for fos gene expression in the transcriptional activation of collagenase by other oncogenes and phorbol esters." *Cell* **54**(3): 325-334.

Schraufstatter, I. U., D. B. Hinshaw, P. A. Hyslop, R. G. Spragg and C. G. Cochrane (1986). "Oxidant injury of cells. DNA strand-breaks activate polyadenosine diphosphate-ribose polymerase and lead to depletion of nicotinamide adenine dinucleotide." *Journal of Clinical Investigation* **77**(4): 1312-1320.

Schreiber, V., J.-C. Amé, P. Dollé, I. Schultz, B. Rinaldi, V. Fraulob, J. Ménissier-de Murcia and G. de Murcia (2002). "Poly(ADP-ribose) Polymerase-2 (PARP-2) Is Required for Efficient Base Excision DNA Repair in Association with PARP-1 and XRCC1." *Journal of Biological Chemistry* **277**(25): 23028-23036.

Sfeir, A. and L. S. Symington (2015). "Microhomology-Mediated End Joining: A Back-up Survival Mechanism or Dedicated Pathway?" *Trends in Biochemical Sciences* **40**(11): 701-714.

Shen, J., E. C. Gilmore, C. A. Marshall, M. Haddadin, J. J. Reynolds, W. Eyaid, A. Bodell, B. Barry, D. Gleason, K. Allen, V. S. Ganesh, B. S. Chang, A. Grix, R. S. Hill, M. Topcu, K. W. Caldecott, A. J. Barkovich and C. A. Walsh (2010). "Mutations in PNKP cause microcephaly, seizures and defects in DNA repair." *Nat Genet* **42**(3): 245-249.

Shieh, W. M., J. C. Ame, M. V. Wilson, Z. Q. Wang, D. W. Koh, M. K. Jacobson and E. L. Jacobson (1998). "Poly(ADP-ribose) polymerase null mouse cells synthesize ADP-ribose polymers." *J Biol Chem* **273**(46): 30069-30072.

Shyu, A. B., M. E. Greenberg and J. G. Belasco (1989). "The c-fos transcript is targeted for rapid decay by two distinct mRNA degradation pathways." *Genes & Development* **3**(1): 60-72.

Singhal, R. K., R. Prasad and S. H. Wilson (1995). "DNA-polymerase-beta conducts the gap-filling step in uracil-initiated base excision-repair in a bovine testis nuclear extract." *Journal of Biological Chemistry* **270**(2): 949-957.

Skourti-Stathaki, K. and N. J. Proudfoot (2014). "A double-edged sword: R loops as threats to genome integrity and powerful regulators of gene expression." *Genes & Development* **28**(13): 1384-1396.

Skourti-Stathaki, K., Nicholas J. Proudfoot and N. Gromak (2011). "Human Senataxin Resolves RNA/DNA Hybrids Formed at Transcriptional Pause Sites to Promote Xrn2-Dependent Termination." *Molecular Cell* **42**(6): 794-805.

Slade, D., M. S. Dunstan, E. Barkauskaite, R. Weston, P. Lafite, N. Dixon, M. Ahel, D. Leys and I. Ahel (2011). "The structure and catalytic mechanism of a poly(ADP-ribose) glycohydrolase." *Nature* **477**(7366): 616-620.

Sleeth, K. M., R. L. Robson and G. L. Dianov (2004). "Exchangeability of Mammalian DNA Ligases between Base Excision Repair Pathways." *Biochemistry* **43**(40): 12924-12930.

Snapp, E. L., R. S. Hegde, M. Francolini, F. Lombardo, S. Colombo, E. Pedrazzini, N. Borgese and J. Lippincott-Schwartz (2003). "Formation of stacked ER cisternae by low affinity protein interactions." *The Journal of Cell Biology* **163**(2): 257-269.

Sobol, R. W., J. K. Horton, R. Kuhn, H. Gu, R. K. Singhal, R. Prasad, K. Rajewsky and S. H. Wilson (1996). "Requirement of mammalian DNA polymerase-beta in base-excision repair." *Nature* **379**(6561): 183-186.

Sobol, R. W., R. Prasad, A. Evenski, A. Baker, X.-P. Yang, J. K. Horton and S. H. Wilson (2000). "The lyase activity of the DNA repair protein [beta]-polymerase protects from DNA-damage-induced cytotoxicity." *Nature* **405**(6788): 807-810.

Sordet, O., S. Larochelle, E. Nicolas, E. V. Stevens, C. Zhang, K. M. Shokat, R. P. Fisher and Y. Pommier (2008). "Hyperphosphorylation of RNA Polymerase II in Response to Topoisomerase I Cleavage Complexes and Its Association with Transcription- and BRCA1-dependent Degradation of Topoisomerase I." *Journal of Molecular Biology* **381**(3): 540-549.

Sordet, O., C. E. Redon, J. Guirouilh-Barbat, S. Smith, S. Solier, C. Douarre, C. Conti, A. J. Nakamura, B. B. Das, E. Nicolas, K. W. Kohn, W. M. Bonner and Y. Pommier (2009). "Ataxia telangiectasia mutated activation by transcription- and topoisomerase I-induced DNA double-strand breaks." *EMBO Rep* **10**(8): 887-893.

Staker, B. L., K. Hjerrild, M. D. Feese, C. A. Behnke, A. B. Burgin and L. Stewart (2002). "The mechanism of topoisomerase I poisoning by a camptothecin analog." *Proceedings of the National Academy of Sciences* **99**(24): 15387-15392.

Stewart, L., M. R. Redinbo, X. Qiu, W. G. J. Hol and J. J. Champoux (1998). "A Model for the Mechanism of Human Topoisomerase I." *Science* **279**(5356): 1534-1541.

Strickfaden, H., D. McDonald, M. J. Kruhlak, J.-F. Haince, J. P. H. Th'ng, M. Rouleau, T. Ishibashi, G. N. Corry, J. Ausio, D. A. Underhill, G. G. Poirier and M. J. Hendzel (2016). "Poly(ADP-ribosyl)ation-dependent Transient Chromatin Decondensation and Histone Displacement following Laser Microirradiation." *Journal of Biological Chemistry* **291**(4): 1789-1802.

Strom, C. E., F. Johansson, M. Uhlen, C. A. Szigyarto, K. Erixon and T. Helleday (2011). "Poly (ADP-ribose) polymerase (PARP) is not involved in base excision repair but PARP inhibition traps a single-strand intermediate." *Nucleic Acids Res* **39**(8): 3166-3175.

Strosznajder, J. B., G. A. Czapski, A. Adamczyk and R. P. Strosznajder (2012). "Poly(ADP-ribose) polymerase-1 in amyloid beta toxicity and Alzheimer's disease." *Mol Neurobiol* **46**(1): 78-84.

Strumberg, D., A. A. Pilon, M. Smith, R. Hickey, L. Malkas and Y. Pommier (2000). "Conversion of topoisomerase 1 cleavage complexes on the leading strand of ribosomal DNA into 5 '-phosphorylated DNA double-strand breaks by replication runoff." *Molecular and Cellular Biology* **20**(11): 3977-3987.

Strumberg, D., A. A. Pilon, M. Smith, R. Hickey, L. Malkas and Y. Pommier (2000). "Conversion of topoisomerase I cleavage complexes on the leading strand of ribosomal DNA into 5'-phosphorylated DNA double-strand breaks by replication runoff." *Mol Cell Biol* **20**(11): 3977-3987.

Sugimura, K., S. Takebayashi, H. Taguchi, S. Takeda and K. Okumura (2008). "PARP-1 ensures regulation of replication fork progression by homologous recombination on damaged DNA." *J Cell Biol* **183**(7): 1203-1212.

Sugiyama, H., T. Fujiwara, A. Ura, T. Tashiro, K. Yamamoto, S. Kawanishi and I. Saito (1994). "Chemistry of thermal degradation of abasic sites in DNA. Mechanistic investigation on thermal DNA strand cleavage of alkylated DNA." *Chem Res Toxicol* **7**(5): 673-683.

Sundin, O. and A. Varshavsky (1980). "Terminal stages of SV40 DNA replication proceed via multiply intertwined catenated dimers." *Cell* **21**(1): 103-114.

Sung, P. (1994). "Catalysis of atp-dependent homologous DNA pairing and strand exchange by yeast RAD51 protein." *Science* **265**(5176): 1241-1243.

Swenberg, J. A., M. A. Bedell, K. C. Billings, D. R. Umbenhauer and A. E. Pegg (1982). "Cell-specific differences in O6-alkylguanine DNA repair activity during continuous exposure to

carcinogen." *Proceedings of the National Academy of Sciences of the United States of America* **79**(18): 5499-5502.

Swenberg, J. A., K. Lu, B. C. Moeller, L. Gao, P. B. Upton, J. Nakamura and T. B. Starr (2011). "Endogenous versus Exogenous DNA Adducts: Their Role in Carcinogenesis, Epidemiology, and Risk Assessment." *Toxicological Sciences* **120**(suppl_1): S130-S145.

Symons, M. C. R. (1994). "Direct and indirect damage to DNA by ionising radiation." *Radiation Physics and Chemistry* **43**(4): 403-405.

Szabo, C., H. Ischiropoulos and R. Radi (2007). "Peroxynitrite: biochemistry, pathophysiology and development of therapeutics." *Nat Rev Drug Discov* **6**(8): 662-680.

Takashima, H., C. F. Boerkoel, J. John, G. M. Saifi, M. A. M. Salih, D. Armstrong, Y. Mao, F. A. Quiocho, B. B. Roa, M. Nakagawa, D. W. Stockton and J. R. Lupski (2002). "Mutation of TDP1, encoding a topoisomerase I-dependent DNA damage repair enzyme, in spinocerebellar ataxia with axonal neuropathy." *Nat Genet* **32**(2): 267-272.

Tan, H. B., P. F. Swann and E. M. Chance (1994). "Kinetic analysis of the coding properties of O6-methylguanine in DNA: the crucial role of the conformation of the phosphodiester bond." *Biochemistry* **33**(17): 5335-5346.

Tao, Z., P. Gao and H.-w. Liu (2009). "Identification of the ADP-Ribosylation Sites in the PARP-1 Automodification Domain: Analysis and Implications." *Journal of the American Chemical Society* **131**(40): 14258-14260.

Taylor, A. M. R., D. G. Harnden, C. F. Arlett, S. A. Harcourt, A. R. Lehmann, S. Stevens and B. A. Bridges (1975). "Ataxia telangiectasia: a human mutation with abnormal radiation sensitivity." *Nature* **258**(5534): 427-429.

Tebbs, R. S., L. H. Thompson and J. E. Cleaver (2003). "Rescue of Xrcc1 knockout mouse embryo lethality by transgene-complementation." *DNA Repair (Amst)* **2**(12): 1405-1417.

Teixeira, M. M., F. Q. Cunha, A. Noronha-Dutra and J. Hothersall (1999). "Production of singlet oxygen by eosinophils activated in vitro by C5a and leukotriene B4." *FEBS Letters* **453**(3): 265-268.

Teloni, F. and M. Altmeyer (2016). "Readers of poly(ADP-ribose): designed to be fit for purpose." *Nucleic Acids Res* **44**(3): 993-1006.

Teytelman, L., D. M. Thurtle, J. Rine and A. van Oudenaarden (2013). "Highly expressed loci are vulnerable to misleading ChIP localization of multiple unrelated proteins." *Proceedings of the National Academy of Sciences* **110**(46): 18602-18607.

Thoma, F., T. Koller and A. Klug (1979). "Involvement of histone H1 in the organization of the nucleosome and of the salt-dependent superstructures of chromatin." *J Cell Biol* **83**(2 Pt 1): 403-427.

Thompson, L. H., K. W. Brookman, L. E. Dillehay, A. V. Carrano, J. A. Mazrimas, C. L. Mooney and J. L. Minkler (1982). "A CHO-cell strain having hypersensitivity to mutagens, a defect in DNA strand-break repair, and an extraordinary baseline frequency of sister-chromatid exchange." *Mutation Research* **95**(2-3): 427-440.

Thompson, L. H., K. W. Brookman, N. J. Jones, S. A. Allen and A. V. Carrano (1990). "Molecular cloning of the human XRCC1 gene, which corrects defective DNA strand break repair and sister chromatid exchange." *Mol Cell Biol* **10**(12): 6160-6171.

Thompson, L. H., K. W. Brookman, J. L. Minkler, J. C. Fuscoe, K. A. Henning and A. V. Carrano (1985). "DNA-mediated transfer of a human DNA repair gene that controls sister chromatid exchange." *Molecular and Cellular Biology* **5**(4): 881-884.

Timinszky, G., S. Till, P. O. Hassa, M. Hothorn, G. Kustatscher, B. Nijmeijer, J. Colombelli, M. Altmeyer, E. H. K. Stelzer, K. Scheffzek, M. O. Hottiger and A. G. Ladurner (2009). "A macrodomain-containing histone rearranges chromatin upon sensing PARP1 activation." *Nat Struct Mol Biol* **16**(9): 923-929.

Ting, N. S., Y. Yu, B. Pohorelic, S. P. Lees-Miller and T. L. Beattie (2005). "Human Ku70/80 interacts directly with hTR, the RNA component of human telomerase." *Nucleic Acids Res* **33**(7): 2090-2098.

Tobey, R. A. (1972). "Effects of Cytosine Arabinoside, Daunomycin, Mithramycin, Azacytidine, Adriamycin, and Camptothecin on Mammalian Cell Cycle Traverse." *Cancer Research* **32**(12): 2720-2725.

Tomkinson, A. E., S. Vijayakumar, J. M. Pascal and T. Ellenberger (2006). "DNA ligases: structure, reaction mechanism, and function." *Chem Rev* **106**(2): 687-699.

Trujillo, K. M., S. S. Yuan, E. Y. Lee and P. Sung (1998). "Nuclease activities in a complex of human recombination and DNA repair factors Rad50, Mre11, and p95." *J Biol Chem* **273**(34): 21447-21450.

Tsao, Y. P., A. Russo, G. Nyamuswa, R. Silber and L. F. Liu (1993). "Interaction between replication forks and topoisomerase-I-DNA cleavable complexes - studies in a cell-free SV40 DNA-replication system." *Cancer Research* **53**(24): 5908-5914.

Tse, Y. C., K. Kirkegaard and J. C. Wang (1980). "Covalent bonds between protein and DNA - formation of phosphotyrosine linkage between certain DNA topoisomerases and DNA." *Journal of Biological Chemistry* **255**(12): 5560-5565.

Tuduri, S., L. Crabbe, C. Conti, H. Tourriere, H. Holtgreve-Grez, A. Jauch, V. Pantesco, J. De Vos, A. Thomas, C. Theillet, Y. Pommier, J. Tazi, A. Coquelle and P. Pasero (2009). "Topoisomerase I suppresses genomic instability by preventing interference between replication and transcription." *Nat Cell Biol* **11**(11): 1315-1324.

Tulin, A. and A. Spradling (2003). "Chromatin Loosening by Poly(ADP)-Ribose Polymerase (PARP) at Drosophila Puff Loci." *Science* **299**(5606): 560-562.

Uttara, B., A. V. Singh, P. Zamboni and R. T. Mahajan (2009). "Oxidative Stress and Neurodegenerative Diseases: A Review of Upstream and Downstream Antioxidant Therapeutic Options." *Current Neuropharmacology* **7**(1): 65-74.

Valko, M., D. Leibfritz, J. Moncol, M. T. D. Cronin, M. Mazur and J. Telser (2007). "Free radicals and antioxidants in normal physiological functions and human disease." *The International Journal of Biochemistry & Cell Biology* **39**(1): 44-84.

van der Horst, G. T., H. van Steeg, R. J. Berg, A. J. van Gool, J. de Wit, G. Weeda, H. Morreau, R. B. Beems, C. F. van Kreijl, F. R. de Gruijl, D. Bootsma and J. H. Hoeijmakers (1997). "Defective transcription-coupled repair in Cockayne syndrome B mice is associated with skin cancer predisposition." *Cell* **89**(3): 425-435.

Vance, J. R. and T. E. Wilson (2002). "Yeast Tdp1 and Rad1-Rad10 function as redundant pathways for repairing Top1 replicative damage." *Proc Natl Acad Sci U S A* **99**(21): 13669-13674.

Verly, W. G. and Y. Paquette (1972). "Endonuclease for depurinated DNA in escherichia-coli b." *Canadian Journal of Biochemistry* **50**(2): 217-&.

Vidal, A. E., S. Boiteux, I. D. Hickson and J. Radicella (2001). "XRCC1 coordinates the initial and late stages of DNA abasic site repair through protein–protein interactions." *The EMBO Journal* **20**(22): 6530-6539.

Vis, J. C., E. Schipper, R. T. de Boer-van Huizen, M. M. Verbeek, R. M. de Waal, P. Wesseling, H. J. ten Donkelaar and B. Kremer (2005). "Expression pattern of apoptosis-related markers in Huntington's disease." *Acta Neuropathol* **109**(3): 321-328.

Vivelo, C. A. and A. K. L. Leung (2015). "Proteomics Approaches to Identify Mono(ADP-ribosyl)ated and Poly(ADP-ribosyl)ated proteins." *Proteomics* **15**(0): 203-217.

Vogt, A., K. A. Cooley, M. Brisson, M. G. Tarpley, P. Wipf and J. S. Lazo (2003). "Cell-active dual specificity phosphatase inhibitors identified by high-content screening." *Chem Biol* **10**(8): 733-742.

Vrouwe, M. G., A. Pines, R. M. Overmeer, K. Hanada and L. H. F. Mullenders (2011). "UV-induced photolesions elicit ATR-kinase-dependent signaling in non-cycling cells through

nucleotide excision repair-dependent and -independent pathways." *Journal of Cell Science* **124**(3): 435-446.

Vyas, S., I. Matic, L. Uchima, J. Rood, R. Zaja, R. T. Hay, I. Ahel and P. Chang (2014). "Family-wide analysis of poly(ADP-ribose) polymerase activity." *Nature Communications* **5**: 4426.

Wacker, D. A., D. D. Ruhl, E. H. Balagamwala, K. M. Hope, T. Zhang and W. L. Kraus (2007). "The DNA binding and catalytic domains of poly(ADP-ribose) polymerase 1 cooperate in the regulation of chromatin structure and transcription." *Mol Cell Biol* **27**(21): 7475-7485.

Wallace, S. S. (1998). "Enzymatic processing of radiation-induced free radical damage in DNA." *Radiat Res* **150**(5 Suppl): S60-79.

Wang, J. C. (2002). "Cellular roles of DNA topoisomerases: a molecular perspective." *Nat Rev Mol Cell Biol* **3**(6): 430-440.

Wang, J. C. (2009). *Untangling the double helix: DNA entanglement and the action of the DNA topoisomerases*, Cold Spring Harbor Laboratory Press.

Wang, L. K., C. D. Lima and S. Shuman (2002). "Structure and mechanism of T4 polynucleotide kinase: an RNA repair enzyme." *Embo j* **21**(14): 3873-3880.

Wang, M., W. Wu, W. Wu, B. Rosidi, L. Zhang, H. Wang and G. Iliakis (2006). "PARP-1 and Ku compete for repair of DNA double strand breaks by distinct NHEJ pathways." *Nucleic Acids Res* **34**(21): 6170-6182.

Wang, R. Y., K. C. Kuo, C. W. Gehrke, L. H. Huang and M. Ehrlich (1982). "Heat- and alkali-induced deamination of 5-methylcytosine and cytosine residues in DNA." *Biochim Biophys Acta* **697**(3): 371-377.

Wang, T. S. F. and D. Korn (1980). "Reactivity of kb cell deoxyribonucleic-acid polymerases-alpha and polymerases-beta with nicked and gapped deoxyribonucleic-acid." *Biochemistry* **19**(9): 1782-1790.

Wang, Y., R. An, G. K. Umanah, H. Park, K. Nambiar, S. M. Eacker, B. Kim, L. Bao, M. M. Harraz, C. Chang, R. Chen, J. E. Wang, T.-I. Kam, J. S. Jeong, Z. Xie, S. Neifert, J. Qian, S. A. Andrabi, S. Blackshaw, H. Zhu, H. Song, G.-l. Ming, V. L. Dawson and T. M. Dawson (2016). "A nuclease that mediates cell death induced by DNA damage and poly(ADP-ribose) polymerase-1." *Science* **354**(6308).

Wang, Z., G. A. Michaud, Z. Cheng, Y. Zhang, T. R. Hinds, E. Fan, F. Cong and W. Xu (2012). "Recognition of the iso-ADP-ribose moiety in poly(ADP-ribose) by WWE domains suggests a general mechanism for poly(ADP-ribosyl)ation-dependent ubiquitination." *Genes Dev* **26**(3): 235-240.

Wang, Z., Z. Ying, A. Bosy-Westphal, J. Zhang, B. Schautz, W. Later, S. B. Heymsfield and M. J. Müller (2010). "Specific metabolic rates of major organs and tissues across adulthood: evaluation by mechanistic model of resting energy expenditure." *The American Journal of Clinical Nutrition* **92**(6): 1369-1377.

Watkins, J. C. and H. J. Olverman (2000). "Agonists and antagonists for excitatory amino acid receptors." *Trends in Neurosciences* **10**(7): 265-272.

Weiss, B. (1976). "Endonuclease II of Escherichia coli is exonuclease III." *Journal of Biological Chemistry* **251**(7): 1896-1901.

Whitehouse, C. J., R. M. Taylor, A. Thistlethwaite, H. Zhang, F. Karimi-Busheri, D. D. Lasko, M. Weinfeld and K. W. Caldecott (2001). "XRCC1 Stimulates Human Polynucleotide Kinase Activity at Damaged DNA Termini and Accelerates DNA Single-Strand Break Repair." *Cell* **104**(1): 107-117.

WHO. (2017). "What is Ionizing Radiation?", from http://www.who.int/ionizing_radiation/about/what_is_ir/en/.

Wiebauer, K. and J. Jiricny (1989). "In vitro correction of G.T mispairs to G.C pairs in nuclear extracts from human cells." *Nature* **339**(6221): 234-236.

Wiebauer, K. and J. Jiricny (1990). "Mismatch-specific thymine DNA glycosylase and DNA polymerase-beta mediate the correction of G.T mispairs in nuclear extracts from human-cells." *Proceedings of the National Academy of Sciences of the United States of America* **87**(15): 5842-5845.

Wiederhold, L., J. B. Leppard, P. Kedar, F. Karimi-Busheri, A. Rasouli-Nia, M. Weinfeld, A. E. Tomkinson, T. Izumi, R. Prasad, S. H. Wilson, S. Mitra and T. K. Hazra (2004). "AP Endonuclease-Independent DNA Base Excision Repair in Human Cells." *Molecular Cell* **15**(2): 209-220.

Williams, R. S., R. Green and J. N. M. Glover (2001). "Crystal structure of the BRCT repeat region from the breast cancer-associated protein BRCA1." *Nat Struct Mol Biol* **8**(10): 838-842.

Williams, R. S., J. S. Williams and J. A. Tainer (2007). "Mre11-Rad50-Nbs1 is a keystone complex connecting DNA repair machinery, double-strand break signaling, and the chromatin template." *Biochem Cell Biol* **85**(4): 509-520.

Wilson, S. H. and T. A. Kunkel (2000). "Passing the baton in base excision repair." *Nat Struct Mol Biol* **7**(3): 176-178.

Wright, R. H. G., A. Lioutas, F. Le Dily, D. Soronellas, A. Pohl, J. Bonet, A. S. Nacht, S. Samino, J. Font-Mateu, G. P. Vicent, M. Wierer, M. A. Trabado, C. Schelhorn, C. Carolis, M. J. Macias, O.

Yanes, B. Oliva and M. Beato (2016). "ADP-ribose–derived nuclear ATP synthesis by NUDIX5 is required for chromatin remodeling." *Science* **352**(6290): 1221-1225.

Wu, J. and L. F. Liu (1997). "Processing of topoisomerase I cleavable complexes into DNA damage by transcription." *Nucleic Acids Research* **25**(21): 4181-4186.

Wyatt, Haley D. M., S. Sarbajna, J. Matos and Stephen C. West (2013). "Coordinated Actions of SLX1-SLX4 and MUS81-EME1 for Holliday Junction Resolution in Human Cells." *Molecular Cell* **52**(2): 234-247.

Xanthoudakis, S., R. J. Smeyne, J. D. Wallace and T. Curran (1996). "The redox/DNA repair protein, Ref-1, is essential for early embryonic development in mice." *Proc Natl Acad Sci U S A* **93**(17): 8919-8923.

Xu, G. P. and P. I. Reed (1993). "N-nitroso compounds in fresh gastric juice and their relation to intragastric pH and nitrite employing an improved analytical method." *Carcinogenesis* **14**(12): 2547-2551.

Yamada, M., M. Miwa and T. Sugimura (1971). "Studies on poly (adenosine diphosphate-ribose)." *Archives of Biochemistry and Biophysics* **146**(2): 579-586.

Yang, K., R. Guo and D. Xu (2016). "Non-homologous end joining: advances and frontiers." *Acta Biochim Biophys Sin (Shanghai)* **48**(7): 632-640.

Yang, L., M. Guell, S. Byrne, J. L. Yang, A. De Los Angeles, P. Mali, J. Aach, C. Kim-Kiselak, A. W. Briggs, X. Rios, P.-Y. Huang, G. Daley and G. Church (2013). "Optimization of scarless human stem cell genome editing." *Nucleic Acids Research* **41**(19): 9049-9061.

Yang, S. W., A. B. Burgin, B. N. Huizenga, C. A. Robertson, K. C. Yao and H. A. Nash (1996). "A eukaryotic enzyme that can disjoin dead-end covalent complexes between DNA and type I topoisomerases." *Proceedings of the National Academy of Sciences* **93**(21): 11534-11539.

Yeh, Y. C., H. F. Liu, C. A. Ellis and A. L. Lu (1994). "Mammalian topoisomerase I has base mismatch nicking activity." *Journal of Biological Chemistry* **269**(22): 15498-15504.

Yeo, A. J., O. J. Becherel, J. E. Luff, J. K. Cullen, T. Wongsurawat, P. Jenjaroenpoon, V. A. Kuznetsov, P. J. McKinnon and M. F. Lavin (2014). "R-Loops in Proliferating Cells but Not in the Brain: Implications for AOA2 and Other Autosomal Recessive Ataxias." *PLoS ONE* **9**(3): e90219.

Yu, S.-W., S. A. Andrabi, H. Wang, N. S. Kim, G. G. Poirier, T. M. Dawson and V. L. Dawson (2006). "Apoptosis-inducing factor mediates poly(ADP-ribose) (PAR) polymer-induced cell death." *Proceedings of the National Academy of Sciences* **103**(48): 18314-18319.

Yu, S.-W., H. Wang, M. F. Poitras, C. Coombs, W. J. Bowers, H. J. Federoff, G. G. Poirier, T. M. Dawson and V. L. Dawson (2002). "Mediation of Poly(ADP-Ribose) Polymerase-1-Dependent Cell Death by Apoptosis-Inducing Factor." *Science* **297**(5579): 259-263.

Zacharias, D. A., J. D. Violin, A. C. Newton and R. Y. Tsien (2002). "Partitioning of Lipid-Modified Monomeric GFPs into Membrane Microdomains of Live Cells." *Science* **296**(5569): 913-916.

Zaidi, N. H., E. Allay, T. C. Ayi, B. F. Li, L. L. Dumenco, M. S. Sy and S. L. Gerson (1995). "The immature thymocyte is protected from N-methylnitrosourea-induced lymphoma by the human MGMT-CD2 transgene." *Carcinogenesis* **16**(5): 1047-1053.

Zaidi, N. H., T. P. Pretlow, M. A. O'Riordan, L. L. Dumenco, E. Allay and S. L. Gerson (1995). "Transgenic expression of human MGMT protects against azoxymethane-induced aberrant crypt foci and G to A mutations in the K-ras oncogene of mouse colon." *Carcinogenesis* **16**(3): 451-456.

Zeng, Z., A. Sharma, L. Ju, J. Murai, L. Umans, L. Vermeire, Y. Pommier, S. Takeda, D. Huylebroeck, K. W. Caldecott and S. F. El-Khamisy (2012). "TDP2 promotes repair of topoisomerase I-mediated DNA damage in the absence of TDP1." *Nucleic Acids Research* **40**(17): 8371-8380.

Zernike, F. (1942). "Phase contrast, a new method for the microscopic observation of transparent objects Part II." *Physica* **9**: 974-986.

Zhang, F., Y. Chen, M. Li and X. Yu (2014). "The oligonucleotide/oligosaccharide-binding fold motif is a poly(ADP-ribose)-binding domain that mediates DNA damage response." *Proc Natl Acad Sci U S A* **111**(20): 7278-7283.

Zhang, H. F., A. Tomida, R. Koshimizu, Y. Ogiso, S. H. Lei and T. Tsuruo (2004). "Cullin 3 promotes proteasomal degradation of the topoisomerase I-DNA covalent complex." *Cancer Research* **64**(3): 1114-1121.

Zhang, Y., Q. He, Z. Hu, Y. Feng, L. Fan, Z. Tang, J. Yuan, W. Shan, C. Li, X. Hu, J. L. Tanyi, Y. Fan, Q. Huang, K. Montone, C. V. Dang and L. Zhang (2016). "Long noncoding RNA LINP1 regulates repair of DNA double-strand breaks in triple-negative breast cancer." *Nat Struct Mol Biol* **23**(6): 522-530.

Zhang, Y., S. M. Liu, C. Mickanin, Y. Feng, O. Charlat, G. A. Michaud, M. Schirle, X. Y. Shi, M. Hild, A. Bauer, V. E. Myer, P. M. Finan, J. A. Porter, S. M. A. Huang and F. Cong (2011). "RNF146 is a poly(ADP-ribose)-directed E3 ligase that regulates axin degradation and Wnt signalling." *Nature Cell Biology* **13**(5): 623-U292.

Zhang, Y.-W., M. Regairaz, J. A. Seiler, K. K. Agama, J. H. Doroshow and Y. Pommier (2011). "Poly(ADP-ribose) polymerase and XPF–ERCC1 participate in distinct pathways for the repair of topoisomerase I-induced DNA damage in mammalian cells." *Nucleic Acids Research* **39**(9): 3607-3620.

Zheng, Y. and T. L. Sheppard (2004). "Half-life and DNA strand scission products of 2-deoxyribonolactone oxidative DNA damage lesions." *Chem Res Toxicol* **17**(2): 197-207.

Zhou, T., K. Akopiants, S. Mohapatra, P. S. Lin, K. Valerie, D. A. Ramsden, S. P. Lees-Miller and L. F. Povirk (2009). "Tyrosyl-DNA phosphodiesterase and the repair of 3'-phosphoglycolate-terminated DNA double-strand breaks." *DNA Repair (Amst)* **8**(8): 901-911.

Zhou, T., J. W. Lee, H. Tatavarthi, J. R. Lupski, K. Valerie and L. F. Povirk (2005). "Deficiency in 3'-phosphoglycolate processing in human cells with a hereditary mutation in tyrosyl-DNA phosphodiesterase (TDP1)." *Nucleic Acids Research* **33**(1): 289-297.

Zhou, W. and P. W. Doetsch (1993). "Effects of abasic sites and DNA single-strand breaks on prokaryotic RNA polymerases." *Proc Natl Acad Sci U S A* **90**(14): 6601-6605.

Zhou, W. and P. W. Doetsch (1994). "Transcription bypass or blockage at single-strand breaks on the DNA template strand: effect of different 3' and 5' flanking groups on the T7 RNA polymerase elongation complex." *Biochemistry* **33**(49): 14926-14934.

Zhou, Y., X. Feng and D. W. Koh (2011). "Activation of cell death mediated by apoptosis-inducing factor due to the absence of poly(ADP-ribose) glycohydrolase." *Biochemistry* **50**(14): 2850-2859.

Zhu, Z., W. H. Chung, E. Y. Shim, S. E. Lee and G. Ira (2008). "Sgs1 helicase and two nucleases Dna2 and Exo1 resect DNA double-strand break ends." *Cell* **134**(6): 981-994.

Zmudzka, B. Z., A. Fornace, J. Collins and S. H. Wilson (1988). "Characterization of DNA polymerase-beta messenger-RNA - cell-cycle and growth-response in cultured human-cells." *Nucleic Acids Research* **16**(20): 9587-9596.

Znojek, P., E. Willmore and N. J. Curtin (2014). "Preferential potentiation of topoisomerase I poison cytotoxicity by PARP inhibition in S phase." *Br J Cancer* **111**(7): 1319-1326.

Zock, J. M. (2009). "Applications of High Content Screening in Life Science Research." *Combinatorial Chemistry & High Throughput Screening* **12**(9): 870-876.

Zou, L. and S. J. Elledge (2003). "Sensing DNA damage through ATRIP recognition of RPA-ssDNA complexes." *Science* **300**(5625): 1542-1548.

Zou, Y., Y. Liu, X. Wu and S. M. Shell (2006). "Functions of human replication protein A (RPA): from DNA replication to DNA damage and stress responses." *J Cell Physiol* **208**(2): 267-273.

Zylka, M. J., J. M. Simon and B. D. Philpot (2015). "Gene length matters in neurons." *Neuron* **86**(2): 353-355.

Published Work

2546–2557 *Nucleic Acids Research, 2017, Vol. 45, No. 5* *Published online 13 December 2016*
doi: 10.1093/nar/gkw1246

Overlapping roles for PARP1 and PARP2 in the recruitment of endogenous XRCC1 and PNKP into oxidized chromatin

Hana Hanzlikova†, William Gittens†, Katerina Krejcikova, Zhihong Zeng and Keith W. Caldecott*

Genome Damage and Stability Centre, School of Life Sciences, University of Sussex, Falmer, Brighton, BN1 9RQ, UK

Received July 01, 2016; Revised November 24, 2016; Editorial Decision November 26, 2016; Accepted December 11, 2016

ABSTRACT

A critical step of DNA single-strand break repair is the rapid recruitment of the scaffold protein XRCC1 that interacts with, stabilizes and stimulates multiple enzymatic components of the repair process. XRCC1 recruitment is promoted by PARP1, an enzyme that is activated following DNA damage and synthesizes ADP-ribose polymers that XRCC1 binds directly. However, cells possess two other DNA strand break-induced PARP enzymes, PARP2 and PARP3, for which the roles are unclear. To address their involvement in the recruitment of endogenous XRCC1 into oxidized chromatin we have established 'isogenic' human diploid cells in which *PARP1* and/or *PARP2*, or *PARP3* are deleted. Surprisingly, we show that either PARP1 or PARP2 are sufficient for near-normal XRCC1 recruitment at oxidative single-strand breaks (SSBs) as indicated by the requirement for loss of both proteins to greatly reduce or ablate XRCC1 chromatin binding following H_2O_2 treatment. Similar results were observed for PNKP; an XRCC1 protein partner important for repair of oxidative SSBs. Notably, concentrations of PARP inhibitor >1000-fold higher than the IC50 were required to ablate both ADP-ribosylation and XRCC1 chromatin binding following H_2O_2 treatment. These results demonstrate that very low levels of ADP-ribosylation, synthesized by either PARP1 or PARP2, are sufficient for XRCC1 recruitment following oxidative stress.

INTRODUCTION

Single-strand breaks (SSBs) are one of the commonest lesions in DNA, arising at a frequency of tens-of-thousands per cell per day (1,2). One major source of SSBs are reactive oxygen species that generate DNA breaks directly by attack of deoxyribose and indirectly by triggering the excision repair of oxidized DNA bases and abasic sites. An early step in the repair of SSBs is the activation of poly (ADP-ribose) polymerases (PARPs); enzymes that covalently modify themselves and other proteins at the site of the break with mono and/or poly (ADP-ribose) and thereby serve as molecular SSB sensors (3–5). Poly (ADP-ribose) (PAR) is then bound by X-ray repair cross-complementing protein 1 (XRCC1), a molecular scaffold protein that interacts with, stabilizes and stimulates multiple enzymatic components of SSB repair and accelerates the overall process (6–9). One of the most important XRCC1 protein partners is DNA polynucleotide kinase phosphatase (PNKP) (10,11). PNKP is a dual function 5′-DNA kinase and 3′-DNA phosphatase that can convert oxidative DNA termini into canonical 5′-phosphate and 3′-hydroxyl termini that can support DNA gap filling and DNA ligation (12,13). The importance of this activity is illustrated by existence of neurological diseases in which PNKP is mutated (14–17).

The first PARP to be identified was PARP1 (ADPRT1), a 113 KDa enzyme that is responsible for ∼85–95% of the total cellular PARP activity triggered in response to DNA breaks (18). Subsequently, following the observation of residual PAR synthesis in *Parp1*$^{-/-}$ mouse embryonic fibroblasts (MEFs) treated with high doses of damaging agents, PARP2 (ADPRT2) was identified (18,19). More recently we, and others, identified PARP3 (ADPRT3) as a third ADP-ribosyl transferase (ADPRT) that is stimulated by DNA breaks (20–23). PARP1, PARP2 and PARP3 share ∼60% homology within their catalytic and tryptophan-glycine-arginine (WGR) domains, but diverge at their N-termini. The N-terminal region of PARP1 is comprised of ∼500 amino acids and includes three zinc finger domains, two of which promote binding to DNA breaks and a third that is believed to trigger stimulation of catalytic activity by up to ∼500-fold. PARP2 and PARP3 lack these zinc finger domains and instead possess shorter N-terminal regions of ∼78 and 40 amino acids, respectively, the functions of which are poorly understood. In contrast to PARP1, PARP2 and

*To whom correspondence should be addressed. Tel: +44 1273 877519; Email: k.w.caldecott@sussex.ac.uk
†These authors contributed equally to the paper as first authors.

PARP3 are reliant on their WGR domains for DNA binding, perhaps explaining their lower catalytic activity.

Despite a great deal of interest in the precise roles of PARP enzymes in DNA repair their relative contribution to specific DNA repair processes remains unclear. Previous studies employing overexpressed GFP-tagged or RFP-tagged XRCC1 have demonstrated that the re-localization of these fusion proteins to focal sites of laser microirradiation or chromatin oxidized by hydrogen peroxide (H_2O_2) is largely or entirely dependent upon PARP1 (24–27). However, the overexpression of tagged XRCC1 might not accurately reflect the behaviour of endogenous XRCC1. Moreover, the role of PARP1 in promoting XRCC1 recruitment to sites of DNA damage has recently been challenged (28–31). Consequently, we have now generated *PARP1*$^{-/-}$, *PARP2*$^{-/-}$, *PARP1*$^{-/-}$/*PARP2*$^{-/-}$ and *PARP3*$^{-/-}$ diploid human hTERT RPE-1 cell lines using CRISPR-Cas9 technology and developed high-content imaging approaches to measure the relative activity and impact of PARP1, PARP2 and PARP3 on the recruitment of endogenous XRCC1 into oxidized human chromatin. Surprisingly, we find that deletion of PARP1 alone does not dramatically impact on XRCC1 recruitment, despite the deletion of this protein reducing total ADP-ribosylation by ∼4- to 5-fold. Indeed, loss of both PARP1 and PARP2 was required to greatly reduce or ablate chromatin binding by endogenous XRCC1. Moreover, similar results were observed for endogenous PNKP, the recruitment of which was dependent on XRCC1. Consistent with these data, we show that relatively small amounts of ADP-ribosylation are required for recruitment of endogenous XRCC1 into chromatin following DNA oxidation, explaining the ability of PARP2 to substitute for PARP1.

MATERIALS AND METHODS

Antibodies and chemicals

The antibodies used in this study were the rabbit polyclonals anti-XRCC1 (Millipore; ABC738), anti-PARP2 (Active Motif; 39743), anti-PARP3 (4699; a kind gift from F. Dantzer), anti-PNKP (SK3195) (32), anti-poly (ADP-ribose) (Trevigen; 4336), rabbit Fc-fused anti-pan-ADP-ribose binding reagent (Millipore; MABE1016) and the mouse monoclonals anti-PARP1 (Serotec; MCA1522G), anti-poly (ADP-ribose) 10H (Enzo; ALX-804-2), anti-nucleophosmin (B23) (Invitrogen; 325200) and anti-actin (Sigma; A4700). The secondary antibodies employed for Western blotting were HRP-conjugated goat anti-rabbit (Bio-Rad; 170-6515) and goat anti-mouse (Bio-Rad; 170-6516) and for indirect immunofluorescence were goat anti-mouse or anti-rabbit Alexa 488 (Invitrogen; A11001 and A31628), goat anti-mouse Alexa 555 (Invitrogen; A21422) and donkey anti-mouse Alexa 647 (Invitrogen; A39571). 8.8 M H_2O_2 was obtained from Fischer Scientific. Olaparib (S1060) was purchased from Selleckchem and KU0058948 hydrochloride from Axon. Both PARP inhibitors were dissolved in dimethyl sulfoxide (Sigma) to a working concentration of 10 mM.

Cell culture, treatment and siRNA transfection

Human hTERT RPE-1 cells obtained from ATCC were cultured in Dulbecco's Modified Eagle's Medium (DMEM/F12; Sigma) supplemented with 10% fetal calf serum (FCS) and 0.01 mg/ml hygromycin B at 37°C and 5% CO_2. Human U2OS cells and MEFs from wild type or *Parp1*$^{-/-}$ mice (33) were cultured in DMEM (Gibco) containing 10% FCS, 2 mM glutamine and the antibiotics *penicillin* (100 units/ml) and *streptomycin* (100 μg/ml) at 37°C and 5% CO_2. Wild-type primary human fibroblasts (1BR) and primary human fibroblasts from a *PNKP*-mutated patient (15) were cultured in Minimum Essential Media (Gibco) containing 15% FCS, 2 mM glutamine and the antibiotics penicillin (100 units/ml) and streptomycin (100 μg/ml) at 37°C and 5% CO_2. Where indicated, cells were treated with H_2O_2 diluted in phosphate buffered saline (PBS) or serum free medium at the indicated concentrations immediately prior to use for 7 min at room temperature (RT) or 10 min on ice. PARP inhibitors (Olaparib or KU0058948) were employed where indicated at a final concentration of 1 μM or 10 μM and were added to the cells 1 h prior to and during H_2O_2 treatment. Non-targeting siRNA (ON-TARGETplus, Dharmacon), siPARP2 or siPARP3 SMARTpool (Dharmacon) were reverse-transfected into the cells using Lipofectamine® RNAiMAX (Invitrogen) according to the manufacturer's instructions. All experiments were carried out 72 h post-transfection, at the observed peak of target protein depletion.

Generation of *PARP1*$^{-/-}$, *PARP2*$^{-/-}$, *PARP1*$^{-/-}$/*PARP2*$^{-/-}$, *PARP3*$^{-/-}$ and *XRCC1*$^{-/-}$ cells

Human hTERT RPE-1 gene edited cell lines were prepared using Cas9 and guides identified using either E-CRISP (http://www.e-crisp.org/E-CRISP/) or CRISPRdirect (http://crispr.dbcls.jp). For XRCC1, the 21-mer Tru-guide (34) sequences were 5′-GACACGACAUGGCGGAGGCGG-3′ and 5′-CCGCCUCCGCCAUGUCGUGUC-3′ (PAM underlined) and spanned nucleotides 12–32 of the human *XRCC1* ORF. The 58-mer synthetic oligonucleotides XCr2F: 5′-TTTCTTGGCTTTATATATCTTGTGGAAAGGACGAAACACCGACACGACATGGCGGAGG-3′ and XCr2R: 5′-GACTAGCCTTATTTTAACTTGCTATTTCTAGCTCTAAAACCCTCCGCCATGTCGTGTC-3′ (Eurofins) encoding the 18 bp Tru-guide sequence (underlined) minus the PAM were annealed and extended into a 98-mer double-stranded fragment using Phusion polymerase (NEB) which was then subcloned into the guide RNA vector (Addgene; #41824) using Gibson Assembly (NEB).

For PARP1 deletion in RPE-1 cells we used the 22-mer Tru-guide sequences 5′-GAAGGUGGGCCACUCCAUCCGG-3′ and 5′-CCGGAUGGAGUGGCCCACCUUC-3′ (PAM underlined) spanning nucleotides 174–195 of the human *PARP1* ORF. For these experiments, the synthetic 59-mers PARP1-4F:5′-TTTCTTGGCTTTATATATCTTGTGGAAAGGACGAAACACCGAAGGTGGGCCACTCCATC-3′ and PARP1-4R: 5′-GACTAGCCTTATTTTAACTTGCTATT

TCTAGCTCTAAAACGATGGAGTGGCCCACCTTC-3′ encoding the 19 bp Tru-guide (underlined) minus the PAM were subcloned as above. For PARP1 deletion in U2OS cells, we used the 20-mer Tru-guide sequences 5′-GCACCCUGACGUUGAGGUGG-3′ and 5′-CCACCUCAACGUCAGGGUGC-3′ (PAM underlined) spanning nucleotides 195–214 of the human *PARP1* ORF. For these experiments, the synthetic 57-mers PARP1-2F: 5′-TTTCTTGGCTTTATATATCTTGTGGAAAGGACGAAACACCGCACCCTGACGTTGAGG-3′ and PARP1-2R: 5′-GACTAGCCTTATTTTAACTTGCTATTTCTAGCTCTAAAACCCTCAACGTCAGGGTGC-3′ encoding the 17 bp Tru-guide (underlined) minus the PAM were subcloned as above. For PARP2, the 20-mer 'Tru-guide' sequences were 5′-GCAUCUACGAGUUUUCUUGG-3′ and 5′-CCAAGAAAACUCGUAGAUGC-3′ (PAM underlined) and spanned nucleotides 107–126 of the human *PARP2* ORF. The synthetic 57-mers PARP2-F: 5′-TTTCTTGGCTTTATATATCTTGTGGAAAGGACGAAACACCGCATCTACGAGTTTTCT-3′ and PARP2-R: 5′-GACTAGCCTTATTTTAACTTGCTATTTCTAGCTCTAAAACAGAAAACTCGTAGATGC-3′ encoding the 17 bp Tru-guide sequence (underlined) minus the PAM were subcloned as above. For PARP3, the 20-mer 'Tru-guide' sequences were 5′-GAUUAUGCGCUUCUCUGCGG-3′ and 5′-CCGCAGAGAAGCGCAUAAUC-3′ (PAM underlined) and spanned nucleotides 119–138 of the human PARP3 ORF. The synthetic 57-mers PARP3-1F: 5′-TTTCTTGGCTTTATATATCTTGTGGAAAGGACGAAACACCGATTATGCGCTTCTCTG-3′ and PARP3-1R: 5′-GACTAGCCTTATTTTAACTTGCTATTTCTAGCTCTAAAACCAGAGAAGCGCATAATC-3′ encoding the 17 bp Tru-guide sequence (underlined) minus the PAM were subcloned as above.

Generation of *PARP1*$^{-/-}$/PARP2$^{-/-}$ RPE-1 cells was carried out by targeting *PARP2* in *PARP1*$^{-/-}$ RPE-1 cells. The 20-mer 'Tru-guide' sequences targeting PARP2 in this case were 5′-GAGGAUUGUAUUCGGGCUGG-3′ and 5′-CCAGCCCGAAUACAAUCCUC-3′ (PAM underlined) and spanned nucleotides 11821–11841 of the human *PARP2* ORF. The synthetic 57-mers PARP2-B-F: 5′-TTTCTTGGCTTTATATATCTTGTGGAAAGGACGAAACACCGAGGATTGTATTCGGGC-3′ and PARP2-B-R: 5′-GACTAGCCTTATTTTAACTTGCTATTTCTAGCTCTAAAACGCCCGAATACAATCCTC-3′ encoding the 17 bp Tru-guide (underlined) minus the PAM were subcloned as above.

For gene editing, hTERT RPE-1 or U2OS cells were co-transfected with the appropriate guide RNA construct indicated above and a Cas9 expression construct (Addgene; #41815) using a NEON Transfection System (Invitrogen). Twenty four hours later, the transfected cells were selected in medium containing 0.5 mg/ml G418 for 5 days and then subcloned into 96-wells plates. Once at sufficient cell density the subclones were analysed for presence of the target protein by indirect immunofluorescence (PARP1, PARP2, XRCC1) or by Western blotting (PARP3). The absence of the targeted protein in cell clones selected as above was confirmed by Western blotting and one clone of each genotype was chosen for further analysis (clone #G7 for *PARP1*$^{-/-}$, #A1 for *PARP2*$^{-/-}$, #E6 for *PARP1*$^{-/-}$/*PARP2*$^{-/-}$, #20 for *PARP3*$^{-/-}$ and #3 for *XRCC1*$^{-/-}$ cells).

Confirmation of gene editing by sanger sequencing

Genomic DNA was purified from WT, *PARP1*$^{-/-}$, *PARP2*$^{-/-}$, *PARP3*$^{-/-}$, *PARP1*$^{-/-}$/*PARP2*$^{-/-}$ and *XRCC1*$^{-/-}$ RPE-1 cells using Extract-N-Amp Tissue PCR kit (Sigma) as per the manufacturer's instructions. PCR was used to amplify regions of interest surrounding the specific gRNA target loci (primer sequences can be found in Supplementary Table S1). Amplicons were cloned and expanded in pCR®2.1-TOPO® (Invitrogen) prior to Sanger sequencing. WT RPE-1 cells were sequenced by whole exome sequencing (Source BioScience). Consensus sequences for each pCR®2.1-TOPO® clone were aligned with the consensus sequences for the corresponding loci from WT RPE-1 exome sequencing, allowing identification of indels close to the gRNA target loci.

SDS-PAGE and Western blotting

Collected cells were lysed in standard 1x Laemmli loading buffer, denaturated for 10 min at 95°C and sonicated for 30 s using Bioruptor® Pico (Diagenode). Protein concentrations were determined using the BCA assay (Pierce). Samples were subjected to SDS-PAGE (8% or gradient gel), proteins transferred onto nitrocellulose membrane and detected by relevant specific antibodies combined with horseradish peroxidase-conjugated secondary antibodies. Peroxidase activity was detected by ECL reagent (GE Healthcare) and Amersham Hyperfilm ECL (GE Healthcare) or ImageQuant LAS-4000 system connected with high-sensitivity Super CCD camera (GE Healthcare).

Immunofluorescence and microscopy

Cells grown on coverslips were washed with PBS and fixed with 4% paraformaldehyde in PBS 10 min at RT. After fixation, cells were washed twice with PBS, treated with ice-cold methanol/acetone solution (1:1) for 5 min, washed twice with PBS and blocked at least 30 min in 10% FCS in PBS. Incubation with the primary antibody (60 min, RT) was followed by wash (3 × 5 min in PBS) and incubation with appropriate fluorescently-labelled secondary antibody (60 min, RT). Coverslips were washed (3 × 5 min in PBS), stained with DAPI (1 μg/ml in water, 2 min) and mounted using VECTASHIELD (Vector Laboratories). To measure chromatin retention of proteins, cells were pre-extracted in cold 0.2% Triton X-100 for 2 min on ice prior to fixation as above. High-resolution microscopy of fixed samples was carried out on a Zeiss AxioObserver.Z1 microscope, equipped with oil immersion objectives (Plan-Apochromat 63x/1.4), Hamamatsu ORCA-Flash4.0 LT camera and ZEN 2 core imaging software. Automated wide-field microscopy was performed on an Olympus ScanR system (motorized IX83 microscope) with ScanR Image Acquisition and Analysis Software, 20x/0.45 (LUCPLFLN 20x PH) and 40x/0.6 (LUCPLFLN 40x PH) dry objectives and Hamamatsu ORCA-R2 digital CCD camera C10600.

Total nuclear ADP-ribose fluorescence signal was quantified in the region colocalizing with DAPI. Non-nucleolar anti-XRCC1 fluorescence signal was quantified in the region colocalizing with DAPI but excluding the nucleolar region defined by B23 colabelling. Fluorescence was plotted relative to that in untreated WT cells. Where indicated, non-specific anti-XRCC1 background fluorescence was measured using *XRCC1*$^{-/-}$cells and is indicated by a black dotted line in the relevant graphs.

Alkaline comet assays

A total of 3×10^6 cells were trypsinized, washed and resuspended in ice cold PBS. A total of 5×10^5 cells were removed and stored on ice ('undamaged' sample). The remaining cells were then treated with H_2O_2 (50 μM) in PBS for 10 min on ice before mixing with complete DMEM/F12 medium prior to recovery of the cells by centrifugation and resuspension in ice cold complete DMEM/F12. A total of 5×10^5 cells were removed and stored on ice ('no repair' sample) and the remaining cells resuspended in complete DMEM/F12 (37°C) and incubated at 37°C for the indicated repair period. At 7.5, 15 and 30 min, 5×10^5 cells were removed and stored on ice. Finally, all samples were resuspended in 200 μl ice cold PBS, rapidly mixed with 200 μl 1.2% low melting point agarose in PBS and plated on 0.6% agarose-coated, frosted glass slides on ice. The agarose was allowed to solidify prior to incubation in lysis buffer (2.5 M NaCl, 100 mM EDTA, 10 mM Tris-HCl pH 10) for 1 h at 4°C. Slides were washed 3 times with 4°C H_2O and incubated for 45 min in electrophoresis buffer (1 mM EDTA, 50 mM NaOH). Electrophoresis was carried out at 12 V for 25 min, prior to overnight neutralization with Tris-HCl (1 M). Finally, slides were stained with Tris-HCl (1 M) containing SYBR-G (1:10000) and Antifade (40 μg/ml), and imaged (Nikon Eclipse 50i). Average tail moments from 100 cells per sample were obtained using Comet Assay IV software (Perceptive Instruments).

RESULTS

To examine the respective roles of PARP1, PARP2 and PARP3 on the recruitment of endogenous XRCC1 at sites of DNA damage we generated a set of diploid human hTERT RPE-1 cell lines (denoted RPE-1 for simplicity) in which these four proteins were deleted individually using CRISPR/Cas9-mediated genome editing. Individual clones in which the relevant protein was absent were identified using Western blotting and immunofluorescence and a single clone of each genotype was chosen for further experiments (Figure 1A and B). That the relevant CRISPR/Cas9 target site was mutated was confirmed by PCR and Sanger sequencing (Supplementary Figure S1A).

The generation of *XRCC1*$^{-/-}$ RPE-1 cells and the identification of a specific anti-XRCC1 antibody for immunofluorescence enabled us to develop a high-content imaging approach for measuring the recruitment of endogenous XRCC1 into oxidized human chromatin. Interestingly, when soluble proteins were extracted with detergent prior to fixation and immunostaining XRCC1 was localized primarily in the nucleoli in undamaged wild-type RPE-1 cells (Figure 1C, *left*). This was not the case in *XRCC1*$^{-/-}$ RPE-1 cells, confirming that the anti-XRCC1 nucleolar signal was specific. More importantly, XRCC1 was rapidly recruited into chromatin globally across the nucleus following treatment with H_2O_2. H_2O_2 is a physiologically relevant source of oxidative stress and SSBs but induces DSBs only very poorly, with a SSB/DSB ratio of >2000/1 (35). To quantify XRCC1 recruitment into global nuclear chromatin following H_2O_2 treatment we employed an Olympus ScanR automated wide-field microscope with image acquisition and analysis software, and excluded signal co-localising with the nucleolar marker, nucleophosmin (B23). These data revealed that the amount of chromatin bound XRCC1 increased 5-fold in wild-type RPE-1 cells following treatment with H_2O_2, but did not increase above background signal in *XRCC1*$^{-/-}$ RPE-1 cells (Figure 1C, *right*).

Next, we examined levels of ADP-ribosylation and XRCC1 chromatin loading in RPE-1 cells deleted of the individual PARP proteins. Importantly, only the level of the targeted PARP was affected in each of the gene-edited cell lines (Figure 2A, *left*). Only in *PARP1*$^{-/-}$ cells were the levels of ADP-ribosylation visibly reduced, as measured by Western blotting and indirect immunofluorescence (Figure 2A, *right* and B). This is consistent with previous observations demonstrating that PARP1 accounts for 80–90% of total ADP-ribosylation following DNA damage (18). In our hands, PARP1 deletion resulted in ∼75–80% reduction in total ADP-ribosylation under the conditions employed (Figures 2B and 4B). Surprisingly, however, the level of XRCC1 recruitment into oxidized chromatin was not significantly reduced by PARP1 deletion (Figures 2B and 4B). This was not an artefact of clonal selection because XRCC1 recruitment into chromatin was not measurably reduced in two other independent *PARP1*$^{-/-}$ clones (Supplementary Figure S1B and C).

The high level of XRCC1 recruitment into oxidized chromatin observed in *PARP1*$^{-/-}$ RPE-1 cells suggests that the residual ADP-ribosylation observed in these cells is sufficient for XRCC1 recruitment. Consistent with this, treatment of wild type or *PARP1*$^{-/-}$ RPE-1 cells with the PARP inhibitor KU0058948 at 10 μM ablated ADP-ribosylation and reduced H_2O_2-induced XRCC1 recruitment by more than 85% (Figure 3). At lower concentrations of KU0058948 (1 μM) we observed a small amount of residual ADP-ribosylation by immunofluorescence analysis, and this correlated with increased residual XRCC1 loading in chromatin (Supplementary Figure S2). It is noteworthy that the residual ADP-ribosylation remaining in cells pre-incubated with lower concentrations of KU0058948 was detected only with highly sensitive ADP-ribose detection reagents and only by immunofluorescence analysis, highlighting the importance of careful analysis when correlating the impact of PARP inhibitors on ADP-ribosylation with biological end points (Supplementary Figure S3).

Collectively, the results described above suggest that the recruitment of endogenous XRCC1 into oxidized chromatin in human diploid RPE-1 cells is largely dependent on ADP-ribosylation but does not require the presence of PARP1. To examine if this was also true in other cell types we employed wild type and *PARP1*$^{-/-}$ U2OS

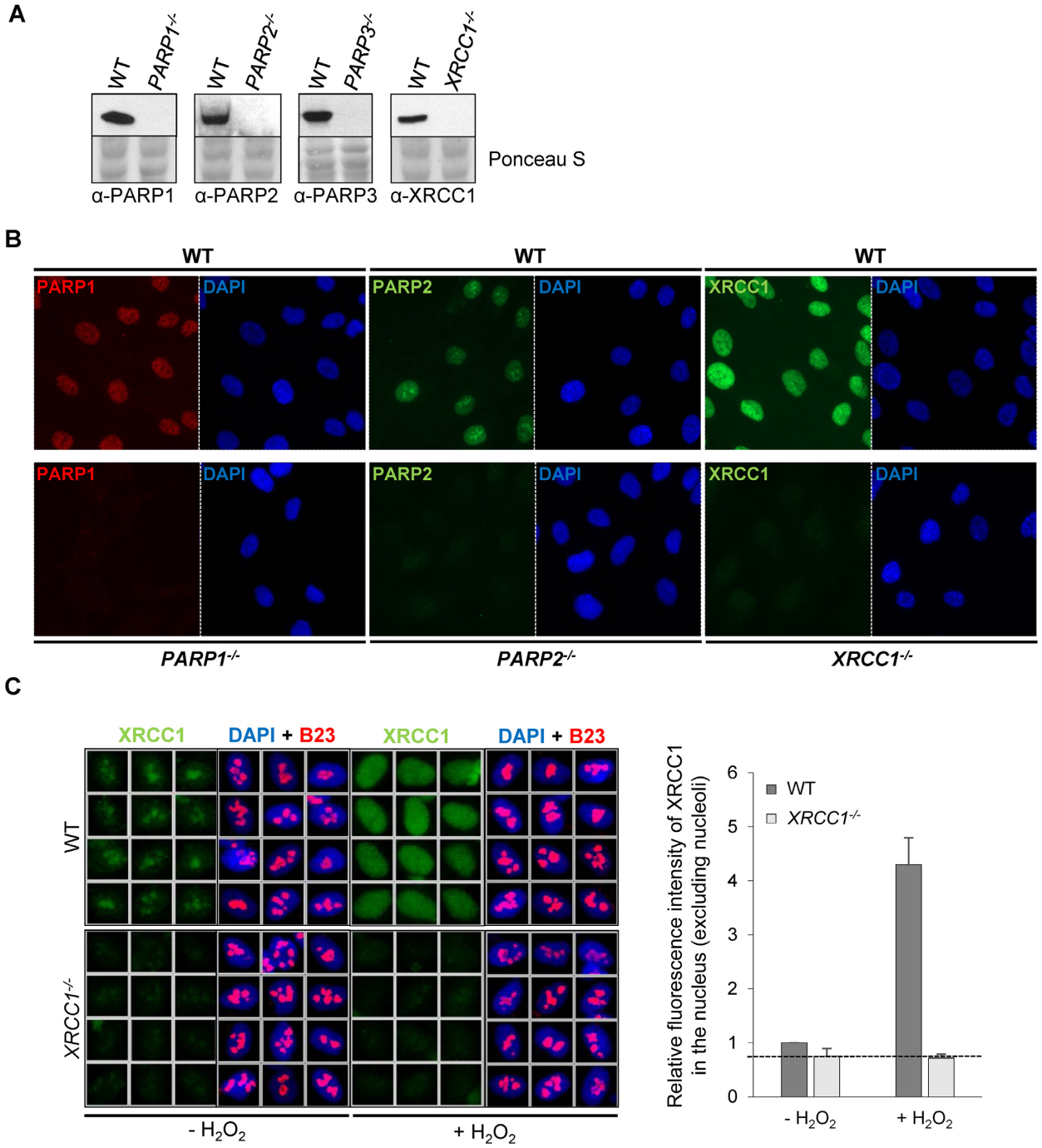

Figure 1. Development of *PARP1*$^{-/-}$, *PARP2*$^{-/-}$, *PARP3*$^{-/-}$ and *XRCC1*$^{-/-}$ RPE-1 cells and XRCC1 high-content imaging. Wild type (WT), *PARP1*$^{-/-}$, *PARP2*$^{-/-}$, *PARP3*$^{-/-}$ and *XRCC1*$^{-/-}$ RPE-1 clonal cell lines were analysed for loss of the targeted protein by (**A**) Western blotting and (**B**) immunofluorescence. Note that the PARP3 antibody available to us was not suitable for immunofluorescence. (**C**) *Left*, representative ScanR images of WT and *XRCC1*$^{-/-}$ RPE-1 cells non-treated or treated with 1 mM hydrogen peroxide (H_2O_2) for 10 min and pre-extracted with detergent prior to fixation and immunostaining for XRCC1 (green), the nucleolar marker B23 (red) and counterstaining with DAPI (blue). *Right*, quantification of detergent-insoluble anti-XRCC1 signal (excluding nucleolar XRCC1 signal) from >1000 cells per sample using Olympus ScanR analysis software. Data are the mean (±SEM) of three independent experiments. The black dotted line denotes non-specific anti-XRCC1 background signal, defined as the residual signal in *XRCC1*$^{-/-}$ RPE-1 cells.

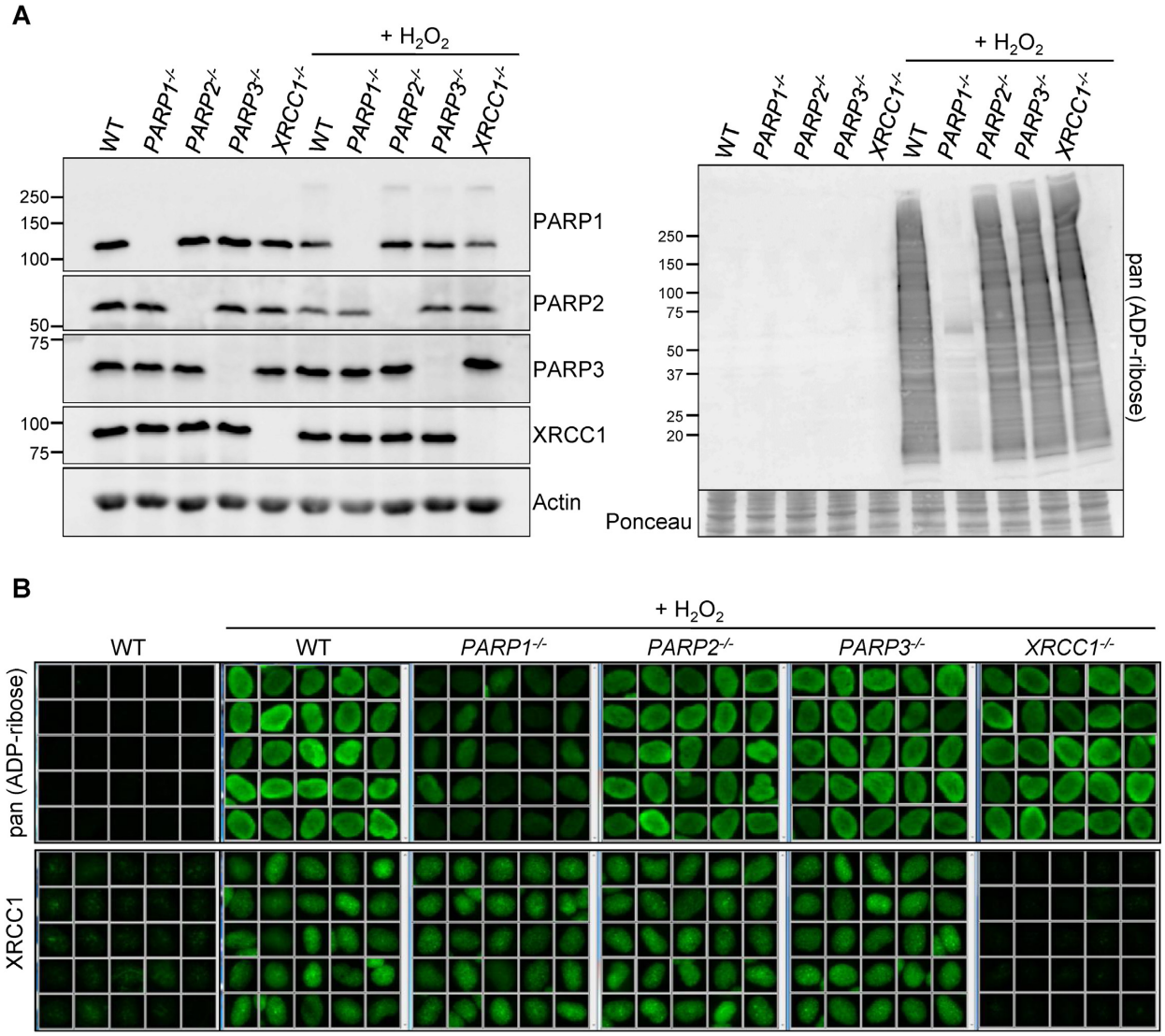

Figure 2. Levels of H_2O_2-induced ADP-ribosylation and XRCC1 recruitment into chromatin in PARP-deleted RPE-1 cells. (**A**) Levels of the indicated proteins (*left*) and ADP-ribosylated proteins (*right*) were compared in cell lysates from the indicated WT or mutant RPE-1 cells harvested before and after treatment with 400 μM H_2O_2 for 7 min by Western blotting using appropriate antibodies and anti-pan-ADP-ribose binding reagent. (**B**) Levels of ADP-ribosylation and chromatin-bound XRCC1 were analysed by indirect immunofluorescence in cells treated or not with H_2O_2 (as above) by fixation and staining with anti-pan-ADP-ribose binding reagent (*top panels*) or by detergent pre-extraction prior to fixation and staining with anti-XRCC1 antibody (*bottom panels*). Representative ScanR images are shown.

cells and MEFs. Indeed, XRCC1 recruitment into oxidized chromatin was not noticeably affected by PARP1 deletion in U2OS and MEFs, respectively (Supplementary Figure S4). Once again, the ability to support XRCC1 chromatin loading reflected residual levels of ADP-ribosylation in *PARP1*$^{-/-}$ cells, because both these residual levels and XRCC1 loading were ablated by incubation with PARP inhibitor (Supplementary Figure S4).

Given the dependence on ADP-ribosylation for recruitment of endogenous XRCC1 into oxidized chromatin, and the individual dispensability of PARP1, PARP2 and PARP3 for this process, we considered the possibility that two or more of these enzymes exhibit redundant or overlapping roles. The possible redundancy between PARP1 and PARP2 was of particular interest, because PARP2 has been reported to account for the residual poly ADP-ribosylation detected in *Parp1*$^{-/-}$ MEFs (18). Indeed, deletion of *PARP2* in *PARP1*$^{-/-}$ RPE-1 cells (denoted *PARP1*$^{-/-}$/*PARP2*$^{-/-}$ cells) reduced the residual ADP-ribosylation below the level of detection under the conditions employed and reduced XRCC1 recruitment into oxidized chromatin to levels that were not significantly above background (Figure 4A and B). XRCC1 recruitment into chromatin was similarly selectively reduced in *PARP1*$^{-/-}$ RPE-1 cells by PARP2 siRNA (Supplementary Figure S5), thereby demonstrating functional overlap between PARP1 and PARP2 using two independent approaches. In contrast, loss of PARP3 alone or together with PARP1 failed to impact on XRCC1 recruitment in RPE-1 cells (Figure 2B and Supplementary Figure S5). Interestingly, PARP2 was not able to functionally re-

place PARP1 with respect the rate of SSBR, because the rate at which DNA breaks declined following H_2O_2 treatment was equally slow in *PARP1*$^{-/-}$ and *PARP1*$^{-/-}$/*PARP2*$^{-/-}$ cells (Figure 4C). This is consistent with our previous findings (27), and suggests that PARP1 fulfils a second role during SSBR that is functionally distinct from PARP2.

Finally, we examined whether the functional overlap between PARP1 and PARP2 in XRCC1 recruitment extended to another component of the XRCC1-dependent SSBR pathway. For this we chose PNKP, an important DNA strand break repair enzyme reported previously to be recruited to SSBs by interaction with XRCC1 (11). Indeed, consistent with this, the level of chromatin-bound nuclear anti-PNKP staining increased 2-fold in wild type RPE-1 cells following H_2O_2 treatment, but failed to do so in *XRCC1*$^{-/-}$ RPE-1 cells (Figure 5A and B). That the PNKP immunostaining in these experiments was specific was confirmed using primary fibroblasts from a patient (15) in which PNKP is mutated and greatly reduced (Supplementary Figure S6A). More importantly, whereas deletion of neither *PARP1* nor *PARP2* alone significantly reduced PNKP recruitment into oxidised chromatin, co-deletion of both of these genes did so (Figure 5A and B). This did not reflect a difference in total PNKP levels because this was similar in wild type and *PARP1*$^{-/-}$/*PARP2*$^{-/-}$ RPE-1 cells (Figure 5C and Supplementary Figure S6B).

In summary, we show here that the SSB sensor proteins PARP1 and PARP2 fulfil overlapping roles in promoting the recruitment of endogenous XRCC1 and PNKP into oxidized human chromatin during chromosomal SSBR, such that either enzyme can support this function.

DISCUSSION

XRCC1 is a scaffold protein that interacts with multiple enzymatic components of SSB repair and thereby accelerates the overall process (2,8). Here, we have applied CRISPR-Cas9 technology and quantitative high-content imaging to investigate, for the first time, the role of PARP1, PARP2 and PARP3 in the recruitment of endogenous XRCC1 to sites of chromosome damage. Detergent pre-extraction suggested that, prior to exogenous DNA damage, chromatin-bound XRCC1 is located predominantly in nucleoli. This is consistent with several previous observations (24,36–38) and suggests that nucleoli are a storage site for this protein and/or that XRCC1 has an as yet undefined role in maintaining ribosomal DNA metabolism.

Importantly, we detected a 5-fold increase in the amount of detergent-insoluble XRCC1 present outside of the nucleolus following H_2O_2 treatment, suggesting that XRCC1 becomes distributed throughout the nuclear chromatin in response to oxidative stress. This is consistent with the observation that, under the conditions employed here, H_2O_2 induces 10 000–20 000 SSBs per cell (unpublished observations). Our experiments employing PARP inhibitors demonstrate unequivocally that the global recruitment of endogenous XRCC1 into oxidized chromatin required poly (ADP-ribose) polymerase activity, a notion that has been questioned recently (28–31). A surprising finding of this work, however, is that relatively little ADP-ribosylation is required for XRCC1 recruitment, compared to the total cellular level of ADP-ribosylation following H_2O_2 treatment. For example, to completely block ADP-ribosylation and ablate XRCC1 recruitment required a concentration of the PARP inhibitor KU0058948 (10 μM) that was 3000-fold higher than the IC50 (3.4 nM) (39). Indeed, residual levels of XRCC1 recruitment were observed at levels of ADP-ribosylation that were too low to be detected by Western blotting. Only by employing highly sensitive ADP-ribose antibodies and detection reagents in immunofluorescence experiments were we able to detect this level of ADP-ribosylation.

XRCC1 binds directly to poly (ADP-ribose) via its central BRCT1 domain, thereby enabling this scaffold protein to accumulate at sites of PARP activity (6,7). The recruitment of XRCC1 at sites of chromosomal SSBs has been reported by us and others to be dependent on PARP1, which is the most abundant and active poly (ADP-ribose) polymerase and is the primary source of poly (ADP-ribose) following oxidative stress (24–27,40). However, we have now found that deletion of PARP1 alone is unable to prevent the recruitment of endogenous XRCC1 into oxidized chromatin globally across the nucleus, suggesting that the level of ADP-ribosylation remaining in *PARP1*$^{-/-}$ cells is sufficient for XRCC1 loading into oxidised chromatin. Indeed, loss of both PARP1 and PARP2 was required to ablate H_2O_2-induced ADP-ribosylation and prevent loading of endogenous XRCC1 into oxidized chromatin. We suggest that this discrepancy reflects the use in previous studies of overexpressed XRCC1 and/or the measurement of XRCC1 accumulation at a limited number of focal or highly damaged sites. Whereas only PARP1 has sufficient activity to load high levels of overexpressed XRCC1 at focal sites of damage, either PARP1 or PARP2 is able to achieve this for endogenous XRCC1 at more physiological levels of oxidized chromatin induced stochastically across the genome.

This functional overlap between PARP1 and PARP2 in protein recruitment into oxidized chromatin was not restricted to XRCC1. Indeed, we observed similar results for recruitment of PNKP, an important partner protein of XRCC1 that is critical for rapid repair of oxidative DNA breaks (10,11). PNKP is a dual function 5′-DNA kinase and 3′-DNA phosphatase which if mutated results in human neurological disease characterized by progressive cerebellar ataxia and early onset seizures with developmental delay (14–16). It has been reported previously that XRCC1 recruits recombinant PNKP at sites of oxidative damage, but our data are the first demonstration that this is true for the endogenous protein. This is important because several recent publications have instead concluded that PNKP is recruited to DNA damage sites by alternative mechanism/s including direct binding of PNKP to DNA and/or poly (ADP-ribose) (6,29,30). However, our experiments show that most if not all chromatin binding by endogenous PNKP is XRCC1-dependent following H_2O_2 treatment.

Our finding that either PARP1 or PARP2 can support loading of endogenous XRCC1 and PNKP into oxidized chromatin is consistent with a functional overlap between these PARP enzymes (41). It has been shown previously that whereas both *Parp1*$^{-/-}$and *Parp2*$^{-/-}$ mice are viable, mice lacking both enzymes die early during embryogenesis, fur-

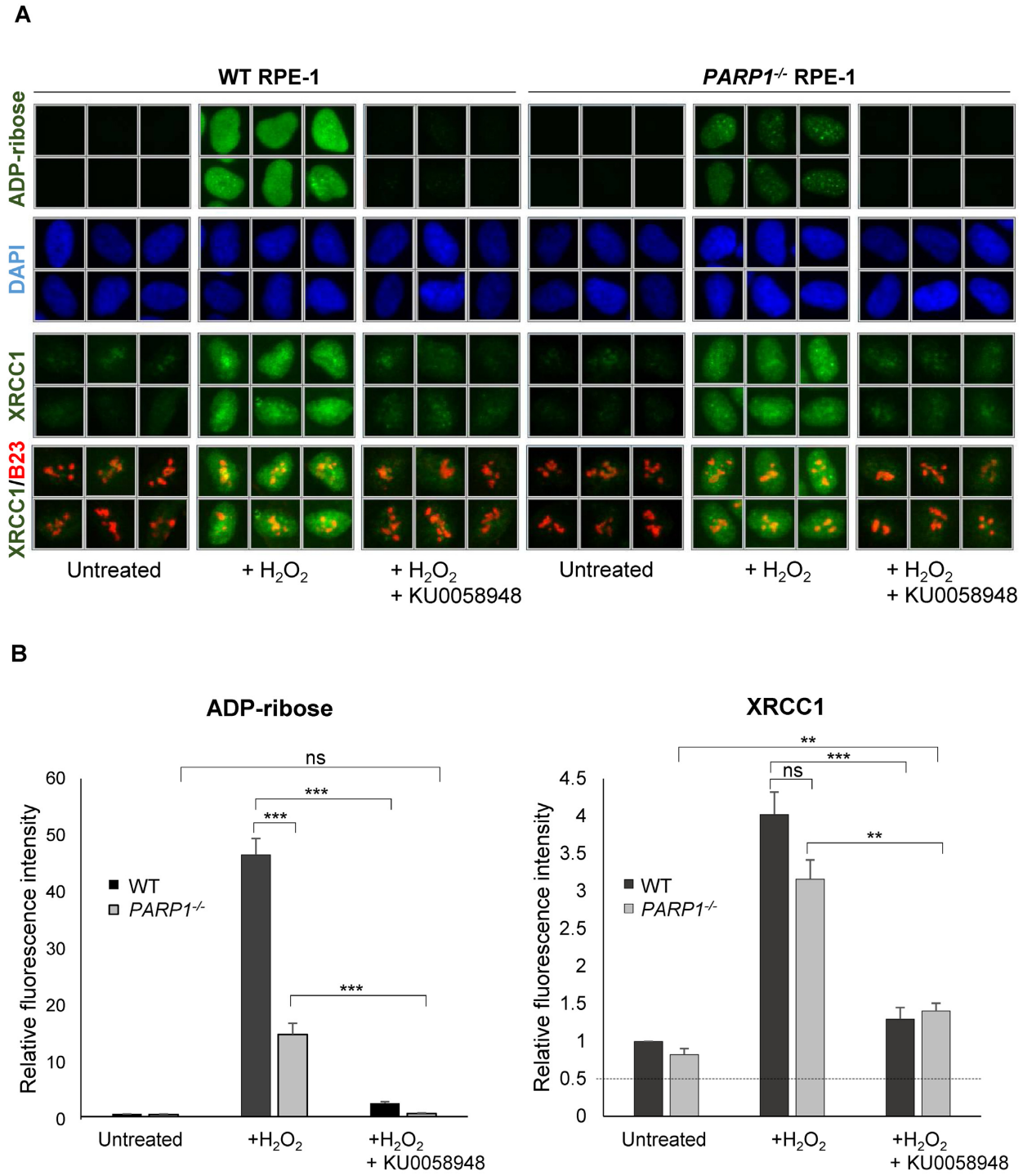

Figure 3. Residual recruitment of endogenous XRCC1 into oxidized chromatin in *PARP1*$^{-/-}$ RPE-1 cells is greatly reduced by PARP inhibitor. (**A**) WT and *PARP1*$^{-/-}$ RPE-1 cells were pre-incubated or not with 10 μM KU0058948 inhibitor for 1 h prior to a 7 min incubation with or without 400 μM H_2O_2. Cells were pre-extracted with detergent to remove non-chromatin bound proteins prior to fixation and immunostaining with the indicated antibodies or anti-pan-ADP-ribose binding reagent. Representative ScanR images are shown. (**B**) Quantification of total nuclear pan-ADP-ribose and chromatin-bound nuclear XRCC1 (excluding nucleolar XRCC1 signal) in cells treated as in panel A. Nucleoli were located using anti-B23 antibodies. All data are the mean (±SEM) of three independent experiments with >1000 cells scored per sample in each experiment. Statistical significance was assessed by two-tailed t-tests. Asterisks ** and *** indicate *P*-values of <0.01 and <0.001, respectively; ns – not significant. The black dotted line denotes non-specific anti-XRCC1 background signal, defined as the residual signal in *XRCC1*$^{-/-}$ cells stained in parallel.

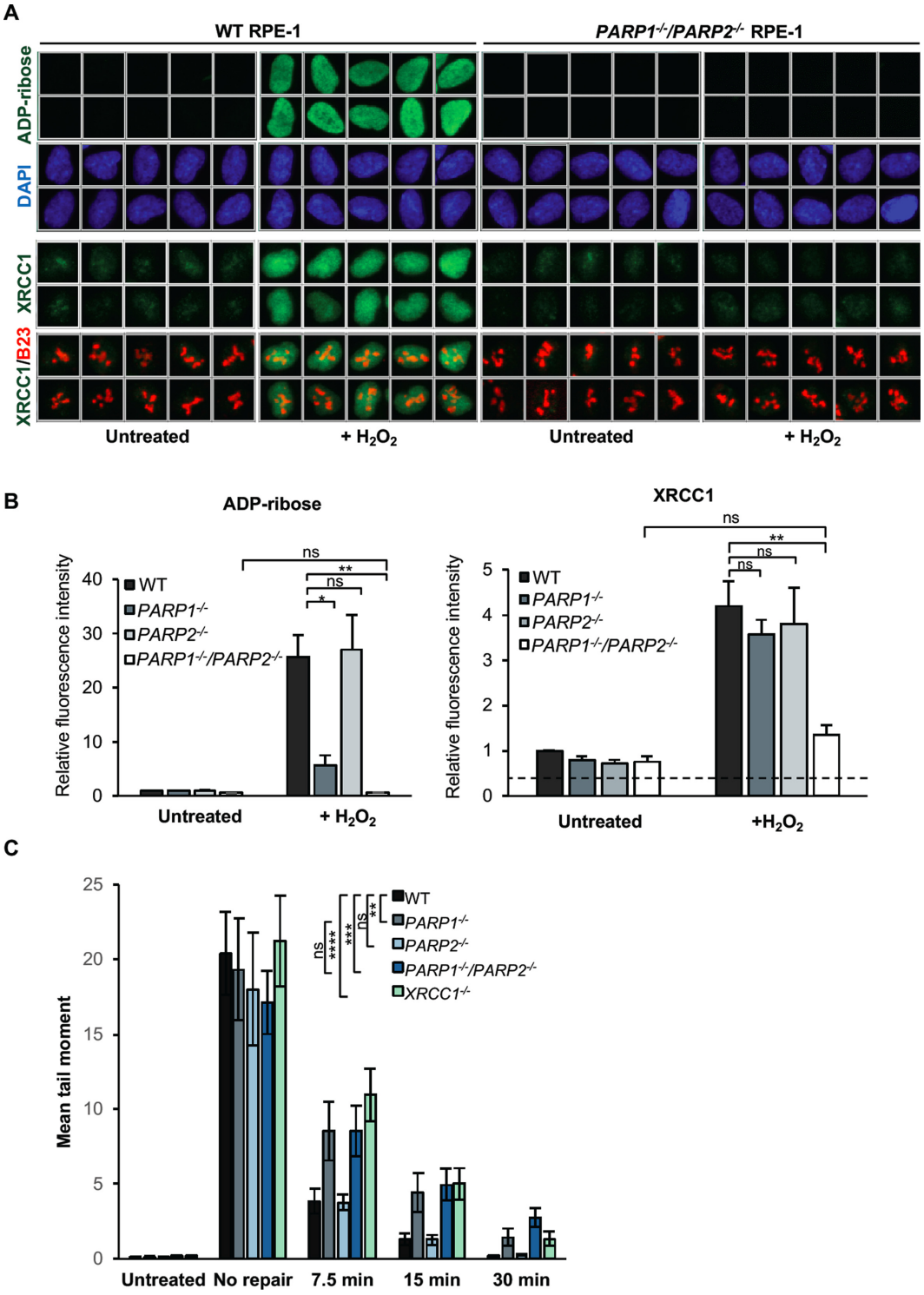

Figure 4. Overlapping roles for PARP1 and PARP2 in recruiting endogenous XRCC1 into oxidized chromatin. (**A**) Levels of ADP-ribosylation and chromatin-bound XRCC1 were measured by indirect immunofluorescence in WT and *PARP1*$^{-/-}$/*PARP2*$^{-/-}$cells treated or not with 400 μM H_2O_2 for 7 min by fixation and staining with anti-pan-ADP-ribose binding reagent and DAPI (*top panels*) or by detergent pre-extraction prior to fixation and staining with anti-XRCC1 and anti-B23 antibodies (*bottom panels*). Representative ScanR images are shown. (**B**) Quantification of total nuclear pan-ADP-ribose and chromatin bound XRCC1 (excluding nucleolar signal). The black dotted line denotes non-specific anti-XRCC1 background signal, measured by XRCC1 immunostaining in *XRCC1*$^{-/-}$ cells in parallel. All data are the mean (±SEM) of three independent experiments with >1000 cells scored per sample in each experiment. Statistical significance was assessed by two tailed t-tests. Asterisks * and ** indicate *P*-values of <0.05 and <0.01, respectively; ns – not significant. (**C**) DNA strand breakage was quantified by alkaline comet assays in indicated RPE-1 cells before, immediately after treatment with 50 μM H_2O_2 on ice and after the depicted repair periods in drug-free medium. Data are the average comet tail moment (an arbitrary unit-measure of DNA strand breaks) of 100 cells per sample and are the mean (±SEM) of three independent experiments. Statistically significant differences (two-way ANOVA) are indicated (**$P < 0.01$; ***$P < 0.001$; ****$P < 0.0001$; ns – not significant).

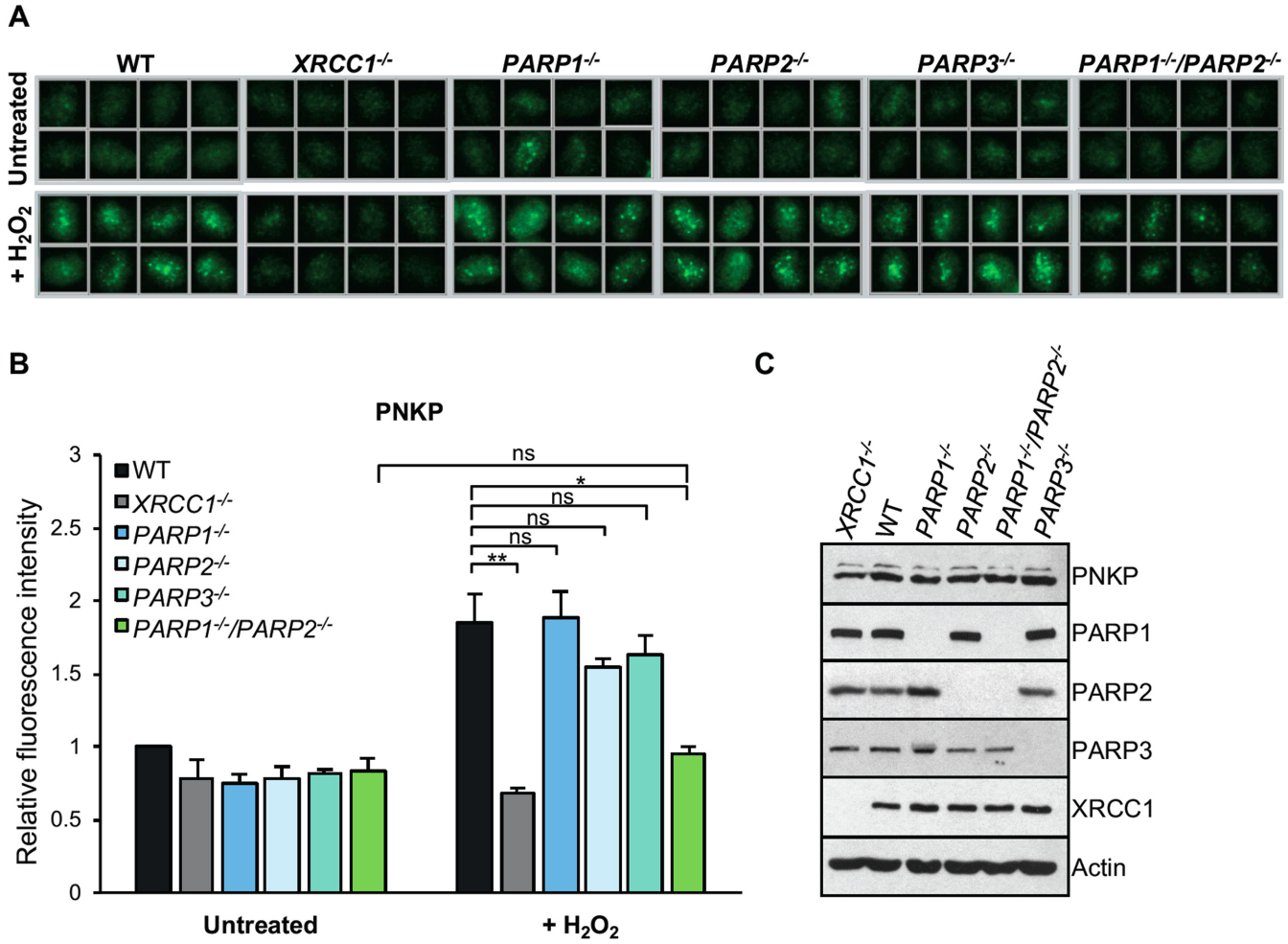

Figure 5. Overlapping roles for PARP1 and PARP2 in recruiting endogenous PNKP into oxidised chromatin. (**A**) Levels of chromatin-bound PNKP were analysed by indirect immunofluorescence in indicated RPE-1 cell lines untreated or treated with 400 μM H_2O_2 for 7 min by detergent pre-extraction prior to fixation and staining with anti-PNKP antibody. Representative ScanR images are shown. (**B**) Quantification of chromatin-bound PNKP in cells measured as above. All data are the mean (±SEM) of three independent experiments with >2000 cells scored per sample in each experiment. Statistical significance was assessed by two-tailed t-tests. Asterisks * and ** indicate *P*-values of <0.05 and <0.01, respectively; ns – not significant. (**C**) Levels of PNKP and the relevant proteins in cell extracts from RPE-1 cells of the indicated genotype.

ther demonstrating a functional interplay between these enzymes (42). One prediction arising from our data is that the loss of both PARP1 and PARP2 should be necessary to reduce the rate of chromosomal SSBR. However, in our previous work we found that only PARP1 depletion reduced this rate, and that PARP2 depletion did not measurably slow SSBR even in cells in which PARP1 was depleted (27). Indeed, we observed the same result in the current work, in which we compared SSBR rates in RPE-1 cells deleted of PARP1 or PARP2 separately and together. This epistatic relationship suggests that whilst loss of both PARP1 and PARP2 is necessary to impact greatly on XRCC1 recruitment, PARP1 fulfils an additional role that is part of the same SSBR pathway but which is downstream of XRCC1/PNKP recruitment into chromatin and cannot be fulfilled by PARP2. That this role is within the XRCC1-dependent SSBR pathway is supported by the observation that PARP1 deletion does not further slow SSBR in *XRCC1*$^{-/-}$ RPE-1 cells (unpublished observations). In contrast to PARP1 and PARP2, we did not observe any impact of PARP3 on XRCC1 recruitment into oxidised chromatin. This may reflect that PARP3 primarily mono ADP-ribosylates proteins in response to SSBs, because the central BRCT1 domain of XRCC1 selectively binds poly (ADP-ribose) (7,43). The role fulfilled by of PARP3 activation at SSBs is currently unknown, but may involve the recruitment of one or more proteins that can bind mono-ADP ribosylated histone H2B (43).

In summary, we demonstrate here that surprisingly little ADP-ribosylation activity is required for the global recruitment of endogenous XRCC1 into oxidized chromatin, and we show that either PARP1 or PARP2 activity is sufficient for this process. It will now be of interest to determine whether these enzymes fulfil similar overlapping roles during the repair of other types of SSBs.

SUPPLEMENTARY DATA

Supplementary Data are available at NAR Online.

ACKNOWLEDGEMENTS

The authors thank Francoise Dantzer for provision of anti-PARP3 antibody and Velibor Savic for access to the Olympus ScanR system. The authors thank Grazia Mancini for provision of PNKP mutated patient fibroblasts.

FUNDING

This work was funded by MRC programme grants to K.W.C [MR/J006750/1 and MR/P010121/1]. Funding for open access charges was from the MRC.
Conflict of interest statement. None declared.

REFERENCES

1. Lindahl,T. (1993) Instability and decay of the primary structure of DNA. *Nature*, **362**, 709–715.
2. Caldecott,K.W. (2008) Single-strand break repair and genetic disease. *Nat. Rev. Genet.*, **9**, 619–631.
3. Caldecott,K.W. (2014) Protein ADP-ribosylation and the cellular response to DNA strand breaks. *DNA Repair (Amst)*, **19**, 108–113.
4. de Murcia,G. and Menissier-de Murcia,J. (1994) Poly(ADP-ribose) polymerase: a molecular nick-sensor. *Trends Biochem. Sci.*, **19**, 172–176.
5. Amé,J.-C., Spenlehauer,C. and de Murcia,G. (2004) The PARP superfamily. *Bioessays*, **26**, 882–893.
6. Li,M., Lu,L.-Y., Yang,C.-Y., Wang,S. and Yu,X. (2013) The FHA and BRCT domains recognize ADP-ribosylation during DNA damage response. *Genes Dev.*, **27**, 1752–1768.
7. Breslin,C., Hornyak,P., Ridley,A., Rulten,S.L., Hanzlikova,H., Oliver,A.W. and Caldecott,K.W. (2015) The XRCC1 phosphate-binding pocket binds poly (ADP-ribose) and is required for XRCC1 function. *Nucleic Acids Res.*, **43**, 6934–6944.
8. Caldecott,K.W. (2003) XRCC1 and DNA strand break repair. *DNA Repair (Amst)*, **2**, 955–969.
9. Caldecott,K.W. (2014) DNA single-strand break repair. *Exp. Cell Res.*, **329**, 2–8.
10. Whitehouse,C.J., Taylor,R.M., Thistlethwaite,A., Zhang,H., Karimi-Busheri,F., Lasko,D.D., Weinfeld,M. and Caldecott,K.W. (2001) XRCC1 stimulates human polynucleotide kinase activity at damaged DNA termini and accelerates DNA single-strand break repair. *Cell*, **104**, 107–117.
11. Loizou,J.I., El-Khamisy,S.F., Zlatanou,A., Moore,D.J., Chan,D.W., Qin,J., Sarno,S., Meggio,F., Pinna,L.A. and Caldecott,K.W. (2004) The protein kinase CK2 facilitates repair of chromosomal DNA single-strand breaks. *Cell*, **117**, 17–28.
12. Karimi-Busheri,F., Daly,G., Robins,P., Canas,B., Pappin,D.J., Sgouros,J., Miller,G.G., Fakhrai,H., Davis,E.M., Le Beau,M.M. *et al.* (1999) Molecular characterization of a human DNA kinase. *J. Biol. Chem.*, **274**, 24187–24194.
13. Jilani,A., Ramotar,D., Slack,C., Ong,C., Yang,X.M., Scherer,S.W. and Lasko,D.D. (1999) Molecular cloning of the human gene, PNKP, encoding a polynucleotide kinase 3′-phosphatase and evidence for its role in repair of DNA strand breaks caused by oxidative damage. *J. Biol. Chem.*, **274**, 24176–24186.
14. Shen,J., Gilmore,E.C., Marshall,C.A., Haddadin,M., Reynolds,J.J., Eyaid,W., Bodell,A., Barry,B., Gleason,D., Allen,K. *et al.* (2010) Mutations in PNKP cause microcephaly, seizures and defects in DNA repair. *Nat. Genet.*, **42**, 245–249.
15. Poulton,C., Oegema,R., Heijsman,D., Hoogeboom,J., Schot,R., Stroink,H., Willemsen,M.A., Verheijen,F.W., van de Spek,P., Kremer,A. *et al.* (2012) Progressive cerebellar atrophy and polyneuropathy: expanding the spectrum of PNKP mutations. *Neurogenetics*, **14**, 43–51.
16. Bras,J., Alonso,I., Barbot,C., Costa,M.M., Darwent,L., Orme,T., Sequeiros,J., Hardy,J., Coutinho,P. and Guerreiro,R. (2015) Mutations in PNKP cause recessive ataxia with oculomotor apraxia type 4. *Am. J. Hum. Genet.*, **96**, 474–479.
17. Paucar,M., Malmgren,H., Taylor,M., Reynolds,J.J., Svenningsson,P., Press,R. and Nordgren,A. (2016) Expanding the ataxia with oculomotor apraxia type 4 phenotype. *Neurol. Genet.*, **2**, e49.
18. Amé,J.C., Rolli,V., Schreiber,V., Niedergang,C., Apiou,F., Decker,P., Muller,S., Höger,T., Menissier-de Murcia,J. and de Murcia,G. (1999) PARP-2, A novel mammalian DNA damage-dependent poly(ADP-ribose) polymerase. *J. Biol. Chem.*, **274**, 17860–17868.
19. Johansson,M. (1999) A human poly(ADP-ribose) polymerase gene family (ADPRTL): cDNA cloning of two novel poly(ADP-ribose) polymerase homologues. *Genomics*, **57**, 442–445.
20. Rulten,S.L., Fisher,A.E.O., Robert,I., Zuma,M.C., Rouleau,M., Ju,L., Poirier,G., Reina-San-Martin,B. and Caldecott,K.W. (2011) PARP-3 and APLF function together to accelerate nonhomologous end-joining. *Mol. Cell*, **41**, 33–45.
21. Langelier,M.-F., Riccio,A.A. and Pascal,J.M. (2014) PARP-2 and PARP-3 are selectively activated by 5′ phosphorylated DNA breaks through an allosteric regulatory mechanism shared with PARP-1. *Nucleic Acids Res.*, **42**, 7762–7775.
22. Boehler,C., Gauthier,L.R., Mortusewicz,O., Biard,D.S., Saliou,J.-M., Bresson,A., Sanglier-Cianferani,S., Smith,S., Schreiber,V., Boussin,F. *et al.* (2011) Poly(ADP-ribose) polymerase 3 (PARP3), a newcomer in cellular response to DNA damage and mitotic progression. *Proc. Natl. Acad. Sci. U.S.A.*, **108**, 2783–2788.
23. Beck,C., Boehler,C., Barbat,J.G., Bonnet,M.-E., Illuzzi,G., Ronde,P., Gauthier,L.R., Magroun,N., Rajendran,A., Lopez,B.S. *et al.* (2014) PARP3 affects the relative contribution of homologous recombination and nonhomologous end-joining pathways. *Nucleic Acids Res.*, **42**, 5616–5632.
24. Okano,S., Lan,L., Caldecott,K.W., Mori,T. and Yasui,A. (2003) Spatial and temporal cellular responses to single-strand breaks in human cells. *Mol. Cell. Biol.*, **23**, 3974–3981.
25. El-Khamisy,S.F., Masutani,M., Suzuki,H. and Caldecott,K.W. (2003) A requirement for PARP-1 for the assembly or stability of XRCC1 nuclear foci at sites of oxidative DNA damage. *Nucleic Acids Res.*, **31**, 5526–5533.
26. Mortusewicz,O., Amé,J.-C., Schreiber,V. and Leonhardt,H. (2007) Feedback-regulated poly(ADP-ribosyl)ation by PARP-1 is required for rapid response to DNA damage in living cells. *Nucleic Acids Res.*, **35**, 7665–7675.
27. Fisher,A.E.O., Hochegger,H., Takeda,S. and Caldecott,K.W. (2007) Poly(ADP-ribose) polymerase 1 accelerates single-strand break repair in concert with poly(ADP-ribose) glycohydrolase. *Mol. Cell. Biol.*, **27**, 5597–5605.
28. Parsons,J.L., Dianova,I.I., Allinson,S.L. and Dianov,G.L. (2005) DNA polymerase beta promotes recruitment of DNA ligase III alpha-XRCC1 to sites of base excision repair. *Biochemistry*, **44**, 10613–10619.
29. Parsons,J.L., Dianova,I.I., Boswell,E., Weinfeld,M. and Dianov,G.L. (2005) End-damage-specific proteins facilitate recruitment or stability of X-ray cross-complementing protein 1 at the sites of DNA single-strand break repair. *FEBS J.*, **272**, 5753–5763.
30. Abdou,I., Poirier,G.G., Hendzel,M.J. and Weinfeld,M. (2014) DNA ligase III acts as a DNA strand break sensor in the cellular orchestration of DNA strand break repair. *Nucleic Acids Res.*, **43**, 875–892.
31. Hanssen-Bauer,A., Solvang-Garten,K., Sundheim,O., Peña-Diaz,J., Andersen,S., Slupphaug,G., Krokan,H.E., Wilson,D.M., Akbari,M. and Otterlei,M. (2011) XRCC1 coordinates disparate responses and multiprotein repair complexes depending on the nature and context of the DNA damage. *Environ. Mol. Mutagen.*, **52**, 623–635.
32. Breslin,C. and Caldecott,K.W. (2009) DNA 3′-phosphatase activity is critical for rapid global rates of single-strand break repair following oxidative stress. *Mol Cell Biol*, **29**, 4653–4662.
33. Masutani,M., Suzuki,H., Kamada,N., Watanabe,M., Ueda,O., Nozaki,T., Jishage,K., Watanabe,T., Sugimoto,T., Nakagama,H. *et al.* (1999) Poly(ADP-ribose) polymerase gene disruption conferred mice resistant to streptozotocin-induced diabetes. *Proc. Natl. Acad. Sci. U.S.A.*, **96**, 2301–2304.
34. Fu,Y., Sander,J.D., Reyon,D., Cascio,V.M. and Joung,J.K. (2014) Improving CRISPR-Cas nuclease specificity using truncated guide RNAs. *Nat. Biotechnol.*, **32**, 279–284.
35. Bradley,M.O. and Kohn,K.W. (1979) X-ray induced DNA double strand break production and repair in mammalian cells as measured by neutral filter elution. *Nucleic Acids Res.*, **7**, 793–804.
36. Antoniali,G., Lirussi,L., Poletto,M. and Tell,G. (2014) Emerging roles of the nucleolus in regulating the DNA damage response: the

noncanonical DNA repair enzyme APE1/Ref-1 as a paradigmatical example. *Antioxid. Redox Signal.*, **20**, 621–639.
37. Andersen,J.S., Lam,Y.W., Leung,A.K.L., Ong,S.-E., Lyon,C.E., Lamond,A.I. and Mann,M. (2005) Nucleolar proteome dynamics. *Nature*, **433**, 77–83.
38. Rancourt,A. and Satoh,M.S. (2009) Delocalization of nucleolar poly(ADP-ribose) polymerase-1 to the nucleoplasm and its novel link to cellular sensitivity to DNA damage. *DNA Repair (Amst)*, **8**, 286–297.
39. McCabe,N., Lord,C.J., Tutt,A.N.J., Martin,N.M.B., Smith,G.C.M. and Ashworth,A. (2005) BRCA2-deficient CAPAN-1 cells are extremely sensitive to the inhibition of Poly (ADP-Ribose) polymerase: an issue of potency. *Cancer Biol. Ther.*, **4**, 934–936.
40. Rulten,S.L., Cortes Ledesma,F., Guo,L., Iles,N.J. and Caldecott,K.W. (2008) APLF (C2orf13) is a novel component of poly(ADP-ribose) signaling in mammalian cells. *Mol. Cell. Biol.*, **28**, 4620–4628.
41. Schreiber,V., Amé,J.-C., Dollé,P., Schultz,I., Rinaldi,B., Fraulob,V., Ménissier-de Murcia,J. and de Murcia,G. (2002) Poly(ADP-ribose) polymerase-2 (PARP-2) is required for efficient base excision DNA repair in association with PARP-1 and XRCC1. *J. Biol. Chem.*, **277**, 23028–23036.
42. Ménissier-de Murcia,J., Ricoul,M., Tartier,L., Niedergang,C., Huber,A., Dantzer,F., Schreiber,V., Amé,J.-C., Dierich,A., LeMeur,M. *et al.* (2003) Functional interaction between PARP-1 and PARP-2 in chromosome stability and embryonic development in mouse. *EMBO J.*, **22**, 2255–2263.
43. Grundy,G.J., Polo,L.M., Zeng,Z., Rulten,S.L., Hoch,N.C., Paomephan,P., Xu,Y., Sweet,S.M., Thorne,A.W., Oliver,A.W. *et al.* (2016) PARP3 is a sensor of nicked nucleosomes and monoribosylates histone H2B(Glu2). *Nat. Commun.*, **7**, 12404.

LETTER

doi:10.1038/nature20790

XRCC1 mutation is associated with PARP1 hyperactivation and cerebellar ataxia

Nicolas C. Hoch[1,2]*, Hana Hanzlikova[1]*, Stuart L. Rulten[1], Martine Tétreault[3], Emilia Komulainen[1], Limei Ju[1], Peter Hornyak[1], Zhihong Zeng[1], William Gittens[1], Stephanie A. Rey[4], Kevin Staras[4], Grazia M. S. Mancini[5], Peter J. McKinnon[6], Zhao-Qi Wang[7], Justin D. Wagner[8], Care4Rare Canada Consortium†, Grace Yoon[9] & Keith W. Caldecott[1]

XRCC1 is a molecular scaffold protein that assembles multi-protein complexes involved in DNA single-strand break repair[1,2]. Here we show that biallelic mutations in the human *XRCC1* gene are associated with ocular motor apraxia, axonal neuropathy, and progressive cerebellar ataxia. Cells from a patient with mutations in *XRCC1* exhibited not only reduced rates of single-strand break repair but also elevated levels of protein ADP-ribosylation. This latter phenotype is recapitulated in a related syndrome caused by mutations in the XRCC1 partner protein PNKP[3–5] and implicates hyperactivation of poly(ADP-ribose) polymerase/s as a cause of cerebellar ataxia. Indeed, remarkably, genetic deletion of *Parp1* rescued normal cerebellar ADP-ribose levels and reduced the loss of cerebellar neurons and ataxia in *Xrcc1*-defective mice, identifying a molecular mechanism by which endogenous single-strand breaks trigger neuropathology. Collectively, these data establish the importance of XRCC1 protein complexes for normal neurological function and identify PARP1 as a therapeutic target in DNA strand break repair-defective disease.

A 47-year-old woman of East Indian descent and non-consanguineous parents was diagnosed at age 41 with cerebellar atrophy, gait and limb ataxia, ocular motor apraxia, and peripheral neuropathy (Fig. 1a, b). Prenatal and early development was completely normal; difficulties with balance and gait were first noticed at 28 years, but this was not fully investigated until age 40. Magnetic resonance imaging and cerebellar examination revealed progressive cerebellar atrophy (Fig. 1c) and multiple ataxic abnormalities including dysmetria, dysdiadochokinesis, and dysarthria; nerve conduction studies revealed chronic length-dependent sensory–motor (predominantly axonal) peripheral neuropathy (Fig. 1b and Supplementary Information). After ruling out more than ten known spinocerebellar ataxias by genetic and metabolic screening (Supplementary Information), exome sequencing of the proband identified compound heterozygous mutations in *XRCC1* (NM_006297). The mutations were confirmed by Sanger sequencing as c.1293G>C (p.K431N) and c.1393C>T (p.Q465*) and were present *in trans*, with the unaffected sibling of the proband heterozygous for c.1293G>C (Fig. 1d). Mutation c.1393C>T has not previously been described in the population, whereas c.1293G>C was previously detected in heterozygous state in four individuals of South Asian descent (ExAC Consortium). After ruling out other rare gene variants on the basis of their presence in the unaffected sibling, presence in the homozygous state in unaffected in-house controls and/or ExAC, and lack of functional and/or disease relevance, no other candidate causative mutations remained.

The c.1393C>T mutation is located within exon 12 and creates a premature stop codon at amino acid 465, most likely triggering nonsense-mediated messenger RNA (mRNA) decay. The c.1293G>C mutation is located at the end of exon 11 and is also part of the donor splice site for intron 11, most likely affecting splicing and inducing premature stop codons/nonsense-mediated decay and/or encoding XRCC1 with the missense mutation K431N. Consistent with this,

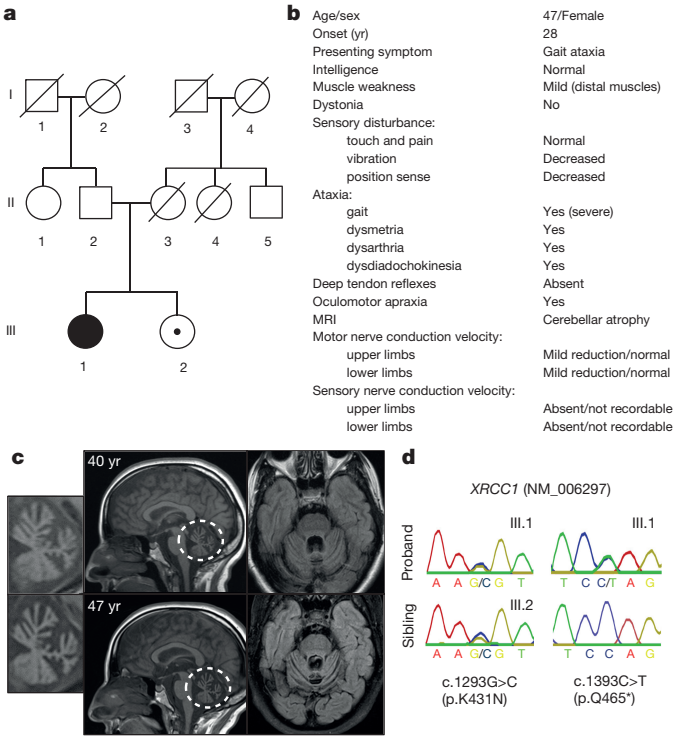

Figure 1 | XRCC1 mutations are associated with cerebellar ataxia, ocular motor apraxia, and axonal neuropathy. a, Pedigree of the proband (III.1; filled circle) and unaffected sibling (III.2; circle/filled dot). **b**, Proband clinical features (see Supplementary Information for full description). **c**, Proband magnetic resonance imaging at 40 and 47 years. Sagittal T_1-weighted images (middle) demonstrating vermian atrophy and axial fluid attenuated inversion recovery (FLAIR) images (right) demonstrating atrophy of the cortex of the vermis and cerebellar hemispheres. The cerebellum is circled and insets (left) are magnifications highlighting the cerebellar atrophy. **d**, Sanger sequencing confirming the mutations c.1293G>C (p.K431N) and c.1393C>T (p.Q465*) in the proband (III.1) and c.1293G>C (p.K431N) in the unaffected sibling (III.2).

[1]Genome Damage and Stability Centre, School of Life Sciences, University of Sussex, Falmer, Brighton BN1 9RH, UK. [2]CAPES Foundation, Ministry of Education of Brazil, Brasilia/DF 70040-020, Brazil. [3]Department of Human Genetics, McGill University and Genome Québec Innovation Centre, Montréal, Québec, H3A 0G4, Canada. [4]Neuroscience, School of Life Sciences, University of Sussex, Falmer, Brighton BN1 9QG, UK. [5]Department of Clinical Genetics, Erasmus MC, PO Box 2040, 3000 CA, Rotterdam, the Netherlands. [6]St. Jude Children's Research Hospital, Memphis, Tennessee 38105, USA. [7]Leibniz Institute for Age Research, Fritz Lipmann Institute, 1107745 Jena, Germany. [8]The Children's Hospital of Eastern Ontario Research Institute, Ottawa, K1L 8H1, Canada. [9]Division of Clinical and Metabolic Genetics, and Division of Neurology, The Hospital for Sick Children, University of Toronto, Toronto, M5G 1X8, Canada.
*These authors contributed equally to this work.
†Steering committee members and their affiliations appear at the end of the paper.

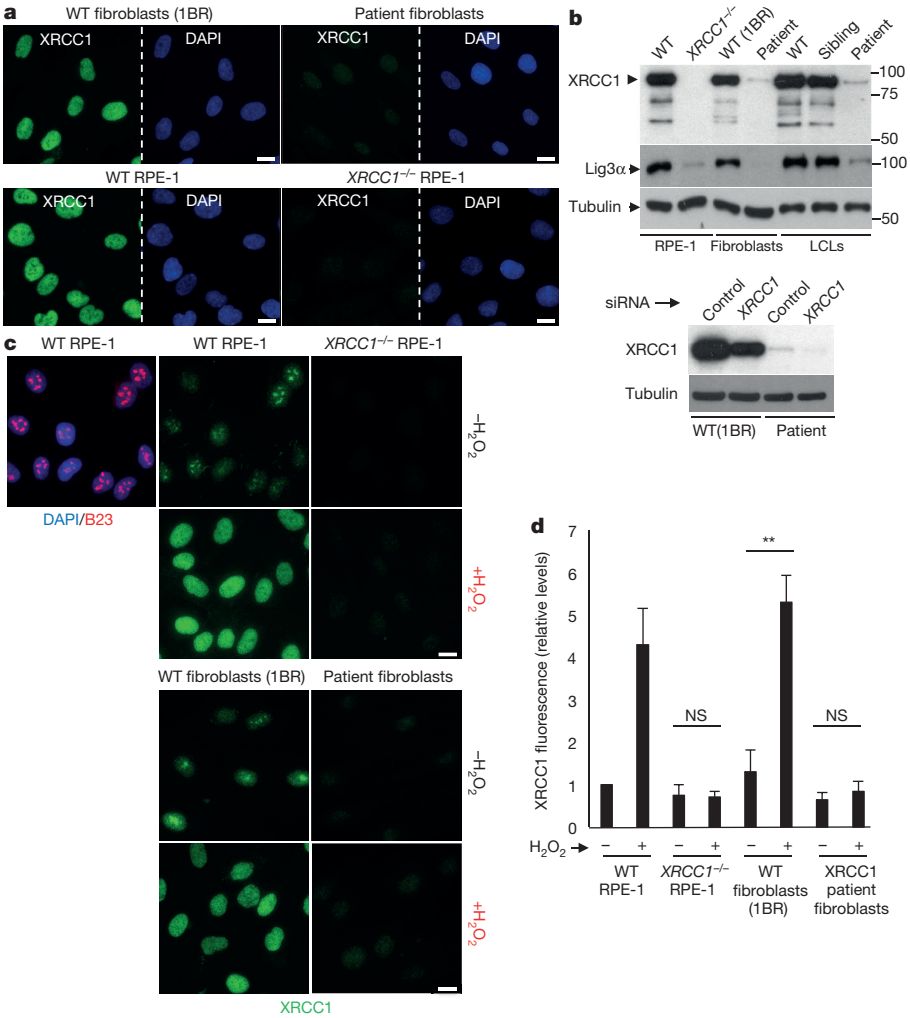

Figure 2 | Mutations in patient-derived XRCC1 reduce XRCC1 levels and recruitment into chromatin. a, XRCC1 levels measured by immunofluorescence in WT 1BR fibroblasts, WT RPE-1 cells, XRCC1-patient fibroblasts, and *XRCC1*$^{-/-}$ RPE-1 cells. **b**, Top: XRCC1 and Lig3α levels measured in the above cells by western blotting and additionally in WT, XRCC1-patient, and sibling LCLs. The source data are included in Supplementary Fig. 1. Bottom: WT or patient fibroblasts were transfected with non-targeting or *XRCC1* siRNA and immunoblotted as above. **c**, XRCC1 chromatin binding measured by immunofluorescence in the indicated cells before and 10 min after treatment with 1 mM H_2O_2. **d**, Quantification of XRCC1 in chromatin (excluding nucleoli) from more than 1,000 cells per sample using ScanR software. Data are the mean (± 1 s.d.) of three independent experiments. Statistical analysis (two-tailed *t*-test) is indicated (**$P < 0.01$; NS, not significant). Representative ScanR images are in Extended Data Fig. 3a. Scale bars, 10 μm.

reduced total levels of *XRCC1* mRNA were observed in patient-derived cells, as well as aberrant splicing of *XRCC1* transcripts if nonsense-mediated decay was inhibited with cycloheximide (Extended Data Fig. 1).

To establish the pathogenic impact of the biallelic *XRCC1* mutations, we examined patient-derived fibroblasts and lymphoblastoid cells (LCLs) for levels of XRCC1 protein by indirect immunofluorescence and western blotting. XRCC1 in patient primary fibroblasts was greatly reduced compared with wild-type (WT) primary human fibroblasts (1BR) by indirect immunofluorescence and was not measurably higher than in human RPE-1 cells in which *XRCC1* was deleted by clustered, regularly interspaced short palindromic repeats (CRISPR)-Cas9 (Fig. 2a). However, western blotting suggested that patient fibroblasts

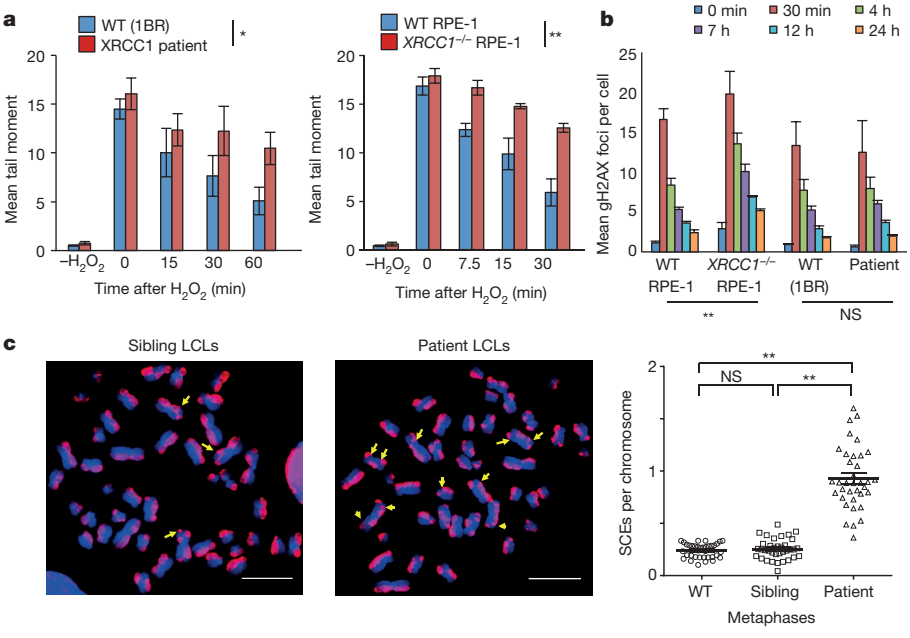

Figure 3 | Mutations in patient-derived XRCC1 reduce SSBR. a, DNA strand breaks quantified in the indicated fibroblasts (left) or RPE-1 cells (right) by alkaline comet assays before and at the indicated times after H_2O_2 treatment. Data are the mean (± s.e.m.) comet tail moments (an arbitrary-unit measure of DNA strand breaks) of three independent experiments. Statistical analyses (two-way analysis of variance) are indicated (*$P < 0.05$; **$P < 0.01$). **b**, Double-strand breaks quantified as γ-H2AX foci in the indicated cell lines before and at the indicated times after ionizing radiation (2 Gy). Data are the mean γ-H2AX foci per cell (± 1 s.d.) from three independent experiments (~1,000 cells per sample per experiment). Statistical analysis as above. Representative images are in Extended Data Fig. 4. **c**, Frequencies of sister chromatid exchange per chromosome (mean ± 1 s.e.m.) quantified in control and XRCC1-patient LCLs (36 metaphases per genotype). Representative metaphases (arrows, sister chromatid exchanges) are shown, left. Statistical analysis, two-tailed *t*-test (**$P < 0.01$; NS, not significant). Scale bars, 10 μm.

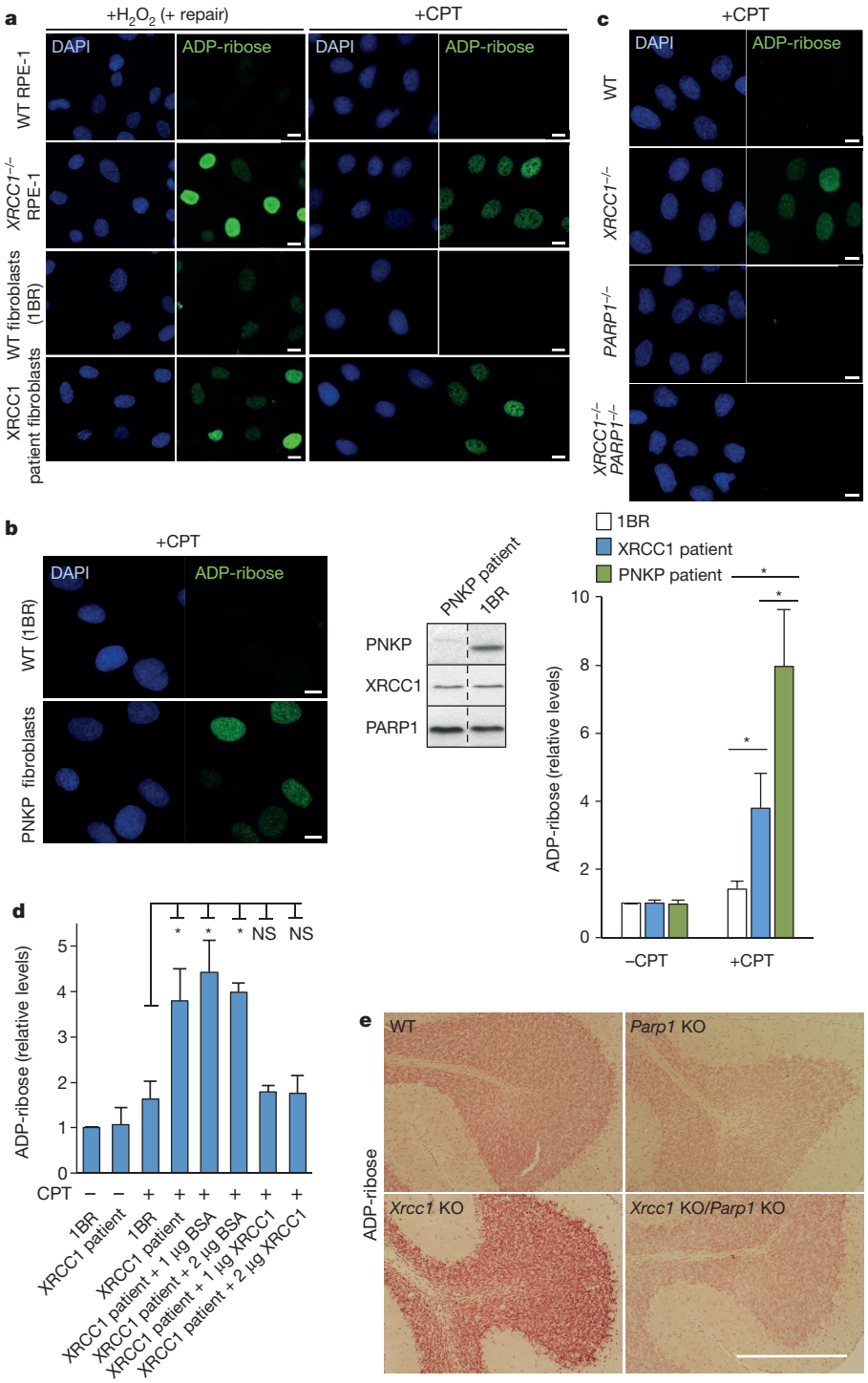

Figure 4 | XRCC1 mutation elevates ADP-ribosylation in cells and cerebellum. a, ADP-ribosylation in WT 1BR fibroblasts, WT RPE-1 cells, XRCC1-patient fibroblasts, and *XRCC1*$^{-/-}$ RPE-1 cells after H_2O_2 or CPT treatment. **b**, Left: ADP-ribosylation levels in 1BR or PNKP-patient fibroblasts after CPT treatment. Middle: PNKP, XRCC1, and PARP1 levels in 1BR and PNKP-patient fibroblasts. The source data are included in Supplementary Fig. 1. Right: ADP-ribose levels quantified by ScanR imaging in 1BR, XRCC1-patient, and PNKP-patient fibroblasts before and after CPT treatment. Data are mean (± 1 s.d.) ADP-ribose levels (relative to untreated 1BR cells) from three independent experiments (>1,000 cells per sample). Statistically significant differences (two-tailed *t*-test) are indicated (*$P < 0.05$). **c**, ADP-ribosylation levels in the indicated RPE-1 cells after CPT treatment. **d**, ADP-ribosylation levels quantified by ScanR imaging before and after CPT treatment in 1BR and XRCC1-patient fibroblasts with or without transfection with 1 or 2 μg of bovine serum albumin (BSA) or recombinant human XRCC1 protein. Statistical analyses as above. Representative ScanR images are in Extended Data Fig. 8. **e**, ADP-ribosylation levels measured by immunohistochemistry in cerebellar sections from WT mice or mice deleted (knockout, 'KO') of *Xrcc1* and/or *Parp1*. Scale bars in immunofluorescence images are 10 μm and in histology images are 1 mm.

and LCLs both retained a small amount (~5%) of residual XRCC1 (Fig. 2b and Extended Data Fig. 2a). Indeed, this was confirmed using *XRCC1* short interfering RNA (siRNA), which reduced the anti-XRCC1 signal on western blots of patient fibroblasts even further (Fig. 2b, bottom). Levels of DNA ligase IIIα (Lig3α) were also greatly reduced (by >80%) in patient cells, consistent with the established impact of XRCC1 on the cellular stability of this partner protein[6,7] (Fig. 2b, top, and Extended Data Fig. 2b). Since germ-line deletion of *Xrcc1* in mouse is embryonic lethal[8], we suggest that the small amount of XRCC1 remaining in the patient was important for embryonic viability. Consistent with this idea, embryonic viability in mice is supported by as little as approximately 10% of normal Xrcc1 levels[9].

To determine whether the residual XRCC1 in patient cells can engage in single-strand break repair (SSBR), we quantified the extent to which it bound oxidized chromatin. XRCC1 was primarily detected in nucleoli in undamaged WT RPE-1 cells and normal primary 1BR fibroblasts, after the extraction of soluble proteins with detergent, but was rapidly recruited into global nuclear chromatin after treatment with H_2O_2 (Fig. 2c, d), a physiological source of oxidative single-strand breaks (SSBs)[10]. By contrast, little or no XRCC1 recruitment into chromatin was detected in XRCC1-patient fibroblasts by high-resolution or high-content imaging (Fig. 2c, d and Extended Data Fig. 3a). Similar results were observed after treatment with camptothecin (CPT), a topoisomerase poison that induces SSBs triggered by abortive topoisomerase I activity (Extended Data Fig. 3b).

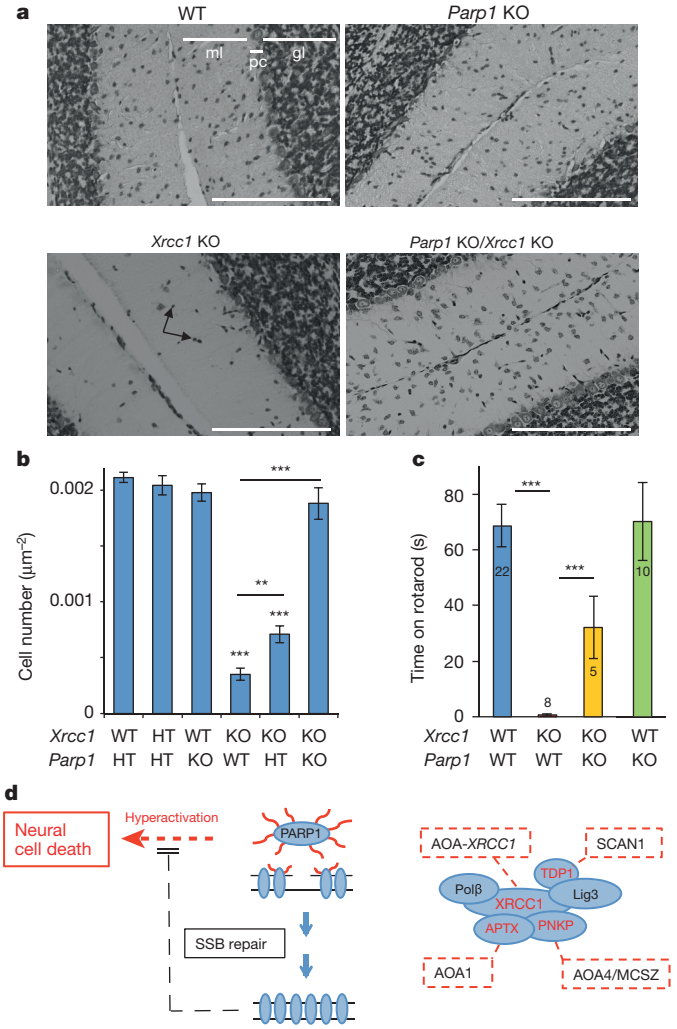

Figure 5 | Parp1 deletion restores normal interneuron density and reduces cerebellar ataxia in *Xrcc1*$^{Nes\text{-}Cre}$ mice. a, Representative cerebellar sections from WT mice or mice deleted ('KO') of *Xrcc1* and/or *Parp1* stained with Nissl to detect neurons. Scale bars, 200 μm. Abbreviations: gl, granule layer; ml, molecular layer; pc, Purkinje cells. Black arrows indicate interneurons. **b**, Interneuron density in the molecular layer of cerebella of the indicated genotype. Data are the mean (± s.e.m.) Nissl-positive cells per square micrometre of 5–10 mice per genotype. Indicated are *t*-test comparisons (**$P < 0.01$; ***$P < 0.001$). **c**, Motor coordination in mice of the indicated genotype measured on a rotarod (mouse numbers analysed indicated in/above the bars). Statistical tests as above. **d**, Model for PARP1 hyperactivation and neural death triggered by unrepaired SSBs. PARP1 activation at SSBs triggers auto- and trans-protein ADP-ribosylation (red wavy lines). XRCC1 binds poly(ADP-ribose) and assembles SSBR protein complexes. Mutated XRCC1 or partner proteins cause delayed SSBR and PARP1 hyperactivation, resulting in cytotoxic levels of poly (ADP-ribose) and/or NAD^+ depletion. SSBR proteins and their associated cerebellar ataxias are highlighted/boxed in red. SCAN1, spinocerebellar ataxia with axonal neuropathy-1 (TDP1-mutated); AOA1, ataxia oculomotor apraxia-1 (APTX-mutated); AOA4, ataxia oculomotor apraxia-4 (PNKP-mutated); AOA-XRCC1, ataxia oculomotor apraxia-*XRCC1* mutated[18].

Importantly, the defect in XRCC1 recruitment in patient fibroblasts was accompanied by a delay in the kinetics of DNA SSBR after H_2O_2 treatment (Fig. 3a). This phenotype was recapitulated in *XRCC1*$^{-/-}$ RPE-1 cells and is consistent with the established molecular role of XRCC1 (ref. 2). By contrast, we failed to detect a major difference in double-strand break repair in XRCC1-patient fibroblasts, as measured by γ-H2AX immunostaining after ionizing radiation (Fig. 3b and Extended Data Fig. 4). In agreement with the defect in SSBR, XRCC1-patient LCLs exhibited a fourfold increase in sister chromatid exchange, a hyper-recombination phenotype resulting from elevated homologous recombination triggered by unrepaired SSBs in the S/G2 phase of the cell cycle[11] (Fig. 3c).

XRCC1 is a scaffold protein that assembles SSBR multi-protein complexes. Importantly, components of these complexes are mutated in the cerebellar ataxias spinocerebellar ataxia with axonal neuropathy-1 (SCAN1; mutated in TDP1)[12,13], ataxia oculomotor apraxia-1 (AOA1; mutated in aprataxin)[14], and ataxia oculomotor apraxia-4 (AOA4; mutated in PNKP)[3,4]. Indeed, it is striking that patients with the *XRCC1* mutation combine features of each of these diseases, consistent with the role played by XRCC1 in coordinating their activity. The discovery that XRCC1 is itself mutated in cerebellar ataxia is thus notable because it demonstrates the importance of these complexes in preventing neurodegeneration in humans.

To investigate the mechanism(s) by which unrepaired SSBs trigger neuropathology, we considered the possibility that persistent unrepaired SSBs might result in prolonged activity of the SSB sensor protein PARP1. This hypothesis was prompted by the observation that excessive synthesis of poly(ADP-ribose) and/or excessive depletion of NAD^+ by PARP1 is neurotoxic and associated with ischaemia reperfusion injury[15,16]. Consistent with this idea, while ADP-ribose was rapidly detected in both WT and patient fibroblasts after H_2O_2 treatment, it persisted at a higher level in the latter cells during subsequent incubation in drug-free medium (Fig. 4a, left). This was also evident in *XRCC1*$^{-/-}$ human RPE-1 cells, confirming that this phenotype was induced by loss of XRCC1. Elevated ADP-ribose levels were also detected in XRCC1-patient fibroblasts and *XRCC1*$^{-/-}$ RPE-1 cells after treatment with CPT (Fig. 4a, right). Indeed, the difference in ADP-ribose levels between WT and *XRCC1*-mutant cells was even greater after CPT than after H_2O_2 treatment. The type of SSB induced by CPT has been linked previously with SSBR-defective neurodegenerative disease and is a possible source of pathogenic SSBs in SSBR-defective individuals[13,17]. Consistent with this idea, CPT-induced ADP-ribose levels were also elevated in fibroblasts from a patient with ataxia oculomotor apraxia-4 (AOA4); the cerebellar ataxia resulting from mutation of the XRCC1 protein partner, PNKP (Fig. 4b and Extended Data Fig. 5). Importantly, the elevated ADP-ribose observed in CPT-treated *XRCC1*$^{-/-}$ RPE-1 cells, XRCC1-patient cells, and PNKP-patient cells was entirely dependent on PARP1 activity (Fig. 4c and Extended Data Figs 6 and 7). Moreover, this phenotype was rescued by introducing WT recombinant XRCC1 into XRCC1-patient fibroblasts by electroporation (Fig. 4d and Extended Data Fig. 8).

Next, to examine directly whether hyperactive PARP1 triggers cerebellar ataxia in the absence of efficient SSBR, we used a mouse model in which Xrcc1 was conditionally deleted in brain (*Xrcc1*$^{Nes\text{-}Cre}$)[7]. *Xrcc1*$^{Nes\text{-}Cre}$ mice exhibit pronounced cerebellar histopathology including increased apoptosis of cerebellar granule neurons, greatly reduced numbers of cerebellar interneurons, and decreased electrophysiological spike activity in Purkinje cells (ref. 4 and Extended Data Fig. 9). Moreover, consistent with the pathology of the patient with the *XRCC1* mutation and other SSBR-defective patients, *Xrcc1*$^{Nes\text{-}Cre}$ mice exhibit cerebellar ataxia[7]. Strikingly, we detected elevated levels of ADP-ribose in the cerebellum of *Xrcc1*$^{Nes\text{-}Cre}$ mice, suggesting that the loss of Xrcc1 can trigger Parp1 hyperactivation in the brain even at endogenous levels of SSBs (Fig. 4e). Indeed, the deletion of Parp1 ablated both the elevated level of ADP-ribose and the characteristic loss of cerebellar interneurons in *Xrcc1*$^{Nes\text{-}Cre}$ mice, thereby increasing neuronal density in the molecular layer approximately fourfold to WT levels (Fig. 5a, b). This did not reflect an impact of Parp1 deletion on the rate of SSBR because the latter was similarly slow in *XRCC1*$^{-/-}$ and *XRCC1*$^{-/-}$/*PARP1*$^{-/-}$ RPE-1 cells (Extended Data Fig. 10). Rather, these data demonstrate that in the absence of Xrcc1-dependent SSBR Parp1 is hyperactivated, resulting in the loss and/or dysfunction of cerebellar neurons. Finally, to examine whether Parp1 deletion also rescued the cerebellar ataxia observed in *Xrcc1*$^{Nes\text{-}Cre}$ mice, we

compared *Xrcc1*$^{Nes\text{-}Cre}$ and *Xrcc1*$^{Nes\text{-}Cre}$/*Parp1*$^{-/-}$ mice for their performance on an accelerating rotarod. Indeed, remarkably, whereas *Xrcc1*$^{Nes\text{-}Cre}$ mice were profoundly ataxic and unable to remain on the rotarod for more than a few seconds, the additional deletion of Parp1 improved the rotarod performance of *Xrcc1*$^{Nes\text{-}Cre}$ mice more than 30-fold, increasing their mean retention time to approximately 30 s (Fig. 5c).

Collectively, these data identify elevated ADP-ribose levels as a biomarker of PARP1 hyperactivity and as a cause of cerebellar ataxia induced by unrepaired SSBs (Fig. 5d). This scenario might also extend to other more common neurodegenerative diseases because elevated levels of oxidative stress and DNA strand breakage are also implicated in disorders such as Alzheimer disease, Huntington disease, and Parkinson disease[17–19]. Intriguingly, patients with mutations in the XRCC1 partner protein PNKP exhibit not only ataxia but also microcephaly and seizures, and we have more recently identified a patient with rare, possibly pathogenic mutations (<0.01% allele frequency and not present in ExAC in homozygous state) in XRCC1 who exhibits this same combination of phenotypes[3–5]. Notably, *Xrcc1*$^{Nes\text{-}Cre}$ mice also present with seizures, raising the prospect that PARP1 hyperactivation may induce not only ataxia, but also more severe pathologies.

Finally, these data identify PARP1 as a possible drug target for treating cerebellar ataxias associated with unrepaired SSBs. Inhibition of PARP1 with currently available chemical inhibitors may not be useful in this context, however, because these inhibitors 'trap' PARP1 on DNA[20] and do not mimic PARP1 genetic deletion (Extended Data Fig. 10). However, the development of selective inhibitors of PARP1 that prevent DNA binding by this enzyme may have substantial therapeutic potential.

Online Content Methods, along with any additional Extended Data display items and Source Data, are available in the online version of the paper; references unique to these sections appear only in the online paper.

Received 27 May 2016; accepted 15 November 2016.
Published online 21 December 2016.

1. Caldecott, K. W. Single-strand break repair and genetic disease. *Nature Rev. Genet.* **9,** 619–631 (2008).
2. Caldecott, K. W. XRCC1 and DNA strand break repair. *DNA Repair (Amst.)* **2,** 955–969 (2003).
3. Shen, J. *et al.* Mutations in PNKP cause microcephaly, seizures and defects in DNA repair. *Nature Genet.* **42,** 245–249 (2010).
4. Bras, J. *et al.* Mutations in PNKP cause recessive ataxia with oculomotor apraxia type 4. *Am. J. Hum. Genet.* **96,** 474–479 (2015).
5. Poulton, C. *et al.* Progressive cerebellar atrophy and polyneuropathy: expanding the spectrum of PNKP mutations. *Neurogenetics* **14,** 43–51 (2013).
6. Caldecott, K. W., Tucker, J. D., Stanker, L. H. & Thompson, L. H. Characterization of the XRCC1-DNA ligase III complex *in vitro* and its absence from mutant hamster cells. *Nucleic Acids Res.* **23,** 4836–4843 (1995).
7. Lee, Y. *et al.* The genesis of cerebellar interneurons and the prevention of neural DNA damage require XRCC1. *Nature Neurosci.* **12,** 973–980 (2009).
8. Tebbs, R. S. *et al.* Requirement for the Xrcc1 DNA base excision repair gene during early mouse development. *Dev. Biol.* **208,** 513–529 (1999).
9. Tebbs, R. S., Thompson, L. H. & Cleaver, J. E. Rescue of Xrcc1 knockout mouse embryo lethality by transgene-complementation. *DNA Repair (Amst.)* **2,** 1405–1417 (2003).
10. Bradley, M. O. & Kohn, K. W. X-ray induced DNA double strand break production and repair in mammalian cells as measured by neutral filter elution. *Nucleic Acids Res.* **7,** 793–804 (1979).
11. Dillehay, L. E., Thompson, L. H., Minkler, J. L. & Carrano, A. V. The relationship between sister-chromatid exchange and perturbations in DNA replication in mutant EM9 and normal CHO cells. *Mutat. Res.* **109,** 283–296 (1983).
12. Takashima, H. *et al.* Mutation of TDP1, encoding a topoisomerase I-dependent DNA damage repair enzyme, in spinocerebellar ataxia with axonal neuropathy. *Nature Genet.* **32,** 267–272 (2002).
13. El-Khamisy, S. F. *et al.* Defective DNA single-strand break repair in spinocerebellar ataxia with axonal neuropathy-1. *Nature* **434,** 108–113 (2005).
14. Moreira, M. C. *et al.* The gene mutated in ataxia-ocular apraxia 1 encodes the new HIT/Zn-finger protein aprataxin. *Nature Genet.* **29,** 189–193 (2001).
15. Eliasson, M. J. *et al.* Poly(ADP-ribose) polymerase gene disruption renders mice resistant to cerebral ischemia. *Nature Med.* **3,** 1089–1095 (1997).
16. Chiarugi, A. Poly(ADP-ribose) polymerase: killer or conspirator? The 'suicide hypothesis' revisited. *Trends Pharmacol. Sci.* **23,** 122–129 (2002).
17. Katyal, S. *et al.* Aberrant topoisomerase-1 DNA lesions are pathogenic in neurodegenerative genome instability syndromes. *Nature Neurosci.* **17,** 813–821 (2014).
18. Marras, C. *et al.* Nomenclature of genetic movement disorders: recommendations of the International Parkinson and Movement Disorder Society task force. *Mov. Disord.* **31,** 436–457 (2016).

Supplementary Information is available in the online version of the paper.

Acknowledgements This work was funded by MRC Programme Grants (MR/J006750/1 and MR/P010121/1) to K.W.C., a 'Science without Borders' postdoctoral fellowship (CAPES Foundation, Ministry of Education, Brazil, BEX9769-13-7) to N.H., and funding to G.Y. from Genome Canada, the Canadian Institutes of Health Research, the Ontario Genomics Institute, Ontario Research Fund, Genome Quebec, the Children's Hospital of Eastern Ontario Foundation, and the Hospital for Sick Children. K.S. was funded by the BBSRC grant BB/K019015/1 and P.J.M. acknowledges the National Institutes of Health (NS-37956, CA-21765), the CCSG (P30 CA21765), and the American Lebanese and Syrian Associated Charities of St. Jude Children's Research Hospital for support. We thank the patient and her family for their contribution to this study. This work was selected for study by the Care4Rare Canada (Enhanced Care for Rare Genetic Diseases in Canada) Consortium Gene Discovery Steering Committee (for committee members, see below). We thank D. Dyment for his advice and discussion. We thank S. van der Velde-Visser and J. Schuurs-Hoeijmakers for Epstein-Barr virus transformation of the patient's and sibling's LCLs. We also thank S. El-Khamisy and A. Ridley for preliminary analyses and assistance with the mouse work.

Author Contributions H.H. generated gene-edited RPE-1 cell lines and designed and conducted the immunofluorescence, high-content imaging (Olympus ScanR), protein complementation, and double-strand break repair experiments. N.H. analysed XRCC1-patient cells by western blotting and RT-qPCR and designed and conducted sister chromatid exchange and comet assays. S.L.R., E.K., and L.J. designed and conducted mouse behaviour and histopathology experiments. S.R. and K.S. designed and conducted electrophysiology experiments. P.H. prepared recombinant XRCC1. Z.Z. generated CRISPR guide constructs. W.G. conducted preliminary CPT/ADP-ribose experiments. G.M.S.M. provided PNKP-patient fibroblasts. P.J.M. and Z.-Q.W. provided mouse models. G.Y. identified and oversaw genetic analysis of the patient, and J.W. and M.T. conducted exome analysis. K.W.C. conceived and managed the project, and wrote the manuscript with H.H. and N.H. All authors edited the manuscript.

Author Information Reprints and permissions information is available at www.nature.com/reprints. The authors declare no competing financial interests. Readers are welcome to comment on the online version of the paper. Correspondence and requests for materials should be addressed to K.W.C. (k.w.caldecott@sussex.ac.uk) or G.Y. (grace.yoon@utoronto.ca).

Care4Rare Canada Consortium

Gene Discovery Steering Committee members are:
Kym Boycott[1], Alex MacKenzie[1], Jacek Majewski[2], Michael Brudno[3], Dennis Bulman[1] & David Dyment[1]

[1]The Children's Hospital of Eastern Ontario Research Institute, Ottawa, Ontario K1L 8H1, Canada. [2]Department of Human Genetics, McGill University and Genome Québec Innovation Centre, Montréal, Québec H3A 0G4, Canada. [3]Program in Genetics and Genome Biology and the Centre for Computational Medicine, The Hospital for Sick Children, Toronto, Ontario M5G 0A4, Canada.

METHODS

Whole-exome sequencing. Whole-exome library preparation, exon capture, and sequencing were performed at the Genome Québec Innovation Center (Montréal, QC, Canada) as previously described[19]. Genomic DNA was captured using the SureSelect Human 50Mb All Exon kit v5 (Agilent Technologies, Santa Clara, California, USA). Sequencing was performed on an Illumina HiSeq2000 (Illumina, San Diego, California, USA) with paired-end 100-base-pair (bp) reads. A mean coverage of 137× was obtained and 97% of the bases were covered at more than 10×. Read alignment, variant calling, and annotations were done with a pipeline on the basis of BWA, SAMtools, Annovar, and custom annotation scripts. All sequences were aligned to Human genome Hg19. We excluded variants with minor allele frequency greater than 5% in either the 1000 Genomes Project (http://browser.1000genomes.org/index.html) or the 6500 NHLBI EVS (http://evs.gs.washington.edu/EVS), and seen in more than 30 samples from our in-house database (containing approximately 2,000 samples). The whole-exome sequencing data were further filtered to keep protein-damaging variants (nonsense, missense, frameshift, indel, and splice variants).

Antibodies and chemicals. The antibodies used in this study were anti-XRCC1 rabbit polyclonal (Millipore; ABC738), anti-Lig3α (TL25) rabbit polyclonal[20], anti-PNKP (SK3195) rabbit polyclonal[21], rabbit Fc-fused Anti-pan-ADP-ribose binding reagent (Millipore; MABE1016), anti-poly(ADP-ribose) rabbit polyclonal (Trevigen; 4336), anti-α-tubulin rat polyclonal (Abcam; ab6160), anti-BrdU rat monoclonal, crossreacting with CldU, (BioRad; OBT0030G), anti-nucleophosmin (B23) mouse monoclonal (Invitrogen; 325200), anti-PARP1 mouse monoclonal (Serotec; MCA1522G), and anti-γ-H2AX mouse monoclonal (Millipore; 05-636). The secondary antibodies used for western blotting were HRP-conjugated goat anti-rabbit (Bio-Rad; 170-6515), goat anti-mouse (Bio-Rad; 170-6516), and rabbit anti-rat (Abcam; ab6734); and for indirect immunofluorescence they were goat anti-mouse or anti-rabbit Alexa 488 (Invitrogen; A11001 and A31628), goat anti-rabbit Alexa 568 (Invitrogen; A11036), donkey anti-mouse Alexa 647 (Invitrogen; A39571), and goat anti-rat Alexa 568 (Invitrogen; A11077). CPT was purchased from Sigma and H_2O_2 was obtained from Fischer Scientific. Veliparib (ABT-888) was purchased from Selleckchem and KU0058948 hydrochloride from Axon.

Cell lines. All cell lines were tested for the absence of mycoplasma. WT human hTERT RPE-1 cells (ATCC; CRL4000) (denoted 'RPE-1' for simplicity) and their *XRCC1*$^{-/-}$ derivative (*XRCC1*$^{-/-}$ RPE-1 cells) were cultured in Dulbecco's modified Eagle's medium (DMEM/F12; Sigma) supplemented with 10% fetal calf serum and 0.01 mg/ml hygromycin B in a humidified atmosphere of 5% CO_2 at 37 °C. WT control cells were 1BR3 (denoted 1BR in the text for simplicity) primary human fibroblasts and the lymphoblastoid cell line (LCL) 11-27 isolated from a normal, unaffected control. XRCC1-patient primary fibroblasts (identifier number 5596502b) were generated from a patient's skin biopsy and the LCL cell lines HEP15-00082 and HEP15-00083 were obtained from fresh blood from, respectively, the unaffected sibling and affected patient by Epstein-Barr virus transformation. Appropriate patient consent was provided for preparation of primary fibroblasts. Primary human fibroblasts from a *PNKP*-mutated patient with cerebellar ataxia have been described previously[5]. Primary human fibroblasts were grown in Minimum Essential Media (MEM; Gibco) containing 15% fetal calf serum, 2 mM glutamine, and the antibiotics penicillin (100 units/ml) and streptomycin (100 μg/ml) at low oxygen (5%) at 37 °C. LCLs were cultured in RPMI medium (Gibco) containing 10% FBS, 2 mM glutamine and penicillin/streptomycin, in a humidified atmosphere of 5% CO_2 at 37 °C.

Generation of gene-edited RPE-1 cells. Guide sequences were identified using either E-CRISP (http://www.e-crisp.org/E-CRISP/) or CRISPRdirect (http://crispr.dbcls.jp). For *XRCC1* gene editing we chose the 23-base CRISPR complementary guide RNA sequences 5′-CCGCCUCCGCCAUGUCGUGUCCU-3′ and 5′-AGGGACACGACAUGGCGGAGGCGG-3′ (PAM underlined) spanning *XRCC1* ORF nucleotides 12–34, and used the 58-base synthetic oligonucleotides (XCr2F; 5′-TTTCTTGGCTTTATATATCTTGTGGAAAGGACGAAACACCGACACGACATGGCGGAGG and XCr2R; 5′-GACTAGCCTTATTTTAACTTGCTATTTCTAGCTCTAAAACCCTCCGCCATGTCGTGTC) (Eurofins) encoding 18 bp Tru-guide[22] versions of the guide (underlined) minus the PAM. For *PARP1* gene editing we chose the 22-base 'Tru-guide' sequences 5′-GAAGGUGGGCCACUCCAUCCGG-3′ and 5′-CCGGAUGGAGUGGCCCACCUUC-3′ (PAM underlined) spanning nucleotides 174–195 of the human *PARP1* ORF, and used the 59-base synthetic oligonucleotides (PARP1-4F: 5′-TTTCTTGGCTTTATATATCTTGTGGAAAGGACGAAACACCGAAGGTGGGCCACTCCATC-3′ and PARP1-4R: 5′-GACTAGCCTTATTTTAACTTGCTATTTCTAGCTCTAAAACGATGGAGTGGCCCACCTTC-3′) encoding the 19 bp Tru-guide versions of the guide (underlined) minus the PAM.

The relevant oligonucleotide guide pairs were annealed and extended into a 98-base oligonucleotide duplexes using Phusion polymerase (NEB) and then subcloned into the guide RNA vector (Addgene 41824)[23] using Gibson Assembly (NEB). hTERT RPE-1 cells were co-transfected with the relevant guide construct/s separately (*XRCC1*$^{-/-}$, *PARP1*$^{-/-}$) or together (*XRCC1*$^{-/-}$/*PARP1*$^{-/-}$) and with the Cas9 expression construct Addgene 41815 (ref. 23) using a NEON Transfection System (Invitrogen). Twenty-four hours later, the transfected cells were selected in medium containing 0.5 mg/ml G418 for 5 days and subcloned into 96-well plates. Once at sufficient cell density, the subclones were analysed for expression of the relevant protein/s by indirect immunofluorescence. Absence of the relevant protein/s in selected clones was then confirmed by western blotting. For *XRCC1*$^{-/-}$, *PARP1*$^{-/-}$, and *XRCC1*$^{-/-}$/*PARP1*$^{-/-}$ RPE-1 cells, we selected clones 3, G7, and D1 for further work, respectively.

Complementation of XRCC1-patient cells with recombinant XRCC1 protein. Recombinant human XRCC1 harbouring a carboxy (C)-terminal decahisitidine tag (denoted XRCC1-His) was expressed in *Escherichia coli* from pET16b-XH and purified by metal-chelate affinity chromatography and gel filtration[6]. Control BSA (1 or 2 μg) or purified XRCC1-His was electroporated into 1×10^5 XRCC1-patient fibroblasts using a NEON Transfection System (Invitrogen) according to the manufacturer's protocol. Eighteen hours later the cells were treated with CPT for 45 min, fixed, and immunostained for levels of XRCC1 and ADP-ribose as indicated.

RNA extraction, cDNA synthesis, and qPCR analysis. LCLs were treated with either 100 μg/ml cycloheximide (Sigma) or vehicle alone for 4 h and total RNA extracted with RNAeasy Kit (Qiagen) essentially as described by the manufacturer but with an additional 15 min DNase I (Promega) digest of the samples on the column. 1 μg total RNA was annealed to oligodT(15) primer and reverse transcribed using M-MuLV RT (NEB) for 2 h at 42 °C. After RNase A digest, the cDNA was purified using PCR purification kit (Qiagen) and 1/40 of the eluate used per reaction. Three replicate qPCR reactions using ABsolute qPCR SYBR Low ROX (Thermo) were performed per experiment in a MX3005P (Agilent) thermocycler and analysed using MxPro software (Agilent). The fold change was calculated from cycle threshold (ΔC_t) values relative to actin and $\Delta\Delta C_t$ values relative to WT untreated for three independent experiments. Primers were as follows: XRCC1 exon10 forward, CAACACCCCCAAGTACAGC; XRCC1 exon 10 reverse, AGTCCAGCACCCACTCCTTAC; XRCC1 exon11 forward, TCCAGCAGTGAGGAGGATG; XRCC1 intron11 reverse, AGGCAAGAGTGGGAAGTTTG; XRCC1 exon 12 reverse, AGTGGGCTTGGTTTTGGTC; actin forward, CTCGTCATACTCCTGCTTGC; actin reverse, GAAGTGTGACGTGGACATCC.

XRCC1 cDNA cloning. cDNA prepared as above from patient cells treated with cycloheximide was used for Phusion polymerase (NEB) amplification of full-length XRCC1 transcripts using primers ATGCCGGAGATCCGCCTCCG and GGCTTGCGGCACCACCCCAT. PCR products were purified using Gel extraction kit (Qiagen), cloned using TOPO cloning kit (Thermo Fischer Scientific) and plasmids originating from single colonies purified using Miniprep kit (Qiagen) and sequenced by Sanger sequencing (Beckman Coulter).

siRNA. WT and patient primary fibroblasts were reverse-transfected with Lipofectamine RNA iMAX (Life Technologies) as indicated by the manufacturer, using non-targeting siRNA (ON-TARGETplus, Dharmacon) and siXRCC1 SMARTpool (Dharmacon).

Western blotting. PBS-washed cells were lysed in Laemmli buffer, heated for 10 min at 95 °C, and sonicated for 30 s using Bioruptor Pico (Diagenode). Protein concentrations were determined using the BCA assay (Pierce). Samples were subjected to SDS–PAGE, proteins transferred onto nitrocellulose membrane and detected by immunoblotting using the relevant primary and horseradish peroxidase-conjugated secondary antibodies. Peroxidase activity was detected by ECL reagent (GE Healthcare) and Amersham Hyperfilm ECL (GE Healthcare). Non-saturated film exposures were digitalized using an EPSONperfection 2400 photo scanner and quantified using ImageJ software.

Immunofluorescence and microscopy. Cells cultured on glass coverslips were fixed in 4% paraformaldehyde for 10 min at room temperature, permeabilized in methanol/acetone solution (1:1), blocked in 10% fetal calf serum, and incubated with primary antibodies for 60 min at room temperature. Following rinsing in PBS, coverslips were incubated with secondary antibodies at room temperature for 60 min. Finally, after washing in PBS, nuclei were counterstained with DAPI (Sigma) and coverslips mounted using anti-fading mounting reagent (Vectashield, Vector Laboratories). To measure chromatin retention of proteins, cells were pre-extracted in cold 0.2% Triton X-100 for 2 min on ice before fixation as above. High-resolution microscopy of fixed samples was performed on a Zeiss AxioObserver.Z1 microscope, equipped with oil immersion objectives (Plan-Apochromat 63×/1.4 and 100×/1.4), Hamamatsu ORCA-Flash4.0 LT camera and ZEN 2 core imaging software. Automated wide-field microscopy was performed on an Olympus ScanR system (motorized IX83 microscope) with ScanR Image Acquisition and Analysis Software, 20×/0.45 (LUCPLFLN 20× PH) and 40×/0.6

(LUCPLFLN 40× PH) dry objectives and Hamamatsu ORCA-R2 digital CCD camera C10600.

ADP-ribosylation. Levels of ADP-ribosylation were measured in the indicated cell lines by indirect immunofluorescence using Anti-pan-ADP-ribose binding reagent (Millipore). Cells were treated where indicated with 150 μM H_2O_2 for 10 min and then incubated in drug-free medium for 60 min to allow DNA repair or were incubated with 30 μM CPT for 45 min. ADP-ribose levels were quantified by Olympus ScanR imaging and plotted relative to the ADP-ribose level in untreated cells. For cerebellar sections, postnatal day ((P)17–P23) mice were anaesthetized using 0.2 mg/g Euthanal (Vetoquinol UK) and perfused transcardially with PBS followed by 4% paraformaldehyde. Brains were postfixed in 4% paraformaldehyde for 48 h and stored in 25% sucrose/PBS until moulding and freezing. Sagittal sections (7 μm) were prepared using a cryostat (Leica CM1850) and immunohistochemistry was conducted essentially as described[7]. Briefly, slides were washed in PBS and heated until boiling in antigen retrieval buffer (Nacalai Tesque, Histo VT One). Endogenous peroxidase was blocked by incubating slides in 0.6% H_2O_2 in methanol. After incubating in blocking solution (5% goat serum, 1% BSA, 0.4% Triton-X-100 in PBS) rabbit anti-poly(ADP-ribose) primary antibody (Trevigen) was applied overnight. Anti-rabbit Biotin-SP-conjugated AffiniPure Goat secondary antibody (JacksonImmuno Research, 1:500) was incubated on the slides for 1 h followed by ABC reagent (Vectastain Elite ABC kit, Vector Laboratories) according to the manufacturer's instructions. The chromogen was developed using VIP reagent (Vector VIP peroxide substrate kit, Vector Laboratories; SK-4600). Images were obtained using a Nikon Eclipse E400 mounted with Electronic Digital Eyepiece Camera CMOS (C-mount UK).

Sister chromatid exchanges. Lymphoblastoid cell lines were incubated in medium containing 8 μM chlorodeoxyuridine, 32 μM thymidine, 10 μM fluorodeoxyuridine, and 200 μM cytidine (such that 20% of incorporated thymidine was replaced with chlorodeoxyuridine)[11,24] for 20 h, washed twice in media, and then allowed to grow for another 20 h in medium containing 10 μM thymidine. Cells were treated with 100 ng/ml colcemid for 1 h, swollen in 75 mM KCl for 5 min at 37 °C, and fixed in Carnoy's fixative before preparation of metaphase spreads. Slides were allowed to dry in air, rehydrated in PBS, incubated in 2 M HCl for 30 min, washed twice in 100 mM borate buffer pH 8.5 for 10 min, and blocked in 10% fetal calf serum in PBS for 30 min. Further immunofluorescence and imaging was performed as above.

Single- and double-strand break assays. Alkaline comet assays were performed essentially as described[25] and DNA breaks induced with 50 μM H_2O_2 (RPE-1 cells) or 25 μM H_2O_2 (primary fibroblasts) for 10 min on ice. Data are plotted as the average comet tail moment (an arbitrary-unit measure of DNA strand breaks) of 100 cells per sample and are the mean (± s.e.m.) of three independent experiments. For double-strand break repair assays, cells were irradiated with 2 Gy using a Gammacell 1000 machine, and γ-H2AX quantified at the indicated times, afterwards. Data are the average number of γ-H2AX foci per cell from about 1,000 cells per sample, scored by Olympus ScanR software, and are the mean (± 1 s.d.) of three independent experiments.

Mouse maintenance and analysis. Animals were maintained and used under the auspices of UK Home Office project licence number 70/8300. The generation of *Parp1*$^{-/-}$ and *Xrcc1*$^{Nes\text{-}Cre}$ mice have been reported previously[7,26]. Intercrosses between *Parp1*$^{-/-}$ and *Xrcc1*$^{+/loxp}$ mice were maintained in a mixed C57/Bl6 × S129 strain and housed on a 12 h light/dark cycle with lights on at 7:00. Temperature and humidity were maintained at 21 °C (± 2 °C) and 50% (± 10%), respectively. All experiments were performed under the UK Animal (Experimental Procedures) Act, 1986. Genomic DNA was extracted from biopsied tail using the REDExtract-N-Amp Tissue PCR Kit in accordance to the manufacturer's instructions (Sigma). For *Parp1*, the following primers were used: *Parp1* F1 (5′-GTT GTG AAC GAC CTT CTG GG-3′), *Parp1* R1 (5′-CCT TCC AGA AGC AGG AGA AG-3′), and *Parp1* R2 (5′-GCT TCA GTG ACA ACG TCG AG-3′). PCR products were generated by an initial denaturation step at 94 °C for 2 min followed by 35 cycles of 94 °C for 30 s, 54 °C for 40 s, and 72 °C for 180 s. *Xrcc1* was amplified using the forward PC1 (5′-TAT GCT TGC TGT ACA GGG ATT GGG-3′) and reverse PC2 (5′-TGG ACC ATG AAA AAG CTG TGT GC-3′) primers. A 400 bp *cre* PCR product was generated using the forward Cre-3 (5′-CTG CCA CGA CCA AGT GAC AGC-3′) and reverse Cre-4 (5′-ACC TGC GGT GCT AAC CAG CG-3′) primers. Both *Xrcc1* and *Cre* PCR products were amplified using the following PCR conditions: initial denaturation for 5 min at 94 °C followed by 35 cycles of 94 °C for 30 s, 59 °C for 45 s and 72 °C for 45 s.

Nissl staining of paraffin-embedded sections. Brains were removed at the indicated times and placed in 10% neutral buffered formalin (3.7% formaldehyde, 3.5 g/l NaH_2PO_4, 6.5 g/l Na_2HPO_4) for 24 h and then transferred to PBS. Paraffin embedding, sagittal sectioning and Nissl staining were performed by Propath UK (Hereford, UK) and UCL IQPath (Institute of Neurology, London, UK). Briefly, deparaffinized sections were stained in 0.1% cresyl violet solution (0.1% cresyl violet, 0.3% glacial acetic acid) for 3–10 min, rinsed in water, then 95% ethanol for 30 s to 5 min, 100% ethanol for 2 × 5 min, and xylene for 2 × 5 min before mounting. Nissl-positive interneurons were counted within three randomly selected 16,875 μm^2 regions of each molecular layer, and the number of cells per square micrometre was calculated.

Rotarod analysis. To evaluate motor coordination/cerebellar ataxia, an accelerating Panlab Rotarod (Harvard Apparatus, UK) was used. The apparatus was composed of a rod with a diameter of 30 mm divided into five opaque methacrylate arnite barriers, separating the rod into five 50 mm sections. Mice were trained for three successive attempts on the day before assessment. For assessment, mice were positioned on the rod facing away from the experimenter while the rod was stationary. Once activated, the rod accelerated at 0–40 r.p.m. at an acceleration rate of 5 r.p.m. per minute. Mice were rested for 15 min between each of the three trials and then positioned back on the rod for the next assessment. The time spent on the rod was recorded for each mouse and the mean time was calculated from the three independent trials.

Purkinje cell recordings. Vermis parasagittal slices (200 μm) were taken from P13–P17 mice using a vibroslicer (VT1200S, Leica Microsystems, Germany) in ice-cold artificial cerebrospinal fluid containing (in mM): 125 NaCl, 2.5 KCl, 25 glucose, 1.25 NaH_2PO_4, 26 $NaHCO_3$, 1 $MgCl_2$, 2 $CaCl_2$ (bubbled with 95% O_2 and 5% CO_2, pH 7.3). Slices were maintained in artificial cerebrospinal fluid at 34–35 °C for 45 min and then at 23–25 °C for electrophysiology. Voltage-clamp recordings of Purkinje cells were performed in cell-attached mode using a Multiclamp 700A amplifier (Molecular Devices) with pipettes (5–7 MΩ) containing 150 mM NaCl. Signals were filtered at 10 kHz and digitized at 50 kHz, and analysis of spike activity performed offline using Clampfit (Molecular Devices).

Data analysis and statistics. The number of experimental repeats and statistical tests (conducted in Microsoft Excel or GraphPad) are indicated in the relevant figure legends. The means of population averages from multiple independent experiments (± s.d. or s.e.m.) are indicated. Where appropriate, power calculations were conducted using online statistical resources. The experiments were not randomized. Samples were not blinded but the collection and analysis of microscopic data were automated and free of user bias. No animals/samples were omitted from data points/data analyses.

Data availability. The data sets generated during and/or analysed during the current study are available from the corresponding authors on reasonable request.

19. Tetreault, M. *et al.* Whole-exome sequencing identifies novel ECHS1 mutations in Leigh syndrome. *Hum. Genet.* **134,** 981–991 (2015).
20. Cappelli, E. *et al.* Involvement of XRCC1 and DNA ligase III gene products in DNA base excision repair. *J. Biol. Chem.* **272,** 23970–23975 (1997).
21. Breslin, C. & Caldecott, K. W. DNA 3′-phosphatase activity is critical for rapid global rates of single-strand break repair following oxidative stress. *Mol. Cell. Biol.* **29,** 4653–4662 (2009).
22. Fu, Y., Sander, J. D., Reyon, D., Cascio, V. M. & Joung, J. K. Improving CRISPR-Cas nuclease specificity using truncated guide RNAs. *Nature Biotechnol.* **32,** 279–284 (2014).
23. Mali, P. *et al.* RNA-guided human genome engineering via Cas9. *Science* **339,** 823–826 (2013).
24. Pinkel, D., Thompson, L. H., Gray, J. W. & Vanderlaan, M. Measurement of sister chromatid exchanges at very low bromodeoxyuridine substitution levels using a monoclonal antibody in Chinese hamster ovary cells. *Cancer Res.* **45,** 5795–5798 (1985).
25. Breslin, C. *et al.* Measurement of chromosomal DNA single-strand breaks and replication fork progression rates. *Methods Enzymol.* **409,** 410–425 (2006).
26. Wang, Z. Q. *et al.* Mice lacking ADPRT and poly(ADP-ribosyl)ation develop normally but are susceptible to skin disease. *Genes Dev.* **9,** 509–520 (1995).